Fractional Calculus
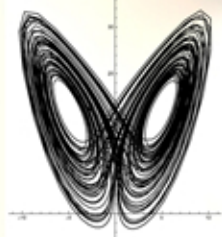
Applications

Roy Abi Zeid Daou
Xavier Moreau

Editors

FRACTIONAL CALCULUS
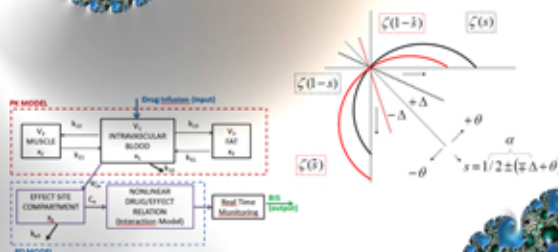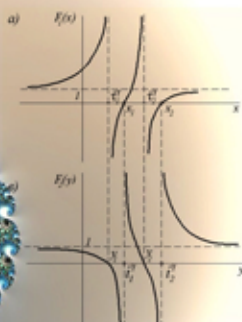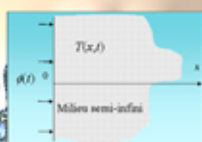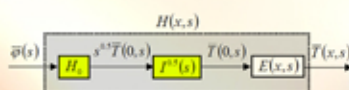
APPLICATIONS

MATHEMATICS RESEARCH DEVELOPMENTS

Additional books in this series can be found on Nova's website
under the Series tab.

Additional e-books in this series can be found on Nova's website
under the e-book tab.

FRACTIONAL CALCULUS

APPLICATIONS

ROY ABI ZEID DAOU
AND
XAVIER MOREAU
EDITORS

Published by Nova Science Publishers, Inc. † New York

CONTENTS

FOREWORD

Non-integer differentiation does not escape to the slogan "different operator, different properties and performances". This is indeed the concise formula that is likely to explain the "why" of this operator, especially as most of its properties and performances favorably distinguish, not only the operator itself, but also the models that use it.

It is true that we have established non-integer models that overcome the mass-damping dilemma in mechanics and the stability-precision dilemma in automatic control, the technological achievements associated with these models have been made possible thanks to an adequate synthesis of the non-integer differentiation operator.

It is indeed the idea to synthesize non-integer differentiation (in a medium frequency range) through a recursive distribution of passive components, of transitional frequencies or of zeros and poles, which is at the origin of the non-integer differentiation operator real-time use and, therefore, of both analogical and numerical applications that arise from it. As for the corresponding dates, the synthesis as we have led it has been developed by stages and thus proposed and experimented in the 70s for half-integer orders, in the 80s for real non-integer orders and in the 90s for complex non-integer orders.

The first technological applications of this operator (henceforth usable in real-time) and notably the first application in 1975 of a "half-integer order controller" to the frequency control of a continuous dye laser, have widely contributed to take the non-integer differentiation out of the mathematician drawers and to arouse new developments likely to enrich the theoretical corpus of circuits and systems.

In this way France has been the first country to know a renewed interest on non-integer differentiation, this renewal having been well relayed thanks to the dynamism of the foreign scientific communities, at the European level as well as at the international level.

In this context, the French institutions have encouraged research in this field through the acknowledgement of major scientific advances and the support of initiatives or actions aiming to favor the synergies between the different themes and between the academic and industrial components, the University-Industry partnership having indeed been nationally rewarded by the AFCET'95 Trophy distinguishing the CRONE suspension as best technological innovation. Concerning the acknowledgements, let us cite the selection of the CRONE control as a "striking fact" of the Centre National de la Recherche Scientifique (CNRS) in 1997 and as "Flagship Innovation" of Alstom in 2000 (Hanover and Baden Baden International Fairs, 2000), a Silver Medal of the CNRS in 1997 and the Grand Prix Lazare Carnot 2011 of the Science Academy (founded by the Ministry of Defense). Concerning the supports, let us cite the actions

financially supported by the CNRS and the Ministry of Research: the edition of "La commande CRONE" (Hermès, 1991) with an exceptional help of the ministry; the International Summer School "Fractal and hyperbolic geometries, fractional and fractal derivatives in engineering, applied physics and economics" (Bordeaux, 1994); the national project of the CNRS, "Non-integer differentiation in vibratory insulation" (1997-1999); the colloquium "Fractional differential systems" (Paris, 1998); the launching in 1999 of the thematic action of the Ministry of Research "Systems with non-integer derivatives"; the launching in 2004 of the IFAC Workshop "Fractional Differentiation and its Applications" through the first Workshop FDA'04 (Bordeaux, 2004) with S. Samko as chairman of the International Program Committee ; the magisterial lecture "From diversity to unexpected dynamic performances" initiated by the French Science Academy (Bordeaux, 5 January 2012).

But this academic support also found a guarantee in the industrial support brought by a strong partnership with major companies as PSA Peugeot-Citroën, Bosch (Stuttgart) and Alstom, such a partnership having indeed led to a high number of patents and technological transfers that have widely proved the industrial interest of non-integer approaches.

Alongside the shared efforts to inscribe these approaches in the realist frame of the University-Industry relations, our efforts have never stopped being shared with those of the international scientific community to develop the best relations and collaborations within this community. Without aiming for exhaustiveness, let us cite the involvement of European countries in the diffusion, promotion and animation within the community: the research group "Fracalmo", which originates from **Fra**ctional **cal**culus **mo**delling, started with a round table discussion in 1996 during the 2nd International Conference "Transform methods and special functions" held in Bulgaria; the journal "Fractional Calculus and Applied Analysis" (FCAA) started in 1998 with V. Kiryakova as managing editor; the survey on the "Recent history of fractional calculus" (*Communications in Nonlinear Science and Numerical Simulation*, 2010) at the initiative of J.T. Machado who desired to make an inventory of the major documents and events in the area of fractional calculus that had been produced or organized since 1974; the symposium "Fractional Signals and Systems" (FSS) launched by M. Ortigueira in 2009 at Lisbon, then held in 2011 at Coimbra (Portugal) and in 2013 at Ghent (Belgium). Both in and out of Europe, let us also recall the various events of the Workshop FDA after its launching at Bordeaux in 2004 (under the aegis of IFAC): Porto (Portugal) in 2006; Ankara (Turkey) in 2008; Badajoz (Spain) in 2010; Nanjing (China) in 2012; Grenoble (France) in 2013; Catania (Italy) in 2014 (under the aegis of IEEE).

Founder of the CRONE team that counts today about ten permanent researchers, I recognize this team to have always escorted me in the federative actions, launched within the national or international scientific community, to energize and harmonize the researches on both theoretical and applicative aspects of non-integer differentiation.

Xavier Moreau, member of the CRONE team, and Roy Abi Zeid Daou, associated member, who are implied in this book as coordinators well attest this will to be at the initiative of collective actions. It is then a pleasure for me, through this foreword, to warmly congratulate them for their efforts of scientific coordination at the international level, especially as the number of proposed contributions in this book well proves the dynamics of the fractional (or non-integer) community.

Alain Oustaloup

PREFACE

After presenting the first volume of this two-volume book, presenting a lot of mathematical and theoretical studies and research related to non-integer calculus, the second volume illustrates lots of applications related to this domain. In the following, we will present the applications discussed in this book.

This volume is made up of 11 chapters. The first chapter presents the heuristic power of the non-integer differential operators in physics starting from the chaos to the emergence, the auto-organizations and the holistic rules. The second chapter shows the dynamics of the fractional order chaotic systems along with some applications. The third chapter represents the pressure control of gas engines by non-integer order controllers by showing a novel trend in the application of the fractional calculus to automotive systems.

Chapter 4 shows the way to model fractional order equations using state space modeling along with some applications. Another application related to this domain is the thermal diffusive interface. Chapter five shows the analysis of a semi-infinite diffuse plane medium along with the equations that model this medium, and some frequency and time domain responses. However, chapter six treats this problem by controlling this plant using the well-known CRONE controller.

Chapter eight presents the adaptive second-order fractional sliding mode control with an application to a water tanks level system. Chapter nine treats the mechanical aspect by showing the features of the fractional operators applied to this domain. Also, chapter nine presents the theory of diffusive stresses based on the fractional advection-diffusion equation.

The modeling of drug diffusion during general anesthesia using Fractional Calculus is shown in chapter ten and is considered as another application related to the biomedical field. At the end, chapter eleven represents an overview of the fractional fuzzy controllers by showing the analysis, the synthesis and the implementation of this module.

To sum up, this second volume presents lot of applications of fractional calculus in several engineering domains as the thermal, the automotive, the mechanical, the biomedical and much more. Note that this volume was preceded by a first volume that focuses on the mathematical and theoretical aspects of fractional calculus.

Chapter 1

The Heuristic Power of the Non Integer Differential Operator in Physics: From Chaos to Emergence, Auto-Organisations and Holistic Rules

Alain Le Méhauté[*]

Physics Department, Kazan Federal University, Kazan, Russia

Abstract

The use of fractional differential equations raises a paradox due to the non-respect of the space time noetherian axioms. In environments characterized by scaling laws (hyperbolic geometry associated with fractional diff-integral) energy is no more the invariant of the dynamics. Nevertheless the experimental action requiring the use of energy, the relevant representation of the fractional-process, must be extended. The extension is carried out using the canonical transfer functions in Fourier space and explained by their links with the Riemann zeta function. Category theory informs the extension problem.

Ultimately the extension can be expressed by a simple change of referential. It leads to embed the time in the complex space. This change unveils the presence of a time singularity at infinity.

The paradox of the energy in the fractality illuminates the heuristic power of the fractional differential equations. In this mathematical frame, it is shown that the dual requirement of the frequency response to differential equations of non-integer order and of the notherian constraints make gushing out a source of negentropique likely to formalize the emergence of macroscopic correlations into self-organized structures as well as holistic rules of behaviour.

1. Introduction

The heuristic power of the fractional derivation operator is based at least upon three theoretical foundations

---

[*] E-mail address: alm@materialsdesign.com

- the canonical link between the fractional operators and fractal geometries. This type of operator expresses the non-differentiability of the geometry (Le Méhauté, 1982a),
- the generalization of exponentiation operation in the frequency space. This generalization is related to partial hyperbolic geodesics (Nivanen, 2005),
- the relation between this generalization and Riemann's (and Goldbach's) hypothesis that gives meaning to the universal approximations of all analytic functions (Voronin, 1975) (Bagshi, 1987).

The assertion of heuristic power of fractional diff-integral operators finds its sources, within the first generalization of Zipf laws in the form of so-called Zipf-Mandelbrot law (Le Méhauté, 1974, 1977). These publications link the recursive structures of the statistical supports (trees and hyperbolic groups) and the thermodynamic laws by merging geometries and singularity distributions. By extending the concept of recursivity into geometry, Mandelbrot published in 1975 his first works on 'fractal geometries' (Mandelbrot 1975, 1982), a word forged for the purposes of the case. To describe the exchange of energy and matter dynamics in heterogeneous environments (ie fractal structures) (here considered as a mathematical distribution ground (Schwartz, 1950)) the author of this paper has developed at the end of the seventies a model of transfer of energy on fractal structure embedded in a physical environment (electrolyte, liquid, air, etc.) named TEISI model (Le Méhauté, 1980, 1982a, 1984). This model merges a class of convolution between fractal structures (geometric factor) and traditional differential operators (dynamics factor). It gives a theoretical base to a new type of irreversible dynamics. After the Oldham and Spanier (Oldham, 1974) and Nigmatullin's senior formal works (Nigmatullin, 1975), the TEISI model and its fractional operators feature the way for a theoretical analysis of processes characterized by an irreversibility based upon geometry. Jointly, the relevance of these operators for the optimization of electrochemical energy storage devices (Le Méhauté, 1982b, 1986) was performed. There followed a 'declension' of many issues about irreversibility that leads to the establishment of a link between fractals and hyperbolic geometries (Nivanen, 2005), number theory (Le Méhauté, 2010) and theory of categories (Riot, 2013).

Despite an undeniable prospective effectiveness and numerous coherent experimental data (Le Méhauté, 1983, 1986, 1992), opinion still mainly given to this work, is the one expressed by Pierre Gilles de Gennes referee to the Academy of Sciences of Paris, in the defense of the first publications of the author (Le Méhauté 1982a). He wrote in footnote page "*L'introduction d'une hypothèse de self similarité sur la structure de certaines électrodes parait extrêmement féconde. Par contre l'équation reliant directement la dépendance en fréquence de l'impédance à un paramètre purement géométrique (...) semble très conjecturale. Dans les quelques exemples connus de transport impliquant un fractal (amas de percolation, réseaux de Sierpinsky,...) l'exposant de conductivité n'est pas lié directement à la dimensionnalité*". Let us see why the assumption of the *transport of species* evoked by P. G. de Gennes, twists the empirical point of view with respect to the hypothesis based on the *transfer of energy*. Due to the range of frequency analysis (Hertz plus microwaves range) the analysis of the efficiency of (i) the batteries and (ii) of the cable impedance served as an excellent compass.

Let us see why despite the approval of the scientific community to de Gennes' reserves, and after the epistemological choice of this community for considering the fractal interface

only as an external boundary conditions with regard to the transportation of physical species (matter, ions, electrons, entropy, energy), the author continued his work in the original direction by addressing the issue of *transport in fractal* media through the theory of distributions as a simple limit case of *transfer process*.

2. A Nice Equation for an Heuristic Power

"Sole a beautiful equation may have a deep meaning!" This is the case of the equation below. It establishes a merging between fractal geometry and the operator of the fractional differentiation in the Fourier space, via the set of the integer numbers:

$$[\eta(\omega)]^d (i\omega\tau) = const \quad , \tag{1}$$

As shown in (Le Méhauté, 1982a), this equation does not *a priori* assume, (as one may understand *a posteriori*) the presence of a link between space and time. In the frame of distribution theory it just assumes the empirical constraint for a measurement of a recursive ordered structure (interface), which canonical expression is given via a set of integers. The emergence, a posteriori, of temporal variables is a simple mathematical consequence of the use of this one dimensional set when it is plunged in the set of pure complex numbers. This mathematical embedding comes from the interpretation of the Hausdorff-Mandelbrot equation

$$\nu\eta^d = const \quad , \tag{2}$$

(Mandelbrot, 1975, 1982) by using the number expressed by. In equation (1) the complex number 'i' expresses the independence of the local measure of the space with regards to the computation required by a global normalization of the fractal interface. The reference 'τ' expresses the requirement for time normalisation. The normalization keeps the scaling invariance to the fractal geometry, when it is used as support of the exchange for the transfer of energy.

Beyond all the outstanding issues about the definition of the operator in time (the whole of this book), this equation expresses the issue open by the non-integer derivation, in its recursive simplicity. For the reasons given above and developed below, we assert that the Fourier space is the natural space of description for all recursive geometries:

$$\eta(\omega) \approx \frac{1}{(i\omega\tau)^{1/d}} \quad . \tag{3}$$

We maintain that, including in a majority of experimental cases, it exists a direct link between the expression of the derivation of non-integer order in this space and the fractal dimension of a substructure that is the support of the transfer of energy. It is expressed physically through a generalization of the concept of capacity that we called 'Fractance' (i.e., capacity on fractal support).

This concept founds the use of non-integer derivative in physics. Moreover the use of this formulation in the frequency domain (Fourier or Laplace) postulates a 'computational foundation' for the emergence of well-ordered variable that we name the 'irreversible time' which is practically useless in mechanics (Rovelli, 2004, 2006) (Connes 1994)

Such a variable must be considered like simple mathematical object in accordance with Hausdorff-Mandelbrot rule. In practice, equation (1) interpolates an invariant factor of the fractal dynamics between the concept of velocity (, $d = 1$) and concept the diffusion coefficient (, $d = 2$). Probably intuitively perceived by de Gennes when assuming exclusively *transport* processes, this interpolation points out an apparent physical 'weakness'. Indeed, due to its dimensions, the new invariant cannot possess a simple physical meaning. Meanwhile at the beginning of the eighties, the heuristic hypotheses of dynamic recursivity described via diff-integral, was already well assured by the results obtained from the efficiency of the batteries, and also supports preliminary development of the CRONE control (Oustaloup, 1983).

There was something of a contradiction. Including with the Mandelbrot's works the engineering was at that time the spearhead of dynamics in fractality and advanced open interrogations. The paradox raised by the contradiction between theory and experiment, (no solved by the use of the concept of transport) unveiled an unquestionable opportunity for making a conceptual breakthrough.

3. SWOT Method, Non Integer Diff-Integral and Co-Dimension

We recall that the TEISI model assumes a 2D symmetry of the macroscopic experimental complex structure which geometry looks like a capacitor. In addition the symmetry of the force-field locates the fractal dimension d in the range given by.

The relevant remark of P. G. de Gennes concerning the weakness of the TEISI model was finally upset as follows: as a matter of fact, the relevant dimensional invariants required in expression (1) are not part of the usual invariants used when energy is exchanged upon integer dimensional interface. In that standard case, the dimensional equation for the energy is:

$$E = ML^2t^{-2} \ , \tag{4}$$

(in Fourier space) and the dimension of the physical action is given by

$$A = ML^2t^{-1}, \tag{5}$$

(in Fourier space). These dimensions cannot be simply applied when environments is characterized by scaling properties. It has to be really 'adapted' to the problem. The standard energy is expressed in space-time by the square of a velocity. This square factor cannot appear naturally when dynamics is deployed in fractal geometry: indeed, the support is not differentiable and therefore, cannot easily have any gradient operator at its disposal.

The second question addressed by the problematic concerns the global point of view upon the interface: the space-time integral, expressed by the macroscopic law

$$x^d \approx t \ , \tag{6}$$

cannot be reduced to the diffusive formulation

$$x^2 \approx t \ , \tag{7}$$

or even to

$$x^{d/2} \approx t \ , \tag{8}$$

initial de Gennes proposal. Because, any experimental process is dissipative it might appear simple to express the problem of fractality as an anomalous diffusive process

$$\left[\eta(\omega)\right]^2 \left(i\omega\tau\right)^{1/d} = const \ . \tag{9}$$

Alas! There was worse to come: these formulations didn't solve, in any manner, the controversial issue *transport* against *transfer* pointed out above. Are these threats, a condemnation of the use of distribution theory and the non-integer order operators? The answer is clearly negative. All attempts to simply mask the defect of fitting between the concept of energy and the concept of fractal, is just a dead end. This question requires, as we have shown very early (1978), a reference to the concept of fractal co-dimension (Tricot, 1999). If the formulation (1) infringes the principles of Emmy Noether (energy cannot more be the expression of the homogeneity of fractal space-time), the difficulties are not mathematically intrinsic but extrinsic. They are strongly related to the contradiction between the Noether's axioms and the scaling properties of the fractal interface measurements. The contradiction between standard theories and experiments, when fractal media is involved, is due to the restrictive requirement imposed by the use of energy for checking the physical properties. This difficulty must be addressed to an epistemological issue that not only assumes an extrinsic meaning of energy (homogeneity of space-time) but uses of balls (in maths) or/and energy (in physics) to perform all practical measurement even if far from homogeneity (complex media). The non-differentiability and the related fractional statistics, hidden behind the transfer TEISI model, unveil precisely the conceptual limitations that must be addressed head on.

If the fractal dimension is *d*, let us observe that the Noetherian homogeneity can be conceptually 'restored' using the concept co-dimensional space by writing

$$E_\omega = \left(ML^d t^{-1}\right)\left(L^{2-d}\right) \ , \tag{10}$$

or, in Fourier space, the geometric co-density of energy

$$E_\omega / L^{2-d} = \left(ML^d t^{-1}\right), \tag{11}$$

is obviously the Hausdorff-Mandelbrot dimensional content of the co-fractal space. Let us also observe that the formulations can be reversed by writing

$$E_\omega = \left(ML^{2-d}t^{-1}\right)\left(L^d\right) \tag{12}$$

and

$$E_\omega / L^d = \left(ML^{2-d}t^{-1}\right) . \tag{13}$$

This inversion points out one of the major symmetry for the transfer of energy in fractal media. The question raised by these formulas is the meaning of the co-fractality (). It is obviously related to the embedding of the fractal interface in the two dimensional space. This embedding is required to perform measurement and experiences as well. As exemplified for a long time in energy storage industry (battery energy/power balance optimization), we can confirm that the fractality, which raises the paradox Energy vs Fractal, also opens up new opportunities for technical breakthrough: the design of the geometry is an extrinsic optimization factor of the irreversibility of the process deployed in fractal media. Energy storage requires 3D structures whereas Power requires 2D interface. Depending of the need, the fractal dimension balance is obviously in between. Conversely, the entropy/negentropy ratio must control the metric and therefore 'curvature' of a fractal geometry.

We will see that the constraint of continuity along the fractal object is a central factor for optimization principle. It is expressed by a geometrical phase. Then the metric of the geometry determines the ratio of the entropy/negentropy production. To easily understand the contents of the role of this ratio we need to consider briefly the fractional generalization of exponentiation.

4. The Generalization of the Exponential Concept

The 'exponential' and 'logarithm' functions play a central role in physics. This role has its origin in the morphism between addition and multiplication. As shown in category theory, this morphism is essential in mathematics and physics because it establishes a strict relationship between the constructivism performance, that is the addition of ordered structures (adding is considered then as a co-product), and the partition or deconstruction of the same structures into substructures (represented by the product). The question addressed by this morphism concerns the content of the 'differance' with 'a' and not 'e' (Derrida, 1973) which controls the irreversibility. We shall find in non-extensive thermodynamic developments, a useful analytic extension of exponential functions and logarithms within the time space (Nivanen, 2005). However, these extensions can only reach a deep geometrical meaning in Fourier space.

The exponential term in the Fourier space is always given through a semicircle

$$Z(\omega\tau) \approx \frac{R}{1+i\omega\tau} . \tag{14}$$

This is a transformation obtained by a geometrical reversing of a straight line with respect to a point located outside of the line. This modular formulation (Ghys, 1990) is canonical and it is rightly adapted to our purposes because it opens the matter of geodesics in hyperbolic space. The impedance takes the dimension of a resistor:. For longtime and R defines a state in the thermodynamic sense. The semicircle, inverse of a straight line, is also a geodesic because its inverse Fourier transform is (i) the classical first order relaxation dynamics solution and (ii) the merging of additive and multiplicative properties. Both properties give to the exponential function a canonical characteristic of a closure (construction, ω-algebra/τ-algebra, deconstruction).

Starting from that observation an heuristic approach built from this canonical form leads to consider the TEISI model as a rather natural 'declension' of exponential function because the introduction of the fractal geometry as an interface for transfer of energy involves geodesics as arcs of circle. We recall that TEISI model leads

$$Z_{1/d}(\omega\tau) \approx \frac{R\cos\varphi}{1+(i\omega\tau)^{1/d}} \quad . \tag{15}$$

Then, we can confirm that

$$\eta(\omega\tau) = \frac{u(\omega\tau)}{v(\omega\tau)} \quad , \tag{16}$$

expresses the hyperbolic distance on . The scaling correlations conditions are deliver for (respectively) where is the phase angle associated with the rotation given by in the complex plan. This phase angle which requires information coming from the environment renders the above Cole and Cole representation incomplete. The paradox is not only the absence of standard thermodynamic equilibrium state function at infinity, (when this infinity is defined by), but also the requirement for a couple of referentials to define the whole representation. Even if the origin of the phase at infinity comes from intrinsic recursive correlations characterizing the fractal support of the process, it requires the embedding within a larger environment. This requirement looks like Kan extension and virtualisation of sets in the frame of the theory of categories (Riot, 2013). In spite of these difficulties Gemant analysis (Gemant, 1935) and Cole-Cole synthetic formulation (Cole, 1942) has a real empirical effectiveness. Let us observe that the fractional process is characterized by. Then the points at infinity contain phase information which reduces relatively to R the entropy. Therefore, beyond the questions raised by the temporal expression, the Fourier space representation reveals a new core of problems concerning the balance between entropy and negentropy production in complex media: the role of the boundary (environment). Then the question of local causality in the traditional sense can be clearly addressed precisely from the incomplete TEISI transfer formulation.
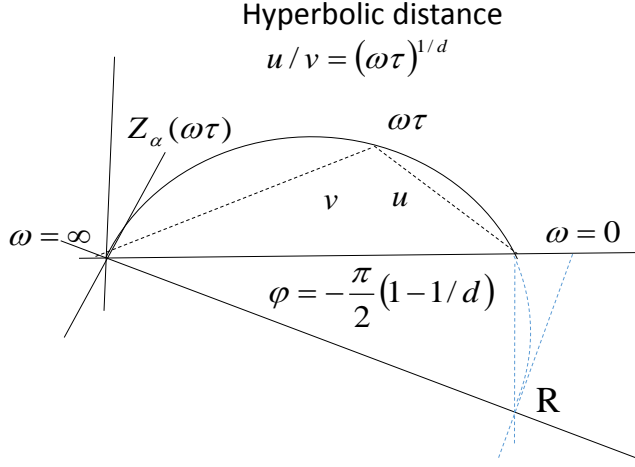
Figure 1. Typical Cole-Cole transfer function for a canonical fractional differential equation (Le Méhauté, 1982).

To give a content to this remarks it is possible to refer to the impedance related to diffusive TEISI degeneration when fractal interface fulfils the 2D space.

5. Diffusion Under Field

The diffusive model can be written in the frame of the TEISI model as . Let us compare this equation with the fractional expression of the diffusion equation that uses non integer differential equations (Oldham, 1974) (Podlubny, 1999):

$$\frac{\partial}{\partial t} - D\frac{\partial^2}{\partial x^2} = \left(\frac{\partial^{1/2}}{\partial t^{1/2}} - \sqrt{D}\frac{\partial}{\partial x}\right)\left(\frac{\partial^{1/2}}{\partial t^{1/2}} + \sqrt{D}\frac{\partial}{\partial x}\right) \ . \tag{17}$$

The second factor of that equation is a non-causal operator, whose physical meaning, to our knowledge, has never been considered. Even hidden, this factor plays a role which is crucial especially if some characteristics can fit the complementary set of

$$Z_{1/2}(\omega\tau) \approx \frac{R\cos(\pi/4)}{1 + (i\omega\tau)^{1/2}} \ , \tag{18}$$

in the complex plan, that is to say, the role played by the co-dimension in the general TEISI analysis. In order to fit this meaning, we have to observe that the thermodynamic 'gradient' must be written

$$\frac{\partial U}{\partial x} \approx U_\infty(t) - U(t) \ . \tag{19}$$

It is expressed by the means of a pivot which is an energy in the process used for measurement. The harmonic ratio

$$\frac{U(\omega\tau)}{U_\infty(\omega\tau)} = Z(\omega\tau) \tag{20}$$

is then precisely the impedance. As shown by J. P. Badiali in the frame of statistical thermodynamics when based on path integrals (Badiali, 2013), this energy is used as a reference point for energy balance. This pivot gives a generalization of the physical concept of equilibrium and a reference for causality principle. The main question is the following: when such a reference is used, is the entropy increasing or decreasing with respect to the fractal correlations along the process? Indeed, the conditions of the existence of a flow of 'negentropy' remain to be clarified to address the issue of non-causal factor. The diffusive example can serve as a guide to address the issue of the absence of energetical dimensional fitting because this absence is clearly related to this non-causal factor.
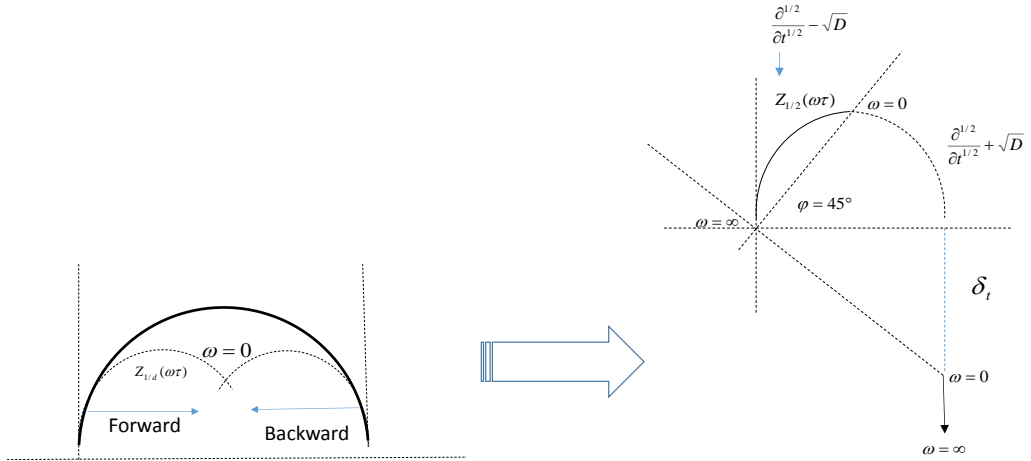
Figure 2. Analysis of diffusive process with field using the merging of forward and backward fractional process in the Poincaré fundamental domain (Nivanen, 2005).

As evoked above, due to the use of energy as the essential experimental factor for defining the equilibrium, the representation of empirical data by the means of a derivative operator of non-integer order, over fit like the ball of measurement the fractal interface properties. So the description of the fractal reality with non-integer operator is almost surely incomplete with respect to the physical experiment. Nevertheless this assertion is paradoxical if coupled to the Godel incompleteness theorems: the set of rational numbers is obviously larger than the set of natural numbers. To precise the content of this paradox we have to analyse the response given when half diff-integral is considered in the frame of non-integer operator application? Unlike transport models and the use of temporal operators without precaution, the Fourier space used to express the TEISI model opens into the origin of a natural incompleteness. We have already shown that the model is related to the chaotic dynamics upon punctuated torus characterized by an angle at boundary (Nivanen, 2005). In the diffusive frame, the angle at infinity is $\varphi = (\pi/2)/2$. This angle is critical: the canonical diffusive process *(d=2)* under field may be

considered as the merging schematized in the diagram given below. A couple of causal (forward) and a-causal (backward) tiles of a generalized Poincaré fundamental domain mapping (Figures 2 and 3) enters in confusion if $\alpha = 1/2$.

Because for *d=2*, the diagram merges a couple of components for stating a new meaning of the resistance *R*, that is to say the role of local energy within the whole dissipative process. The merging renders obvious the role played by the referential of the representation. The passing from the non-integer order differential equation (irrelevance of the energy) to its integer counterpart (relevance of the energy) requires a rotation of the external referential with respect to the angle. The referential attached to the fractal interface (external with regard to energy) is opposed to the overall-referential (qualified as internal). In the first referential (limited to the harmonic analysis) the operational time is associated with the inverse Fourier transform of omega. The process is linearly approximated. In the frame of the second referential, the relevance of the time requires to take into account a singularity at boundary. In the diffusive traditional equation, an initialization of a process in the Atlantic east coast of United States, involved an immediate modification of the state of the sea in the west coast of Britany. This non-physical singularity is fortunately a forgotten non-physical characteristic of integer representation of a diffusive process. This paradox refers to internal equation referential. In the first referential, nonobstant the singularity at infinity, the process states a pseudo-equilibrium, as 'Zeit Objekt'. This object is given under the sole linear constraint. It is qualified as a pseudo-equilibrium because it satisfies independence from the clock-time variable, seen as an inverse transform of Fourier frequency. However this time is not the relevant variable with respect to the energy balance. This balance requires a meaning for the local concept of differentiation. It forgets the singularity on the time variable mainly ignores on the way of fractional representation when taking into account the sole fractality. Somehow paradoxically, the singularity involved with the complex time, restores the Noetherian-homogeneity of lost space-time via the sole fractality.

We shall show that this singularity contributes to the emergence of a negentropique factor. This factor balances the disequilibrium of the 'energy' between the fractal interface characterized by the forward process, using 'something happening' in the co-fractal environment. The theory of the categories may explain this emergence as a Kan extension of the fractal space-time (Riot, 2013). At this stage the controversy opened in 1982 reaches its heuristic pungency. The will stays focused on the TEISI transfer process supported by a huge undeniable set of experimental data that ignores transportation. The angle at infinity appears naturally as a key factor of the paradoxes concerning the energy. Since the incompleteness of non-integer operators is pointed out, it also asks for understanding the precise choice of the space time referential. From that point of view, the problem looks like the issue of the Coriolis momentum within a rotational referential. The analogy is peculiarly relevant because fractal geometry is strongly linked to the hyperbolic geometry. In this frame the fractal dimension *d* is related to a curvature of the geodesics, i.e., their common acceleration. This acceleration is characterized by the singularity of the dynamics that characterizes an extended 'time' at infinity. Then, the paradox of the energy, led by the role of the resistance *R*, that is to say, the term of dissipation of energy, is related to the geometrical phase angle. According to the canonical model TEISI this angle carries a factor related to the internal correlations upon recursion which states, as for Coriolis momentum, the duality of the referential system when

fractal space is considered from inside or from outside. This is clearly unveiled when we relate both Natural and Fourier spaces.

For example, the inverse Fourier transform of gives a measure of local Dirac (Angot, 1972), but also gives meaning to the ball for measurement upon the fractal object. Conversely, the measurement of the gauge η, does not have any analytic expression in Fourier space. The gauge η is the only variable which may simply be expressed in physical space via except if we forget the Fourier Transform limitations

$$1/(i\omega\tau)^{\frac{1}{d}+1} := \eta(t) = t^{\frac{1}{d}} / \Gamma\left(1 + \frac{1}{d}\right) . \tag{21}$$

After analysis, the splitting between natural and Fourier space is normal, but may be surprising especially since the changes associated with $d = 2$, lead the exact identity of the diffusion operators involving a simple square roots:

$$\frac{1}{(i\omega\tau)^{1/2}} := \frac{1}{(\pi t/\tau)^{1/2}} . \tag{22}$$

This simplicity is not general if. Therefore we cannot consider the diffusive process (respectively the deterministic case) as a mere extension of the general fractal process. As already pointed by Peano and Cantor for recursive geometries and in another area by Galois and Abel with non-solvable groups, the diffusive process leads to face a degenerate form which cannot easily be derived from the general fractal process. This explains the reported link within others notes between our analysis and Gromov's hyperbolic groups: due to the absence of sharpness on branching (small-triangle at infinity), the scaling process cannot be completely defined from the hyperbolic tree seen as a set of branches. There is an uncertainty at branching. The difficulty lies precisely in the degenerate nature of this issue if $d = 2$ (respectively if $d = 1$). In the case $d = 1$ the semi-circle fully explains the local exchange of energy. In the case $d = 2$, we can consider the isometry between the arc and the euclidean process by passing the nonlinear scaling. As shown in the scheme below, due to equivalence of metric between hyperbolic and Euclidean (Nash theorem), we can use the fundamental Poincaré's group to lead an isometry represented as a pseudo-linear application.

The illustration of the isomorphism gives a simple obvious form to the geometric content of the Laplace operator $d=2$. This isomorphism, well understood from external algebra, manages the relationship between Euclidean space, associated to the local exchange of energy (gradient) and the hyperbolic geometry of the whole set of exchanges upon the interface characterized by a Peano structure (divergence of the gradient *vs.* TEISI). Insofar $d = 2$, the interface environment is none other than the interface itself. It prohibits any leakage of energy out of the local entropy production zone.
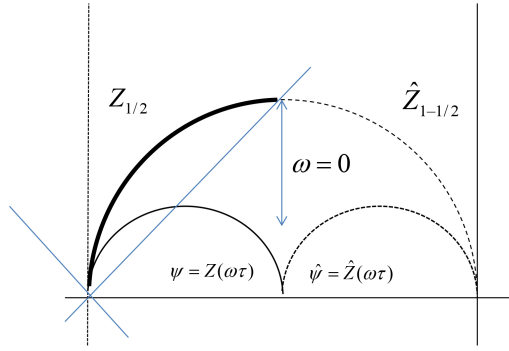
Figure 3. Illustration of the Nash isomorphism in the case of diffusive process with field (d=2).

Although Nash's theorem ensures that, such an isometry exists almost surely, even for a more complex hyperbolic structure than a Peano one, that is to say , intuition is much less immediate and the associated application is in this case, no longer linear as shown in the diagram below. In this diagram the tilling of the automorphism (related to the dynamics with) is very distinct of the Poincaré's mapping.
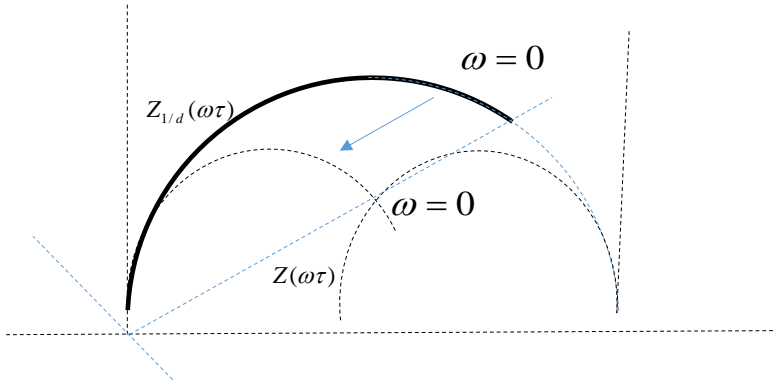
Figure 4. Representation in the frame of TEISI model of Nash's isomorphism in the general case.

The difficulties already pointed out can then be summarized as follows: merged in the same 'object', the sums of building (constructivist view and co-product) and of the products of processes (leading to partitions or reverse engineering), the extension of the concept of exponential in Fourier space, offers almost all the good properties of a generic functions. These functions are strongly connected with fractal metrics. Its representation in the complex plan is indeed a piece of hyperbolic geodesic. Nevertheless, this piece cannot possess one of the crucial properties required to perform a rigorous reverse engineering of the process: the distributivity. A 'difference' remains after any proceeding along a loop of building and deconstruction. This 'difference' is expressed by a phase factor (time irreversibility). Once again, for understanding this subtle issue we have to refer to the theory of categories. It explains the paradox of the energy, by suggesting the Kan extension as an operation to be considered for understanding the storage of information within the phase factor.

The use of any types of generalized exponential must be done with caution. It requires a deep understanding of physical phenomena in its own and external space time structure. A geometric understanding must guide the use of related fractional operators for the physical

representation of complex systems. Recall that what is behind the will of the representation of the reality is almost always the desire to find a causal reason. Here, this must be carefully considered only as a linear will. It may be a non-relevant extension of standard paradigms in the case of complex environment. In spite of the non-linearity of power laws, the scientist can easily fall into the trap of an artificial linearization. It is precisely to avoid this trap that it is necessary to understand the link between non-integer dynamics and Riemann zeta function as a topologic, or more precisely, homotopic parametrization of fractional dynamics.

6. Riemann Zeta Function and Non-Integer Differentiation

We recall that the expressions of the Zeta functions and are arithmetically related. We do not enter below in the subtilies of this relationship insofar it is well known for the experts in number theory. We considered only the function assuming that generalizations in the frame TEISI model are obvious. We recall that this function is expressed in the set of integers by (i) a power law under a form of a co-product:

$$\zeta(s) = \sum_{n=1}^{\infty} \frac{1}{n^s} \ , \tag{23}$$

with and also (ii) as a product based on the prime numbers (Tenenbaum2011):

$$\zeta(s) = \prod_{p_i \in \wp} \left[\frac{1}{1 - \dfrac{1}{p_i^{\ s}}} \right] . \tag{24}$$

The Riemann function therefore carries the combination of sums and products merged together. This merging recalls all the problems mentioned above. As consequence, the relationship between zeta function and fractality seems rather natural and the author has developed this question in details (Le Méhauté, 2010). The theory of categories makes echoes to this proximity in relation with the punctuated torus. In addition we have already derived a physical demonstration of the Riemann hypothesis based on the TEISI model by using a transition phase geometrical model. The basic diagram of the proof is given below (Figure 5).

According to the parametrizations of the hyperbolic distance $v/u = 1/(\omega\tau)^{1/d}$ this diagram suggests to introduce and then for building a topological morphism between each terms of the sum $\zeta(\alpha + i\theta)$ and each integer point upon $Z_\alpha(i\omega\tau)$. Each couple of points is obviously parametrized using integer frequency.
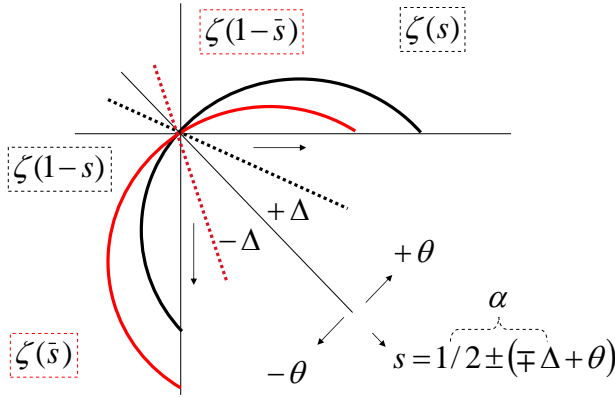
Figure 5. Key representation of the Riemann Zeta Function hearth in the frame of the TEISI model (Le Méhauté, 2010). Also representation of macro KMS condition *versus* Fractional Differentiation Riemann Approach through exchange of axis.

More generally, the zeta function (respectively its inverse) is part of a larger set, taking into account the sign of the rotation in the complex plan especially and according to the new set $\{\zeta(s), \zeta(1-s), \zeta(\bar{s}), \zeta(1-\bar{s})\}$. This set is obviously centered upon $\alpha = 1/2$. This set may be associated through a morphism to a new set of transfer functions which appear clearly in the diagram above. Both sets authorize the construction of a new morphism upon the sets $\{\cdots\}$. The phase characterizing the rotations, and coupling the components of the sets $\{\cdots\}$, it constrains the morphism between the sets, and this constraint allows a thorough understanding of Riemann as well as Goldbach's hypothesis. The trapping of a geometric phase for defining the thermodynamic states is the key factor of the fractal approach of Riemann's hypothesis (Le Méhauté, 2010).

The Riemann hypothesis establishes that there are zeros for the zeta function in the only event . This constraint establishes a direct link between the diffusive process analysed via fractional operators and Riemann zeros. The Goldbach hypothesis asserts in this case that any even number is a sum of two primes. Zeros being related to a static state, the first condition implicitly says that there is no assignable stable equilibrium from, except for .The Zeit objekt character is therefore irreducible in the general case. Fractal system is always dynamic. The second conjecture leads to more subtle conclusions that we examine elsewhere.

At this stage a crucial property of zeta functions amplifies the heuristic power of the derivation of non-integer order. This property is the functional relation:

$$\pi^{\frac{-s}{2}}\,\Gamma\left(\frac{s}{2}\right)\zeta(s) = \pi^{\frac{-(1-s)}{2}}\,\Gamma\left(\frac{1-s}{2}\right)\zeta(1-s) \ . \tag{25}$$

The morphism between transfer functions and zeta functions leads one to say that the functional relationship on zeta gives credit to a homologous relation upon the impedances. In other respects, due to morphism in the couple of sets, another functional relation exists between them. A brief analysis of its properties shows that this relation relates from the disjoint sum of the dual transfer functions and in the complex plan. As shown schematically above (Figure 5), by coupling both impedances, this relationship resets the invariance of the

energy and raises the time singularity at infinity. This statement requires a theoretical and mathematical work currently in progress (Riot, 2013). Restoring the notherian consistency by extension (Kan extension), the understanding of the Riemann hypothesis through the theory of categories solves the paradox of a dynamic responses for which the energy is not an invariant. The sum hidden behind Kan extension closes the fractional process not upon a transport process as assumed usually, but upon a deterministic process that constitutes the underlying (or horizon) of the process when it is performed by an experimentalist (respectively via the test function in distribution theory). This assertion does not mean that the diffusive process could not constitute an underlying; quite the contrary. We may not to forget that determinism and diffusive process are strongly linked together. The issue that arises here is the question of the functional content of this Kan's sum and its links with the un-causal component of the diffusion process, which is given through component even if it is not accessible just via a physical measurement. It is here that the prime numbers enter the lists for giving a statistical meaning to the Kan extension, and therefore for stating the concept of Kan entropy. Each integer number, being associated with point upon the set (seen as hyperbolic distance), is indeed the product of prime numbers. It is written as a product in a set of primes each of them having a position upon. Each point can be seen as both (i) the time constant of the process which is a freedom factor of the experimentalist and (ii) the reference distance as the hyperbolic metric upon.

Surjection

$$Z_\alpha \Rightarrow Z_{1-\alpha}$$

$$n = 2\pi\nu\tau$$

$$\tau$$

$$\nu\tau \in N$$

$$\nu\tau = \prod_{p_i \in \wp} (p_i)^{k_i}$$
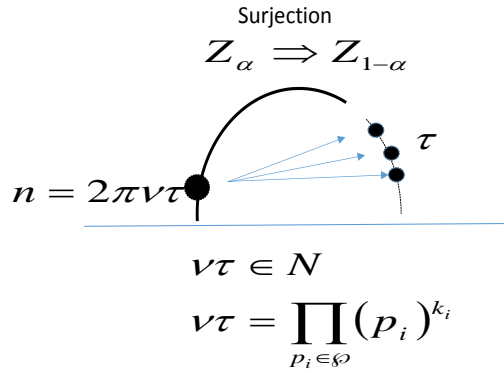
Figure 6. Simplified representation of Kan extension in the frame of the TEISI model.

This operation is a canonical surjection, that is to say an epimorphism. A part of information contained in is then lost within the product decomposition, whereas another data are supplied through. Clearly mixed upon the information coming from through the Kan extension requires a statistic entropic calculus. Only merging all data coming from and its complement provides the whole physical information. This was evident since frequency measurement assumes, notwithstanding the choice of the exchange interface, the choice of the reaction developed on the interface; therefore an a priori choice of a time constant (chosen within a discrete set of numbers). This freedom limited by the natural set of integer number must be taken into account. Even constrained experimentally the choice for observing the geometry using a dedicated process is an epistemological choice. The operation of surjection of the time constant upon forces the representation of the process to break his pure thermodynamic state, and to plunge into a disordered set of primes, that, due to the mixing,

has a higher cardinal than the one of the primes; irreversible time appears at this step. From surjection both complex structure and its complement merges pure and partitioned states, multiplication and addition. The linear reference being always the pure states is solely given by a prime number. One can indeed observe that certain values n (respectively τ) may themselves be primes. In this case the value τ is pinned upon the unit (respectively n). The surjection becomes a simple application. Then, by inversion, the application is an injection. This shows that if is an ordinate distribution of frequencies, the correlations are only controlled via. may then be associated with a prime numbers distribution, rightly ordinated according to its own structure, but mixed with respect the distribution of the frequencies upon . This function of mixing via the surjection leads the negentropic/entropic balance. It is not only the origin of the closure of the fractional processes upon the Noether axiomes but the source of the auto organization and of the emergence. These new phenomena is required to close experimentally 'non causal components' and to regularize the singularity at infinity. Due to the use of energy to do that, it must be related to a competition between hyperbolic distances upon and. Let us notice that the second term, strongly related to zeta function, provides the pure stable states used as references after Kan extension. This observation requires more comments.

7. Auto Organization and Emergence

The origin of emergence in Complex Systems (Holland, 1998) is an open question that always baffles the scientists. Like phase transition, the phenomenon of emergence is indeed a highly nonlinear process led by generally unknown criterions. Nevertheless we know that emergence, characterized by holistic properties, must be sourced within local chaotic behaviour. The Riemann zeta function remarkably illustrates this feature. The local chaos is associated with the stochastic occurrence of the prime numbers whereas, the global behaviour is ordered according to the mathematical well known distribution

$$\pi(n) \approx \frac{\log n}{n} \ . \tag{26}$$

Similarly (i) the ideal gas rules PV=NRT that comes from the molecular chaos, (ii) the WLF law of renormalization for polymers comes from the molecular properties of the monomers, (iii) the Peukert law (Peukert, 1897) comes from the surface disorder of the electrodes of batteries, (iv) the processes of aggregation with or without fields raise dendritic fractal structures, etc. From the considerations given above let us seek to understand why macroscopic rules emerge so naturally, from chaotic local process. Especially, from above analysis, we would like to know why the competition between internal and external referential plays a so crucial role in the emergence of auto organization. As noticed previously the relation

$$R_{1/2} = R\cos(\pi/2) < R_{\alpha} = R\cos\varphi < R \tag{27}$$

means that the fractional process represented by is less dissipative than the deterministic process that serves as the underlying. Nevertheless it is more dissipative than the diffusive process which bounds via *d=2* the geometrical embedding. However, since the energy is not the invariant of the fractional process, it seems impossible at this general stage to evoke a variable that we could call entropy. For giving a meaning to his concept the analysis requires a precise analysis of the Kan extension, that is to say the embedment of the fractal structure of dissipation into a larger infinite set. The surjection using the set of prime number then gives a statistical status of the concept of entropy. Moreover, the properties of scaling of allows to define two distinct types of statistical entropy namely which has a thermodynamic and statistical meaning of the ball of measurement, and which has only a statistical signification evoked in the frame of the interpretation of the Kan extension. Within the standard statistical meaning, the relation ordering the impedances leads the inequality. Because it is empirically based on the performing of energy, the fractional process involves only local dissipative properties (for all integer point of the transfer function) but it involves also global correlations that can be pointed via by means of a distribution of prime adequate time constants. The categorical analysis of Riemann's conjecture (Riot, 2013) then suggests designing a set of infinite orthogonal of primes, in which natural numbers can find their locations. Such a referential is natural for fractional process because any scaling is simply a change of unit. It follows that, the deterministic process Z_1 may use as Euclidean dynamic external referential to source the fractional processes Z_α, whereas diffusive process $Z_{1/2}$ defines in the same referential an hyperbolic distance able to minimize the geometrical entropy. Along the browsing upon process Z_α from high to low frequencies, the partition function associated with the distribution of prime decreases dually.
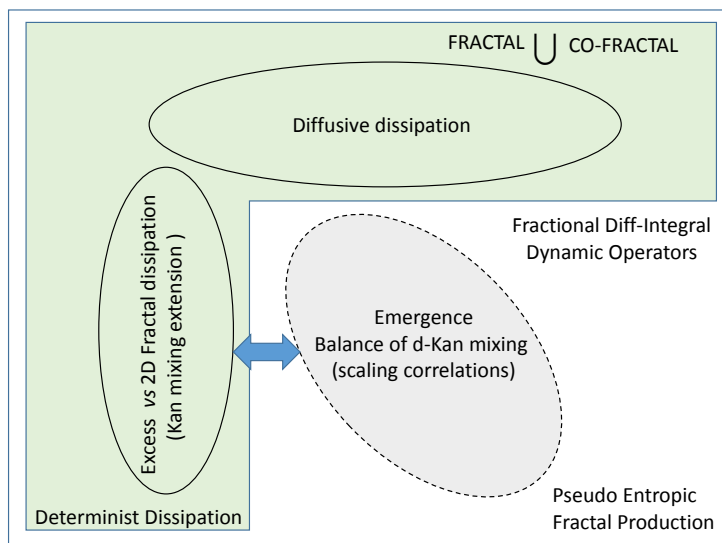

Figure 7. Schematic representation of the problematic of 'entropy' production on self-similar structure, within integer environment (Fractal merged with a co Fractal). In order to balance the energy between deterministic and diffusive process, the irreversible process leads the creation of holistic emerging properties.

On one hand it decreases because the number of primes at stake decreases with frequency. Therefore the configurationl entropy goes down. On the other hand, because the only entropy that may be involved in the process, the *2d*-entropy, is lower than the statistical entropy that would result from backward (Kan extension) and forward approximation of the 'Zeit Objekt' characterized by $Z_\alpha(\omega = 0)$, a Kan entropy appears. It must lead holistic characteristics. In other words, the lowering of the dissipation within the competition between two types of metric (Euclidean and *2d*-hyperbolic) contributes to the building of an auto organization (and/or Holistic rules) during the frequency deployment of the dissipative process. This would be a general property of all dissipative processes except for the diffusive one. The emergence is clearly a constructive-dissipation. Up to now this issue was hidden by implicit hypothesis of limitation of dissipative processes by diffusive transportation.

Conclusion

Far from inconsistency, the fractional diff-integral operator enlarges the epistemological perspectives, open by integer analysis. Due to the fact that the set of rational numbers is larger than the set of integers and according to the couple of Godel's theorems about incompleteness, we cannot reduce the fractional analysis to the paradigmatic point of view of integer dynamics. In particular, the energy is no more an invariant of space time dynamics. It has to take into account the behaviour at infinity, that is to say the structure of the environment. This assertion is clearly a key point of what is often called 'inconsistency' of fractional analysis. This apparent 'inconsistency' is due to the fact that energy stays the main factor of experimental performance as well as the application of the theory of fractal distribution requires regularization via a test function. The paradoxes are due to the incompleteness of the paradigmatic analysis with respect to the fractional one. This incompleteness of the standard paradigms, explains the divergence characterizing the behaviour of complex systems analysis with respect to the system able to accept a reverse engineering. Far from the very nice artefact of renormalization technics, how to overcome in physics the divergence between Euclidean and hyperbolic systems? The physical systems do that naturally through what we call 'emergence', a response of the system to bypass the paradox led by non notherian internal structure. The theory of categories highlights this question through the concepts of Kan extension and the related virtual sets which close precisely the systems upon fractality as shown by Bagshi and recently Riot.

This analysis shows why the expression of a dissipative process by means of a derivative operator of non-integer order is relevant within the meaning of fractality (recursive structures), but also why it requires a tricky physical analysis involving the introduction of Kan entropy. In fact, the energy being not a natural invariant of the fractional operator, the practical use of this operator for the representation of physical systems and its extensions in engineering (for example as in the CRONE control devices) requires to understand a subtle problem of closure at infinity. This question can be expressed in various ways. For his part, the author chooses to express this problem in Fourier space by considering the link between the dynamic transfer functions, the hyperbolic spaces with angle at infinity (or equivalently the Gromov hyperbolic groups) and finally the Riemann zeta properties in theory of numbers. P. Riot chooses another way. He has shown recently that incompleteness can be analysed using the category theory. In all cases, the complex systems require, for being analysed, an

embeddement, that is to say at least two points of view. The paradox of compatibility between the experience that requires the use of energy and the theory ends into the emergence of self similarity and vice versa. New holistic hierarchies then appear and contribute to the emergence of new properties or geometrical features such as aggregation, dendritic growth, the geographical contours, etc... The model TEISI contributes for his part to show why the concept of complex time is the hearth of the problematic.

Alongside the traditional time (seen as inverse transform of the Fourier frequency) the concept of complex time contributes to the emergence of a singular time which is precisely the time of the holistic emergence, self-organization and innovation. The emergence is expressed by splitting between internal and external referential during the frequencial deployment of the process.

We have seen that all the considerations that are needed to understand the physical meaning of the fractional differential equations naturally open upon heuristics issues. Recall that these opportunities were very early noticed. It concerned in particular (i) the physical sense of the wave function in quantum mechanics ($d = 2$) now illuminated by zeta functions and Kan extension, (ii) the topological superconductivity; (iii) the question of the topological gravity by inversion of space-time variable. All these questions and associated opportunities remain yet open upon future developments.

Acknowledgment

References

(Angot, 1972) Angot A., *Compléments de mathématiques à l'usage des ingénieurs de l'électrotechnique et des télécommunications*, Masson, Paris, 1972.

(Badiali, 2013) Badiali J.P., Toward a new fundations of statistical mechanics, arXiv: 1311.4995, V1, *cond-math.stat-mech*, 20 nov., 2013.

(Bagshi, 1987) Bagshi B., Recurence into topological dynamics and Riemann Hypothesis, *Acta Math Hungar*, 50, p. 227-240, 1987.

(Cole, 1942) Cole K.S. and Cole R.H., Dispersion and absorption in dielectric. Direct current characteristics, *J. Phys. Chem* 10, p. 98-105, 1942.

(Connes, 1994) Connes A. *Non Commutative Geometry*, Acad. Press. San Diego C.A. 1994.

(Derrida, 1973) Derrida Jacques, *'Différance' in speech and phenomena*, Northwest University Press Ilinois, 1973.

(Gemant, 1935) Gemant A. The conception of concept viscosity and application to dielectric, *Transaction of the faraday society*, V.31, pp. 1582-1590, 1935.

(Ghys, 1990) Ghys E and de La Harpe P : sur les groupes hyperboliques d'après Gromov, (Bern 1988) 1-25, *Prog. Math.,* 83, Birkhäuser Boston, MA, 1990.

(Holland, 1998) Holland J. H., *Emergence: from chaos to order*, Helix books Addison-Wesley MA, 1998.

(Le Méhauté, 1974) Le Méhauté A, Application à la hiérarchie départementale française d'un modèle d'adaptation des individus à une structure de désutilité en arbre, *Annales du Centre de Recherche de l'urbanisme Presses du CRU,* Paris, 1974.

(Le Méhauté, 1977) Le Méhauté A. and Apelby J., A parametric analysis of the structure of international energy consumption, *Energy,* 2, p 105-114, 1977.

(Le Méhauté, 1980) Le Méhauté A., de Guibert A., Delaye M. et Filippi C., Phénoménologie du transfert de matière et d'énergie en milieu présentant une similitude interne. Rapport de Recherche, Laboratoire de Marcoussis, *Division Electrochimie*, 458, Décembre 1980.

(Le Méhauté, 1982a) Le Méhauté A., de Guibert A., Delaye M. et Filippi C., Note d'introduction à la cinétique des échanges d'énergies et de matières sur des interfaces fractales, *C.R. Acad. Sci.,* Paris, t. 294, Paris, pp.835-837, 1982.

(Le Méhauté, 1982b) Le Méhauté A. et Crepy G., Sur quelques propriétés de transferts électrochimiques en géométrie fractales*, C.R. Acad. Sci*., T. 294, Paris, pp.685-688, 1982.

(Le Méhauté, 1983) Le Méhauté A., Dugast A., Introduction of scaling properties in electrochemistry: from TEISI model to lithium layered structure, *Solid State Ionics*, 9/10, P 17-30, 1983.

(Le Méhauté, 1984) Le Méhauté A, Transfer process in fractal media, *J. Stat. Phys*. Vol. 36 N°5/6 N.Y. 665-676, 1984.

(Le Méhauté, 1986) Le Méhauté A, Frushter L., Crépry G., le Méhauté A., Batteries, Identified Fractal objects, *J. power Sources*, 18, 51-62, 1986.

(Le Méhauté, 1992) Le Méhauté A., Heliodore F, Cottevieille D., Propagation des ondes en milieux hétérogènes, *Revue scientifique et technique de la défense*, p 22-33, 1992.

(Le Méhauté, 2010) Le Méhauté A., El Kaabouchi A., Nivanen N., Riemann's conjecture and fractal derivative, Computer and mathematics with application *Chaos Solitons and Fractals,* Vol 59 (6), pp. 1610-1613, 2010.

(Mandelbrot, 1975) Mandelbrot B., *Les géométries fractales*, Flammarion Paris 1975.

(Mandelbrot, 1982) Mandelbrot B., *The fractal geometry of nature*, Freeman, San Francisco, 1982.

(Nigmatullin, 1975) Nigmatullin R. Sh., Kader B.A., Krylov V.S., Sokolov L.A., Electrochemical methods of transfer processes research in liquids. //*Success in Chemistry Uspekhi Khimii*, v. XLIV, issue.11, pp.2008-2034, 1975.

(Nivanen, 2005) Nivanen L, Wang Q.A., le Méhauté A. 'from complexe systems to generalized statistics and algebra In fractional differentiation and application Eds A. le Méhauté, J.A. Tenreiro-Machado, J.C. Trigeassou, and J. Sabatier U-Book, 2005

(Oldham, 1974) Oldham K.B. and Spanier J., *The fractional calculus*, Academic Press NY, 1974.

(Oustaloup, 1983) Oustaloup A., Systèmes asservis linéaires d'ordre fractionnaire: théorie et pratique. *Masson*, Paris, 1983.

(Peukert, 1897) Peukert W., Über die Abhängigkeit der Kapazität von der Entladestromstärke bei Bleiakkumulatoren, *Electrotech. Z.* V.18, pp.287-292, 1897.

(Podlubny, 1999) Podlubny I, *Fractional differential Equations*, Academic press NY, 1999.

(Riot, 2013) Riot P. http://repmus.ircam.fr/mamux/saisons/saison13-2013-2014/2013-12-06

(Rovelli, 2004) Rovelli C., *Quantum Gravity*, Cambridge University Press, 2004.

(Rovelli, 2006) Rovelli C., *Qu'est ce que le temps? Qu'est ce que l'espace?,* Bernard Gilson, 2006.

(Schwartz, 1950) Schwartz L., *Théorie des distributions*, Herman, Paris, 1950.

(Tenenbaum, 2011) Tenenbaum G. et Mendes France M., *Les nombres premiers entre ordre et chaos*, Dunod, Paris, 2011.

(Tricot, 1999) Tricot Claude, *Courbes et dimensions fractales*, Springer Verlag, 1999.

(Voronin, 1975) Voronin S., Theorem of the universality of Riemann zeta function, *Izv. Akad. Nauk. SSSR Ser. Matem.*, Vol. 39, p. 476-486, 1975, Reprinted: *Math SSSR. Izv,* Vol.9, pp.443-445, 1975.

Chapter 2

DYNAMICS OF FRACTIONAL ORDER CHAOTIC SYSTEMS

*Sachin Bhalekar**
Department of Mathematics, Shivaji University, Kolhapur, India

Abstract

This chapter deals with the fractional order generalization of the chaotic system proposed by Li et al [Nonlinear Analysis: Modelling & Control, 18 (2013) 66-77]. We discuss the dynamical properties such as symmetry, dissipativity, stability of equilibrium points and chaos. Further we control the chaos in proposed system and present the synchronization phenomenon.

Keywords: Chaos, fractional order, stability

AMS Subject Classification: 26A33, 65P20, 34L30

1. Introduction

Differential equation is one of the basic tools to model the motion of a physical system. When the solutions of these differential equations are bounded, they either settle down to an equilibrium state or oscillates in a periodic or quasi-periodic state. If the order of the system is three or more and the system is nonlinear then there is a possibility of another type of solutions. Such solutions exhibit aperiodic motion for all time and never settles. These solutions are highly sensitive to initial conditions also. Thus, it is not possible to predict the behavior of the solution for a long time. Such systems are termed as chaotic dynamical systems [1].

If the order of the derivative in the system is not an integer then it is called as fractional order system [2, 3, 4]. There are two very important advantages of the fractional order derivative over a conventional integer order derivative. The first advantage is the nonlocal nature of fractional order derivative. The integer order derivative of a function at a point can be approximated using the nearby values whereas the fractional derivative needs the

---

*E-mail addresses: sbb_maths@unishivaji.ac.in, sachin.math@yahoo.co.in

total history from an initial point. This nonlocality of fractional derivative (FD) is playing a vital role in modelling memory and hereditary properties in the system. Hence the models involving FD are more realistic than those involving integer order ones. Second advantage is the FD is capable of modelling intermediate processes. In some physical problems such as the diffusion of fluid in porous media, the integer order derivative cannot model the real phenomena because the processes are intermediate. In such case, one has to consider a model involving the intermediate (fractional) order derivative.

The generalized dynamical systems involving fractional order derivative are extensively studied by researchers. In the seminal paper, Grigorenko and Grigorenko [5] proposed a fractional order generalization of Lorenz system. Further, various fractional order systems such as Chen system [6], Lü system [7], Rossler system [8]and Liu [9] system are studied in the literature.

In this chapter, we propose a fractional order generalization of the chaotic system proposed by Li et al. [17] and discuss its properties.

2. Preliminaries

2.1. Stability Analysis

We discuss the stability results of the following fractional order system

$$
\begin{aligned}
D^{\alpha_1} x_1 &= f_1(x_1, x_2, \cdots, x_n), \\
D^{\alpha_2} x_2 &= f_2(x_1, x_2, \cdots, x_n), \\
&\vdots \\
D^{\alpha_n} x_n &= f_n(x_1, x_2, \cdots, x_n),
\end{aligned} \tag{2.1}
$$

where $0 < \alpha_i < 1$ are fractional orders. The system (2.1) is called as a commensurate order if $\alpha_1 = \alpha_2 = \cdots = \alpha_n$ otherwise an incommensurate order.

A point $p = (x_1^*, x_2^*, \cdots, x_n^*)$ is called an equilibrium point of system (2.1) if $f_i(p) = 0$ for each $i = 1, 2, \cdots, n$.

Theorem 2.1. *[10, 11] Consider $\alpha = \alpha_1 = \alpha_2 = \cdots = \alpha_n$ in (2.1). An equilibrium point p of the system (2.1) is locally asymptotically stable if all the eigenvalues of the Jacobian matrix*

$$
J = \begin{pmatrix}
\partial_1 f_1(p) & \partial_2 f_1(p) & \cdots & \partial_n f_1(p) \\
\partial_1 f_2(p) & \partial_2 f_2(p) & \cdots & \partial_n f_2(p) \\
\vdots & \vdots & \vdots & \vdots \\
\partial_1 f_n(p) & \partial_2 f_n(p) & \cdots & \partial_n f_n(p)
\end{pmatrix}. \tag{2.2}
$$

evaluated at p satisfy the following condition

$$
|arg(Eig(J))| > \alpha \pi / 2. \tag{2.3}
$$

Theorem 2.2. *[12, 13] Consider the incommensurate fractional ordered dynamical system given by (2.1). Let $\alpha_i = v_i/u_i$, $(u_i, v_i) = 1$, u_i, v_i be positive integers. Define M to be the least common multiple of u_i's.*

Define

$$\Delta(\lambda) = diag\left(\left[\lambda^{M\alpha_1}, \lambda^{M\alpha_2}, \cdots, \lambda^{M\alpha_n}\right]\right) - J \qquad (2.4)$$

where J is the Jacobian matrix as defined in (2.2) evaluated at point p. Then p is locally asymptotically stable if all the roots of the equation $det\,(\Delta(\lambda)) = 0$ satisfy the condition $|arg(\lambda)| > \pi/(2M)$.

This condition is equivalent to the following inequality

$$\frac{\pi}{2M} - \min_i\left\{|arg(\lambda_i)|\right\} < 0. \qquad (2.5)$$

Thus an equilibrium point p of the system (2.1) is asymptotically stable if the condition (2.5) is satisfied. The term $\frac{\pi}{2M} - min_i\left\{|arg(\lambda_i)|\right\}$ is called as the instability measure for equilibrium points in fractional order systems (IMFOS). Hence, a necessary condition for fractional order system (2.1) to exhibit chaotic attractor is [12]

$$\text{IMFOS} \geq 0. \qquad (2.6)$$

Theorem 2.3. *[18] Consider the polynomial*

$$P(\lambda) = \lambda^3 + a_1\lambda^2 + a_2\lambda + a_3 = 0. \qquad (2.7)$$

Define the discriminant for equation (2.7) as

$$D(P) = 18a_1a_2a_3 + (a_1a_2)^2 - 4a_3(a_1)^3 - 4(a_2)^3 - 27(a_3)^2. \qquad (2.8)$$

1. *If $D(P) > 0$ then all the roots of $P(\lambda)$ satisfy the condition*

$$|arg(\lambda)| > \alpha\pi/2 \qquad (2.9)$$

   where $0 \leq \alpha \leq 1$.

2. *If $D(P) < 0$, $a_1 \geq 0$, $a_2 \geq 0$, $a_3 > 0$, $\alpha < 2/3$ then (2.9) is satisfied.*

3. *If $D(P) < 0$, $a_1 > 0$, $a_2 > 0$, $a_1a_2 = a_3$ then (2.9) is satisfied for all $0 \leq \alpha < 1$.*

2.2. Numerical Method for Solving Fractional Differential Equations

The numerical methods developed for solving equations involving integer order derivatives are not useful to solve those involving fractional derivatives. A modification of Adams-Bashforth-Moulton algorithm is proposed by Diethelm et al. in [14, 15, 16] to solve FDEs.

Consider for $\alpha \in (m-1, m]$ the initial value problem (IVP)

$$D^\alpha y(t) = f\left(t, y(t)\right), \quad 0 \leq t \leq T, \qquad (2.10)$$

$$y^{(k)}(0) = y_0^{(k)}, \quad k = 0, 1, \cdots, m-1. \qquad (2.11)$$

The IVP (2.10)–(2.11) is equivalent to the Volterra integral equation

$$y(t) = \sum_{k=0}^{m-1} y_0^{(k)}\frac{t^k}{k!} + \frac{1}{\Gamma(\alpha)}\int_0^t (t-\tau)^{\alpha-1} f\left(\tau, y(\tau)\right) d\tau. \qquad (2.12)$$

Consider the uniform grid $\{t_n = nh/n = 0, 1, \cdots, N\}$ for some integer N and $h := T/N$. Let $y_h(t_n)$ be approximation to $y(t_n)$. Assume that we have already calculated approximations $y_h(t_j)$, $j = 1, 2, \cdots, n$ and we want to obtain $y_h(t_{n+1})$ by means of the equation

$$y_h(t_{n+1}) = \sum_{k=0}^{m-1} \frac{t_{n+1}^k}{k!} y_0^{(k)} + \frac{h^\alpha}{\Gamma(\alpha+2)} f(t_{n+1}, y_h^P(t_{n+1})) + \frac{h^\alpha}{\Gamma(\alpha+2)} \sum_{j=0}^{n} a_{j,n+1} f(t_j, y_n(t_j))$$

(2.13)

where

$$a_{j,n+1} = \begin{cases} n^{\alpha+1} - (n-\alpha)(n+1)^\alpha, & \text{if } j = 0, \\ (n-j+2)^{\alpha+1} + (n-j)^{\alpha+1} - 2(n-j+1)^{\alpha+1}, & \text{if } 1 \le j \le n, \\ 1, & \text{if } j = n+1. \end{cases}$$

The preliminary approximation $y_h^P(t_{n+1})$ is called predictor and is given by

$$y_h^P(t_{n+1}) = \sum_{k=0}^{m-1} \frac{t_{n+1}^k}{k!} y_0^{(k)} + \frac{1}{\Gamma(\alpha)} \sum_{j=0}^{n} b_{j,n+1} f(t_j, y_n(t_j)),$$

(2.14)

where

$$b_{j,n+1} = \frac{h^\alpha}{\alpha} \left((n+1-j)^\alpha - (n-j)^\alpha \right).$$

(2.15)

Error in this method is

$$max_{j=0,1,\cdots,N} |y(t_j) - y_h(t_j)| = O(h^p),$$

(2.16)

where $p = min(2, 1 + \alpha)$.

3. The Model

A new 3D chaotic system proposed by Li et al. in [17] is

$$\begin{aligned} \dot{x} &= a(y-x) + yz, \\ \dot{y} &= (c-a)x - xz + cy, \\ \dot{z} &= ey^2 - bz, \end{aligned}$$

(3.17)

where a, b, c and e are constants. We propose a modification in system (3.17) involving fractional order derivatives as below:

$$\begin{aligned} D^\alpha x &= a(y-x), \\ D^\alpha y &= (c-a)x - xz + cy, \\ D^\alpha z &= ey^2 - bz, \end{aligned}$$

(3.18)

where $0 < \alpha \le 1$. Now we discuss some dynamical properties of the system (3.18).

1. **Symmetry.** The system is symmetric about z-axis because the transformation $(x, y, z) \longrightarrow (-x, -y, z)$ does not change the system.

2. **Dissipativity.** Consider

$$
\begin{aligned}
div(V) &= \frac{\partial \dot{x}}{\partial x} + \frac{\partial \dot{y}}{\partial y} + \frac{\partial \dot{z}}{\partial z} \\
&= c - (a + b).
\end{aligned}
\tag{3.19}
$$

The system is dissipative if $c < a + b$.

3. **Non-generalized Lorenz system.** The generalized Lorenz system (GLS) discussed in [20] is of the form

$$
\dot{X} = \begin{pmatrix} A & 0 \\ 0 & \lambda_3 \end{pmatrix} + x \begin{pmatrix} 0 & 0 & 0 \\ 0 & 0 & -1 \\ 0 & 1 & 0 \end{pmatrix} X,
\tag{3.20}
$$

where $X = [x, y, z]^T$, $\lambda_3 \in \Re$ and A is a 2×2 matrix with eigenvalues $\lambda_1, \lambda_2 \in \Re$ such that $-\lambda_2 > \lambda_1 > -\lambda_3 > 0$. Since our system

$$
\dot{X} = \begin{pmatrix} -a & a & 0 \\ c-a & c & 0 \\ 0 & 0 & -b \end{pmatrix} + x \begin{pmatrix} 0 & 0 & 0 \\ 0 & 0 & -1 \\ 0 & 1 & 0 \end{pmatrix} X + \begin{pmatrix} yz \\ 0 \\ ey^2 \end{pmatrix}
\tag{3.21}
$$

is having different structure than the system (3), it is not a GLS.

4. **Equilibrium points and their stability.** The system (3.18) has three equilibrium points viz. $E_0 = (0,0,0)$, $E_{1,2} = \left(\mp\sqrt{-b(a-2c)/e}, \mp\sqrt{-b(a-2c)/e}, -a+2c \right)$. The Jacobian matrix evaluated at an arbitrary point $X = (x, y, z)$ is given by

$$
J(X) = \begin{pmatrix} -a & a & 0 \\ c-a-z & c & -x \\ 0 & 2ey & -b \end{pmatrix}.
\tag{3.22}
$$

The characteristic equation of $J(E_0)$ is therefore,

$$
P = \lambda^3 + (a+b-c)\lambda^2 + (a^2 + ab - 2ac - bc)\lambda + (a^2 b - 2abc) = 0. \tag{3.23}
$$

The following expression defines the descriminant of the equation (3.23).

$$
D(P) = -(3a^2 - 6ac - c^2)(a^2 + b^2 + bc - ab - 2ac)^2.
\tag{3.24}
$$

The sign of $D(P)$ is same as the sign of $-(3a^2 - 6ac - c^2) = -(a - (1 + 2/\sqrt{3})c(a - (1 - 2/\sqrt{3})c))$. The sufficient conditions for the stability of E_0 are discussed in the following theorem which are consequences of Theorem 2.3.

Theorem 3.1. *(a) If $2c < a < \sqrt{13/3}c$ then the equilibrium point E_0 is asymptotically stable.*

(b) If $c = 0$, $b > 0$ and $a > 0$ then E_0 is asymptotically stable for $\alpha < 2/3$.

4.   Numerical Simulations

We consider the system(3.18) with $a = 41$, $c = 31$, $e = 3.2$ and $b = 4$. The equilibrium points are now $E_0 = (0, 0, 0)$ and $E_{1,2} = (\pm 5.123475, \pm 5.123475, 21)$. The saddle equilibrium E_0 is useful in connecting chaotic scrolls and the scrolls will be around $E_{1,2}$. The eigenvalues of Jacobian at $E_{1,2}$ are $-20.3789, 3.18947 \pm 18.1059\imath$ and the minimum effective dimension is turned out to be 0.888994. Numerical observations also show that the system is chaotic for $\alpha > 0.88$. The stable orbits for $\alpha = 0.88$ are shown in Figs. 1 whereas the chaotic attractors for $\alpha = 0.89$ are shown in Figs. 2.
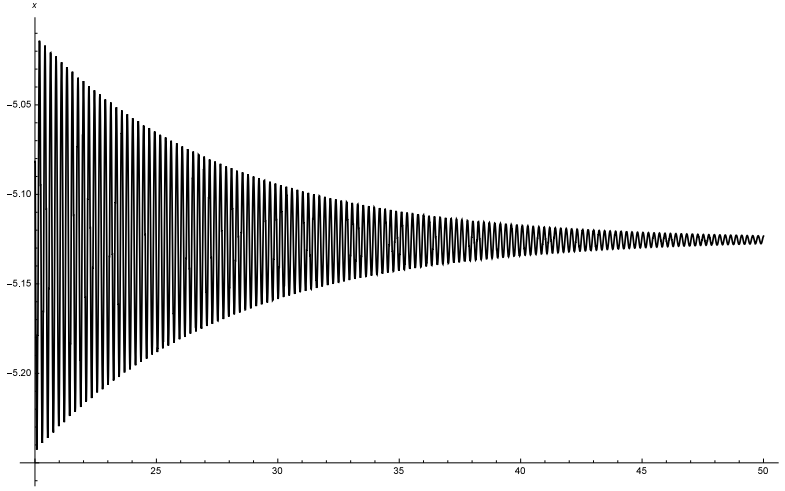
Figure 1a. Stable time series $x(t)$ for $\alpha = 0.88$.
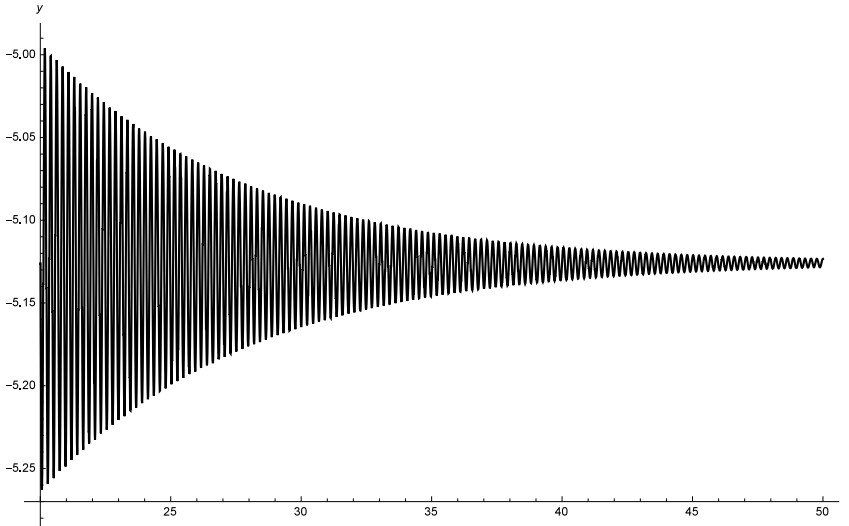
Figure 1b. Stable time series $y(t)$ for $\alpha = 0.88$.
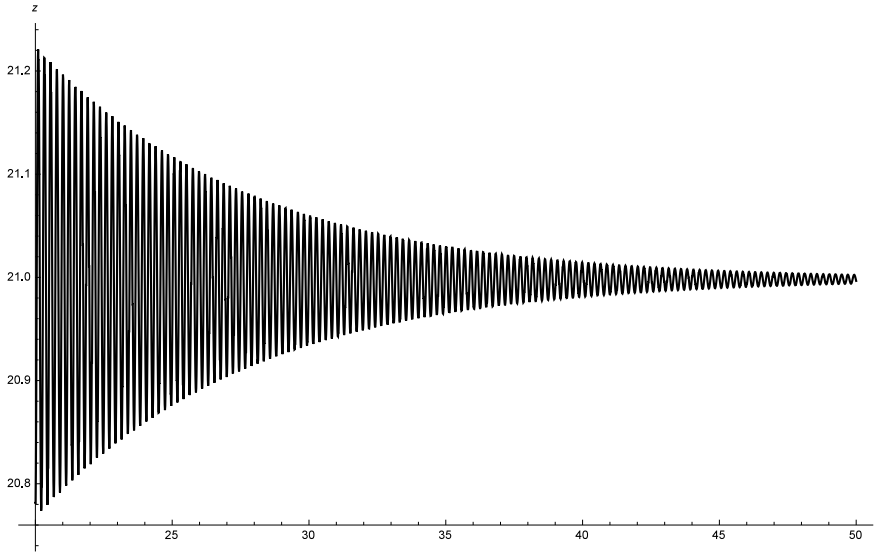
Figure 1c. Stable time series $z(t)$ for $\alpha = 0.88$.
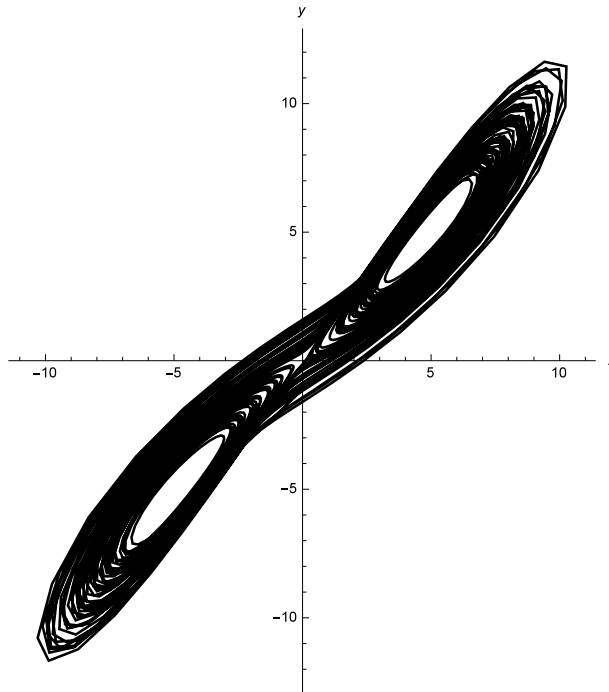
Figure 2a. Chaotic xy-phase portrait for $\alpha = 0.89$.

5.   Synchronization

Though the chaotic trajectories are aperiodic in nature, two different chaotic trajectories can oscillate together if the appropriate controller is applied [21, 22].

The chaos synchronization technique has been explored in secure communications [23]
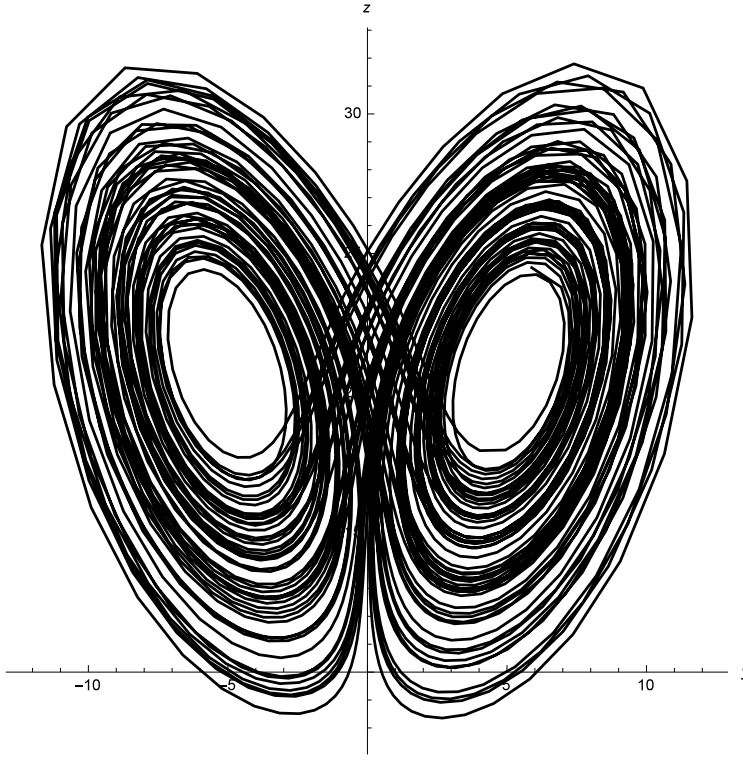
Figure 2b. Chaotic yz-phase portrait for $\alpha = 0.89$.

and cryptographic systems [24].

Deng and Li introduced the synchronization of fractional order chaotic systems in [25]. Since then various researchers presented different techniques of synchronization of chaos in fractional order systems. Now we utilize the nonlinear feedback control technique to synchronize the proposed fractional order chaotic system.

Consider the drive system as

$$
\begin{aligned}
D^\alpha x &= 41(y - x), \\
D^\alpha y &= -10x - xz + 31y, \\
D^\alpha z &= 3.2y^2 - 4z
\end{aligned}
\tag{5.25}
$$

and response system as

$$
\begin{aligned}
D^\alpha x_1 &= 41(y_1 - x_1), \\
D^\alpha y_1 &= -10x_1 - x_1 z_1 + 31y_1 + u_2, \\
D^\alpha z_1 &= 3.2y_1^2 - 4z_1 + u_3.
\end{aligned}
\tag{5.26}
$$

The nonlinear feedback controllers u_i's are chosen as $u_2 = x_1 z_1 - xz + 22y - 22y_1$ and $u_3 = 3.2(y^2 - y_1^2)$. If the errors in synchronization are termed as $e_1 = x - x_1$, $e_2 = y - y_1$ and $e_3 = z - z_1$ then the error system can be obtained by subtracting the system (5.26)
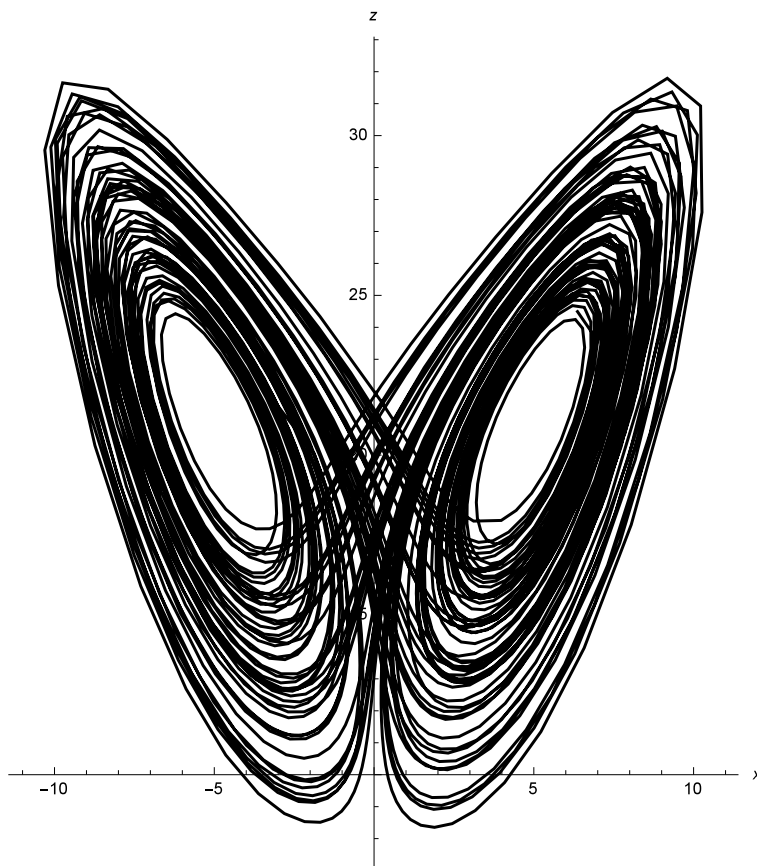
Figure 3c. Chaotic xz-phase portrait for $\alpha = 0.89$.

from the system (5.25) as below

$$
\begin{aligned}
D^\alpha e_1 &= 41(-e_1 + e_2), \\
D^\alpha e_2 &= -10e_1 + 9e_2, \\
D^\alpha e_3 &= -4e_3.
\end{aligned}
\tag{5.27}
$$

The eigenvalues of the coefficient matrix of the error system (5.27) are $-30.6629, -1.33712, -4$. This shows that the errors will tend to zero as t tends to infinity. In the figs. 3 and 4 we show the synchronization of the system for fractional orders $\alpha = 0.80$ and $\alpha = 0.98$ respectively. The dashed lines in synchronized signals show the response signals whereas the solid lines show the drive signals. The solid lines, the dotted lines and the dot-dashed lines in Figs. 3(b) and 4(b) show the errors e_1, e_2 and e_3 respectively.

6. Conclusion

In this chapter, we discussed the dynamics of fractional order chaotic system. It is observed that the nonlinear system with fractional system order less than three can exhibit
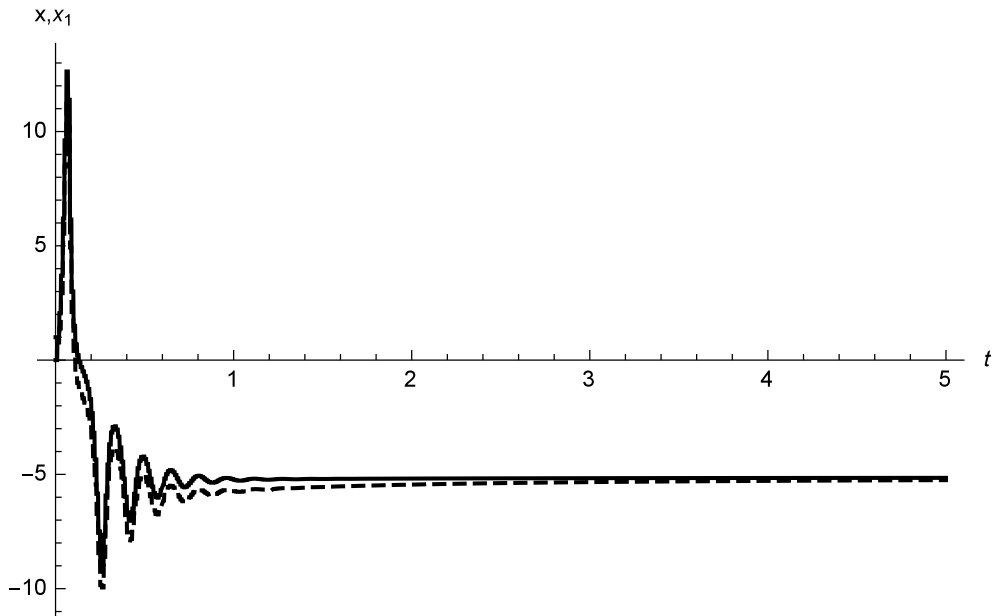
Figure 3a. Synchronized signals $x(t)$ and $x_1(t)$ for $\alpha = 0.80$.
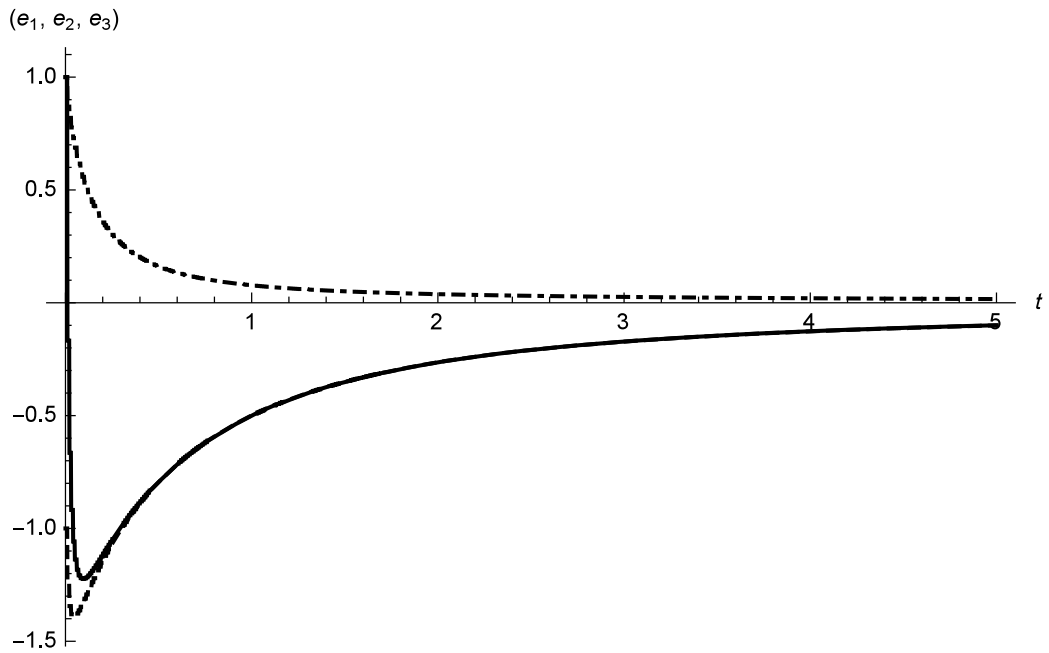
Figure 3b. Errors in synchronization for $\alpha = 0.80$.

chaos. Further, the synchronization of chaos is presented using nonlinear feedback control technique.
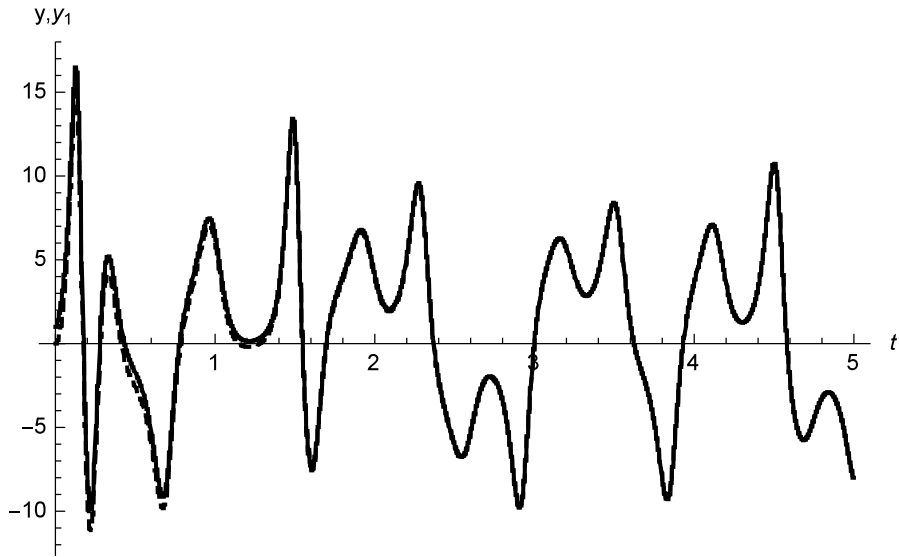
Figure 4a. Synchronized signals $y(t)$ and $y_1(t)$ for $\alpha = 0.98$.
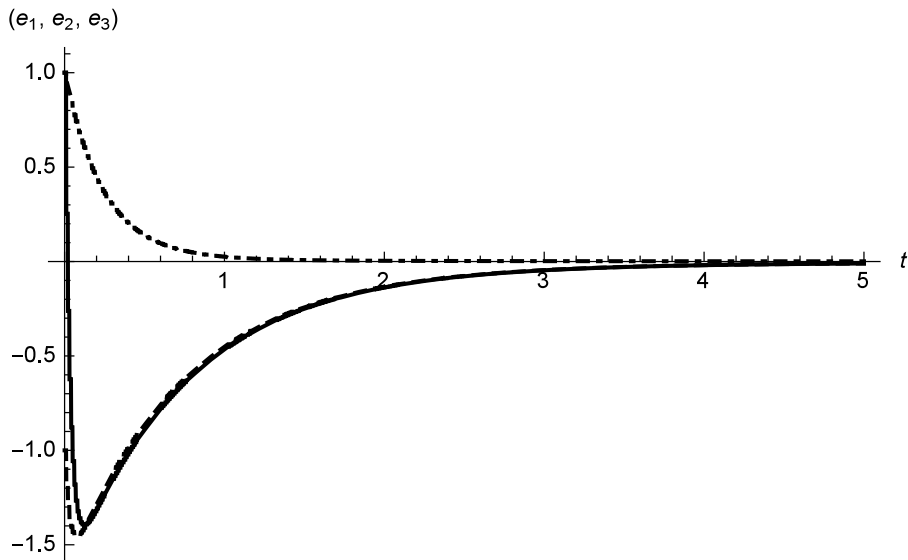
Figure 4b. Errors in synchronization for $\alpha = 0.98$.

Acknowledgments

References

[1] K.T. Alligood, T.D. Sauer, J. A. Yorke, *Chaos: An Introduction to Dynamical Systems*, Springer, New York, 2008.

[2] Podlubny, I., *Fractional Differential Equations*, Academic Press, San Diego (1999).

[3] Samko, S. G., A. A. Kilbas and O. I. Marichev, *Fractional Integrals and Derivatives: Theory and Applications*, Gordon and Breach, Yverdon (1993).

[4] Kilbas, A. A., H. M. Srivastava and J. J. Trujillo, *Theory and Applications of Fractional Differential Equations*, Elsevier, Amsterdam (2006).

[5] I. Grigorenko and E. Grigorenko, Chaotic dynamics of the fractional Lorenz system, *Phys. Rev. Lett.* 91 (2003) 034101.

[6] C. Li, G. Peng, Chaos in Chen's system with a fractional order, *Chaos Solitons Fractals* 22 (2004) 443–450.

[7] J. G. Lü, Chaotic dynamics of the fractional order Lü system and its synchronization, *Phys. Lett. A* 354(4) (2006) 305–311.

[8] Li, C. G. and G. Chen, Chaos and hyperchaos in the fractional order Rossler equations, *Phys. A: Stat. Mech. Appl.*, 341, (2004) 55–61.

[9] Daftardar-Gejji, V. and S. Bhalekar, Chaos in fractional ordered Liu system, *Comput. Math. Appl.*, 59, (2010) 1117–1127.

[10] M. S. Tavazoei and M. Haeri, Regular oscillations or chaos in a fractional order system with any effective dimension, *Nonlinear Dynamics*, 54(3) (2008) 213–222.

[11] D. Matignon, Stability results for fractional differential equations with applications to control processing. In: Computational Engineering in Systems and Application multiconference, vol. 2, pp. 963-968, *IMACS, IEEE-SMC Proceedings*, Lille, France, July (1996).

[12] M. S. Tavazoei and M. Haeri, Chaotic attractors in incommensurate fractional order systems, *Physica D*, 237 (2008) 2628-2637.

[13] W. Deng, C. Li and J. Lu, Stability analysis of linear fractional differential system with multiple time delays, *Nonlinear Dynamics*, 48 (2007) 409-416.

[14] K. Diethelm, N. J. Ford and A. D. Freed, A predictor-corrector approach for the numerical solution of fractional differential equations, *Nonlinear Dynamics* 29 (2002) 3–22.

[15] K. Diethelm, An algorithm for the numerical solution of differential equations of fractional order, *Elec. Trans. Numer. Anal.* 5 (1997) 1–6.

[16] K. Diethelm and N. J. Ford, Analysis of fractional differential equations, *J. Math. Anal. Appl.* 265 (2002) 229-48.

[17] C. Li, L. Wu, H. Li, Y. Tong, A novel chaotic system and its topological horseshoe, *Nonlinear Analysis: Modelling and Control*, 18(1) (2013) 66–77.

[18] E. Ahmed, A.M.A. El-Sayed, H. A.A. El-Saka, On some RouthHurwitz conditions for fractional order differential equations and their applications in Lorenz, Rossler, Chua and Chen systems, *Physics Letters A* 358 (2006) 1–4.

[19] E.N. Lorenz, Deterministic nonperiodic flow, *J. Atmos. Sci.* 20 (1963) 130.

[20] S. Celikovsky, G. Chen, On the generalized Lorenz canonical form, *Chaos Solitons Fractals*, 26 (2005), 1271

[21] L. M. Pecora and T. L. Carroll, Synchronization in chaotic systems, *Phys. Rev. Lett.* 64(8) (1990) 821.

[22] L. M. Pecora and T. L. Carroll, Driving systems with chaotic signals, *Phys. Rev. A* 44 (1991) 2374.

[23] R. Hilfer, *Applications of Fractional Calculus in Physics*, World Scientific, USA, 2001.

[24] R. He and P. G. Vaidya, Implementation of chaotic cryptography with chaotic synchronization, *Phys. Rev. E* 57(2) (1998) 1532.

[25] W. H. Deng and C. P. Li, Chaos synchronization of the fractional Lü system, *Physica A* 353 (2005) 61–72.

Chapter 3

Pressure Control of CNG Engines by Non-integer Order Controllers: A New Trend in Application of Fractional Calculus to Automotive Systems

Paolo Lino*and Guido Maione†
Dipartimento di Ingegneria Elettrica e dell'Informazione,
Politecnico di Bari, Bari, Italy

Abstract

The massive use of electronic control in automotive vehicles improved performance, comfort, safety and reduced pollutant emissions and consumption. In particular, the accurate control of the fuel injected into cylinders allowed the common rail fuel injection system to increase engine performance while reducing emissions, noise and fuel consumption. In this context, compressed natural gas (CNG) engine systems can further reduce emissions to adhere to environmental policy regulations. However, the injection process is strongly non-linear, time-variant and highly coupled, so suitable control systems must be designed to guarantee the desired performance.

This chapter describes how to synthesize and realize non-integer order controllers for pressure control in common rail injection systems of CNG engines. The realization is relatively simple and cheap, as required by the industrial application. Namely, not only low sensitivity to parameter variations and load disturbances must be achieved, but also a limited cost with respect to implementation by consolidated PID controllers.

The CNG common rail injection system includes: a tank storing high pressure gas; a main chamber and a control chamber; a solenoid valve; an electronic control unit; a common rail and electro-injectors. The tank feeds the downstream circuit. The main and control chambers are separated by a moving piston. Both chambers receive fuel from the tank and send it to the common rail, which is a constant volume accumulator connected to the electro-injectors. The inlet flow to the main chamber is regulated by a shutter that is integral with the piston, whose position depends on the equilibrium of the pressures acting on its surfaces. Adjusting the pressure in the control circuit by the

---

*E-mail address: paolo.lino@poliba.it
†E-mail address: guido.maione@poliba.it

solenoid valve regulates the main chamber inflow. Moreover, as the main chamber and the common rail have almost equal pressures, accurate metering of the injected fuel is allowed by setting the injection timings at the same time.

This work reports recent advancements in the design and simulation of switched fractional order PI controllers, in which the integral action is of non-integer order. Performance, robustness and disturbance rejection are tested by simulation of virtual prototypes based on non-linear models. The basic idea is to perform a loop-shaping of the open-loop transfer function to obtain frequency domain performance specifications and achieve an optimal feedback system. To this aim, the fractional integrator is profitably used and robust stability of the closed-loop system is guaranteed by a D-decomposition method. There are several benefits of the design approach. Closed formulas determine the controller gains by frequency domain specifications and can be used for an automatic synthesis of the controller. Moreover, the realization of the non-integer operator is by an efficient approximation method that prevents numerical problems and leads to a rational transfer function characterized by interlaced minimum-phase zeros and stable poles, so that a reduced approximation error is obtained and easy implementation is possible. To conclude, the non-integer order controllers allow higher accuracy in metering the injected fuel and promptness in setting the rail pressure to the desired reference values.

PACS: 02.30.Yy, 05.45-a., 07.05.Dz, 88.85.mf

Keywords: Compressed natural gas engines, injection systems, non-integer-order controllers, fractional-order controllers, fractional-order proportional-integral controllers, loop-shaping, approximation of irrational operators, continued fractions, zero-pole interlacing, control systems, stability, frequency-response methods

AMS Subject Classification: 93C, 93D, 93C80

1. Introduction: A Short Literature Review

The automotive industry is undergoing a deep transformation due to the massive introduction of electronic control systems within vehicles. Electronic control has helped practitioners to improve performance, comfort and safety and to reduce pollutant emissions and fuel consumption. Among the control-engineered systems, the fuel injection system received great benefits from electronic control. Specifically, the advent of the common rail injection system led to improved engine performance and reduced emissions, noise and fuel consumption by accurate control of the amount of fuel injected into the cylinders. Recently, to further reduce emissions and adhere to environmental policy regulations, innovative compressed natural gas (CNG) engine systems have also been studied, designed and analyzed. Suitable control systems must guarantee the desired performance of the injection process, which is non-linear and time-variant, even in the presence of large variations and uncertainties of parameters and working points.

This chapter concerns a new and interesting application of the paradigm of fractional calculus (e.g., see [3, 47, 55] for mathematical background) in this context. The authors' interest in this subject is motivated by recent research results [27, 28] that are focused on a methodology for designing non-integer (fractional) order controllers of the pressure in the common rail injection system of CNG engines [23]. For high engine performance, indeed,

it is necessary to regulate the injection pressure for properly metering the air-fuel mixture, notwithstanding the large variations of working conditions due to gas compressibility. Moreover, control also has to adapt the working point of injection to changes of the power request, speed, load, etc. To this aim, a suitable model is necessary for analyzing and controlling the process dynamics, and both the controllers' performance and their robustness must be evaluated and analyzed.

The motivation for employing non-integer order controllers and their origin can be traced back to the famous and seminal works by Bode, Manabe, and Tustin [7, 40, 65]. Bode found that a non-integer (fractional) order integrator is the ideal open-loop transfer function for designing feedback amplifiers. Manabe investigated the dynamics of flexible spacecraft structures and used non-integer integration for modeling purposes [40]. Tustin worked on robust control of massive objects, approximated a fractional integrator of order 0.5, and achieved a phase margin of $45°$ over a sufficiently wide frequency range around the gain crossover frequency. However, a renewed interest in fractional calculus applications has only been observed in recent decades. This interest grew especially thanks to successful results in controlling car suspensions and other systems by using the CRONE (Commande Robuste d'Ordre Non Entièr) control approach developed by the French team headed by Oustaloup [48, 49, 51–53]. Besides the several generations of the CRONE approach [53], there are many ways to design and tune non-integer order controllers for automotive, mechatronics and industrial systems (e.g., see [5, 9, 10, 13, 21, 30, 42, 43, 54, 63, 64]).

These and many other works let researchers understand that non-integer (fractional) order differential and integral operators could offer more flexibility to the familiar PID controllers. Derivatives and integrals of non-integer order were proposed in $PI^{\lambda}D^{\mu}$-controllers [56, 57], where λ and μ are the non-integer orders of integration and differentiation, respectively. However, one can use any non-integer order (a real or even complex number) [50]. Another way is to consider fractional power poles [10, 11] or transfer functions powered to a non-integer order, from which the term fractional order proportional-integral-derivative (or FOPID) controllers is derived [43, 58]. To synthesize, the term Fractional Order Controllers (FOCs) is commonly used because the integral and derivative actions are often of a fractional order. The common factor among all solutions is the extension of the potentialities of the common PID controllers by offering more design degrees of freedom and enhanced robustness.

Namely, FOCs may overcome PID or more complex integer order controllers because they may guarantee better closed-loop performance and higher robustness for parametric variations, both in the case of plants described as integer order systems and especially in the case of plants characterized by non-integer order models [13]. Therefore, the potential impact of FOCs in industrial loops is high. Recent results justify the efforts to exploit these potentialities [43], even if there is no established and widely accepted method for designing or tuning FOCs. In fact, there are still many issues to consider, especially for applications requiring a relatively simple and cheap realization of non-integer order controllers. Namely, the developed solutions should not only be less sensitive to parameter variations and load disturbances, but should also have economic benefits with respect to standard PID controllers of consolidated practice and limited cost. In conclusion, for automotive industries it is important to obtain both efficient and low-cost controllers.

This chapter describes an approach for rail pressure control in injection systems of

CNG engines. The approach combines a gain scheduling technique and a systematic design methodology of FOCs to be applied for different working conditions of the injection system. After the linearization of a non-linear state-space model, the process is modeled as a first order lag plus a time delay (FOLPD) system. In particular, the chapter shows the benefits provided by fractional order proportional-integral (FOPI) controllers, in which the integral action is of non-integer order and is added to a standard proportional action. The basic idea is to perform a loop-shaping [26] of the open-loop transfer function to obtain frequency domain performance specifications and achieve an optimal feedback system [19]. The loop-shaping by the fractional integrator is inspired by the classical symmetrical optimum principle. Deadtime in the plant is also taken into account. Gain scheduling is used to adapt the FOC parameters to the various working points, then to switch between different controllers. Moreover, robust stability of the closed-loop controlled system during the switching between working points is guaranteed by a D-decomposition method [46] and effective simulation tools.

To show the effectiveness of the approach, performance and robustness are tested by simulation of virtual prototypes based on non-linear models and developed by commercially available software.

2. The Injection System

The CNG common rail injection system includes the following main components (see Figure 1): a tank storing high pressure gas that goes up to 200 bars; a pressure regulator that is electronically driven by a solenoid valve and an electronic control unit (ECU); a fuel metering system, consisting of a common rail and electro-injectors. The tank is a constant volume steel cylinder that feeds the downstream circuit, so that pressure in the tank slowly decreases because of the injection flow. The pressure regulator includes a main chamber and a control chamber, which are separated by a moving piston. Both chambers receive fuel from the tank, then send it to the common rail, which is a constant volume accumulator connected to the electro-injectors. The inlet flow to the main chamber is regulated by a shutter that is integral with the moving piston, whose position depends on the equilibrium of the pressures acting on its surfaces. Therefore, adjusting the pressure in the control circuit by means of a solenoid valve allows the regulation of the main chamber inflow. Moreover, the main chamber and the common rail have almost equal pressures (p_2 in Figure 1), so that control of the rail pressure is indirectly achieved by operating on the valve. Then, the ECU accurately meters the amount of injected fuel by operating on the valve control circuit to determine the rail pressure and by setting the injection timings.

2.1. Modeling the CNG Injection System

The state-space model of the CNG injection system is derived by the Eulerian approach. Two control volumes are considered, i.e., the regulator control chamber and the rail circuit. These volumes have a uniform, time-varying, pressure distribution: p_1 is the pressure in the control circuit, p_2 is the pressure in the main chamber and common rail. The tank pressure $p_3 = p_{tk}$ is considered an input rather than a state variable, because its measure is always available on board as it is related to the fuel supply. Pressure p_{tk} is approximately constant
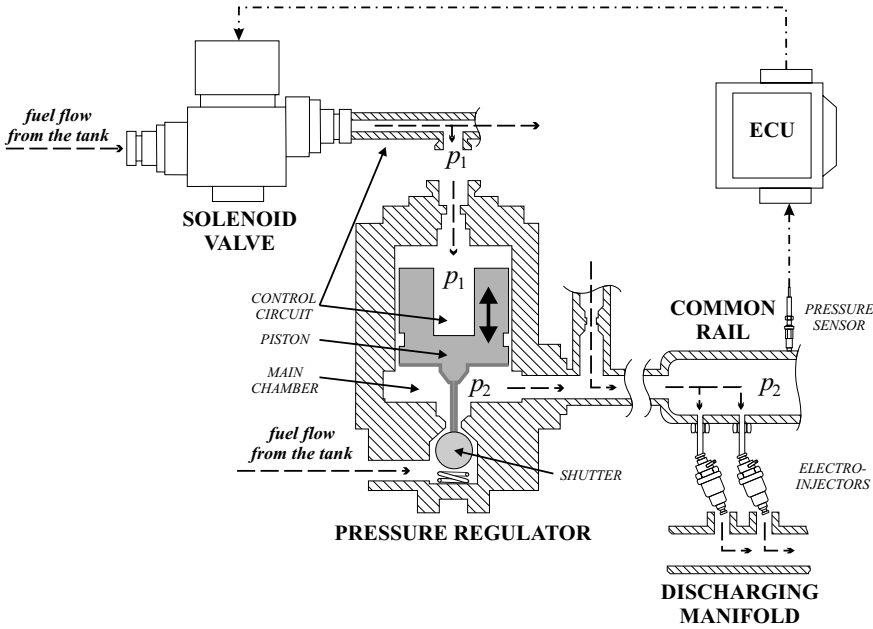
Figure 1. Scheme of the CNG common rail injection system.

within a large time interval, even if the fuel reservoir is slowly decreasing. Moreover, it is likely to assume that injection and rail pressures are equal, so that injectors are not modeled apart and are included in the rail circuit as electronic control valves. Finally, the temperature is assumed to be constant in the whole injection system, so that the system dynamics is completely defined by the pressure variations in the control chamber and the rail circuit.

State-space equations of control volumes derive from the perfect gas law and can be written in terms of the continuity equation [23]:

$$\dot{p} = \frac{R\,\Theta}{V}\left(\dot{m}_{in} - \dot{m}_{out}\right) \tag{1}$$

where p is the pressure of the considered control volume, R is the gas constant, Θ is the temperature, and $\dot{m}_{in}$ and $\dot{m}_{out}$ are the input and output mass flows, respectively, the sum of which has to be equal to the overall mass variation in the control volume V. Possible volume changes due to mechanical part motions are disregarded, since they do not considerably affect the pressure dynamics. Mass flows through control chamber and regulator inlet orifices are considered to be isoentropic transformations, where an output/input pressure ratio $p_{out}/p_{in} \le 0.5444$ is assumed (critical flow condition resulting in a sonic speed flow). Applying the momentum equation leads to the following formula that holds for sonic speed flow [68]:

$$\dot{m}_{in} = c_d\,\rho_{in}\,A\,\sqrt{k\,R\,\Theta\left(\frac{2}{k+1}\right)^{\frac{k+1}{k-1}}} \tag{2}$$

where A is the area of the inflow section, ρ_{in} is the intake gas density, k is the gas elastic constant and c_d is a discharge coefficient accounting for non-uniformity of the mass flow

rate.

In the case of a fluid-dynamic stationary flow, the following formula is used [68]:

$$\dot{m}_{in} = c_d\, c_L\, A_{n,min}\, \sqrt{\rho_{out}\,(p_{in} - p_{out})} \tag{3}$$

where c_L takes into account the effect of kinetic energy losses in the nozzle minimal section $A_{n,min}$. Equation (3) also assumes that no reversal flow occurs. This is the case of the flow between the control chamber and rail circuit.

The inflow section of the pressure regulator, i.e., A in (2), changes with the axial displacement h_s of the shutter and piston [23]. Then, to compute A, the shutter and piston dynamics are determined by applying Newton's second law of motion to the forces acting upon each of them. If the viscous friction and the inertias of the piston and the shutter are disregarded with respect to the large hydraulic forces, then the force balance is:

$$\sum_i p_i\, S_i - k_s\, h_s + F_{so} - F_c = 0 \tag{4}$$

where S_i is area of the surfaces on which pressure p_i acts. It is assumed that pressure gradients are applied to the flow minimal sections. Moreover, k_s is the spring constant, F_{so} is the spring pre-load, i.e., the force applied when the shutter is closed, and F_c is the assumed constant coulomb friction. Hence, equation (4) provides h_s and then A.

The shutter displacement of the electro-hydraulic valve regulates the incoming flux in the control chamber. Since the shutter inertia is negligible, it is assumed that the inflow section can be completely opened ($A_s = A_{s,max}$) or closed ($A_s = 0$), depending on the actual driving current of the valve (energized/not-energized circuit). Consequently, the value of the inflow section can be calculated as $A_s = ET_{sv} \cdot A_{s,max}$, where ET_{sv} is a square signal defining the energizing phase of the solenoid valve. ET_{sv} takes values in $\{0; 1\}$ representing the valve energizing conditions.

In this model, the injector opening and closing transients are disregarded. Hence only two conditions can occur: injectors are closed or opened with a flow section A_{inj}. In this way, system order and computational effort are reduced, without introducing a considerable error. Thus, the injector flow section can be expressed as $ET_{inj} \cdot A_{inj}$, where ET_{inj} is a square signal of amplitude $\{1; 2; \ldots; n\}$, where n is the number of injectors. The amplitude depends on the number of simultaneously opened injectors and on the signal period that varies with the engine speed. Since critical flow condition always holds true, the injection mass flow can be calculated by applying (2).

Now define two state variables, i.e., the control chamber pressure ($x_1 = p_1$) and the rail pressure ($x_2 = p_2$). Moreover, assume as inputs the signals driving the solenoid valve, $u_1 = ET_{sv}$, and the injectors, $u_2 = ET_{inj}$, respectively. Then the CNG injection system resulting from (1)-(4) is described by the following second order non-linear state-space model [23]:

$$\begin{cases} \dot{x}_1(t) = c_{11}\, p_{tk}(t)\, u_1(t) - c_{12}\, \sqrt{x_2(t)\,[x_1(t) - x_2(t)]} \\ \dot{x}_2(t) = c_{21}\, p_{tk}(t)\,[c_{24}\, x_1(t) - c_{25}\, x_2(t) - c_{26}\, p_{tk}(t) - c_{27}] - c_{22}\, x_2(t)\, u_2(t) + \\ \qquad + c_{23}\, \sqrt{x_2(t)\,[x_1(t) - x_2(t)]} \end{cases} \tag{5}$$

where c_{ii} are constant coefficients that depend on the fluid-dynamics gas characteristics and on the system geometrical parameters.

Now, the state-space equations (5) are linearized around different equilibrium points $(\bar{\mathbf{x}}, \bar{\mathbf{u}})$, so that each tuning of the controller parameters refers to a current working point. This simplification is justified because control must keep the pressure close to a reference value, depending on the working conditions set by the driver power request, engine speed and load. Linearization with respect to $\bar{\mathbf{x}}$ and $\bar{\mathbf{u}}$ yields: $\delta\dot{\mathbf{x}}(t) = \mathbf{A}\,\delta\mathbf{x}(t) + \mathbf{B}\,\delta\mathbf{u}(t)$, where $\delta\mathbf{x}(t) = \mathbf{x}(t) - \bar{\mathbf{x}}$ and $\delta\mathbf{u}(t) = \mathbf{u}(t) - \bar{\mathbf{u}}$, with $\mathbf{u}(t) = \begin{bmatrix} u_1(t) \\ u_2(t) \end{bmatrix}$, $\mathbf{x}(t) = \begin{bmatrix} x_1(t) \\ x_2(t) \end{bmatrix}$.

Choosing $\delta x_2(t)$ as output gives $\delta y(t) = \mathbf{C}\,\delta\mathbf{x}(t)$, with $\mathbf{C} = \begin{bmatrix} 0 & 1 \end{bmatrix}$. The following matrices $\mathbf{A} = [a_{ij}]$ and $\mathbf{B} = [b_{ik}]$ are obtained:

$$\mathbf{A} = \begin{bmatrix} -c_{12}\,\dfrac{\bar{x}_2}{2\sqrt{\bar{x}_2\,(\bar{x}_1-\bar{x}_2)}} & -c_{12}\,\dfrac{\bar{x}_1-2\,\bar{x}_2}{2\sqrt{\bar{x}_2\,(\bar{x}_1-\bar{x}_2)}} \\ c_{21}\,c_{24}\,\bar{p}_{tk} + c_{23}\,\dfrac{\bar{x}_2}{2\sqrt{\bar{x}_2\,(\bar{x}_1-\bar{x}_2)}} & -c_{21}\,c_{25}\,\bar{p}_{tk} - c_{22}\,\bar{u}_2 + c_{23}\,\dfrac{\bar{x}_1-2\,\bar{x}_2}{2\sqrt{\bar{x}_2\,(\bar{x}_1-\bar{x}_2)}} \end{bmatrix} \tag{6}$$

$$\mathbf{B} = \begin{bmatrix} c_{11}\,\bar{p}_{tk} & 0 \\ 0 & -c_{22}\,\bar{x}_2 \end{bmatrix} \tag{7}$$

The Laplace transform of the linearized model yields:

$$\begin{cases} X_1 = \dfrac{a_{12}}{s - a_{11}}\,X_2 + \dfrac{b_{11}}{s - a_{11}}\,U_1 = G_{11}\,X_2 + G_{12}\,U_1 \\[2mm] X_2 = \dfrac{a_{21}}{s - a_{22}}\,X_1 + \dfrac{b_{22}}{s - a_{22}}\,U_2 = G_{21}\,X_1 + G_{22}\,U_2 \end{cases} \tag{8}$$

where, with some notational abuse, symbol δ has been dropped and the dependence of X_1, X_2, U_1, U_2 and of G_{ij} on the complex variable s has been omitted. Equations (8) show that the equilibrium tank pressure $\bar{p}_{tk}$ greatly affects the effectiveness of the control action through G_{12}, while the injection process can be considered to be a disturbance on the rail pressure. Clearly, the pressure dynamics in the control chamber and rail are strongly coupled. From (8), it is straightforward to obtain the relationship between U_1 and X_2:

$$X_2 = \frac{G_{12}\cdot G_{21}}{1 - G_{11}\cdot G_{21}}U_1 = \frac{a_{21}b_{11}}{s^2 - (a_{11} + a_{22})s + a_{11}a_{22} - a_{12}a_{21}}U_1 \tag{9}$$

Then, by putting $U = U_1$ and $Y = X_2$, the input-output transfer function is given by:

$$\frac{Y(s)}{U(s)} = \frac{a_{21}\cdot b_{11}}{s_1\cdot s_2}\cdot\frac{1}{(1 - \frac{1}{s_1}s)(1 - \frac{1}{s_2}s)} \tag{10}$$

in which the constant coefficients depend on the working point and the transfer function poles are $s_{1/2} = 0.5[a_{11} + a_{22} \pm \sqrt{\Delta}]$, with $\Delta = (a_{11} - a_{22})^2 + 4a_{12}a_{21}$. It always holds that $a_{11}, a_{22} < 0$ and $a_{12}, a_{21} > 0$, then $\Delta > 0$. Furthermore, $\{a_{21}, |a_{22}|\} \gg \{|a_{11}|, a_{12}\}$ and $(a_{11} - a_{22})^2 \gg 4a_{12}a_{21}$. Then $s_1 = 0.5[a_{11} + a_{22} + \sqrt{\Delta}]$ dominates the transient response, independently of the working point, whereas $s_2 \approx a_{22}$. To sum up, if the smaller time constant is neglected and a time delay τ is introduced to take into account the pressure propagation from the main chamber to the common rail, a family of models described by a first-order lag plus a time delay (FOLPD) system is obtained:

$$Y(s) = G_p(s)\cdot U(s) = \frac{Ke^{-\tau s}}{1 + Ts}\cdot U(s) \tag{11}$$

where $K = a_{21} \cdot b_{11}/(s_1 \cdot s_2)$ and $T = -1/s_1$. The delay τ of pressure propagation can be experimentally determined.

To determine K and T, (5) is manipulated to evaluate equilibrium pressures. However, the valve and injectors' driving signals, $\bar{u}_1$ and $\bar{u}_2$, cannot be directly plugged into the model equations because they result from modulation of discrete values. For this reason, their mean values within an injection cycle are considered instead of the instantaneous values. In particular, $\bar{u}_1$ is the driving current duty cycle, while $\bar{u}_2 = 4 \cdot t_j \cdot \upsilon/120$, i.e., the ratio between the injection time interval t_j and the duration of the whole injection cycle, multiplied by the number (four) of injectors and by the engine speed υ (in rpm). Under this assumption, the linear model coefficients of $\mathbf{A}$ and $\mathbf{B}$ are determined as follows.

First, some considerations on operation modes are useful. As shown by (5) and by the coefficients of the linearized system, operation strongly depends on the tank pressure $\bar{p}_{tk}$. The ECU takes into account the driver power request, speed and load, then it specifies the proper amount of injected fuel by setting the rail pressure reference and the injection timings. Namely, the injection flow rate only depends on the rail pressure because critical flow conditions hold true [23]. Then, the ECU stores static look-up tables that specify the rail pressure and injection timings, in terms of opening time interval t_j (as a function of load and rail pressure) and frequency $4t_j\upsilon/120$ (as a function of speed). This guarantees that the optimal injection profile is set for each working point that refers to specific values of tank pressure, rail pressure and injection timings.

Therefore, a set of linearized models can be determined for each value of $\bar{p}_{tk}$. As a matter of fact, $\bar{p}_{tk}$ depends on the fuel supply, so it is almost constant in a large time interval compared to the dynamics of x_1 and x_2. Moreover, $\bar{p}_{tk}$ affects the efficacy of the control action u_1 because it is included in coefficient b_{11} appearing in G_{12}. Each linearized model in the set related to $\bar{p}_{tk}$ depends on the rail pressure $\bar{x}_2$ and the injection timings $\bar{u}_2$, as specified by the ECU. Then, the control input $\bar{u}_1$, which is able to keep $\bar{x}_2$, and the resulting control pressure $\bar{x}_1$ can be computed from (5) by setting derivatives to 0, and by fixing $\bar{p}_{tk}$, $\bar{x}_2$, and $\bar{u}_2$. In particular, the first equation in (5) gives the control chamber pressure:

$$\bar{x}_1 = \bar{x}_2 + \frac{(c_{11}\bar{p}_{tk}\bar{u}_1)^2}{c_{12}^2\bar{x}_2}. \tag{12}$$

Then, solving the equilibrium condition resulting from the second equation of (5) gives $\bar{u}_1$:

$$\frac{c_{11}^2 c_{21} c_{24}}{c_{12}^2 \bar{x}_2}\bar{p}_{tk}^3\bar{u}_1^2 + \frac{c_{11}c_{23}}{c_{12}}\bar{p}_{tk}\bar{u}_1 + c_{21}(c_{24}\bar{x}_2 - c_{25}\bar{x}_2 - c_{26}\bar{p}_{tk} - c_{27})\bar{p}_{tk} - c_{22}\bar{u}_2\bar{x}_2 = 0 \tag{13}$$

Finally, given $\bar{u}_1$, $\bar{x}_2$, and $\bar{x}_1$, one can determine elements of $\mathbf{A}$ and $\mathbf{B}$ that affect K and T.

2.2.   Scheduling of Parameters

Since the system has several equilibrium points, the parameters K and T in (11) assume different values to which the FOC design will refer. A gain scheduling approach is adopted to adjust the controller settings to variations in the CNG system parameters. Each equilibrium has an associated triple (K, T, τ). More specifically, for each value of $\bar{p}_{tk}$, two 2-D maps can be obtained for K and T by varying the rail pressure and the injection timings at the same time in the whole working range. To synthesize, a fixed value of $\bar{p}_{tk}$ is chosen

to select the proper 2-D look-up tables, which are used to compute K and T based on the equilibrium actual rail pressure $\bar{x}_2$ and injection timings $\bar{u}_2$. The choice of equilibrium conditions, and thus of the scheduling strategy, is based on a sensitivity analysis of the linear model coefficients. Clearly, the larger the number of operating conditions for the scheduling strategy, the larger the amount of memory to store controller parameters. However, the computational effort does not increase. Namely, the complete set of controller parameters is computed off-line and stored in static look-up tables as a function of the chosen operating conditions.

3.   The Control Strategy: Switching of Fractional Order Controllers by Gain Scheduling

To take into account different equilibrium points of the controlled system and to achieve a good trade-off between performance and robustness, a possible solution is to implement switching among fractional order controllers by a scheduling strategy. This is a natural extension of the common approach in automotive applications that frequently employ scheduling of different integer order PI controllers [14, 45, 62]. However, a PI controller is employed for all operating conditions and its tuning is obtained by conventional rules like Ziegler-Nichols [2, 15, 23, 66]. In what follows, the controller parameters depend on the CNG engine working conditions. In other words, for each of these equilibrium points, there is a different fractional order controller that is properly designed to achieve performance and robustness specifications (see Section 4).

Scheduling works as follows. Firstly, the working point is established by the rail pressure and by the average duration, say $\overline{I}$, of the injection process, for each value of the approximately constant tank pressure. More specifically, $\overline{I}$ depends on the injector opening time intervals and on the engine speed. Secondly, the values of the rail pressure and $\overline{I}$ are considered for the new working point that is required to be reached, and the variation between the two working points is computed. Thirdly, the controller is designed with reference to the set (K, T, τ) of parameters associated with the new equilibrium point.

This method is used when the variations between the two operating points are bounded by 2 bar for the rail pressure and by 6 seconds for $\overline{I}$. However, if the variations are higher than these limit values, then several intermediate rail pressure and $\overline{I}$ reference values are considered. Then, several sets (K, T, τ) are determined and several associated controllers are designed. In this way, maps of controller gains are built for the different equilibrium points.

As regards stability of gain scheduling, the pressure reference and $\overline{I}$ are the scheduling variables subject to step changes between the equilibrium points. Then, the amplitudes of these steps must be limited, because each local linear fractional order controller guarantees stability only close to the equilibrium point. If this holds true, then the initial equilibrium point is in the region of attraction of the changed equilibrium point, and a smooth transition is achieved [20].

If variations of variables are fast, then assessing stability in switching for classical gain scheduling is impossible. In this case, only simulation can be used [59], for which the reader can refer to Section 5. There are recent design approaches, such as those based on linear

parameter-varying systems (LPV) [44], that explicitly take into account time dependency of scheduling variables, so that global closed-loop stability is *a priori* achieved [45]. However, the number and variation rate of scheduling parameters, as well as complexity of the non-linear model, make the LPV framework inappropriate for the considered application. Namely, analysis and design are complex and the computational effort is high [45].

To better analyze closed-loop stability with respect to variations in working conditions of the injection process, one may refer to the classical D-decomposition methodology [46] that is well known for designing integer order controllers [1] but that was also recently applied to FOPID controllers operating on fractional order systems with delays [16,18,29]. Namely, this approach determines all the stabilizing controllers, i.e., the set of controller parameters that guarantee a stable closed-loop system. A stability domain, say $\mathcal{D}$, is defined in the so-called parameter space and the designed controller is associated with a point inside this space. If the point is far from the boundaries of the stability domain, then closed-loop stability is obtained for (small) bounded variations of the controller gains.

To extend the D-decomposition methodology to the case of fractional order controllers, consider the procedure shown by [16,29]. The starting point is the characteristic equation of a closed loop containing a FOPI controller. If the open-loop transfer function is

$$G(s) = \frac{K\,K_I\,(1 + T_I s^\nu)}{(1 + Ts)\,s^\nu}\,e^{-\tau s} \tag{14}$$

then the closed-loop transfer function is

$$F(s) = \frac{K\,K_I\,(1 + T_I s^\nu)\,e^{-\tau s}}{(1 + Ts)\,s^\nu + K\,K_I\,(1 + T_I s^\nu)\,e^{-\tau s}} \tag{15}$$

where ν is the fractional order of integration, $T_I = K_P/K_I$, and K_P and K_I are the proportional and integral gain, respectively. To analyze closed-loop stability, consider the solutions of the fractional order characteristic pseudo-polynomial equation

$$E(s) = (1 + Ts)\,s^\nu + K\,K_I\,(1 + T_I s^\nu)\,e^{-\tau s} = 0 \tag{16}$$

Then, if all solutions lie in the open left-half of the s-plane (LHP roots), then the closed-loop system is BIBO stable [8, 16, 18].

So, if $(K_P, K_I, \nu) \in \mathcal{D}$ (the set of all stabilizing controllers in the parameter space), then all closed-loop roots are LHP. The domain $\mathcal{D}$ is defined by boundaries: the real root boundary (RRB), the infinite root boundary (IRB), and the complex root boundary (CRB) [1, 16]. The RRB is associated with the solutions of $E(s = 0) = 0$:

$$K\,K_I = 0 \Rightarrow K_I = 0 \tag{17}$$

The CRB comes from $E(s = j\omega) = 0$

$$\begin{aligned}(1 + Tj\omega)\,\omega^\nu\,(C + jS)+ \\ + K\,K_I\,[1 + T_I \omega^\nu (C + jS)]\,[\cos(x) - j\sin(x)] = 0\end{aligned} \tag{18}$$

with $C = \cos(\theta), S = \sin(\theta), \theta = \frac{\pi}{2}\nu, x = \omega\tau$. Taking the real and imaginary parts of the complex equation (18) leads to the following solutions:

$$K_I = \frac{\omega^\nu\,(\sin(x) + \omega T \cos(x))}{K\,S}, K_P = \frac{(\omega TS - C)\,\sin(x) - (S + \omega TC)\,\cos(x)}{K\,S} \tag{19}$$

which can be used to plot a curve in the 2-D-space (K_P, K_I), when ν is fixed and ω is varied from 0 to ∞, since the gains are functions of ω. If a different pair of controller gains is chosen, analogous curves can be drawn in the 2-D-spaces (K_P, T_I) or (T_I, K_I).

The IRB for $s \to \infty$ does not exist, because the condition $\alpha_n \le \beta_n$ provided in [16] is not satisfied, where α_n and β_n are, respectively, the integer (in general fractional) orders of the denominator and numerator polynomials of $G_p(s)$ in (11).

To simplify the identification of the complete stability domain $\mathcal{D}$, two steps can be followed. Firstly, one of the parameters (e.g., the order ν) is fixed so that the RRB and CRB boundaries are determined inside the plane defined by the remaining two parameters (e.g., the (K_P, K_I)-plane). Secondly, the fixed parameter is varied and the complete 3-D stability domain is obtained by sweeping over all the admissible values of the parameter fixed initially.

If the analysis focuses on the plane (K_P, K_I), then the boundaries divide it into unstable and stable regions that can be checked by a test point. If a region is stable, then it does not contain any closed-loop root in the closed right-half of the s-plane (RHP root); if a region is unstable, then it includes some RHP root. For the stability check, algorithms were proposed by [18] and [41].

For example, Figure 2a shows the stability regions obtained for $\nu = 1.3, 1.4, 1.5, 1.6$, when a FOPI controller is designed according to the procedure of Section 4, with reference to an equilibrium point defined by $K = 165$ bar and $T = 1.74$ s. In particular, the equilibrium points are determined by (K, T)-values corresponding to values of the rail pressure p_2 and injection timing t_{inj}, for an engine speed of 2500 rpm. Note that the τ parameter is approximately constant in the whole operating range, if an accurate model of the CNG injection system is considered. Moreover, for a different equilibrium point, a different FOPI controller and a different stability region are defined. Figure 2b shows the case of $K = 127$ bar and $T = 1.97$ s. The values of the gains in Figures are indicated but for a multiplying factor of 10^{-2}.

Finally, it is remarked that, for each value of ν, the design point P (marked with $\times$ in the Figure 2) lies in the stability region and belongs to a peculiar curve; this curve is called a "relative stability curve" and is obtained by the technique of the phase margin tester [16, 29]. This curve is associated with the specified phase margin PM_s and, for each point, provides a possible gain crossover frequency. Then, the point $\times$ determined by the designed values of K_P and K_I corresponds to the specified gain crossover frequency, ω_c. Moving the design point along the relative stability curve changes the controller gains, by keeping the same PM_s while changing ω_c. Moreover, another curve (not shown) can be defined for a specified gain margin GM_s and passes through a design point that is associated with the phase crossover frequency.

4.   Fractional Order Control Design

In this section, the focus is on the PI^ν type of controllers, because they recently obtained promising results in mechatronics and automotive control systems. Namely, a systematic design methodology has been applied [24, 26] and is extendable to a wide class of systems. Moreover, this kind of controller is the closest one to PI controllers that are typically employed in industrial contexts [4]. Hence it is quite natural to compare the PI
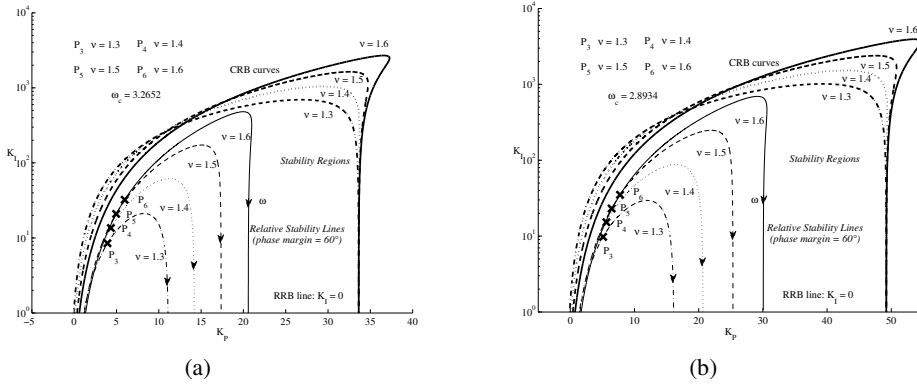
Figure 2. Design of FOPI controllers ($u_c = 5.7$, $PM_s = 60°$) for two working points and position of design points P in stability regions with respect to stability boundaries (CRB curves) and relative stability curves: (a) $K = 165$ bar, $T = 1.74$ s, (b) $K = 127$ bar, $T = 1.97$ s.

to the flexible and robust PI^ν, with its high performance due to the additional freedom of choosing the non-integer order ν of integration. The limited complexity of PI^ν could also help practitioners to make comparisons with various tuning rules of PI controllers and, above all, to promote their acceptance of the fractional order control paradigm. Finally, as shown below, the choice of the free controller parameters is determined by closed-form formulas that combine a low computational complexity with analytic satisfaction of design specifications (robustness and performance).

The design is guided by basically two ideas:

- the *optimality* of the closed-loop system, to obtain a system which is a good approximation of an optimal system in a frequency band of interest [19];

- the *loop-shaping* of the open-loop frequency response, to obtain high robustness to parametric variations and uncertainties, in a sufficiently wide frequency range.

The design obviously requires a realization phase. Namely, implementation of FOC requires approximating the irrational operators that are basic units in Laplace representation of FOC. Then, a rational transfer function must be obtained by a proper approximation technique. Among the available techniques, a continued fractions approach is chosen that shows several benefits:

a) good convergence properties and reduced approximation errors;

b) stability and minimum-phase characteristics, which are very important for control applications;

c) interlacing between real poles and real zeros of the rational transfer function.

These properties are verified both in the analog and in the discrete domain. The implementation of the approximating transfer functions can be achieved by using interface equipment allowing use of the Matlab/Simulink environment or micro-controllers or low cost components.

4.1. Design Procedure

The design of robust FOPI controllers for each operating point is based on a loop-shaping approach. By applying relatively easy closed-form formulas, the methodology directly relates performance and robustness specifications to the values of the controller parameters. More specifically, to achieve robustness to gain variations in a sufficiently wide frequency range around the crossover [26], an integrator of non-integer order ν is particularly suitable. Namely, it leads to a nearly flat phase diagram and a constant slope of the magnitude diagram of the open-loop gain in that range. Moreover, to pursue optimality of the feedback system [19], the open-loop frequency response is so shaped that the gain is high at low frequencies and rolls off at high frequencies to avoid stability problems [61]. A good input-output tracking is obtained in a specified bandwidth.

The proposed design procedure was conceived for controlling plants with transfer function $G_p(s) = \frac{K}{s(1+Ts)}$ [26]. In particular, the background idea was inspired by the symmetrical optimum method that is often used to tune integer order PI controllers for electric drives [39]. Subsequently, the effect of time delay τ has been added [24, 25]. To cover a wide range of applications, processes characterized by $G_p(s) = \frac{K}{1+Ts}e^{-\tau s}$ have also been considered [27, 28].

Here, the controlled plant of a unitary feedback control system is considered, in which sensor dynamics are neglected for the sake of simplicity, and with a model defined by:

$$G_p(s) = \frac{K}{1+T\,s}\,e^{-\tau s} \tag{20}$$

where K is the static dc-gain, T is the time constant of the dominant dynamics and τ is the dead time of the injection system. Moreover, the system includes a FOPI controller that is characterized by a standard proportional element and an integral action of non-integer order $1 < \nu < 2$:

$$G_c(s) = K_P + \frac{K_I}{s^\nu} = \frac{K_I}{s^\nu}\left(1 + T_I\,s^\nu\right) \tag{21}$$

with $T_I = \frac{K_P}{K_I}$ and where K_P and K_I are the proportional and integral gain, respectively. In this way, the open-loop gain $G(s) = G_c(s)\,G_p(s)$ is:

$$G(s) = \frac{K\,K_I\,(1+T_I\,s^\nu)}{s^\nu\,(1+T\,s)}\,e^{-\tau s} \tag{22}$$

The non-integer order is chosen $1 < \nu < 2$ so that an integer unitary integration s^{-1} is included to allow compensation of disturbances on the plant. The reason for this choice is that, if the non-integer operator s^ν with $0 < \nu < 1$ is approximated by a rational transfer function, then a non-zero dc-gain would be obtained by this realization and a steady-state error would occur. Instead, by using $1 < \nu < 2$, an integer integrator (with order equal to 1) and a non-integer integrator (with order $\lambda = \nu - 1$ and $0 < \lambda < 1$) ensue. Therefore,

increased flexibility is gained due to three design parameters (K_P, K_I, ν), i.e., to one more degree of freedom with respect to a PI controller. However, reliable and effective rules to design and tune the parameters must also be established.

Putting $s = j\omega$, the open-loop frequency response (OLFR for brevity) associated with $G(s) = G_c(s)\,G_p(s)$ is given by:

$$
\begin{aligned}
G(j\omega) &= \frac{K\,K_I\,[1 + T_I\,(j\omega)^\nu]}{(j\omega)^\nu\,(1 + j\omega\,T)}\,e^{-j\omega\tau} \\
&= \frac{K\,K_I\,\{1 + T_I\,\omega^\nu\,[\cos(\frac{\pi}{2}\nu) + j\sin(\frac{\pi}{2}\nu)]\}}{\omega^\nu\,[\cos(\frac{\pi}{2}\nu) + j\sin(\frac{\pi}{2}\nu)]\,(1 + j\omega\,T)}\,e^{-j\omega\tau}.
\end{aligned}
\tag{23}
$$

Now, after simple algebraic computations, putting $\theta = \frac{\pi}{2}\nu$, $S = \sin(\theta)$, and $C = \cos(\theta)$ and introducing a nondimensional frequency $u = \omega\,T$ lead to:

$$
G(ju) = \frac{K\,K_I\,T^\nu\,\left\{1 + T_I\,(\frac{u}{T})^\nu\,[C + jS]\right\}}{u^\nu\,[C + jS]\,(1 + j\,u)}\,e^{-j\frac{u\tau}{T}}
\tag{24}
$$

Then the magnitude and phase angle frequency behaviors are given by:

$$
|G(ju)| = \frac{K\,K_I\,T^\nu}{u^\nu}\sqrt{\frac{1 + 2\,T_I\,(\frac{u}{T})^\nu\,C + T_I^2\,(\frac{u}{T})^{2\nu}}{1 + u^2}}
\tag{25}
$$

$$
\angle G(ju) = \arctan\left(\frac{T_I\,(\frac{u}{T})^\nu\,S}{1 + T_I\,(\frac{u}{T})^\nu\,C}\right) - \arctan(u) - \theta - \frac{u\tau}{T}
\tag{26}
$$

Now, the closed-loop frequency response $F(ju) = \frac{1}{1+G^{-1}(ju)}$ is considered and the optimality requirement $|F(ju)| \equiv 1$ is approximated in a sufficiently large bandwidth u_B. In theory, however, an optimal feedback system that provides perfect input-output tracking should be achieved only if this holds true for all frequencies. i.e., $|G(ju)| \gg 1, \forall u$ should be verified. Namely, *"a feedback system is optimal if and only if the absolute value of the return difference is at least one at all frequencies"* [19], but this condition cannot be satisfied by the return difference $|1 + G^{-1}(j\omega)|$. Instead, $|G(ju)|$ is shaped around the crossover u_c so that a high gain is obtained at low frequencies, whereas it rolls off at high frequencies to avoid stability problems [61]. The appropriate shaping guarantees robust stability and desired performance despite parameter variations in the controlled injection system. Namely, the non-integer order integrator provides a magnitude plot with a fractional slope of -20 dB/decade and a nearly flat phase diagram in a range around u_c so that a nearly constant phase margin is achieved in this range.

To synthesize, start by fixing u_B where optimal tracking is desired. In particular, a trade-off is reached. Namely, the higher u_B is, the lower the rise time in the response of the closed-loop system. Moreover, the lower is u_B, the more the crossover u_c is shifted toward a centered position in the flat region of the phase characteristic. For the sake of convenience, u_B is chosen higher than the plant bandwidth.

Then the normalized crossover frequency is estimated by a commonly used relation [31]: $u_c \in [\frac{u_B}{1.7}, \frac{u_B}{1.3}]$, e.g., $u_c = \frac{u_B}{1.5}$. The estimate may be changed inside the indicated

range to adjust T_I. Then, to achieve a specified phase margin PM_s at u_c, T_I is properly selected. Namely, the phase margin $PM = \pi + \angle G(ju_c)$ is:

$$PM = \arctan\left(\frac{T_I\left(\frac{u_c}{T}\right)^\nu S}{1 + T_I\left(\frac{u_c}{T}\right)^\nu C}\right) - \arctan(u_c) - \frac{u_c \tau}{T}$$

$$+ \pi - \theta = \varphi_1(u_c) - \varphi_2(u_c) - \frac{u_c \tau}{T} + \pi - \theta \qquad (27)$$

where $\varphi_1(u_c)$ and $\varphi_2(u_c)$ are the first two arguments on the right side of (27). Then, T_I is determined to compensate the delay by putting $\varphi_1(u_c) - \varphi_2(u_c) - u_c\frac{\tau}{T} = 0$ and obtain a closed-form formula:

$$T_I = \frac{T^\nu \left[u_c + \tan(\frac{u_c \tau}{T})\right]}{u_c^\nu \left[S - u_c\,C - (C + u_c\,S)\tan(\frac{u_c \tau}{T})\right]}. \qquad (28)$$

This choice yields:

$$PM_s = \pi - \theta = (2 - \nu)\,\pi/2 \Leftrightarrow \nu = 2 - 2PM_s/\pi \qquad (29)$$

which represents a direct and easy design relation between the fractional order ν and the specification provided on PM_s. Note that $\nu > 1$ is always obtained for a plant without an integrator. Obviously, at the end of the design procedure, it is always verified that the FOPI controller ensures a nearly flat Bode plot of $\angle G(ju)$, so that the obtained phase margin is nearly constant in a range around u_c.

To complete the design procedure, $|G^{-1}(ju_c)|^2 = 1$ is helpful to get another closed-form formula for determining K_I:

$$K_I = \frac{1}{K}\left(\frac{u_c}{T}\right)^\nu \sqrt{\frac{1 + u_c^2}{1 + 2\,T_I\left(\frac{u_c}{T}\right)^\nu C + T_I^2\left(\frac{u_c}{T}\right)^{2\nu}}} \qquad (30)$$

The (30) also leads to $K_P = K_I\,T_I$.

It is to be noted that the value and sign of T_I in (28) depend on the choice of ν (i.e., the specified PM_s), which affects C and S, and on the choice of u_c (i.e., the specified u_B). Then, if u_B is fixed, ν is restricted to allow $T_I > 0$, i.e., a minimum-phase and stable compensated system. This means that restrictions apply on the achievable phase margin. Vice versa, if PM_s is fixed, the same kind of restriction applies on u_c. In other words, restrictions apply on the achievable bandwidth. For example, for $PM_s = \pi/4$ with $\nu = 1.5$, Table 1 provides the values of T_I for several values of the pairs (r, u_c), where r is the delay ratio $r = \tau/T$ and $u_c \in \{u_B/1.7, u_B/1.5, u_B/1.3\}$, with $u_B = 2\pi$.

Finally, another point must be noted. Given T from the plant model, u_c, and ν, the maximum plant time delay allowing $T_I > 0$ is: $\tau_{max} = \left(\frac{T}{u_c}\right)\arctan\left(\frac{S - u_c\,C}{C + u_c\,S}\right)$. Then, τ_{max} satisfying this requirement depends on plant parameters and specifications on u_B and PM_s. Moreover, values $\nu \geq 1.6$ are not convenient because they imply a too low phase margin, which is usually taken as greater than $35°$ [61]. Table 2 reports the values of T_I corresponding to $u_c = u_B/1.5 = 4.1888$, $\tau = 0.18$ seconds and $T = 1.6857$ seconds ($r = 0.1068$), which are the parameters of the CNG injection system model for a particular working condition. In all cases, $\tau_{max} > \tau$ so the controller design is possible.

Table 1. Values of T_I (s) corresponding to pairs (r, u_c) **for** $PM_s = 54°, 45°, 36°$ **(with** $\nu = 1.4, 1.5, 1.6$**)**

(r, u_c)	$\nu = 1.4$	$\nu = 1.5$	$\nu = 1.6$
$(0.8, 3.6960)$	0.3408	0.2940	0.2607
$(0.8, 4.1888)$	0.4599	0.3523	0.2830
$(0.8, 4.8332)$	1.8525	0.6835	0.3930
$(1.0, 3.6960)$	0.9623	0.6210	0.4495
$(1.0, 4.1888)$	-1.0476	-6.3933	1.2395
$(1.0, 4.8332)$	-0.0251	-0.0265	-0.0297
$(1.2, 3.6960)$	-0.4398	-0.6572	-1.6913
$(1.2, 4.1888)$	0.0261	0.0267	0.0286
$(1.2, 4.8332)$	0.1828	0.1600	0.1435

Table 2. Values of T_I and τ_{max} for a given working condition ($T = 1.6857$ **s,** $\tau = 0.18$**s)**

ν	PM_s	T_I (s)	τ_{max} (s)
1.3	63°	1.1719	0.2839
1.4	54°	0.6773	0.3472
1.5	45°	0.4606	0.4104
1.6	36°	0.3418	0.4736
1.7	27°	0.2684	0.5368

4.2. Realization

The final step of the design procedure requires realization of the irrational non-integer order operator s^ν. To this aim, a rational transfer function approximation is required. Many approximation methods exist, starting with the well-known recursive Oustaloup's technique [48]. Other approaches are based on truncation of continued fraction expansions (CFEs) and interpolation techniques [12, 67] or signal processing techniques [6]. Here, an efficient method is used that derives approximations from the Lagrange's CFE [33].

This CFE-based method *a priori* guarantees minimum-phase zeros and stable poles of the approximating rational transfer function and is based on closed-form formulas expressing coefficients of the numerator and denominator polynomials in the transfer function. Moreover, zeros and poles are interlaced on the negative real half-axis [35], and this property also holds for digital realization [32, 34, 36]. This is very important for controller synthesis, because right-half plane (RHP) zeros and RHP poles in the open-loop transfer function imply inherent limitations to the benefits of feedback [17, 60]. More specifically, RHP poles imply constrained large gain bandwidth, which leads to a highly amplified sensor noise at the input to the plant. Finally, the method can obtain a reduced approximation

error by a relatively low number of zeros and poles, so an easy implementation is possible in the analog or digital domain. The closed-form formulas are valid for s^ν when $0 < \nu < 1$. Then, since $\nu > 1$ in the non-integer order integrator of the FOPI controller, given that $s^\nu = s\, s^{\nu-1}$, only $s^{\nu-1}$ is approximated. To synthesize, if $\lambda = \nu - 1$, the approximation is as follows:

$$s^\lambda \approx \frac{\alpha_{N,0}(\lambda)\, s^N + \alpha_{N,1}(\lambda)\, s^{N-1} + \ldots + \alpha_{N,N}(\lambda)}{\beta_{N,0}(\lambda)\, s^N + \beta_{N,1}(\lambda)\, s^{N-1} + \ldots + \beta_{N,N}(\lambda)} \tag{31}$$

where $N \geq 1$ is the number of zero-pole interlaced pairs and the coefficients $\alpha_{N,j}(\lambda) = \beta_{N,N-j}(\lambda)$, for $j = 0, \ldots, N$, depend on λ and are determined by the following closed-form formula:

$$\alpha_{N,j}(\lambda) = (-1)^j \binom{N}{j} (\lambda + j + 1)_{(N-j)} (\lambda - N)_{(j)} \tag{32}$$

in which the so-called Pochhammer functions are $(\lambda + j + 1)_{(N-j)} = (\lambda + j + 1)(\lambda + j + 2) \ldots (\lambda + N)$ and $(\lambda - N)_{(j)} = (\lambda - N)(\lambda - N + 1) \ldots (\lambda - N + j - 1)$, with $(\lambda + N + 1)_{(0)} = (\lambda - N)_{(0)} = 1$. Simple algebraic manipulations allow us to express the previous formula differently [37, 38]:

$$\alpha_{N,j} = C(N, j)\, (j + 1 + \lambda)_{(N-j)}\, (N - \lambda)_{(j)^*} \tag{33}$$

$$\beta_{N,j} = C(N, j)\, (N - j + 1 + \lambda)_{(j)}\, (N - \lambda)_{(N-j)^*} \tag{34}$$

where $(N - \lambda)_{(j)^*} := (N - \lambda)(N - \lambda - 1) \ldots (N - \lambda - j + 1)$ and $(N - \lambda)_{(N-j)^*} := (N - \lambda)(N - \lambda - 1) \ldots (j - \lambda + 1)$ are falling factorials. It holds $(N - \lambda)_{(0)^*} = 1$.

5.   Simulation Results

This section shows the effectiveness, performance and robustness of the described control strategy. To this aim, a detailed non-linear simulation model is created by the commercial AMESim developing package [22]. AMESim is a simulation tool based on a virtual prototyping environment. It enables modeling and integration of different physical components, supports and combines different levels of abstraction. The polymorphism concept of AMESim allows the analysis of a multi-disciplinary system as a whole and the representation of many different scenarios. All its peculiarities and properties make AMESim capable of replacing real experiments for validation, so that the non-linear model of this study accurately represents the complex fluid-dynamic phenomena characterizing the injection system at different working points.

The AMESim model makes some assumptions. First, the distribution of pressure in the control chamber, the common rail and the injectors is uniform; the elastic deformations of solid parts by pressure changes are negligible; the pipes, which are considered incompressible ducts with friction, are subject to non-uniform pressure distribution. Vice versa, the model considers temperature variations affecting the pressure dynamics in each component and only takes into account heat exchanges through pipes, by properly computing a thermal exchange coefficient. The tank pressure plays the role of a maintenance input and it is modeled by a constant pneumatic pressure source. Finally, to simplify the AMESim model construction, some supercomponents have been created to group multiple elements.

The operating ranges of the main variables in the system are the following:

- pressure in the tank: $p_{tk} \in [30, 200]$ bar;

- pressure in the control chamber: $x_1 \in [4, 25]$ bar;

- pressure in the common rail: $x_2 \in [4, 25]$ bar;

- injector opening time: $t_{inj} \in [025]$ ms;

- duty-cycle of the command signal for the valve: $[0, 100]\%$;

- engine speed: $\omega_{rpm} \in [1000, 4000]$ rpm.

As a consequence, the model parameters vary in the following ranges: $K \in [134, 1129]$ bar, $T \in [1.059, 18.546]$ seconds.

In the most representative simulation tests, the tank pressure, the engine speed and the injector opening time are kept constant at $p_{tk} = 50$ bar, $\omega_{rpm} = 2500$ rpm and $t_{inj} = 5ms$, respectively. However, Table 3 shows the system parameters in several conditions.

Table 3. Engine parameters in working points

t_{inj} (ms)	x_2 (bar)	p_{tk} (bar)	K (bar)	T (s)
5	4	50	156	1.52
5	5	50	178	1.75
5	6	50	200	1.96
5	8	50	243	2.38
5	10	50	288	2.82
20	5	50	176	1.73
25	20	50	526	5.18

To test their efficiency and robustness, the gain-scheduled FOPI controllers, with $\nu = 1.3, 1.4, 1.5$, are compared to a standard integer order PI that is typically used for injection control and usually tuned by the open-loop Ziegler-Nichols rules. The PI is gain-scheduled for fairness of comparison. Values of $\nu < 1.3$ or $\nu > 1.6$ are discarded because they lead to too high or low (below $36°$) phase margins. With reference to the typical working conditions in Table 3, two different cases are simulated.

In the first one, the reference pressure undergoes a small variation from 5 to 6 bar and the system variables are perturbed slightly from their working point. Hence, the local behavior can be analyzed by the linearized model. The parameters of the injection system are $K = 200$ bar, $T = 1.96$ seconds (see Table 3). A single FOPI or PI controller is used and designed according to these parameters associated with the final reference pressure that must be reached.

Figure 3 shows the closed-loop step response.

With respect to a standard PI, the FOPI controllers improve the performance indices: even if the rise time is slightly longer, the overshoot is highly reduced, so that a better injection accuracy is achieved; the settling times are comparable for $\nu \leq 1.5$. With the PI controller, the performance is influenced primarily by disturbances and nonlinearities
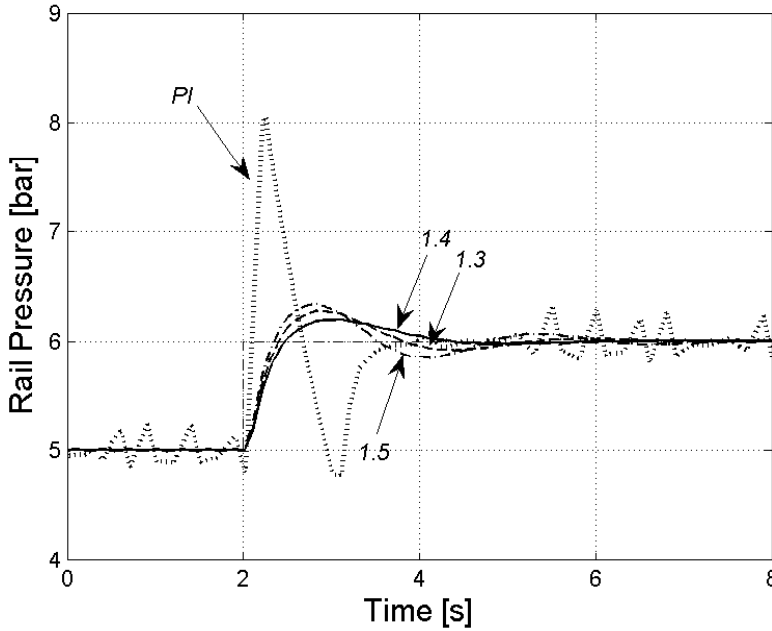
Figure 3. Response to a 5-to-6 bar step in the reference pressure.

related to operations of injectors, by PWM modulation of the solenoid valve command. Large variations of the control signal cause high frequency pressure oscillations around the equilibrium point. Moreover, the saturation in the control signal, which is associated with a complete closure of the valve, determines large rail pressure overshoots and undershoots. Conversely, performances of fractional controllers are less sensitive to system disturbances and nonlinearities.

The second case simulates a large variation in the reference pressure from 6 to 10 bar, with a step of 2 bar, and then back from 10 to 6 bar, with the same step. Then, the scheduling switches between several controllers. In particular, since the variation is divided into two steps, two FOPI/PI controllers are used. This choice is justified by simulation. Several tests, indeed, verified that stability is achieved if variations of the rail reference pressure and of injector opening times are within operating ranges.

This second experiment aims at testing control robustness. Namely, the emptying and filling of the common rail follow different dynamics. This is due to several reasons. First, the gradient between the tank pressure and the main chamber is higher than between the common rail and the discharging manifold. Secondly, the rail fills more rapidly because the feeding tank has a higher pressure than the rail. In contrast, the rail empties more slowly because of the much lower rail pressure and the injection outflow. However, injection timings do not vary because they are set by the ECU based on the amount of fuel to inject. Therefore, the emptying process can be accelerated only by closing the solenoid valve.

Figure 4 shows that, for rising transients, FOPIs remarkably reduce the overshoots and responses are similar to the first case. FOPIs are very prompt in resetting the rail pressure
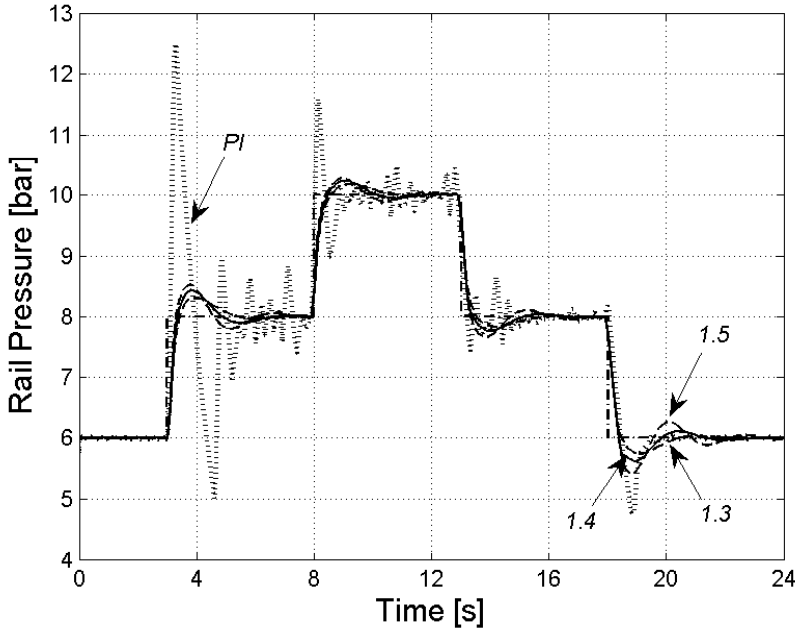
Figure 4. Response to large variations in the reference pressure.

to the set-point.

Conversely, the PI controller reacts poorly to larger variations, and the previously described non-linear phenomena considerably affect overall performance.

For descending transients starting from $t = 13$ s, owing to the request of a quick pressure reduction, a duty cycle equal to zero closes the valve completely. Thanks to injections, the rail pressure decreases to the final reference values (8 and 6 bar, respectively), with a time constant depending on the system geometry. The error cannot be reduced with a higher rate than that achieved, due to the saturation of the actuation variable. This is reflected by the same slope of pressure plots by FOPIs or PI. Figure 4 clearly shows a better tracking of the PI during the descending transient with respect to the rising transient. At the same time, a large undershoot of the rail pressure still remains before reaching the steady state.

Therefore, FOPIs achieve an overall better quality of the response, so they may also improve injection pressure regulation for large perturbations of working conditions.

All the achieved results confirm the higher robustness and performance of the FOPI controllers in all simulated conditions. The tests show that FOPIs significantly improve the usual performance indices for injection pressure control, by reducing undershoots/overshoots, steady-state errors and settling times [14].

This remarkable result can be explained by the proposed control approach. Namely, on one side, it is already well known that fractional order control may help to improve robustness and closed-loop performance. But the added value here is the robust stability properties enforced by the D-decomposition. If one considers the variation of the working points of the injection system, then the approach guarantees that, for each new working

point associated with a reference rail pressure and injection timing, the representative point P of the designed controller (for each value of ν) belongs to the stability domain. In particular it lies on the relative stability curve associated with the designed phase margin (see Figure 2 for two different points).

This occurs because, for each value of ν, the position and amplitude of both the CRB boundary curves and the relative stability curves change, but their shape and mutual position do not. In addition, consider parametric variations, uncertainties and model inaccuracies that bring the design point P closer to a modified actual CRB curve than to an initially used nominal CRB curve. In this case, the distance between the nominal CRB curve and the relative stability curve on which P lies is sufficient to guarantee stability. If needed, this distance can also be enlarged by shifting the point P along the relative stability curve with the same phase margin specification (see possible different locations in Figure 2) with increasing ω. In this way, P is relocated away from the CRB curve provided that ω_c, then ω_B, can be increased.

Finally, the employed scheduling strategy guarantees stability when switching the fractional order controllers. Namely, as far as variations in the reference pressure are bounded by 2 bar and those in injection duration by 6 s (which is a good indication for real practice), simulation results always verify closed-loop stable responses.

6.   Conclusion

Injection pressure regulation is currently an important control problem in the automotive industry because of the ever-growing focus on reducing pollutant emissions and consumption and increasing engine efficiency. In this chapter, the case of CNG engines was approached by an innovative fractional order control strategy. The typical advantages offered by FOCs are amplified by combining the D-decomposition methodology and appropriate controller scheduling for the specific injection system working points. To synthesize, injection pressure is regulated by tuning different FOPI controllers based on the reference working points to achieve. Variations between working points and disturbances are compensated by scheduling the FOPI controller gains. Moreover, several simulation studies verify that switching between controllers does not lead to stability problems. To sum up, the main benefits of the proposed approach for controlling rail pressure in injection systems of CNG engines are the following.

Closed-form and relatively simple design formulas are applied to obtain the controller gains in terms of frequency domain specifications; such formulas could be used for an automatic synthesis of the controller. As far as relative stability is concerned, a specification on the phase margin can be analytically achieved and is strictly related to the required non-integer order ν and, vice versa, the selected order ν determines the phase margin that can be obtained (see formulas in (29)).

The integral (or derivative) operator of the fractional order controller is realized by an efficient approximation method that prevents numerical problems and leads to a rational transfer function characterized by a low number of zeros and poles. Both reduced approximation errors and easy implementation are guaranteed by the proposed realization. The approximating rational transfer function shows remarkable properties: the poles of the transfer function are stable, the zeros are minimum-phase, and all singularities are interlaced

on the negative real half-axis of the s-plane [35]; interlacing, stability and minimum-phase characteristics are also achieved by the discrete transfer function used for digital realization [34, 36, 37].

Robust stability of the designed FOPI controllers is guaranteed by the D-decomposition, which allows a greater robustness with respect to the usual solutions employed in the automotive industry, even if large variations of working points are considered. Finally, if switching between sufficiently close working points is done such that variations of injection timings are below 6 seconds and changes of rail pressure are below 2 bar, then nonlinearity effects, oscillations and instability problems in the rail pressure are prevented.

Acknowledgment

References

[1] Ackermann, J., and D. Kaesbauer (2003). Stable polyhedra in parameter space. *Automatica*, 39 (5), 937–943.

[2] Amorese, C., De Matthaeis, S., De Michele, O., and A. Satriano. The gaseous fuel option: LPG and CNG. In *Proc. Int. Conf. on Vehicles Alternative Fuel System & Envir. Protection*, Dublin, Ireland, 6–9 July 2004.

[3] Arena, P., Caponetto, R., Fortuna, L., and D. Porto (2000). *Nonlinear Noninteger Order Circuits and Systems: An Introduction*. In L. O. Chua (Ed.) *World Scientific Series on Nonlinear Science, Series A* (Vol. 38). Singapore: World Scientific.

[4] Åström, K. J., and T. Hägglund (1995). *PID Controllers: Theory, Design, and Tuning*. 2nd edition. Research Triangle Park, NC: Instrument Society of America.

[5] Barbosa, R. S., Tenreiro Machado, J. A., and J. M. Ferreira (2004). Tuning of PID controller based on Bode's ideal transfer function. *Nonlinear Dynamics*, 38, 305–321.

[6] Barbosa, R. S., Tenreiro Machado, J. A., and M. F. Silva (2006). Time domain design of fractional differintegrators using least squares. *Signal Process.*, 86 (10), 2567–2581.

[7] Bode, H.-W. (1945). *Network Analysis and Feedback Amplifier Design*. New York: D. Van Nostrand Co., Inc..

[8] Bonnet, C., and J. R. Partington (2001). Stabilization of fractional exponential systems including delays. *Kybernetika*, 37 (3), 345–353.

[9] Caponetto, R., Dongola, G., Fortuna, L., and I. Petráš (2010). *Fractional Order Systems: Modeling and Control Applications*. World Scientific Series on Nonlinear Science Series A: Vol. 72. Singapore: World Scientific.

[10] Charef, A. C., Sun, H. H., Tsao, Y. Y., and B. Onaral (1992). Fractal systems as represented by singularity function. *IEEE Trans. Autom. Contr.*, 37 (9), 1465–1470.

[11] Charef, A. C., (2006). Analogue realisation of fractional-order integrator, differentiator and fractional $PI^\lambda D^\mu$ controller. *IET Contr. Theory and Appl.*, 153 (6), 714–720.

[12] Chen, Y.-Q., Vinagre, B. M., and I. Podlubny (2004). Continued fraction expansion approaches to discretizing fractional order derivatives – An expository review. *Nonlinear Dynamics*, 38 (1-2), 155–170.

[13] Chen, Y.-Q. (2006). Ubiquitous Fractional Order Controls? In *Proc. of the Second IFAC Symposium on Fractional Derivatives and its Applications (IFAC FDA'06)*, Porto, Portugal, 19-21 July 2006, vol. 2, part 1, 168–173.

[14] di Gaeta, A., Montanaro, U., Fiengo, G., Palladino, A., and V. Giglio (2012). A model-based gain scheduling approach for controlling the common-rail system for GDI engines. *International Journal of Control*, 85 (4), 419–436.

[15] Fiengo, G., di Gaeta, A., Palladino, A., and V. Giglio (2013). *Common Rail System for GDI Engines: Modelling, Identification, and Control*. London: Springer Briefs in Electrical and Computer Engin., Springer.

[16] Hamamci, S. E. (2007). An algorithm for stabilization of fractional-order time delay systems using fractional-order PID controllers. *IEEE Trans. Automatic Control*, 52 (10), 1964–1969.

[17] Horowitz, I. (1963). *Synthesis of Feedback Systems*. New York, London: Academic Press.

[18] Hwang, C., and Y. C. Cheng (2006). A numerical algorithm for stability testing of fractional delay systems. *Automatica*, 42 (5), 825–831.

[19] Kalman, R.-E. (1964). When is a linear control system optimal? *Transactions of the ASME, Journal of Basic Engineering*, 86, series D, 84–90.

[20] Khalil, H. K. (2002). *Nonlinear Systems*. 3rd edition. Upper Saddle River, NJ: Prentice-Hall.

[21] Li, H. S., Luo, Y., and Y. Q. Chen (2010). A fractional order proportional and derivative (FOPD) motion controller: tuning rule and experiments. *IEEE Trans. Control Systems Technology*, 18 (2), 516–520.

[22] Lino, P., and B. Maione (2007). Integrated design of a mechatronic system - The pressure control in common rails. In *Proc. 4th Int. Conf. on Informatics in Control, Autom. and Robot. (ICINCO 2007)*, Angers, France, 9-12 May 2007, 11–18.

[23] Lino, P., Maione, B., and C. Amorese (2008). Modelling and predictive control of a new injection system for compressed natural gas engines. *Control Engineering Practice*, 16 (10), 1216–1230.

[24] Lino, P., and G. Maione (2012). Fractional Order PI Tuning for Integrating Plants with Time Delay. In R. Vilanova and A. Visioli (Eds.), *2nd IFAC Conf. on Advances in PID Control (PID'12)*, Brescia, Italy, 28-30 Mar. 2012, IFAC Proceedings on line: Vol. 2, Part I, 649–654.

[25] Lino, P., and G. Maione (2013). Laboratory experiments on fractional order PI control of a servo system with delay. In E. Witrant, J. Sabatier, J.A. Tenreiro Machado, O. Sename, and L. Dugard (Eds.), *First IFAC Joint Conference on System Structure and Control, Time-Delay Systems and Fractional Differentiation (2013 IFAC Joint Conference SSSC-TDS-FDA) – Track FDA: Sixth Workshop on Fractional Differentiation and Its Applications*, Grenoble, France, 4-6 Feb 2013, IFAC Proceedings on line: Vol. 6, Part I, 899–904.

[26] Lino, P., and G. Maione (2013). Loop-Shaping and Easy Tuning of Fractional-Order Proportional Integral Controllers for Position Servo Systems, *Asian Journ. of Control*, 5 (3), 1–10.

[27] Lino, P., and G. Maione (2013). Fractional order control of the injection system in a CNG engine. In *2013 Europ. Contr. Conf.*, Zürich, Switzerland, 17-19 July 2013, 3997–4002.

[28] Lino, P., and G. Maione (2013). Design and simulation of fractional-order controllers of injection in CNG engines. In T. Kawabe (Ed.), *7th IFAC Symp. Adv. Automot. Contr.*, Tokyo, Japan, 4-7 Sep. 2013, IFAC Proceedings on line: Vol. 7, Part 1, 582–587.

[29] Luo, Y., and Y. Q. Chen (2012). Stabilizing and robust fractional order PI controller synthesis for first order plus time delay systems. *Automatica*, 48 (9), 2159–2167.

[30] Ma, C. B., and Y. Hori (2007). Fractional order control: Theory and applications in motion control. *IEEE Industrial Electronics Magazine*, Winter 2007 (4), 6–10.

[31] Maciejowski, J. M. (1989). *Multivariable Feedback Design*. Wokingham, UK: Addison-Wesley.

[32] Maione, G. (2006). Concerning continued fractions representations of noninteger order digital differentiators. *IEEE Signal Processing Letters*, 13 (12), 725–728, 2006.

[33] Maione, G. (2008). Continued fractions approximation of the impulse response of fractional order dynamic systems. *IET Contr. Theory and Appl.*, 2 (7), 564–572, 2008.

[34] Maione, G. (2011). High-speed digital realizations of fractional operators in the delta domain. *IEEE Trans. Autom. Control*, 56 (3), 697–702.

[35] Maione, G. (2011). Conditions for a class of rational approximants of fractional differentiators/integrators to enjoy the interlacing property. In S. Bittanti, A. Cenedese, and S. Zampieri (Eds.), *Proc. 18th IFAC World Congr.*, Università Cattolica del Sacro Cuore, Milan, Italy, 28 Aug. - 2 Sept. 2011, IFAC Proceedings on line: Vol. 18, Part 1, 13984–13989.

[36] Maione, G. (2013). On the Laguerre rational approximation to fractional discrete derivative and integral operators. *IEEE Trans. Autom. Control*, 58 (6), 1579–1585.

[37] Maione, G. (2013). Closed-form rational approximations of fractional, analog and digital differentiators/integrators. *IEEE J. on Emerging and Selected Topics in Circuits and Systems*, 3 (3), 322–329.

[38] Maione, G. (2013). Correction to "Closed-form rational approximations of fractional, analog and digital differentiators/integrators". *IEEE J. on Emerging and Selected Topics in Circuits and Systems*, 3 (4), 654.

[39] Maione, G., and P. Lino (2007). New tuning rules for fractional PI^α controllers. *Nonlin. Dyn.*, 49 (1-2), 251–257.

[40] Manabe, S. (1961). The non-integer integral and its application to control systems. *Japanese Inst. Electrical Engineers Journal*, 6 (3-4), 83–87.

[41] Matignon, D. (1996). Stability result on fractional differential equations with applications to control processing. In *Proc. of IMACS-IEEE SMC Conf.*, Lille, France, 9-12 July 1996, vol. 2, 963–968.

[42] Monje, C. A., Chen, Y. Q., Vinagre, B. M., Xue, D., and V. Feliu-Batlle (2010). *Fractional-order Systems and Controls: Fundamentals and Applications*. London, U.K.: Springer-Verlag.

[43] Monje, C. A., Vinagre, B. M., Feliu, V., and Y. Q. Chen (2008). Tuning and auto-tuning of fractional order controllers for industry applications. *Control Engineering Practice*, 16, 798–812.

[44] Moze, M., Sabatier, J., and A. Oustaloup (2010). Air-fuel ratio control of an internal combustion engine using CRONE control extended to LPV systems. In D. Baleanu, Z. B. Güvenç, and J. A. Tenreiro Machado (Eds.) *New Trends in Nanotechnology and Fractional Calculus Applications* (71–86). Dordrecht, The Netherlands: Springer.

[45] Naus, G. J. L. (2010). Model-based control for automotive applications. PhD Thesis, Technische Universiteit Eindhoven, http://dx.doi.org/10.6100/IR690571, 2010.

[46] Neimark, Yu.I. (1949). *Ustoichivost' linearizovannykh sistem upravleniya (Stability of Linearized Control Systems)*. LKVVIA, Leningrad.

[47] Oldham, K. B., and J. Spanier (1974). *The fractional calculus: Integrations and Differentiations of Arbitrary Order*. New York, NY: Academic Press.

[48] Oustaloup, A. (1991). *La Commande CRONE: Command Robuste d'Ordre Non Entièr*. Paris: Editions Hermès.

[49] Oustaloup, A. (1999). *La Commande CRONE: du Scalaire au Multivariable*. Paris: Editions Hermès.

[50] Oustaloup, A., Levron, F., Nanot, F., and B. Mathieu (2000). Frequency band complex non integer differentiator: Characterization and synthesis. *IEEE Trans. Circuits Syst. I, Fundam. Theory Appl.*, 47 (1), 25–40.

[51] Oustaloup, A., Moreau, X., and M. Nouillant (1996). The CRONE suspension. *Control Engineering Practice*, 4 (8), 1101–1108.

[52] Oustaloup, A., Sabatier, J., and P. Lanusse (1999). From fractal robustness to CRONE control. *Fractional Calculus and Applied Analysis*, 2 (1), 1–30.

[53] Oustaloup, A., Sabatier, J., Lanusse, P., Malti, R., Melchior, P., Moreau, X., and M. Moze (2008). An overview of the crone approach in system analysis, modeling and identification, observation and control. In M. J. Chung and P. Misra (Eds.), *Proc. of the 17th IFAC World Congress*, Seoul, Korea, 2008, Vol. 17, Part 1, 14254–14265.

[54] Petráš, I. (2009). Fractional-order feedback control of a dc motor. *Journal of Electrical Engineering*, 60 (3), 117–128.

[55] Podlubny, I. (1999). *Fractional Differential Equations*. San Diego, CA: Academic Press.

[56] Podlubny, I. (1999). Fractional-order systems and $PI^\lambda D^\mu$ controllers. *IEEE Trans. Aut. Contr.*, 44 (1), 208–214.

[57] Podlubny, I., Dorcak, L., and I. Kostial (1997). On fractional derivatives, fractional-order dynamic systems and $PI^\lambda D^\mu$-controllers. In *Proc. 36th IEEE Conf. on Decision and Control*, San Diego, CA, USA, 10-12 Dec. 1997, vol. 5, 4985–4990.

[58] Raynaud, H.-F., and A. Zergaïnoh (2000). State-space representation for fractional order controllers. *Automatica*, 36, 1017–1021.

[59] Rugh, W. J., and J. S. Shamma (2000). Research on gain scheduling. *Automatica*, 36 (10), 1401–1425.

[60] Sidi, M. J. (2001). *Design of Robust Control Systems: From Classical to Modern Practical Approaches*. Malbar (FLA), USA: Krieger Publishing Company.

[61] Skogestad, S., and I. Postlethwaite (2005). *Multivariable Feedback Control: Analysis and Design*. 2nd edition. Chichester, England: Wiley & Sons, Ltd..

[62] Sun, Z., and S. S. Ge (2005). *Switched Linear Systems: Control and Design*. London: Springer-Verlag.

[63] Tenreiro Machado, J. A. (1997). Analysis and design of fractional-order digital control systems. *Journal Systems Analysis Modelling Simulation*, 27 (2-3), 107–122.

[64] Tenreiro Machado, J. A. (2001). Discrete-time fractional-order controllers. *Journal of Fractional Calculus & Applied Analysis*, 4 (1), 47-66.

[65] Tustin, A. (1958). The design of systems for automatic control of the position of massive objects. *Proc. Institution of Electrical Engineers*, 105, Part C, Suppl. No. 1, 1–57.

[66] Ulsoy, A. G., Peng, H., and M. Çakmakci (2012). *Automotive Control Systems*. 1st edition. Cambridge: Cambridge University Press.

[67] Vinagre, B. M., Podlubny, I., Hernandez, A., and V. Feliu (2000). Some approximations of fractional order operators used in control theory and applications. *J. Frac. Calc. Appl. Anal.*, 13 (3), 231–248.

[68] Zucrow, M., and J. Hoffman (1976). *Gas Dynamics*. New York: John Wiley & Sons.

Chapter 4

LINEAR INTEGER ORDER SYSTEM CONTROL BY FRACTIONAL PI-STATE FEEDBACK

Rachid Mansouri[1], Maamar Bettayeb[2,3], Chahira Boussalem[1] and Ubaid M. Al-Saggaf [3]

[1]L2CSP Laboratory, University Mouloud Mammeri of Tizi-Ouzou, Algeria
[2]Electrical & Computer Engineering Department, University of Sharjah, UAE
[3] Center of Excellence in Intelligent Engineering Systems (CEIES),
King Abdulaziz University, Jeddah, KSA

Abstract

This book chapter deals with a linear non-fractional order system control by a PI-state feedback fractional-controller. The fractional aspect of the control law is introduced by a dynamic state feedback as $u(t) = K_p x(t) + K_I \mathcal{J}_\alpha(x(t))$.

Two methods, based on pole placement principle, are then proposed to design the feedback vector gains K_p and K_I.

The first one uses the augmented system method. In this case, the closed-loop characteristic polynomial is of order $(qn + \mu)$ where n is the order of the integer system and q is the fractional ratio of the non integer order α ($\alpha = \mu/\text{q}$).

The second proposed method allows to decompose the closed-loop characteristic polynomial into a fractional polynomial of order α, $(0 < \alpha < 2)$ and an integer order polynomial of order $n - 1$. In this case, a suitable choice of the poles provides to obtain, in closed-loop, the Bode's ideal transfer function.

These two methods are then applied to stabilize an inverted pendulum-car system and the effectiveness and robustness of the proposed controllers are examined by experiments on a real system.

Keywords: Fractional calculus, Fractional systems, PI-state feedback, Pole placement, Inverted pendulum-cart system stabilization

Introduction

The idea of fractional calculus has been known since the development of the regular integer order calculus, with the first reference being associated with Leibnitz and L'Hopital in 1695 where half order derivatives were mentioned. A detailed chronology of this notion is given in [23, 36]. The books [31, 41, 44] and more recently [18, 22, 33] constitute currently the main references of this theory. Non integer differentiation is currently considered among emerging thematics applied to many science and technology disciplines. All works undertaken on systems modeling by linear differential equations using the usual integer differentiation must be re-examined. From the automation point of view, the fundamental notions analysis and simulation of fractional systems and the fractional controllers design constitute highly promising fields of research.

In control theory, the non integer differentiation/integration has also proven its efficiency. Indeed, Oustaloup, [40] with the CRONE-controller (Commande Robuste d'Ordre Non Entier) and Podlubny, [42] with the $PI^\lambda D^\mu$-controller, involving the fractional-order integrator and differentiator, have shown the advantage of the fractional-controllers over the classical ones. Fractional-order controllers have received a considerable attention in the last three decades (see [7, 12, 24, 33] for example). In fact, in principle, they provide more flexibility in the controller design, with respect to the integer order controllers, because they have more parameters to select.

However, almost all fractional controller design methods use the transfer function representation because of the simplicity of the mathematical manipulations. There is still a lack of strategies for introducing fractional dynamics in state space methods. The state space representation of fractional order systems is introduced in [13, 19, 43, 49]. It has been exploited in order to analyze performance of fractional order systems. Indeed, the stability of the fractional order system has been investigated [28, 30]. Further, the controllability and the observability properties have been defined and some algebraic criteria of these two properties have been derived [8, 29, 51]. Recently, some new results on the minimal state space realization for fractional order systems [47, 48] and approximation of fractional order state space SISO and MIMO models in both commensurate and non-commensurate cases are derived [25-27].

Control systems can include both the fractional order system to be controlled and the fractional order controller. However, in practice, it is more common to consider only the controller to be of fractional order. This is due to the fact that the plant model may have been already obtained as an integer order model in the classical sense. In state space representation, the introduction of the concept of fractional differentiation is not obvious because it does not appear explicitly in the model. As in the transfer function representation, the fractional aspect will be introduced by the control law. However, in state space, the control law is usually used as a static state feedback that does not allow the introduction of the fractional aspect. In [34, 46], the authors present a fractional order state space control strategy for integer order systems. It is based on rearranging integer order system equations into a set of fractional (rational) order equations using system augmentation. By doing so, fractional order dynamics can be introduced in the controlled system by using traditional state-space methods for controller design. System augmentation is also used in [14, 15] to study the stabilization

problem of commensurate fractional order systems by a pseudo-state feedback. However, the non-integer order must be rational.

Pole placement via state feedback has been known for several decades [35]. Recently, state-derivative feedback has been proposed [1-3, 18, 36] due to considerably low gain and fast response. In this chapter, new approach is presented to design the fractional PI-state feedback gain, two solutions are then proposed. In the first one, the integer PI-state feedback solution proposed in [50] is generalized to the fractional PI-state feedback. We show that we find the same solution but also the same problems as the solution proposed in [46] by using system augmentation principle. Our second approach [10] provides a very simple method to achieve the gain vectors of the fractional PI-state feedback. The desired closed-loop characteristic polynomial is composed of two polynomials: The first one is integer and permits to impose $n - 1$ integer poles and the second one is a non-integer polynomial having the form $(s^{\alpha+1} + p_f)$, $(0 < \alpha < 1)$ imposed to the closed-loop when CRONE principle [38-40] (phase flatness of the open-loop) is used. These two methods are then applied to stabilize an inverted pendulum-car system.

This chapter contains six sections including the introduction. In Section 2, some basic definitions are recalled. These definitions include the fractional integral operation, the Bode's ideal transfer function and the stability condition of fractional order systems. Pole placement by integer PI-state feedback algorithm is also presented in this section. The main results are presented in Sections 3 and 4. In Section 3, the pole placement method by integer PI-state feedback is generalized to the fractional one. Limits of this method are also investigated and presented through a first order system. Section 4 contains the second method which is more general and simpler to implement. After presenting the inverted pendulum-car system in Section 5, those two methods are used in Section 6 to stabilize it. Experimental results are also presented in this section.

1. Basic Definitions and Preliminaries

1.1. Fractional Integral Operation

Let $f(t)$ be a real function, of real variable t, continuous and differentiable on $[0, \infty]$, the k-th repeated integration, denoted $I^k(f(t))$, is given by the Cauchy formula

$$I^k\big(f(t)\big) = \int_{t_0}^t \frac{(t-\tau)^{k-1}}{(k-1)!} f(\tau) d\tau \tag{1}$$

k is an integer number. The generalization of the Cauchy formula (1) to a non-integer number $\alpha \in \mathbb{R}_+^*$ is given by [20]

$$I^\alpha\big(f(t)\big) = \int_{t_0}^t \frac{(t-\tau)^{\alpha-1}}{\Gamma(\alpha)} f(\tau) d\tau \tag{2}$$

$\Gamma(\alpha)$ is the Euler Gamma function

$$\Gamma(\alpha) = \int_0^\infty \nu^{\alpha-1} e^{-\nu} d\nu \ \forall \ \alpha \in \mathbb{R}_+^* \tag{3}$$

Note that, in Equation (2), the term $\frac{(t-\tau)^{\alpha-1}}{\Gamma(\alpha)}$ is equal to 1 when $\alpha = 1$. We thus find the usual definition of the integration. When α is a real number, Equation (2) can be written as

$$I^\alpha\big(f(t)\big) = \mathcal{P}_\alpha(t) \otimes f(t) \tag{4}$$

$\otimes$ being the convolution product, and $\mathcal{P}_\alpha(t)$ is given by

$$\mathcal{P}_\alpha(t) = \frac{(t-\tau)^{\alpha-1}}{\Gamma(\alpha)} \tag{5}$$

Oustaloup [38] calls the weight function $\mathcal{P}_\alpha(t)$ the forgetting factor ("le facteur d'oubli").

1.2. Bode's Ideal Transfer Function

In his study on the design of feedback amplifiers, Bode [10] suggested an ideal shape of the open-loop transfer function of the form

$$L(s) = \frac{1}{\tau_c s^\alpha} \ \alpha \in \mathbb{R} \tag{6}$$

where $1/\tau_c^{-\alpha} = \omega_c$ is the gain crossover frequency, that is, $|L(\omega_c)| = 1$. The parameter α is the slope of the magnitude curve, on log-log scale, and may assume integer as well as non-integer values. In fact, the transfer function $L(s)$ is a fractional-order differentiator when $\alpha < 0$ and a fractional-order integrator for $\alpha > 0$. In the Bode diagram, the amplitude curve of $L(s)$ is a straight line of constant slope -20α dB/dec, and the phase curve is a horizontal line at $-\alpha\pi/2$ rad.

Let us now consider the unity feedback system represented in Figure (1) with Bode's ideal transfer function $L(s)$ inserted in the forward path. This choice of $L(s)$ gives a closed-loop system with the desirable property of being insensitive to gain changes, also called the "iso-damping" property [38]. If the gain changes, the crossover frequency ω_c will vary but the phase margin of the system remains equal to $\pi(1-\alpha/2)$rad, independently of the value of the gain.
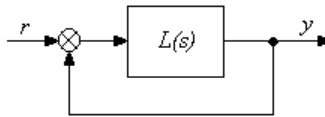
Figure 1. Fractional-order control system with Bode's ideal transfer function.

The closed-loop system of Figure (1) is given by

$$f(s) = \frac{L(s)}{1 + L(s)} = \frac{1}{1 + \tau_c s^\alpha} \ \alpha \in \mathbb{R}^+ \tag{7}$$

It exhibits important properties such as infinite gain margin and constant phase margin (dependent only on α). Thus, this closed-loop system is robust to process gain variations and the

step response exhibits iso-damping property. The order α and the time constant τ_c determine the overshoot (dependent on α)) and the settling time (dependent on τ_c), respectively [38, 40].

1.3. Stability of the Fractional Order Systems

The definition of stability adopted here is the Bounded Input Bounded Output (BIBO) stability, also called external stability. For commensurate non-integer order systems, the stability condition is, as for the integer system, that the roots of the characteristic equation lie in the left-hand s-plane.

In practice, checking the stability condition by calculating the roots of the characteristic equation is very difficult due to the complexity of their calculation. Instead of using the roots of the characteristic polynomial in s, Matignon has established a stability condition by using the integer order polynomial, of complex variable p, obtained by the change of variable $p = s^\alpha$. This condition can therefore be applied only to commensurate non-integer order systems.

Theorem 1. *[28-30] A non-integer system of commensurate order α, $(0 < \alpha < 2)$ is BIBO stable, if and only if, the roots of the integer polynomial $\Delta(p)$, obtained from the characteristic equation of the non-integer system $\Delta(s)$, by the change of variable $p = s^\alpha$, satisfy the condition*

$$|arg(p_i)| > \alpha\frac{\pi}{2} \; i = 1, ..., n \tag{8}$$

n is the order of $\Delta(p)$, p_i, $(i = 1, ..., n)$ are the roots, and $arg(p_i)$ is the argument of the root p_i.

Remark: The commensurability condition of the fractional order is a necessary condition. Indeed, when this condition is not verified, the study of fractional order system stability based on the roots of its characteristic polynomial only is not feasible.

1.4. Pole Placement by Integer PI-State Feedback

State feedback is a well established tool for the stabilization and control of dynamic systems, and it is widely used in the field of control engineering.

The idea of using state-PID feedback is relatively new, and so far only few applications can be found in the literature. In [1-3, 18], the motivation for using state derivative feedback instead of conventional state feedback is given by the easy implementation in mechanical applications where accelerometers and velocity sensors are used for measuring the system motion.

Thus, the accelerations and velocities are the sensed variables, as opposed to the displacement. Typical applications are in the vibration control of mechanical systems [2, 3, 18]. The use of acceleration feedback in vibration suppression problems has also been discussed at length in [37].

The application of state derivative feedback to vibration problems has been discussed from the perspective of robust control in [21]. In what follows, we recall the pole placement method in the integer PI-state feedback case, see [50] for more details.

Let's consider a controllable LTI integer order system described by

$$\begin{cases} \dot{x}(t) = Ax(t) + Bu(t) \; x(0) = x_0 \\ \qquad\qquad y(t) = Cx(t) \end{cases} \tag{9}$$

where $x \in \mathbb{R}^n$ is the state vector, and $u \in \mathbb{R}$ is the control input, $y \in \mathbb{R}$ is the output. $A \in \mathbb{R}^{n \times n}$, $B \in \mathbb{R}^{n \times 1}$, $C \in \mathbb{R}^{1 \times n}$ are the system matrix, the control and the output gain vectors respectively.

The control law by PI-state feedback is

$$u(t) = K_p x(t) + K_I \int_0^t x(\tau) d\tau \tag{10}$$

where $K_p = [K_{p1} \quad K_{p2} \cdots \quad K_{pn}]$ and $K_I = [K_{I1} \quad K_{I2} \cdots \quad K_{In}]$ are the designed gain vectors to achieve a desired closed-loop characteristic polynomial. The block diagram of Figure (2) represents a LTI system with PI-state feedback.
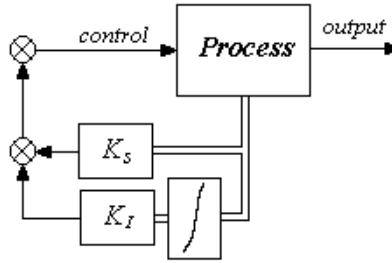
Figure 2. Block diagram representation of a linear system with PI-state feedback.

The corresponding characteristic polynomial is given by

$$\Delta_\Sigma(s) = \det(sI - A) = s^n + a_1 s^{n-1} + a_2 s^{n-2} + \cdots + a_{n-1}s + a_n \tag{11}$$

Since the system is controllable, there exists a linear transformation T such that $x = Tz$, System (9) becomes

$$\begin{cases} \dot{z}(t) = A_c z(t) + B_c u(t) \; z(0) = z_0 \\ \qquad\qquad y(t) = C_c z(t) \end{cases} \tag{12}$$

and the control law by PI-state feedback (10) becomes

$$u(t) = K_{pc} z(t) + K_{Ic} \int_0^t z(\tau) d\tau \tag{13}$$

where

$$A_c = \begin{bmatrix} 0 & 1 & 0 & \cdots & 0 \\ 0 & 0 & 1 & \cdots & 0 \\ \vdots & & & \ddots & \vdots \\ 0 & 0 & 0 & \cdots & 1 \\ -a_n & -a_{n-1} & -a_{n-2} & \cdots & -a_1 \end{bmatrix} \quad B_c = \begin{bmatrix} 0 \\ 0 \\ \vdots \\ 0 \\ 1 \end{bmatrix}$$

The closed-loop model is then given by

$$\begin{cases} \dot{z}(t) = \left(A_c + B_c K_{pc} \right) z(t) + B_c K_{Ic} \int_0^t z(\tau) d\tau \quad z(0) = z_0 \\ \qquad\qquad\qquad y(t) = C_c z(t) \end{cases} \tag{14}$$

The closed-loop characteristic equation is

$$\Delta_{\mathrm{cl}}(s) = \det(A_{cl}(s)) = det\left[sI - \left(A_c + B_c K_{pc} \right) - B_c K_{Ic} \frac{1}{s} \right] \tag{15}$$

$A_{cl}(s)$ is given by

$$A_{cl}(s) = \begin{bmatrix} s & -1 & 0 & \cdots & 0 & 0 \\ 0 & s & -1 & \cdots & 0 & 0 \\ \vdots & & & \vdots & \ddots & \vdots \\ 0 & 0 & 0 & \cdots & s & -1 \\ a_{cln}(s) & a_{cln-1}(s) & a_{cln-2}(s) & \cdots & a_{cl2}(s) & a_{cl1}(s) \end{bmatrix}$$

where

$$\begin{cases} a_{cln}(s) = a_n - K_{pc1} - \dfrac{K_{Ic1}}{s} \\ a_{cln-1}(s) = a_{n-1} - K_{pc2} - \dfrac{K_{Ic2}}{s} \\ \qquad\qquad \vdots \\ a_{cl1}(s) = s + a_1 - K_{pcn} - \dfrac{K_{Icn}}{s} \end{cases}$$

$A_{cl}(s)$ having the controllable canonical form, the characteristic polynomial of the closed-loop $\Delta_{cl}(s)$ is given by

$$\Delta_{\mathrm{cl}}(s) = s^n + \left(a_1 - K_{pcn} - \frac{K_{Icn}}{s} \right) s^{n-1} + \left(a_2 - K_{pcn-1} - \frac{K_{Icn-1}}{s} \right) s^{n-2}$$
$$+ \left(a_3 - K_{pcn-2} - \frac{K_{Icn-2}}{s} \right) s^{n-3} + \cdots + \left(a_n - K_{pc1} - \frac{K_{Ic1}}{s} \right) \tag{16}$$

which can be written as

$$\Delta_{\mathrm{cl}}(s) = s^n + \left(\frac{(a_1 - K_{pcn})s - K_{Icn}}{s} \right) s^{n-1} + \left(\frac{(a_2 - K_{pcn-1})s - K_{Icn-1}}{s} \right) s^{n-2}$$
$$+ \left(\frac{(a_3 - K_{pcn-2})s - K_{Icn-2}}{s} \right) s^{n-3} + \cdots + \left(\frac{(a_n - K_{pc1})s - K_{Ic1}}{s} \right) \tag{17}$$

so

$$\Delta_{cl}(s) = s^{n+1} + \left(a_1 - K_{pcn}\right)s^n + \left(a_2 - K_{pcn-1} - K_{Icn}\right)s^{n-1}$$
$$+\left(a_3 - K_{pcn-2} - K_{Icn-1}\right)s^{n-2} + \cdots + \left(a_n - K_{pc1} - K_{Ic2}\right)s^n - K_{Ic1} \tag{18}$$

$\Delta_{cl}(s)$ is of order $n + 1$ when the system is of order n. Therefore, it is necessary to impose $n + 1$ poles to the closed-loop system. The desired polynomial is then

$$\Delta_{d}(s) = \prod_{i=1}^{n+1}(s - s_i) = s^{n+1} + \beta_1 s^n + \beta_2 s^{n-1} + \cdots + \beta_n s + \beta_{n+1} \tag{19}$$

term by term identifying between the polynomials (18) and (19) gives

$$\begin{cases} \beta_1 = a_1 - K_{pcn} \\ \beta_2 = a_2 - K_{pcn-1} - K_{Icn} \\ \beta_3 = a_2 - K_{pcn-2} - K_{Icn-1} \\ \quad\vdots \\ \beta_n = a_n - K_{pc1} - K_{Ic2} \\ \beta_{n+1} = -K_{Ic1} \end{cases} \tag{20}$$

Equation (20) shows that when the integral function is not used ($K_{Ic} = 0$), we find the formulas of the usual static state feedback.

To calculate the coefficients of the feedback gain K_{pc} and K_{Ic}, we can ensure that the coefficients of K_{pc} compensate the coefficients a_i ($i = 2, \cdots, n$) of the open-loop characteristic polynomial, except the coefficient K_{pcn} which is equal to $(a_1 - \beta_1)$. Coefficients of K_{Ic} are used to impose the coefficients β_i ($i = 2, \cdots, n$) of the closed-loop characteristic polynomial.

Feedback gains K_{pc} and K_{Ic} are then given by

$$\begin{cases} K_{pc} = [a_n \quad a_{n-1} \quad \cdots \quad a_2 \quad (a_1 - \beta_1)] \\ K_{Ic} = [-\beta_{n+1} \quad -\beta_n \quad \cdots \quad -\beta_3 \quad -\beta_2] \end{cases} \tag{21}$$

The PI-state feedback gains K_p and K_I of the original System (9) are then given by

$$K_p = K_{pc}T \text{ and } K_I = K_{Ic}T \tag{22}$$

2. Pole Placement Based Design of the Fractional Pi-State Feedback

The generalization of the PI-state feedback involves replacing the integer order integration by a fractional order operator. Figure (3) shows the block diagram of an integer system controlled by the fractional PI-state feedback. The generalization is given by the following result.
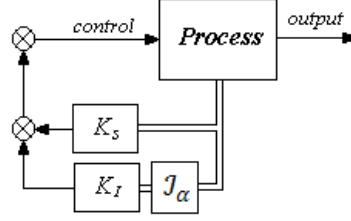
Figure 3. Block diagram of a fractional PI-state feedback.

Theorem 2. *Consider a controllable LTI integer order SISO system described by Equation (9) and let the control law*

$$u(t) = K_p x(t) + K_I \mathcal{I}_\alpha(x(t)) \tag{23}$$

where, $K_p \epsilon \mathbb{R}^{1 \times n}$, and $K_p \epsilon \mathbb{R}^{1 \times n}$, are gain vectors designed to impose the characteristic polynomial of the closed-loop. $\mathcal{I}_\alpha(x(t))$ is the non-integer integration operator of order α defined by Equation (2). Vectors K_p and K_I that can arbitrarily place the poles of the closed-loop characteristic polynomial written in the form

$$\Delta_d(s) = s^{n+\alpha} + \beta_1 s^{n-1+\alpha} + \beta_2 s^{n-1} + \beta_3 s^{n-2+\alpha} + \cdots + \beta_{2n-2} s + \beta_{2n-1} s^\alpha + \beta_{2n} \tag{24}$$

are given by

$$\begin{cases} K_p = [a_n \quad a_{n-1} \quad \cdots \quad a_2 \quad (a_1 - \beta_1)] \, T \\ \\ K_I = [-\beta_{n+1} \quad -\beta_n \quad \cdots \quad -\beta_3 \quad -\beta_2] \, T \end{cases} \tag{25}$$

T being the linear transformation that gives the controllable canonical form.

Proof. The characteristic polynomial of the integer model of Equation (9) is given by (11). Since the model (9) is controllable, it can be rewritten as (12). The control law (23) becomes

$$u(t) = K_{pc} z(t) + K_{Ic} \mathcal{I}_\alpha(z(t)) \tag{26}$$

where

$$K_{pc} = K_p T^{-1} \text{ and } K_{Ic} = K_I T^{-1} \tag{27}$$

The state model in closed-loop is then

$$\begin{cases} \dot{z}(t) = A_c z(t) + B_c \big[K_{pc} z(t) + K_{Ic} \mathcal{I}_\alpha(z(t)) \big] \, z(0) = z_0 \\ \qquad\qquad y(t) = C_c z(t) \end{cases} \tag{28}$$

Laplace transform of Equation (28) yields

$$sz(s) - z_0 = A_c z(s) + B_c K_{pc} z(s) + B_c K_{Ic} \frac{1}{s^\alpha} z(s) \tag{29}$$

which can be written as

$$A_{cl}(s) z(s) = z_0 \tag{30}$$

Matrix $A_{cl}(s)$ has the general form

$$A_{cl}(s) = sI - A_c - B_c K_{pc} - B_c K_{Ic} \frac{1}{s^\alpha} \tag{31}$$

where

$$A_{cl}(s) = \begin{bmatrix} s & -1 & 0 & \cdots & 0 & 0 \\ 0 & s & -1 & \cdots & 0 & 0 \\ \vdots & & & \vdots & \ddots & & \vdots \\ 0 & 0 & 0 & \cdots & s & -1 \\ \tilde{a}_n(s) & \tilde{a}_{n-1}(s) & \tilde{a}_{n-2}(s) & \cdots & \tilde{a}_2(s) & \tilde{a}_1(s) \end{bmatrix}$$

and

$$\begin{cases} \tilde{a}_n(s) = a_n - K_{pc1} - \dfrac{K_{Ic1}}{s^\alpha} \\ \tilde{a}_{n-1}(s) = a_{n-1} - K_{pc2} - \dfrac{K_{Ic2}}{s^\alpha} \\ \qquad\qquad \vdots \\ \tilde{a}_1(s) = s + a_1 - K_{pcn} - \dfrac{K_{Icn}}{s^\alpha} \end{cases}$$

The determinant of is $A_{cl}(s)$

$$\det(A_{cl}(s)) = s^n + \left(a_1 - K_{pcn} - \frac{K_{Icn}}{s^\alpha} \right) s^{n-1} + \left(a_2 - K_{pcn-1} - \frac{K_{Icn-1}}{s^\alpha} \right) s^{n-2}$$
$$+ \cdots + \left(a_{n-1} - K_{pc2} - \frac{K_{Ic2}}{s^\alpha} \right) s + \left(a_n - K_{pc1} - \frac{K_{Ic1}}{s^\alpha} \right) \tag{32}$$

which can be written as

$$\det(A_{cl}(s)) = s^n + \left(\frac{(a_1 - K_{pcn})s^\alpha - K_{Icn}}{s^\alpha} \right) s^{n-1} + \left(\frac{(a_2 - K_{pcn-1})s^\alpha - K_{Icn-1}}{s^\alpha} \right) s^{n-2}$$
$$+ \cdots + \left(\frac{(a_{n-1} - K_{pc2})s^\alpha - K_{Ic2}}{s^\alpha} \right) s + \left(\frac{(a_n - K_{pc1})s^\alpha - K_{Ic1}}{s^\alpha} \right)$$

The characteristic polynomial of the closed-loop system is then

$$\Delta_{cl}(s) = s^{n+\alpha} + \left(a_1 - K_{pcn} \right) s^{n-1+\alpha} - K_{Icn} s^{n-1} + \left(a_2 - K_{pcn-1} \right) s^{n-2+\alpha}$$
$$- K_{Icn-1} s^{n-2} + \cdots + \left(a_{n-1} - K_{pc2} \right) s^{1+\alpha} - K_{Ic2} s + \left(a_n - K_{pc1} \right) s^\alpha - K_{Ic1} \tag{33}$$

Let $\Delta_d(s)$ the polynomial that we want to impose to the closed-loop

$$\Delta_{\text{d}}(s) = s^{n+\alpha} + \beta_1 s^{n-1+\alpha} + \beta_2 s^{n-1} + \beta_3 s^{n-2+\alpha} + \cdots + \beta_{2n-2}s + \beta_{2n-1}s^{\alpha} + \beta_{2n} \quad (34)$$

Identification term by term between $\Delta_{cl}(s)$ of Equation (33) and $\Delta_{\text{d}}(s)$ of Equation (34) gives

$$\begin{cases} \beta_1 = a_1 - K_{pcn} \\ \beta_3 = a_2 - K_{pcn-1} \\ \quad \vdots \\ \beta_{2n-3} = a_{n-1} - K_{pc2} \\ \beta_{2n-1} = a_n - K_{pc1} \end{cases} \text{ and } \begin{cases} \beta_2 = -K_{Icn} \\ \beta_4 = -K_{Icn-1} \\ \quad \vdots \\ \beta_{2n-2} = -K_{Ic2} \\ \beta_{2n} = -K_{Ic1} \end{cases} \quad (35)$$

Therefore, K_{pc} and K_{Ic} are calculated by

$$\begin{cases} K_{pc} = [(a_n - \beta_{2n-1}) \quad (a_{n-1} - \beta_{2n-3}) \quad \cdots \quad (a_2 - \beta_3) \, (a_1 - \beta_1)] \\ \\ \qquad K_{Ic} = [-\beta_{2n} \quad -\beta_{2n-2} \quad \cdots \quad -\beta_4 \quad -\beta_2] \end{cases} \quad (36)$$

Vector gains K_p and K_I of the original control law (23) are finally given by

$$K_p = K_{pc}T \text{ and } K_I = K_{Ic}T \quad (37)$$

This completes the proof.

The fractional PI-state feedback design is based on the coefficients β_i ($i = 1, \cdots, 2n$) of the desired polynomial (34). The problem is how one can find the values of these coefficients β_i from the poles imposed to the desired polynomial, as in the integer case. The polynomial (34) being fractional, the number and the values of its roots depend on the value of α.

Let $\alpha = q/k$ (k and q being two integer numbers). The fractional polynomial (34) can then be put in the form

$$\Delta_{\text{d}}(s) = s^{n+\frac{k}{q}} + \beta_1 s^{n-1+\frac{k}{q}} + \beta_2 s^{n-1} + \beta_3 s^{n-2+\frac{k}{q}} + \cdots + \beta_{2n-2}s + \beta_{2n-1}s^{\frac{k}{q}} + \beta_{2n} \quad (38)$$

or also by making the change of variable $p = s^{\frac{1}{q}}$

$$\Delta_{\text{d}}(p) = p^{nq+k} + \beta_1 p^{(n-1)q+k} + \beta_2 p^{(n-1)q} + \cdots + \beta_{2n-2}p^q + \beta_{2n-1}p^k + \beta_{2n} \quad (39)$$

The resulting polynomial is integer and of order $(nq + k)$ but includes only $(2n)$ parameters. So, there are powers of p whose coefficients are zero. These constitute constraints to be checked when one chooses the poles of the integer polynomial (39). In addition, to ensure the stability of the closed-loop system, poles must verify the Matignon's stability conditions given in Theorem 1. To illustrate the solution, consider the simple example of a first order system $n = 1$ and $\alpha = 1/2$ ($q = 2$ and $k = 1$). In this case, the integer polynomial (39) is written as

$$\Delta_{\mathrm{d}}(p) = p^3 + \beta_1 p^1 + \beta_2 \tag{40}$$

This polynomial is thus of order 3 where the coefficient of p^2 is zero. Therefore, we must choose three poles whose sum is zero. But, when $\alpha = 1/3$ ($q = 3$ and $k = 1$) the integer polynomial (39) becomes

$$\Delta_{\mathrm{d}}(p) = p^4 + \beta_1 p^1 + \beta_2 \tag{41}$$

In this case, we must choose four poles so that the coefficients of p^3 and p^2 must be zero.

The computation of the fractional PI-state feedback is summarized in the following algorithm.

Consider the state space model of an integer order system for which the characteristic polynomial is written as

$$\Delta_{\Sigma}(s) = s^n + a_1 s^{n-1} + a_2 s^{n-2} + \cdots + a_{n-1} s + a_n$$

Step 1. Compute the linear transformation T that gives the controllable canonical form. Matrix T can be computed as follows

$$T = [q_1' \quad (q_1 A)' \quad \cdots \quad (q_1 A^{n-1})']'$$

q_1 is a row vector

$$q_1 = e_n' \, W_c^{-1}$$

W_c is the controllability matrix

$$W_c = [B \quad AB \quad \cdots \quad A^{n-1} B]$$

e_n is a unit vector

$$e_n = [0 \quad 0 \quad \cdots \quad 0 \; 1]'$$

Step 2. Choose the fractional order variable $\alpha = k/q$, k and q must be integers.

Step 3. Write the integer order polynomial, representing the closed-loop characteristic polynomial, in the form

$$\Delta_{\mathrm{d}}(p) = p^{nq+k} + \beta_1 p^{(n-1)q+k} + \beta_2 p^{(n-1)q} + \cdots + \beta_{2n-2} p^q + \beta_{2n-1} p^k + \beta_{2n}$$

Step 4. Select the powers of the variable p for which the coefficient is zero.

Step 5. Choose $nq + k$ poles of the integer polynomial of Step 3 with respect the constraints of Step 4, and with respect the Matignon's stability conditions.

Step 6. The feedback gain vectors K_p and K_I of the PI-state feedback $u(t) = K_p x(t) + K_I \mathcal{J}_\alpha(x(t))$ that place the poles of the system $(\dot{x} = Ax + Bu, y = Cx)$ in closed-loop are given by

$$\begin{cases} K_p = [(a_n - \beta_{2n-1}) \quad (a_{n-1} - \beta_{2n-3}) \quad \cdots \quad (a_2 - \beta_3) \, (a_1 - \beta_1)] \, T \\ \qquad\qquad K_I = [-\beta_{2n} \quad -\beta_{2n-2} \quad \cdots \quad -\beta_4 \quad -\beta_2] \, T \end{cases}$$

3. Bode's Ideal Transfer Function Based Design of Fractional Pi-State Feedback

We presented, in Section 2, the generalization of the integer PI-state feedback. The pole placement design method, although it can be used to determine the feedback gains K_p and K_I, is not practical because the non-integer order α must be rational and its value is not chosen according to a specified objective. In addition, the poles of the corresponding integer polynomial are not arbitrary since they must verify constraints because some of the polynomial coefficients are zero. In this section, another method based on the Bode's ideal transfer function is proposed.

Theorem 3. *Let's consider a controllable LTI integer order SISO system described by Equation (9) and let the control law given by Equation (23). Vectors K_p and K_I that can arbitrarily place the closed-loop characteristic polynomial written in the form*

$$\Delta_d(s) = \left(s^\alpha + p_f\right)\left(s^{n-1} + \beta_1 s^{n-2} + \beta_2 s^{n-3} + \cdots + \beta_{n-2}s + \beta_{n-1}\right) \qquad (43)$$

are given by

$$\begin{cases} K_p = [a_n \; (a_{n-1} - \beta_{n-1}) \quad \cdots \quad (a_2 - \beta_2) \, (a_1 - \beta_1)] \, T \\ \\ \qquad K_I = -p_f[\beta_0 \quad \beta_1 \quad \cdots \quad -\beta_{n-2} \quad 1] \, T \end{cases} \qquad (43)$$

T being the linear transformation that gives the controllable canonical form.

Proof. The closed-loop characteristic polynomial of the state space model (12) using the fractional control law (26) being calculated by $\Delta_{cl}(s)$ (see Equation (33), it is given by

$$\Delta_{cl}(s) = s^{n+\alpha} + \left(a_1 - K_{pcn}\right)s^{n-1+\alpha} - K_{Icn}s^{n-1} + \left(a_2 - K_{pcn-1}\right)s^{n-2+\alpha}$$
$$-K_{Icn-1}s^{n-2} + \cdots + \left(a_{n-1} - K_{pc2}\right)s^{1+\alpha} - K_{Ic2}s + \left(a_n - K_{pc1}\right)s^\alpha - K_{Ic1} \qquad (44)$$

It can be written as

$$\Delta_{cl}(s) = s^\alpha \, \Delta_{cl\,1}(s) - K_{Icn}\Delta_{cl\,2}(s) \qquad (45)$$

where

$$\Delta_{cl\,1}(s) = s^n + (a_1 - K_{pcn})s^{n-1} + \cdots + (a_{n-1} - K_{pc2})s + (a_n - K_{pc1}) \qquad (46)$$

$$\Delta_{cl2}(s) = s^{n-1} + \frac{K_{Icn-1}}{K_{Icn}}s^{n-2} + \cdots + \frac{K_{Ic2}}{K_{Icn}}s + \frac{K_{Ic1}}{K_{Icn}} \qquad (47)$$

$\Delta_{cl\,1}(s)$ and $\Delta_{cl\,2}(s)$ are two integer polynomials of order n and $n-1$, respectively.

K_{pc} and K_{Ic} are then calculated as follows. First we require

$$a_n - K_{pc1} = 0 \;\Rightarrow\; K_{pc1} = a_n \qquad (48)$$

$\Delta_{cl\,1}(s)$ of Equation (46) can thus be written in the form

$$\Delta_{cl\,1}(s) = s\,\tilde{\Delta}_{cl\,1}(s) \qquad (49)$$

where

$$\tilde{\Delta}_{cl\,1}(s) = s^{n-1} + (a_1 - K_{pcn})s^{n-2} + (a_2 - K_{pcn-1})s^{n-3} + \cdots + (a_{n-1} - K_{pc2}) \quad (50)$$

The closed-loop characteristic polynomial (Equation (45)) becomes

$$\Delta_{cl}(s) = s^{\alpha+1}\,\tilde{\Delta}_{cl\,1}(s) - K_{Icn}\Delta_{cl\,2}(s) = (s^{\alpha+1} - K_{Icn})\,\tilde{\Delta}_d(s) \qquad (51)$$

$\tilde{\Delta}_{cl\,1}(s)$ and $\Delta_{cl\,2}(s)$ have now the same order $(n-1)$. Their respective coefficients K_{pci}, $(i = 1, \cdots, n)$ and K_{Ici}, $(i = 1, \cdots, n-1)$ are finally calculated so that

$$\tilde{\Delta}_{cl\,1}(s) = \Delta_{cl\,2}(s) = \tilde{\Delta}_d(s) \qquad (52)$$

$\tilde{\Delta}_d(s)$ is an integer polynomial of degree $(n-1)$ which allows to choose $(n-1)$ poles of the closed-loop characteristic polynomial $\Delta_{cl}(s)$.

Let, then, $\Delta_d(s)$ the desired closed-loop polynomial given by

$$\Delta_d(s) = (s^{\alpha+1} + p_f)\prod_{i=1}^{n-1}(s - s_i)$$
$$= (s^{\alpha+1} + p_f)(s^{n-1} + \beta_1 s^{n-2} + \beta_2 s^{n-3} + \cdots + \beta_{n-2}s + \beta_{n-1}) \qquad (53)$$

$\Delta_d(s)$ consists of two polynomials. A first one is integer and made from $(n-1)$ integer poles and the second one is a non-integer polynomial $(s^\alpha + p_f)$. Thus, when the pole $(-p_f)$ is dominant, the open-loop system will be similar to the Bode's ideal function [9]. Pole $(-p_f)$ is chosen to impose the dynamics of the closed-loop step response and the non-integer order α (with $0 < \alpha < 1$) is chosen to impose its overshoot [7].

Identification term by term between $\Delta_{cl\,2}(s)$ and $\tilde{\Delta}_{cl\,1}(s)$, on one hand, and $\Delta_d(s)$, on other hand, and taking into account Equation (48), gives

$$K_{Icn} = -\mathrm{p}_f \tag{54}$$

and

$$\begin{cases} \beta_1 = a_1 - K_{pcn} = \frac{K_{Icn-1}}{K_{Icn}} \\ \beta_2 = a_2 - K_{pcn-1} = \frac{K_{Icn-2}}{K_{Icn}} \\ \quad \vdots \\ \beta_{n-2} = a_{n-2} - K_{pc3} = \frac{K_{Ic2}}{K_{Icn}} \\ \beta_{n-1} = a_{n-1} - K_{pc2} = \frac{K_{Ic1}}{K_{Icn}} \end{cases} \tag{55}$$

As $K_{pc1} = a_n$ (Equation (48)) and $K_{Icn} = -\mathrm{p}_f$ (Equation (54)), K_{pc} and K_{Ic} are given by

$$\begin{cases} K_{pc} = [a_n \ (a_{n-1} - \beta_{n-1}) \quad \cdots \quad (a_2 - \beta_2) \ (a_1 - \beta_1)] \\ \quad K_{Ic} = -p_f[\beta_{n-1} \quad \beta_{n-2} \quad \cdots \ \beta_1 \quad 1] \end{cases} \tag{56}$$

The pole placement of the closed-loop for the original system (9) is achieved by using the gain vectors

$$K_p = K_{pc}T \text{ and } K_I = K_{Ic}T \tag{57}$$

This completes the proof.

The following algorithm, for the computation of the fractional PI-state feedback, results directly from the proof of the theorem.

Let the state space model of an integer order system for which the characteristic polynomial is written as

$$\Delta_\Sigma(s) = s^n + a_1 s^{n-1} + a_2 s^{n-2} + \cdots + a_{n-1}s + a_n$$

Step 1. Compute the linear transformation T that gives the controllable canonical form. Matrix T can be computed as follows

$$T = [q_1' \quad (q_1 A)' \quad \cdots \quad (q_1 A^{n-1})']'$$

q_1 is a row vector

$$q_1 = e_n' \ W_c^{-1}$$

W_c is the controllability matrix

$$W_c = [B \quad AB \quad \cdots \ A^{n-1}B]$$

e_n is a unit vector

$$e_n = [0 \quad 0 \quad \cdots \ 0 \ 1]'$$

Step 2. Choose the fractional order polynomial $s^{\alpha+1} + p_f$

Step 3. Choose the $(n-1)$ poles $s_i,\ i = 1, \cdots, n-1$ of the integer part of the desired closed-loop polynomial.

Step 4. Put the desired closed-loop polynomial in the form

$$\Delta_d(s) = \left(s^{\alpha+1} + p_f\right)\left(s^{n-1} + \beta_1 s^{n-2} + \beta_2 s^{n-3} + \cdots + \beta_{n-2}s + \beta_{n-1}\right)$$

Step 5. The feedback gain vectors K_p and K_I of the PI-state feedback $u(t) = K_p x(t) + K_I \mathcal{I}_\alpha(x(t))$ that place the poles of the system $(\dot{x} = Ax + Bu, y = Cx)$ in closed-loop are given by

$$\begin{cases} K_p = [a_n\ (a_{n-1} - \beta_{n-1}) \quad \cdots \quad (a_2 - \beta_2)\ (a_1 - \beta_1)]\ T \\ \qquad K_I = -p_f[\beta_{n-1} \quad \beta_{n-2} \quad \cdots \beta_1 \quad 1]\ T \end{cases}$$

5. Inverted Pendulum-Cart System Modeling and Swing-Up Control

The inverted pendulum problem is a challenging problem in control theory and has been studied extensively in the control literature [11, 16, 17, 45]. It is a well established benchmark problem that provides many challenging issues in control design. The system is nonlinear, unstable, non-minimum phase and underactuated. The dynamics are quite similar to two-wheeled mobile robots, flexible link robot, biped robot limbs, missiles and so on. Because of their nonlinear nature, pendulums have maintained their usefulness and they are now used to illustrate many of the ideas emerging in the field of non-linear control. The control of the inverted pendulum can be divided into three aspects. The first aspect that is widely researched is the swing-up control of the inverted pendulum. The second aspect is the stabilization of the inverted pendulum. The third aspect is the tracking control of the inverted pendulum. In practice, stabilization and tracking control are more useful for applications.

The pendulum-cart system is shown in Figure (4) and consists of

- A cart moving along a line on two rails of limited length 0.8 m,
- A pendulum hinged in the cart by means of ball bearings rotating freely in the plane containing this line,
- A cart driving device containing a DC motor, a DC amplifier and a pulley-belt transmission system.

The control input is the supply voltage of the DC motor and the outputs are the cart position x_p and the pendulum angle θ.

The complete model describing the dynamic behaviour of the pendulum-cart system is given by [4, 5]

$$\begin{cases} hx_p + b\dot{x}_p + ml\cos(\theta)\dot{\theta} - ml\sin(\theta)\dot{\theta}^2 = F \\ ml\ddot{x}_p\cos(\theta) + N\ddot{\theta} + d\dot{\theta} - mgl\sin(\theta) = 0 \end{cases} \tag{58}$$

where $h = (M + m)$ and $N = (ml^2 + J)$.
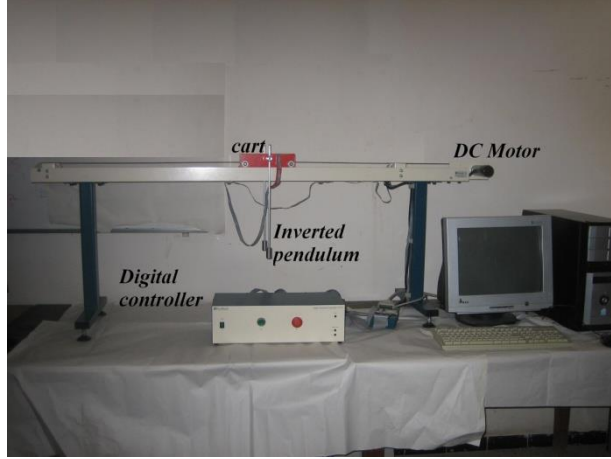
Figure 4. Inverted pendulum-cart system.

To avoid complicating the model of the pendulum-cart system, the DC motor dynamics are neglected. The relationship between the force F applied on the cart and the supply voltage V_c of the DC motor is a simple linear relationship $F = g_t V_c$. (where $g_t = 0.2$). The pendulum parameters are:

$m = 0.2\ kg$ is its mass, $M = 2.3\ kg$ is the cart mass, $l = 0.36\ m$ is the pendulum half length, $J = 0.099\ kgm^2$ is the moment of inertia, $b = 0.05\ kg.m^2/s$ is the friction coefficient of the cart wheels, $b = 0.005\ kg.m^2/s$ is the rotation friction coefficient of the pendulum, and $g = 9.81\ m/s^2$ is the acceleration constant due to the gravity.

Swinging up an inverted pendulum will return it from the stable equilibrium point in position $\theta = \pi$ to an unstable equilibrium point in upright position $\theta = 0$ or $\theta = 2\pi$. The swing-up strategy used here is based on the Lyapunov stability theorem that allows the convergence of the system energy to its energy value in an upright position. The Lyapunov function used is the difference between the mechanical energy of the pendulum and the desired mechanical energy $E^* = 0$. The swing up control is thus given by $u = K_e\ \dot{\theta}\cos(\theta)$ [4]. K_e is a design parameter.

The swing-up control is implemented using a PC Pentium IV, $1\ GHz$, the sampling time is $0.001\ s$ and the design parameter $K_e = 0.15$. A saturation block between ±2.5 Volts is added to protect the DC motor against the control effort. Figure (5) shows the evolution of the cart position x_p, the pendulum position θ and the control voltage V_c.

The results obtained show that $K_e = 0.15$ is sufficient to return the pendulum from its stable equilibrium position $\theta = \pi$ to the unstable equilibrium point $\theta = 2\pi$, respecting the limits of the rail length ±0.4 m, and the control is less than ±2.5 Volts.
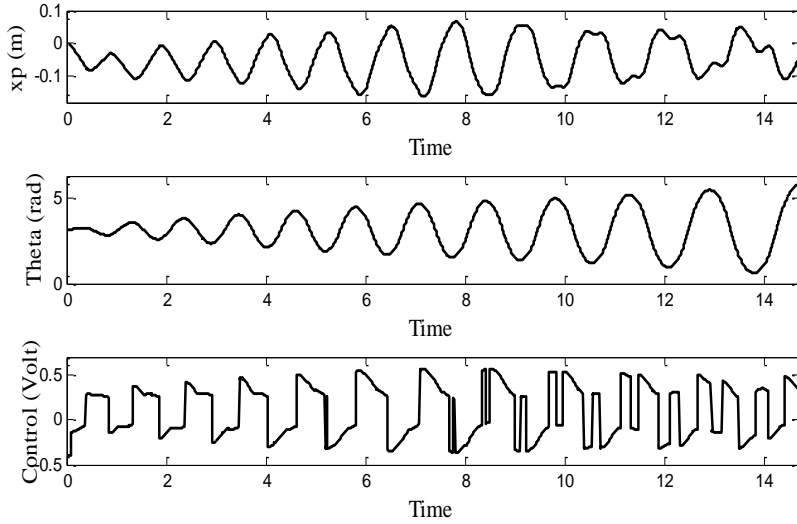
Figure 5. Experimental results of the swing-up control.

5. Implementation of the Fractional PI-State Feedback to Stabilize the Inverted Pendulum-Cart System

To test the theoretical results elaborated in Sections 3 and 4, the linearized model of the inverted pendulum-cart system around $\theta = 0$ is used. It is given by

$$A = \begin{bmatrix} 0 & 1 & 0 & 0 \\ 0 & \frac{-bN}{hN-m^2l^2} & \frac{-m^2l^2g}{hN-m^2l^2} & \frac{mlb}{hN-m^2l^2} \\ 0 & 0 & 0 & 1 \\ 0 & \frac{mlb}{hN-m^2l^2} & \frac{-mgl}{N}+\frac{m^3l^3g}{N(hN-m^2l^2)} & \frac{-d}{N}+\frac{m^2l^2d}{N(hN-m^2l^2)} \end{bmatrix} B = \begin{bmatrix} 0 \\ \frac{N}{hN-m^2l^2} \\ 0 \\ \frac{-ml}{hN-m^2l^2} \end{bmatrix}$$

$$C = \begin{bmatrix} 1 & 0 & 0 & 0 \\ 0 & 0 & 1 & 0 \end{bmatrix} \tag{59}$$

The state vector is

$$x = [x_p \quad \dot{x}_p \, \theta \quad \dot{\theta}]' \tag{60}$$

numerical values of A and B are

$$A = \begin{bmatrix} 0 & 1 & 0 & 0 \\ 0 & -2.1\,10^{-5} & -0.5339 & 0.0045 \\ 0 & 0 & 0 & 1 \\ 0 & 4.5\,10^{-5} & 22.2449 & -0.189 \end{bmatrix}, B = \begin{bmatrix} 0 \\ 0.4218 \\ 0 \\ -0.970 \end{bmatrix} \tag{61}$$

The system is unstable since its poles are $p_{1,2} = 0$, $p_3 = 4.6229$ and $p_4 = -4.8119$.

To implement the fractional PI-state feedback control on the inverted pendulum-car system, all the state variables, the cart position x_p, the pendulum position θ, the cart linear

velocity $\dot{x}_p$ and the angular velocity of the pendulum $\dot{\theta}$ must be measured. These two last measurements, being not available on the real system, we have used a differentiator followed by a low-pass filter whose transfer functions are

$$f_x = \frac{8 \ 10^4}{s^2+90s+10^4} \ f_\theta = \frac{2 \ 10^4}{s^2+90s+10^4} \tag{62}$$

Furthermore, The association between swing-up control and stabilization control requires adding a suitable switching law [5, 45]. In our case, the switching is applied when the absolute value of the angle is close to $\pm 20°$.

5.1. Implementation of the Fractional PI-State Feedback Obtained Using the First Method

The linear model of the inverted pendulum-car system being unstable and as $n = 4$ and we choose $\alpha = k/q = 1/2$, the method requires choosing $qn + k = 9$ poles of the integer polynomial corresponding to the closed-loop characteristic polynomial. The integer polynomial is given by

$$\Delta_d(p) = p^9 + \beta_1 p^7 + \beta_2 p^6 + \beta_3 p^5 + \beta_4 p^4 + \beta_5 p^3 + \beta_6 p^2 + \beta_7 p + \beta_8 \tag{63}$$

This polynomial is of order $qn + k = 9$, however there are only $nk = 8$ coefficients. The zero coefficient is that corresponding to p^8. So, the chosen poles must verify this constraint

$$\sum_{i=1}^{9} p_i = 0 \tag{64}$$

There are several ways to choose these 9 poles. Equations (65) show the solution adopted

$$\begin{cases} p_{1,2} = Re_1 \pm jIm_1, p_{3,4} = Re_2 \pm jIm_2 \\ p_{5,6} = Re_3 \pm jIm_3, p_{7,8} = Re_4 \pm jIm_4 \\ p_9 = -2(Re_1 + Re_2 + Re_3 + Re_4) \end{cases} \tag{65}$$

The numerical values are

$$\begin{cases} p_{1,2} = 0.001 \pm j, p_{3,4} = 0.002 \pm 2j \\ p_{5,6} = 0.05 \pm j, p_{7,8} = 0.04 \pm 2.5j \\ p_9 = -0.186 \end{cases} \tag{66}$$

The numerical value of the parameter g_t representing the DC motor model is $g_t = 0.13$, and by using the algorithm summarized in Section 3, gain vectors K_p and K_I of the fractional PI-state feedback control are

$$\begin{cases} K_p = 0.13 \ [2.7568 \ 6.7194 \quad 77.3854 \quad 16.3982] \\ K_I = 0.13 \ [0.524 \ 0.9413 \quad 5.0553 \quad 1.1213] \end{cases} \tag{67}$$

Figure (6) shows the experimental results obtained. This figure shows the effectiveness of the fractional PI-state feedback control on the experimental test bench. Indeed, it maintains the stability of the pendulum in its unstable equilibrium position $\theta = 2\pi$ and controls the cart position at $x_p = 0$. In addition, the control law values do not exceed ± 2.5 Volts.
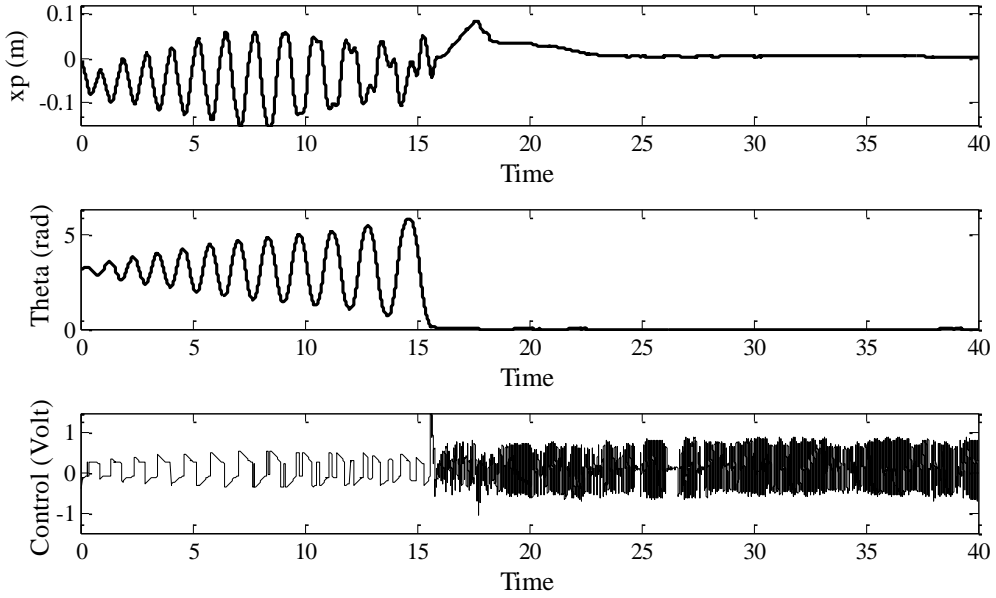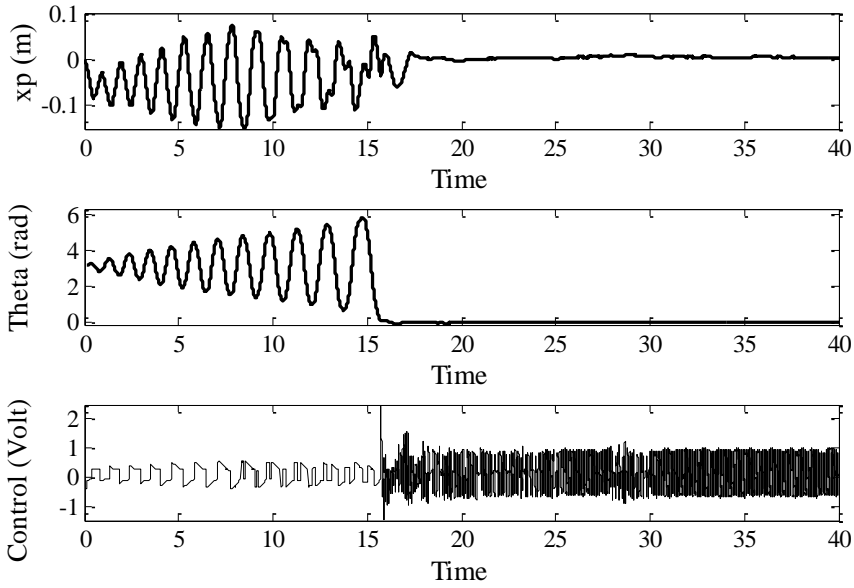

Figure 6. Experimental results swing-up + stabilization control using the first method.
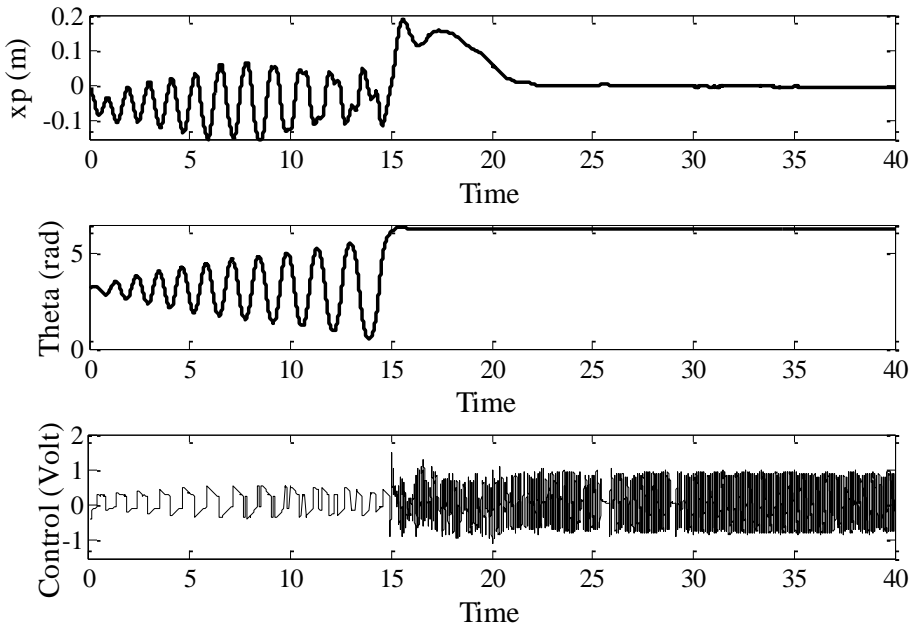
Figure 7. Experimental results with variation of 40% of the cart mass, using the first method.

Figure (7) shows the influence of the variation of 40% of the cart mass (this perturbation is obtained by adding a small mass of aluminum on the cart just after the end of the swinging up step). Figure (8) shows the results obtained when the pendulum is subjected to disturbance in the form of forces applied on it (by hitting the pendulum with a pen at different times). Figures (7) and (8) show the robustness of the stabilization by the fractional PI-state feedback. Indeed, despite the variation of 40% of the cart mass and external disturbances on the pendulum, it remains stable.
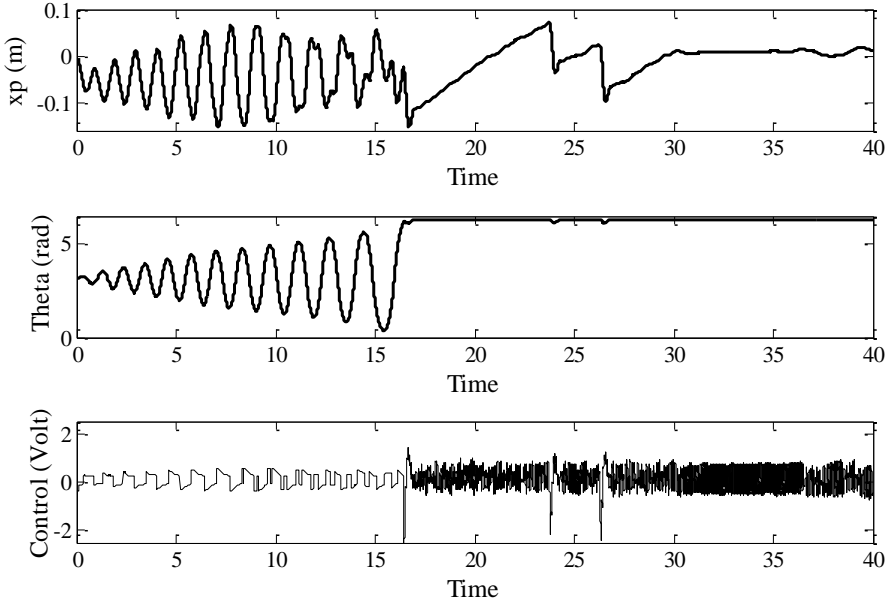
Figure 8. Experimental results with disturbance on the control at $t = 24\ s$, and $t = 26\ s$, using the first method.

5.2. Implementation of the Fractional PI-State Feedback Obtained by Using the Second Method

For the purpose of fractional order PI-state feedback control design, the linearized model of the inverted pendulum-cart system (Equation 59) is considered again. The linear model being of order 4, to achieve the closed-loop characteristic polynomial (Equation (43)), three poles $p_1 = -1.5$, $p_2 = -7$ and $p_3 = -5$ of the integer order polynomial are chosen. An additional pole at $p_f = -0.15$ of the fractional order polynomial is considered. The fractional order considered is $\alpha = 1/2$.

Gain vectors K_p and K_I of the fractional order PI-state feedback control obtained by using the algorithm summarized in Section 4, are

$$\begin{cases} K_p = 0.13\ [0\ 5.9 \quad 83.45 \quad 17.419] \\ K_I = 0.13\ [0.885\ 0.9 \quad 2.719 \quad 0.584] \end{cases} \tag{68}$$

Figure (9) shows the experimental results obtained. This figure shows the effectiveness of the fractional PI-state feedback control on the experimental test bench. Indeed, it maintains the stability of the pendulum in its unstable equilibrium position $\theta = 2\pi$ and controls the cart position at $x_p = 0$.

Figure 9. Swing-up and fractional order PI-state feedback control experimental results, using the second method.
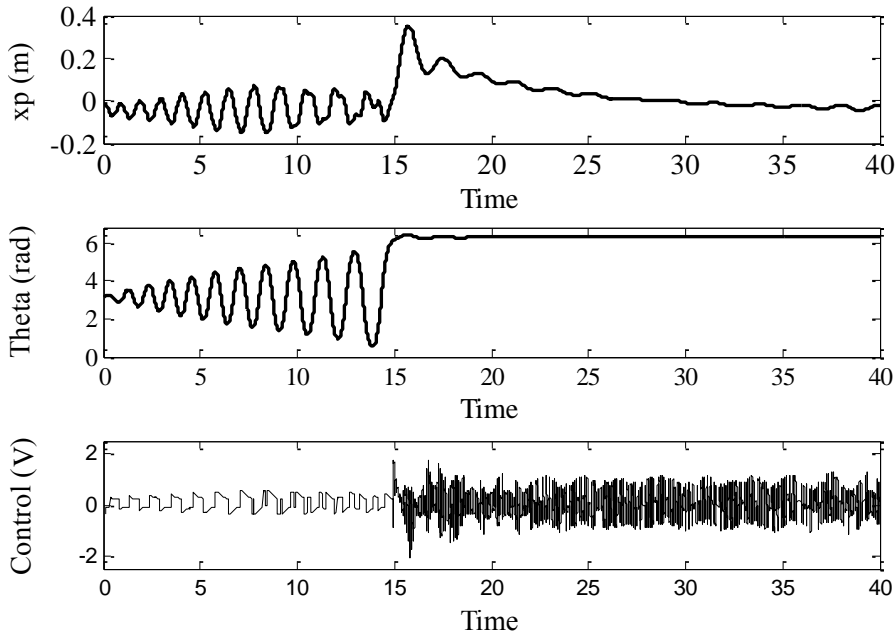
Figure 10. Fractional order PI-state feedback control experimental results with 40% mass variation, using the second method.

Figures (10) and (11) show the experimental results obtained with disturbance. Figure (10) shows the influence of the variation of 40% of the cart mass. Figure (11) shows the results obtained when the pendulum is subjected to disturbance applied at $t = 21\,s$ and $t = 24\,s$. Figures (10) and (11) show, in this case also, the robustness of the stabilization by the fractional PI-state feedback. Indeed, despite the variation of 40% of the cart mass and despite external disturbances on the pendulum, it remains stable.
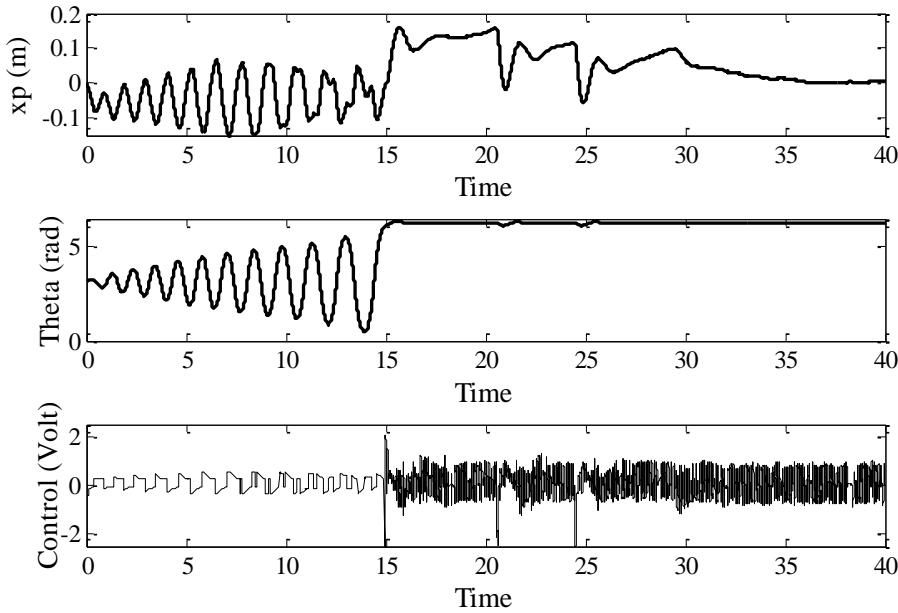
Figure 11. Fractional order PI-state feedback control experimental results with disturbance on the pendulum at $t = 21\,s$ and $t = 24\,s$, using the second method.

Conclusion

Two new pole placement fractional PI-state feedback designs algorithms are presented in this book chapter. The first one consists in choosing $qn + k$ poles of an integer polynomial corresponding to the closed-loop fractional characteristic polynomial. Matignon's stability condition can thus be used to ensure the stability of the closed-loop. Nevertheless, the non-integer order α must be rational. In addition, the poles of the integer polynomial are not arbitrary since they must verify constraints because some of the polynomial coefficients are zero. The second method is simple to implement, it consists in choosing $n - 1$ poles of an integer polynomial and one pole of a fractional polynomial. A judicious choice of these poles provides a closed-loop particular response obtained when the Bode's ideal transfer function is used, that is, an overshoot of the step response imposed by the fractional order α and its dynamics by the pole of the fractional polynomial. These methods are then used to stabilize an inverted pendulum-cart system. The implementation on an experimental test-bed gave good results, especially in terms of stability, accuracy and robustness with respect to the variation of the cart mass as well as external disturbances applied on the pendulum.

Acknowledgments

References

[1]   Abdelaziz T.H.S. and Valasek M., (2003). A direct algorithm for pole placement by state derivative feedback for single-input linear systems. *Acta Polytechnica,* 43, 52-60.

[2]   Abdelaziz T.H.S. and Valasek M., (2004). Pole-placement for SISO linear systems by state-derivative feedback. *IEE Proceedings Control Theory and Application,* 151, 377-385.

[3]   Abdelaziz T.H.S. and Valasek M., (2005). State derivative feedback by LQR for linear time-invariant systems. *Proceeding of 16th IFAC World Congress,* Prague, Czech Republic, July 3-8.

[4]   Astrom K J, and Furuta K., (1996). Swinging up a pendulum by energy control. *Proceeding of IFAC 13th IFAC World Congress, San Francisco*, CA, USA, June 30-July 05.

[5]   Astrom K.J., Aracil J., and Gordillo F., (2008). A family of smooth controllers for swinging up a pendulum. *Automatica,* vol. 44, 1841-1848.

[6]   Axtell, M., and Bise, E. M., (1990). Fractional calculus applications in control systems. *In Proceedings of the IEEE Nat. Aerospace and Electronics Conference,* New York, 8 (3-4), 563-566.

[7]   Barbosa R.S., Machado J.A.T., and Ferreira I.M., (2004). Tuning of PID controllers based on Bode's ideal transfer function. *Nonlinear dynamics,* vol. 38, 305-321.

[8]   Bettayeb M., and Djennoune S., (2008). New results on controllability and observability of fractional dynamical systems. *Journal of Systems Engineering and Electronics,* vol. 14 (9-10), 376-381.

[9]   Bettayeb M., C. Boussalem, Mansouri R. and Al-Saggaf U. M., (2014), Stabilization of an inverted pendulum-cart system by fractional PI-state feedback, *ISA transactions,* vol. 53 (2), 508-516.

[10] Bode H.W., (1945). Network Analysis and Feedback Amplifier Design. Van Nostrand, New York.

[11] Chung C.C. and Hauser J., (1995). Non linear control of a swinging pendulum. *Automatica,* vol. 31 (6), 851-862.

[12] Das S. Saha S. Das S. and Gupta A., (2011). On the selection of tuning methodology of FOPID controllers for the control of higher order processes. *ISA Transactions,* vol. 50, 376-388.

[13] Dorcak, L., Petras, I., and Kostial, I., (2000). Modeling and analysis of fractional-order regulated systems in the state space. *In Proceedings of ICCC'2000,* vol.45, High Tatras, Slovak Republic, 185-188.

[14] Farges C. Moze M. and Sabatier J., (2009). Pseudo-state feedback stabilization of commensurate fractional order systems. *Proceedings of the 10th European control conference*, Budapest, Hungary, August 23-26.

[15] Farges C. Moze M. and Sabatier J., (2010). Pseudo-state feedback stabilization of commensurate fractional order systems. *Automatica,* vol. 46, 1730-1734.

[16] Furuta K. and Yamakita, M. (1991). Swing up control of inverted pendulum. *IEEE Proceedings 1991 International Conference on Industrial Electronics, Control and Instrumentation,* Kobe, Japan, October 28-November 1.

[17] Furuta K., Yamakita M. and Kobayashi S. (1992). Swing-up control of inverted pendulum using pseudo-state feedback. *Journal of Systems and Control Engineering,* vol. 206, 263-269.

[18] Guo G. and Ma Z., (2006). State-PID feedback control with application to a robot vibration absorber. *International Journal of Modelling, Identification and Control,* vol. 1 (1), 38-43.

[19] Hotzel R., and Fliess, M., (1998). On linear system with a fractional derivation: introductory theory and examples. *Mathematics and Computers in Simulation,* vol. 45, 385-395.

[20] Kilbas A.A., Srivastava H.M. and Trujillo J.J., (2006). *Theory and Applications of Fractional Differential Equations*. Elsevier, North-Holland.

[21] Leitmann G. and Reithmeier E. (2003) Robust vibration control of dynamical system based on the derivative of the state. *Archive of Applied mechanics*, Vol. 72, 856-864.

[22] Magin R.L., (2006). Fractional Calculus in Bioengineering. Begell House Punlishers, Inc., Connecticut.

[23] Machado, J.T., Kityakova V. and Mainardi F., (2011). Recent History of fractional calculus. *Communications in Nonlinear Science and Numerical Simulation,* vol. 16 (3), 1140-1153.

[24] Manabe, S., (1963). The system design by the use of a model consisting of a saturation and non-integer integrals. *ETJ of Japan,* vol. 8 (3-4), 147-150.

[25] Mansouri R., Bettayeb M., and Djennoune S., (2007). Multivariable fractional order system approximation using derivative representation. *International Journal of Applied Mathematics,* vol. 20 (7) 983-1003.

[26] Mansouri R., Bettayeb M., and Djennoune S., (2008). Non integer order system approximation by an integer reduced model. *in a special issue on fractional calculus in the Journal Européen des Systèmes Automatisés,* vol. 42, 689-700.

[27] Mansouri R., Bettayeb M., and Djennoune S., (2010). Multivariable fractional system approximation with Initial conditions using integral state space representation. *Int. Journal on Computers and Mathematics with Applications,* vol.59 (5), 1842-1851.

[28] Matignon, D., (1996). Stability results on fractional differential with application to control processing. *In IAMCS, IEEE SMC Proceedings Conference,* Lille, France, 963-968.

[29] Matignon, D., and d'Andréa-Novel, B., (1996). Some results on controllability and observability of finite dimensional fractional differential systems. *In IAMCS, IEEE-SMC Proceedings Conference,* Lille, France, pp. 952-956.

[30] Matignon D., (1998). Stability properties for generalized fractional differential systems. In *Systèmes différentiels fractionnaires* (Paris 1998), vol.5 of *ESAIM: Proceedings,* 145–158, Society for Industrial and Applied Mathematics, Paris, France.

[31] Miller K.S. and Ross B., (1974). *An introduction to the Fractional Calculus and Fractional Differential Equations.* A Wiley Interscience Publication.

[32] Monje C.A., Vinagre B.M., Feliu V. and Chen Y.Q., (2008). Tuning and auto-tuning of fractional order controllers for industry applications. *Control Engineering Practice,* vol. 16, 798–812.

[33] Monje, C.A., Chen, Y., Vinagre, B.M., Xue, D., and Feliu-Batlle, V., (2010). *Fractional-order Systems and Controls: Fundamentals and Applications*. Springer Verlag.

[34] Nia S.H.H., Sierociuk D., Calderon A.J. and Vinagre B.M., (2010). Augmented System Approach for Fractional Order SMC of a DC-DC Buck Converter. *Proceedings of the 4th IFAC Workshop on Fractional Differentiation and its Applications,* Badajoz, Spain, october 18-20.

[35] Ogata, K., (1997). *Modern Control Engineering*. Third Edition, Prentice Hall.

[36] Oldham K.B. and Spanier J., (1974). *The Fractional Calculus*. Academic Press, New York and London.

[37] Olgac N., Elmali H., Hosek M. and Renzulli M., (1997). Active vibration control of distributed systems using delayed resonator with acceleration feedback. *Journal of Dynamic Systems, Measurement and Control,* vol.119 (3), 380-389.

[38] Oustaloup A., (1991). *La Commande CRONE*. Hermès Edition, Paris.

[39] Oustaloup, A., (1995). *La Dérivation Non Entière: Théorie, Synthèse et Applications*. Hermès Edition, Paris, France.

[40] Oustaloup A. and Mathieu B., (1999). *La Commande CRONE du Scalaire au Multivariable*. Hermès Editeur, Paris.

[41] Podlubny I., (1999). *Fractional Differential Equations*. Academic Press, San Diego.

[42] Poblubny I., (1999). Fractional-Order System and $PI^\lambda D^\mu$. *JIEEE Transactions on automatic control,* vol. 44 (1), 208-214.

[43] Raynaud, H. F., and Zergainoh, A., (2000). State space representation for fractional order controllers. *Automatica,* vol. 36, 1017-1021.

[44] Samko S.G., Kilbas A.A. and Marichev O.I., (1993). *Fractional Integrals and Derivatives*. Gordon and Breach Science Publishers.

[45] Srinivasan B., Huguenin P., and Bonvin D., (2009). Global stabilization of an inverted pendulum - Control stategy and experimental verification. *Automatica,* vol. 45, 265-269.

[46] Sierociuk D. and Vinagre B.M., (2010). State and Output Feedback Fractional Control by System Augmentation. *Proceedings of the 4th IFAC Workshop on Fractional Differentiation and its Applications,* Badajoz, Spain, october 18-20.

[47] Tavakoli-Kakhki M., and Haeri M., (2010). The minimal state space realization for a class of fractional order transfer functions. *SIAM Journal on Control and Optimization,* vol. 48 (7), 4317-4326.

[48] Tavakoli-Kakhki M, Haeri M, and Tavazoei M.S, (2011). Notes on the state space realizations of rational order transfer functions. *IEEE Transactions on Circuits and Systems I: Regular Papers,* vol. 58 (5), 1099-1108.

[49] Vinagre, B. M., Monje, C. A., and Caldero, A. J., (2002). Fractional order systems and fractional order actions. *Tutorial Workshop # 2: Fractional Calculus Applications in Automatic Control and Robotics,* 41st IEEE CDC, Las Vegas.

[50] Wiboonjaroen W., and Sujitjorn S., (2011). Stabilization of an Inverted Pendulum System via State-PI Feedback. *International Journal of Mathematical models and methods in applied sciences,* vol. 5. (41), 763-772.

[51] Zeng Q., Cao G., and Zhu X., (2005). Research on controllability for a class of fractional-order linear control systems. *Journal of Vibration and Control,* vol. 14 (9-10), 1531-1541.

Chapter 5

FROM THE FORMAL CONCEPT ANALYSIS TO THE NUMERICAL SIMULATION OF THE THERMAL DIFFUSION PHENOMENA IN A FINITE MEDIUM

Riad Assaf[1,2,], Roy Abi Zeid Daou[2,†],
Xavier Moreau[1,‡] and Fady Christophy[1,2,#]*

[1]University of Bordeaux, IMS Laboratory, Talence, Bordeaux, France
[2]Lebanese German University, Faculty of Public Health,
Biomedical Technologies department, Sahel Alma, Jounieh, Lebanon

Abstract

This chapter shows the use of the fractional order approach in the study of the thermal interface behavior in view to facilitate the identification of this phenomenon and the optimization of its process control. After a short introduction, the main parameters are defined then the semi-infinite plane case study is considered. A representative model is developed based on the system equations. The operational, frequency and time responses are studied. The case study of a finite plane follows using the same methodology, nevertheless exact analytical solutions in the time domain don't exist; their approximations will be treated in other publications.

1. Context and Problematic

In general, the development of diffusion phenomena equations naturally leads to fractional order systems (Podlubny, 2002). There are many examples in the fields of physics such as electrochemistry (Kuhn, 2005), electromagnetism (Benchellal, 2005) (Canat, 2005), or thermal (Agrawal, 2004) (Battaglia, 2001) (Kusiak, 2005).

---

[*] E-mail addresses: riad.assaf@u-bordeaux.fr; r.assaf@lgu.edu.lb.
[†] E-mail address: r.abizeiddaou@lgu.edu.lb.
[‡] E-mail address: xavier.moreau@u-bordeaux.fr.
[#] E-mail addresses: fady.chrystophy@u-bordeaux.fr; f.christophy@lgu.edu.lb.

Actually, the recognition of fractional order behavior when identifying physical systems flourished starting the second half of the twentieth century (Oldham, 1974). One of these fields where the fractional order integration can show up is the thermal diffusive interfaces. In fact, for some special conditions, an integration of order 0.5 appears when identifying such system (Abi Zeid Daou, 2012, Assaf, 2012). The objective of this chapter is to study the presence of the fractional order and its effects on the system behavior, and to determine the relation between the applied flux, the conduction and the point of measurement of the temperature in a plane medium.

This objective is a milestone towards the definition of valid approximations for reliable numerical simulations of the thermal diffusion phenomena in a finite medium where exact analytical time response solutions don't exist. For instance, one can define conditions for which a finite medium can be considered as a semi-infinite medium, and can define other conditions for which analytical approximations generate accurate time response simulations.

The understanding of the thermal diffusion phenomena, hence the establishment of a validation model has two main goals:

- As part of the identification process: to facilitate the definition of the model structure, and to pass from a black box approach to a gray box approach.
- As part of a process control model: to deduct from the validation model not only a nominal model of synthesis, but also structural and parametric uncertainties.

This chapter contains six main paragraphs other than the Abstract and the Introduction at the beginning; the Conclusion and the References at the end. A reminder of the main physical characteristics needed to describe the thermal diffusion are found in Para 2, in Para 3 a model of the diffusion phenomena in the semi-infinite medium is developed, then the relative operational, frequency and time responses are studied in Para 4. In Para 5 a model of the diffusion phenomena in the finite medium is developed, then only the corresponding operational and frequency responses are studied in Para 6 since no exact analytical solutions exist to represent the time response for the finite medium. In Para 7 one can find some step responses using Simulink, it opens the door for the need for simple and accurate approximations.

2. Parameters and Definitions

The main thermal parameters and definitions characterizing any thermal interface are presented in this paragraph.

- Heat flow in the x direction is represented by Q_x (W).
- Heat flux in the x direction is represented by φ_x (W/m^2).
- Thermal conductivity λ $(W.m^{-1}.K^{-1})$ [Özişik, 1980] is the material property which controls the rate of heat flow in the medium. For aluminum $\lambda = 237\ Wm^{-1}K^{-1}$.
- Homogeneous and Isotropic medium [Özişik, 1980] is a material in which thermal conductivity is independent of direction.
- Density of a material is represented by ρ (kg/m^3). For aluminum $\rho = 2,700\ kg/m^3$.

- Specific heat capacity C_p $(J.kg^{-1}.K^{-1})$ is [Schneider, 1957] the heat energy required to raise the temperature of a unit weight of the material by one degree. For aluminum $C_p = 908\ J.kg^{-1}K^{-1}$.

- Thermal diffusivity $\alpha\ (m^2/s)$ of a medium [Özişik, 1980] is associated with the speed of propagation of heat into the solid during changes of temperature with time. For aluminum $\alpha = \frac{\lambda}{\rho.C_p} = 9.67 \times 10^{-5}\ m^2/s$.

- Thermal effusivity $T_{iu}(kg.K^{-1}.s^{-2.5})$ is [de Wit, 2009] a measure of the material's ability to exchange thermal energy with its surroundings. For aluminum $T_{iu} = \sqrt{\lambda.\rho.C_p} = 24.1 \times 10^3\ kg.K^{-1}.s^{-2.5}$.

- Volumetric heat capacity C_{th} $(J.K^{-1}.m^{-2})$. $C_{th} = \rho C_p L$ is a variant of the volumetric heat capacity [US Army, 1988]; it describes the ability of a given volume (crossed by a heat flux through its area A along its length L) of finite medium to store internal energy while undergoing a temperature change.

3. Semi-Infinite Plane

We consider a semi-infinite, homogeneous, isotropic, one-dimensional plane medium of conductivity λ, diffusivity α and of initial temperature zero all over the medium (Figure 1) [Sabatier, 2008]. A heat flux $\varphi(t)$ is normally applied on its surface. Consequently, a temperature gradient $T(x,t)$ appears, which is a function of the independent time variable t as well as the abscissa x of the temperature measurement point, inside the medium.
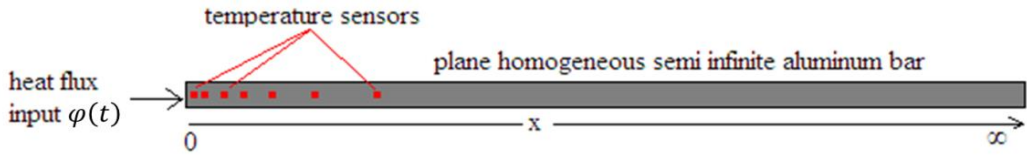
Figure 1. Diffusion in a semi-infinite plane medium.

3.1. System Definition

The one-dimensional heat conduction equation (Özişik, 1985) is given by a partial differential equation:

$$\frac{\partial T(x,t)}{\partial t} = \alpha\ \frac{\partial^2 T(x,t)}{\partial x^2},\ 0 < x < \infty,\ t > 0\ . \tag{1}$$

Since the initial temperature is zero all over the medium:

$$T(x,t) = 0,\ 0 \leq x < \infty,\ t = 0 \tag{2}$$

The Fourier law states the boundary condition (Özişik, 1985) where the flux is applied, the second condition is trivial:

$$-\lambda \frac{\partial T(x,t)}{\partial x} = \varphi(t), \ x = 0, \ t > 0;$$

(3)

$$T(x,t) = 0, \ x \to \infty, \ t > 0.$$

(4)

3.2. System Resolution

The use of the fractional calculus to resolve the problems of the diffusive interfaces dates back to the beginning of the 20th century [Battaglia, 2001]. The system of (Eq. 1-4) represents the relations that model this interface knowing that the input signal is the flux $\varphi(t)$ whereas the output signal is the temperature $T(x,t)$ as shown in Figure 1.

The initial condition of the temperature being zero, Laplace transform $\mathcal{L}\{\cdot\}$ of (Eq. 1) is:

$$\frac{\partial^2 \bar{T}(x,s)}{\partial x^2} - \frac{s}{\alpha}\bar{T}(x,s) = 0, \text{ where } \bar{T}(x,s) = \mathcal{L}\{T(x,t)\}.$$

(5)

This is a differential equation of the 2nd order in *x*. Its general solution is:

$$\bar{T}(x,s) = e^{r(s)x},$$

(6)

leading to the characteristic equation:

$$r^2(s) - \frac{s}{\alpha} = 0 \ ,$$

(7)

which has the following 2 roots $r_1(s)$ and $r_2(s)$:

$$r_i = \pm\sqrt{\frac{s}{\alpha}} \ , \ i \in \{1,2\}$$

(8)

Hence the solution of (Eq. 5) is:

$$\bar{T}(x,s) = K_1(s)e^{x\sqrt{s/\alpha}} + K_2(s)e^{-x\sqrt{s/\alpha}}$$

(9)

Resolving (Eq. 9) for the boundary conditions (*Eq. 3-4*) gives the values of $K_1(s)$ and $K_2(s)$, let:

$$\begin{cases} K_1(s) = 0 \\ K_2(s) = \frac{1}{\lambda\sqrt{\frac{s}{\alpha}}} \bar{\varphi}(s) \end{cases}$$

(10)

Taking into consideration the definitions of the characteristic parameters and the outcome of (Eq. 10) then resolving (Eq. 9), the solution of (Eq. 5) is found to be:

$$\bar{T}(x,s) = \frac{1}{\sqrt{\lambda\rho C_p s}} e^{-x\sqrt{s/\alpha}} \bar{\varphi}(s).$$

(11)

Under the assumption of an initial condition of the temperature being zero, the transfer function $H(x,s)$ between the input flux $\bar{\varphi}(s)$ and the output temperature $\bar{T}(x,s)$ is:

$$H(x,s) = \frac{\bar{T}(x,s)}{\bar{\varphi}(s)} = \frac{1}{\sqrt{\lambda \rho C_p s}} \, e^{-x\sqrt{s/\alpha}}, \tag{12}$$

or rewritten as:

$$H(x,s) = H_0 \, I^{0.5}(s) \, E(x,s), \tag{13}$$

with the following considerations:

$$\begin{cases} H_0 = \dfrac{s^{0.5}\bar{T}(0,s)}{\bar{\varphi}(s)} = \dfrac{1}{\sqrt{\lambda \rho C_p}} = \dfrac{1}{T_{iu}} \\[2mm] I^{0.5}(s) = \dfrac{\bar{T}(0,s)}{s^{0.5}\bar{T}(0,s)} = \dfrac{1}{s^{0.5}} \\[2mm] E(x,s) = \dfrac{\bar{T}(x,s)}{\bar{T}(0,s)} = e^{-\left(\frac{s}{\omega_x}\right)^{0.5}} \end{cases} \tag{14}$$

and defining a cutoff frequency ω_x as:

$$\omega_x = \alpha/x^2. \tag{15}$$

Consequently, the transfer function $H(x,s)$ of the system can be seen as three cascading functions represented in Figure 2.
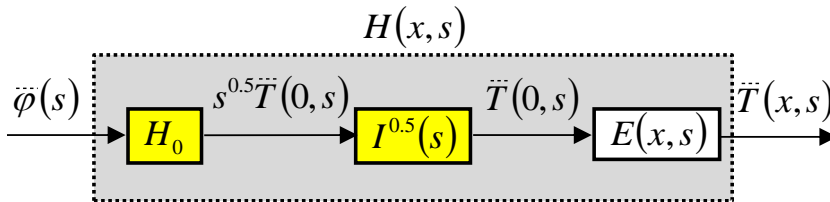
Figure 2. Block diagram illustrating the transfer function $H(x,s)$ of the semi-infinite medium.

The function H_0 depends on the medium physical characteristics, it links the input flux $\bar{\varphi}(s)$ and the fractional derivative of order 0.5 of the temperature at $x = 0$.

Then, $I^{0.5}(s)$ is a fractional integrator of order 0.5 that gives the temperature at $x = 0$.

The last function $E(x,s)$ generates the output temperature $\bar{T}(x,s)$ at any point of the semi-infinite medium.

This new approach allows understanding the link existing between the two kinds of study encountered in the dynamics of thermal systems, i.e.:

- When the boundary condition at $x = 0$ is the flux $\bar{\varphi}(s)$; it is recognized as Neumann (second-type) boundary condition.
- When the boundary condition at $x = 0$ is the temperature $\bar{T}(0,s)$; it is recognized as Dirichlet (first-type) boundary condition.

In both cases, for a semi-infinite medium the transfer $E(x, s)$ is the same.

4. Responses in the Semi-Infinite Plane

4.1. Asymptotic Behavior Analysis at $x = 0$

At $x = 0$, $E(0, s) = 1$; thus the transfer function $H(x, s)$ becomes:

$$H(0, s) = H_0 \, I^{0.5}(s) \tag{16}$$

which asymptotic behaviors are given by:

$$\begin{cases} \lim_{s \to 0} H(0, s) = \lim_{s \to 0} I^{0.5}(s) = \infty \\ \lim_{s \to \infty} H(0, s) = \lim_{s \to \infty} I^{0.5}(s) = 0 \end{cases} \tag{17}$$

The fractional integration behavior of order 0.5 between the input flux $\bar{\varphi}(s)$ and the temperature $\bar{T}(0, s)$ is at mid-way between an integration behavior of order 1 which is characteristic of a capacitive behavior, and a proportional behavior (integration of order 0) characteristic of a resistive behavior.

4.2. Asymptotic Behavior Analysis at $x > 0$

The analysis of the influence of $E(x, s)$ on the transfer function $H(x, s)$ through its asymptotic behaviors leads to:

$$\begin{cases} \lim_{s \to 0} E(x, s) = 1 \\ \lim_{s \to \infty} E(x, s) = \lim_{s \to \infty} e^{-\left(\frac{s}{\omega_x}\right)^{0.5}} = 0 \end{cases} \tag{18}$$

Hence,

$$\begin{cases} \lim_{s \to 0} H(x, s) = \lim_{s \to 0} I^{0.5}(s) = \infty \\ \lim_{s \to \infty} H(0, s) = \lim_{s \to \infty} \frac{H_0}{s^{0.5}} e^{-\left(\frac{s}{\omega_x}\right)^{0.5}} = 0 \end{cases}. \tag{19}$$

The same asymptotic behavior is noticed at any place of the semi-infinite medium.

4.3. Frequency Response Analysis at $x = 0$

The frequency response $H(x, j\omega)$ is given by:

$$H(x, j\omega) = H_0 \, I^{0.5}(j\omega) \, E(x, j\omega). \tag{20}$$

At $x = 0$, the block $E(0, j\omega) = 1$ thus the transfer function $H(x, j\omega)$ becomes:

$$H(0, j\omega) = H_0 \, I^{0.5}(j\omega). \tag{21}$$

The gain and the phase of the transfer function $\bar{H}(0, j\omega)$ are:

$$\begin{cases} |H(0, j\omega)| = \dfrac{H_0}{\omega^{0.5}} \\ arg\big(H(0, j\omega)\big) = -\dfrac{\pi}{4} \end{cases} \tag{22}$$

Bode diagrams and Black-Nichols diagram of $H(0, j\omega)$ are represented in (*Figure 3*) and (*Figure 4*), respectively.

4.4. Frequency Response Analysis at $x > 0$

At $x > 0$, the 3rd block $E(x, j\omega)$ becomes:

$$E(j\omega, s) = e^{-\left(\frac{j\omega}{\omega_x}\right)^{0.5}} \tag{23}$$

Knowing that $j^{0.5} = cos\left(\dfrac{\pi}{4}\right) + j sin\left(\dfrac{\pi}{4}\right) = \dfrac{\sqrt{2}}{2} + j\dfrac{\sqrt{2}}{2}$, the block $E(x, j\omega)$ is written as:

$$E(x, j\omega) = e^{-\left(\frac{\omega}{2\omega_x}\right)^{0.5}} e^{-j\left(\frac{\omega}{2\omega_x}\right)^{0.5}} \tag{24}$$

thus the gain and the phase of this block are:
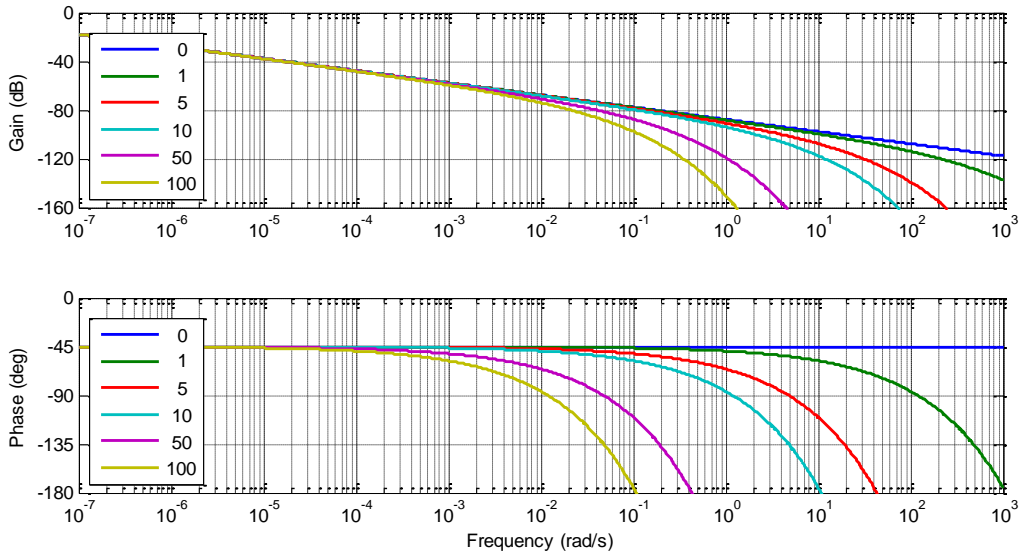
Figure 3. Bode diagrams of $H(x, j\omega)$ for different positions of the temperature sensor in a semi-infinite aluminum medium.
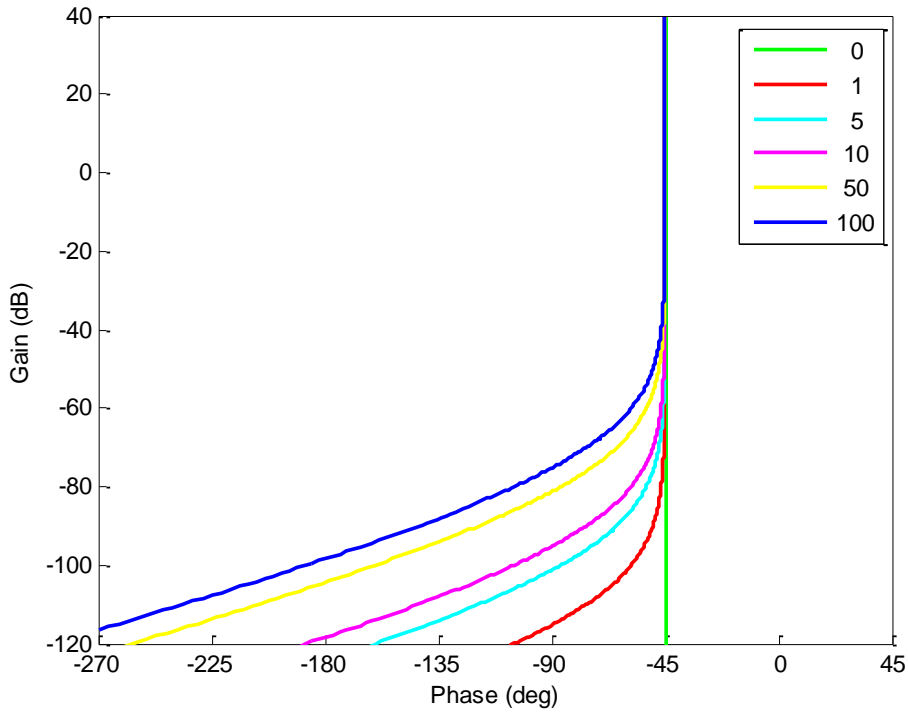
Figure 4. Black-Nichols plots of $H(x, j\omega)$ for different positions of the sensor in a semi-infinite aluminum medium.

$$\begin{cases} |E(x, j\omega)| = e^{-\left(\frac{\omega}{2\omega_x}\right)^{0.5}} \\ arg\big(E(x, j\omega)\big) = -\left(\frac{\omega}{2\omega_x}\right)^{0.5}. \end{cases} \tag{25}$$

- At the low frequencies, the behavior of this block is similar to the one observed when $x = 0$:

$$\begin{cases} \lim_{\omega \to 0} |E(x, j\omega)| = 1 \\ \lim_{\omega \to 0} arg\big(E(x, j\omega)\big) = 0. \end{cases} \tag{26}$$

- At the medium frequencies, especially when $\omega = \omega_x = \alpha/x^2$, the cutoff frequency:

$$\begin{cases} |E(x, j\omega)| = 0.493 \ (-6.14 dB) \\ arg\big(E(x, j\omega)\big) = -40.5° \end{cases}. \tag{27}$$

- At the high frequencies, the behavior of this block is like:

$$\begin{cases} \lim_{\omega \to \infty} |E(x, j\omega)| = 0 \\ \lim_{\omega \to \infty} arg\big(E(x, j\omega)\big) = -\infty. \end{cases} \tag{28}$$

Now, we can look deeply into the transfer function:

$$\bar{H}(x, j\omega) = \frac{H_0}{(j\omega)^{0.5}} \; e^{-\left(\frac{\omega}{2\omega_x}\right)^{0.5}} e^{-j\left(\frac{\omega}{2\omega_x}\right)^{0.5}}. \tag{29}$$

The asymptotic behaviors of $H(x, j\omega)$ are found to be:

- At low frequencies:

$$\begin{cases} \lim_{\omega \to 0} |H(x, j\omega)| = \frac{H_0}{\omega^{0.5}} \\ \lim_{\omega \to 0} arg\big(H(x, j\omega)\big) = -\frac{\pi}{4} \end{cases}. \tag{30}$$

The behavior is similar to the one observed when $x = 0$.
- At high frequencies:

$$\begin{cases} \lim_{\omega \to \infty} |H(x, j\omega)| = \lim_{\omega \to \infty} \frac{H_0}{\omega^{0.5}} e^{-\left(\frac{\omega}{2\omega_x}\right)^{0.5}} = 0 \\ \lim_{\omega \to \infty} arg\big(H(x, j\omega)\big) = \lim_{\omega \to \infty} \left(-\frac{\pi}{4} - \left(\frac{\omega}{2\omega_x}\right)^{0.5}\right) = -\infty \end{cases}. \tag{31}$$

Bode diagrams and Black-Nichols plots in a semi-infinite aluminum medium are merged in Figure 3 and Figure 4 with various values of $x \geq 0$. The fractional integration behavior of order 0.5 is present all over the frequency range for $x = 0$, it disappears gradually at higher frequencies when x increases.

4.5. Time Response Analysis

When analyzing this system in time domain, a special attention should be taken. In fact, because of the presence of the exponent in the expression of $E(x, s)$, the inverse Laplace transfer in simulation is not always possible when taking into consideration special inputs $\bar{\varphi}(s)$. (*Eq. 32*) shows the inverse Laplace transform $\mathcal{L}^{-1}\{\cdot\}$ of the output temperature.

$$T(x, t) = \mathcal{L}^{-1}\{\bar{T}(x, s)\} = \mathcal{L}^{-1}\{H(x, s)\bar{\varphi}(s)\} \tag{32}$$

Nevertheless, some time domain simulations could be made without using approximations. In fact, three time domain simulations for three well known input types are proposed: the impulse, the step and the sinusoidal inputs.

4.5.1. Impulse Response

The impulse response is obtained by substituting $H(x, s)$ by its value shown in (Eq. 12) and $\bar{\varphi}(s)$ by $\mathcal{L}\{\delta(t)\} = 1$. Accordingly, the impulse response is given by:

$$T(x,t) = \mathcal{L}^{-1}\left(\frac{1}{\sqrt{\lambda \rho C_p s}} \; e^{-x\sqrt{s/\alpha}}\right) = \mathcal{L}^{-1}\left(\frac{H_0}{\sqrt{s}} \; e^{-x\sqrt{s/\alpha}}\right) \tag{33}$$

Knowing that (Battaglia, 2008):

$$\mathcal{L}^{-1}\left(\frac{1}{\sqrt{s}} \; e^{-a\sqrt{s}}\right) = \frac{1}{\sqrt{\pi t}} \; e^{\left(\frac{-a^2}{4t}\right)} \tag{34}$$

where $a > 0$, the impulse response can be presented as follows:

$$T(x,t) = \frac{H_0}{\sqrt{\pi t}} \; e^{\left(\frac{-x^2}{4\alpha t}\right)} \tag{35}$$

Figure 5 shows the outputs for the impulse at different locations of x and different values of t in a semi-infinite aluminum medium.

4.5.2. Step Response

The step $u(t)$ response of magnitude U_0 is obtained by substituting $H(x,s)$ by its value shown in (Eq. 12) and $\bar{\varphi}(s)$ by $\mathcal{L}\{u(t)\} = U_0/s$. Accordingly, the step response is given by:

$$(x,t) = \mathcal{L}^{-1}\left(\frac{1}{\sqrt{\lambda \rho C_p s}} \; e^{-x\sqrt{s/\alpha}} \frac{U_0}{s}\right) = \mathcal{L}^{-1}\left(\frac{H_0 U_0}{s^{3/2}} \; e^{-x\sqrt{s/\alpha}}\right) \tag{36}$$
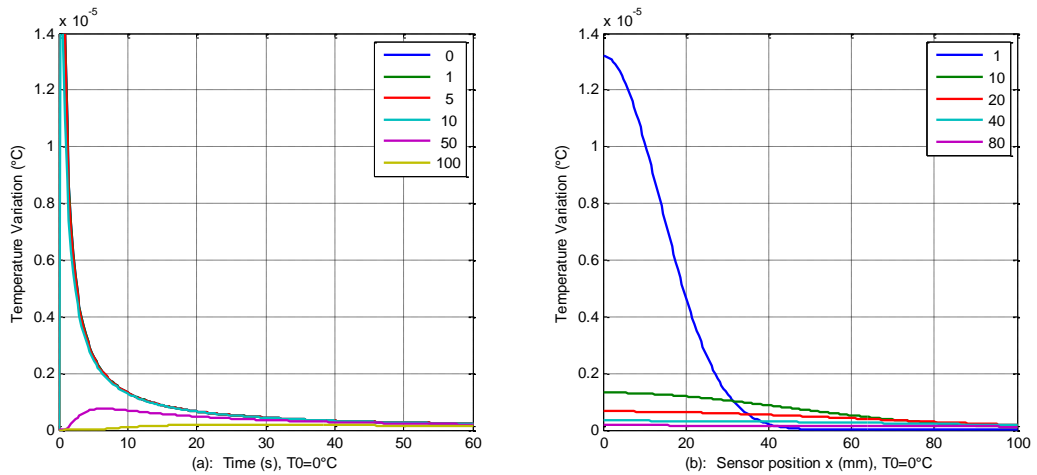
Figure 5. Impulse responses of $T(x,t)$ for (a) $x = 0\,mm, 1mm, 5mm, 10mm, 50mm$ and $100mm$; and (b) $t = 1s, 10s, 20s, 40s$ and $80s$.

Knowing that (Battaglia, 2008):

$$\mathcal{L}^{-1}\left(\frac{1}{s^{3/2}} \; e^{-a\sqrt{s}}\right) = 2\sqrt{\frac{t}{\pi}} \; e^{\left(\frac{-a^2}{4t}\right)} - a.erfc\left(\frac{a}{2\sqrt{t}}\right) \tag{37}$$

where $erfc(\cdot)$ is the complementary error function and $a > 0$, the step response can be presented as follows:

(a): Time (s), T0=0°C, Flux=2000W/m^2

(b): Sensor position x (mm), T0=0°C, Flux=2000W/m^2
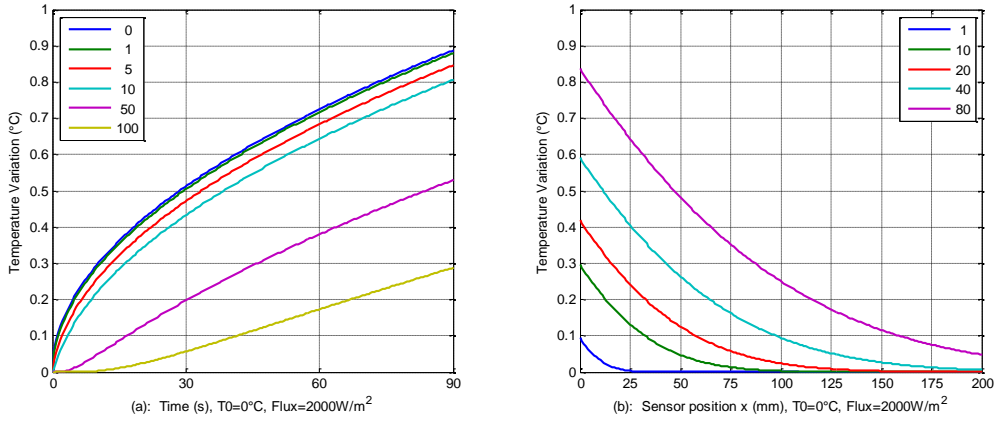
Figure 6. Step responses of $T(x,t)$ for (a) $x = 0mm, 1mm, 5mm, 10mm, 50mm$ and $100mm$; and (b) $t = 1s, 10s, 20s, 40s$ and $80s$.

$$T(x,t) = H_0 U_0 \left(2\sqrt{\frac{t}{\pi}} e^{\left(\frac{-x^2}{4\alpha t}\right)} - \frac{x}{\sqrt{\alpha}} erfc\left(\frac{x}{2\sqrt{\alpha t}}\right) \right) \tag{38}$$

Figure 6 shows the outputs for the step function at different locations of x and different values of t in a semi-infinite aluminum medium.

4.5.3. Stationary Harmonic Response

The entry at $x = 0$ is supposed to be

$$\varphi(t) = \varphi_0 cos(\omega t). \tag{39}$$

The system being supposed linear, the expression of the output temperature is given by:

$$T(x,t,\omega) = \varphi_0 |H(x,j\omega)| cos\left(\omega t + arg\big(H(x,j\omega)\big)\right) \tag{40}$$

then replacing $H(x,j\omega)$ by its value in (Eq. 29)

$$T(x,t,\omega) = \varphi_0 \frac{H_0}{\omega^{0.5}} e^{-\left(\frac{\omega}{2\omega_x}\right)^{0.5}} cos\left(\omega t + arg\left(e^{-j\left(\frac{\omega}{2\omega_x}\right)^{0.5}}\right)\right) \tag{41}$$

Let

$$\Omega = \omega/2\alpha \text{ and } \Omega_1 = H_0{}^2/2\alpha \tag{42}$$

Then

$$T(x,t,\Omega) = \varphi_0 \left(\frac{\Omega_1}{\Omega}\right)^{0.5} e^{-\sqrt{\Omega}x} cos\left(2\alpha\,\Omega\,t - \frac{\pi}{4} - \sqrt{\Omega}x\right) \tag{43}$$
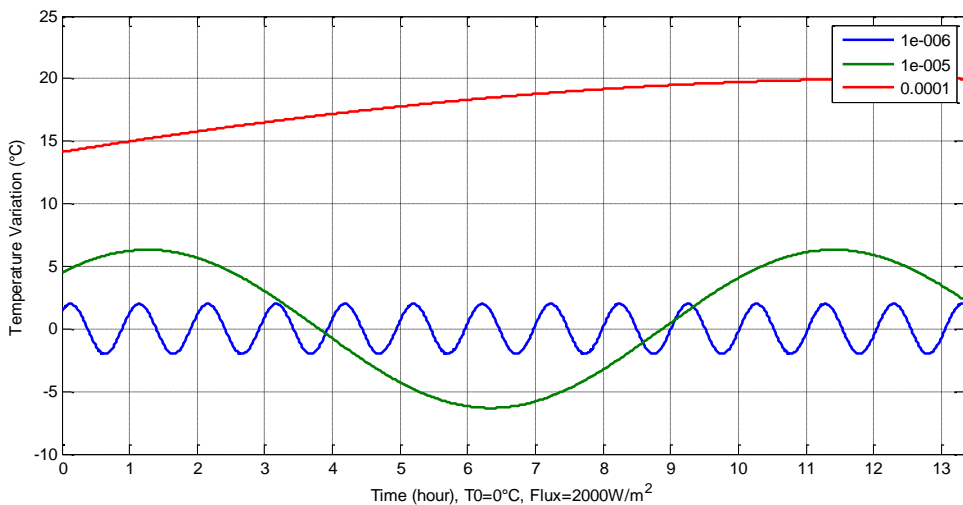
Figure 7. Harmonic responses of $T(0,t,\Omega)$ for $(\Omega_1/\Omega) \in \{10^{-4}, 10^{-5}, 10^{-6}\}$ and $\varphi_0 = 2\,kW/m^2$.

At $x = 0$:

$$T(0,t,\Omega) = \varphi_0 \left(\frac{\Omega_1}{\Omega}\right)^{0.5} cos\left(2\alpha\,\Omega\,t - \frac{\pi}{4}\right). \tag{44}$$

Figure 7 illustrates the outputs for a harmonic function input for different values of $(\Omega_1/\Omega) \in \{10^{-4}, 10^{-5}, 10^{-6}\}$ and for $\varphi_0 = 2\,kW/m^2$ in a semi-infinite aluminum medium.
At $\boldsymbol{x} > \boldsymbol{0}$:

In order to make the analysis easier, let's consider the temperature at $x = 0$ as a reference, thus we can write:

$$T(0,t,\Omega) = T_0\,cos(2\alpha\,\Omega\,t). \tag{45}$$

Hence the temperature at $x > 0$ will be written as:

$$T(x,t,\Omega) = T_0\,e^{-\sqrt{\Omega}x}cos(2\alpha\,\Omega\,t - \sqrt{\Omega}x). \tag{46}$$

For illustration purposes, let $T_0 = 1°C$ with $0 < x < 1m$. Figure 8 shows the outputs for a harmonic function input for different values of $\Omega \in \{0.001, 0.01, 0.1, 1, 10, 100\}$ in a semi-infinite aluminum medium.
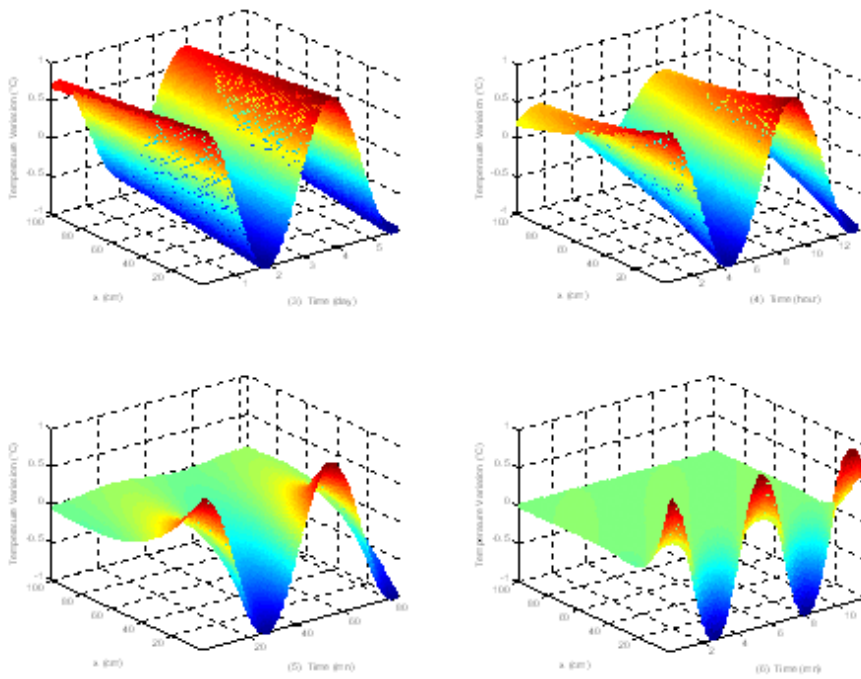
Figure 8. Harmonic responses of $T(x,t,\Omega)$ when $T_0 = 1°C$, for (1): $\Omega = 0.001$, (2): $\Omega = 0.01$, (3): $\Omega = 0.1$, (4): $\Omega = 1$, (5): $\Omega = 10$ and (6): $\Omega = 100$.
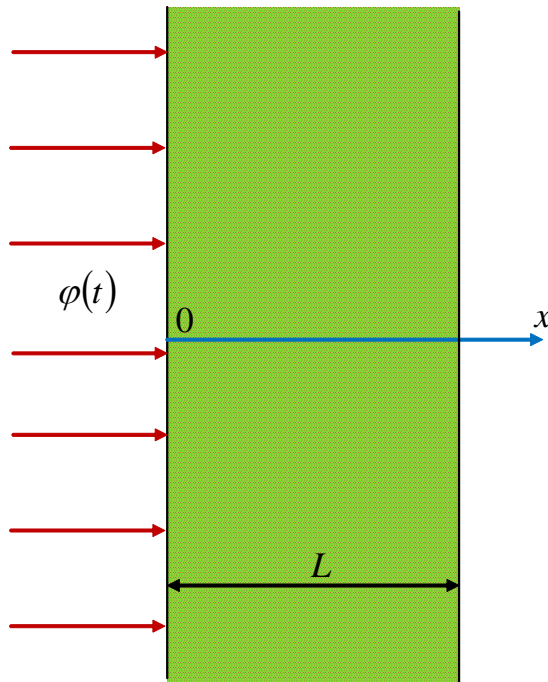
Figure 9. Finite unidirectional plane of thickness L.

Note that, as long as the frequency of variation of the temperature ω is low relatively to the diffusivity α, the temperature variation is uniform and harmonic.

When the frequency of variation of the temperature ω increases, the diffusion depth of the temperature decreases in the semi-infinite medium.

5. Finite Plane

We consider a finite, homogeneous, isotropic, one-dimensional plane medium of thickness L, conductivity λ, diffusivity α, and of initial temperature zero all over the medium (Figure 9). A heat flux $\varphi(t)$ is normally applied on its surface at $x = 0$; it is assumed that there are no losses at this point. Consequently, a temperature gradient $T(x,t)$ appears, which is a function of the independent time variable t as well as the abscissa x of the temperature measurement point, with $x \in [0; L]$ inside the medium.

5.1. System Definition

The one-dimensional heat conduction equation (Özişik, 1985) is given by a partial differential equation:

$$\frac{\partial T(x,t)}{\partial t} = \alpha \frac{\partial^2 T(x,t)}{\partial x^2}, \; 0 < x < L, \; t > 0. \tag{47}$$

Since the initial temperature is zero all over the medium:

$$T(x,t) = 0, \; 0 \leq x < L, \; t = 0 \; . \tag{48}$$

The Fourier law states the boundary conditions (Özişik, 1985) where the flux is applied, as well as at the second end:

$$-\lambda \frac{\partial T(x,t)}{\partial x} = \varphi(t), \; x = 0, \; t > 0 \tag{49}$$

$$-\lambda \frac{\partial T(x,t)}{\partial x} = 0, \; x = L, \; t > 0 \; . \tag{50}$$

5.2. System Resolution

The system of (Eq. 47-50) represents the relations that model the diffusive interface knowing that the input signal is the flux $\varphi(t)$ whereas the output signal is the temperature $T(x,t)$ as shown in Figure 9.

The initial condition of the temperature being zero, Laplace transform $\mathcal{L}\{\cdot\}$ of (Eq. 47) is:

$$\frac{\partial^2 \overline{T}(x,s)}{\partial x^2} - \frac{s}{\alpha} \overline{T}(x,s) = 0, \text{ where } \overline{T}(x,s) = \mathcal{L}\{T(x,t)\} \tag{51}$$

The solution of (*Eq. 51*) is similar to the previous case, hence:

$$\bar{T}(x,s) = K_1(s)e^{x\sqrt{s/\alpha}} + K_2(s)e^{-x\sqrt{s/\alpha}} \ . \tag{52}$$

Resolving (Eq. 52) for the boundary conditions (Eq. 49-50) gives the values of $K_1(s)$ and $K_2(s)$, let:

$$\begin{cases} K_1(s) - K_2(s) = -\dfrac{1}{\lambda\sqrt{\frac{s}{\alpha}}} \ \bar{\varphi}(s) \\[2ex] K_1(s)e^{L\sqrt{\frac{s}{\alpha}}} - K_2(s)e^{-L\sqrt{\frac{s}{\alpha}}} = 0 \end{cases} \tag{53}$$

Taking into consideration the definitions of the characteristic parameters and the outcome of (Eq. 53), thus:

$$\begin{cases} K_1(s) = \dfrac{1}{\sqrt{\lambda\rho C_p s}} \ \dfrac{e^{-L\sqrt{s/\alpha}}}{e^{L\sqrt{s/\alpha}} - e^{-L\sqrt{s/\alpha}}} \ \bar{\varphi}(s) \\[2ex] K_2(s) = \dfrac{1}{\sqrt{\lambda\rho C_p s}} \ \dfrac{e^{L\sqrt{s/\alpha}}}{e^{L\sqrt{s/\alpha}} - e^{-L\sqrt{s/\alpha}}} \ \bar{\varphi}(s) \end{cases} \tag{54}$$

then the solution of (Eq. 51) is found to be:

$$\bar{T}(x,s) = \dfrac{1}{\sqrt{\lambda\rho C_p s}} \ \dfrac{e^{(x-L)\sqrt{s/\alpha}} + e^{(L-x)\sqrt{s/\alpha}}}{e^{L\sqrt{s/\alpha}} - e^{-L\sqrt{s/\alpha}}} \ \bar{\varphi}(s) \ . \tag{55}$$

Under the assumption of an initial condition of the temperature being zero, the transfer function $H(x,s)$ between the input flux $\bar{\varphi}(s)$ and the output temperature $\bar{T}(x,s)$ is:

$$H(x,s,L) = \dfrac{\bar{T}(x,s)}{\bar{\varphi}(s)} = \dfrac{1}{\sqrt{\lambda\rho C_p s}} \ \dfrac{e^{(x-L)\sqrt{s/\alpha}} + e^{(L-x)\sqrt{s/\alpha}}}{e^{L\sqrt{s/\alpha}} - e^{-L\sqrt{s/\alpha}}} \ , \tag{56}$$

then, introducing the hyperbolic functions $cosh$ and $tanh$ the transfer function $H(x,s)$ becomes:

$$H(x,s,L) = \dfrac{\bar{T}(x,s)}{\bar{\varphi}(s)} = \dfrac{1}{\sqrt{\lambda\rho C_p s}} \ \dfrac{1}{tanh\left(L\sqrt{s/\alpha}\right)} \ \dfrac{cosh\left((L-x)\sqrt{s/\alpha}\right)}{cosh\left(L\sqrt{s/\alpha}\right)} \ , \tag{57}$$

or rewritten as:

$$H(x,s,L) = H_0 \, I^{0.5}(s) \, F(0,s,L) \, G(x,s,L) \ , \tag{58}$$

where:

$$\begin{cases} H_0 = \dfrac{s^{0.5}\overline{T}(0,s,\infty)}{\overline{\varphi}(s)} = \dfrac{1}{\sqrt{\lambda \rho C_p}} = \dfrac{1}{T_{iu}} \\[2mm] I^{0.5}(s) = \dfrac{\overline{T}(0,s,\infty)}{s^{0.5}\overline{T}(0,s,\infty)} = \dfrac{1}{s^{0.5}} \\[2mm] F(0,s,L) = \dfrac{\overline{T}(0,s,L)}{\overline{T}(0,s,\infty)} = \dfrac{1}{tanh\left(\sqrt{s/\omega_L}\right)} \\[4mm] G(x,s,L) = \dfrac{\overline{T}(x,s,L)}{\overline{T}(0,s,L)} = \dfrac{cosh\left(\sqrt{s/\omega_{Lx}}\right)}{cosh\left(\sqrt{s/\omega_L}\right)} \end{cases} \qquad (59)$$

with the following considerations:

$$\begin{cases} w_l = \dfrac{1}{\lambda \rho C_p} = \left(\dfrac{1}{T_{iu}}\right)^2 = H_0{}^2 \\[2mm] \omega_L = \dfrac{\alpha}{L^2} \\[2mm] \omega_{Lx} = \dfrac{\alpha}{(L-x)^2} \end{cases} \qquad (60)$$

One can derive from (Eq. 60) that ω_L and ω_{Lx} are linked by the following relation:

$$\omega_L = \left(1 - \frac{x}{L}\right)^2 \omega_{Lx}. \qquad (61)$$

One can derive also the thermal diffusion time constant defined as:

$$\tau_d = \frac{1}{\omega_L} = \frac{L^2}{\alpha}. \qquad (62)$$

To clarify, the different temperatures found in the system (Eq. 59) are as follows:

- $\overline{T}(0,s,\infty)$ is the measured temperature at $x = 0$ if the medium is considered to be a semi-infinite medium.
- $\overline{T}(0,s,L)$ is the measured temperature at $x = 0$ of the finite medium of length L.
- $\overline{T}(x,s,L)$ is the measured temperature at x, $\forall\, x \in [0; L]$.

Consequently, the transfer function $H(x,s,L)$ of the system can be seen as four cascading functions represented in (Figure 10).

The function H_0 depends on the medium physical characteristics, it links the input flux $\overline{\varphi}(s)$ and the fractional derivative of order 0.5 of the temperature at $x = 0$.

Then, $I^{0.5}(s)$ is a fractional integrator of order 0.5 that gives the temperature at $x = 0$. Its output is the temperature $\overline{T}(0,s,\infty)$.

The third block is the transfer function $F(0,s,L)$ between the temperatures $\overline{T}(0,s,\infty)$ and $\overline{T}(0,s,L)$.

The fourth part is the transfer function $G(x, s, L)$ having as input $\bar{T}(0, s, L)$ and as output the temperature $\bar{T}(x, s, L)$.
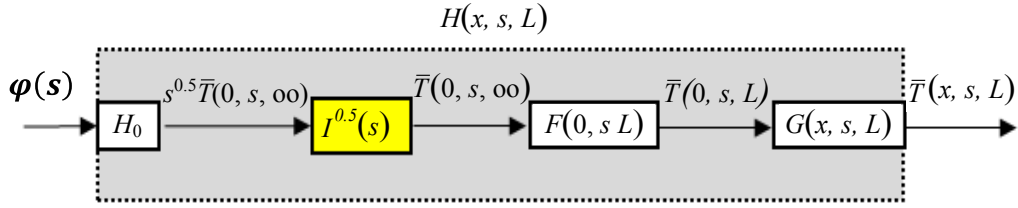
$$H(x, s, L)$$

Figure 10. Block diagram illustrating the transfer function $H(x, s, L)$ of the finite medium.

6. Responses in Finite Plane

6.1. Asymptotic Behavior Analysis at $x = 0$

At $x = 0$, $G(x, s, L) = G(0, s, L) = 1$, thus the temperature $\bar{T}(0, s, L)$ of the finite medium of length L is given by:

$$\bar{T}(0, s, L) = H_0\, I^{0.5}(s)\, F(0, s, L)\, \bar{\varphi}(s). \tag{63}$$

The transfer function $F(0, s, L)$ allows the analysis of the influence of the medium finite character on the temperature at $x = 0$. As such, let the change of variable $z = \sqrt{s/\omega_L}$. Considering the definitions in *(Para 2.)* and (Eq. 60, 61), as a start the following is verified: if $L \to \infty$ then $z \to \infty$, as $\lim_{z \to \infty} tanh(z) = 1$, thus $\lim_{L \to \infty} F(0, s, L) = 1$, accordingly it is found that:

$$\lim_{L \to \infty} H(0, s, L) = H_0\, I^{0.5}(s) \tag{64}$$

which is a result similar to what was found in a semi-infinite medium at $x = 0$.

Now consider when $s \to 0$ then $\to 0$, as $\lim_{z \to 0} tanh(z) = z$, thus:
$\lim_{s \to 0} F(0, s, L) = \dfrac{1}{\sqrt{s/\omega_L}}$, accordingly it is found that:

$$\lim_{s \to 0} H(0, s, L) = \frac{H_0\, I^{0.5}(s)}{\sqrt{s/\omega_L}} \tag{65}$$

Once again, considering the definitions in *(Para 2.)* and (Eq. 60, 61), the (Eq. 65) is rewritten as:

$$\lim_{s \to 0} H(0, s, L) = \frac{1}{C_{th}s}\ . \tag{66}$$

Thus for high instances, corresponding to low frequencies (i.e. $s \to 0$), the asymptotic behavior of a finite medium is of capacitive type characterized by an integrator of order 1. It is different than the behavior in a semi-infinite medium characterized by a fractional integrator of order 0.5.

For low instances, corresponding to high frequencies, when $s \to \infty$ then $\to \infty$, as $\lim_{z \to \infty} tanh(z) = 1$, thus:

$$\lim_{s \to \infty} H(0, s, L) = H_0 \, I^{0.5}(s) \tag{67}$$

Accordingly an asymptotic fractional order behavior appears when $s \to \infty$ between the input flux and the temperature at the boundary where the flux is applied; in fact, it is the same result that appears in the semi-infinite medium.

6.2. Asymptotic Behavior Analysis for $0 < x \leq L$

For high instances, corresponding to low frequencies, when $s \to 0$ then $\lim_{s \to 0} G(x, s, L) = 1$, thus:

$$\lim_{s \to 0} H(x, s, L) = \frac{1}{C_{th}s} \tag{68}$$

The same asymptotic behavior applies as at $x = 0$. It is of capacitive type characterized by an integrator of order 1; it is different than the behavior in a semi-infinite medium characterized by a fractional integrator of order 0.5.

For low instances, corresponding to high frequencies, when $s \to \infty$ then $\to \infty$, as $\lim_{z \to \infty} e^{-z} = 0$, thus $\lim_{s \to \infty} G(x, s, L) = \dfrac{e^{\sqrt{s/\omega_{Lx}}}}{e^{\sqrt{s/\omega_L}}}$; it is resolved introducing (Eq. 61) a relation between ω_{Lx} and ω_L; accordingly:

$$\lim_{s \to \infty} G(x, s, L) = e^{-\sqrt{\frac{s}{\alpha/x^2}}} = e^{-\sqrt{\frac{s}{\omega_x}}} \tag{69}$$

then,

$$\lim_{s \to \infty} H(x, s, L) = \lim_{s \to \infty} H_0 \, I^{0.5}(s) \, e^{-\sqrt{\frac{s}{\omega_x}}} = 0 \tag{70}$$

It is the same asymptotic behavior as it appears in a semi-infinite medium.

6.3. Frequency Response Analysis at $x = 0$

Now that the mathematical model is established, frequency domain analyses $(s = j\omega)$ can be done. The resulting transfer function $H(x, j\omega, L)$ is the concatenation of four cascading

blocks as shown on the (Figure 10) and represented in the (*Eq. 58-60*). When the study is on the boundary where the flux is applied, $x = 0$, the transfer function is expressed by:

$$H(0, j\omega, L) = H_0 \, I^{0.5}(j\omega) \, F(0, j\omega, L) \, G(0, j\omega, L) \tag{71}$$

with $G(0, j\omega, L) = 1$, then $H(0, j\omega, L)$ reduces to::

$$H(0, j\omega, L) = H_0 \, I^{0.5}(j\omega) \, F(0, j\omega, L) \tag{72}$$

Bode diagrams of the classic fractional integrator of order 0.5 in a finite aluminum medium are represented in Figure 11.

The frequency response study of the function $F(0, j\omega, L)$ allows understanding the influence of the finite character of the medium on the temperature at $x = 0$. Actually Figure 12 represents Bode diagrams of this transfer for three different values of $L \in \{1,10,100\}cm$ in a finite aluminum medium.
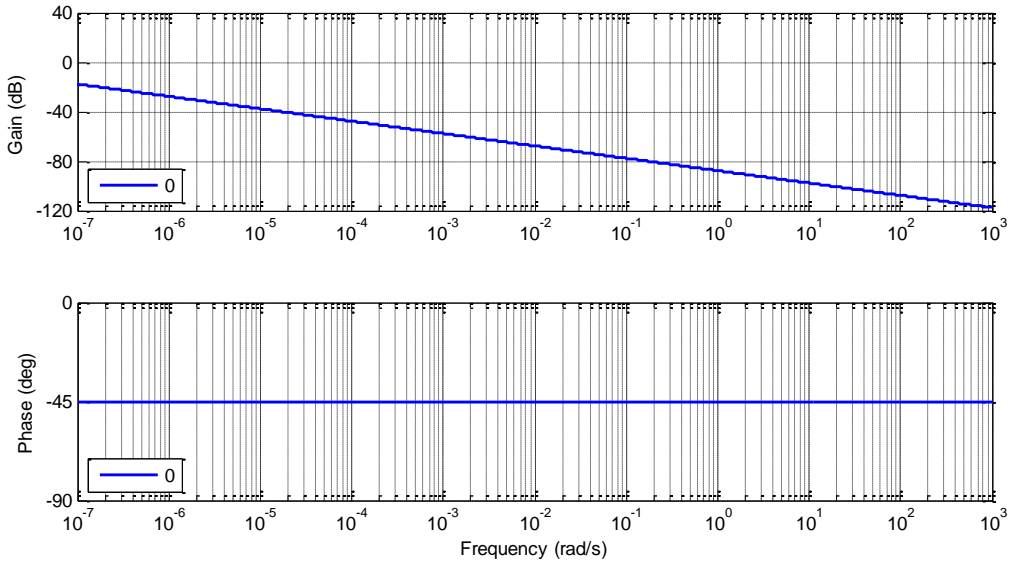
Figure 11. Bode diagrams of $H_0 I^{0.5}(j\omega)$ in a finite medium at $x = 0$.

Two asymptotic behaviors clearly appear:

At the low frequencies, a fractional integration behavior of order 0.5 prevails. Actually, $\forall \omega \ll \omega_L = \frac{\alpha}{L^2}$, $F(0, j\omega, L)_{\omega \ll \omega_L} \approx \left(\frac{\omega_L}{j\omega}\right)^{0.5} \Rightarrow$

$$\begin{cases} |F(0, j\omega, L)| = \left(\frac{\omega_L}{\omega}\right)^{0.5} \\ arg\big(F(0, j\omega, L)\big) = -\frac{\pi}{4} \end{cases} \tag{73}$$

t the high frequencies, a proportional behavior prevails. Actually, $\forall \omega \gg \omega_L = \frac{\alpha}{L^2}$, $F(0, j\omega, L)_{\omega \gg \omega_L} = 1 \Rightarrow$

$$\begin{cases} |F(0, j\omega, L)| = 1 \\ arg\big(F(0, j\omega, L)\big) = 0 \end{cases} \tag{74}$$

The transitional zone between the two asymptotic behaviors is four decades wide and it is centered on the transitional frequency ω_L.
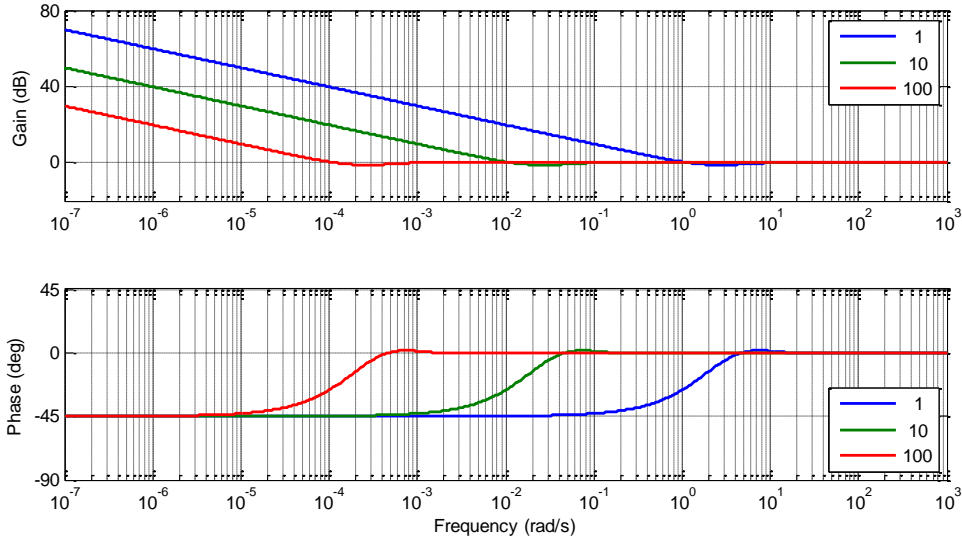
Figure 12. Bode diagrams of $of\ F(0, j\omega, L)\ for\ L \in \{1, 10, 100\} cm$.

Now it is time to study the influence of each of the three cascading blocks on the global transfer function $H(0, j\omega, L)$. For this purpose, for $x = 0$ and $L = 1m$, Figure 13 visualizes the contribution of each block to the global response in a finite aluminum medium.

Two asymptotic behaviors clearly appear:

At the low frequencies, an integration behavior of order 1 prevails. Actually, $\forall \omega \ll \omega_L = \frac{\alpha}{L^2}$, $H(0, j\omega, L)_{\omega \ll \omega_L} \approx \frac{1}{C_{th} j\omega} \Rightarrow$

$$\begin{cases} |H(0, j\omega, L)| = \frac{1}{C_{th} \omega} \\ arg\big(H(0, j\omega, L)\big) = -\frac{\pi}{2} \end{cases} \tag{75}$$
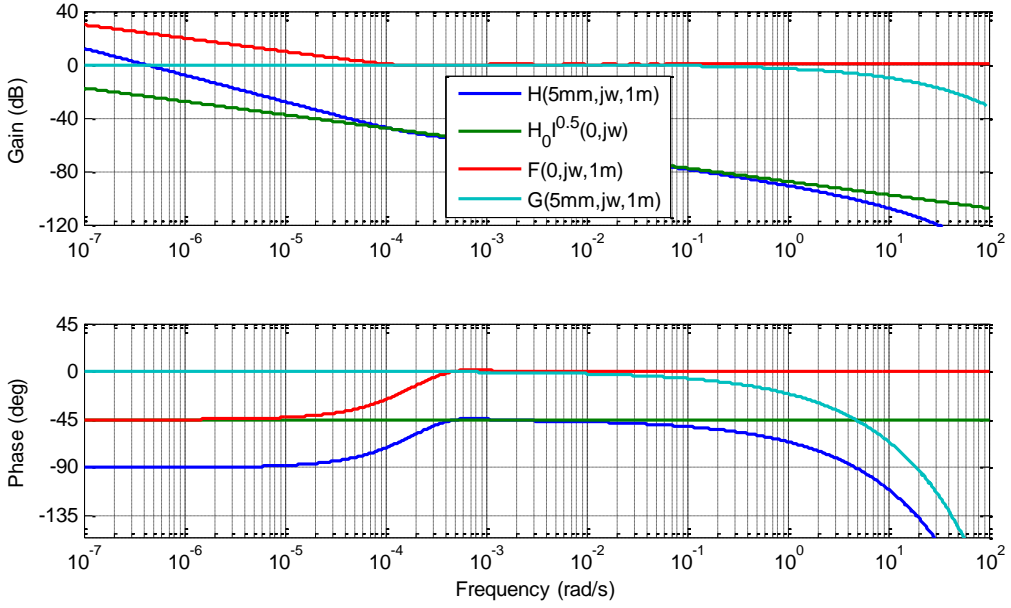
At the high frequencies, a fractional integration behavior of order 0.5 prevails. Actually, $\forall \omega \gg \omega_L = \frac{\alpha}{L^2}$, $H(0, j\omega, L)_{\omega \gg \omega_L} = \left(\frac{w_l}{j\omega}\right)^{0.5} \Rightarrow$

$$\begin{cases} |H(0, j\omega, L)| = \left(\frac{w_l}{\omega}\right)^{0.5} \\ arg\big(H(0, j\omega, L)\big) = -\frac{\pi}{4} \end{cases} \tag{76}$$

Here also, the transitional zone between the two asymptotic behaviors is four decades wide and it is centered on the transitional frequency ω_L.
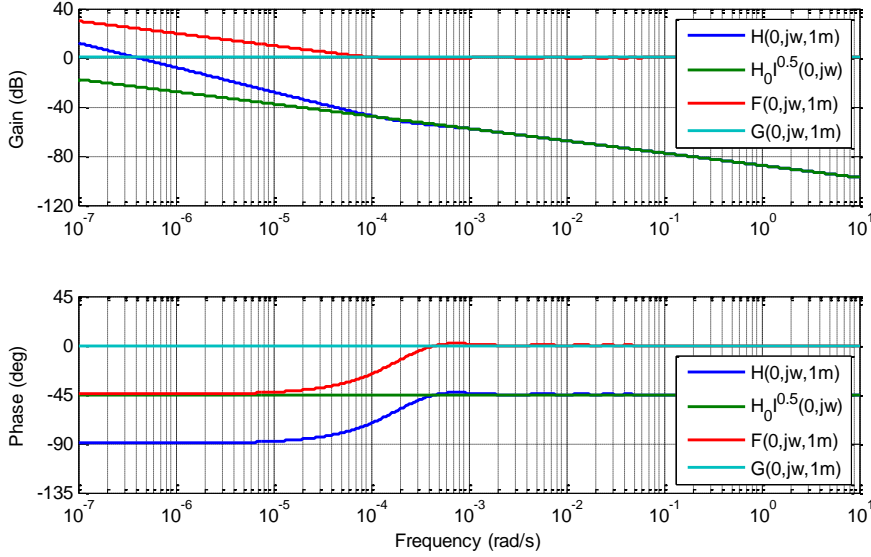
Figure 13. Bode diagrams of $H(0, j\omega, L), H_0 I^{0.5}(j\omega), F(0, j\omega, L)$ and $G(0, j\omega, L)$.

For different values of $L \in \{1,10,100\}cm$, (Figure 14 represents the respective Bode diagrams in a finite aluminum medium illustrating the translation of the transitional zone towards the high frequencies when L decreases.
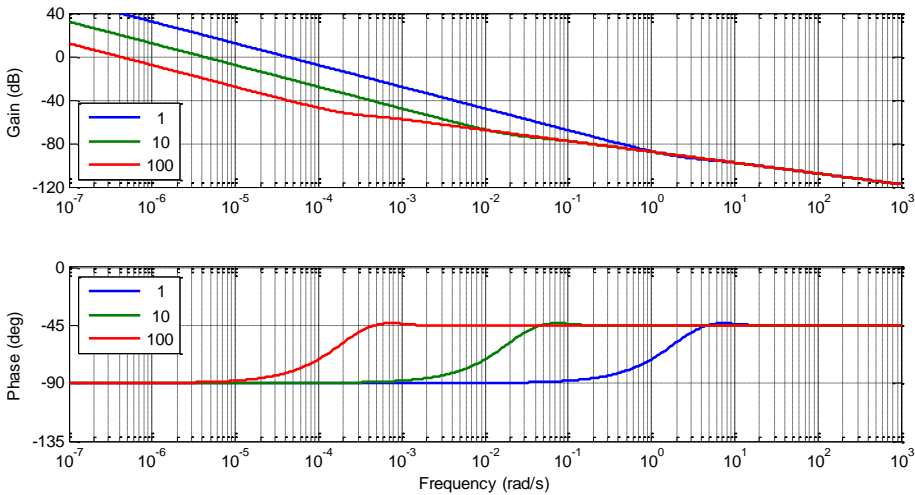
Figure 14. Bode diagrams of $H(0, j\omega, L)$ for $L \in \{1,10,100\}cm$.

For different values of $L \in \{1,10,100\}cm$, Figure 15 represents respectively $H(0, s, L)$ in Black-Nichols plane in a finite aluminum medium.

6.4. Frequency Behavior Analysis for $0 < x \leq L$

For $0 < x \leq L$, $G(x, j\omega, L) \neq 1$. Thus it is interesting to begin with the study of its frequency behavior in order to understand its influence on the global response $H(x, j\omega, L)$. (Eq. 56-59) reformulate the expression of the third block:

$$G(x, s, L) = \frac{e^{(x-L)\sqrt{s/\alpha}} + e^{(L-x)\sqrt{s/\alpha}}}{e^{L\sqrt{s/\alpha}} - e^{-L\sqrt{s/\alpha}}} \tag{77}$$

Figure 16 represents Bode diagrams of the transfer of $G(x, j\omega, L)$ for a finite aluminum medium of length $L = 1m$ and for four different values x of the temperature sensor position, let $x \in \{0,5,10,50\}mm$.

Two behaviors clearly appear:

At the low frequencies,

$$\lim_{\omega \to 0} G(x, j\omega, L) = 1 \Rightarrow \begin{cases} |G(x, j\omega, L)| = 1 \\ arg\big(G(x, j\omega, L)\big) = 0 \end{cases} \tag{78}$$
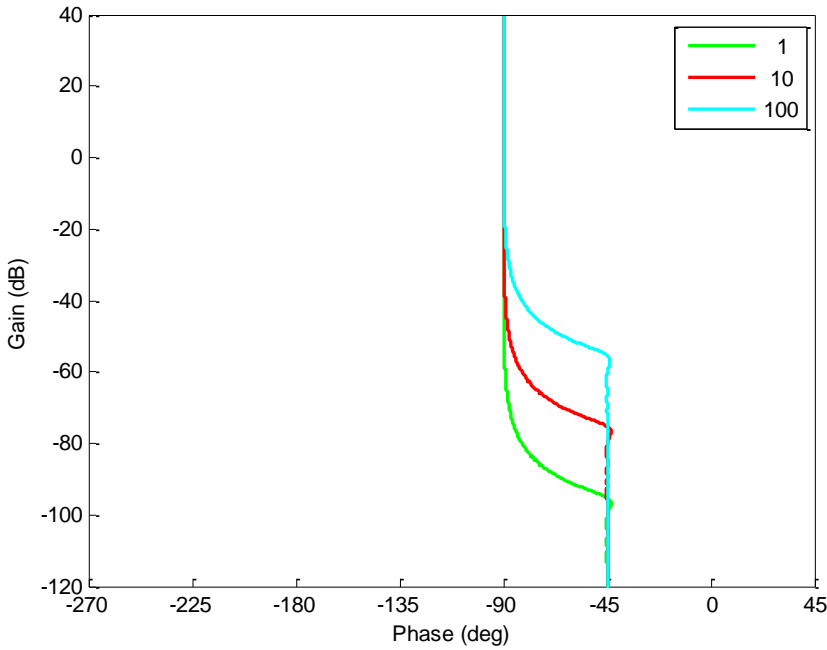
Figure 15. Black-Nichols plots of $H(0, j\omega, L)$ for $L \in \{1,10,100\}cm$.
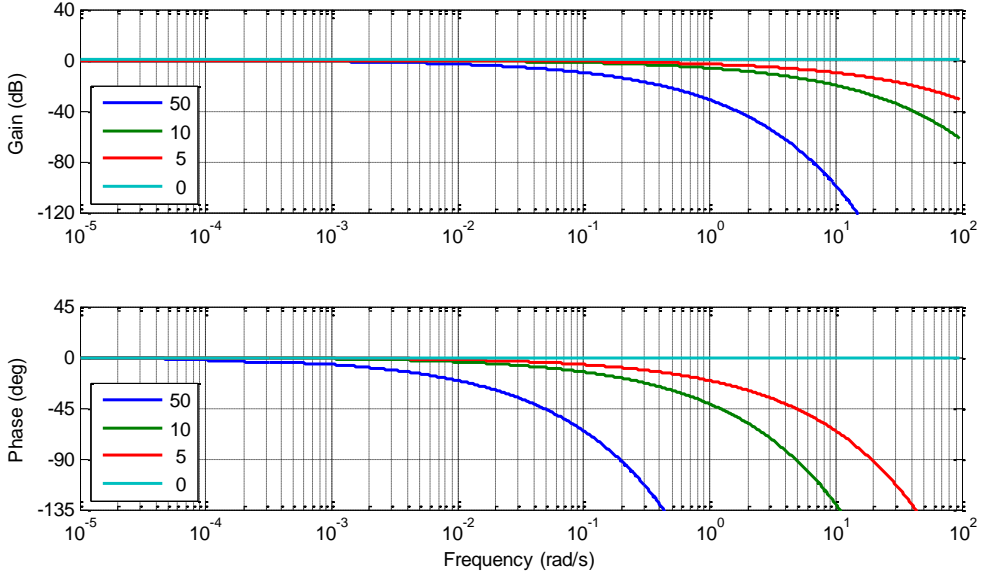
Figure 16. Bode diagrams of $G(x, j\omega, L)$ for $x \in \{0,5,10,50\} mm$.

At the high frequencies,

$$\lim_{\omega \to \infty} G(x, j\omega, L) = e^{-\sqrt{j\frac{\omega}{\omega_x}}} \Rightarrow \begin{cases} |G(x, j\omega, L)| \approx e^{-\left(\frac{\omega}{2\omega_x}\right)^{0.5}} = 0 \\ arg\big(G(x, j\omega, L)\big) \approx -\left(\frac{\omega}{2\omega_x}\right)^{0.5} = -\infty \end{cases} \quad (79)$$

In order to make the analysis easier, a special frequency ω_c is introduced; it is defined as:

$$|G(x, j\omega_c, L)| = 1/\sqrt{2} \Rightarrow -3dB \quad (80)$$

The frequency ω_c decreases when x increases. This is why, for a given frequency ω, the gain and the phase are as smaller as x is big as it is evident in Figure 16.

Now it is time to study the influence of each of the four cascading blocks on the global transfer function $H(x, j\omega, L)$. For this purpose, for $x = 5mm$ and $L = 1m$, Figure 17 visualizes the contribution of each block to the global response in a finite aluminum medium.

Three behaviors clearly appear:

At the low frequencies, an integration behavior of order 1 prevails similar to the one found at $x = 0$. Actually, $\forall \omega \ll \omega_L = \frac{\alpha}{L^2}$, $H(x, j\omega, L)_{\omega \ll \omega_L} \approx \frac{1}{C_{th}j\omega} \Rightarrow$

$$\begin{cases} |H(x, j\omega, L)| = \frac{1}{C_{th}\omega} \\ arg\big(H(x, j\omega, L)\big) = -\frac{\pi}{2} \end{cases} \quad (81)$$

Figure 17. Bode diagrams of $H(x, j\omega, L), H_0 I^{0.5}(j\omega), F(0, j\omega, L)$ and $G(x, j\omega, L)$.

At the medium frequencies, a fractional integration behavior of order 0.5 prevails. Actually, $\omega_L \ll \omega \ll \omega_c$, $H(x, j\omega, L) \approx I^{0.5}(j\omega) \Rightarrow$

$$\begin{cases} |H(x, j\omega, L)| = \left(\frac{w_l}{\omega}\right)^{0.5} \\ arg\big(H(x, j\omega, L)\big) = -\frac{\pi}{4} \end{cases} \tag{82}$$

At the high frequencies, a behavior identical to the one in the semi-infinite medium prevails. Actually, $\forall \omega \gg \omega_c, H(x, j\omega, L)_{\omega \gg \omega_c} \approx I^{0.5}(j\omega)e^{-\sqrt{j\frac{\omega}{\omega_x}}} \Rightarrow$

$$\begin{cases} |H(x, j\omega, L)| \approx \left(\frac{w_l}{\omega}\right)^{0.5} e^{-\left(\frac{\omega}{2\omega_x}\right)^{0.5}} \\ arg\big(H(x, j\omega, L)\big) \approx -\frac{\pi}{4} - \left(\frac{\omega}{2\omega_x}\right)^{0.5} \end{cases} \tag{83}$$

Figure 18 represents Bode diagrams of the transfer of $H(x, j\omega, L)$ for a finite aluminum medium of length $L = 1m$ and for four different values x of the temperature sensor position, let $x \in \{0,5,10,50\}mm$.

For a finite aluminum medium of length $L = 1m$ and for four different values x of the temperature sensor position, let $x \in \{0,5,10,50\}mm$, Figure 19 represents respectively $H(x, s, L)$ in Black-Nichols plane.
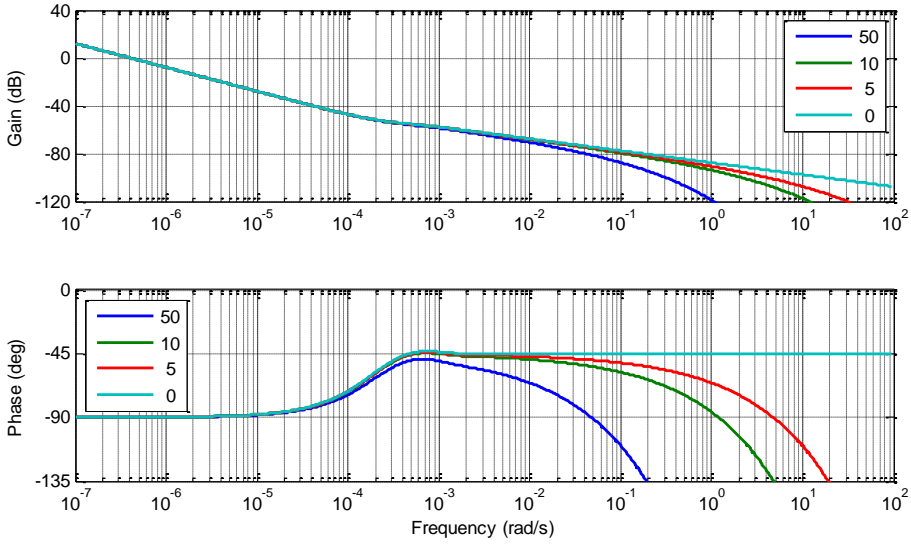
Figure 18. Bode diagrams of $H(x, j\omega, L)$ for $x \in \{0,5,10,50\}mm$.
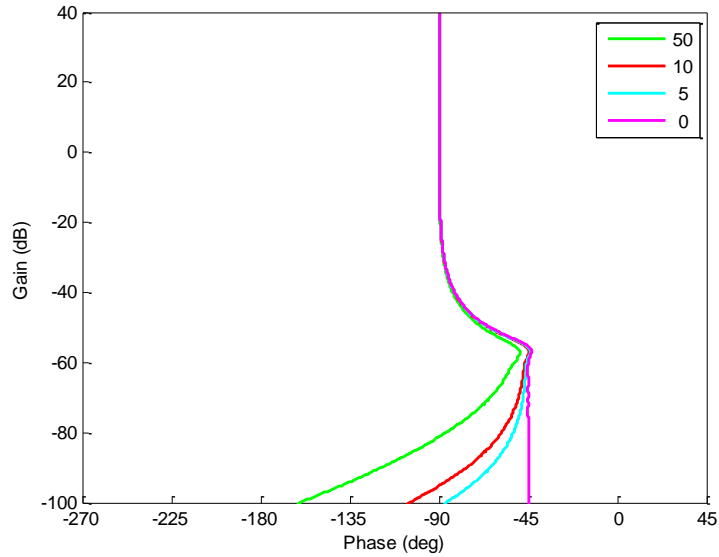
Figure 19. Black-Nichols plots of $H(x, j\omega, L)$ for $x \in \{0,5,10,50\}mm$.

7. Simulink Responses

In this last part of the chapter, the *Simulink* responses will be presented for both the semi-infinite and the finite aluminum media. For both cases, the exact system is implemented on *Simulink*.

So, Figure 20 shows the *Simulink* system whereas Figure 21 represents the temperature variation with respect to time for different values of the sensor placement.
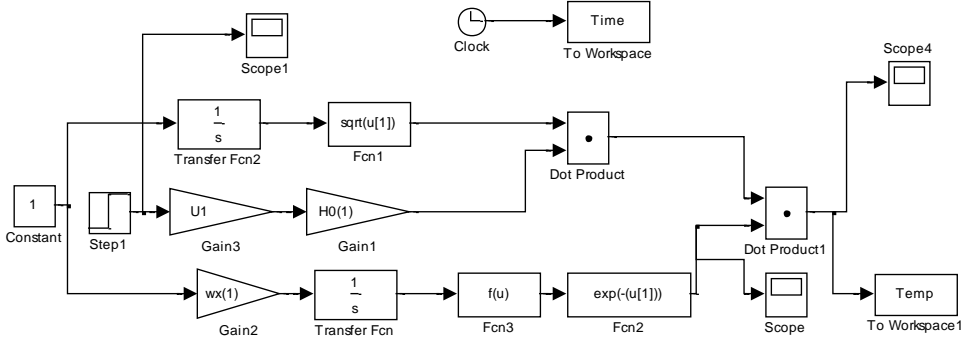
Figure 20. Simulink representation for the semi-infinite homogeneous plane.
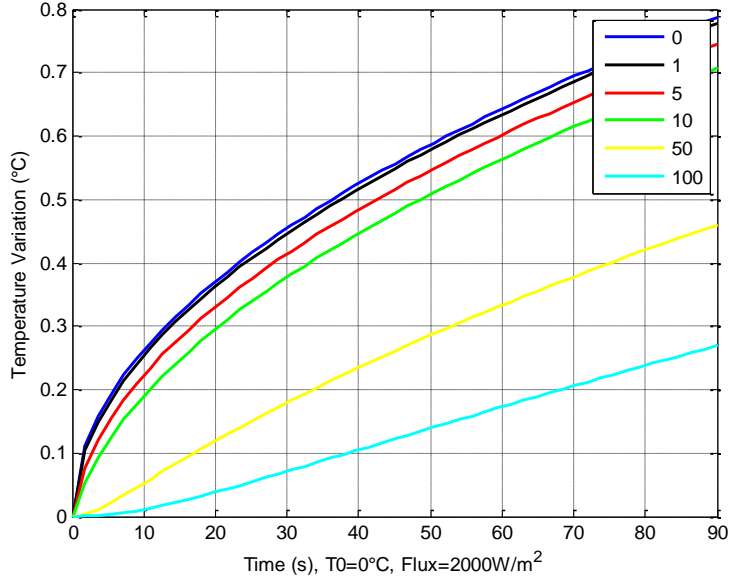
Figure 21. Step responses of $T(x, t)$ using Simulink for $x \in \{0,1,5,10,50,100\}mm$.

Note that, when comparing Figure 6 to Figure 21, a small time variation of about $8 \, seconds$ appears due to the simulation time needed in *Simulink* that didn't show up when using *Matlab*.

As for the finite medium, Figure 22 and Figure 23 show the *Simulink* system and the temperature variation with respect to time for different values of the sensor placement and for two values of L:

- for *Figure 23a*, L is equal to $1m$
- for *Figure 23b*, L is equal to $20cm$.
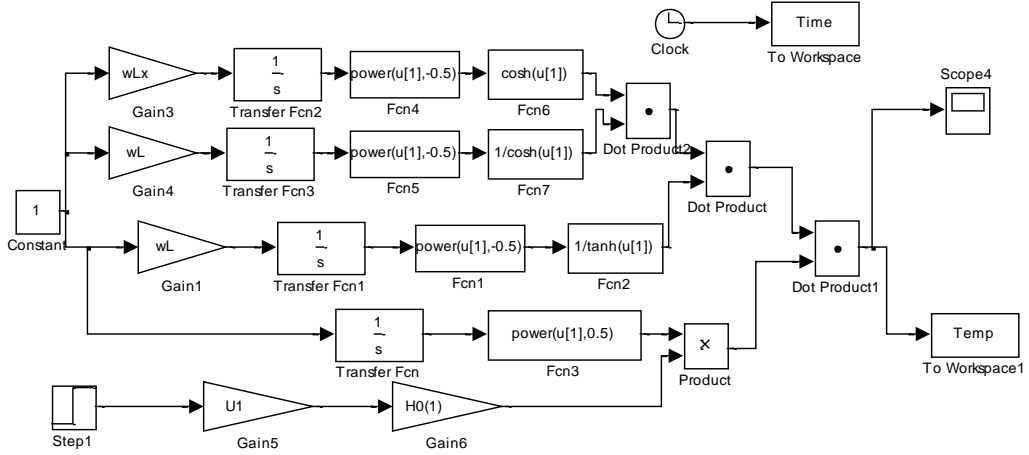
Figure 22. Simulink representation for the finite homogeneous plane.
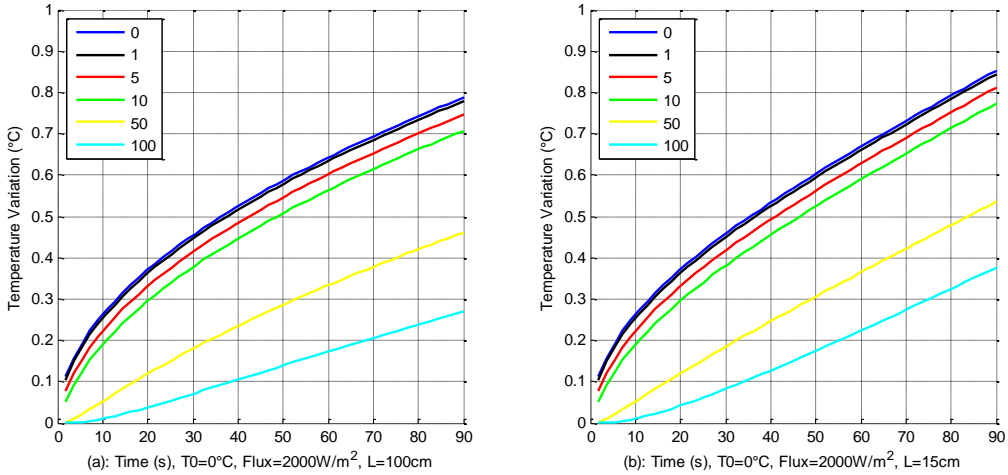
Figure 23. Step responses of $T(x, t)$ using Simulink for $x \in \{0,1,5,10,50,100\}$mm and for (a) $L = 1$m and (b) $L = 15$cm.

Conclusion

In this chapter we have studied the thermal interface behavior using the fractional order approach. The identification of the diffusion phenomena as well as the optimization of their process control were made easier using the fractional order approach, especially when both operational and frequency domains are considered. In fact, based on the pseudo-state (Sabatier, 2013) equations of the conduction phenomenon, representative models for both semi-infinite and finite media were easily developed.

On the other hand, when it comes to time responses, it is more complicated as the analytical solutions of Inverse Laplace transforms don't exist for all the types of equations. Nevertheless, approximations do exist and others are still a contemporary research subject of our interest; they are the core of advanced studies related to fractional order applications.

References

Abi Zeid Daou R., Moreau X., Assaf R. and Christophy F. - Analysis of the Fractional Order System in the thermal diffusive interface – Part 1: application to a semi-infinite plane medium – *2nd International Conference on Advances in Computational Tools for Engineering Applications (ACTEA)*, December 2012, Lebanon.

Agrawal O. M. P. – Application of Fractional Derivatives in Thermal Analysis of Disk Brakes – *Journal of Nonlinear Dynamics*, Vol. 38, pp. 191-206, 2004, Kluwer Academic Publishers.

Assaf R., Moreau X., Abi Zeid Daou R. and Christophy F. - Analysis of the Fractional Order System in the thermal diffusive interface – Part 2: application to a finite plane medium – *2nd International Conference on Advances in Computational Tools for Engineering Applications (ACTEA)*, December 2012, Lebanon.

Battaglia J. L., Cois O., Puissegur L. and Oustaloup A. – Solving an inverse heat conduction problem using a non-integer identified model – *International Journal of Heat and Mass Transfer,* Vol. 44, N 14, pp. 2671-2680, 2001.

Battaglia J. L. – Heat Transfer in Materials Forming Processes – ISTE Ed., London, 2008.

Benchellal A., Bachir S., Poinot T. and Trigeassou J. C. – Identification of non-integer model of induction machines – Chapter in *Fractional differentiation and its applications*, U-Books Edition, pp. 471-482, 2005.

Canat S. and Faucher J. – Modeling, identification and simulation of induction machine with fractional derivative – Chapter in *Fractional Differentiation and its Applications*, U-Books Edition, pp. 459-470, 2005.

Cois O. - Systèmes linéaires non entiers et identification par modèle non entier: application en thermique - *Thèse de Doctorat* de l'Université Bordeaux 1, 2002.

de Wit M. H. – Heat, air and moisture in building envelopes – *Course book*, Eindhoven University of Technology, 2009.

Kuhn E., Forgez C. and Friedrich G. – Fractional and diffusive representation of a 42 V Ni-mH battery – Chapter in *Fractional differentiation and its applications*, U-Books Edition, pp. 423-434, 2005.

Kusiak A., Battaglia J. L. and Marchal R. – Heat flux estimation in CrN coated tool during MDF machining using non integer system identification technique – Chapter in *Fractional differentiation and its applications*, U-Books Edition, pp. 377-388, 2005.

Melchior P., Cugnet M., Sabatier J., Poty A. and Oustaloup A. – Flatness control of a fractional thermal system – Chapter in *Advances in Fractional Calculus: Theoretical Developments and Applications in Physics and Engineering*, Springer Ed., pp. 493-509, 2007.

Oldham K. B. and Spanier J. – *The fractional calculus* – Academic Press, Inc., New York, 1974.

Özişik M. N. – *Heat Conduction* – John Wiley & Sons, New York, 1980.

Özişik M. N. – *Heat Transfer – A basic Approach* – McGraw-Hill, New York, 1985.

Podlubny I. – Geometric and physical interpretation of fractional integration and fractional differentiation – Chapter in *Fractional differentiation and its applications*, U-Books Edition, pp. 3-18, 2005.

Sabatier J., Melchior P. and Oustaloup A. – A testing bench for fractional order systems education – *JESA*, Vol. 42, N°6-7-8, pp. 839-861, 2008.

Sabatier J., Farges C. and Trigeassou J.-C. – Fractional systems state space description: some wrong ideas and proposed solutions – *Journal of Vibration and Control,* 1077546313481839, 02-Jul-2013.

Schneider P. J. – *Conduction Heat Transfer* – Addison-Wesley Publishing Company Inc., Reading Massachusetts, 1957.

U.S. Army Corps of Engineers Technical Manual - Arctic and Subarctic Construction: *Calculation Methods for Determination of Depths of Freeze and Thaw in Soils* - TM 5-852-6/AFR 88-19, Volume 6, 1988.

Chapter 6

TEMPERATURE CONTROL OF A DIFFUSIVE MEDIUM USING THE CRONE APPROACH

Fady Christophy[1,2,∗], Xavier Moreau[1,†], Roy Abi Zeid Daou[2] and Riad Assaf[1,2,‡]

[1]University of Bordeaux, Laboratory IMS, Talence, Bordeaux, France
[2]Lebanese German University, Faculty of Public Health,
Biomedical Technologies department, Sahel Alma, Jounieh, Lebanon

Abstract

This chapter presents the design of the temperature control of a diffusive medium by using a unique robust controller for three different materials: aluminum, copper and iron. For the control-system design, the aluminum is selected as the material defining the nominal model. Then, the second generation CRONE control is used because the parametric uncertainty (due to the copper and the iron) leads to variations of open-loop gain. Finally, the responses in frequency-domain and in time-domain illustrate the influence of the position of the sensor versus the actuator on the stability degree robustness.

1. Introduction

The concept of fractional differentiation is an old one that was born at the end of the 17th century when L'Hospital and Leibniz exchanged on the meaning of half order derivatives [Oldham, 1974]. Since that date, many mathematicians worked on this concept from a mathematical point of view. The most important contributions in this domain came in the 19th century with Riemann and Liouville [Miller, 1993] when they gave a coherent definition of a fractional derivation.

However, the applications on the fractional order systems started in the last quarter of the 20th century [Oustaloup, 1981]. In the last forty years, work on such systems propagated in

---

[∗] E-mail address: fady.chrystophy@u-bordeaux.fr.
[†] E-mail address: xavier.moreau@u-bordeaux.fr.
[‡] E-mail address: riad.assaf@u-bordeaux.fr.

several fields as the electrochemical processes [Kuhn, 2005] [Sabatier, 2006], dielectric polarization [Bohannan, 2000], induction machines [Benchellal, 2005] [Canat, 2005], viscoelastic materials [Moreau, 2002], suspension system [Abi Zeid Daou, 2010] [Abi Zeid Daou, 2011.a], automatic control [Oustaloup, 1983] [Oustaloup, 1995] [Lanusse, 1994] [Abi Zeid Daou, 2011.b], physiological movements as the muscle contraction [Sommacal, 2008], the respiratory process [Ionescu, 2011], thermal diffusion [Battaglia, 2001] [Agrawal, 2004] [Kusiak, 2005] [Melchior, 2007], and so on. In general, the development of diffusion phenomena equations naturally leads to fractional order systems [Podlubny, 2005].

The aim of this study is to design the temperature control of a diffusive medium by using an unique robust controller for three different materials (aluminum, copper and iron) constituting the medium. In more details, this chapter is divided as follows. In section 2, the material properties and the diffusive interface relations are recalled. Section 3 presents the SISO Crone control-system design used in the frequency-domain for the temperature control of the uncertain diffusive medium. Responses in frequency-domain and in time-domain are given to illustrate the influence of the position of the sensor versus the actuator on the stability degree robustness. At the end, a conclusion sums up all the results and some future works are proposed.

2. Modelling

Consider a homogeneous one-dimensional semi-infinite medium, of conductivity λ, of diffusivity α and of initial temperature zero at every point (figure 1). It is subjected to a flux density $\varphi(t)$ (W/m^2) on the outgoing normal surface $\vec{n}$. This results in a temperature change, denoted $T(x,t)$, function of time t and of abscissa x ($x \in [0\,;\infty[$) of the measuring temperature point inside the medium.
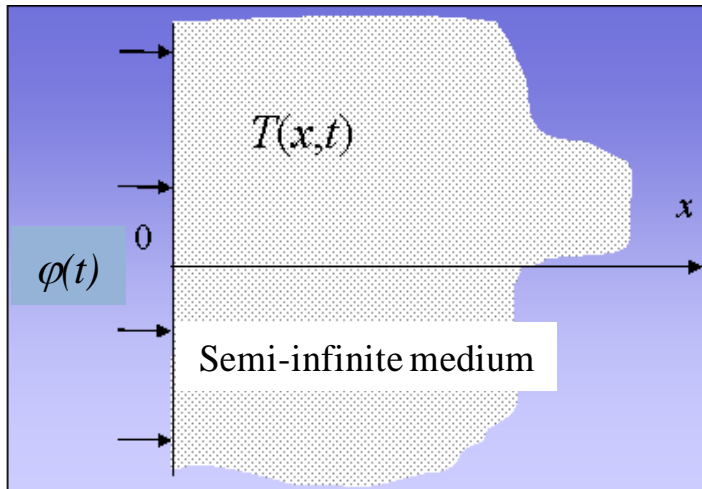
Figure 1. Illustration of the study area defining the process.

Initially, the goal is to achieve control of the temperature $T(0,t)$ at $x = 0$ with a sensor placed in this position. For this we have a heating resistor bonded to a surface S of 1 cm^2 at

the end $x = 0$ of a bar (high thermal conductivity glue) for generating a command $u(t)$ of flux $f(t)$, or a flux density $\varphi(t) = f(t)/S$. The maximum flux U_{max} produced by the resistance is 12 W (1 A under 12 V over 1 cm^2, thus 12 10^4 W/m^2). The medium temperature is measured with a platinum sensor of type PT100 via a voltage amplifier [Sabatier, 2008].

In a second step, the goal is always to regulate the temperature $T(0,t)$ at $x = 0$ but with a sensor placed at a position $x > 0$. An analysis of the influence of the position x of the sensor on the performance of the command is given.

2.1. Fractional Model at $x = 0$

At $x = 0$, the transfer function $G(0,s)$ of the process is given by [Abi Zeid Daou, 2012]:

$$G(0,s) = \frac{\overline{T}(0,s)}{U(s)} = \omega_0^{0.5} \, I^{0.5}(s), \tag{1}$$

with

$$\begin{cases} \omega_0 = \dfrac{1}{S^2 \, \lambda \, \rho \, C_p} \\ I^{0.5}(s) = \dfrac{1}{s^{0.5}} \end{cases}, \tag{2}$$

ω_0 is an uncertain parameter, $\omega_0 \in [\omega_{0\min} \,; \omega_{0\max}]$, not only because the parameters λ, ρ et C_p (relation (2)) are given with an uncertainty (data values at 20°C), but also because the objective of the robust control for this study is to use the same control for different materials constituting the semi-infinite medium (aluminum, copper, iron, …).

In this study, we chose three materials: aluminum, copper and iron. Table 1 summarizes the materials' characteristics necessary to calculate ω_0.

Table 1. Characteristics of the materials used

Materials at 20°C	ρ (kg/m^3)	C_p (J.kg^{-1}.K^{-1})	λ (W.m^{-1}.K^{-1})	ω_0 (rad/s) for $S = 10^{-4}$ m^2
Aluminium	2700	889	237	1,76 10^{-1}
Copper	8930	382	399	0,735 10^{-1}
Iron	7860	452	81	3,475 10^{-1}

For these three materials, we get $\omega_0 \in [\, 0.735 \,; 3.475 \,] 10^{-1} \text{rad/s}$.

For the remainder of the control-system design, the aluminum is selected as a material defining the nominal model, hence $\omega_{0nom} = 1.76 \ 10^{-1}$ rad/s. Thus, the uncertainties of ω_0 result in gain variations of $G(0,j\omega)$ of a factor 2.17 (between the iron and copper we have: $(3.475/0.735)^{0.5} = 2.17$). These gain variations cause gain variations $\Delta\beta$ in open loop, $\Delta\beta = 2.17$, hence the use of the second generation CRONE control [Oustaloup, 1995].

Figure 2 shows the Bode plots of $G(0,j\omega)$ for the three materials.
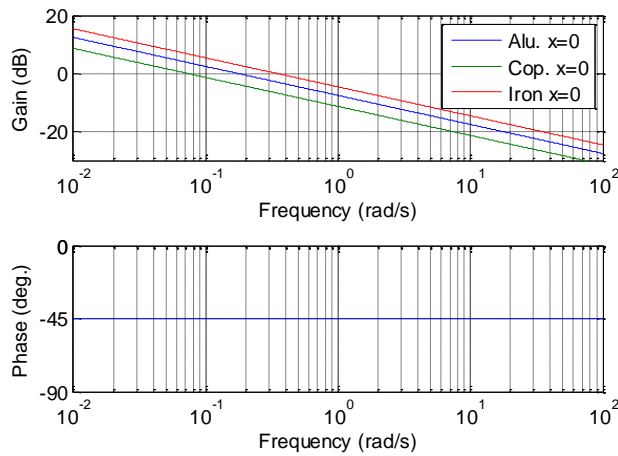
Figure 2. Bode diagram of G(0,jω).

Moreover, the analytical expression of the step response $T(0,t)$ for a flux $f(t)$ of amplitude U_0 is given by [Schneider, 1957] [Özisik, 1980] [Özisik, 1985] [Battaglia, 2008]:

$$T(0,t) = \frac{2\,U_0}{S\,\sqrt{\pi\,\lambda\,\rho\,C_p}}\,\sqrt{t} = 2\,U_0\sqrt{\frac{\omega_0}{\pi}}\,\sqrt{t}\;. \tag{3}$$

Figure 3 shows for the three materials the step responses at $x = 0$ for an input of amplitude $U_0 = 1$ W.
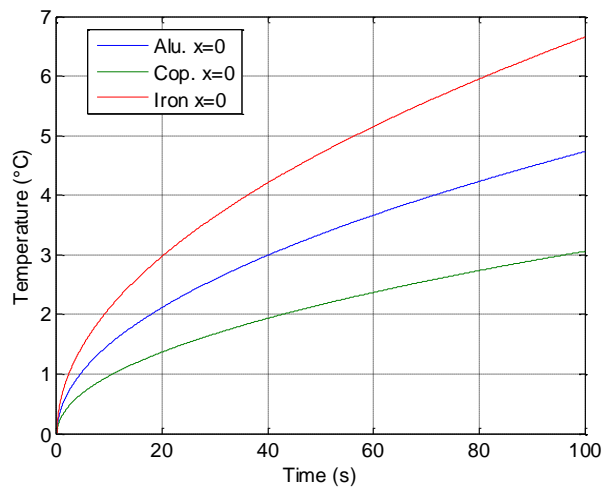
Figure 3. Step responses of the process at x = 0 for a flux of amplitude U0 = 1 W.

2.2. Fractional Model at $x > 0$

At $x > 0$, the transfer function $G(x,s)$ of the process is expressed by [Assaf, 2012]:

$$G(x,s) = \frac{\overline{T}(x,s)}{U(s)} = \omega_0^{0.5} \, I^{0.5}(s) \, E(x,s), \tag{4}$$
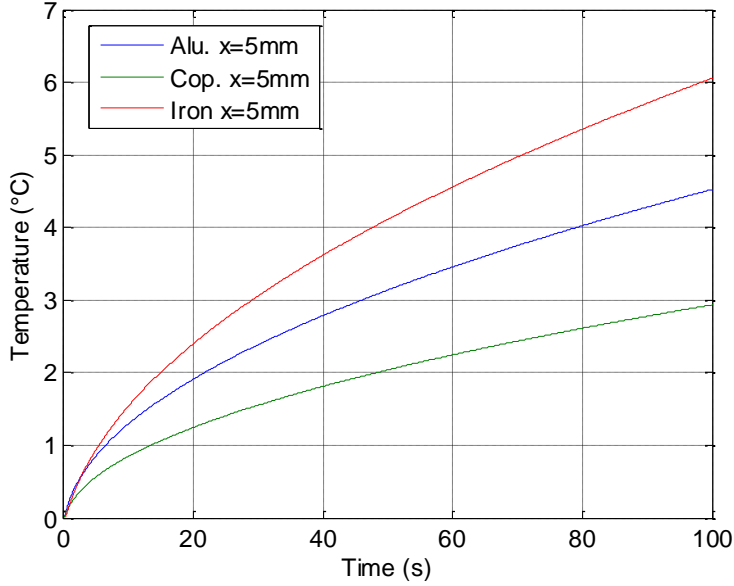
Figure 4. Step responses of the process at x = 5mm for a flux of amplitude U0 = 1 W.

with

$$\begin{cases} E(x,s) = e^{-\left(\frac{s}{\omega_x}\right)^{0.5}} \\ \\ \omega_x = \dfrac{\alpha}{x^2} \end{cases}, \tag{5}$$

or, by introducing the nominal transfer function $G_{nom}(0,s)$ established with the aluminum at $x = 0$,

$$G(x,s) = G_{nom}(0,s) \, e^{-\left(\frac{s}{\omega_x}\right)^{0.5}}. \tag{6}$$

Remark. The exponential function can be interpreted as a multiplicative structural uncertainty $\Delta_m(x)$:

$$\Delta_m(x) = e^{-\left(\frac{s}{\omega_x}\right)^{0.5}} = e^{-x\left(\frac{s}{\alpha}\right)^{0.5}}. \tag{7}$$

Moreover, the analytical expression of the step response T(x,t) for a flux f(t) of amplitude U_0 is given by [Battaglia, 2008]:

$$T(x,t) = U_0 \sqrt{\omega_0} \left(2 \sqrt{\frac{t}{\pi}} \, e^{\frac{-1}{4\,\omega_x\,t}} - \frac{1}{\sqrt{\omega_x}} \, \mathrm{erfc} \left(\frac{1}{2\sqrt{\omega_x\,t}} \right) \right), \tag{8}$$

where erfc(.) is the complementary error function.

Figure 4 shows for the three materials the step responses at x = 5mm for an input of amplitude $U_0 = 1$ W.

2.3. Rational Model for Temporal Simulation $\forall\, x \geq 0$

If the numerical simulation of the fractional integrator $I^{0.5}(s)$ and of function $E(x,s)$ cause no problem in the frequency domain, it's not the same for the time domain. In fact, apart from some analytical signals such as the Dirac pulse or unit step for which analytical expressions of time responses are well known, time simulation of the responses of the process model to any of the other inputs is more problematic. This is the case in particular when the process model is immersed in a control loop. It is then necessary to implement methods for approximating the fractional model to have a rational model.

Thus, the fractional integrator $I^{0.5}(s)$ is first approximated by a fractional integrator bounded in frequency between ω_a and ω_b that can be written as $_{\omega_a} I_{\omega_b}^{0.5}(s)$ where:

$$\begin{cases} I^{0.5}(s) = \dfrac{1}{s^{0.5}} \\ {}_{\omega_a} I_{\omega_b}^{0.5}(s) = \dfrac{K_0}{s} \left(\dfrac{1+s/\omega_a}{1+s/\omega_b} \right)^{0.5} \end{cases} \Rightarrow \quad \dfrac{1}{s^{0.5}} \approx \dfrac{K_0}{s} \left(\dfrac{1+s/\omega_a}{1+s/\omega_b} \right)^{0.5}, \tag{9}$$

with $\omega_a < \omega_b$ and K_0 a constant computed for the two integrators to have the same gain at midband $\omega_m = \sqrt{\omega_a\,\omega_b}$:

$$K_0 = \omega_m^{0.5} \left(\frac{1+(\omega_m/\omega_b)^2}{1+(\omega_m/\omega_a)^2} \right)^{0.25}, \tag{10}$$

or by introducing the constant $A = \omega_b/\omega_a > 1$,

$$K_0 = \frac{\omega_m^{0.5}}{A^{0.25}} . \tag{11}$$

Then the fractional integrator bounded in frequency is approximated by a rational integrator frequency bounded [Oustaloup, 1995]:

$$\omega_a I_{\omega_b}^{0.5}(s) = \lim_{N \to \infty} I_N^{0.5}(s) \,, \tag{12}$$

with

$$I_N^{0.5}(s) = \frac{K_0}{s} \prod_{i=1}^{N} \left(\frac{1 + \dfrac{s}{\omega_i^{'}}}{1 + \dfrac{s}{\omega_i}} \right) \,, \tag{13}$$

where

$$\alpha \eta = \left(\frac{\omega_b}{\omega_a} \right)^{1/N} \,, \ \eta = (\alpha \eta)^{-0.5}, \ \alpha = (\alpha \eta)^{0.5},$$

$$\omega_1^{'} = \sqrt{\eta} \, \omega_a \quad, \ \omega_N = \frac{1}{\sqrt{\eta}} \omega_b \,, \ \frac{\omega_i}{\omega_i^{'}} = \alpha > 1, \ , \tag{14}$$

$$\frac{\omega_{i+1}^{'}}{\omega_i^{'}} = \eta > 1 \quad \text{et} \quad \frac{\omega_{i+1}^{'}}{\omega_i^{'}} = \frac{\omega_{i+1}}{\omega_i} = \alpha \eta > 1 \,.$$

Finally, concerning the exponential function $E(x,s)$, we use the limited Taylor expansion of e^z when z tends to zero:

$$\lim_{z \to 0} e^z = 1 + z + \frac{z^2}{2!} + \frac{z^3}{3!} + \ldots + \frac{z^k}{k!} + \ldots = \sum_{k=0}^{\infty} \frac{z^k}{k!} \,. \tag{15}$$

By taking $z = (s/\omega_x)^{0.5}$, we obtain:

$$\frac{1}{e^{\left(\frac{s}{\omega_x} \right)^{0.5}}} \approx \frac{1}{1 + \left(\dfrac{s}{\omega_x} \right)^{0.5} + \dfrac{s}{2!\omega_x} + \dfrac{1}{3!}\left(\dfrac{s}{\omega_x} \right)^{1.5} + \ldots + \dfrac{1}{K!}\left(\dfrac{s}{\omega_x} \right)^{0.5K}} = \frac{1}{\displaystyle\sum_{k=0}^{K} \frac{1}{k!}\left(\dfrac{s}{\omega_x} \right)^{0.5k}} \,. \tag{16}$$

Remark. *z tends to zero is equivalent to tendering s to zero, and therefore ω to zero and t to infinity (time-frequency duality), or, considering the expression (5) of ω_x, x tends to zero. Thus, this approximation is more accurate than the truncation order K is high, when x is small and it is with long time. In fact, this approximation is legitimate when $\omega << \omega_x$ or equivalently, when $t >> \tau_x = 1/\omega_x$.*

In a first step, K is limited to 1, hence:

$$E(x,s) = \frac{\overline{T}(x,s)}{\overline{T}(0,s)} \approx \frac{1}{1 + \left(\dfrac{s}{\omega_x} \right)^{0.5}} = \frac{\left(\dfrac{\omega_x}{s} \right)^{0.5}}{1 + \left(\dfrac{\omega_x}{s} \right)^{0.5}} \,, \tag{14}$$

the expression of order 0.5 could be interpreted as a closed loop system (figure 5), the open loop transfer function is equal to the product of a constant $\omega_x^{0.5}$ and a fractional integrator $I^{0.5}(s)$, the latter having already been subjected to the approximation described above.
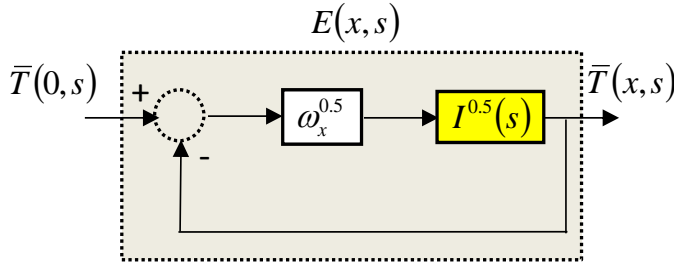
Figure 5. Block diagram associated with the approximation of the function E(x,s).

In summary, obtaining the rational model for temporal simulation, $\forall\, x \geq 0$, is due to the rational integrator $I_N^{0.5}(s)$ whose center frequency ω_m is chosen equal to the crossover frequency, ω_{unom}, in nominal open loop.

Figure 6 shows the block diagram of the rational model used in Simulink for time response simulation.
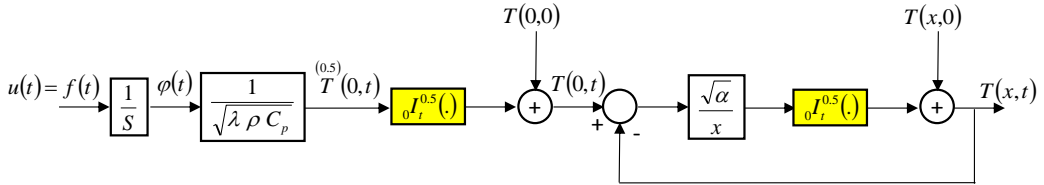
Figure 1. Block diagram of the rational model used in Simulink for time response simulation.

Remark. *In a second step, an optimal approach to managing the dilemma between the fidelity of the approximation which may be improved by increasing the order K of the truncation of the series (16) (by increasing the complexity), and the simulation time which unfortunately also increases with the degree of complexity is proposed. A fractional representation of order 0.5 is studied in particular for the formulation of the optimal approach, the value of the order K directly fixing the number of fractional integrators. Similarly, the optimum choice of the number of decades and cells in the synthesis of rational integrator will be a specific study.*

Finally, the approximation errors of the rational model may be considered as uncertainties and used for the control-system design.

3. Temperature Control

3.1. Scheme for the Control-System Design

Figure 7 shows the scheme used for the control-system design.
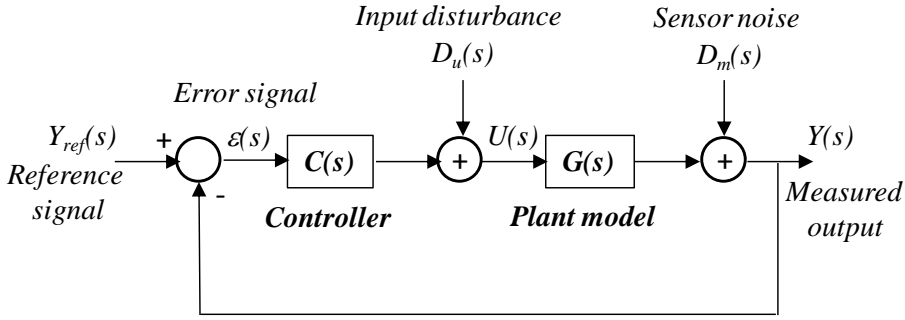
Figure 7. Scheme used for the control-system design.

The equations associated with the scheme of figure 7 are:

for the output signal:

$$Y(s) = S(s)D_m(s) + S(s)G(s)D_u(s) + T(s)Y_{ref}(s); \qquad (18)$$

for the error signal:

$$\varepsilon(s) = -S(s)D_m(s) - S(s)G(s)D_u(s) + S(s)Y_{ref}(s); \qquad (19)$$

for the control signal:

$$U(s) = -S(s)C(s)D_m(s) + T(s)D_u(s) + S(s)C(s)Y_{ref}(s), \qquad (20)$$

with

$$\begin{cases} S(s) = \dfrac{1}{1 + \beta(s)}: & \text{Sensitivity function} \\ T(s) = 1 - S(s): & \text{Complementary sensitivity function} \\ \beta(s) = C(s)G(s): & \text{Open loop transfer function} \end{cases} \qquad (21)$$

3.2. Summary Data

The required data for the control-system design are divided into two groups:

−   Signals models (often difficult to obtain, especially regarding the measurement noise) and the uncertain especially linear model of the process which in the case of a frequency approach is in the form of a transfer function $G(s)$ (Figure 7), the areas of uncertainty parameters θ_i are specified, for example, in the form of bounded intervals, $\theta_i \in \left[\underline{\theta_i} ; \overline{\theta_i} \right]$;

−   Translating specifications:

    o   Degree of stability, through the stability margins, M_Φ, M_G, M_M;

    o   Speed, through the unit gain frequency in open loop, $\omega_u \in [\omega_{u\,min} \; ; \omega_{u\,max}]$;

    o   Accuracy in the steady state, through the relative error, $\varepsilon(\%)$;

    o   Saturation, through the maximum value of the command, U_{max}.

Remark. It should be noted that the translation of specifications requires preliminary work, especially regarding the choice of ω_u.

In the absence of additional information, particularly regarding the measurement noise, it is difficult (or impossible) to determine precisely $\omega_{u\,nom}$.

However, a simplified approach leading to a first iteration can be made by taking $\omega_{u\,nom} = 3\,\omega_{0\,nom}$, initial choice based on experience…

Another approach is to set the contribution c_m of measurement noise relative to the maximum value U_{max} of control signal (for instance $c_m = 10\%$). In the absence of precise model of the measurement noise, knowing that its frequency spectrum is more concentrated towards the high frequencies, we place ourselves in stationary harmonic, we estimate the amplitude D_m of measurement noise over the full scale range E_m of the sensor (for instance $D_m = 1\%\ E_m$) and from equation (3) we impose:

$$\lim_{\omega \to \infty} |U(j\omega)| = \lim_{\omega \to \infty} |S(j\omega)C(j\omega)|\ D_m \leq c_m\,U_{max}\,, \tag{22}$$

knowing that $\displaystyle\lim_{\omega \to \infty} |S(j\omega)| = 1$,

$$\lim_{\omega \to \infty} |U(j\omega)| \approx \lim_{\omega \to \infty} |C(j\omega)|\ D_m \leq c_m\,U_{max}\,. \tag{23}$$

Thus, a strain is obtained regarding the controller gain at high frequencies:

$$C_\infty = \lim_{\omega \to \infty} |C(j\omega)| \leq \frac{c_m\,U_{max}}{D_m}\,, \tag{24}$$

constraint leads to limit ω_u.

3.3. Loop Shaping

There are three generations of the CRONE controller [Oustaloup, 1995]. When parametric uncertainties result in gain variations $\Delta\beta$ in open loop, the second generation is used. Hence, the expression of the open loop transfer function $\beta(s)$ is given by:

$$\beta(s) = \beta_0 \left(\frac{1 + s/\omega_l}{s/\omega_l} \right)^{n_l} \left(\frac{1 + s/\omega_h}{1 + s/\omega_l} \right)^{n} \left(1 + s/\omega_h \right)^{-n_h}\,, \tag{25}$$

where ω_l and ω_h represent the transitional low and high frequencies, n the non-integer order between 1 and 2 near the frequency ω_u, n_l and n_h are the orders of the asymptotic behavior at

low and high frequencies (figure 8) and β_0 a constant which ensures unity gain at frequency ω_u. β_0 is given by:

$$\beta_0 = \left(\omega_u / \omega_l\right)^{n_l} \left(1 + \left(\omega_u / \omega_l\right)^2\right)^{(n-n_l)/2} \left(1 + \left(\omega_u / \omega_h\right)^2\right)^{(n_h-n)/2}. \tag{26}$$

The fractional asymptotic behavior (figure 8) is set to a frequency interval $[\omega_A, \omega_B]$ around the nominal frequency ω_{unom}. To meet the robustness of the degree of stability, it is necessary to impose:

$$\forall\, \omega_u \in \left[\omega_{u\min}\; ;\; \omega_{u\max}\right],\ \omega_A \leq \omega_u \leq \omega_B \quad \Rightarrow \quad \begin{cases} \omega_A \leq \omega_{u\min} \\ \omega_B \geq \omega_{u\max} \end{cases}. \tag{27}$$
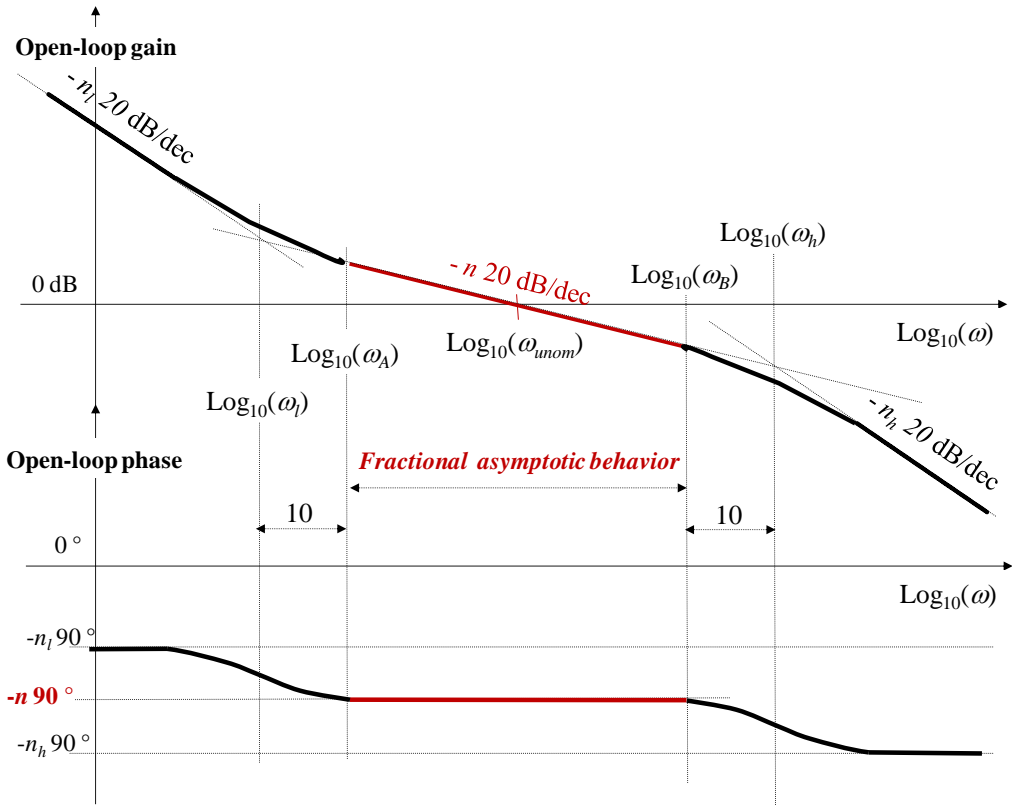
Figure 8. Asymptotic Bode diagrams of $\beta(j\omega)$.

In addition, to obtain a fractional asymptotic behavior on the interval $[\omega_A, \omega_B]$ (Figure 8), a practical rule leads to choose [Oustaloup, 1995]

$$\begin{cases} \omega_l = \omega_A /10 \\ \omega_h = 10\,\omega_B \end{cases}. \tag{28}$$

Taking ω_l and ω_h geometrically distributed around ω_{unom} and introducing $a = \omega_B/\omega_A$:

$$\begin{cases} \sqrt{\omega_l\ \omega_h} = \omega_{unom} \\ a = \dfrac{\omega_B}{\omega_A} \end{cases}, \tag{29}$$

ω_l and ω_h are given by:

$$\begin{cases} \sqrt{\omega_l\ \omega_h} = \omega_{unom} \\ \dfrac{\omega_h}{\omega_l} = 100\ a \end{cases} \Rightarrow \begin{cases} \omega_l = \omega_{unom}/\left(10\ \sqrt{a}\right) \\ \omega_h = \omega_{unom}\,10\ \sqrt{a} \end{cases}. \tag{30}$$
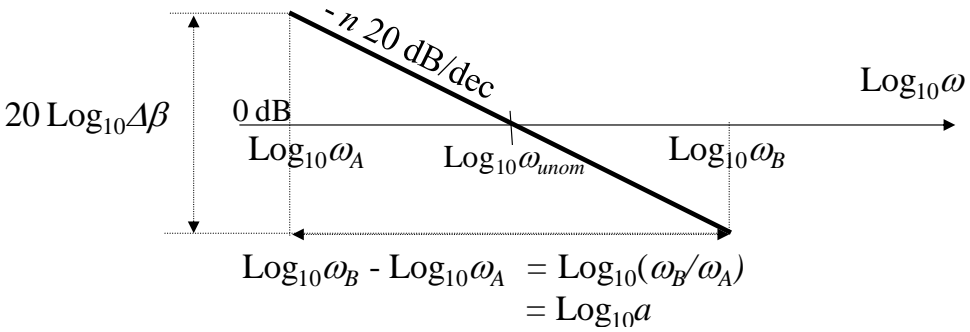
Figure 9. Illustration of computing a.

As for the calculation of the ratio a, it is derived from the slope of $-n20$dB/dec near ω_{unom} and the gain variation $\Delta\beta$ in open loop due to parametric uncertainties (figure 9). Thus, we find out:

$$a = \Delta\beta^{1/n}\ . \tag{31}$$

Finally, given that

$$\beta(s) = C_{crone}(s)\ G(s)\ , \tag{32}$$

the fractional form $C_F(s)$ of the transfer function of the CRONE regulator $C_{crone}(s)$ is deduced from the transfer function $G_{nom}(s)$ of the nominal process:

$$C_F(s) = \beta(s)/G_{nom}(s)\ . \tag{33}$$

Finally, one last step is necessary to determine the rational form $C_R(s)$ of the fractional transfer function $C_F(s)$ which is obtained either analytically using a recursive distribution of poles and zeros [Oustaloup, 1995], either numerically from the frequency response of $C_F(j\omega)$ and a specific module of the CRONE Toolbox [Oustaloup, 2005].

Remark. *Be careful, if the process is non minimum phase (positive real part zeros) and if it has a delay and / or very little damped modes, then there are precautions to take [Oustaloup, 2005].*

3.4. Specifications and Results

Finally, the translation of specifications led to choose:

o   for the degree of stability, phase margin $M_\Phi \geq 45$;
o   for the speed, crossover frequency, ω_{unom}, in nominal open loop the greatest possible;
o   for accuracy in the steady state, a static error equal to zero;
o   to saturation, a maximum value of the control signal, $U_{max} = 12$ W.

Given the summary data, we choose:

– $n_l = 1.5$, to ensure zero steady-state error;
– $n = (180° - M_\Phi)/90° = 1.5$, to ensure a phase margin $M_\Phi = 45$;
– $n_h = 1.5$, to limit the input sensitivity;
– $\omega_{unom} = 3\omega_{0nom} = 0.53$ rad/s (simplified approach).

From these data and taking into consideration the relation (31), we deduce:

$$a = 2.17^{1/1.5} = 1.68 \quad \Rightarrow \quad \begin{cases} \omega_A = \omega_{u\min} = 0.41 \text{ rad/s} \\ \omega_B = \omega_{u\max} = 0.684 \text{ rad/s} \end{cases} \quad \Rightarrow \quad \begin{cases} \omega_l = 0.041 \text{ rad/s} \\ \omega_h = 6.84 \text{ rad/s} \end{cases}. \tag{34}$$

The expression of the transfer function is given by:

$$\beta(s) = \beta_0 \left(\frac{1 + s/\omega_l}{s/\omega_l} \right)^{1.5} \left(\frac{1 + s/\omega_h}{1 + s/\omega_l} \right)^{1.5} \left(1 + s/\omega_h \right)^{-1.5}, \tag{35}$$

with

$$\beta_0 = 46.6. \tag{36}$$

From the relations (32) and (33), we deduce the expression of the fractional form $C_F(s)$ of the CRONE regulator:

$$C_F(s) = \beta_0 \left(\frac{1 + s/\omega_l}{s/\omega_l} \right)^{1.5} \left(\frac{1 + s/\omega_h}{1 + s/\omega_l} \right)^{1.5} \left(1 + s/\omega_h \right)^{-1.5} \left(\frac{s}{\omega_{1nom}} \right)^{0.5}, \tag{37}$$

after simplification,

$$C_F(s) = \frac{C_0}{s} \quad , \qquad\qquad (38)$$

with

$$C_0 = \beta_0 \left(\frac{\omega_l^{1.5}}{\omega_{lnom}^{0.5}} \right) \quad \Rightarrow \quad C_0 = 9.145\,10^{-1}\,W/K . \qquad (39)$$

Remark. The nature of the plant (integrator of order 0.5) and the choice of orders asymptotic behavior at low ($n_l = 1.5$), at average ($n = 1.5$) and at high ($n_h = 1.5$) frequencies lead to a particular case where the expression $C_F(s)$ is already in a very simple rational form (an integrator of order 1). In fact, for this particular case, the transfer function $\beta(s)$ in open loop is an integrator of order 1.5:

$$\beta(s) = \left(\frac{\omega_u}{s} \right)^{1.5} . \qquad\qquad (40)$$

Sensitivity function S(s) and complementary sensitivity function T(s) have the following expressions:

$$S(s) = \frac{1}{1+\beta(s)} = \frac{(s/\omega_u)^{1.5}}{1+(s/\omega_u)^{1.5}} \qquad\qquad (41)$$

and

$$T(s) = \frac{\beta(s)}{1+\beta(s)} = \frac{1}{1+(s/\omega_u)^{1.5}} \quad . \qquad\qquad (42)$$
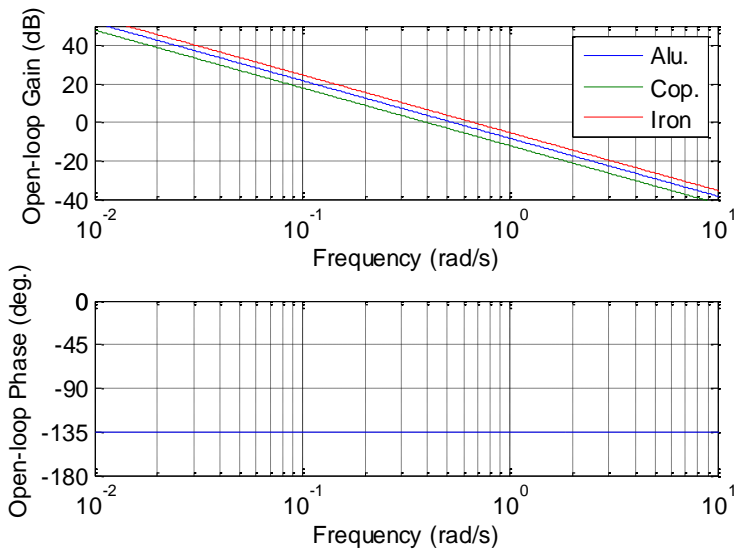
Figure 10. Bode diagrams of $\beta(j\omega)$.

3.4.1. Frequency Responses at x = 0

Figures 10 and 11 show Bode diagrams and Black-Nichols diagrams of the transfer function in open loop $\beta(s)$ for the nominal parametric state, and for the extreme values of gain. The robustness of the degree of stability is ensured, due to the insensitivity of the phase margin M_Φ to parametric uncertainties.
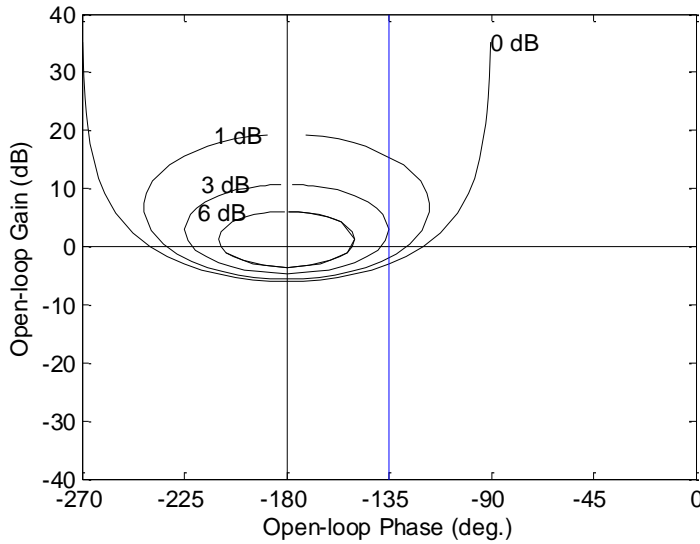
Figure 11. Black-Nichols diagram of β(jω).
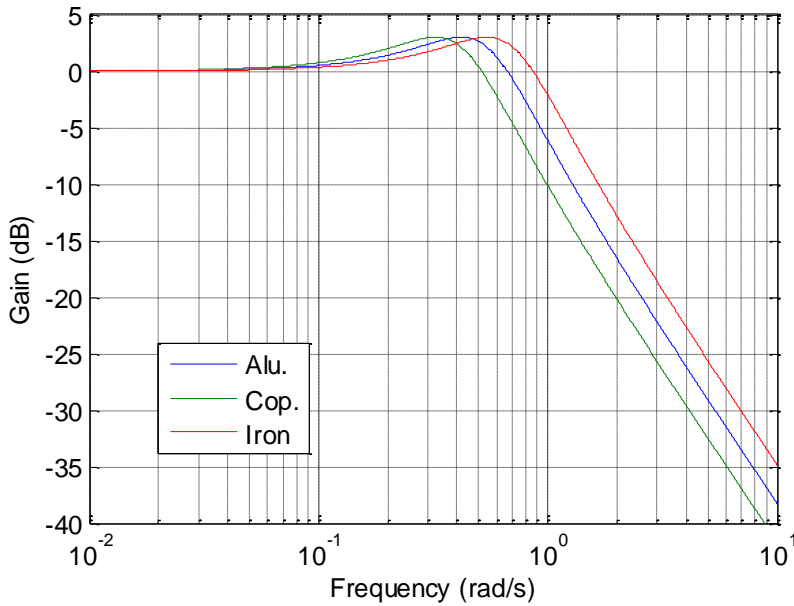
Figure 12. Gain diagram of the complementary sensitivity function T(s).

Figures 12 and 13 show diagrams of the complementary sensitivity function *T(s)* (figure 12) and the sensibility function *S(s)* (figure 13) for the nominal parametric state, and for the extreme values of the uncertainties. The robustness of the degree of stability appears with insensitivity of the resonance factors *T(jω)* et *S(jω)* to parametric uncertainties.

Figure 14 shows diagrams of the sensitivity function input *R(s) = S(s)C(s)*. We can notice that the gains *R(jω)* are maximum at medium frequencies.
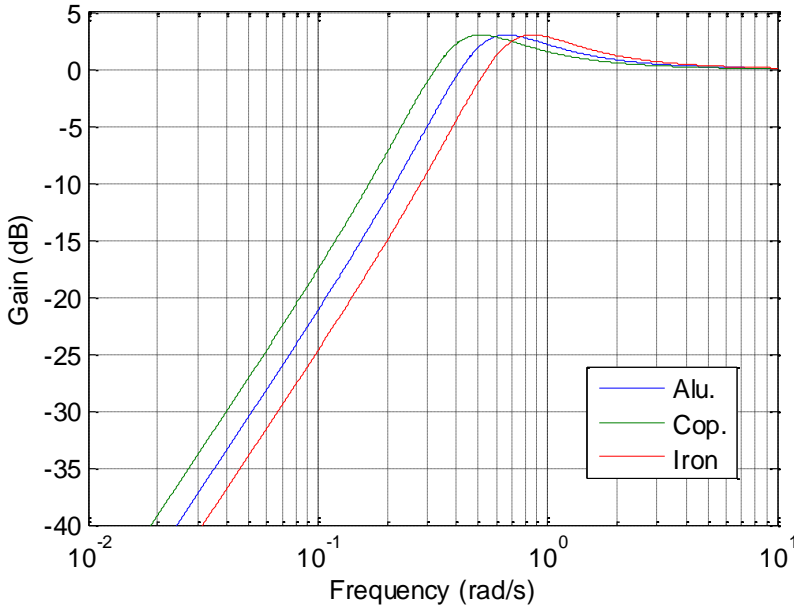
Figure 13. Gain diagram of the sensibility function S(s).
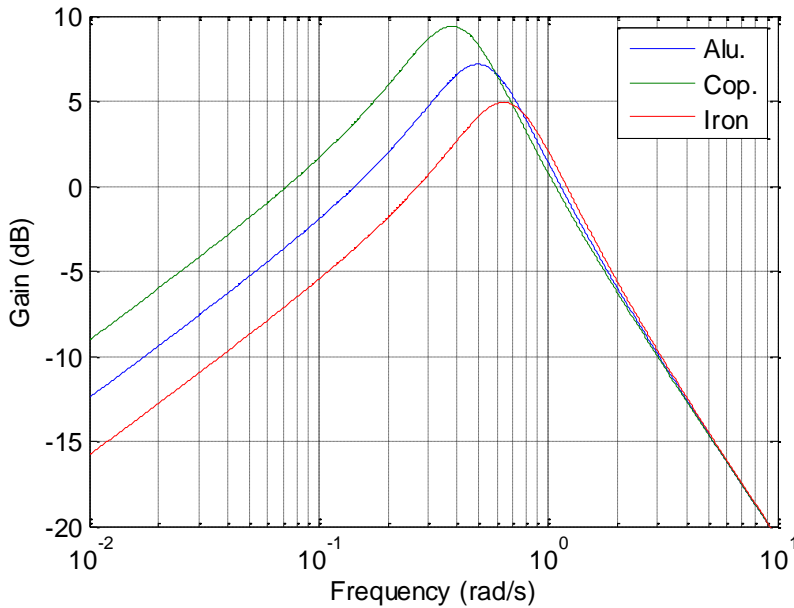
Figure 14. Gain diagram of the sensitivity function of the input R(s)= S(s)C(s).

3.4.2. Time Responses at x = 0

The rational model of the process used for the time simulation is derived from the rational integrator $I_N^{0.5}(s)$ (relation (13)) obtained by taking a median frequency $\omega_m = \omega_{unom} = 0.53$ rad/s, a constant $A = \omega_b/\omega_a = 10^8$ (an approximation of 8 decades) and a number of cells $N = 20$.

Figure 15 shows, at $x = 0$ and for aluminum, the step responses of the temperature to a flux of amplitude 1 W obtained from the exact response (relation (3)) and the response of the approximated model.
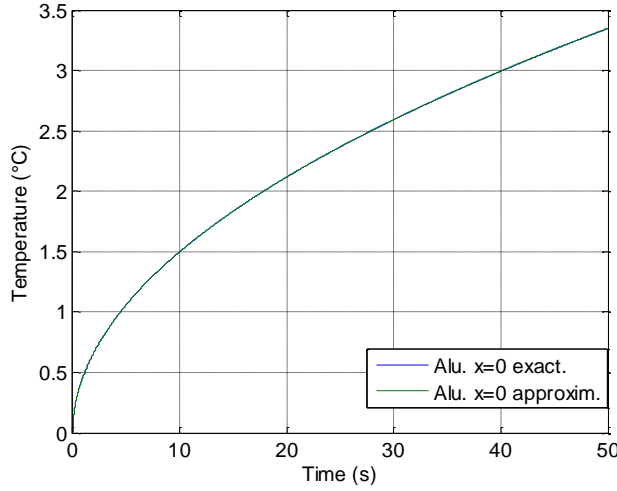
Figure 15. Step responses of the temperature at a flux of amplitude 1 W, at $x = 0$, for aluminum, obtained from the exact response (relation (3)) and the response of the approximated model.
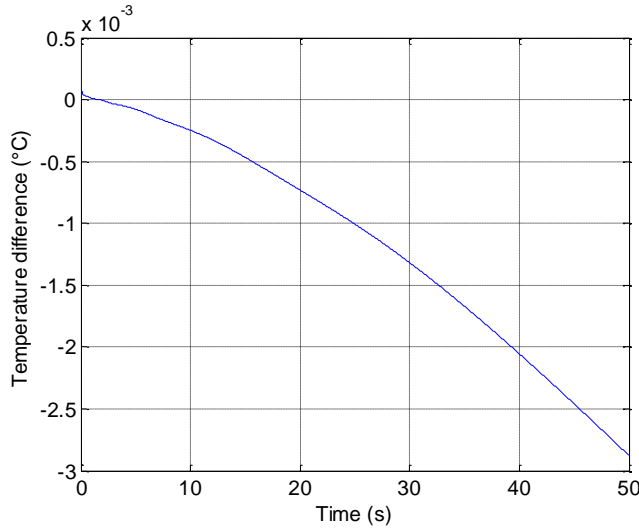
Figure 16. Temperature difference, at $x = 0$ and for aluminum, between the exact step response (relation (3)) and the approximated model.

Figure 16 shows, always at $x = 0$ and for aluminum, the temperature difference between the exact step response and the approximated model, to assess the quality of the approximation since the maximum error in 50 seconds is less than 3/1000 of °C.

Figure 17 shows the step responses of the output at a step input of amplitude 1°C for the nominal parametric state, and for the extreme values of the uncertainties. The robustness of the degree of stability clearly appears with the insensitivity of the first overshoot and the damping factor.
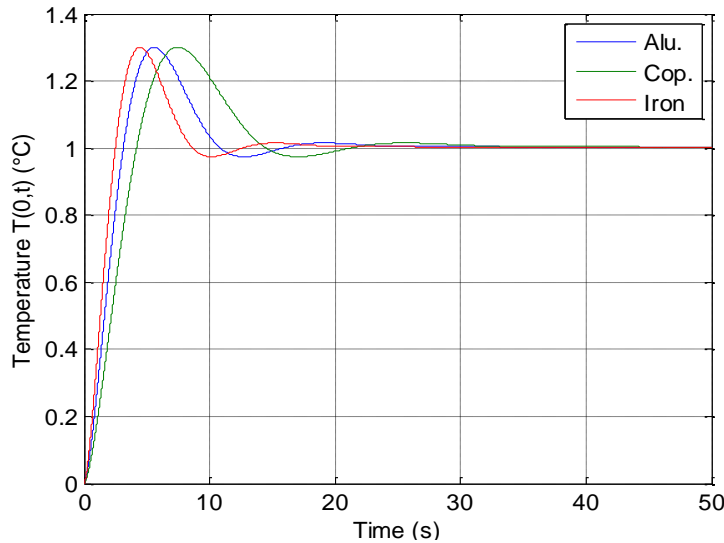
Figure 17. Step responses of the output to an input step of 1°C: for aluminum (⎯⎯⎯), copper (⎯⎯⎯) and iron (⎯⎯⎯).
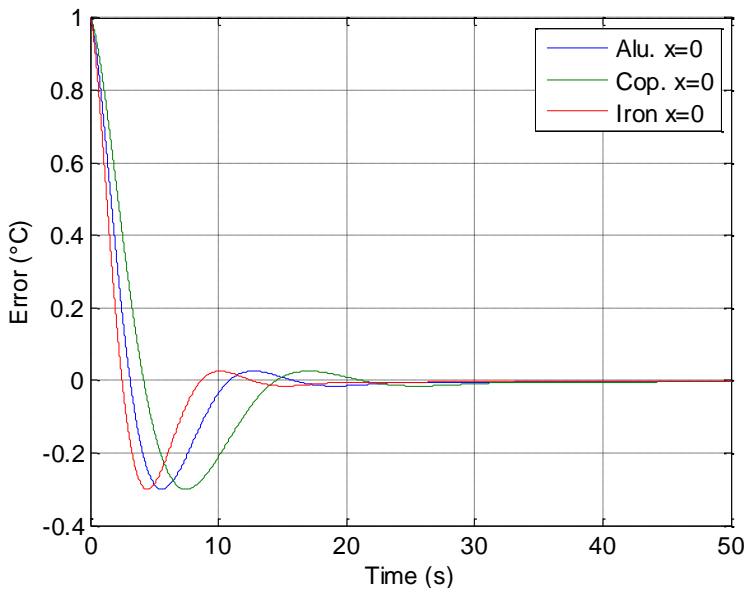
Figure 18. Step responses of the error to a step input of 1°C: for aluminum (⎯⎯⎯), copper (⎯⎯⎯) and iron (⎯⎯⎯).

Figure 18 shows the step responses of the error for the same simulation conditions. According to specifications, the static error is zero.

Finally, figure 19 shows the corresponding step responses of the control signal where the maximum value $U_{max} = 12$ W is never reached.
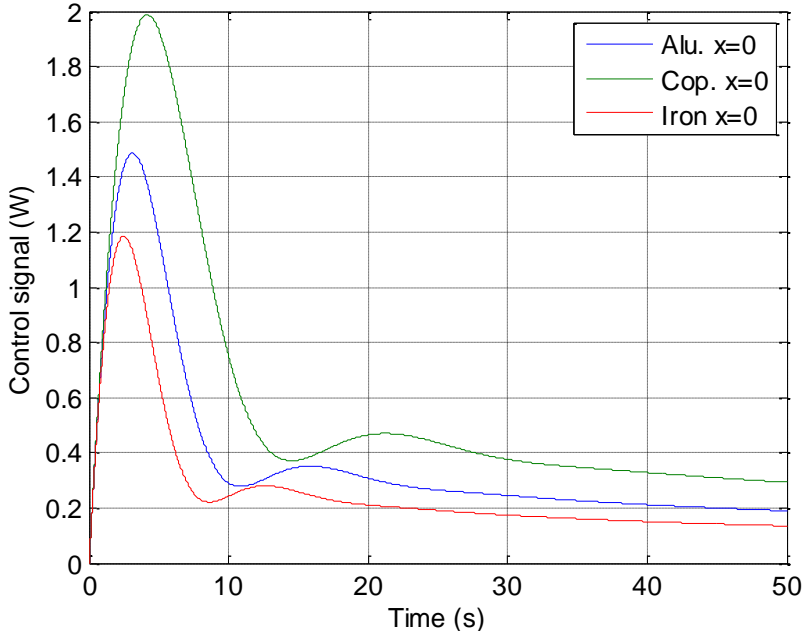
Figure 19. Step responses of the control signal to a step input of 1°C: for aluminum (———), copper (———) and iron (———).

3.4.3. Frequency Responses at x > 0

The objective is always to control the temperature $T(0,t)$ *at* $x = 0$, but by analyzing the influence of the position x of the temperature sensor when it can't be positioned at $x = 0$.

Thus, the transfer function of open loop $\beta(x,s)$ is then given by:

$$\beta(x,s) = C(s)G(0,s) \, e^{-\left(\frac{s}{\omega_x}\right)^{0.5}}, \tag{43}$$

by introducing the nominal transfer function of the open loop $\beta_{nom}(0,s)$,

$$\beta(x,s) = \beta_{nom}(0,s) \, e^{-\left(\frac{s}{\omega_x}\right)^{0.5}}, \tag{44}$$

whose frequency response $\beta(x,j\omega)$ is expressed by:

$$\beta(x,j\omega) = \beta_{nom}(0,j\omega) \, e^{-\left(j\frac{\omega}{\omega_x}\right)^{0.5}}. \tag{45}$$

Knowing that

$$e^{-\left(j\frac{\omega}{\omega_x}\right)^{0.5}} = m(x,\omega)\ e^{-j\theta(x,\omega)} \quad \text{avec} \quad \begin{cases} m(x,\omega) = e^{-\left(\frac{\omega}{2\omega_x}\right)^{0.5}} = e^{-x\left(\frac{\omega}{2\alpha}\right)^{0.5}} \\ \theta(x,\omega) = -\left(\frac{\omega}{2\omega_x}\right)^{0.5} = -x\left(\frac{\omega}{2\alpha}\right)^{0.5} \end{cases}, \quad (46)$$

the gain and the argument of the open loop are given by:

$$\begin{cases} |\beta(x,j\omega)| = |\beta_{nom}(0,j\omega)|\ m(x,\omega) \\ \arg \beta(x,j\omega) = \arg \beta_{nom}(0,j\omega) + \theta(x,\omega) \end{cases}. \quad (47)$$

Illustratively, the controller synthesized for $x = 0$ is applied to the process at $x = 0.5$ cm. This value is selected to 0.5 cm to compare the results with those shown in [Sabatier, 2008].

Figures 20 and 21 show Bode diagrams of Black-Nichols diagram for the transfer function of open loop $\beta(x,s)$ for the nominal case (aluminum at $x = 0$) and at $x = 0.5$ cm with aluminum, copper and iron.
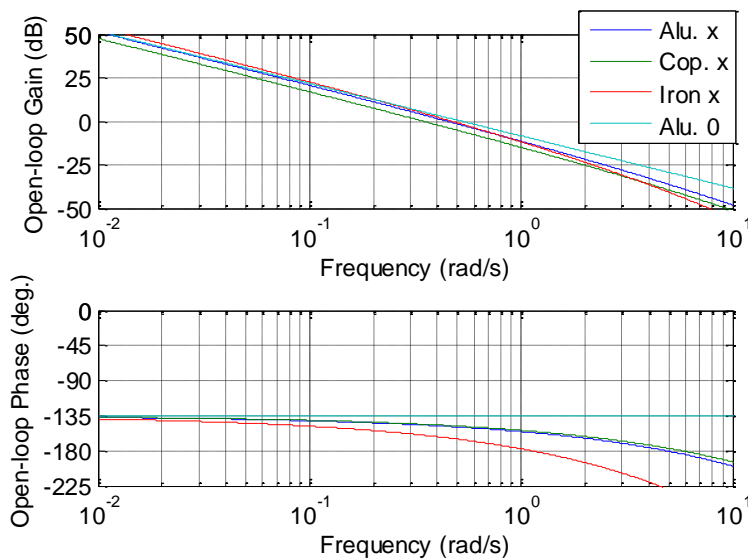
Figure 20. Bode diagrams of $\beta(x,j\omega)$ at x = 0.5 cm for aluminum (———), copper (———) and iron (———), and for the nominal case (———).

3.4.4. Time Response at x > 0

Figure 22 shows, at $x = 0.5$ cm and for aluminum, the step responses of the temperature to a flux of amplitude 1 W obtained from the exact response (relation (8)) and the response of the approximated model.

Figure 23 shows, still at $x = 0.5$ cm and for aluminum, the temperature difference between the exact step response and the approximated model, to assess the quality of the approximation since the maximum error in 50 seconds is less than 33/1000 of °C.
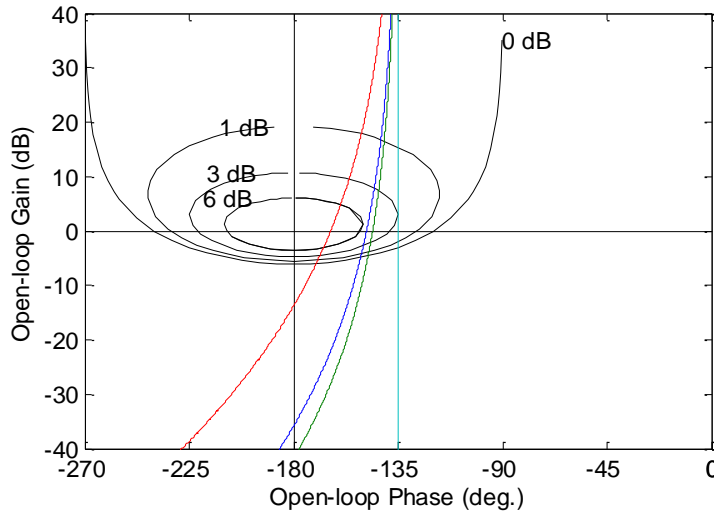
Figure 21. Black-Nichols diagrams of $\beta(x,j\omega)$ at x = 0.5 cm for aluminum (——), copper (——) and iron (——), and for the nominal case (——).
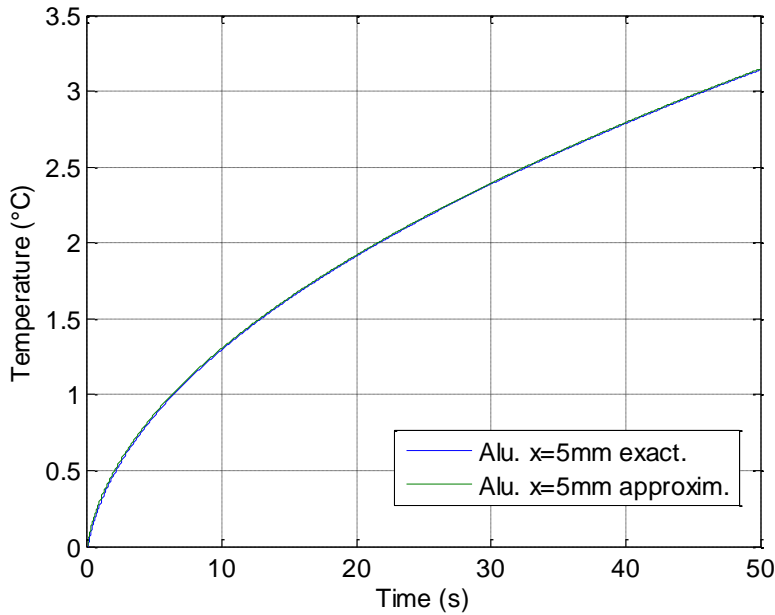
Figure 22. Step responses of the temperature at a flux with an amplitude of 1 W, at x = 0.5 cm and for aluminum, obtained from the exact response (relation (8)) and the response of the approximated model.
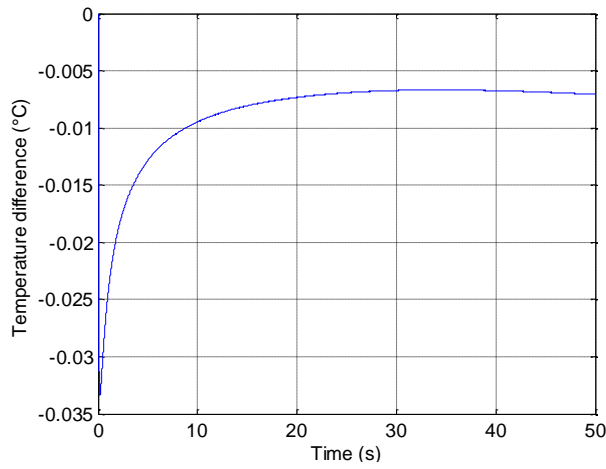
Figure 23. Temperature difference, at x = 0.5 cm and for aluminum, between the exact step response (relation (8)) and the approximated model.

(a)

(b)
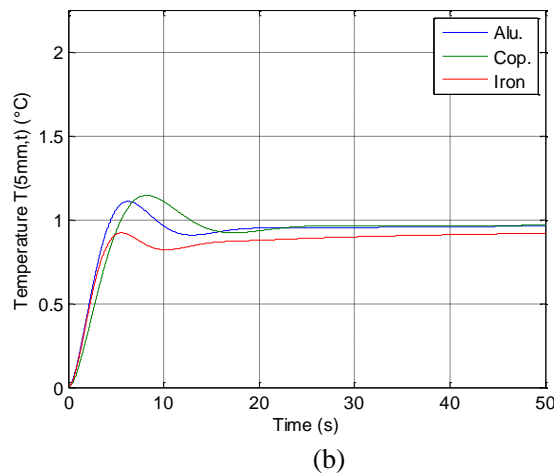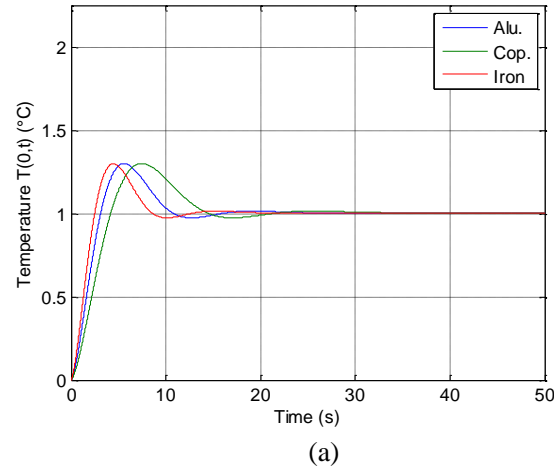
Figure 24. Simulated step responses of the temperature T(0,t) at x = 0 (a) and T(5mm,t) at x = 5mm (b) for a step input of 1°C for aluminum, copper and iron, in the case of a position sensor x_{capt} = 0 mm.

To facilitate comparison, figure 24 recalls for a position sensor $x_{capt} = 0$ mm the simulated step responses of the temperature to a step input of 1°C for aluminum, copper and iron, not only at $x = 0$ mm (figure 24.a), but also at $x = 5$ mm (figure 24.b).

Figure 25 shows for a position sensor $x_{capt} = 5$ mm the simulated step responses of the temperature at a step input of 1 ° C for aluminum, copper and iron, at $x = 0$ mm (figure 25.a) and at $x = 5$ mm (figure 25.b).

Thus, with a position sensor $x_{capt} = 5$ mm, not only the specifications regarding degree of stability and precision for steady-state temperature $T(0,t)$ are not complied with whatever material, but also the robustness of the degree of stability achieved with sensor position $x_{capt} = 0$ mm disappears. This result was predictable by viewing figure 21.
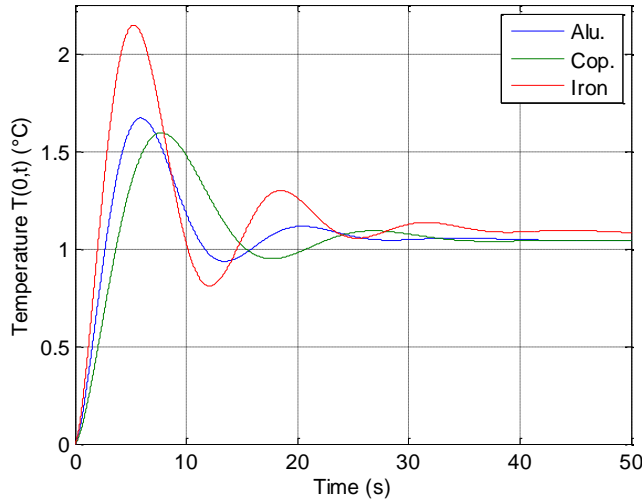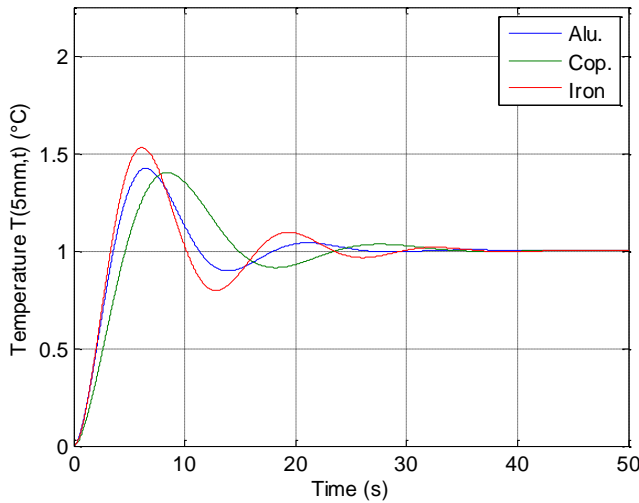
Figure 25. Simulated step responses of the temperature T(0,t) at x = 0 (a) and T(5mm,t) at x = 5mm (b) for a step input of 1°C for aluminum, copper and iron, in the case of a position sensor x_{capt} = 5 mm.

4. Conclusion

In this chapter we have studied the design of the temperature control of a diffusive medium by using an unique robust controller for three different materials, namely: aluminum, copper and iron. For the control-system design, the aluminum has been selected as the material defining the nominal model. Then, the second generation CRONE control has been chosen because the parametric uncertainty (due to the copper and the iron) leads to variations of open-loop gain. Finally, the responses in frequency-domain and in time-domain have illustrated the influence of the position of the sensor versus the actuator on the stability degree robustness.

As a future work, three tracks will be studied during the design of robust control:

- the first will be to take into account the uncertainties associated with the sensor position x_{capt};
- the second will be to estimate the temperature $T(0,t)$ from the measurement of the temperature $T(x_{capt},t)$;
- the third will be to combine the first two.

References

[Abi Zeid Daou, 2010] Abi Zeid Daou R., Francis C. and Moreau X. – *Study of the inertial effect and the nonlinearities of the CRONE suspension based on the hydropneumatic technology* – Nonlinear Dynamics, an *International Journal of Nonlinear Dynamics and Chaos in Engineering Systems*, Vol.63, N°1-2, pp.1-17, 2010.

[Abi Zeid Daou, 2011.a] Abi Zeid Daou R., Moreau X. and Francis C. – *Effect of hydropneumatic components nonlinearities on the CRONE suspension* – *IEEE Transactions on Vehicular Technology*, Vol. 61, N°2, pp. 466-474, 2011.

[Abi Zeid Daou, 2011.b] Abi Zeid Daou R., Moreau X. and Francis C. – *Control of hydro-electromechanical system using the generalized PID and the CRONE controllers* - 18th World Congress of the International Federation of Automatic Control (IFAC), Milano, Italy, August 18 – September 2, 2011.

[Abi Zeid Daou, 2012] Abi Zeid Daou R., Moreau X., Assaf R. and Christophy F. - Analysis of the Fractional Order System in the thermal diffusive interface – Part 1: application to a semi-infinite plane medium – *2nd International Conference on Advances in Computational Tools for Engineering Applications (ACTEA),* December 2012, Lebanon.

[Agrawal, 2004] Agrawal O.M.P. – Application of Fractional Derivatives in Thermal Analysis of Disk Brakes – *Journal of Nonlinear Dynamics*, Vol. 38, pp. 191-206, 2004, Kluwer Academic Publishers.

[Assaf, 2012] Assaf R., Moreau X., Abi Zeid Daou R. and Christophy F. - Analysis of the Fractional Order System in the thermal diffusive interface – Part 2: application to a finite plane medium – *2nd International Conference on Advances in Computational Tools for Engineering Applications (ACTEA),* December 2012, Lebanon.

[Battaglia, 2001] Battaglia J.L., Cois O., Puissegur L. and Oustaloup A. – Solving an inverse heat conduction problem using a non-integer identified model – *International Journal of Heat and Mass Transfer*, Vol. 44, N°14, pp. 2671-2680, 2001.

[Battaglia, 2008] Battaglia J.L. – *Heat Transfer in Materials Forming Processes* – ISTE Ed., London, 2008.

[Benchellal, 2005] Benchellal A., Bachir S., Poinot T. and Trigeassou J.C. – Identification of non-integer model of induction machines – Chapter in *Fractional differentiation and its applications*, U-Books Edition, pp. 471-482, 2005.

[Bohannan, 2000] Bohannan G. W. - *Application of Fractional Calculus to Polarization Dynamics in Solid Dielectric Materials* - Ph. D. Thesis, Montana State University, 2000.

[Canat, 2005] Canat S. and Faucher J. – Modeling, identification and simulation of induction machine with fractional derivative – Chapter in *Fractional Differentiation and its Applications*, U-Books Edition, pp. 459-470, 2005.

[Ionescu, 2011] Ionescu C., Desager K., De Keyser R. - *Fractional order model parameters for the respiratory input impedance in healthy and in asthmatic children* - Computer Methods and Programs in Biomedicine, Vol. 101, Issue 3, pp. 315-323, March 2011.

[Kuhn, 2005] Kuhn E., Forgez C. and Friedrich G. – Fractional and diffusive representation of a 42 V Ni-mH battery – Chapter in *Fractional differentiation and its applications*, U-Books Edition, pp. 423-434, 2005.

[Kusiak, 2005] Kusiak A., Battaglia J.L. and Marchal R. – Heat flux estimation in CrN coated tool during MDF machining using non integer system identification technique – Chapter in *Fractional differentiation and its applications*, U-Books Edition, pp. 377-388, 2005.

[Lanusse, 1994] P. Lanusse, De la commande CRONE de première génération à la commande CRONE de troisième génération, *PhD Thesis*, Bordeaux I University, France, 1994.

[Melchior, 2007] Melchior P., Cugnet M., Sabatier J., Poty A. and Oustaloup A. – Flatness control of a fractional thermal system – Chapter in *Advances in Fractional Calculus: Theoretical Developments and Applications in Physics and Engineering*, Springer Ed., pp. 493-509, 2007.

[Miller, 1993] Miller K.S. and Ross B. – *An Introduction to the Fractional Calculus and Fractional Differential Equations* – Wiley, New York, 1993.

[Moreau, 2002] Moreau X., Ramus-Serment C. and Oustaloup A. – Fractional Differentiation in Passive Vibration Control – Nonlinear Dynamics, An *International Journal of Nonlinear Dynamics and Chaos in Engineering Systems*, ISSN 0924-090X, Vol. 29, pp. 343-362, 2002.

[Oldham, 1974] Oldham K.B. and Spanier J. – *The Fractional Calculus* – Academic Press, New York, 1974.

[Oustaloup, 1981] Oustaloup A. - *Fractional order sinusoïdal oscillators: optimization and their use in highly linear FM modulation* - IEEE Transactions on Circuits and Systems, vol. cas 28, n°10, pp. 1007-1009, 1981.

[Oustaloup, 1983] Oustaloup A., Systèmes asservis linéaires d'ordre fractionnaire: théorie et pratique. *Masson*, Paris, 1983.

[Oustaloup, 1995] Oustaloup A., La dérivation non entière: théorie, synthèse et applications. *Hermès*, Paris, 1995.

[Oustaloup, 2005] Oustaloup A., Melchior P., Lanusse P., User's Guide, CRONE Control Design Module, CRONE Toolbox for MatLab, Version 3.5, May 27, 2005.

[Özişik, 1980] Özişik M.N. – *Heat Conduction* – John Wiley & Sons, New York, 1980.

[Özişik, 1985] Özişik M.N. – *Heat Transfer – A basic Approach* – McGraw-Hill, New York, 1985.

[Podlubny, 2005] Podlubny I. – Geometric and physical interpretation of fractional integration and fractional differentiation – Chapter in *Fractional differentiation and its applications*, U-Books Edition, pp. 3-18, 2005.

[Sabatier, 2006] Sabatier J., Aoun M., Oustaloup A., Grégoire G., Ragotand F., Roy P. - *Fractional system identification for lead acid battery sate charge estimation* - Signal Processing, 86 (10), 2645–2657, 2006.

[Sabatier, 2008] Sabatier J., Melchior P. and Oustaloup A. – *A testing bench for fractional order systems education* – JESA, Vol. 42, N°6-7-8, pp. 839-861, 2008.

[Schneider, 1957] Schneider P.J. – *Conduction Heat Transfer* – Addison-Wesley Publishing Company Inc., Reading Massachusetts, 1957.

[Sommacal, 2008] Sommacal A., Melchior P., Cabelguen J-M., Oustaloup A., Ijspeert A-J. - *Fractional Multi-Models of the Gastrocnemius Frog Muscle - Journal of Vibration and Control.* Sage Publishing, Vol. 14, No. 9-10, pp. 1415-1430, 2008.

Chapter 7

ADAPTIVE SECOND-ORDER FRACTIONAL SLIDING MODE CONTROL WITH APPLICATION TO WATER TANKS LEVEL CONTROL

Danial Senejohnny[1],*, Mohammadreza Faieghi[2],†
and Hadi Delavari [3],‡

[1]School of Electrical Engineering,
Sharif University of Technology, Tehran, Iran
[2]School of Electrical Engineering, Iran University of Science
and Technology, Tehran, Iran
[3]Faculty of Electrical Engineering, Hamedan University
of Technology, Hamedan, Iran

Abstract

Combining the fractional calculus with second-order sliding mode control, a novel type of control strategy called second order fractional sliding mode control is introduced for a class of nonlinear dynamical systems subject to uncertainty. A fractional-order switching manifold is proposed and the corresponding control law is formulated based on the Lyapunov stability theory to guarantee the sliding condition. A novel adaptation algorithm is derived to ensure perfect tracking, diminish chattering effect and steady state error by estimating switching controller parameters. Finally, numerical simulation results utilizing the dynamic model of interconnected twin tank system are presented to illustrate the effectiveness of the proposed method.

---

* E-mail address: d.senejohnny@gmail.com (Corresponding author).
† E-mail address: mfaieghi@gmail.com.
‡ E-mail address: hdelavary@gmail.com.

1. Introduction

Among existing control methodologies, the sliding mode control method, first proposed in the early fifties, is one of the control design methods to dominate the uncertainties and disturbances (i.e., the so-called 'matched' disturbances) acting on the systems. The method has gained significant research attention since early sixties in the former USSR and in the modern world since the late seventies and has been widely applied in a variety of applications [1, 2].

In first order sliding mode controller design, the sliding surface is selected such that it has relative degree one with respect to the control input. That means the control input acts on the first derivative of the sliding surface. Higher-order sliding mode is the generalization of the first-order sliding mode and the control input is performed so that it acts on higher derivatives of the sliding surface. The chattering is due to the inclusion of the sign function in the switching term and it can cause the control input to start oscillating around the zero sliding surface, resulting in unwanted wear and tear of the actuators. In general two approaches have been proposed in the literature to solve the problem. The first is to smoothen the switching term as the sliding surface gets closer to zero (soft switching) by using the continuous approximations of the discontinuous sign function, and the second is to generate "higher-order sliding modes", first introduced by Levant in 1987 [3, 4].

The second-order and higher-order sliding mode approaches have been actively developed over the last two decades for chattering attenuation and robust control of uncertain systems in variety of applications with relative degree two and higher respectively [3-12]. The second-order sliding mode control compared to first-order SMC has the advantage of providing a smooth control and better performance in the control implementation yielding less chattering and better convergence accuracy while preserving the robustness properties.

In recent years, numerous studies and applications of fractional-order systems in many areas of science and engineering have presented [13-16]. Fractional calculus, as old as the ordinary differential calculus, goes back to times when Leibniz and Newton invented differential calculus. Emergence of effective methods in differentiation and integration of non-integer order equations make fractional-order systems and controllers more and more attractive to the control engineers.

In most cases, researchers consider the fractional order controllers applied to the integer or fractional order plants to enhance the system control performance [17-25]. In [17] a new tuning method for fractional order proportional and derivative controller (FO-PD) is proposed for a class of typical second-order plants, existence of fractional adaptive controller based on high gain output feedback for linear, time-invariant, minimum phase, and single input single output systems of relative degree one is investigated in [18], several alternative methods for the control of power electronic buck converters applying fractional order control (FOC) [19], a fractional order disturbance observer for robust vibration suppression in [20], fractional order reference models in model-reference adaptive control investigated in [21], and various kind of fractional sliding mode control strategies with different fractional sliding surfaces in [22-25].

In this paper, the objective is to construct a second-order sliding mode control based on a fractional PIDD$^\alpha$ sliding surface with independent gain coefficients. Although the theme of 2-SMC is inherently proposed for high frequency chattering suppression, but an adaptive algorithm for of parameter estimation in switching surface is proposed to further suppress this phenomenon. As a way of illustrating the control scheme, simulations are carried out on interconnected twin tank system.

The rest of this paper is organized as follows, basic mathematical definitions of fractional calculus and problem statement are presented in Section 2. Second-order fractional sliding mode control strategy with fractional PIDD$^\alpha$ sliding surface, widely investigated in section 3. Adaptive algorithm for estimating switching surface parameters is given in Section 4. In Section 5, simulation results are given to support the theoretical analysis of the proposed second order fractional sliding mode control and validate its usefulness. A summary of the present research is given in Section 6.

2. Preliminaries

2.1. Basic Definition of Fractional-Order Calculus

Fractional-order integration and differentiation are the generalization of the integer-order ones. Efforts to extend the specific definitions of the traditional integer-order to the more general arbitrary order context led to different definitions for fractional derivatives [13-16]. One of the most commonly used definitions is Caputo definition. In this paper, authors have used Caputo fractional operators $_{t_0}^{c}D_t^\alpha$ as a main tool. The Caputo fractional derivative of order α of a continuous function $f(t)$ is defined as follows

$$_{t_0}^{c}D_t^\alpha f(t) = \frac{1}{\Gamma(\alpha-1)} \int_{t_0}^{t} \frac{\dot{f}(\tau)}{(t-\tau)^\alpha} d\tau, \quad 0 < \alpha < 1 \tag{1}$$

where t_0 and t are the limits of operation, and Γ is the Gamma function.

The initial conditions for the fractional order differential equations with the Caputo's derivatives are in the same form as for the integer-order differential equations. The formula for the Laplace transform of the Caputo's fractional derivative for $t_0 = 0$ has the form [13-16]:

$$\int_0^\infty e^{-st} \left\{ _0^{c}D_t^\alpha f(t) \right\} dt = s^\alpha F(s) - s^{\alpha-1} f(0) \quad 0 < \alpha \le 1 \tag{2}$$

where s denotes the Laplace operator and $F(s)$ is the Laplace transform of $f(t)$. Laplace transform of the Caputo derivative allows utilization of initial values of classical integer order derivatives. For zero initial conditions, Laplace transform of any fractional derivatives reduces to:

$$L\left\{ _0D_t^\alpha f(t) \right\} = s^\alpha F(s) \tag{3}$$

2.2. Problem Statement

Suppose a generalized nonlinear dynamic model can be described by a coupled second-order nonlinear system of the form

$$
\begin{aligned}
\dot{x}_{2k-1}(t) &= x_{2k}(t) \\
\dot{x}_{2k}(t) &= f_k(x) + b_k u_k(t) + \Delta f_k(x), \quad k = 1, \dots, n
\end{aligned}
\tag{4}
$$

where $\Delta f_k(x)$ is the lumped model uncertainty, and $x(t)$ is state vector

$$
x(t) = \left[x_1(t), x_2(t), x_3(t), \dots, x_{2n}(t) \right]^T \in R^{2n}
\tag{5}
$$

also $u_k(t) \in R$ is a control action, $b_k(x)$ and $f_k(x,t)$, are the control gains and the nonlinear dynamics of the system, respectively.

The desired state variables are defined as:

$$
x_d(t) = \left[x_1^d(t), x_2^d(t), x_3^d(t), \dots, x_{2n}^d(t) \right]^T \in R^{2n}
\tag{6}
$$

The tracking error can be defined as:

$$
\begin{aligned}
e_{2k-1}(t) &= x_{2k-1}^d(t) - x_{2k-1}(t) \\
e_{2k}(t) &= x_{2k}^d(t) - x_{2k}(t)
\end{aligned}
\tag{7}
$$

Replacing (4) in (7) yields:

$$
\begin{aligned}
\dot{e}_{2k-1}(t) &= e_{2k}(t) + \dot{x}_{2k-1}^d(t) - x_{2k}^d(t) \\
\dot{e}_{2k}(t) &= \dot{x}_{2k}^d(t) - f_k(x) - b_k u_k(t) - \delta_k(t) - \Delta f_k(x),
\end{aligned}
\tag{8}
$$

The control objective is to steer the system's states $x(t)$ to the desired trajectory $x^d(t)$. In next section the theory of second order sliding mode control with fractional $PIDD^{\alpha}$ sliding surface is studied.

3. Second Order Sliding Mode Control Strategy

In first order sliding mode controller design a desirable sliding surface, namely S, is selected and the feedback control law, acting discontinuously on $\dot{S}$, aims to fulfill the constraint $S = 0$ in finite time.

Provided that $S, \dot{S}, \dots, S^{(r-1)}$ are continuous functions and the rth order sliding set $S = \dot{S} = \dots = S^{(r-1)} = 0$, the rth order sliding mode control objective is to steer to zero not only the sliding surface S in finite time, but also its (r-1) first successive time derivatives by defining a suitable discontinuous control function acting on the rth time derivative of S [9, 12].

In the particular case of the second-order sliding mode control, the control acting on the second derivative of the sliding variable, namely $\ddot{S}$, aims to steer to zero not only the sliding surface S, but also its first-order time derivative as $S = \dot{S} = 0$ [11].

The idea of the proposed second-order sliding mode, designed for the special class of nonlinear systems (4), is based on the controller proposed in [10]. The selected sliding surface in this research is a fractional PIDD$^\alpha$ function of error (section 3.1) and the switching controller parameters are estimated according to an adaptation law (section 4). The block diagram of the proposed control scheme is depicted in Figure 1
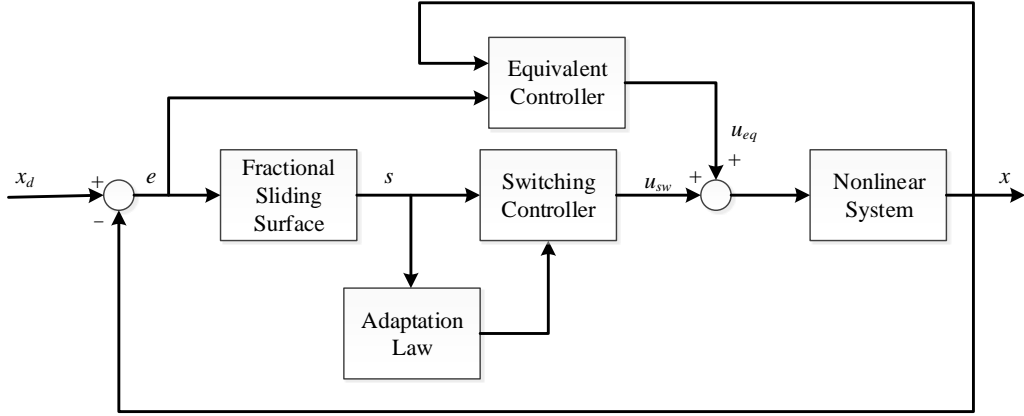
Figure 1. Block diagram of second-order sliding mode controller with fractional sliding surface.

3.1. Second Order Fractional Slidng Surface Synthesis

The problem of interest in the present case is to generate a second-order sliding mode control on a chosen sliding surface $S(t)$. In the literature, some different sliding functions were used in the derivation of sliding mode controllers such as, Terminal and fractional sliding surface [24, 26], fractional integral sliding surface [27], PD and fractional PD$^\alpha$ sliding surface [25, 28]. In order to utilize the robustness properties of fractional order controller and reduce the sliding surface settling time, we used the term $^cD^\alpha e(t)$ beside the term PID where unanimously construct a robust fractional sliding surface PIDD$^\alpha$ [22, 29].

The PIDD$^\alpha$ fractional sliding surface with constant coefficients can be introduced as:

$$\dot{S}_k(t) + \beta_k S_k(t) = k_k^P e_{2k-1}(t) + k_k^D \dot{e}_{2k-1}(t) + k_k^{FD} D^{\alpha_k} e_{2k-1}(t) + k_k^I \int_0^t e_{2k-1}(\tau)d\tau \qquad (9)$$

where k_k^P, k_k^D, k_k^I and k_k^{FD} are the independent positive constants denoting proportional derivative and fractional derivative gains, respectively, α_k is the order of fractional derivative action, $\alpha_k \in [0,1)$, β_k is also a positive constant, that determines $S_k(t)$ rate of decay. Substituting (8) in (9) one obtains

$$\dot{S}_k(t) + \beta_k S_k(t) = k_k^P e_{2k-1}(t) + k_k^D \left(e_{2k}(t) + \dot{x}_{2k-1}^d(t) - x_{2k}^d(t) \right) + k_k^{FD} D^{\alpha_k} e_{2k-1}(t) + k_k^I \int_0^t e_{2k-1}(\tau)d\tau \quad (10)$$

Taking time derivative from sliding surface given in (10) one gets

$$\ddot{S}_k(t) + \beta_k \dot{S}_k(t) = k_k^P \dot{e}_{2k-1}(t) + k_k^D \left(\dot{e}_{2k}(t) + \ddot{x}_{2k-1}^d(t) - \dot{x}_{2k}^d(t) \right) + k_k^{FD} D^{\alpha_k} \dot{e}_{2k-1}(t) + k_k^I e_{2k-1}(t) \quad (11)$$

The control input can be given as $u_k = u_k^{eq} + u_k^{sw}$, where u_k^{eq} and u_k^{sw} are the equivalent control and the switching control, respectively. The equivalent control, u_k^{eq}, proposed by Utkin [30] is based on the nominal (estimated) plant parameters (i.e. model uncertainty are not considered) and provides the main control action, while the switching control, u_k^{sw}, ensures the discontinuity of the control law across sliding surface, supplying additional control to account for the presence of model uncertainty.

By substituting (8) into (11) and then equating $\ddot{S}_k(t)$ to zero, the overall control signal become as:

$$u_k(t) = b_k^{-1} \left[\left(k_k^D \right)^{-1} \left(k_k^{FD} D^{\alpha} e_{2k-1}(t) + k_k^I e_{2k-1}(t) + k_k^P \dot{e}_{2k-1}(t) - \beta_k \dot{S}_k(t) \right) - f_k(x) + \ddot{x}_{2k-1}^d(t) \right] + u_k^{sw} \quad (12)$$

where u_k^{sw} is the switching function and is introduced to be as

$$u_k^{sw} = \left[\lambda_k^s S_k(t) + k_k^s \, \text{sgn}(\dot{S}_k(t)) \right] \quad (13)$$

where λ_k^s, k_k^s are switching feedback control gains to be chosen in sequel, and

$$\text{sgn}(\dot{S}_k(t)) = \begin{cases} +1 & \text{if } \dot{S}_k(t) > 0 \\ 0 & \text{if } \dot{S}_k(t) = 0 \\ -1 & \text{if } \dot{S}_k(t) < 0 \end{cases} \quad (14)$$

Substitution of (12) into (11), results in:

$$\ddot{S}_k(t) = -k_k^D \Delta f_k(x) - k_k^D b_k \lambda_k^s S_k(t) - k_k^D b_k k_k^s \, \text{sgn}(\dot{S}_k(t)) \quad (15)$$

The switching controllers (13) involve a discontinuous control action owing to the term $\text{sgn}(\dot{S}_k(t))$. There arises the practical issue of chattering due to imperfections in switching devices and delays. In addition, the chattering causes oscillations of the control input around the zero sliding surface, resulting in unwanted wear and tear of actuators. Recently, researchers have utilized the adaptive techniques together with the sliding mode control for many engineering systems to smooth the output from a sliding mode controller and alleviate the chattering in the pure sliding mode control [31]. Therefore, an adaptation law is derived in section 4 to estimate switching control gains λ_k^s, k_k^s. Stability and Lyapunov analysis are carried out in the next subsection.

3.2. Stability Analysis

If the system is trapped on the sliding surface, namely $S_k = \dot{S}_k = \ddot{S}_k = 0$, then the tracking error e_{2k-1} converges to zero exponentially if the coefficients, k_k^P, k_k^D, k_k^I and k_k^{FD}, are selected properly, in turn, the fractional-order differential equation (FODE) $k_k^P \dot{e}_{2k-1} + k_k^D \ddot{e}_{2k-1} + k_k^{FD} D^\alpha \dot{e}_{2k-1} + k_k^I e_{2k-1} = 0$ is stable. This implies that the closed-loop system is globally asymptotically stable.

The following *Lemma* addresses that how sliding surface parameters k_k^P, k_k^D, k_k^I and k_k^{FD} could be chosen such that FODE $k_k^P \dot{e}_{2k-1} + k_k^D \ddot{e}_{2k-1} + k_k^{FD} D^\alpha \dot{e}_{2k-1} + k_k^I e_{2k-1} = 0$ be asymptotically stable.

Lemma 1. FODE $k_k^P \dot{e}_{2k-1} + k_k^D \ddot{e}_{2k-1} + k_k^{FD} D^\alpha \dot{e}_{2k-1} + k_k^I e_{2k-1} = 0$ is asymptotically stable if $\Theta = \left\{ \lambda \mid \left| \arg(\lambda) \right| > \dfrac{\pi}{2q_k} \right\}$ [32].

Proof. Regardless of initial conditions, the Laplace transform of $k_k^P \dot{e}_{2k-1} + k_k^D \ddot{e}_{2k-1} + k_k^{FD} D^\alpha \dot{e}_{2k-1} + k_k^I e_{2k-1} = 0$ is $F_k(s) E_{2k-1}(s)$, where $E_{2k-1}(s)$ is the Laplace transform of $e_{2k-1}(t)$ and $F_k(s)$ is

$$F_k(s) = k_k^P s + k_k^D s^2 + k_k^{FD} s^{1+\alpha} + k_k^I \tag{16}$$

Assuming $\alpha_k = p_k/q_k$ where, p_k, q_k are positive constants so that $(p_k, q_k) = 1$, and $\lambda = s^{(\frac{1}{q_k})}$, then (16) can be rewritten as

$$F_k(\lambda) = k_k^P \lambda^{q_k} + k_k^D \lambda^{2q_k} + k_k^{FD} \lambda^{p_k+q_k} + k_k^I \tag{17}$$

Then it is obvious that the FODE $k_k^P \dot{e}_{2k-1} + k_k^D \ddot{e}_{2k-1} + k_k^{FD} D^\alpha \dot{e}_{2k-1} + k_k^I e_{2k-1} = 0$ is asymptotically stable if parameters k_k^P, k_k^D, k_k^I and k_k^{FD} could be chosen so that $\Theta = \left\{ \lambda \mid \left| \arg(\lambda) \right| > \dfrac{\pi}{2q_k} \right\}$.

According to the proposed *Lemma 1* the sliding surface is asymptotically stable; $e_{2k-1}(t) \to 0$ as $t \to \infty$. □

In order to analyze the stability analysis of the proposed second order sliding mode control, under control action (12) take the following Lyapunov function

$$V_k = \frac{1}{2}\left(S_k^2 + \dot{S}_k^2 \right) \tag{18}$$

The stability is guaranteed if the derivative of the Lyapunov function is negative definite, also known as the reaching condition. Taking the first time derivative from (18) one gets:

$$\dot{V}_k = S_k \dot{S}_k (1 - \lambda_k^s b_k k_k^D) - k_k^D \dot{S}_k \Delta f_k(x) - k_k^D b_k k_k^s \left| \dot{S}_k \right| \tag{19}$$

Assuming that $\Delta f_k(x)$ are bounded, namely $\eta_k = \left| \sup_x \{ \Delta f_k(x) \} \right|$, and $\lambda_k^s > 1/k_k^D b_k$, then one gets $1 - \lambda_k^s k_k^D b_k < 0$. As a result, the expression (19) can be rewritten as

$$\begin{aligned}
\dot{V}_k &\leq -\left| \dot{S}_k \right| \left| S_k \right| \left(1 - \lambda_k^s b_k k_k^D \right) + k_k^D \eta_k \left| \dot{S}_k \right| - k_k^D b_k k_k^s \left| \dot{S}_k \right| \\
&\leq -\left| \dot{S}_k \right| \left(\left| S_k \right| \left(1 - \lambda_k^s b_k k_k^D \right) + k_k^D b_k k_k^s - k_k^D \eta_k \right)
\end{aligned} \tag{20}$$

Therefore, provided $k_k^s > \dfrac{1}{b_k} \left[\dfrac{\left| S_k \right| \left(\lambda_k^s k_k^D b_k - 1 \right)}{k_k^D} + \eta_k \right]$ to dominate the model matched uncertainties [33], then $\dot{V}_k$ will be negative which implies asymptotic stability of the system and $S_k(t)$ and $\dot{S}_k(t)$ tend to zero as $t \to \infty$.

4. Adaptation Law Synthesis

In this section an adaptive scheme based on Lyapunov function for switching feedback control gains is derived. The adaptation law guarantees the system stability regardless of model uncertainty bound. Take the following Lyapunov function

$$V_k = \frac{1}{2} \left(S_k^2 + \dot{S}_k^2 + \xi_{2k-1}^{-1} (\tilde{\lambda}_k^s)^2 + \xi_{2k}^{-1} (\tilde{k}_k^s)^2 \right) \tag{21}$$

where $\tilde{\lambda}_k^s = \hat{\lambda}_k^s - \lambda_k^s$, $\tilde{k}_k^s = \hat{k}_k^s - k_k^s$ denote the estimation error. Taking time derivative from (21) with respect to time and with the sense of (20), one has:

$$\dot{V}_k = -\left| S_k \right| \left| \dot{S}_k \right| \left(1 - \lambda_k^s b_k k_k^D \right) + \left(k_k^D b_k k_k^s - k_k^D \eta_k \right) \left| \dot{S}_k \right| - \xi_{2k-1}^{-1} \tilde{\lambda}_k^s \dot{\tilde{\lambda}}_k^s - \xi_{2k}^{-1} \tilde{k}_k^s \dot{\tilde{k}}_k^s \tag{22}$$

adding and subtracting some terms, Eq. (22) can be rewritten as follows

$$\begin{aligned}
\dot{V}_k &\leq -\left| \dot{S}_k \right| \left(\left| S_k \right| \left(1 - \hat{\lambda}_k^s k_k^D b_k \right) + \hat{k}_k^s b_k k_k^D - k_k^D \eta_k \right) - \tilde{k}_k^s b_k k_k^D \left| \dot{S}_k \right| - \tilde{\lambda}_k^s b_k k_k^D \left| S_k \right| \left| \dot{S}_k \right| \\
&- \xi_{2k-1}^{-1} \tilde{\lambda}_k^s \dot{\tilde{\lambda}}_k^s - \xi_{2k}^{-1} \tilde{k}_k^s \dot{\tilde{k}}_k^s
\end{aligned} \tag{23}$$

It is clear that $\hat{k}_k^s$ and $\hat{\lambda}_k^s$ can be chosen such that

$$-\left|\dot{S}_k\right|\left(\left|S_k\right|\left(1-\hat{\lambda}_k^s b_k k_k^D\right)+\hat{k}_k^s b_k k_k^D - k_k^D \eta_k\right)<0\,,$$

so the adaptation law can be derived directly from (23) as follow

$$
\begin{aligned}
-\tilde{\lambda}_k^s b_k k_k^D \left|S_k\right|\left|\dot{S}_k\right| - \xi_{2k-1}^{-1} \tilde{\lambda}_k^s \dot{\lambda}_k^s = 0 &\rightarrow \dot{\lambda}_k^s = -\xi_{2k-1} k_k^D b_k \left|S_k\right|\left|\dot{S}_k\right| \\
-\tilde{k}_k^s b_k k_k^D \left|\dot{S}_k\right| - \xi_{2k}^{-1} \tilde{k}_k^s \dot{k}_k^s = 0 &\rightarrow \dot{k}_k^s = -\xi_{2k} k_k^D b_k \left|\dot{S}_k\right|
\end{aligned}
\tag{24}
$$

The switching controller parameters λ_k^s and k_k^s in switching control (13) are evaluated through the adaptive algorithm derived in (24).

As the bound of uncertainty is not available, choosing switching controller gains manually can make chattering effect worst. Therefore, by virtue of adaptation law (24) switching controller parameters assume their gains by making a compromise between chattering suppression and reaching condition.

5. Numerical Studies

The twin-tanks system comprised of two small tanks mounted above a reservoir which provides storage for the water, Figure 2. Water is pumped into the bottom of each tank by two independent pumps. The pump only increases the liquid level and is not responsible for pumping the water out of the tank [8].
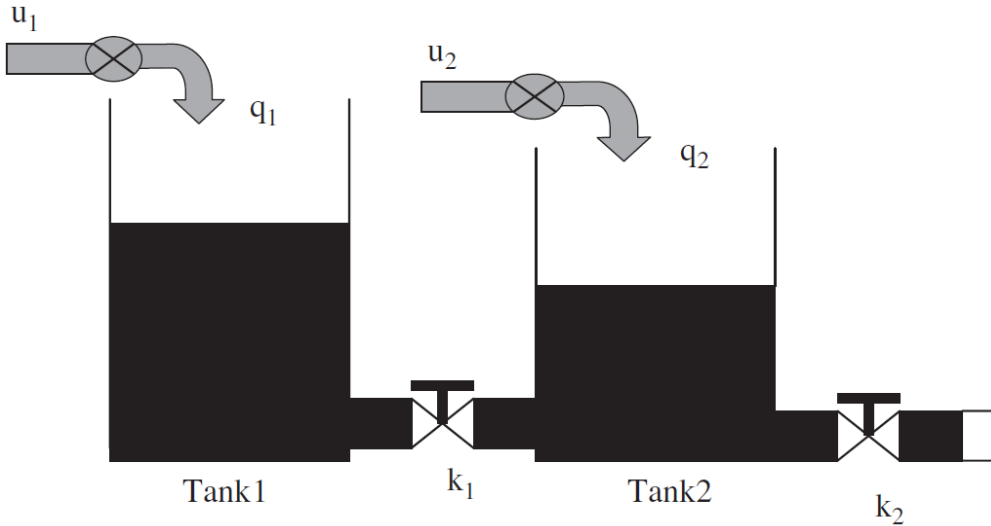
Figure 2. The plant of a liquid-level control system.

The twin-connected tanks system is a nonlinear dynamical system and the governing dynamical equations can be written as [8, 34]

$$\dot{h_1} = -\frac{k_1}{A_1}\sqrt{|h_1 - h_2|}\,sign(h_1 - h_2) + \frac{1}{A_1}q_1$$

$$\dot{h_2} = \frac{k_1}{A_2}\sqrt{|h_1 - h_2|}\,sign(h_1 - h_2) - \frac{k_2}{A_2}\sqrt{h_2} + \frac{1}{A_2}q_2$$

(25)

where h_1 and h_2 are the total water heads in Tank 1 and Tank 2 respectively, which are the two outputs of interest, and q_1, q_2 are the two inflows into the tanks. It is assumed that A_1 and A_2 are the capacities of Tank-1 and Tank-2 respectively. Both tanks assumed to have the same cross sectional area i.e. $A_1 = A_2 = A$.

It has been seen in [35] that in chemical plants, selecting the flow rate as an input is more effective than using flow as the input. Thus, if the flow rates are considered as the inputs, i.e., $\dot{q_1} = u_1$ and $\dot{q_2} = u_2$, the system dynamics can be written as

$$\ddot{h_1} = -\frac{k_1}{2A}\frac{\dot{h_1} - \dot{h_2}}{\sqrt{|h_1 - h_2|}} + \frac{1}{A}u_1$$

$$\ddot{h_2} = \frac{k_1}{2A}\frac{\dot{h_1} - \dot{h_2}}{\sqrt{|h_1 - h_2|}} - \frac{k_2}{2A\sqrt{h_2}}\dot{h_2} + \frac{1}{A}u_2$$

(26)

It seems from (25) and (26) that there is a discontinuity at $h_1 = h_2$, so desired water level is selected as $h_{d1} \neq h_{d2}$.

A mathematical model of Twin Tank can be expressed as follows:

$$\dot{x_1}(t) = x_2(t)$$

$$\dot{x_2}(t) = -\frac{k_1}{2A}\frac{x_2 - x_4}{\sqrt{|x_1 - x_3|}} + \frac{1}{A}u_1$$

$$\dot{x_3}(t) = x_4(t)$$

$$\dot{x_4}(t) = \frac{k_1}{2A}\frac{x_2 - x_4}{\sqrt{|x_1 - x_3|}} - \frac{k_2}{2A\sqrt{x_3}}x_4 + \frac{1}{A}u_2$$

(27)

System constraints: The flowed fluid into the tanks (q_1 and q_2) cannot be negative because the pumps can only pump water into the tanks. Therefore constraints on the inflow are given by $q_1, q_2 \geq 0$. In the steady state, for constant water level set points, the respective derivatives must be zero separately i.e. $\dot{h_1} = 0, \dot{h_2} = 0$. Therefore, the inequality $\frac{k_1^2}{k_1^2 + k_2^2} \leq \frac{h_2}{h_1} \leq 1$ must hold [8].

Both tanks have the same area of $70\,cm^2$, $k_1 = 14$ and $k_2 = 10$, the set point water level is selected as $h_{d,1} = x_{d,1} = 8\,cm$ and $h_{d,3} = x_{d,3} = 6\,cm$, with initial water level $h_1(0) = 4$, $h_2(0) = 2$.

In Eq. (9) sliding surface parameters are selected to be as $k_1^P = 3$, $k_1^D = 7$, $k_1^{FD} = 1$, $k_1^I = 0.5$, $\beta_1 = 1$, $\alpha_1 = 0.8$, $k_2^P = 3$, $k_2^D = 7$, $k_2^{FD} = 1$, $\beta_2 = 1$, $k_2^I = 0.5$, $\alpha_2 = 0.8$. The initial conditions are chosen as $S_1(0) = 0.5$ and $S_2(0) = 0.5$ as well. In order to smooth the control action, instead of sgn(.) function tanh(.) is used.

The simulation results with $+20\%$ variations in system's nominal parameters (i.e $A = 84\,cm^2$, $k_1 = 16.8$ and $k_2 = 12$) shows good stabilization of the water levels in both tanks Figs. 3, dashed-line and solid-line represents system's response and desired trajectory, respectively. The value of inflow in both tanks settles to the steady state values shown in Figure 3, the pumps only increases the liquid level, so their value is always positive.
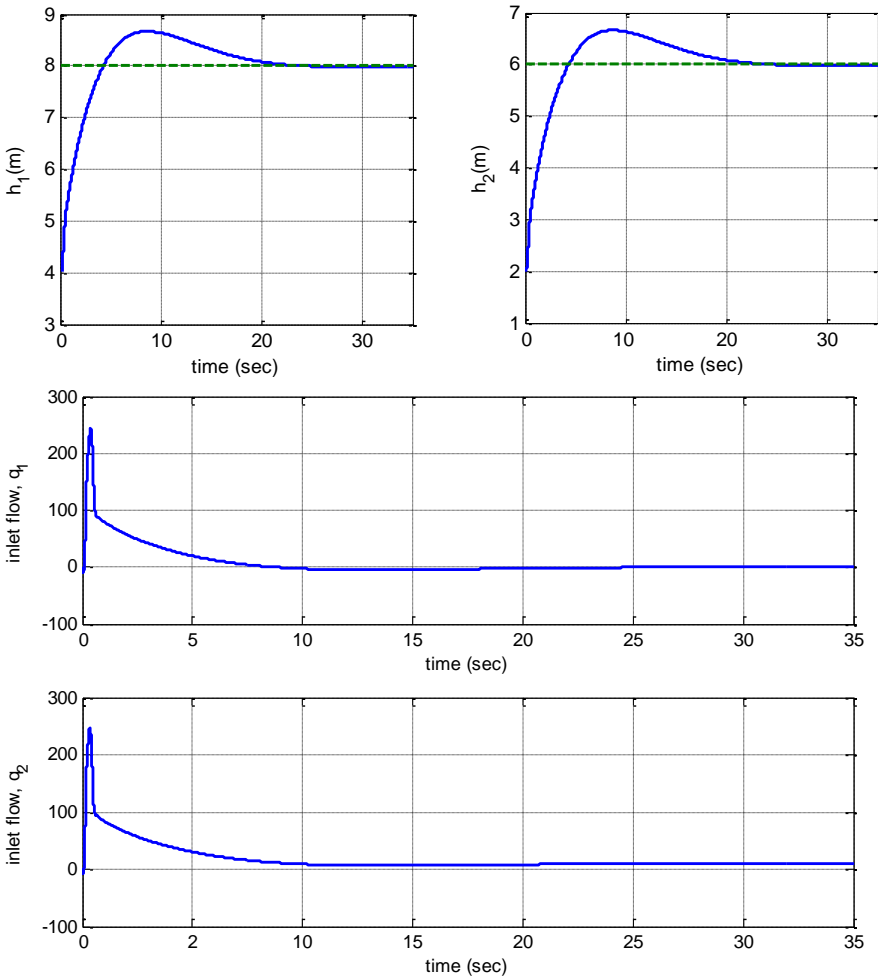
Figure 3. 2-SMC with PIDD$^\alpha$ surface and +20% variation in parameters of Twin Tank system.
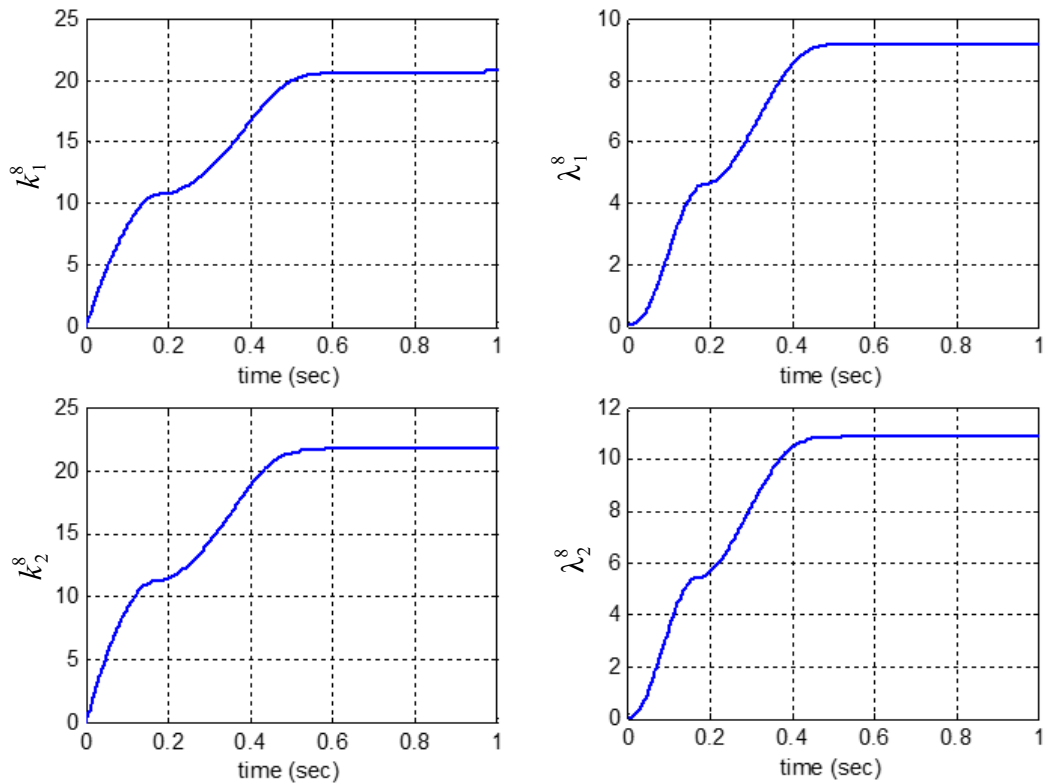
Figure 4. Adaptive parameters versus time.
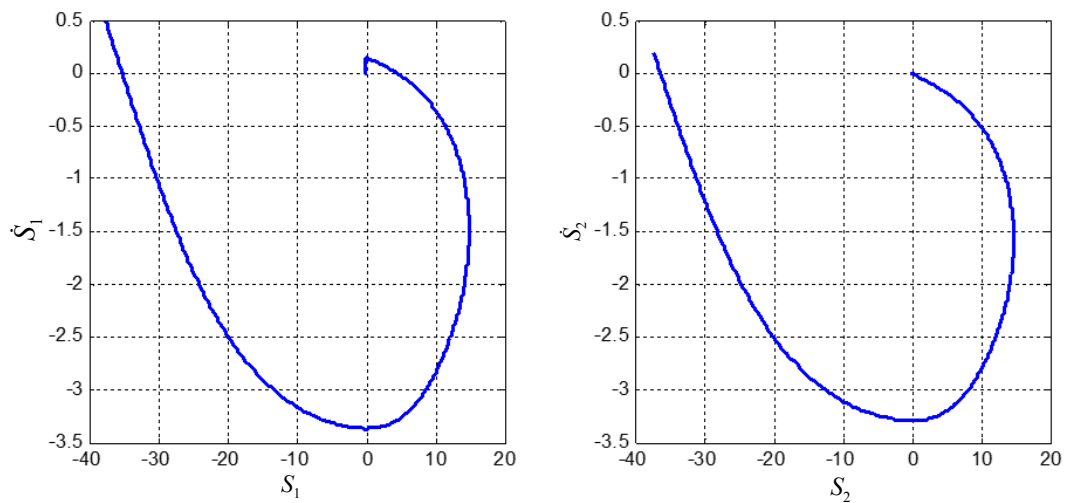
Figure 5. Phase plot.

Adaptive parameters λ_1^s, k_1^s, λ_2^s, k_2^s in (24) are estimated as follow with zero initial conditions shown in Figure 4.

$$\dot{\lambda}_1^s = -\xi_1 k_1^D b_1 |S_1| |\dot{S}_1| , \dot{k}_1^s = -\xi_2 k_1^D b_1 |\dot{S}_1|, \ \dot{\lambda}_2^s = -\xi_3 k_2^D b_2 |S_2| |\dot{S}_2| \ \ \dot{k}_2^s = -\xi_4 k_2^D b_2 |\dot{S}_2|$$

where $\xi_1 = 0.8$, $\xi_2 = 2.8$, $\xi_3 = 1$, $\xi_4 = 3.2$. In order to depict the transient behavior of estimated parameters figures are zoomed with respect to time access and are depicted for 1 second.

The trajectories of the proposed control algorithm are demonstrated on the phase portrait of the sliding variable in Fig 5, where S_1 - $\dot{S_1}$ and S_2 - $\dot{S_2}$ converge to zero.

Conclusion

In this study chattering-free robust second order sliding mode controller with PIDD^α sliding surface for nonlinear systems is investigated. The main virtue of this study relies on fractional PIDD^α sliding surface which provides more flexibility in the controller design. The other objective is to find an effective chattering-free robust method for nonlinear dynamic systems, by applying appropriate control action (12). Adaptation algorithm is derived based on second order sliding mode control, to estimate switching controller parameters without any knowledge about model uncertainty bound.

References

[1]   U. Itkis, *Control Systems of Variable Structure*. NewYork: Wiley, 1976.

[2]   W. Perruquetti, J. P. Barbot, *Sliding mode control in engineering*, New York, NY, Marcel Dekker Inc., 2002.

[3]   Levant A. Sliding order and sliding accuracy in sliding mode control. *Internat. J. Control.* 1993; 58:1247-63.

[4]   Ferrara A, Rubagotti MA. Sub-optimal second order sliding mode controller for systems with saturating actuators. *IEEE Trans Automat. Control.* 2009; 54: 1082_7.

[5]   Boiko I, Fridman L, Iriarte R, Pisano A, Usai E. Parameter tuning of second-order sliding mode controllers for linear plants with dynamic actuators. *Automatica* 2006; 42:833-9.

[6]   Davila J, Fridman L, Levant A. Second-order sliding mode observer for mechanical systems. *IEEE Trans Automat. Control.* 2005; 50:1785-9.

[7]   Bartolini G, Pisano A, Usai E, Second-order sliding-mode control of container cranes, *Automatica* 38 (2002) 1783 – 1790.

[8]   Khan MK, Spurgeon SK. Robust MIMO water level control in interconnected twin-tanks using second order sliding mode control. *Control Eng. Pract.* 2006; 14:375-86.

[9]   Levant A. Principles of 2-sliding mode design. *Automatica* 2007, 43(4), 576–86.

[10]   Eker l, Second-order sliding mode control with experimental application, *ISA Transactions* 49 (2010) 394-405.

[11]   Mihoub M, Nouri AS, Abdennour RR. Real-time application of discrete second order sliding mode control to a chemical reactor, *Control. Eng. Pract.* 2009; 17: 1089_95.

[12]   Levant A. Homogeneity approach to high-order sliding mode design. *Automatica*, 2005, 41,823–30.

[13]   I. Podlubny, *Fractional differential equations*. New York: Academic Press; 1999.

[14] R. Hilfer, *Applications of fractional calculus in physics*. Singapore: World Scientific; 2001.

[15] K. Miller, B. Ross, *An Introduction to the Fractional Calculus and Fractional Differential Equations*, Wiley, New York, 1993.

[16] K. Oldham, J. Spanier, *The Fractional Calculus*, Academic Press, New York.

[17] H. Li, Y. Luo, Y. Chen, A Fractional Order Proportional and Derivative (FOPD) Motion Controller: *Tuning Rule and Experiments, IEEE Transaction on Control System Technology*, VOL. 18, NO. 2, MARCH 2010, 516 – 520.

[18] S. Ladacia, J. J. Loiseaua, A. Charefb, Fractional order adaptive high-gain controllers for a class of linear systems, *Communication in nonlinear science and numerical simulation*, Volume 13, Issue 4, July 2008, Pages 707–714.

[19] Y. Luo, Y.Q. Chen, *Fractional order [proportional derivative] controller for a class of fractional order systems*, Volume 45, Issue 10, October 2009, Pages 2446–2450.

[20] Y. Q. Chen, B. M. Vinagre, I. Podlubny, Fractional Order Disturbance Observer for Robust Vibration Suppression, *Nonlinear Dynamics* 38:355-367, 2004.

[21] B. M. Vinagre, I. Petras, I. Podlubny, Y. Q. Chen, Using Fractional Order Adjustment Rules and Fractional Order Reference Models in Model-Reference Adaptive Control, *Nonlinear Dynamics* 29: 269–279, 2002.

[22] H. Delavari, D.M. Senejohnny, Fractional-order controllers for robot manipulator, In: Legnani G, Fassi I, editors. *Robotics: state of the art and future trends*, New York: Nova Science Publishers; 2012, pp. 187–209. ISBN: 978-1-62100-403-5.

[23] B. Zhang, Y. Pi, Y. Luo, Fractional order sliding-mode control based on parameters auto-tuning for velocity control of permanent magnet synchronous motor, *ISA Transactions*, Volume 51, Issue 5, September 2012, Pages 649–656.

[24] Dadras S, Momeni HR. Fractional terminal sliding mode control design for a class of dynamical systems with uncertainty. *Commun Nonlinear Sci Numer Simulat*, Volume 17, Issue 1, January 2012, Pages 367–377.

[25] M.Ö. Efe. Fractional fuzzy adaptive sliding-mode control of a 2-DOF direct-drive robot arm. *IEEE Trans Syst Man Cybern Part B: Cybern*. 388 2008; 38:1561–70.

[26] Z. Man, A.P. Paplinski, H.R. Wu. A robust MIMO terminal sliding mode control for rigid robotic manipulators. IEEE Trans Autom Control 1994; 39:2464–9.

[27] S. Dadras, H. Momeni. "Passivity-based fractional-order integral sliding-mode control design for uncertain fractional-order nonlinear systems." *Mechatronics*, 23(7) (2013): 880-887.

[28] H. Delavari, R. Ghaderi, A. Ranjbar, S. Momani, Fuzzy fractional order sliding mode controller for nonlinear systems, *Communication in Nonlinear Science and Numerical Simulation* 15 (2010) 963–978.

[29] L. Bruzzone, G. Bozzini, Non dimensional Analysis of Fractional-Order PDD$^{1/2}$ Control of Purely Inertial Systems, *Journal of Mechatronics and Applications*, 2010. doi:10.1155/2010/903420.

[30] VI. Utkin. *Sliding modes in optimization and control problems*. New York: Springer-Verlag; 1992.

[31] W. Perruquetti, J. P. Barbot, *Sliding mode control in engineering*, New York, NY, Marcel Dekker Inc., 2002.

[32] W.Deng, C.Li, J.Lu, Stability analysis of linear fractional differential system with multiple time delays, *Nonlinear Dynamic* (2007) 48:409–416, Springer.

[33] M. Naderi, MR. Faieghi, Comments on second-order sliding mode control with experimental application, *ISA Transations*, 2012;51(6):861–862.

[34] L.Chang, A MIMO sliding control with a second order sliding condition. In *ASME winter annual meeting*, Dallas, Texas, (1990), paper No. 90-WA/DSC-5.

[35] J. Kantor, Non-linear sliding mode controller and objective function for surge tanks. *International Journal of Control*, (1989) 50, 2025–2047.

Chapter 8

FEATURES OF FRACTIONAL OPERATORS INVOLVING FRACTIONAL DERIVATIVES AND THEIR APPLICATIONS TO THE PROBLEMS OF MECHANICS OF SOLIDS

Yury A. Rossikhin[*]**and Marina V. Shitikova**[†]
Research Center on Dynamics of Solids,
Voronezh State University of Architecture and Civil Engineering,
Voronezh, Russia

Abstract

The given Chapter consists of Introduction, 8 paragraphs and Conclusion. The state-of-the-art review of papers devoted to the fractional derivatives, fractional operators and their applications is presented in paragraph 1. In first four original paragraphs, from 2 to 5, the theoretical foundations of Rabotnovs fractional operators are presented, namely: the definition of the fractional operators, their connection with fractional derivatives, the multiplication theorem of fractional operators, the class of resolvent operators originated by Rabotnov operator. Besides, the definitions of the generalized Rabotnov operators are formulated, which are represented in terms of finite sums of the fractional Rabotnov operators with one and the same fractional parameter. The class of the resolvent operators, which are originated by the generalized Rabotnov operator, has been constructed. The main viscoelastic operators of frequent use in applications, and particularly, the operator of cylindrical rigidity, are calculated under two assumptions: (1) when the operator of volume expansion-compression is constant, and (2) when it is an operator involving the Rabotnov fractional operator. The connection between the Rabotnov fractional operator and Koellers operators is shown in paragraph 5. The applications of the presented theories to the problems of vibrations of oscillators, propagation of stationary shock waves in hereditarily elastic media, and of impact interaction of an elastic sphere with viscoelastic beams are given, respectively, in paragraphs from 6 to 8.

[*]E-mail address: yar@vgasu.vrn.ru
[†]E-mail address: mvs@vgasu.vrn.ru

1. Introduction

The number of researchers who utilize fractional derivatives in their studies is growing steadily year after year. It hardly probable that many of them even realize the reasons to insert the fractional derivatives in all conceivable and inconceivable processes, even to the detriment of the processes in themselves [1, 2, 82]. It seems likely that the exotic character of the equations describing such processes charm researchers. As this takes place, some slighting treatment of research advances of other scientists in the field, sometimes bordering through one's ignorance. Thus, for example, Usuki [85] when investigating Rayleigh waves in a fractional derivative viscoelastic medium cited the second review paper by Rossikhin and Shitikova [64] completely ignoring their first state-of-the-art article [55], wherein both volume harmonic waves in a three-dimensional fractional derivative viscoelastic medium (fractional derivative standard linear solid model) and Rayleigh waves in the same medium have been considered in detail.

Recently our attention was attracted by a paper by Dal [16], wherein the author has argued that Caputo derivative along with Riemann-Liouville derivative had been utilized by Samko et. al. [73] and Rossikhin and Shitikova [64], what is a pure invention. It seems likely that the author of [16] has read neither [73] nor [64].

In 1998, Rossikhin and Shitikova in their paper [58] devoted to the application of fractional calculus in nonlinear vibrations of suspension bridges under the conditions of different internal resonances pioneered in utilizing the approximate formula

$$D^\gamma e^{i\omega t} \approx (i\omega)^\gamma e^{i\omega t}, \tag{1}$$

which differs from the exact formula by one term

$$D^\gamma e^{i\omega t} = (i\omega)^\gamma e^{i\omega t} + \frac{\sin \pi\gamma}{\pi} \int_0^\infty \frac{u^\gamma}{u + i\omega}\, e^{-ut} du, \tag{2}$$

where ω is the frequency, t is the time, $i = \sqrt{-1}$, γ $(0 < \gamma \leq 1)$ is the fractional parameter,

$$D^\gamma x(t) = \frac{1}{\Gamma(1 - \gamma)}\, \frac{d}{dt} \int_0^t \frac{x(s)ds}{(t - s)^\gamma}, \tag{3}$$

$\Gamma(1 - \gamma)$ is the gamma-function, and $x(t)$ is an arbitrary function.

And this approximate formula (1), together with a nontraditional definition of the fractional derivative (see formula (5.82) in Samko et al [73] referring to Krasnosel'skii et al [35] and Iosida [30])

$$D^\gamma = \left(\frac{d}{dt}\right)^\gamma, \tag{4}$$

which is a good combination with the method of multiple time scales, allowed the authors of [54, 58] to solve completely the stated problem.

The same authors in 2009 [69] and 2012 [66] succeeded in showing that if one uses the method of multiple time scales for the analysis of nonlinear vibration of mechanical systems and restricts oneself by the zero- and first-order approximations, then the utilization of the approximate formula is quite reasonable, since the second term of the exact formula (2) does not enter into this approximation. This result is rather important, and it could not be ignored. However, this practice recently was applied repeatedly by various authors without any reference to its originators [16, 17].

This list could be continued, but we restrict ourselves by the enumerated examples, because there is more important problem. This problem is connected with the fact that the willingness of some researchers to accustom by all means to the usage of fractional integro-differential calculus results in inept findings published in scientific literature. Thus, equations with fractional forces of inertia made its appearance [3, 32, 37, 79, 82, 87], as well as rheological models inconsistent with the laws of thermodynamics [34], intrinsic damping [82] instead of the internal friction due to Zener [38, 66, 91], contradictions in the evaluation of the applicability of different definitions of a fractional derivative, and in particular, Riemann-Liouville definition and so-called Caputo definition [16], etc.

Many of enumerated and unstated absurdities could be prevented if instead of fractional derivatives one uses fractional operators which connected at once with fractional integro-differentiation, in so doing they possess pictorial physical meaning.

Investigation of properties of the fractional operators and their applications to the problems of Mechanics of Solids were carried out with a great success by the Russian school of thought leaded by the prominent scientist of the XXth century, Academician Yury N. Rabotnov [47, 48] (the authors of this Chapter also belong to this school of mechanicians).

The chronological list of the main contributions made prior to 1980 by Western and Russian researchers in the field of fractional calculus applications in linear viscoelasticity was presented by Rossikhin in his retrospective article [50], wherein they have been summarized in Table 1 showing to the present generation of researchers applying fractional calculus in many branches of science that the work of these pioneers was primarily responsible for the development of the *theory of fractional calculus viscoelasticity*. The simplest fractional calculus equations modeling the viscoelastic features of materials using the two approaches, i.e., via the Boltzmann-Volterra relationships with weakly singular kernels and via fractional derivatives or fractional integrals, as well as other types of fractional operators, are presented in the first column, while the Russian and Western authors who proposed them for the first time (to our knowledge) in problems of viscoelasticity are cited in the second and third columns, respectively. The last column shows the papers wherein these models were implemented for the first time for solving different dynamic problems of mechanics of solids and geophysics.

The enumeration of the models is started from the fractional Newtonian model suggested by Scott Blair [8] and Gerasimov [20] using the second and first approaches, respectively. This simplest fractional calculus element was further named by Koeller [33] as the *spring-pot* with the memory parameter γ, because it has the property that its constitutive equation has continuity from the ideal solid state at $\gamma = 0$, to the ideal fluid state at $\gamma = 1$. This model was used by Caputo [13] to study vibrations of an infinite viscoelastic layer.

The fractional calculus standard linear solid model proposed by Gross [21] and Rabotnov [46] was employed with great success in the 1970s by Russian scholars for solving a

rich variety of dynamic engineering problems [22, 23, 24, 40, 42, 70, 88]. Thus, in 1966, Rozovskii and Sinaiskii [70] were the first to study the impulse response of an oscillator representing the order of the fractional exponent as the proper fraction, $\gamma = q/n$, where q and n are integers, that results in the rationalization of the corresponding characteristic equation. This procedure is now widely used by the authors dealing with numerical algorithms in treating equations with fractional operators. The Green functions for the fractional standard linear solid and Maxwell oscillators were obtained in 1970 by Zelenev et al. in Refs. [88] and [89], respectively.

As for the wave propagation in hereditarily elastic media, then harmonic bulk waves were investigated in 1968 by Meshkov and Rossikhin [42], and the impulse load propagation in a rod made of the fractional standard linear solid material was studied by Gonsovskii and Rossikhin [23] (since this paper was originally published in a hard-to-get Russian volume, then the main results of Ref. [23] were presented in Sec. 4.3 of Ref. [55]). The impact of a hereditarily elastic rod with the Rabotnov kernel of heredity against a rigid barrier was studied by Gonsovskii et al. [22] in 1972. The nearby-front asymptotic of the stress waves in a semi-infinite rod originated by the constant load application to its free end at the initial time was obtained in 1973 by Gonsovskii and Rossikhin [24]. Two years later, the asymptotic solution in the neighborhood of the step pulse onset in a similar problem for a viscoelastic rod made of the fractional Maxwell material was presented by Buchen and Mainardi [9], using the second approach for $\gamma = 1/2$.

Rabotnov [47] was a ground breaker in the generalization of the fractional calculus standard solid model suggesting in 1966 the rheological models which describe the dissipative processes with several relaxation (retardation) times based on the fractional exponential function proposed by him in Ref. [47]. He further used such models in Ref. [48] for an approximation of the relaxation and creep functions determined experimentally for several polymeric materials. The presence of a large variety of rheological parameters allows one to describe adequately the behavior of the advanced polymeric materials possessing the complex relaxation and creep functions involving several plateau and several transition zones.

Rzhanitsyn [49] proposed in 1949 another weakly singular kernel of heredity as a creep kernel, which was written in the form of a fractional operator different from the fractional derivative or fractional integral. Its resolvent kernel of relaxation was found by Vulfson [86] in 1960. In 1967, Meshkov [38] suggested the equivalent form for the Rzhanitsyn model, while Slonimsky [77] employed it for describing relaxation processes in polymers with a chain structure of macromolecules. Four years later, Meshkov and Rossikhin [43] suggested to use the Rzhanitsyn kernel as the relaxation kernel in the Boltzmann-Volterra equation and utilized this model to study the impulse response of a viscoelastic oscillator. Belov and Bogdanovich [6] used the model proposed in Ref. [43] for investigating the propagation of a load impulse in a semi-infinite rod and constructed its asymptotic solution.

Table 1. A historical overview of Russian and Western contributors to the use of Fractional Calculus in Mechanics of Solids, from the 1940's to the 1970's

The simplest fractional calculus models	Russian researchers	Western researchers	Applications carried out prior to 1980
fractional Newtonian model $$\sigma(t) = E_\infty \tau_\varepsilon^\gamma D^\gamma \varepsilon(t)$$ $$\sigma(t) = E_\infty \tau_\varepsilon^\gamma I^{1-\gamma} d\varepsilon(t)$$	Gerasimov (1948) [20]	Scott Blair (1944) [8] Bland (1960) [93]	Caputo (1976) [13]
standard linear solid model (a) via Boltzmann − Volterra relationships $$\sigma = E_\infty \left[\varepsilon - \nu_\varepsilon \int_0^t \ni_\gamma (-t'/\tau_\varepsilon)\varepsilon(t-t')dt' \right]$$ $$\varepsilon = J_\infty \left[\sigma + \nu_\sigma \int_0^t \ni_\gamma (-t'/\tau_\sigma)\sigma(t-t')dt' \right]$$	Rabotnov (1948) [46]	Gross (1947) [21]	Rozovskii and Sinaiskii (1966) [70] Meshkov and Rossikhin (1968) [42] Zelenev et al. (1970) [89] Meshkov et al. (1971) [40] Gonsovskii et al. (1972) [22] Gonsovskii and Rossikhin (1972) [23], (1973) [24]
(b) via fractional derivatives $$\sigma + \tau_\varepsilon^\gamma D^\gamma \sigma = E_0(\varepsilon + \tau_\sigma^\gamma D^\gamma \varepsilon)$$ (b) via fractional operators $$\sigma = E_\infty \left[1 - \nu_\varepsilon \frac{\tau_\varepsilon^{-\gamma} I^\gamma}{1+\tau_\varepsilon^{-\gamma} I^\gamma} \right] \varepsilon$$	Meshkov (1967) [38] Rabotnov (1966) [47]	Caputo and Mainardi (1971) [14]	Caputo and Mainardi (1971) [14, 15]
Kelvin − Voigt model (a) via Boltzmann − Volterra relationships $$\varepsilon = J_0 \int_0^t \ni_\gamma (-t'/\tau_\sigma)\sigma(t-t')dt'$$ (b) via fractional derivatives $$\sigma = E_0(\varepsilon + \tau_\sigma^\gamma D^\gamma \varepsilon)$$	Shermergor (1966) [76] Shermergor (1966) [76]	Caputo (1967) [11] Smit and de Vries (1970) [78]	Caputo (1967) [11], (1974) [12] Bagley and Torvik (1979) [4]

Table 1. (Continued)

The simplest fractional calculus models	Russian researchers	Western researchers	Applications carried out prior to 1980
Maxwell model (a) via Boltzmann − Volterra relationships $\sigma = E_\infty \left[\varepsilon - \int_0^t \ni_\gamma (-t'/\tau_\varepsilon)\varepsilon(t-t')dt' \right]$	Shermergor (1966) [76]		Zelenev et al. (1970) [88]
(b) via fractional derivatives $\sigma + \tau_\varepsilon^{1/2} D^{1/2}\sigma = \eta\dot{\varepsilon}$ $\sigma + \tau_\varepsilon^\gamma D^\gamma \sigma = E_\infty \tau_\varepsilon^\gamma D^\gamma \varepsilon$	Meshkov (1967) [38]	Gemant (1936) [19] Caputo and Mainardi (1971) [15]	Buchen and Mainardi (1975) [9]
(c) via fractional integral $\varepsilon = J_\infty(\sigma + \tau_\varepsilon^{-\gamma} I^\gamma \sigma)$	Shermergor (1966) [76]		
generalized standard linear solid model $\sigma = E_\infty \left[\varepsilon - \int_0^t \sum_{j=1}^n e_j \ni_\gamma (-t'/\tau_{\varepsilon j})\varepsilon(t-t')dt' \right]$	Rabotnov (1966) [47]		
Fractional operator with Rzhanitsyn kernel (a) as a creep kernel $\varepsilon = J_\infty \left[1 + \nu_\sigma \left(1 + \tau_\sigma \frac{d}{dt} \right)^{-\gamma} \right] \sigma$ $\varepsilon = J_\infty \left[\sigma + \nu_\sigma \int_0^t \frac{t^{\gamma-1} e^{-t'/\tau_\sigma}}{\tau_\sigma^\gamma \Gamma(\gamma)} \sigma(t-t')dt' \right]$ $\sigma = E_\infty \left[\varepsilon - \int_0^t e^{-t'/\tau_\sigma} \ni_\gamma (-\nu_\sigma t'/\tau_\sigma)\varepsilon(t-t')dt' \right]$ (b) as a relaxation kernel $\sigma = E_\infty \left[\varepsilon - \nu_\varepsilon \int_0^t \frac{t^{\gamma-1} e^{-t'/\tau_\varepsilon}}{\tau_\varepsilon^\gamma \Gamma(\gamma)} \varepsilon(t-t')dt' \right]$	Meshkov (1967) [38] Slonimsky (1967) [77] Rzhanitsyn (1949) [49] Vulfson (1960) [86] Meshkov and Rossikhin (1971) [43]		 Meshkov and Rossikhin (1971) [43] Belov and Bogdanovich (1976) [6]

The fractional derivative Kelvin-Voigt and standard linear solid models were first proposed by Shermergor [76] and Meshkov [38] in 1966 and 1967, respectively, and then independently but at a somewhat later time by Caputo [11] and Caputo and Mainardi [14], respectively. The early applications of these models were made by Caputo [11] in 1967 and Caputo and Mainardi [14, 15] in 1971 for solving the problems dealing with geophysics. In 1974, the fractional derivative Kelvin-Voigt model was utilized by Caputo [12] to study vibrations of an infinite viscoelastic layer.

In the late 1970s, an investigation on fractional derivative models and their application to the problems of structural dynamics was initiated in the USA by Torvik and Bagley. Their first paper in the field [4] dated to 1979 was devoted to modeling an elastomer damper as a fractional derivative Kelvin-Voigt oscillator. During the next decade, these authors contributed significantly to incorporate the fractional derivative standard linear solid model into the numerical procedures for investigating viscoelastically damped structures [5, 83, 84].

Thus, from the papers cited in the forth column of Table 1 it is clearly evident what a tremendous work was carried out in the late 60's and 70's by Russian and Italian researchers in the application of fractional calculus viscoelastic models (formulated earlier or in the same period using the two approaches as shown in the first three columns of Table 1) for solving dynamic problems in the mechanics of solids and geophysics.

2.   Rabotnov's Fractional Operators and Main Formulas of Algebra of Fractional Operators

We shall proceed our presentation in this Section from the analysis of the rheological model, which is called as *the fractional derivative standard linear solid model*

$$\sigma + \tau_\varepsilon^\gamma D^\gamma \sigma = E_0(\varepsilon + \tau_\sigma^\gamma D^\gamma \varepsilon), \tag{5}$$

in so doing

$$\tau_\varepsilon^\gamma \tau_\sigma^{-\gamma} = E_0 E_\infty^{-1}, \tag{6}$$

where σ is the stress, ϵ is the strain, τ_ϵ and τ_σ are the relaxation and retardation times, respectively, E_0 and E_∞ are the relaxed (prolonged modulus of elasticity, or the rubbery modulus) and nonrelaxed (instantaneous modulus of elasticity, or the glassy modulus) magnitudes of the elastic modulus, respectively.

Meshkov [38] was the first to derive formula (5) in 1967.

Expressing σ in terms of ε or ε in terms of σ from (5) with due account for (6) yields

$$\sigma = E_\infty \left(\varepsilon - \nu_\varepsilon \frac{1}{1 + \tau_\varepsilon^\gamma D^\gamma} \varepsilon \right), \tag{7}$$

$$\varepsilon = J_\infty \left(\sigma + \nu_\sigma \frac{1}{1 + \tau_\sigma^\gamma D^\gamma} \sigma \right), \tag{8}$$

where $E_0 = J_0^{-1}$, $E_\infty = J_\infty^{-1}$,

$$\nu_\varepsilon = \frac{E_\infty - E_0}{E_\infty} = \frac{J_0 - J_\infty}{J_0}, \quad \nu_\sigma = \frac{E_\infty - E_0}{E_0} = \frac{J_0 - J_\infty}{J_\infty}. \tag{9}$$

Relationships (7) and (8) involve one and the same operator which will be denoted further as $\ni_\gamma^* (\tau_i^\gamma)$, i.e.,

$$\ni_\gamma^* (\tau_i^\gamma) = \frac{1}{1 + \tau_i^\gamma D^\gamma} \quad (i = \sigma, \varepsilon). \tag{10}$$

Operator (10) was introduced into consideration by Yu. N. Rabotnov in a little bit another form [46].

In order to obtain operator (10) in another form, we multiply the numerator and denominator of the fraction in (10) by $I^\gamma \tau_i^{-\gamma}$, where

$$I^\gamma x(t) = \int_0^t \frac{(t - s)^{\gamma - 1}}{\Gamma(\gamma)} x(s) ds \tag{11}$$

is the fractional integral.

Considering that $D^\gamma I^\gamma = 1$, we find

$$\ni_\gamma^* (\tau_i^\gamma) = \frac{I^\gamma \tau_i^{-\gamma}}{1 - \left(-I^\gamma \tau_i^{-\gamma}\right)}. \tag{12}$$

If we suppose that the right part of formula (12) is the sum of an infinite decreasing geometrical progression, the denominator of which is equal to $d = -I^\gamma \tau_i^{-\gamma}$, then $\ni_\gamma^* (\tau_i^\gamma)$ could be represented as

$$\ni_\gamma^* (\tau_i^\gamma) = \sum_{n=0}^\infty (-1)^n \tau_i^{-\gamma(n+1)} I^{\gamma(n+1)}, \tag{13}$$

or

$$\ni_\gamma^* (\tau_i^\gamma) x(t) = \int_0^t \ni_\gamma (-s/\tau_i) x(t - s) ds, \tag{14}$$

where

$$\ni_\gamma (-t/\tau_i) = \frac{t^{\gamma - 1}}{\tau_i^\gamma} \sum_{n=0}^\infty \frac{(-1)^n (t/\tau_i)^{\gamma n}}{\Gamma[\gamma(n + 1)]}. \tag{15}$$

Considering (14), formulas (7) and (8) take the form

$$\sigma = E_\infty \left[\varepsilon - \nu_\varepsilon \int_0^t \ni_\gamma (-s/\tau_\varepsilon) \varepsilon(t - s) ds \right], \tag{16}$$

$$\varepsilon = J_\infty \left[\sigma + \nu_\sigma \int_0^t \ni_\gamma (-s/\tau_\sigma) \sigma(t - s) ds \right]. \tag{17}$$

Formulas (16) and (17) are Boltzmann-Volterra relationships with weakly singular kernels of heredity $\ni_\gamma (-t/\tau_i)$, which attenuate at $t \to \infty$, in so doing resolvent kernels occur to be the same. Only exponential kernels possess this feature, and the kernels (15) go over into exponential kernels at $\gamma = 1$, i.e.,

$$\ni_\gamma (-t/\tau_i) = \tau_i^{-1} \exp(-t/\tau_i). \tag{18}$$

These properties of $\ni_\gamma (-t/\tau_i)$-function allowed Rabotnov to call it as a *fractional exponential function*.

Relationships (16) and (17) sometimes are written in the form

$$\sigma = \widetilde{E}\varepsilon, \qquad \widetilde{E} = E_\infty \left[1 - \nu_\varepsilon \ni_\gamma^* (\tau_\varepsilon^\gamma)\right], \tag{19}$$

$$\varepsilon = \widetilde{J}\sigma, \qquad \widetilde{J} = J_\infty \left[1 + \nu_\sigma \ni_\gamma^* (\tau_\sigma^\gamma)\right]. \tag{20}$$

In conclusion of this Section we present the important formula for the multiplication of the operators

$$\ni_\gamma^* (\tau_\varepsilon^\gamma) \ni_\gamma^* (\tau_\sigma^\gamma) = \frac{\tau_\varepsilon^\gamma \ni_\gamma^* (\tau_\varepsilon^\gamma) - \tau_\sigma^\gamma \ni_\gamma^* (\tau_\sigma^\gamma)}{\tau_\varepsilon^\gamma - \tau_\sigma^\gamma}. \tag{21}$$

In fact

$$\ni_\gamma^* (\tau_\varepsilon^\gamma) \ni_\gamma^* (\tau_\sigma^\gamma) = \frac{1}{(1 + \tau_\varepsilon^\gamma D^\gamma)(1 + \tau_\sigma^\gamma D^\gamma)} = \frac{A_1}{1 + \tau_\varepsilon^\gamma D^\gamma} + \frac{A_2}{1 + \tau_\sigma^\gamma D^\gamma}, \tag{22}$$

where

$$A_1 = \frac{\tau_\varepsilon^\gamma}{\tau_\varepsilon^\gamma - \tau_\sigma^\gamma}, \quad A_2 = -A_1 \frac{\tau_\sigma^\gamma}{\tau_\varepsilon^\gamma} = -\frac{\tau_\sigma^\gamma}{\tau_\varepsilon^\gamma - \tau_\sigma^\gamma}.$$

It should be noted that formula (21) does not coincide with that presented in Rabotnov [48] (see formula (5.10) there), since we use the dimensionless operator $\ni_\gamma^* (\tau_i^\gamma)$, while the dimensional operator was utilized in [48].

3.   Generalized Rabotnov Operators

Generalized Rabotnov operators are written in the form

$$E_* = E_\infty \left[1 - \sum_{j=1}^n m_j \ni_\gamma^* \left(t_j^\gamma\right)\right], \tag{23}$$

$$J_* = J_\infty \left[1 + \sum_{i=1}^n n_i \ni_\gamma^* (\tau_i^\gamma)\right], \tag{24}$$

where m_j, t_j $(j = 1, 2, ..., n)$ and n_i, τ_i^γ $(i = 1, 2, ..., n)$ are constants.

Since operators (19) and (20) are reciprocal, i.e., $E_* J_* = J_* E_* = 1$, then the following relationship should be valid:

$$1 = \left[1 + \sum_{i=1}^n n_i \ni_\gamma^* (\tau_i^\gamma)\right] \left[1 - \sum_{j=1}^n m_j \ni_\gamma^* \left(t_j^\gamma\right)\right]. \tag{25}$$

Assume that the constants n_i and τ_i^γ $(i = 1, ..., n)$ are known, and it is necessary to determine the constants m_j and t_j^γ $(j = 1, ..., n)$. Using formula (21), let us rewrite (25) in the form

$$\sum_{i=1}^n n_i \ni_\gamma^* (\tau_i^\gamma) - \sum_{j=1}^n m_j \ni_\gamma^* \left(t_j^\gamma\right) - \sum_{i=1}^n \sum_{j=1}^n n_i m_j \frac{\tau_i^\gamma \ni_\gamma^* (\tau_i^\gamma) - t_j^\gamma \ni_\gamma^* \left(t_j^\gamma\right)}{\tau_i^\gamma - t_j^\gamma} = 0,$$

whence it follows that

$$\sum_{i=1}^{n} n_i \ni_\gamma^* (\tau_i^\gamma) \left[1 - \sum_{j=1}^{n} \frac{m_j \tau_i^\gamma}{\tau_i^\gamma - t_j^\gamma} \right] - \sum_{j=1}^{n} m_j \ni_\gamma^* \left(t_j^\gamma \right) \left[1 - \sum_{i=1}^{n} \frac{n_i t_j^\gamma}{\tau_i^\gamma - t_j^\gamma} \right] = 0. \quad (26)$$

From (26) we find

$$1 - \sum_{j=1}^{n} \frac{m_j \tau_i^\gamma}{\tau_i^\gamma - t_j^\gamma} = 0, \quad (27)$$

$$1 - \sum_{i=1}^{n} \frac{n_i t_j^\gamma}{\tau_i^\gamma - t_j^\gamma} = 0, \quad (28)$$

or in another form

$$1 + \sum_{j=1}^{n} \frac{m_j t_j^{-\gamma}}{\tau_i^{-\gamma} - t_j^{-\gamma}} = 0, \quad (29)$$

$$1 + \sum_{i=1}^{n} \frac{n_i \tau_i^{-\gamma}}{\tau_i^{-\gamma} - t_j^{-\gamma}} = 0. \quad (30)$$

From the n-th order Eqs. (28) or (30) we could define n magnitudes of $t_j^{\pm\gamma}$ ($j = 1, ..., n$), while knowing $t_j^{\pm\gamma}$ from the set of n Eqs. (27) or (29) we find the values m_j ($j = 1, ..., n$).

Suppose now that constants m_j and t_j^γ ($j = 1, ..., n$) are known, and it is a need to determine constants n_i and τ_i^γ ($i = 1, ..., n$). In this case, from the n-th order Eqs. (27) or (29) we could define n magnitudes of $\tau_i^{\pm\gamma}$, while knowing $\tau_i^{\pm\gamma}$, we could find the values of n_i from the set of n Eqs. (28) or (30).

The set of equalities (30) implies that the values $t_j^{-\gamma}$ are the roots of the equation

$$F_1(x) = 1 + \sum_{i=1}^{n} \frac{n_i \tau_i^{-\gamma}}{\tau_i^{-\gamma} - x} = 0. \quad (31)$$

Equation (31) possesses n real positive roots if $\tau_i^{-\gamma} > 0$ and $n_i > 0$.

If we suppose that $\tau_{k+1}^{-\gamma} > \tau_k^{-\gamma}$, then zeros of the function $F_1(x)$ are located between the poles, thus

$$\tau_k^{-\gamma} < t_k^{-\gamma} < \tau_{k+1}^{-\gamma}, \qquad \tau_n^{-\gamma} < t_n^{-\gamma}. \quad (32)$$

The plot of the function $F_1(x)$ for $n = 2$ is presented in Fig. 1a, where $x = t^{-\gamma}$.

The set of equalities (29) represents a system of n linear equations for n unknown coefficients m_j. Assign that

$$F_2(y) = 1 + \sum_{j=1}^{n} \frac{m_j t_j^{-\gamma}}{y - t_j^{-\gamma}}, \quad (33)$$

where $y = \tau^{-\gamma}$.

Function $F_2(y)$ (33) possesses n zeros at $y = \tau_i^{-\gamma}$, while at $y \to t_j^{-\gamma}$ it tends to $+\infty$ or $-\infty$ depending on the sign of m_j and the direction of the transition to the limit. Since the
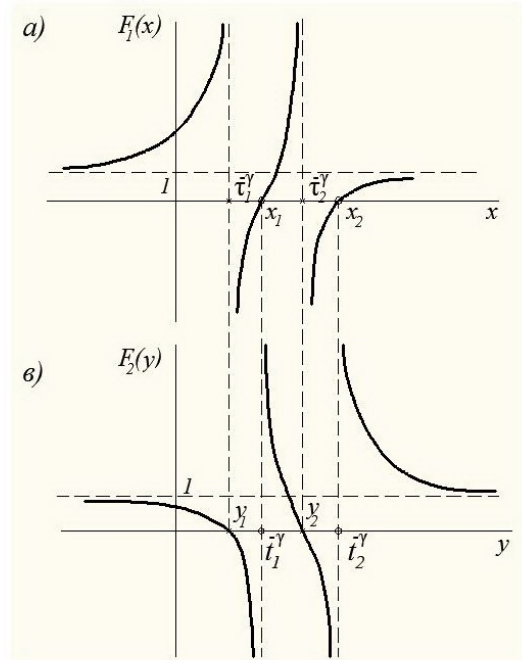
Figure 1. Functions $F_1(x)$ and $F_2(y)$.

points $\tau_i^{-\gamma}$ are located between the points $t_j^{-\gamma}$, except the point $\tau_1^{-\gamma}$ (see formula (32)), then the plot for the function $F_2(y)$ for $n = 2$ should be as that in Fig. 1b, but this is possible only when all m_j are positive.

At $n = 1$, from (27) and (28), (19) and (20) we obtain

$$1 + \nu_\varepsilon \, \frac{\tau_\sigma^\gamma}{\tau_\varepsilon^\gamma - \tau_\sigma^\gamma} = 0, \tag{34}$$

$$1 + \nu_\sigma \, \frac{\tau_\varepsilon^\gamma}{\tau_\varepsilon^\gamma - \tau_\sigma^\gamma} = 0, \tag{35}$$

whence it follows

$$1 - \nu_\varepsilon = \left(\frac{\tau_\varepsilon}{\tau_\sigma}\right)^\gamma, \qquad 1 + \nu_\sigma = \left(\frac{\tau_\sigma}{\tau_\varepsilon}\right)^\gamma. \tag{36}$$

Considering (9), formulas (36) go over in relationships (6).

At $n = 2$, operators J_* and E_* take the form

$$J_* = J_\infty \left[1 + n_1 \ni_\gamma^* (\tau_1^\gamma) + n_2 \ni_\gamma^* (\tau_2^\gamma)\right], \tag{37}$$

and

$$E_* = E_\infty \left[1 - m_1 \ni_\gamma^* (t_1^\gamma) - m_2 \ni_\gamma^* (t_2^\gamma)\right]. \tag{38}$$

Multiplying reciprocal operators (37) and (38) yields

$$1 + \frac{n_1 \tau_1^{-\gamma}}{\tau_1^{-\gamma} - x} + \frac{n_2 \tau_2^{-\gamma}}{\tau_2^{-\gamma} - x} = 0, \qquad x = t_i^{-\gamma}, \tag{39}$$

$$\begin{cases} a_1 m_1 + a_2 m_2 = 1, \\ b_1 m_1 + b_2 m_2 = 1, \end{cases} \tag{40}$$

where it is evident from Fig. 1 that

$$a_1 = \frac{t_1^{-\gamma}}{t_1^{-\gamma} - \tau_1^{-\gamma}} > 0, \qquad a_2 = \frac{t_2^{-\gamma}}{t_2^{-\gamma} - \tau_1^{-\gamma}} > 0,$$

$$b_1 = \frac{t_1^{-\gamma}}{t_1^{-\gamma} - \tau_2^{-\gamma}} < 0, \qquad b_2 = \frac{t_2^{-\gamma}}{t_2^{-\gamma} - \tau_2^{-\gamma}} > 0.$$

Note that the signs of the values a_1, a_2, b_1, and b_2 could be established with help of Fig. 1.

Equation (39) could be written in the form

$$x^2 - \left[\tau_1^{-\gamma}(1 + n_1) + \tau_2^{-\gamma}(1 + n_2) \right] x + \tau_1^{-\gamma} \tau_2^{-\gamma}(1 + n_1 + n_2) = 0, \tag{41}$$

and its roots are defined by formula

$$\begin{aligned} x_{1,2} &= \left(t^{-\gamma} \right)_{1,2} = \frac{1}{2} \left[\tau_1^{-\gamma}(1 + n_1) + \tau_2^{-\gamma}(1 + n_2) \right] \\ &\pm \frac{1}{2} \sqrt{ \left[\tau_1^{-\gamma}(1 + n_1) - \tau_2^{-\gamma}(1 + n_2) \right]^2 + 4\tau_1^{-\gamma} \tau_2^{-\gamma} n_1 n_2 }, \end{aligned} \tag{42}$$

and both roots are positive.

Substituting the found roots (42) in (40), we have

$$m_1 = \frac{b_2 - a_2}{a_1 b_2 - a_2 b_1} > 0, \qquad m_2 = \frac{a_1 - b_1}{a_1 b_2 - a_2 b_1} > 0, \tag{43}$$

which are positive as well.

If, vice versa, it is necessary to determine the values of $\tau_i^{-\gamma}$ and n_i, then using Eqs. (29) and (30), we have

$$1 - \frac{m_1 t_1^{-\gamma}}{t_1^{-\gamma} - x} - \frac{m_2 t_2^{-\gamma}}{t_2^{-\gamma} - x} = 0, \quad x = \tau_i^{-\gamma}, \tag{44}$$

$$\begin{cases} \frac{\tau_1^{-\gamma}}{t_1^{-\gamma} - \tau_1^{-\gamma}} \, n_1 + \frac{\tau_2^{-\gamma}}{t_1^{-\gamma} - \tau_2^{-\gamma}} \, n_2 = 1, \\ \frac{\tau_1^{-\gamma}}{t_2^{-\gamma} - \tau_1^{-\gamma}} \, n_1 + \frac{\tau_2^{-\gamma}}{t_2^{-\gamma} - \tau_2^{-\gamma}} \, n_2 = 1. \end{cases} \tag{45}$$

It is convenient to rewrite (44) in the form

$$x^2 - \left[t_1^{-\gamma}(1 - m_1) + t_2^{-\gamma}(1 - m_2) \right] x + t_1^{-\gamma} t_2^{-\gamma}(1 - m_1 - m_2) = 0. \tag{46}$$

The solution of (46) gives us the values of $\tau_1^{-\gamma}$ and $\tau_2^{-\gamma}$, and then substituting $\tau_1^{-\gamma}$ and $\tau_2^{-\gamma}$ in (45), we find n_1 and n_2.

Let us present here two more useful formulas, which are the immediate generalization of formulas (36).

Using the Viéte theorem, from (41) and (46) we have

$$t_1^{-\gamma} t_2^{-\gamma} = \tau_1^{-\gamma} \tau_2^{-\gamma} (1 + n_1 + n_2),$$

$$\tau_1^{-\gamma} \tau_2^{-\gamma} = t_1^{-\gamma} t_2^{-\gamma} (1 - m_1 - m_2),$$

or

$$\frac{t_1^{-\gamma} t_2^{-\gamma}}{\tau_1^{-\gamma} \tau_2^{-\gamma}} = 1 + n_1 + n_2, \tag{47}$$

$$\frac{\tau_1^{-\gamma} \tau_2^{-\gamma}}{t_1^{-\gamma} t_2^{-\gamma}} = 1 - m_1 - m_2. \tag{48}$$

Formulas (47) and (48) are generalized easily over the case of the operators defined by relationships (23) and (24). In this case, they look like as follows:

$$\left(\frac{\prod_{i=1}^{n} \tau_i}{\prod_{j=1}^{n} t_j} \right)^{\gamma} = 1 + \sum_{i=1}^{n} n_i, \tag{49}$$

$$\left(\frac{\prod_{j=1}^{n} t_j}{\prod_{i=1}^{n} \tau_i} \right)^{\gamma} = 1 - \sum_{j=1}^{n} m_j. \tag{50}$$

4. Calculation of the Main Viscoelastic Operators

4.1. The Case of Constant Operator of the Bulk Extension-Compression $\widetilde{K}$

For the majority of viscoelastic materials, the bulk modulus remains a constant value during the process of mechanical deformation, i.e.,

$$\frac{\widetilde{E}}{1 - 2\widetilde{\nu}} = \frac{E_\infty}{1 - 2\nu_\infty}, \tag{51}$$

where ν_∞ is the nonrelaxed Poisson's ratio, and $\widetilde{\nu}$ is Poisson's operator.

From (51) with due account for (19) we have

$$\widetilde{\nu} = \nu_\infty + \frac{1}{2} \left(1 - 2\nu_\infty \right) \nu_\varepsilon \ni_\gamma^* \left(\tau_\varepsilon^\gamma \right). \tag{52}$$

Further we will require the operators $(1 + \widetilde{\nu})^{-1}$ and $(1 - \widetilde{\nu})^{-1}$, which are determined considering (52) according to the above developed procedure, i.e.,

$$\frac{1}{1 + \nu_\infty + \frac{1}{2} \left(1 - 2\nu_\infty \right) \nu_\varepsilon \ni_\gamma^* \left(\tau_\varepsilon^\gamma \right)} = \frac{1}{1 + \nu_\infty} \left[1 - B \ni_\gamma^* \left(t_1^\gamma \right) \right], \tag{53}$$

$$\frac{1}{1 - \nu_\infty - \frac{1}{2}(1 - 2\nu_\infty)\nu_\varepsilon \ni_\gamma^* (\tau_\varepsilon^\gamma)} = \frac{1}{1 - \nu_\infty} \left[1 + D \ni_\gamma^* (t_2^\gamma) \right], \qquad (54)$$

where B, t_1^γ, and D, t_2^γ are yet unknown constants.

Multiplying the operators in the right-hand sides of Eqs. (53) and (54), respectively, by the denominator of the fraction in their left-hand side parts and considering (21), we are led to the following equations:

$$\frac{1}{2} \frac{(1 - 2\nu_\infty)\nu_\varepsilon}{1 + \nu_\infty} \left[1 - B \frac{\tau_\varepsilon^\gamma}{\tau_\varepsilon^\gamma - t_1^\gamma} \right] \ni_\gamma^* (\tau_\varepsilon^\gamma) - B \left[1 - \frac{1}{2} \frac{(1 - 2\nu_\infty)\nu_\varepsilon}{1 + \nu_\infty} \frac{t_1^\gamma}{\tau_\varepsilon^\gamma - t_1^\gamma} \right] \ni_\gamma^* (t_1^\gamma) = 0,$$
$$(55)$$

$$-\frac{1}{2} \frac{(1 - 2\nu_\infty)\nu_\varepsilon}{1 - \nu_\infty} \left[1 + D \frac{\tau_\varepsilon^\gamma}{\tau_\varepsilon^\gamma - t_2^\gamma} \right] \ni_\gamma^* (\tau_\varepsilon^\gamma) + D \left[1 + \frac{1}{2} \frac{(1 - 2\nu_\infty)\nu_\varepsilon}{1 - \nu_\infty} \frac{t_2^\gamma}{\tau_\varepsilon^\gamma - t_2^\gamma} \right] \ni_\gamma^* (t_2^\gamma) = 0. \quad (56)$$

Vanishing to zero the terms in square brackets in (55) and (56), we could determine the unknown constants

$$B = \frac{(1 - 2\nu_\infty)\nu_\varepsilon}{2(1 + \nu_\infty) + \nu_\varepsilon(1 - 2\nu_\infty)} = \frac{\tau_\varepsilon^\gamma - t_1^\gamma}{\tau_\varepsilon^\gamma}, \qquad (57)$$

$$t_1^{-\gamma} = \tau_\varepsilon^{-\gamma} \left[1 + \frac{(1 - 2\nu_\infty)\nu_\varepsilon}{2(1 + \nu_\infty)} \right], \qquad t_1^\gamma = \frac{\tau_\varepsilon^\gamma}{A}, \qquad (58)$$

$$D = \frac{(1 - 2\nu_\infty)\nu_\varepsilon}{2(1 - \nu_\infty) - \nu_\varepsilon(1 - 2\nu_\infty)} = -\frac{\tau_\varepsilon^\gamma - t_2^\gamma}{\tau_\varepsilon^\gamma}, \qquad (59)$$

$$t_2^{-\gamma} = \tau_\varepsilon^{-\gamma} \left[1 - \frac{(1 - 2\nu_\infty)\nu_\varepsilon}{2(1 - \nu_\infty)} \right], \qquad t_2^\gamma = \frac{\tau_\varepsilon^\gamma}{C}, \qquad (60)$$

where

$$A = \frac{2(1 + \nu_\infty) + \nu_\varepsilon(1 - 2\nu_\infty)}{2(1 + \nu_\infty)} > 1, \quad C = \frac{2(1 - \nu_\infty) - \nu_\varepsilon(1 - 2\nu_\infty)}{2(1 - \nu_\infty)} < 1.$$

Now we could calculate operators $\widetilde{\mu}$ and $\widetilde{\lambda}$. Really, considering (19) and (53), (57), (58), we find

$$\widetilde{\mu} = \frac{\widetilde{E}}{2(1 + \widetilde{\nu})} = \frac{E_\infty}{2} \left[1 - \nu_\varepsilon \ni_\gamma^* (\tau_\varepsilon^\gamma) \right] \frac{1}{1 + \nu_\infty} \left[1 - B \ni_\gamma^* (t_1^\gamma) \right]. \qquad (61)$$

Multiplying operators entering in (61) and considering (21), we have

$$\widetilde{\mu} = \mu_\infty \left[1 - \nu_\varepsilon \left(1 - B \frac{\tau_\varepsilon^\gamma}{\tau_\varepsilon^\gamma - t_1^\gamma} \right) \ni_\gamma^* (\tau_\varepsilon^\gamma) - B \left(1 + \nu_\varepsilon \frac{t_1^\gamma}{\tau_\varepsilon^\gamma - t_1^\gamma} \right) \ni_\gamma^* (t_1^\gamma) \right], \quad (62)$$

where μ_∞ is the nonrelaxed shear modulus.

But according (57)

$$1 - B\tau_\varepsilon^\gamma (\tau_\varepsilon^\gamma - t_1^\gamma)^{-1} = 0,$$

and

$$B \left(1 + \nu_\varepsilon \, \frac{t_1^\gamma}{\tau_\varepsilon^\gamma - t_1^\gamma} \right) = \frac{3\nu_\varepsilon}{2(1 + \nu_\infty)A}, \tag{63}$$

and finally relationship (62) with due account for (63) takes the form

$$\widetilde{\mu} = \mu_\infty \left[1 - \frac{3\nu_\varepsilon}{2(1 + \nu_\infty)A} \, \ni_\gamma^* \left(\frac{\tau_\varepsilon^\gamma}{A} \right) \right]. \tag{64}$$

To define operator $\widetilde{\lambda}_1$, let us use the following formula:

$$\widetilde{\lambda} = \frac{\widetilde{E}\,\widetilde{\nu}}{(1 - 2\widetilde{\nu})(1 + \widetilde{\nu})} = \frac{1}{3} \frac{\widetilde{E}}{1 - 2\widetilde{\nu}} - \frac{1}{3} \frac{\widetilde{E}}{1 + \widetilde{\nu}}. \tag{65}$$

The first operator in the right-hand side of (65), according to (51), is a constant, while the second one within an accuracy of a constant coincides with formula (64). Thus,

$$\widetilde{\lambda} = \frac{1}{3} \frac{E_\infty}{1 - 2\nu_\infty} - \frac{1}{3} \frac{E_\infty}{1 + \nu_\infty} \left[1 - \frac{3\nu_\varepsilon}{2(1 + \nu_\infty)A} \, \ni_\gamma^* \left(\frac{\tau_\varepsilon^\gamma}{A} \right) \right],$$

or

$$\widetilde{\lambda} = \lambda_\infty \left[1 + \frac{(1 - 2\nu_\infty)\nu_\varepsilon}{2(1 + \nu_\infty)A} \, \ni_\gamma^* \left(\frac{\tau_\varepsilon^\gamma}{A} \right) \right], \tag{66}$$

where λ_∞ is the nonrelaxed magnitude of the second Lame parameter.

In conclusion of this Subsection, we will calculate the operator

$$\frac{\widetilde{E}}{1 - \widetilde{\nu}^2} = \frac{\widetilde{E}}{2} \left(\frac{1}{1 + \widetilde{\nu}} + \frac{1}{1 - \widetilde{\nu}} \right), \tag{67}$$

which within an accuracy of a constant coincides with the operator of cylindrical rigidity and is of frequent use in the problems dealing with mechanical behavior of thin bodies.

Substituting (19), (53), and (54) in (67), multiplying the operators involving in the enumerated relationships and using (21), we obtain

$$\frac{\widetilde{E}}{1 - \widetilde{\nu}^2} = \frac{E_\infty}{1 - \nu_\infty^2} \left[1 - m_1 \, \ni_\gamma^* \left(t_1^\gamma \right) - m_2 \, \ni_\gamma^* \left(t_2^\gamma \right) \right], \tag{68}$$

where

$$m_1 = \frac{3}{2} \frac{B(1 - \nu_\infty)}{(1 - 2\nu_\infty)}, \qquad m_2 = \frac{1}{2} \frac{D(1 + \nu_\infty)}{(1 - 2\nu_\infty)}. \tag{69}$$

In order to find an operator reverse to the operator (68), let us represent it in the form

$$\frac{1 - \widetilde{\nu}^2}{\widetilde{E}} = \frac{1 - \nu_\infty^2}{E_\infty} \left[1 + n_1 \, \ni_\gamma^* \left(\tau_1^\gamma \right) + n_2 \, \ni_\gamma^* \left(\tau_2^\gamma \right) \right], \tag{70}$$

where τ_1^γ, τ_2^γ, and n_1, n_2 are yet unknown constants which are determined from Eqs. (44) and (45). It is convenient to rewrite these equations in another form. Thus, the equation for defining the values τ_i^γ has the form

$$1 + m_1 \frac{x}{t_1^\gamma - x} + m_2 \frac{x}{t_2^\gamma - x} = 0, \quad x = \tau_i^\gamma \ \ (i = 1, 2), \tag{71}$$

or with due account for (69)

$$1 + \frac{3}{2} \frac{B(1 - \nu_\infty)}{(1 - 2\nu_\infty)} \frac{x}{(t_1^\gamma - x)} + \frac{1}{2} \frac{D(1 + \nu_\infty)}{(1 - 2\nu_\infty)} \frac{x}{(t_2^\gamma - x)} = 0. \tag{72}$$

A set of equations for finding n_1 and n_2 is the following:

$$\begin{cases} \frac{t_1^\gamma}{\tau_1^\gamma - t_1^\gamma} n_1 + \frac{t_1^\gamma}{\tau_2^\gamma - t_1^\gamma} n_2 = 1, \\ \frac{t_2^\gamma}{\tau_1^\gamma - t_2^\gamma} n_1 + \frac{t_2^\gamma}{\tau_2^\gamma - t_2^\gamma} n_2 = 1. \end{cases} \tag{73}$$

It could be shown that if substitute τ_ε^γ instead of x in (71) or (72), then the following identity could be obtained:

$$1 \equiv -m_1 \frac{\tau_\varepsilon^\gamma}{t_1^\gamma - \tau_\varepsilon^\gamma} - m_2 \frac{\tau_\varepsilon^\gamma}{t_2^\gamma - \tau_\varepsilon^\gamma}. \tag{74}$$

In order to find the second root of Eq. (71) or (72), let us rewrite it in the form

$$(1 - m_1 - m_2) x^2 - (t_1^\gamma + t_2^\gamma - m_1 t_2^\gamma - m_2 t_1^\gamma) x + t_1^\gamma t_2^\gamma = 0. \tag{75}$$

Due to the Viéte theorem, if the first root is $x_1 = \tau_1^\gamma = \tau_\varepsilon^\gamma$, then the second root $x_2 = \tau_1^\gamma$ satisfies the relationship

$$\tau_\varepsilon^\gamma x_2 = \frac{t_1^\gamma t_2^\gamma}{1 - m_1 - m_2}. \tag{76}$$

Calculations show that

$$\frac{t_1^\gamma t_2^\gamma}{1 - m_1 - m_2} = \frac{\tau_\varepsilon^{2\gamma}}{1 - \nu_\varepsilon}. \tag{77}$$

But $\tau_\varepsilon^\gamma (1 - \nu_\varepsilon)^{-1} = \tau_\sigma^\gamma$, and from (77) it follows that $x_2 = \tau_2^\gamma = \tau_\sigma^\gamma$.
Substituting the found $\tau_1^\gamma = \tau_\varepsilon^\gamma$ and $\tau_2^\gamma = \tau_\sigma^\gamma$ in the set of Eqs. (73), we obtain

$$\begin{cases} \frac{2(1-\nu_\infty)}{(1-2\nu_\infty)\nu_\varepsilon} n_1 - \frac{2(1-\nu_\infty)}{\nu_\sigma} n_2 = -1, \\ \frac{2(1+\nu_\infty)}{(1-2\nu_\infty)\nu_\varepsilon} n_1 + \frac{2}{3} \frac{1+\nu_\infty}{\nu_\sigma} n_2 = 1, \end{cases} \tag{78}$$

whence it follows

$$n_1 = \frac{(1 - 2\nu_\infty)^2 \nu_\varepsilon}{4(1 - \nu_\infty^2)}, \qquad n_2 = \frac{3\nu_\sigma}{4(1 - \nu_\infty^2)}. \tag{79}$$

Considering aforesaid, we have

$$\frac{1 - \widetilde{\nu}^2}{\widetilde{E}} = \frac{1 - \nu_\infty^2}{E_\infty} \left[1 + \frac{(1 - 2\nu_\infty)^2 \nu_\varepsilon}{4(1 - \nu_\infty^2)} \ni_\gamma^* (\tau_\varepsilon^\gamma) + \frac{3\nu_\sigma}{4(1 - \nu_\infty^2)} \ni_\gamma^* (\tau_\sigma^\gamma) \right]. \tag{80}$$

Thus, we obtain two important mutually reciprocal operators (68) and (80) which are widely used in different applications.

Besides, two useful formulas have been found

$$t_1^\gamma t_2^\gamma = \tau_\varepsilon^\gamma \tau_\sigma^\gamma (1 - m_1 - m_2), \tag{81}$$

$$t_1^\gamma (1 - m_2) + t_2^\gamma (1 - m_1) = (\tau_\varepsilon^\gamma + \tau_\sigma^\gamma) (1 - m_1 - m_2). \tag{82}$$

4.2. The Main Case

In the previous Subsection we have not take the second, or bulk, viscosity into account, in spite the fact that there are numerous evidence of its existence in scientific literature [36, 39, 74, 75].

One of the first papers in the field was published by Meshkov and Pachevskaya [39], wherein the attempt for considering the influence of the bulk relaxation on the internal friction phenomenon was carried out on the example of longitudinal harmonic vibrations of a three-dimensional hereditary elastic rod under the conditions of homogeneous deformation. A fractional exponential function has been used as a hereditary kernel. Investigation of the frequency dependence of the tangent of the phase shift between the stress and deformation, i.e., mechanical loss tangent, has revealed two peaks, namely, shear and bulk, in so doing the peak due to the shear deformation is five times larger than that resulting from the bulk deformation.

Assume that operators $\widetilde{\mu}$ and $\widetilde{K}$ are given in the form

$$\widetilde{\mu} = \mu_\infty \left[1 - \nu_{\varepsilon 1} \ni_\gamma^* (\tau_{\varepsilon 1}^\gamma) \right], \tag{83}$$

$$\widetilde{K} = K_\infty \left[1 - \nu_{\varepsilon 2} \ni_\gamma^* (\tau_{\varepsilon 2}^\gamma) \right], \tag{84}$$

where $\nu_{\varepsilon 1} = 1 - \mu_0 \mu_\infty^{-1} = 1 - \tau_{\varepsilon 1}^\gamma \tau_{\sigma 1}^{-\gamma}$, $\nu_{\varepsilon 2} = 1 - K_0 K_\infty^{-1} = 1 - \tau_{\varepsilon 2}^\gamma \tau_{\sigma 2}^{-\gamma}$, μ_0 and μ_∞, K_0 and K_∞ are relaxed and nonrelaxed shear and bulk moduli, respectively, $\tau_{\varepsilon 1}$ and $\tau_{\sigma 1}$, $\tau_{\varepsilon 2}$ and $\tau_{\sigma 2}$ are relaxation and retardation times, the subscript l relates to shear relaxation and the subscript 2 to bulk relaxation.

Starting from formulas (83) and (84), reciprocal operators have the form

$$\frac{1}{\widetilde{\mu}} = \mu_\infty^{-1} \left[1 + \nu_{\sigma 1} \ni_\gamma^* (\tau_{\sigma 1}^\gamma) \right], \tag{85}$$

$$\frac{1}{\widetilde{K}} = K_\infty^{-1} \left[1 + \nu_{\sigma 2} \ni_\gamma^* (\tau_{\sigma 2}^\gamma) \right], \tag{86}$$

where $\nu_{\sigma 1} = \mu_\infty \mu_0^{-1} - 1 = \tau_{\sigma 1}^\gamma \tau_{\varepsilon 1}^{-\gamma} - 1$, and $\nu_{\sigma 2} = K_\infty K_0^{-1} - 1 = \tau_{\sigma 2}^\gamma \tau_{\varepsilon 2}^{-\gamma} - 1$.

First we calculate the operator of compliance

$$\widetilde{J} = \frac{1}{\widetilde{E}} = \frac{1}{3} \frac{3\widetilde{K} + \widetilde{\mu}}{3\widetilde{K}\widetilde{\mu}} = \frac{1}{3} \left(\frac{1}{\widetilde{\mu}} + \frac{1}{3\widetilde{K}} \right). \tag{87}$$

Substituting (85) and (86) in (87) yields

$$\widetilde{J} = J_\infty \left[1 + \frac{1}{3} \frac{\nu_{\sigma 1} E_\infty}{\mu_\infty} \ni_\gamma^* (\tau_{\sigma 1}^\gamma) + \frac{1}{9} \frac{\nu_{\sigma 2} E_\infty}{K_\infty} \ni_\gamma^* (\tau_{\sigma 2}^\gamma) \right],$$

or

$$\widetilde{J} = J_\infty \left[1 + \frac{2}{3} (1 + \nu_\infty) \nu_{\sigma 1} \ni_\gamma^* (\tau_{\sigma 1}^\gamma) + \frac{1}{3} (1 - 2\nu_\infty) \nu_{\sigma 2} \ni_\gamma^* (\tau_{\sigma 2}^\gamma) \right]. \tag{88}$$

Let us consider longitudinal harmonic vibrations of a three-dimensional hereditary elastic rod under the conditions of homogeneous deformation when harmonic force acts infinitely long. If rod's axis coincides with the z-axis, then its longitudinal strain is

$$\varepsilon_{zz} = p_0 J^* e^{i\omega t}, \tag{89}$$

where p_0 and ω are the amplitude and frequency of the external force.

Let us introduce the following operators:

$$\ni^*_{\gamma+} (\tau_i^\gamma) x(t) = \int_{-\infty}^t \ni_\gamma (-s/\tau_i) x(t-s) ds, \tag{90}$$

$$I_+^\gamma x(t) = \int_{-\infty}^t \frac{(t-s)^{\gamma-1}}{\Gamma(\gamma)} x(s) ds. \tag{91}$$

Then according to (13)

$$\ni^*_{\gamma+} (\tau_i^\gamma) e^{i\omega t} = \sum_{n=0}^\infty (-1)^n \tau_i^{-\gamma(n+1)} I_+^\gamma e^{i\omega t}, \tag{92}$$

but

$$\sum_{n=0}^\infty (-1)^n \tau_i^{-\gamma(n+1)} I_+^\gamma e^{i\omega t} = \sum_{n=0}^\infty (-1)^n (i\omega\tau_i)^{-\gamma(n+1)} e^{i\omega t},$$

and the sum in the right-hand side could be interpreted as an infinite decreasing geometrical progression with the denominator $d = -(i\omega t)^{-\gamma}$. In other words,

$$e^{i\omega t} \sum_{n=0}^\infty (-1)^n (i\omega\tau_i)^{-\gamma(n+1)} = \frac{(i\omega\tau_i)^{-\gamma} e^{i\omega t}}{1 - [-(i\omega\tau_i)^{-\gamma}]} = \frac{e^{i\omega t}}{1 + (i\omega\tau_i)^\gamma},$$

and

$$\begin{aligned}
\ni^*_{\gamma+} (\tau_i^\gamma) e^{i\omega t} &= \frac{1}{1 + (i\omega\tau_i)^\gamma} e^{i\omega t} \\
&= \left(\frac{æ_i^{-\gamma} + \cos\psi}{æ_i^{-\gamma} + æ_i^\gamma + 2\cos\psi} - i \frac{\sin\psi}{æ_i^{-\gamma} + æ_i^\gamma + 2\cos\psi} \right) e^{i\omega t}, \quad (93)
\end{aligned}$$

where $æ_i = \omega\tau_i$, and $\psi = \frac{1}{2}\pi\gamma$.

Considering (93), the complex compliance $J(i\omega)$ has the form

$$J(i\omega) = J'(\omega) - iJ''(\omega) = \frac{1}{3} J_\infty \left\{ 2(1+\nu_\infty) \frac{æ_{\sigma1}^\gamma + æ_{\varepsilon1}^{-\gamma} + [1 + (æ_{\sigma1}/æ_{\varepsilon1})^\gamma]\cos\psi}{æ_{\sigma1}^{-\gamma} + æ_{\sigma1}^\gamma + 2\cos\psi} \right.$$

$$\left. + (1-2\nu_\infty) \frac{æ_{\sigma2}^\gamma + æ_{\varepsilon2}^{-\gamma} + [1 + (æ_{\sigma2}/æ_{\varepsilon2})^\gamma]\cos\psi}{æ_{\sigma2}^{-\gamma} + æ_{\sigma2}^\gamma + 2\cos\psi} \right\}$$

$$-i\frac{1}{3} J_\infty \left\{ 2(1+\nu_\infty) \frac{[(æ_{\sigma1}/æ_{\varepsilon1})^\gamma - 1]\sin\psi}{æ_{\sigma1}^{-\gamma} + æ_{\sigma1}^\gamma + 2\cos\psi} + (1-2\nu_\infty) \frac{[(æ_{\sigma2}/æ_{\varepsilon2})^\gamma - 1]\sin\psi}{æ_{\sigma2}^{-\gamma} + æ_{\sigma2}^\gamma + 2\cos\psi} \right\}. \tag{94}$$

Now knowing the value $J(i\omega)$, it is possible to find the tangent of the mechanical loss angle characterizing the internal friction in a viscoelastic rod

$$\tan\delta = \frac{J''}{J'}. \tag{95}$$

Meshkov and Pachevskaya [39] considered a numerical example with $\nu_\infty = 0.3$, $\mu_0/\mu_\infty = K_0/K_\infty = 0.8$, $\tau_{\varepsilon1}/\tau_{\varepsilon2} = 10^3$, and $\omega = 1$ in order to establish whether, in principle, a relaxation peak due to bulk deformation can occur. The $\ln \mathfrak{x}_{\varepsilon2}$-dependence of $\tan \delta$ and phase diagram for the compliance $J'' = f(J')$ were presented in [39] in Figures 1a and 1b, respectively, where the values of the fractional parameter γ were indicated by figures near the corresponding curves. The limiting value $\gamma = 1$ in Figure 1a of [39] indicates that the shear and bulk relaxations are described by the standard linear solid model, and it leads to clear separation of the two peaks. If the bulk and shear moduli have equal degrees of relaxation, they make unequal contributions to the total effect defined by Poisson's ratio ν_∞, namely: the shear peak being about 5.5 times larger than the bulk one. Reduction in γ corresponds to broadening of the relaxation spectrum [41], and the difference between the peaks vanishes. The value $\gamma = 0.5$ may be considered in this case to correspond to the lower limit for the bulk effect, i. e., bulk relaxation is not seen for all $\gamma < 0.5$, although it exists. The possibility of observing bulk relaxation is thus dependent not only on the ratio of the relaxation times for shear and bulk stresses, but also on the parameter that characterizes the width of the relaxation spectrum.

Now we calculate the operator

$$\widetilde{\nu} = \frac{1}{2} \frac{3\widetilde{K} - 2\widetilde{\mu}}{3\widetilde{K} + \widetilde{\mu}}. \tag{96}$$

We will proceed from the operator

$$3\widetilde{K} + \widetilde{\mu} = (3K_\infty + \mu_\infty) \left[1 - m_1 \ni_\gamma^* \left(\tau_{\varepsilon1}^\gamma \right) - m_2 \ni_\gamma^* \left(\tau_{\varepsilon2}^\gamma \right) \right], \tag{97}$$

where $m_1 = \frac{1}{3}(1 - 2\nu_\infty)\nu_{\varepsilon1}$, and $m_2 = \frac{2}{3}(1 + \nu_\infty)\nu_{\varepsilon2}$.

Operator inverse to operator (97) has the form

$$\left(3\widetilde{K} + \widetilde{\mu} \right)^{-1} = \frac{1}{3K_\infty + \mu_\infty} \left[1 + n_1 \ni_\gamma^* \left(t_{\sigma1}^\gamma \right) + n_2 \ni_\gamma^* \left(t_{\sigma2}^\gamma \right) \right], \tag{98}$$

where the values $t_{\sigma1}^\gamma$ and $t_{\sigma2}^\gamma$ are defined from the quadratic equation

$$(1 - m_1 - m_2)x^2 - \left[\tau_{\varepsilon1}^\gamma (1 - m_2) + \tau_{\varepsilon2}^\gamma (1 - m_1) \right] x + \tau_{\varepsilon1}^\gamma \tau_{\varepsilon2}^\gamma = 0, \tag{99}$$

while the values n_1 and n_2 are determined from the set of two equations with due account for the magnitudes of $t_{\sigma1}^\gamma$ and $t_{\sigma2}^\gamma$ found from Eq. (99)

$$\begin{cases} \dfrac{\tau_{\varepsilon1}^\gamma}{\tau_{\varepsilon1}^\gamma - t_{\sigma1}^\gamma}\, n_1 + \dfrac{\tau_{\varepsilon1}^\gamma}{\tau_{\varepsilon1}^\gamma - t_{\sigma2}^\gamma}\, n_2 = -1, \\[2mm] \dfrac{\tau_{\varepsilon2}^\gamma}{\tau_{\varepsilon2}^\gamma - t_{\sigma1}^\gamma}\, n_1 + \dfrac{\tau_{\varepsilon2}^\gamma}{\tau_{\varepsilon2}^\gamma - t_{\sigma2}^\gamma}\, n_2 = -1. \end{cases} \tag{100}$$

Then from (96) we find

$$\widetilde{\nu} = \nu_\infty \left[1 - s_1 \ni_\gamma^* \left(\tau_{\varepsilon1}^\gamma \right) + s_2 \ni_\gamma^* \left(\tau_{\varepsilon2}^\gamma \right) \right] \left[1 + n_1 \ni_\gamma^* \left(t_{\sigma1}^\gamma \right) + n_2 \ni_\gamma^* \left(t_{\sigma2}^\gamma \right) \right], \tag{101}$$

where

$$s_1 = \frac{3K_\infty \nu_{\varepsilon2}}{3K_\infty - 2\mu_\infty}, \qquad s_2 = \frac{2\mu_\infty \nu_{\varepsilon1}}{3K_\infty - 2\mu_\infty}.$$

Opening the brackets in (101) with due account for (21) yields

$$
\begin{aligned}
\widetilde{\nu} = \nu_\infty \Bigg[1 + & \left(n_1 + \frac{s_1 n_1 t_{\sigma 1}^\gamma}{\tau_{\varepsilon 2}^\gamma - t_{\sigma 1}^\gamma} - \frac{s_2 n_1 t_{\sigma 1}^\gamma}{\tau_{\varepsilon 1}^\gamma - t_{\sigma 1}^\gamma} \right) \ni_\gamma^* (t_{\sigma 1}^\gamma) \\
& + \left(n_2 + \frac{s_1 n_2 t_{\sigma 2}^\gamma}{\tau_{\varepsilon 2}^\gamma - t_{\sigma 2}^\gamma} - \frac{s_2 n_2 t_{\sigma 2}^\gamma}{\tau_{\varepsilon 1}^\gamma - t_{\sigma 2}^\gamma} \right) \ni_\gamma^* (t_{\sigma 2}^\gamma) \\
& - \left(s_1 + \frac{s_1 n_1 \tau_{\varepsilon 2}^\gamma}{\tau_{\varepsilon 2}^\gamma - t_{\sigma 1}^\gamma} + \frac{s_1 n_2 \tau_{\varepsilon 2}^\gamma}{\tau_{\varepsilon 2}^\gamma - t_{\sigma 2}^\gamma} \right) \ni_\gamma^* (\tau_{\varepsilon 2}^\gamma) \\
& + \left(s_2 + \frac{s_2 n_1 \tau_{\varepsilon 1}^\gamma}{\tau_{\varepsilon 1}^\gamma - t_{\sigma 1}^\gamma} + \frac{s_2 n_2 \tau_{\varepsilon 1}^\gamma}{\tau_{\varepsilon 1}^\gamma - t_{\sigma 2}^\gamma} \right) \ni_\gamma^* (\tau_{\varepsilon 1}^\gamma) \Bigg] .
\end{aligned} \tag{102}
$$

In order to find operator $\widetilde{E}$, it is necessary to rewrite operator $\widetilde{J}$ in the form

$$
\widetilde{J} = J_\infty \left[1 + n_1 \ni_\gamma^* (\tau_{\sigma 1}^\gamma) + n_2 \ni_\gamma^* (\tau_{\sigma 2}^\gamma) \right] , \tag{103}
$$

where $n_1 = \frac{2}{3}(1 + \nu_\infty)\nu_{\sigma 1}$, and $n_1 = \frac{1}{3}(1 - 2\nu_\infty)\nu_{\sigma 2}$.

Then operator $\widetilde{E}$ takes the form

$$
\widetilde{E} = E_\infty \left[1 - m_1 \ni_\gamma^* (t_{\varepsilon 1}^\gamma) - m_2 \ni_\gamma^* (t_{\varepsilon 2}^\gamma) \right] , \tag{104}
$$

where values $t_{\varepsilon 1}^\gamma$ and $t_{\varepsilon 2}^\gamma$ are determined from the following equation:

$$
\frac{n_1 x}{\tau_{\sigma 1}^\gamma - x} + \frac{n_2 x}{\tau_{\sigma 2}^\gamma - x} = 1, \quad x = t_{\varepsilon i}^\gamma \ (i = 1, 2),
$$

or

$$
(1 + n_1 + n_2)x^2 - \left[\tau_{\sigma 1}^\gamma(1 + n_2) + \tau_{\sigma 2}^\gamma(1 + n_1) \right] x + \tau_{\sigma 1}^\gamma \tau_{\sigma 2}^\gamma = 0, \tag{105}
$$

and values m_1 and m_2 are defined from the set of equations

$$
\begin{cases}
\frac{\tau_{\sigma 1}^\gamma}{\tau_{\sigma 1}^\gamma - t_{\varepsilon 1}^\gamma} m_1 + \frac{\tau_{\sigma 1}^\gamma}{\tau_{\sigma 1}^\gamma - t_{\varepsilon 2}^\gamma} m_2 = 1, \\
\frac{\tau_{\sigma 2}^\gamma}{\tau_{\sigma 2}^\gamma - t_{\varepsilon 1}^\gamma} m_1 + \frac{\tau_{\sigma 2}^\gamma}{\tau_{\sigma 2}^\gamma - t_{\varepsilon 2}^\gamma} m_2 = 1.
\end{cases} \tag{106}
$$

In conclusion of this Subsection we will show how to define the operator proportional to the operator of cylindrical rigidity. With this purpose we will use the operators

$$
\frac{1}{1 + \widetilde{\nu}} = \frac{2}{9} \frac{3\widetilde{K} + \widetilde{\mu}}{\widetilde{K}}, \quad \frac{1}{1 - \widetilde{\nu}} = \frac{2(3\widetilde{K} + \widetilde{\mu})}{3\widetilde{K} + 4\widetilde{\mu}}, \quad \widetilde{E} = \frac{9\widetilde{K}\widetilde{\mu}}{3\widetilde{K} + 4\widetilde{\mu}}. \tag{107}
$$

Then considering (107) we have

$$
\frac{\widetilde{E}}{1 - \widetilde{\nu}^2} = \frac{\widetilde{E}}{2(1 + \widetilde{\nu})} + \frac{\widetilde{E}}{2(1 - \widetilde{\nu})} = \widetilde{\mu} + \frac{9\widetilde{K}\widetilde{\mu}}{3\widetilde{K} + 4\widetilde{\mu}} = \widetilde{\mu} + \widetilde{s}^{-1}. \tag{108}
$$

First we will calculate the operator

$$
\begin{aligned}
\widetilde{s} &= \frac{3\widetilde{K} + 4\widetilde{\mu}}{9\widetilde{K}\widetilde{\mu}} = \frac{1}{3} \left(\frac{1}{\widetilde{\mu}} + \frac{4}{3} \frac{1}{\widetilde{K}} \right) \\
&= \frac{3K_\infty + 4\mu_\infty}{9K_\infty \mu_\infty} \left[1 + \frac{3K_\infty \nu_{\sigma 1}}{3K_\infty + 4\mu_\infty} \ni_\gamma^* (\tau_{\sigma 1}^\gamma) + \frac{3\mu_\infty \nu_{\sigma 2}}{3K_\infty + 4\mu_\infty} \ni_\gamma^* (\tau_{\sigma 2}^\gamma) \right]
\end{aligned} \tag{109}
$$

In order to find an operator reverse to operator (109), let us rewrite it in the form

$$\widetilde{s} = s_\infty \left[1 + n_1 \ni^*_\gamma (\tau^\gamma_{\sigma 1}) + n_2 \ni^*_\gamma (\tau^\gamma_{\sigma 2}) \right], \tag{110}$$

where

$$s_\infty = \frac{3K_\infty + 4\mu_\infty}{9K_\infty \mu_\infty}, \quad n_1 = \frac{3K_\infty \nu_{\sigma 1}}{3K_\infty + 4\mu_\infty}, \quad n_2 = \frac{3\mu_\infty \nu_{\sigma 2}}{3K_\infty + 4\mu_\infty}.$$

Then

$$\widetilde{s}^{-1} = \frac{9\widetilde{K}\widetilde{\mu}}{3\widetilde{K} + 4\widetilde{\mu}} = s_\infty^{-1} \left[1 - m_1 \ni^*_\gamma (t^\gamma_{\varepsilon 1}) - m_2 \ni^*_\gamma (t^\gamma_{\varepsilon 2}) \right], \tag{111}$$

where values $t^\gamma_{\varepsilon 1}$ and $t^\gamma_{\varepsilon 2}$ are determined from Eq. (105), and values m_1 and m_2 are defined from the set of Eqs. (106).

Finally, to calculate operator (108), it is necessary to take formulas (83) and (111) into account. As a result we obtain

$$
\begin{aligned}
\frac{\widetilde{E}}{1 - \widetilde{\nu}^2} &= \frac{\mu_\infty s_\infty + 1}{s_\infty} \left[1 - \frac{\mu_\infty s_\infty \nu_{\varepsilon 1}}{\mu_\infty s_\infty + 1} \ni^*_\gamma (\tau^\gamma_{\varepsilon 1}) \right. \\
&\quad \left. - \frac{m_1}{\mu_\infty s_\infty + 1} \ni^*_\gamma (t^\gamma_{\varepsilon 1}) - \frac{m_2}{\mu_\infty s_\infty + 1} \ni^*_\gamma (t^\gamma_{\varepsilon 2}) \right].
\end{aligned} \tag{112}
$$

The reverse operator has the form

$$\frac{1 - \widetilde{\nu}^2}{\widetilde{E}} = \frac{s_\infty}{\mu_\infty s_\infty + 1} \left[1 + s_1 \ni^*_\gamma (T^\gamma_{\sigma 1}) + s_2 \ni^*_\gamma (T^\gamma_{\sigma 2}) + s_3 \ni^*_\gamma (T^\gamma_{\sigma 3}) \right]. \tag{113}$$

Values $T^\gamma_{\sigma 1}$, $T^\gamma_{\sigma 2}$, and $T^\gamma_{\sigma 3}$ could be found from the following equation:

$$\frac{\eta_1 x}{\tau^\gamma_{\varepsilon 1} - x} + \frac{\eta_2 x}{\tau^\gamma_{\varepsilon 2} - x} + \frac{\eta_3 x}{\tau^\gamma_{\varepsilon 3} - x} = -1,$$

or

$$
\begin{aligned}
\left(1 - \eta_1 - \eta_2 - \eta_3 \right) x^3 &+ \left[\left(\tau^\gamma_{\varepsilon 2} + \tau^\gamma_{\varepsilon 3} \right) \eta_1 + \left(\tau^\gamma_{\varepsilon 3} + \tau^\gamma_{\varepsilon 1} \right) \eta_2 + \left(\tau^\gamma_{\varepsilon 1} + \tau^\gamma_{\varepsilon 2} \right) \eta_3 \right. \\
&\left. - \tau^\gamma_{\varepsilon 1} - \tau^\gamma_{\varepsilon 2} - \tau^\gamma_{\varepsilon 3} \right] x^2 + \left[\tau^\gamma_{\varepsilon 2} \tau^\gamma_{\varepsilon 3}(1 - \eta_1) + \tau^\gamma_{\varepsilon 3} \tau^\gamma_{\varepsilon 1}(1 - \eta_2) + \tau^\gamma_{\varepsilon 1} \tau^\gamma_{\varepsilon 2}(1 - \eta_3) \right] x \\
&- \tau^\gamma_{\varepsilon 1} \tau^\gamma_{\varepsilon 2} \tau^\gamma_{\varepsilon 3} = 0, \tag{114}
\end{aligned}
$$

where

$$\eta_1 = \frac{\mu_\infty s_\infty \nu_{\varepsilon 1}}{\mu_\infty s_\infty + 1}, \quad \eta_2 = \frac{m_1}{\mu_\infty s_\infty + 1}, \quad \eta_3 = \frac{m_2}{\mu_\infty s_\infty + 1}, \quad \tau^\gamma_{\varepsilon 2} = t^\gamma_{\varepsilon 1}, \quad \tau^\gamma_{\varepsilon 3} = t^\gamma_{\varepsilon 2},$$

and values s_1, s_2, and s_3 are determined from following set of equations

$$
\begin{cases}
\frac{s_1 \tau^\gamma_{\varepsilon 1}}{\tau^\gamma_{\varepsilon 1} - T^\gamma_{\sigma 1}} + \frac{s_2 \tau^\gamma_{\varepsilon 1}}{\tau^\gamma_{\varepsilon 1} - T^\gamma_{\sigma 2}} + \frac{s_3 \tau^\gamma_{\varepsilon 1}}{\tau^\gamma_{\varepsilon 1} - T^\gamma_{\sigma 3}} = -1, \\
\frac{s_1 \tau^\gamma_{\varepsilon 2}}{\tau^\gamma_{\varepsilon 2} - T^\gamma_{\sigma 1}} + \frac{s_2 \tau^\gamma_{\varepsilon 2}}{\tau^\gamma_{\varepsilon 2} - T^\gamma_{\sigma 2}} + \frac{s_3 \tau^\gamma_{\varepsilon 2}}{\tau^\gamma_{\varepsilon 2} - T^\gamma_{\sigma 3}} = -1, \\
\frac{s_1 \tau^\gamma_{\varepsilon 3}}{\tau^\gamma_{\varepsilon 3} - T^\gamma_{\sigma 1}} + \frac{s_2 \tau^\gamma_{\varepsilon 3}}{\tau^\gamma_{\varepsilon 3} - T^\gamma_{\sigma 2}} + \frac{s_3 \tau^\gamma_{\varepsilon 3}}{\tau^\gamma_{\varepsilon 3} - T^\gamma_{\sigma 3}} = -1.
\end{cases} \tag{115}
$$

Applying the Viéte theorem to Eq. (114), we have

$$T^\gamma_{\sigma 1} T^\gamma_{\sigma 2} T^\gamma_{\sigma 3} = \frac{\tau^\gamma_{\varepsilon 1} \tau^\gamma_{\varepsilon 2} \tau^\gamma_{\varepsilon 3}}{1 - \eta_1 - \eta_2 - \eta_3},$$

what completely corresponds to relationship (50) at $n = 3$.

5.   Relationship of Rabotnov Fractional Operators with Other Fractional Operators

Along with Rabotnov fractional operators there are exist other fractional operators which are used to solve different problems of viscoelasticity. In this Section, we consider those fractional operators which are somehow or other connected with Rabotnov operators.

5.1.   Rzhanitsyn Operator

Let us consider Boltzmann-Volterra relationships with different kernels of relaxation K_ε and retardation K_σ

$$\sigma = E_\infty \left[\varepsilon - \nu_\varepsilon \int_0^t K_\varepsilon(t - t')\varepsilon(t')dt' \right], \tag{116}$$

$$\varepsilon = J_\infty \left[\sigma + \nu_\sigma \int_0^t K_\sigma(t - t')\sigma(t')dt' \right]. \tag{117}$$

As a hereditary kernel we chose Rzhanitsyn kernel [71]

$$K_i = \frac{t^{\gamma-1}}{\Gamma(\gamma)\tau_i^\gamma} \exp\left(-\frac{t}{\tau_i}\right) \quad (i = \varepsilon, \sigma), \;\; (0 < \gamma < 1), \tag{118}$$

which could be both the kernel of relaxation and the kernel of retardation, although Rzhanitsyn himself used it only as the creep kernel [72].

Putting $i = \sigma$ in (118) and substituting it in (117), we have

$$\varepsilon(t) = J_\infty \left[\sigma(t) + \nu_\sigma \int_0^t \frac{t^{\gamma-1}}{\Gamma(\gamma)\tau_\sigma^\gamma} \exp\left(-\frac{t}{\tau_\sigma}\right) \sigma(t - t')dt' \right]. \tag{119}$$

In the Laplace domain, function K_σ has the form

$$\bar{K}_\sigma(p) = \frac{1}{\left(p + \tau_\sigma^{-1}\right)^\gamma}. \tag{120}$$

Considering (120) from (119) we find

$$\bar{\varepsilon} = J_\infty \left[1 + \nu_\sigma \left(p + \tau_\sigma^{-1}\right)^{-\gamma} \tau_\sigma^{-\gamma} \right] \bar{\sigma}, \tag{121}$$

whence it follows that

$$\bar{\sigma} = \frac{E_\infty}{1 + \nu_\sigma \left(p + \tau_\sigma^{-1}\right)^{-\gamma} \tau_\sigma^{-\gamma}} \, \bar{\varepsilon}. \tag{122}$$

In order to reverse from the frequency domain to the time domain in relationship (122), it is necessary to calculate the integral

$$K(t) = \frac{E_\infty}{2\pi i} \int_{c-i\infty}^{c+i\infty} e^{pt} \frac{dp}{1 + \nu_\sigma \tau_\sigma^{-\gamma} \left(p + \tau_\sigma^{-1}\right)^{-\gamma}}. \tag{123}$$

Carrying out the substitution

$$s = p + \tau_\sigma^{-1}, \quad ds = dp, \quad c' = c + \tau_\sigma^{-1},$$

let us rewrite integral (123) in the form

$$K(t) = \frac{E_\infty}{2\pi i} e^{-t/\tau_\sigma} \int_{c'-i\infty}^{c'+i\infty} e^{st} \left(1 - \frac{1}{1 + s^\gamma T_\sigma^\gamma}\right) ds, \tag{124}$$

where $T_\sigma^\gamma = \tau_\sigma^\gamma \nu_\sigma^{-1}$.

Considering that

$$\frac{1}{2\pi i} \int_{c'-i\infty}^{c'+i\infty} e^{st} \, ds = \delta(t), \quad \frac{1}{2\pi i} \int_{c'-i\infty}^{c'+i\infty} \frac{e^{st} \, ds}{1 + s^\gamma T_\sigma^\gamma} = \ni_\gamma \left(-t/T_\sigma\right),$$

where $\delta(t)$ is the Dirac function, we obtain

$$K(t) = E_\infty \left[\exp\left(-\frac{t}{\tau_\sigma}\right) \delta(t) - \exp\left(-\frac{t}{\tau_\sigma}\right) \ni_\gamma \left(-\frac{t}{T_\sigma}\right)\right]. \tag{125}$$

Reversing from the frequency domain to the time domain in (122) with due account for (125), finally we obtain

$$\sigma(t) = E_\infty \left\{\varepsilon(t) - \nu_\sigma \int_0^t \exp\left(-\frac{t'}{\tau_\sigma}\right) \frac{(t')^{\gamma-1}}{T_\sigma^\gamma} \sum_{n=0}^\infty \frac{(-1)^n \nu_\sigma^n (t'/T_\sigma)^{\gamma n}}{\Gamma[\gamma(n+1)]} \varepsilon(t - t')dt'\right\}. \tag{126}$$

If we reverse from the image to the original in (121) considering the expansion of the function $(1 + p\tau_\sigma)^{-\gamma}$ in a series

$$(1 + p\tau_\sigma)^{-\gamma} = 1 - \gamma \, p\tau_\sigma + \frac{\gamma(\gamma + 1)}{2!} (p\tau_\sigma)^2 - \frac{\gamma(\gamma + 1)(\gamma + 2)}{3!} (p\tau_\sigma)^3 + ...,$$

then as a result we obtain

$$\varepsilon(t) = J_\infty \left[1 + \nu_\sigma \left(1 + \tau_\sigma \frac{d}{dt}\right)^{-\gamma}\right] \sigma(t). \tag{127}$$

From (125) it is seen that the resolvent kernel

$$K_\varepsilon(t) = e^{-t/\tau_\sigma} \ni_\gamma \left(-\frac{t}{T_\sigma}\right) \tag{128}$$

involves the fractional-exponential function, the attenuation of which with time is strengthened by decaying exponent.

If we take the Abel kernel as K_σ kernel

$$K_\sigma(t) = \frac{t^{\gamma-1}}{\Gamma(\gamma)\tau_\sigma^\gamma},$$

which in the Laplace domain has the form

$$\bar{K}_\sigma(p) = (p\tau_\sigma)^{-\gamma},$$

then in this case

$$\bar{\sigma} = E_\infty \left[1 - \frac{1}{1 + p^\gamma T_\sigma^\gamma}\right] \bar{\varepsilon},$$

and

$$\sigma(t) = E_\infty \left[\varepsilon(t) - \int_0^t \ni_\gamma \left(-\frac{t'}{T_\sigma}\right) \varepsilon(t - t')dt'\right]. \tag{129}$$

Relationship (129) is equivalent to the Maxwell model, wherein ordinary time-derivatives are substituted by fractional derivatives.

Although Rzhanitsyn fractional operator $(1 + \tau_\sigma d/dt)^{-\gamma}$ entering in (127) does not involve the fractional derivative in the explicit form, as Rabotnov operator $[1 + \tau_\sigma^\gamma (d/dt)^\gamma)^{-1}]$ does, however, as it will be shown below on the example of a viscoelastic oscillator, possesses similar features.

Rzhanitsyn and Rabotnov kernels could be generalized with help of the operator

$$[1 + \tau_i^\alpha (d/dt)^\alpha)]^{-\beta} \quad (0 < \alpha, \beta < 1), \tag{130}$$

the features of which have been studied in [59].

From (130) it is evident that the combinational Rabotnov-Rzhanitsyn operator (130) at $\beta = 1$ goes over into the Rabotnov operator, while at $\alpha = 1$ it transforms into the Rzhanitsyn operator, respectively.

5.2. Koeller Viscoelastic Models

In 1986 Koeller suggested two viscoelastic models involving fractional derivatives with several fractional parameters and several relaxation (retardation) times [34]

$$\sum_{i=0}^n a_i D^{i\gamma} \varepsilon = \sum_{j=0}^n b_j D^{j\gamma} \sigma, \tag{131}$$

$$E_\infty \prod_{i=1}^n (D^\gamma + \beta_i) \varepsilon = \prod_{j=1}^n (D^\gamma + \gamma_j) \sigma, \tag{132}$$

where a_i, b_j and β_i, γ_j $(i, j = 1, 2, ..., n)$ are certain coefficients, $0 < \gamma < 1$ is the fractional parameter, $E_\infty = a_n/b_n$, and

$$D^{i\alpha} f(t) = \begin{cases} \frac{d^m}{dt^m} \left[\frac{1}{\Gamma(m-i\alpha)} \int_0^t \frac{f(\tau)d\tau}{(t-\tau)^{i\alpha+1-m}}\right], & m - 1 < i\alpha < m \\ \frac{d^m}{dt^m} f(t), & i\alpha = m \end{cases}$$

is the Riemann-Liouville fractional derivative [55].

The model (132) is equivalent to the model (131). In order to show this, it is necessary to find the roots of equations

$$\sum_{j=0}^{n} b_j Z^j = 0, \qquad \sum_{i=0}^{n} a_i Y^i = 0 \tag{133}$$

and suppose that all of them are simple real negative roots $Z_j = -t_j^{-\alpha} = -\gamma_j \ (j = 1, ..., n)$ and $Y_i = -\tau_i^{-\alpha} = -\beta_i \ (i = 1, ..., n)$, and they are different in magnitude. Knowing the roots, it is possible to change the sums in (131) by the products.

However, the thermodynamic analysis of the models (131) and (132) was not carried out, what did not allow Koeller [34] to determine the physical meaning of the involving parameters, as well as to define the admissible boundaries of their domains.

Such analysis was performed in Rossikhin and Shitikova [62, 63, 65, 67], wherein it has been shown that the both models (131) and (132) could be reduced to the generalized Rabotnov model under the appropriate choice of entering constant values. Moreover, only with such a choice of the constants the both models become to be thermodynamically admissible. Really, the model (132) could be rewritten as

$$\sigma = E_\infty \frac{\prod\limits_{i=1}^{n} (D^\gamma + \beta_i)}{\prod\limits_{j=1}^{n} (D^\gamma + \gamma_j)} \, \varepsilon, \tag{134}$$

and the fraction in the right-hand side of (134) could be expanded in simple fractions

$$\frac{\prod\limits_{i=1}^{n} (D^\gamma + \beta_i)}{\prod\limits_{j=1}^{n} (D^\gamma + \gamma_j)} = (D^\gamma + \beta_1) \sum_{j=1}^{n} \frac{A_j}{D^\gamma + \gamma_j}$$

$$= \sum_{j=1}^{n} \left(A_j - \frac{A_j(\gamma_j - \beta_1)}{D^\gamma + \gamma_j} \right) = 1 - \sum_{j=1}^{n} m_j \left(1 + t_j^\gamma D^\gamma \right)^{-1}, \tag{135}$$

where

$$A_j = \frac{\prod\limits_{i=2}^{n} (\beta_i - \gamma_j)}{\prod\limits_{\substack{i=1 \\ (i \neq j)}}^{n} (\gamma_i - \gamma_j)}, \quad m_j = A_j \frac{\gamma_j - \beta_1}{\gamma_j}.$$

The value $\sum\limits_{j=1}^{n} A_j = 1$, since the operator $D^{\gamma n}$ with the coefficient equal to unit enters into the numerator and denominator of the fraction in the left-hand side of formula (135).

Considering formula (10), from (135) we have

$$\sigma = E_\infty \varepsilon - E_\infty \sum_{j=1}^{n} m_j \int_0^t \ni_\gamma \left(-t'/t_j \right) \varepsilon \left(t - t' \right) dt', \tag{136}$$

or

$$\sigma = E_\infty \left[1 - \sum_{j=1}^{n} m_j \ni_\gamma^* \left(t_j^\gamma \right) \right] \varepsilon. \tag{137}$$

As a result we are led to generalized Rabotnov's rheological equation with the operator (23).

Putting $\varepsilon = \varepsilon_0 = const$ in (137), we obtain the relationship

$$\sigma = E_\infty \left\{ 1 - \sum_{j=1}^{n} m_j \left[1 - E_\gamma \left(- (t/t_j)^\gamma \right) \right] \right\} \varepsilon_0, \tag{138}$$

which describes the stress relaxation, where

$$E_\gamma \left[- (t/t_j)^\gamma \right] = \sum_{n=0}^{\infty} \frac{(-1)^n (t/t_j)^{\gamma n}}{\Gamma(1 + \gamma n)}$$

is Mittag-Leffler function.

Tending t to ∞ in (138) and considering that in so doing $E_\gamma \left[- (t/t_j)^\gamma \right]$ tends to zero, we have

$$\sigma_0 = E_\infty \left(1 - \sum_{j=1}^{n} m_j \right) \varepsilon_0, \tag{139}$$

or

$$\sigma_0 = E_0 \varepsilon_0, \tag{140}$$

where $E_0 = E_\infty \left(1 - \sum_{j=1}^{n} m_j \right)$ is the relaxed elastic modulus.

If we express ε in terms of σ from relationship (132)

$$\varepsilon = J_\infty \frac{\prod_{j=1}^{n} (D^\gamma + \gamma_j)}{\prod_{i=1}^{n} (D^\gamma + \beta_i)} \sigma \tag{141}$$

and expand the fraction in the right-hand side of (141) in simple fractions

$$\frac{\prod_{j=1}^{n} (D^\gamma + \gamma_j)}{\prod_{i=1}^{n} (D^\gamma + \beta_i)} = (D^\gamma + \gamma_1) \sum_{i=1}^{n} \frac{B_i}{D^\gamma + \beta_i} = \sum_{i=1}^{n} \left(B_i + \frac{g_i}{1 + \tau_i^\gamma D^\gamma} \right), \tag{142}$$

where

$$B_i = \frac{\prod_{j=2}^{n} (\gamma_j - \beta_i)}{\prod_{\substack{i=1 \\ (i \neq j)}}^{n} (\beta_j - \beta_i)}, \quad g_i = B_i \frac{\gamma_1 - \beta_i}{\beta_i}, \quad \sum_{i=1}^{n} B_i = 1, \quad J_\infty = b_n / a_n,$$

then with due account for (10), we obtain relationship

$$\varepsilon = J_\infty \left[1 + \sum_{i=1}^{n} g_i \ni_\gamma^* (\tau_i^\gamma) \right] \sigma. \tag{143}$$

Putting $\sigma = \sigma_0 = const$ in (143), we find the expression which describes the creep

$$\varepsilon = J_\infty \left\{ 1 + \sum_{i=1}^{n} g_i \left[1 - E_\gamma \left(- (t/t_i)^\gamma \right) \right] \right\} \sigma_0. \tag{144}$$

Tending t to ∞ in (144), we have

$$\varepsilon_0 = J_\infty \left(1 + \sum_{i=1}^{n} g_i \right) \sigma_0, \tag{145}$$

or

$$\varepsilon_0 = J_0 \sigma_0, \tag{146}$$

where $J_0 = J_\infty \left(1 + \sum_{i=1}^{n} g_i \right)$ is the relaxed compliance.

Thus, for the model (132) it has been possible to find the thermodynamic constrains on the rheological parameters by reducing the given model involving fractional derivatives to the known Rabotnov model, representing itself Boltzmann-Volterra relationships with the sum of $\ni_\gamma^*$-operators which possess one fractional parameter and several relaxation (retardation) times, namely: the values $\tau_i^{-\gamma}$ and $t_j^{-\gamma}$ should alternate with each other (32) as it is shown in Fig. 1.

In other words, in order the models (137) and (143) are to be resolvent, as it has been shown by Rabotnov [48], it is necessary that the relaxation times $\tau_i^{-\gamma}$ and the retardation times $t_j^{-\gamma}$ should obey the inequalities according to (32).

In conclusion it should be noted that if any two hereditarily elastic operators, $\tilde{K}$ and $\tilde{E}$, or $\tilde{\mu}$ and $\tilde{E}$, as examples, are given in terms of the Rabotnov-type operators, then it is rather easy to determine all other operators of the model under consideration, which depend on the two given viscoelastic operators.

6. Free Vibrations of Oscillators on the Basis of Fractional Operator Viscoelastic Models

Assume that viscoelastic features of operators are described by the Bolzmann-Volterra relationships with the relaxation kernel $K_\varepsilon(t)$ and retardation kernel $K_\sigma(t)$. Then the equations of motion of such an oscillator could be written in two different but equivalent forms [56]

$$\ddot{x} + \omega_\infty^2 \left[x - \nu_\epsilon \int_0^t K_\epsilon(t - t') x(t') dt' \right] = F\delta(t), \tag{147}$$

$$\ddot{x} + \omega_\infty^2 x + \nu_\sigma \int_0^t K_\sigma(t - t') \ddot{x}(t') dt' = F \left[\delta(t) + \nu_\sigma K_\sigma(t) \right], \tag{148}$$
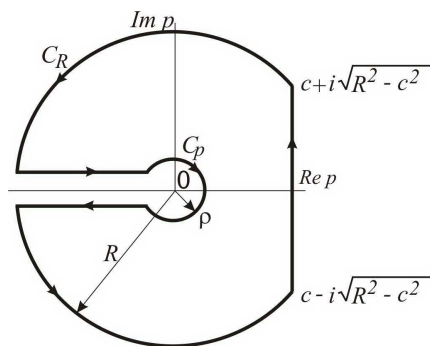
Figure 2. Contour of integration.

where x is the coordinate, F is the amplitude of force impulse per unit mass, ω_∞ is the frequency of elastic vibrations corresponding to the nonrelaxed magnitude of the elastic modulus, and overdots denote time derivatives.

Applying the Laplace transformation to Eqs. (147) and (148) yields

$$\bar{x}(p) = \frac{F}{p^2 + \omega_\infty^2[1 - \nu_\epsilon \bar{K}_\epsilon(p)]} = \frac{F[1 + \nu_\sigma \bar{K}_\sigma(p)]}{\omega_\infty^2 + p^2[1 + \nu_\sigma \bar{K}_\sigma(p)]}. \tag{149}$$

The solution of (149) in the time domain according to the inversion Mellin-Fourier formula has the form

$$x(t) = \frac{1}{2\pi i} \int_{c-i\infty}^{c+i\infty} \bar{x}(p)e^{pt}dp. \tag{150}$$

Functions $\bar{x}(p)$ considered here are multi-valued functions with the branch points $p = 0$ and $p = -\infty$ or $p = -s_*$, $s_* \geq 0$ and $p = -\infty$. In other words, the inversion should be carried out on the first sheet of Riemannian surface with a cut along the real negative semi-axis from 0 to $-\infty$ or from $-s_*$ to $-\infty$. Figure 2 shows the closed contour of integration for the function with the branch points $p = 0$ and $p = -\infty$. If a function possesses the branch points $p = -s_*$ and $p = -\infty$, then the center of a small circumference should locate at the point $p = -s_*$. Due to the Jordan lemma, the curvilinear integrals taken along the arcs c_R tend to zero at $R \to \infty$. For weakly singular kernels, the integral taken along c_ρ also tends to zero when $\rho \to 0$. Besides, the function $\bar{x}(p)$ possesses the ordinary poles at the same magnitudes of p which vanish the denominator in the formula (149), i.e., they are the roots of the characteristic equations:

$$p^2 + \omega_\infty^2 \left[1 - \nu_\epsilon \bar{K}_\epsilon(p)\right] = 0, \tag{151}$$

$$\omega_\infty^2 + p^2 \left[1 + \nu_\sigma \bar{K}_\sigma(p)\right] = 0. \tag{152}$$

Representing the variable p in the form

$$p = r\, e^{i\psi}$$

and introducing notations

$$\rho_\alpha = \sqrt{\Re_\alpha^2[\ \ ] + \Im_\alpha^2[\ \ ]}, \quad \tan\chi_\alpha = \frac{\Im_\alpha[\ \ ]}{\Re_\alpha[\ \ ]} \quad (\alpha = 1, 2),$$

$$\Re_1 \left[1 - \nu_\varepsilon \bar{K}_\varepsilon(p)\right] = \Re_1 \left[\ \right], \quad \Im_1 \left[1 - \nu_\varepsilon \bar{K}_\varepsilon(p)\right] = \Im_1 \left[\ \right],$$

$$\Re_2 \left[1 + \nu_\sigma \bar{K}_\sigma(p)\right] = \Re_2 \left[\ \right], \quad \Im_2 \left[1 + \nu_\sigma \bar{K}_\sigma(p)\right] = \Im_2 \left[\ \right],$$

we obtain

$$r^2 \rho_1^{-1} e^{i(2\psi - \chi_1)} + \omega_\infty^2 = 0, \tag{153}$$

$$r^2 \rho_2^{-1} e^{i(2\psi + \chi_2)} + \omega_\infty^2 = 0. \tag{154}$$

Separating the real and imaginary parts in Eqs. (153) and (154), we find

$$\begin{cases} r^2 \rho_1^{-1} \cos\left(2\psi - \chi_1\right) + \omega_\infty^2 = 0, \\ r^2 \rho_1^{-1} \sin\left(2\psi - \chi_1\right) = 0, \end{cases} \tag{155}$$

$$\begin{cases} r^2 \rho_2^{-1} \cos\left(2\psi + \chi_2\right) + \omega_\infty^2 = 0, \\ r^2 \rho_2^{-1} \sin\left(2\psi + \chi_2\right) = 0. \end{cases} \tag{156}$$

From the sets of Eqs. (153) and (154), we find

$$\begin{cases} 2\psi - \chi_1 = \pm\pi, \\ r^2 \rho_1^{-1} = \omega_\infty^2, \end{cases} \tag{157}$$

$$\begin{cases} 2\psi + \chi_2 = \pm\pi, \\ r^2 \rho_2^{-1} = \omega_\infty^2. \end{cases} \tag{158}$$

From relationships (157) and (158), we find the values of r and ψ which are, respectively, the modulus and argument of the root of characteristic Eqs. (151) and (152).

Using the Jordan lemma and the main theorem of the theory of residues, the solution to Eqs. (157) and (158) may be written as

$$x(t) = x^{\text{drift}}(t) + x^{\text{vibr}}(t) = \frac{1}{2\pi i} \int_0^\infty \left[\bar{x}(se^{-i\pi}) - \bar{x}(se^{i\pi})\right] e^{-st} ds + \sum_k \text{res}\left[\bar{x}(p_k)e^{p_k t}\right], \tag{159}$$

or

$$x(t) = \frac{1}{2\pi i} \int_0^\infty \left[\bar{x}(se^{-i\pi}) - \bar{x}(se^{i\pi})\right] H(s - s_*)e^{-st} ds + \sum_k \text{res}\left[\bar{x}(p_k)e^{p_k t}\right], \tag{160}$$

where $H(s - s_*)$ is the Heaviside function, the summation is taken over all isolated singular points (poles).

Since characteristic equations possess, as a rule, two complex conjugate roots

$$p_{1,2} = -\alpha \pm i\omega = r\, e^{\pm i\psi}, \tag{161}$$

then relationships (159) and (160) take the form

$$x(t) = A_0(t) + A \exp(-\alpha t) \sin(\omega t - \varphi), \tag{162}$$

where

$$A_0(t) = \int_0^\infty \tau^{-1} B(\tau) e^{t/\tau} d\tau, \tag{163}$$

and $B(\tau)$ is the function of distribution of the relaxation parameters (retardation parameters) of the dynamic system.

From Eq. (162) it is seen that the relationship describing vibrations of an oscillator with the natural frequency ω and the damping factor α possesses two terms, one of which describes the drift of the equilibrium position and is represented by the integral involving the distribution function of dynamic and rheological parameters, while the other term is the product of two time-dependent functions, exponent and sine, and it describes damped vibrations around the drifting equilibrium position, in so doing the drift is defined by the function $A_0(t)$. The first term $x^{\mathrm{drift}}(t)$ is governed by an improper integral taken along two sides of the cut along the negative real semi-axis of the complex plane (see Fig. 2), while the second term $x^{\mathrm{vibr}}(t)$ is determined by two complex conjugate roots of the characteristic equation, which locate in the left half-plane of the complex plane.

The original method for solving characteristic equation with fractional powers without its rationalization has been suggested in [40, 89], when the roots and model's parameters (relaxation or retardation times) are found at a time. It has been established that the characteristic equation lacks real negative roots and possesses only two complex conjugate roots. The behavior of the characteristic equation roots in the complex plane depends on the type of relaxation or creep kernel involved in the model of an oscillator under consideration. The interested reader is referred to Refs. [55, 60, 64] for a fully comprehensive description of the mathematical formulation.

Note that 25 years later than it was published in [40, 89], this result was re-discovered in [7].

Thus, in order to obtain the final solution, it is necessary to specify the type of the relaxation or creep kernel. Below we consider a few such examples.

6.1. Rabotnov Model

If we use the Rabotnov model as a relaxation kernel (16), then the solution (159) takes the form of (162) [57], where

$$A = 2F \left[(a^2 + b^2)^{-1} (\tau_\epsilon^{-2\gamma} + r^{2\gamma} + 2\tau_\epsilon^{-\gamma} r^\gamma \cos \gamma\psi) \right]^{1/2}, \tag{164}$$

$$\tan \varphi = -\frac{\tau_\epsilon^{-\gamma} \cos \beta + r^\gamma \cos(\beta - \gamma\psi)}{\tau_\epsilon^{-\gamma} \sin \beta + r^\gamma \sin(\beta - \gamma\psi)}, \qquad \beta = \frac{b}{a}, \qquad r^2 = \omega^2 + \alpha^2, \qquad \tan \psi = -\frac{\omega}{\alpha},$$

$$a = (2 + \gamma) r^{1+\gamma} \cos(1 + \gamma)\psi + 2\tau_\epsilon^{-\gamma} r \cos \psi + \gamma \omega_\infty^2 r^{\gamma-1} \cos(\gamma - 1)\psi,$$

$$b = (2 + \gamma) r^{1+\gamma} \sin(1 + \gamma)\psi + 2\tau_\epsilon^{-\gamma} r \sin \psi + \gamma \omega_\infty^2 r^{\gamma-1} \sin(\gamma - 1)\psi,$$

and

$$B(\tau, \tau_\epsilon^{-\gamma}) = \frac{\sin \gamma\pi}{\pi} \frac{\nu_\epsilon \omega_\infty^2 F [\theta_\infty(\tau)]^{-1} [\theta_0(\tau)]^{-1} \tau^3}{\theta_\infty(\tau) [\theta_0(\tau)]^{-1} \tau^{-\gamma} \tau_\epsilon^{-\gamma} + \theta_0(\tau) [\theta_\infty(\tau)]^{-1} \tau^\gamma \tau_\epsilon^\gamma + 2 \cos \pi\gamma}, \tag{165}$$

$$\theta_\infty(\tau) = \tau^2 \omega_\infty^2 + 1, \qquad \theta_0(\tau) = \tau^2 \omega_0^2 + 1,$$

and ω_0 is the frequency of elastic vibrations corresponding to the relaxed magnitude of the elastic modulus.

The behavior of the roots of the characteristic equation (151) as function of the parameter $\tau_\epsilon^{-\gamma}$ is shown in Figs. 3 a-d for $\omega_\infty = 1$ and four values $\xi = 0,\ 1/50,\ 1/9$ and $1/6$, respectively, where figures near curves denote the magnitudes of the value γ, and $\xi = E_0/E_\infty = 1 - \nu_\epsilon$.
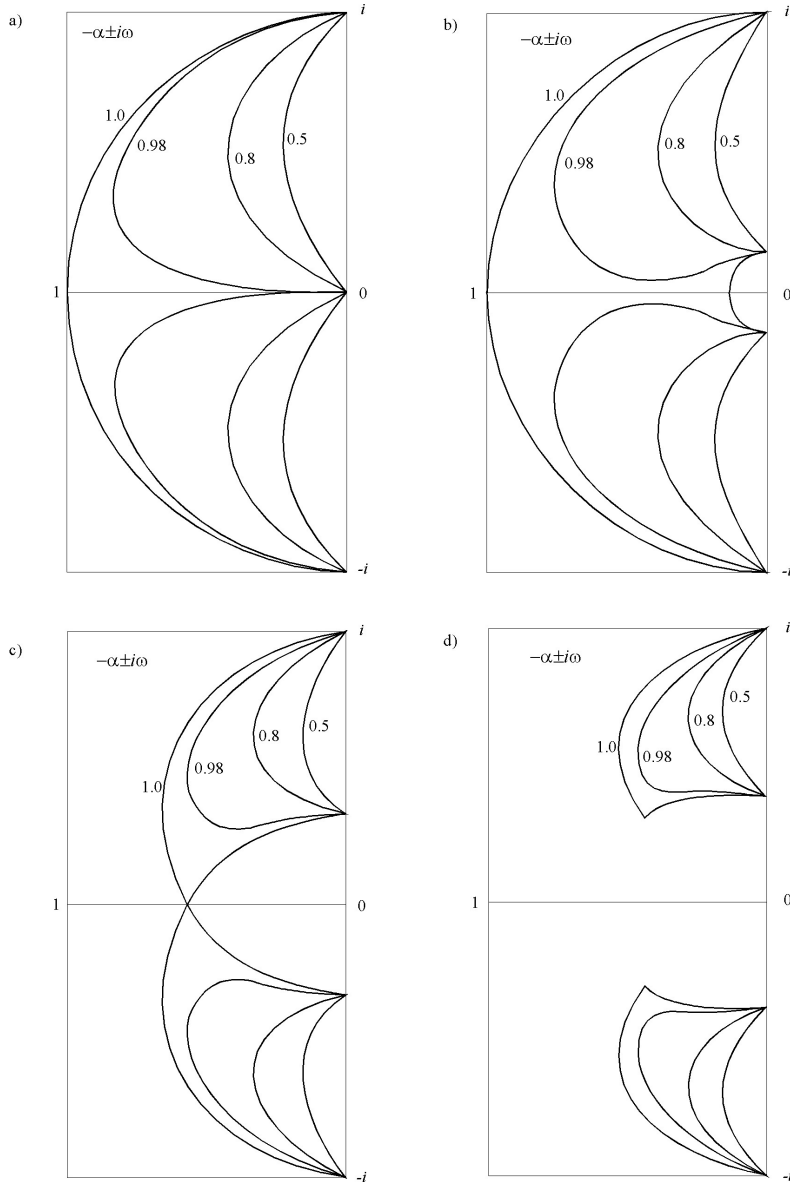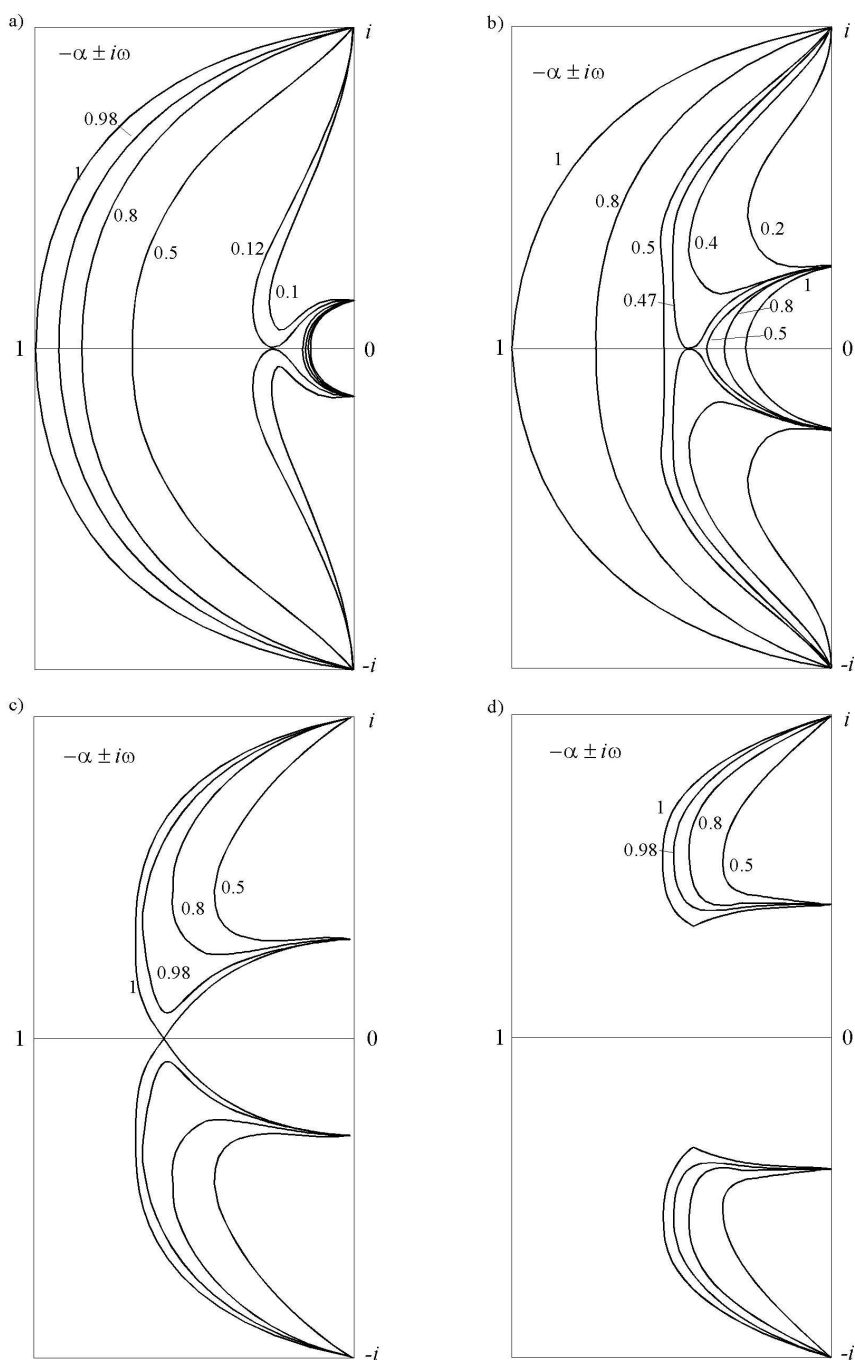

Figure 3. Behavior of the complex conjugate roots $p_{1,2} = -\alpha \pm i\omega$ for an oscillator based on the Rabotnov model: (a) $\xi = 0$, (b) $\xi = 1/50$, (c) $\xi = 1/9$, and (d) $\xi = 1/6$.

It is seen that the $\tau_\epsilon^{-\gamma}$-dependence of the two complex conjugate roots $p_{1,2} = -\alpha \pm i\omega$ at $\gamma \neq 1$ leave the points $\pm i$ and converge in the points $\pm i\xi^{1/2}$ when $\tau_\epsilon^{-\gamma}$ changes from

0 to ∞; in so doing it does not meet the real negative semi-axes and remains inside the curves for the $\tau_\epsilon^{-\gamma}$-dependencies of three roots of the characteristic equation with $\gamma = 1$ (the ordinary standard linear solid model). The behavior of the two roots of three at $\gamma = 1$ (the third root is the real root all the time and changes from 0 to ∞ as $\tau_\epsilon^{-\gamma}$ varies from 0 to ∞) essentially depends on the magnitude of the value ξ. Thus, at the values ξ taken from the interval $(0, 1/9)$ the two complex conjugate roots first become real as $\tau_\epsilon^{-\gamma}$ changes from 0 to ∞. But then during further increase in $\tau_\epsilon^{-\gamma}$, they again become complex conjugate roots, i.e., the domain of aperiodicity (the values of $\tau_\epsilon^{-\gamma}$ wherein $\omega = 0$) has finite dimensions contracting with increase in ξ (Figs. 3a,b). At $\xi = 0$ the ordinary Maxwell model with a semi-infinite domain of aperiodicity is obtained (Fig. 3a) [57], but at $\xi = 1/9$ the domain of aperiodicity degenerates into a point (Fig. 3c). When $\xi > 1/9$, the domain of aperiodicity completely disappears (Fig. 3d).

In other words, at $\gamma \neq 1$ the behavior character of the roots of the characteristic equation for the Rabotnov model is governed by the magnitudes of the value ξ, which may be considered as the deficiency of the elastic modulus.

6.2.   Rzhanitsyn Model

It has been already mentioned in Sect. 5.1 that the Rzhanitsyn kernel (118) [71] could be utilized as the kernel of relaxation and the kernel of retardation, so we will consider these two cases separately.

6.2.1.   Rzhanitsyn After-effect Kernel

Hereditary elastic oscillator model with the Rzhanitsyn creep, or after-effect, kernel (120) was studied in [56], wherein it had been shown that knowing the behavior of roots of the characteristic equation (152) and considering that the branch points are $s_* = \tau_\sigma^{-1}$ and $-\infty$, the solution (159) may be written in the form of (162) with

$$A = 2F\left[(h^2 + q^2)^{-1}(\nu_\sigma^2 + 2R^\gamma \nu_\sigma \cos\gamma\Phi + R^{2\gamma})\right]^{1/2}, \tag{166}$$

where

$$\tan\varphi = -\frac{\nu_\sigma \sin\chi + R^\gamma \sin(\gamma\psi + \chi)}{\nu_\sigma \cos\chi + R^\gamma \cos(\gamma\psi + \chi)}, \qquad \chi = \frac{h}{q},$$

$$R^2 = 1 + 2\tau_\sigma r \cos\psi + \tau_\sigma^2 r^2, \qquad \tan\Phi = \tau_\sigma r \sin\psi(1 + \tau_\sigma r \cos\psi)^{-1},$$

$$h = 2rR^\gamma \cos(\psi+\Phi)+r^2 R^{\gamma-1}\gamma\tau_\sigma \cos[2\psi+(\gamma-1)\Phi]+\tau_\sigma\omega_\infty^2\gamma R^{\gamma-1}\cos(\gamma-1)\Phi+2r\nu_\sigma \cos\psi,$$

$$q = 2rR^\gamma \sin(\psi+\Phi)+r^2 R^{\gamma-1}\gamma\tau_\sigma \sin[2\psi+(\gamma-1)\Phi]+\tau_\sigma\omega_\infty^2\gamma R^{\gamma-1}\sin(\gamma-1)\Phi+2r\nu_\sigma \sin\psi,$$

and

$$B(\tau, \tau_\sigma) = \frac{\sin\pi\gamma}{\pi}\frac{F\omega_\infty^2(1 + \omega_\infty^2\tau^2)^{-1}\tau^3 H(\tau_\sigma - \tau)}{[D_\sigma(\tau)]^{-1} + D_\sigma(\tau) + 2\cos\pi\gamma}, \tag{167}$$

$$D_\sigma(\tau) = \tau^\gamma(1 + \omega_\infty^2\tau^2)^{-1}(\tau_\sigma - \tau)^{-\gamma}\nu_\sigma.$$

The root locus in the complex plane as function of the parameter τ_σ for three magnitudes $\nu_\sigma = 49, 8$, and 5 ($\xi = 1/50, 1/9$ and $1/6$) at $\omega_\infty = 1$ was presented in Figs. 2a-c in [56]. Its analysis reveals that the behavior of the characteristic equation roots in the case under consideration is identical to that of the oscillator with the Rabotnov relaxation kernel shown in Figs. 3b-d for the corresponding magnitudes of the parameter ξ.

6.2.2. Rzhanitsyn Relaxation Kernel

Let us take the Rzhanitsyn kernel (118) at $i = \epsilon$ as the relaxation kernel in the Boltzmann-Volterra relationships (116). Then the characteristic equation (151) takes the form

$$(p^2 + \omega_\infty^2)(1 + p\tau_\epsilon)^\gamma - \omega_\infty^2 \nu_\epsilon = 0. \tag{168}$$

The behavior of the roots of the characteristic equation (168) in the complex plane as function of the parameter τ_ϵ for four magnitudes $\nu_\epsilon = 0.98, 14/15, 8/9$, and $5/6$ ($\xi = 1/50, 1/15, 1/9$ and $1/6$) at $\omega_\infty = 1$ is presented in Figs. 4(a),(b),(c), and (d), respectively, wherein the magnitudes of γ are indicated by figures. Reference to Figs. 4 shows that as τ_ϵ changes from 0 to ∞, the curves for two complex conjugate roots $p_{1,2} = -\alpha \pm i\omega$ at any $0 < \gamma < 1$ issue out of the points $\pm i\xi^{1/2}$ and converge at the points $\pm i$. At $\nu_\epsilon = 0.98$ and $0.12 \leq \gamma < 1$ (Fig. 4(a)) or $\nu_\epsilon = 14/15$ and $0.47 \leq \gamma < 1$ (Fig. 4(b)) the domain of aperiodicity is observed, which narrows with decrease in γ from 1 to 0.12 or from 1 to 0.47 and degenerates into a point at $\gamma = 0.12$ or $\gamma = 0.47$. This domain disappears completely at $0 \leq \gamma < 0.12$ or $0 < \gamma < 0.47$, respectively. At $\nu_\epsilon = 8/9$ (Fig. 4(c)) and $5/6$ (Fig. 4(d)) the domain of aperiodicity is entirely absent, although the domain of aperiodicity at $\nu_\epsilon = 8/9$ and $\gamma = 1$ exists in the form of a point.

In other words, the structural parameter γ along with the parameter ξ influences not only the dimensions of the aperiodicity domain, but the existence of this domain as well. This circumstance profitably distinguishes the model under consideration from the previous model, since it allows one to use this model for describing dissipative processes of high intensity.

Now knowing the behavior of roots of the characteristic equation (168) and considering that the branch points are $s_* = \tau_\sigma^{-1}$ and $-\infty$, the solution (162) is as follows [56]:

for the domains of vibration motions (one real and two complex conjugate roots)

$$x(t) = A_0(t) + A_1 \exp(-\alpha_1 t) + A_2 \exp(-\alpha_2 t)\sin(\omega t - \varphi), \tag{169}$$

or (real root disappears)

$$x(t) = A_0(t) + A_2 \exp(-\alpha_2 t)\sin(\omega t - \varphi); \tag{170}$$

for the domain of aperiodic motions (three real different roots)

$$x(t) = A_0(t) + \sum_{i=1}^{3} H_i \exp(-\beta_i t); \tag{171}$$

for the boundaries of the domain of aperiodic motions (one real root, for example, β_1 is the simple root, and the other real root $\beta = \beta_2 = \beta_3$ is one repeated root)

$$x(t) = A_0(t) + H_1 \exp(-\beta_1 t) + B_1 \exp(-\beta t) + B_2 t \exp(-\beta t), \tag{172}$$

or (in the case, if the domain of the aperiodic motions degenerates into a point, the real root $\beta^* = \beta_1 = \beta_2 = \beta_3$ becomes a 3-fold root)

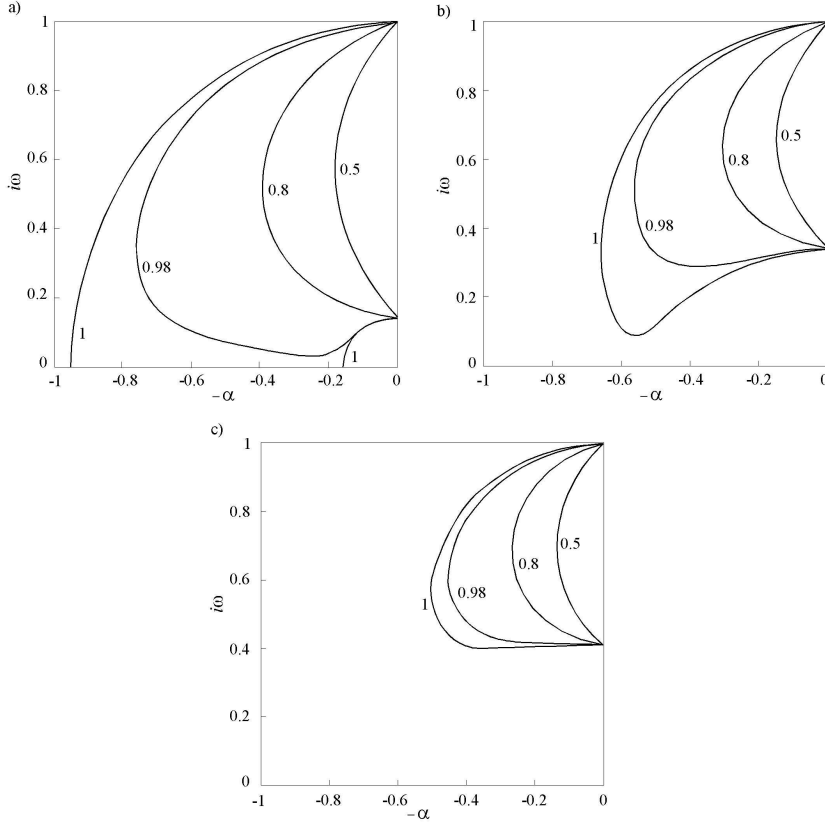$$x(t) = A_0(t) + B_1^* \exp(-\beta^* t) + B_2^* t \exp(-\beta^* t) + B_3^* t^2 \exp(-\beta^* t), \tag{173}$$

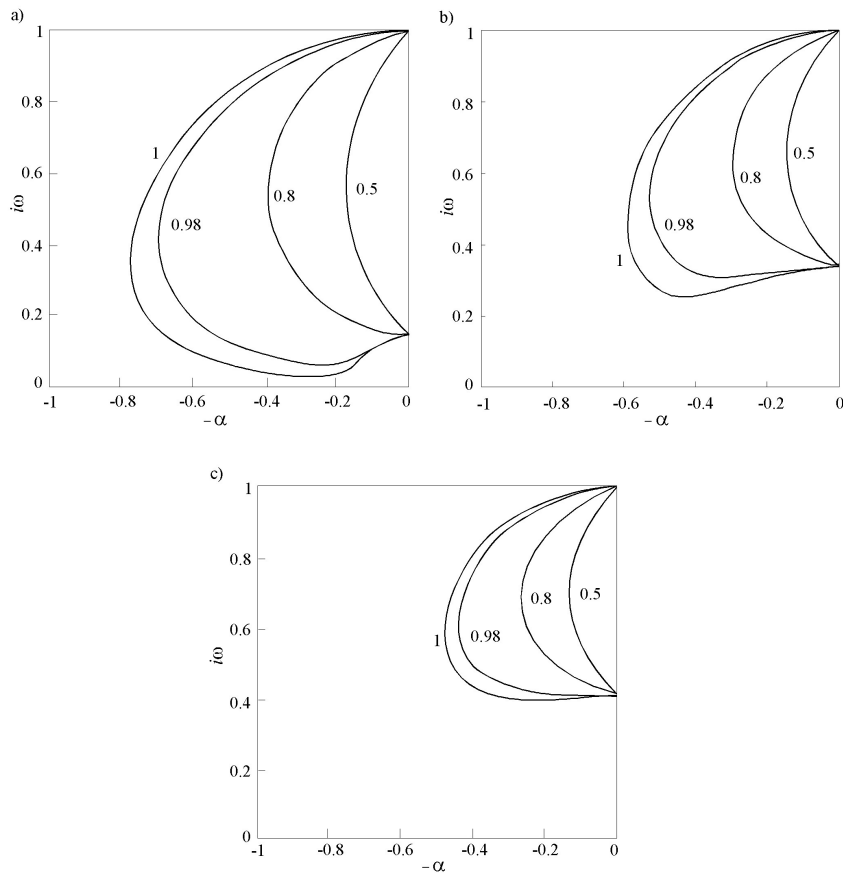Figure 4. Behavior of the complex conjugate roots $p_{1,2} = -\alpha \pm i\omega$ for an oscillator based on the fractional calculus model with the Rzhanitsyn relaxation kernel: (a) $\xi = 1/50$, (b) $\xi = 1/15$, (c) $\xi = 1/9$, and (d) $\xi = 1/6$.

where α_1, β_i $(i = 1, 2, 3)$, β and β^* are the real roots of Eq. (168) which are located between $\tau_\epsilon^{-1}(1 - \nu_\epsilon^{1/\gamma})$ and the branch point τ_ϵ^{-1}, and $\alpha_2 \pm i\omega$ are the complex conjugate roots of Eq. (168).

The amplitudes A_i, H_i, B_i^* $(i = 1, 2, 3)$, B_1, and B_2, as well as φ are expressed in terms of the damping coefficients $\alpha_1, \alpha_2, \beta_i, \beta, \beta^*$ and natural frequency ω as follows:

$$A_1 = \frac{F(1 - \alpha_1\tau_\epsilon)}{\alpha_1^2\tau_\epsilon(2 + \gamma) - 2\alpha_1 + \gamma\tau_\epsilon\omega_\infty^2}, \qquad H_i == \frac{F(1 - \beta_i\tau_\epsilon)}{\beta_i^2\tau_\epsilon(2 + \gamma) - 2\beta_i + \gamma\tau_\epsilon\omega_\infty^2},$$

$$A_2 = 2FR^\gamma(h^2 + q^2)^{-1/2}, \qquad \varphi = -(\gamma\psi + \chi), \qquad \chi = h/q,$$

$$h = 2rR^\gamma \cos(\psi + \gamma\Phi) + \gamma r^2 R^{\gamma-1}\tau_\epsilon \cos[2\psi + (\gamma - 1)\Phi] + \gamma\omega_\infty^2 R^{\gamma-1}\tau_\epsilon \cos(\gamma - 1)\Phi,$$

$$R^2 = 1 + 2\tau_\epsilon r \cos\psi + \tau_\epsilon^2 r^2, \qquad \tan\Phi = \tau_\epsilon r \sin\psi(1 + \tau_\epsilon r \cos\psi)^{-1},$$

$$q = 2rR^\gamma \sin(\psi + \gamma\Phi) + \gamma r^2 R^{\gamma-1}\tau_\epsilon \sin[2\psi + (\gamma - 1)\Phi] + \gamma\omega_\infty^2 R^{\gamma-1}\tau_\epsilon \sin(\gamma - 1)\Phi,$$

$$B_1 = 2F\gamma(1 - \beta\tau_\epsilon)\tau_\epsilon l^{-1}, \qquad B_2 = 2F(1 - \beta\tau_\epsilon)^2 l^{-1},$$

$$l = \beta^2\tau_\epsilon^2(2 + \gamma)(1 + \gamma) - 4\beta\tau_\epsilon(1 + \gamma) + \gamma(\gamma - 1)\tau_\epsilon^2\omega_\infty^2,$$

$$B_1^* = 3F\gamma(\gamma-1)(1-\beta\tau_\epsilon)\tau_\epsilon^2 l_1^{-1}, \quad B_2^* = 6F\gamma(1-\beta\tau_\epsilon)^2\tau_\epsilon l_1^{-1}, \quad B_3^* = 3F(1-\beta\tau_\epsilon)^3 l_1^{-1},$$

$$l_1 = \beta^2\tau_\epsilon^3(2 + \gamma)(1 + \gamma)\gamma - 6\beta\tau_\epsilon^2(1 + \gamma)\gamma + 4\tau_\epsilon(1 + \gamma) + \gamma(\gamma - 1)(\gamma - 2)\tau_\epsilon^2\omega_\infty^2.$$

The value $A_0(t)$ is determined by Eq. (162), wherein the distribution function $B(\tau, \tau_\epsilon)$ of the relaxation and creep parameters of the dynamical system under consideration has the form

$$B(\tau, \tau_\epsilon) = \frac{\sin\pi\gamma}{\pi} \frac{F(1 + \omega_\infty^2\tau^2)^{-1}\tau^3 H(\tau_\epsilon - \tau)}{[D_\epsilon(\tau)]^{-1} + D_\epsilon(\tau)\tau^4 + 2\tau^2 \cos\pi\gamma}, \tag{174}$$

$$D_\epsilon(\tau) = \tau^\gamma(1 + \omega_\infty^2\tau^2)^{-1}(\tau_\epsilon - \tau)^{-\gamma}\omega_\infty^2\nu_\epsilon.$$

Comparison studies of damped vibrations of the hereditary elastic oscillators, whose hereditary properties are described by the fractional calculus models with the weakly singular Rzhanitsyn kernel, allow us to make the following conclusions: (1) the peculiarity of the vibrational process of the viscoelastic single-mass systems, which are modeled by the fractional calculus models with the weakly singular Rzhanitsyn kernel as the creep kernel, resides in impossibility of the transition from the vibrating motions to the aperiodic regime in spite of the known fact that under the sufficiently large intensity of dissipative processes real vibrating systems may experience the aperiodic regime; (2) the more complicated rheological model, i.e., the model with the weakly singular Rzhanitsyn kernel as the relaxation kernel, utilized for describing the viscoelastic properties of a single-mass system, allows one to trace the influence of the fractional operator parameter γ on the dynamic characteristics of the system not only in the region of vibration, but in the domain of the aperiodic motions as well. Moreover, it has been shown that the occurrence or vanishing of the region of the aperiodic motions for the model put forward is governed not only by the magnitudes of the value ν_ϵ, but by the magnitudes of the value γ as well.

6.3.   Combinational Rabotnov-Rzhanitsyn Model

The comparison between theoretical and experimental results in the field of application of fractional calculus models in viscoelasticity carried out in [59] has shown that the fractional models with more than one fractional parameters seem to be very flexible for describing relaxation (retardation) behavior over wide frequency ranges and for different materials. One distinct advantage of the fractional calculus models is their ability to describe real material behavior using only a small number of parameters.

However, the analysis of many of such models [59] revealed the fact that at some magnitudes of rheological parameters they are not thermodynamically admissible, i.e., the loss tangent takes on negative values in some frequency domain and the relaxation (retardation) function becomes non-monotonic in some time intervals.

It has been proved in [59] that the rheological models involving fractional operators (130) with two independent fractional parameters $0 < \alpha, \beta \leq 1$, which represent the combination of Rabotnov and Rzhanitsyn models

$$\sigma = E_\infty[\varepsilon - \nu_\varepsilon(1 + \tau_\varepsilon^\alpha D^\alpha)^{-\beta}\varepsilon], \tag{175}$$

$$\varepsilon = J_\infty[\sigma + \nu_\sigma(1 + \tau_\sigma^\alpha D^\alpha)^{-\beta}\sigma] \tag{176}$$

are thermodynamically well-conditioned at all magnitudes of the rheological parameters.

Note that the models (175) and (176) at $0 < \alpha, \beta < 1$ are not resolvent despite of the Rabotnov models at $0 < \alpha < 1$ and $\beta = 1$.

Havriliak and Negami [26, 27] used these models for the analysis of dielectric and mechanical dispersion for five polymers (polycarbonate and polyisophthalat on the basis of bisphenol A, isotaclic polymethyl methacrylate, polymethylacrylate, and co-polymers of phenylmethacrylate and acrylonitrile), while Hartmann *et al.* [25] utilized them for approximation of the loss factor for polymer relaxation on the basis of experimental data for different polymers. It has been shown close agreement between theoretical and experimental findings.

6.3.1.   Rabotnov-Rzhanitsyn Relaxation Kernel

Now let us first consider viscoelastic oscillators (147), the behavior of which is described by the model (175), following Rossikhin and Shitikova [59]. For this case, Eq. (149) takes the form

$$\bar{x}(p) = \frac{F[1 + (p\tau_\varepsilon)^\alpha]^\beta}{(p^2 + \omega_\infty^2)[1 + (p\tau_\varepsilon)^\alpha]^\beta - \omega_\infty^2\nu_\varepsilon}. \tag{177}$$

To determine the poles of the function $\bar{x}(p)$ (177), it is necessary to find the roots of the characteristic equation

$$(p^2 + \omega_\infty^2)[1 + (p\tau_\varepsilon)^\alpha]^\beta - \omega_\infty^2\nu_\varepsilon = 0. \tag{178}$$

The procedure of solving characteristic Eq. (178) is described in detail in [59].

The behavior of the roots in the complex plane as function of the parameter τ_ε at $\omega_\infty^2 = 1$ for three magnitudes of $\nu_\varepsilon = 0.98, \ 8/9, \ 5/6$ and $\beta = 0.98$ is presented in Figures 5 (a)-(c), respectively, where figures near curves denote the magnitudes of the fractional

Figure 5. Behavior of the complex conjugate roots $p_{1,2} = -\alpha \pm i\omega$ for an oscillator based on the fractional calculus model with the Rabotnov-Rzhanitsyn relaxation kernel at $\omega_\infty = 1$: (a) $\nu_\varepsilon = 0.98$, (b) $\xi = 8/9$, and (c) $\xi = 5/6$ when $\beta = 0.98$.

parameter α. From Figure 5 it is seen that the curves describing the roots behavior do not cut the real axis, i.e., the fundamental possibility for the transition of the vibrational process to an aperiodic regime is absent. Note that at $\alpha = 1$ and fractional β this model, as it has been discussed above in Sec. 6.2.2, behaves similarly to the standard linear solid model with derivatives of an integer order, that is, the system may be both in vibrational and aperiodic regimes depending on the magnitudes of the parameter τ_ε.

Knowing the behavior of the characteristic equation roots, the solution (159) takes the form of (162) [55], where

$$A = 2FR_\varepsilon^\beta(h^2 + q^2)^{-1/2}, \tag{179}$$

$$\tan\varphi = -\tan(\beta\Phi_\varepsilon + \chi), \quad \tan\chi = \frac{h}{q},$$

$$R_\epsilon = \sqrt{1 + 2r^\alpha\tau_\epsilon^\alpha\cos\alpha\psi + r^{2\alpha}\tau_\epsilon^{2\alpha}}, \qquad \tan\Phi_\epsilon = \frac{r^\alpha\tau_\epsilon^\alpha\sin\alpha\psi}{1 + r^\alpha\tau_\epsilon^\alpha\cos\alpha\psi},$$

$$h = 2rR_\varepsilon^\beta\cos(\psi + \beta\Phi_\varepsilon) + r^{1+\alpha}\alpha\beta\tau_\varepsilon^\alpha R_\varepsilon^{\beta-1}\cos[(\beta-1)\Phi_\varepsilon + (\alpha+1)\psi]$$
$$+\omega_\infty^2 r^{\alpha-1}\alpha\beta\tau_\varepsilon^\alpha R_\varepsilon^{\beta-1}\cos[(\beta-1)\Phi_\varepsilon + (\alpha-1)\psi],$$

$$q = 2r R_\varepsilon^\beta \sin(\psi + \beta\Phi_\varepsilon) + r^{1+\alpha}\alpha\beta\tau_\varepsilon^\alpha R_\varepsilon^{\beta-1} \sin[(\beta-1)\Phi_\varepsilon + (\alpha+1)\psi]$$
$$+ \omega_\infty^2 r^{\alpha-1}\alpha\beta\tau_\varepsilon^\alpha R_\varepsilon^{\beta-1} \sin[(\beta-1)\Phi_\varepsilon + (\alpha-1)\psi],$$

$$B(s) = \frac{F\pi^{-1}s^{-1}(s^2 + \omega_\infty^2)^{-1}\sin\beta\Phi_\varepsilon^*}{(s^2 + \omega_\infty^2)R_\varepsilon^{*\beta}\nu_\varepsilon^{-1}\omega_\infty^{-2} + (s^2 + \omega_\infty^2)^{-1}R_\varepsilon^{*-\beta}\nu_\varepsilon\omega_\infty^2 - 2\cos\beta\Phi_\varepsilon^*},$$

$$R_\epsilon^* = R_\epsilon|_{\psi=\pi}, \qquad \Phi_\epsilon^* = \Phi_\epsilon|_{\psi=\pi}.$$

The character of the solution $x(t)$ is presented in Figure 6, where figures near curves denote the magnitude of the fractional parameter α.

6.3.2.   Rabotnov-Rzhanitsyn Retardation Kernel

Now let us consider viscoelastic oscillators (148), the behavior of which is described by the model (176), following Rossikhin and Shitikova [59]. For this case, Eq. (149) takes the form

$$\bar{x}(p) = \frac{F\left\{[1 + (p\tau_\sigma)^\alpha]^\beta + \nu_\sigma\right\}}{(p^2 + \omega_\infty^2)[1 + (p\tau_\sigma)^\alpha]^\beta + p^2\nu_\sigma}. \tag{180}$$

To determine the poles of the function $\bar{x}(p)$ (180), it is necessary to find the roots of the characteristic equation

$$(p^2 + \omega_\infty^2)[1 + (p\tau_\sigma)^\alpha]^\beta + p^2\nu_\sigma = 0. \tag{181}$$

The behavior of the roots in the complex plane as function of the parameter τ_σ is presented in Figs. 7 for three magnitudes of $\nu_\sigma = 49, 8$ and 5, respectively, when $\beta = 0.98$.

Knowing the behavior of the characteristic equation roots, the solution (159) takes the form of (162) [55], where

$$A = 2F\sqrt{(h^2 + q^2)^{-1}(R_\sigma^{2\beta} + 2R_\sigma^\beta\nu_\sigma\cos\beta\Phi_\sigma + \nu_\sigma^2)}, \tag{182}$$

$$\tan\varphi = -\frac{\nu_\sigma\sin\chi + R_\sigma^\beta\sin(\beta\Phi_\sigma + \chi)}{\nu_\sigma\cos\chi + R_\sigma^\beta\cos(\beta\Phi_\sigma + \chi)}, \quad \tan\chi = \frac{h}{q},$$

$$R_\sigma = \sqrt{1 + 2r^\alpha\tau_\sigma^\alpha\cos\alpha\psi + r^{2\alpha}\tau_\sigma^{2\alpha}}, \quad \tan\Phi_\sigma = \frac{r^\alpha\tau_\sigma^\alpha\sin\alpha\psi}{1 + r^\alpha\tau_\sigma^\alpha\cos\alpha\psi},$$

$$h = 2r R_\sigma^\beta\cos(\psi + \beta\Phi_\sigma) + r^{1+\alpha}\alpha\beta\tau_\sigma^\alpha R_\sigma^{\beta-1}\cos[(\beta-1)\Phi_\sigma + (\alpha+1)\psi]$$
$$+ \omega_\infty^2\alpha\beta\tau_\sigma^\alpha r^{\alpha-1} R_\sigma^{\beta-1}\cos[(\beta-1)\Phi_\sigma + (\alpha-1)\psi] + 2r\nu_\sigma\cos\psi,$$

$$q = 2r R_\sigma^\beta\sin(\psi + \beta\Phi_\sigma) + r^{1+\alpha}\alpha\beta\tau_\sigma^\alpha R_\sigma^{\beta-1}\sin[(\beta-1)\Phi_\sigma + (\alpha+1)\psi]$$
$$+ \omega_\infty^2\alpha\beta\tau_\sigma^\alpha r^{\alpha-1} R_\sigma^{\beta-1}\sin[(\beta-1)\Phi_\sigma + (\alpha-1)\psi] + 2r\nu_\sigma\sin\psi,$$

$$B(s) = \frac{F\pi^{-1}\omega_\infty^2 s^{-3}(s^2 + \omega_\infty^2)^{-1}\sin\beta\Phi_\sigma^*}{(s^2 + \omega_\infty^2)R_\sigma^{*\beta}\nu_\sigma^{-1}s^{-2} + (s^2 + \omega_\infty^2)^{-1}R_\sigma^{*-\beta}\nu_\sigma s^2 + 2\cos\beta\Phi_\sigma^*},$$

$$R_\sigma^* = R_\sigma|_{\psi=\pi}, \qquad \Phi_\sigma^* = \Phi_\sigma|_{\psi=\pi}.$$

The character of the solution $x(t)$ is presented in Figure 8, where figures near curves denote the magnitude of the fractional parameter α.
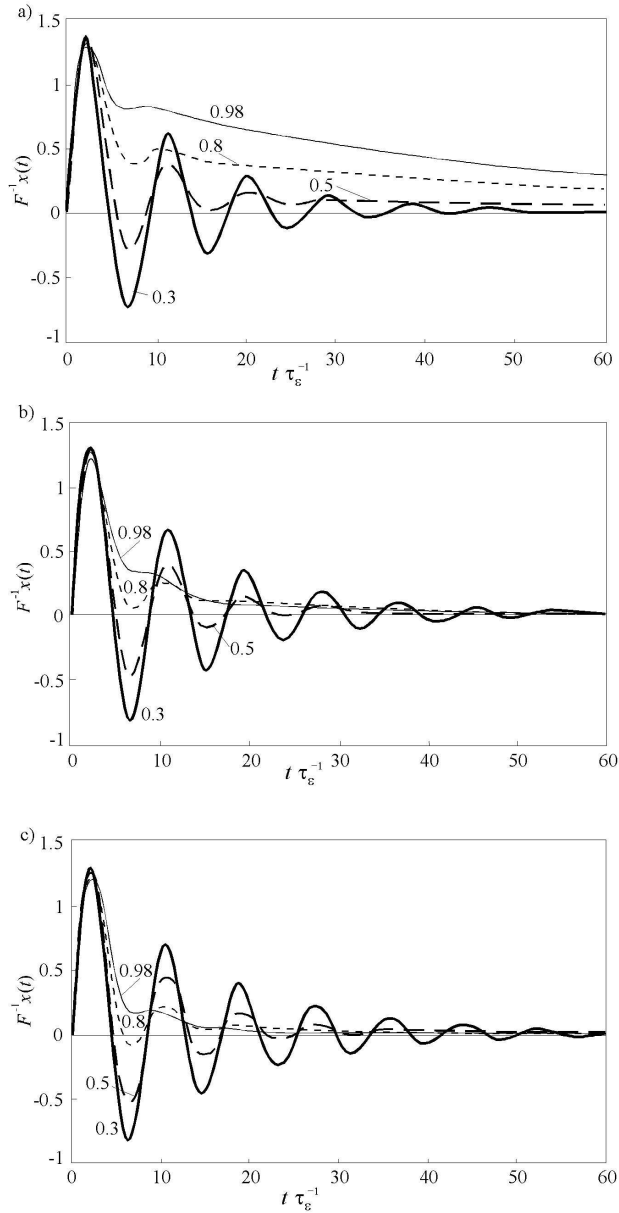
Figure 6. Character of the solution $x(t)$ behavior for an oscillator based on the fractional calculus model with the Rabotnov-Rzhanitsyn relaxation kernel at $\omega_\infty = 1$: (a) $\nu_\varepsilon = 0.98$, (b) $\nu_\varepsilon = 8/9$, and (c) $\nu_\varepsilon = 5/6$ for $\beta = 0.98$ and $\tau_\varepsilon = 1$.

As it has been noted in Sec 6.2.1, when $\alpha = 1$ and $\beta = \gamma$, the model under consideration goes over into the oscillator model with the Rzhanitsyn retardation operator, for which the behavior of the characteristic equation roots resembles the character of the roots behavior for the generalized standard linear solid model with the only difference that in this case the

noticeable asymmetry is observed in the behavior of the roots.

Figure 7. Behavior of the complex conjugate roots $p_{1,2} = -\alpha \pm i\omega$ for an oscillator based on the fractional calculus model with the Rabotnov-Rzhanitsyn retardation kernel at $\omega_\infty = 1$: (a) $\nu_\sigma = 49$, (b) $\nu_\sigma = 8$, and (c) $\nu_\sigma = 5$ when $\beta = 0.98$.

6.4. Generalized Rabotnov Model

The equation of motion of an oscillator, hereditary features of which are described by the model (137) has the form [63]:

$$\ddot{x} + \omega_\infty^2 \left[1 - \sum_{j=1}^{n} m_j \ni_\gamma^* \left(t_j^\gamma \right) \right] x = F\delta(t). \tag{183}$$

Applying the Laplace transformation to Eq. (183) yields

$$\bar{x}(p) = \frac{F}{p^2 + \omega_\infty^2 \{ 1 - \sum_{j=1}^{n} m_j [1 + (pt_j)^\gamma]^{-1} \}}. \tag{184}$$
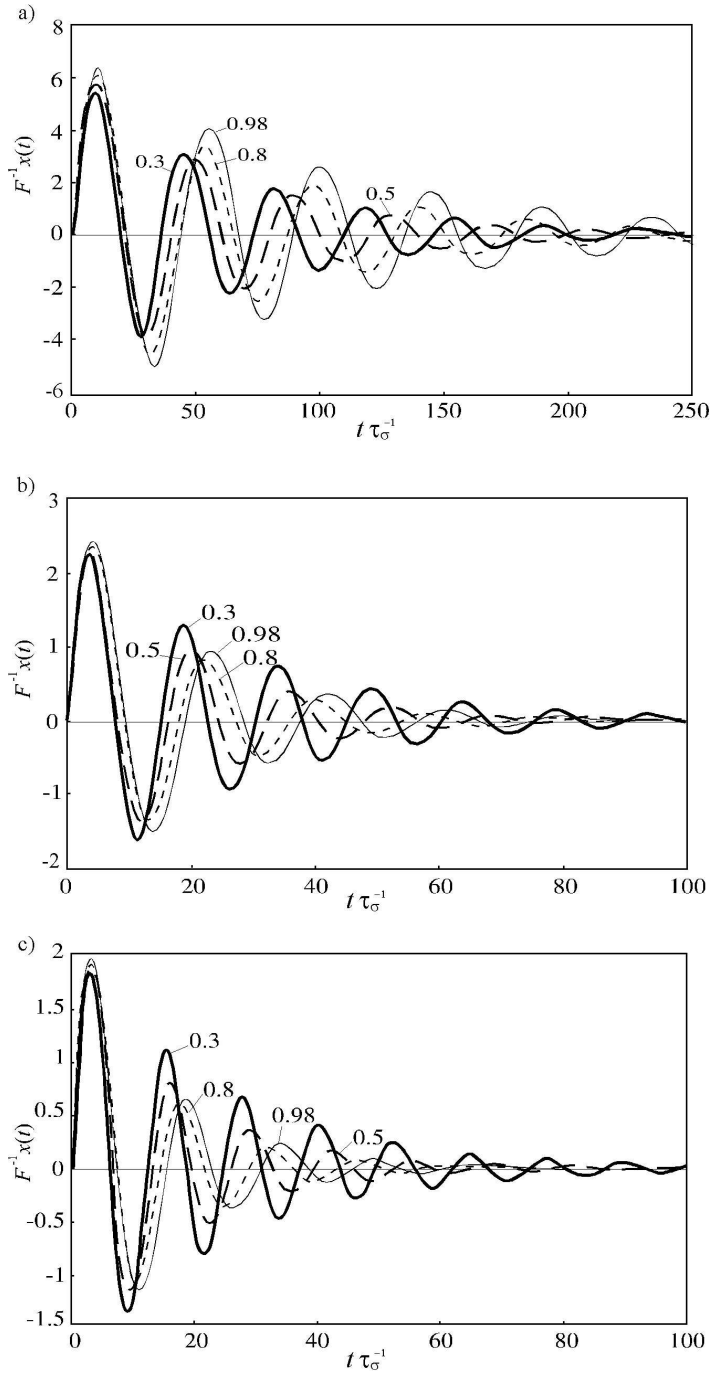
Figure 8. Character of the solution $x(t)$ behavior for an oscillator based on the fractional calculus model with the Rabotnov-Rzhanitsyn retardation kernel at $\omega_\infty = 1$: (a) $\nu_\sigma = 49$, (b) $\nu_\sigma = 8$, and (c) $\nu_\sigma = 5$ for $\beta = 0.98$ and $\tau_\sigma = 1$.

The solution in the time domain is determined by the Mellin-Fourier inversion formula (150). To calculate the integral in (150), it is necessary to determine all singular points of the complex function (184). This function has the branch points $p = 0$ and $p = \infty$ and simple poles at the same magnitudes of p which vanish the denominator of formula (184), i.e., they are the roots of the characteristic equation

$$f(p) = p^2 + \omega_\infty^2 \left\{ 1 - \sum_{j=1}^{n} m_j [1 + (pt_j)^\gamma]^{-1} \right\} = 0. \tag{185}$$

Since for the multivalued functions possessing branch points the inversion formula is valid only for the first sheet of the Riemann surface, then for calculating integral (150) we shall use the closed contour presented in Fig. 2. Using the main theorem of the residue theory, it could be written in the form of (159).

The value $x^{\text{drift}}(t)$ in (159) is calculated immediately and has the form [63]

$$x^{\text{drift}}(t) = \frac{F\omega_\infty^2}{\pi} \int_0^\infty \frac{\sum_{j=1}^{n} m_j R_j^{-1} \sin \Phi_j \, e^{-st} ds}{(s^2 + \omega_\infty^2 - \omega_\infty^2 \sum_{j=1}^{n} m_j R_j^{-1} \cos \Phi_j)^2 + \omega_\infty^4 (\sum_{j=1}^{n} m_j R_j^{-1} \sin \Phi_j)^2}, \tag{186}$$

where

$$R_j = \sqrt{1 + 2(st_j)^\gamma \cos \gamma\pi + (st_j)^{2\gamma}}, \quad \tan \Phi_j = \frac{(st_j)^\gamma \sin \gamma\pi}{1 + (st_j)^\gamma \cos \gamma\pi}.$$

In order to calculate $x^{\text{vibr}}(t)$, it is necessary to investigate the roots of the characteristic equation (185). It has been proved in [63] that (185) lacks real roots and possesses for each fixed magnitude of t_j ($j = 1, ..., n$) only two complex conjugate roots $p_{1,2} = r^{i\psi} = -\delta \pm i\omega$. For example, in the case of $n = 2$, the character of the root locus behavior as function of $Z_1(t_1) = (rt_1)^\gamma$ at fixed magnitudes of $Z_2(t_1) = (rt_2)^\gamma$ is shown in Figs. 9 for $\xi = 1 - (m_1 + m_2) = 1/9$ at $m_1 = m_2 = 4/9$. The values of the fractional parameter γ are indicated by digits near the corresponding curves. In all Figs. 9 a-f only one from each pair of complex conjugate roots is shown in the upper quadrant of the negative half-plane of the complex plane.

Knowing the behavior of the characteristic equation roots, the function $x^{\text{vibr}}(t)$ could be represented as

$$x^{\text{vibr}}(t) = Ae^{-\delta t} \cos(\omega t + \varphi), \tag{187}$$

where

$$A = \frac{2F}{\sqrt{[\Re f'(re^{i\psi})]^2 + [\Im f'(re^{i\psi})]^2}}, \quad \tan \varphi = \frac{\Im f'(re^{i\psi})}{\Re f'(re^{i\psi})},$$

$$\frac{f(p)}{dp} = f'(p) = 2p + \omega_\infty^2 \sum_{j=1}^{n} m_j [1 + (pt_j)^\gamma]^{-2} \gamma p^{\gamma-1},$$

$$\Re f'(re^{i\psi}) = 2r \cos \psi + \omega_\infty^2 \sum_{j=1}^{n} m_j t_j^\gamma \gamma r^{\gamma-1} \bar{R}_j^{-2} \cos \left[2\bar{\Phi}_j + (1 - \gamma)\psi \right],$$

a) $Z_2=0$
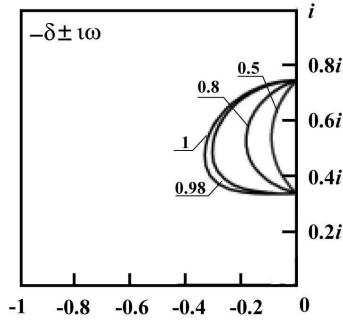
b) $Z_2=0.2$
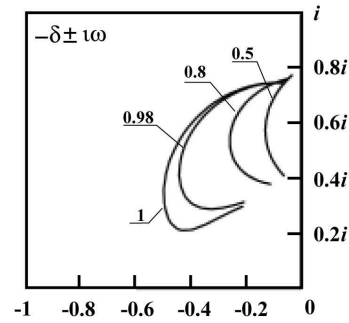
c) $Z_2=0.5$
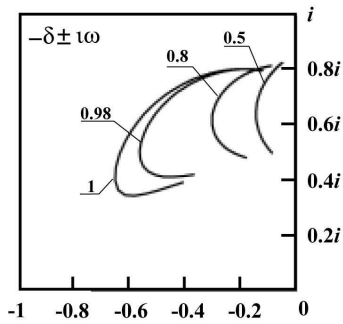
d) $Z_2=0.9$
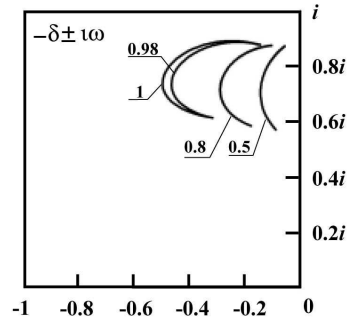
e) $Z_2=3$
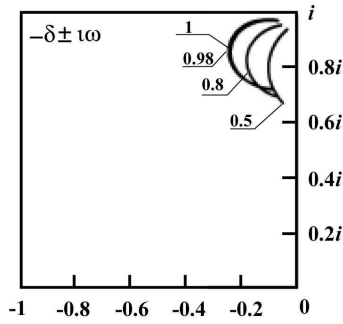
f) $Z_2=100$
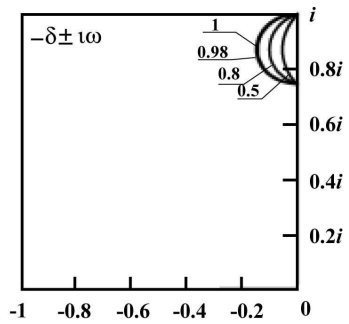
Figure 9. Behavior of the complex conjugate roots $p_{1,2} = -\delta \pm i\omega$ for an oscillator based on the fractional calculus model with the generalized Rabotnov relaxation kernel for $\xi = 1/9$ at $m_1 = m_2 = 4/9$ and $\omega_\infty^2 = 1$.

$$\Im f'\left(re^{i\psi}\right) = 2r\sin\psi - \omega_\infty^2 \sum_{j=1}^{n} m_j t_j^\gamma \gamma r^{\gamma-1} \bar{R}_j^{-2} \sin\left[2\bar{\Phi}_j + (1-\gamma)\psi\right],$$

$$\bar{R}_j = \sqrt{1 + 2(rt_j)^\gamma \cos\gamma\psi + (rt_j)^{2\gamma}}, \quad \tan\bar{\Phi}_j = \frac{(rt_j)^\gamma \sin\gamma\psi}{1 + (rt_j)^\gamma \cos\gamma\psi}.$$

Reference to Figs. 9 shows that under the presence of two relaxation times the curves on the complex plane, which characterize the relaxation time dependence of two complex conjugate roots of the characteristic equation, at the fixed magnitude of t_2 $(0 < t_2 < \infty)$ are detached from the imaginary axis, so that even for the magnitudes $t_1 = 0$ $(Z_1 = 0)$ or $t_1 = \infty$ $(Z_1 = \infty)$ the vibratory process remains dissipative one. In other words, if one of the relaxation mechanisms ceases to work or works under a degenerate regime, then the other mechanism begins to dominate.

However, when $t_2 = 0$ $(Z_2 = 0)$ and $t_2 = \infty$ $(Z_2 = \infty)$, the curves are attached to the imaginary axis at their initial and terminal points (see the cases (a) and (f) in Fig. 9), since in these cases the limiting values of the characteristic equation roots have the following form: when $t_2 = 0$ $(Z_2 = 0)$

$$\text{at } t_1 \to 0 \ (Z_1 \to 0): \quad r_0^2 = \omega_\infty^2(1 - m_1 - m_2), \quad \psi_0 = \pm\frac{\pi}{2},$$

$$\text{at } t_1 \to \infty \ (Z_1 \to \infty): \quad r_\infty^2 = \omega_\infty^2(1 - m_2), \quad \psi_\infty = \pm\frac{\pi}{2},$$

while $t_2 = \infty$ $(Z_2 = \infty)$

$$\text{at } t_1 \to 0 \ (Z_1 \to 0): \quad r_0^2 = \omega_\infty^2(1 - m_1), \quad \psi_0 = \pm\frac{\pi}{2},$$

$$\text{at } t_1 \to \infty \ (Z_1 \to \infty): \quad r_\infty^2 = \omega_\infty^2, \quad \psi_\infty = \pm\frac{\pi}{2}.$$

Thus, if both relaxation processes go on very quickly or very slowly, then the given hereditary elastic model behaves itself as the elastic one.

In a particular case, when $\omega_0 = 0$ or $\sum_{j=1}^{n} m_j = 1$, the curves in the complex plane issue from zero, (what is characteristic of the Maxwell-like model) at the angles $\psi = \pm\frac{\pi}{2-\delta}$, when all $Z_j \to 0$, and arrive at the points $\pm i\omega_\infty$, when all $Z_j \to \infty$. For the case of $n = 2$, this is evident in Figs. 10a and 10f, respectively.

Note that the procedure proposed for the construction and the analysis of the characteristic equation roots' locus can be utilized for an arbitrary number n of terms in the governing equation (183), though it was demonstrated for $n = 2$ in the examples provided above, while the example of retaining three terms in (185) can be found in [68].

7. Stationary Shock Waves in Viscoelastic Media with the Rabotnov Operator

For constructing the evolutionary equations describing the behavior of nonlinear waves in one-dimensional media three methods of simplification - the iterative, the spectral and the asymptotic - are used [18, 31, 44]. The ray method [52] which allows one to derive evolutionary equations both for weak and strong (shock) waves is found to be the most
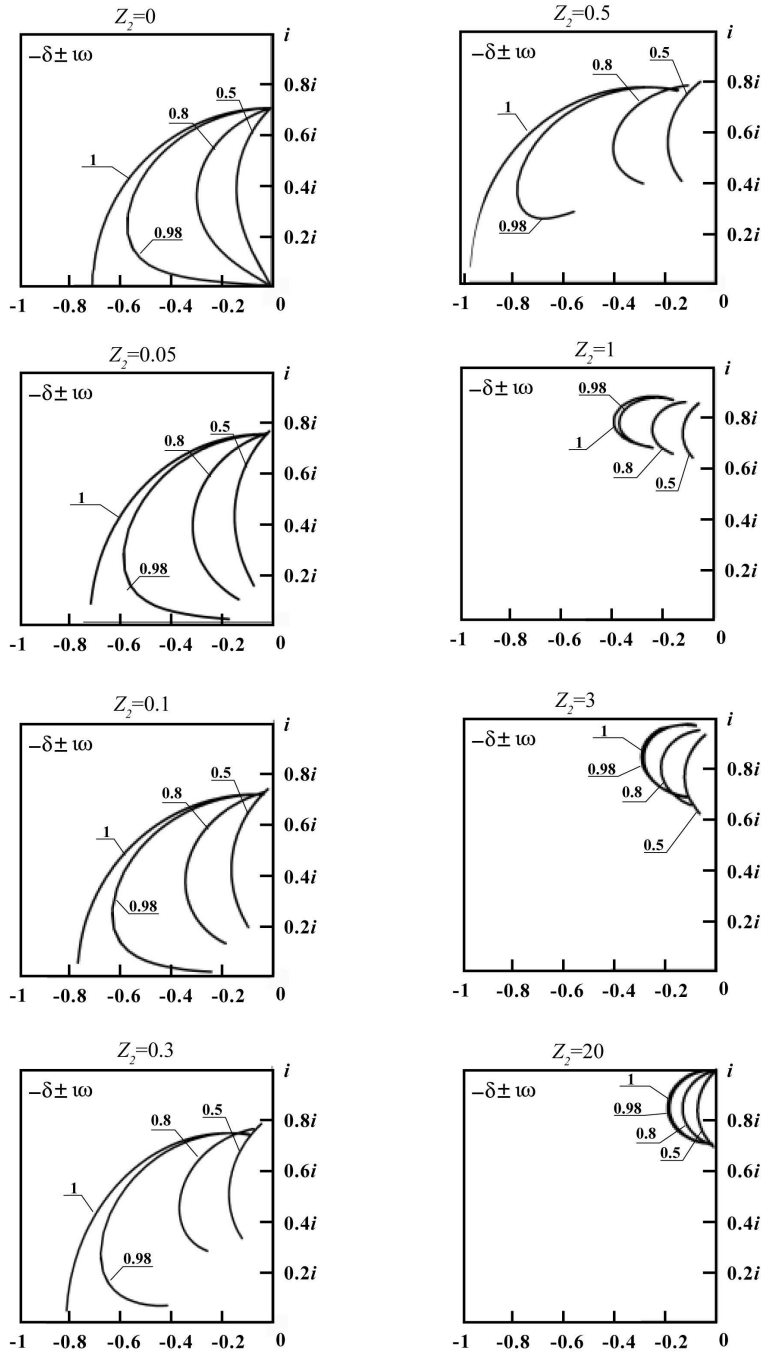
Figure 10. Behavior of the complex conjugate roots $p_{1,2} = -\delta \pm i\omega$ for an oscillator based on the fractional calculus model with the generalized Rabotnov relaxation kernel for $\xi = 0$ at $\omega_\infty^2 = 1$.

efficient among the asymptotic methods. However, in some nonlinear media, shock waves do not propagate in the form of strong discontinuity surfaces but exist only in the form of a shock layer of finite thickness. Among such media are, as an example, linear and nonlinear hereditary elastic media with weakly singular kernels of heredity [10, 24]. It turns out that for such media the application of the ray method within the shock layer allows one to obtain simplified equations describing evolution of shock waves of finite thickness, which admit the solution in the form of a stationary shock wave.

Let us consider, following [53], a nonlinear hereditarily elastic half-space. Equations describing the motion of such a half-space in Eulerian description in the rectangular Cartesian coordinate system x_1, x_2, x_3 have the form

$$\sigma = k\frac{\partial u}{\partial x} + \alpha\left(\frac{\partial u}{\partial x}\right)^2 - \gamma\int_0^t K(t-t')\frac{\partial u}{\partial x}(t')dt', \tag{188}$$

$$\frac{\partial \sigma}{\partial x} = \rho_0\left(\frac{\partial^2 u}{\partial t^2} + 2\frac{\partial u}{\partial x}\frac{\partial u^2}{\partial t\partial x}\right), \tag{189}$$

where $\sigma = \sigma_{11}$ is the stress, $u = u_1$ is the nonzero component of the displacement vector, $k = \lambda + 2\mu$, λ and μ are the equilibrium Lame constants, $\alpha = 3(l + m + n) - 7k/2$, l, m and n are the third-order elastic moduli, t is the time, $x = x_1$ is the coordinate measured along the normal to the boundary $x = 0$ of the hereditarily elastic half-space $x > 0$, $K(t)$ is the kernel of heredity, ρ_0 is the density, and γ is a small parameter taking into consideration the effect of viscosity.

Let beginning from the moment $t = 0$ the boundary $x = 0$ of the half-space $x > 0$ is loaded so that its initial velocity and acceleration are equal to v_0 and a_0, respectively.

As it has been shown in [10, 51], impact loading of the hereditarily elastic half-space boundary gives rise to the shock wave in the half-space, i.e., the geometric surface on which stresses and strains have a discontinuity, in so doing the shock wave velocity is as follows

$$G = c(1 + b\kappa_1), \qquad \kappa_1 = v_0\left\{1 - (a_0b + \beta)t\right\}, \tag{190}$$

where $\kappa_1 = \left[\frac{\partial u}{\partial t}\right] = \left(\frac{\partial u}{\partial t}\right)^+ - \left(\frac{\partial u}{\partial t}\right)^-$ is the discontinuity of the value $\frac{\partial u}{\partial t}$, $c^2 = k\rho_0^{-1}$, $b = (\alpha - k)k^{-1}(2c)^{-1}$, the signs " + " and " − " denote that the value $\frac{\partial u}{\partial t}$ is calculated immediately ahead of and behind the wave front, respectively, and $\beta = K(0)(2k)^{-1}$.

Reference to Eq. (190) shows that at $\beta \leq -ba_0$ $(b < 0)$ the value κ_1 increases with time, but when $\beta > -ba_0$, the value κ_1 is damped out to zero in the finite time lapse between 0 and t^*, where $t^* = (\beta + ba_0)^{-1}$. If the kernel of heredity possesses weak singularity, i.e., $\beta \to \infty$ [48], then damping of the discontinuity κ_1 takes place in an infinitely short time interval, and in that case $G = c$.

Thus, in the nonlinear hereditarily elastic media with weakly singular kernels of heredity, the shock waves cannot propagate in the form of geometrical surfaces of strong discontinuity.

Suppose that in such a medium the shock layer of thickness h propagates with the velocity $G = c$, in so doing within the layer the functions σ, $\frac{\partial u}{\partial x}$ and $\frac{\partial u}{\partial t}$ change monotonically and uninterruptedly from the magnitudes σ^+, $\left(\frac{\partial u}{\partial x}\right)^+$ and $\left(\frac{\partial u}{\partial t}\right)^+$ to the magnitudes σ^-, $\left(\frac{\partial u}{\partial x}\right)^-$ and $\left(\frac{\partial u}{\partial t}\right)^-$.

To construct the solution within the shock layer, let us eliminate the stress σ from Eqs. (188) and (189). As a result, we obtain

$$\frac{\partial^2 u}{\partial x^2} + 2\kappa \frac{\partial u}{\partial x} \frac{\partial^2 u}{\partial x^2} - \gamma_0 \frac{\partial^2 \Phi}{\partial x^2} = c^{-2} \left(\frac{\partial^2 u}{\partial t^2} + 2 \frac{\partial u}{\partial t} \frac{\partial^2 u}{\partial t \partial x} \right), \qquad (191)$$

where $\gamma_0 = \gamma k^{-1}$, $\Phi = \int_0^t K(t - t')u(t')dt'$, $K(0) = \infty$, and $\kappa = \alpha k^{-1}$.

Using the conditions of compatibility which link derivatives in the two coordinate systems: the stationary coordinate system and the moving coordinate system traveling together with the layer

$$\frac{\partial u}{\partial t} = -c \frac{\partial u}{\partial n} + \frac{\delta u}{\delta t}, \qquad \frac{\partial u}{\partial x} = \frac{\partial u}{\partial n}, \qquad \frac{\partial^2 u}{\partial x^2} = \frac{\partial^2 u}{\partial n^2},$$

$$\frac{\partial^2 u}{\partial x \partial t} = -c \frac{\partial^2 u}{\partial n^2} + \frac{\delta}{\delta t} \left(\frac{\partial u}{\partial n} \right), \qquad \frac{\partial^2 u}{\partial t^2} = c^2 \frac{\partial^2 u}{\partial n^2} - 2c \frac{\delta}{\delta t} \left(\frac{\partial u}{\partial n} \right) + \frac{\delta^2 u}{\delta t^2}, \qquad (192)$$

where $\partial/\partial n$ is the derivative with respect to the normal to the wave layer, and $\delta/\delta t$ is the Thomas δ-derivative [81], from Eq. (191) we obtain

$$\frac{\partial^2 u}{\partial n^2} + 2\kappa \frac{\partial u}{\partial n} \frac{\partial^2 u}{\partial n^2} - \gamma_0 \frac{\partial^2 \Phi}{\partial n^2} = c^{-2} \left\{ c^2 \frac{\partial^2 u}{\partial n^2} - 2c \frac{\delta}{\delta t} \left(\frac{\partial u}{\partial n} \right) + \frac{\delta^2 u}{\delta t^2} \right.$$

$$\left. + 2 \left(-c \frac{\partial u}{\partial n} + \frac{\delta u}{\delta t} \right) \left(-c \frac{\partial^2 u}{\partial n^2} + \frac{\delta}{\delta t} \frac{\partial u}{\partial n} \right) \right\}. \qquad (193)$$

Let us reduce Eq. (193) to the dimensionless form introducing the following dimensionless values: $w = v_0^{-2} a_0 u$, $\theta = v_0^{-1} a_0 t$, $z = v_0^{-3/2} c^{-1/2} a_0 n$, and $\epsilon = v_0^{1/2} c^{-1/2}$. As a result, we have

$$2\kappa\epsilon \frac{\partial w}{\partial z} \frac{\partial^2 w}{\partial z^2} - \nu \frac{\partial^2 \Phi^*}{\partial z^2} = -2\epsilon \frac{\delta}{\delta\theta} \left(\frac{\partial w}{\partial z} \right) + \epsilon^2 \frac{\delta^2 w}{\delta\theta^2} + 2\epsilon \frac{\partial w}{\partial z} \frac{\partial^2 w}{\partial z^2}$$

$$-2\epsilon^2 \frac{\partial w}{\partial z} \frac{\delta}{\delta\theta} \left(\frac{\partial w}{\partial z} \right) - 2\epsilon^2 \frac{\delta w}{\delta\theta} \frac{\partial^2 w}{\partial z^2} + 2\epsilon^3 \frac{\delta w}{\delta\theta} \frac{\delta}{\delta\theta} \left(\frac{\partial w}{\partial z} \right), \qquad (194)$$

where $\Phi^* = \int_0^\theta K(\theta - \theta')w(\theta')d\theta'$, $\nu = \gamma_0 \tau$, and $\tau = v_0 a_0^{-1}$.

Considering that ϵ is a small value, we seek the solution of Eq. (194) in the form

$$w = w_0 + \epsilon w_1 + \epsilon^2 w_2 + \dots. \qquad (195)$$

Substituting (195) into Eq. (194) and limiting ourselves by the zeroth term of the series (195) yields

$$(\kappa - 1)\frac{\partial w_0}{\partial z} \frac{\partial^2 w_0}{\partial z^2} + \frac{\delta}{\delta\theta} \left(\frac{\partial w_0}{\partial z} \right) = \nu^* \frac{\partial^2}{\partial z^2} \int_0^\theta K(\theta - \theta')w_0(\theta')d\theta', \qquad (196)$$

where $\nu^* = \nu(2\epsilon)^{-1}$.

Carrying out the change of the variable $v = (\kappa - 1)\partial w_0/\partial z$ in Eq. (196) yields

$$v\frac{\partial v}{\partial z} + \frac{\delta v}{\delta \theta} = \nu^* \frac{\partial}{\partial z}\int_0^\theta K(\theta - \theta')v(\theta')d\theta'. \tag{197}$$

Equation (197) describes variations in the value v within the shock layer which moves with the constant speed c. It could be rewritten in the form

$$\frac{1}{2}\frac{\partial v^2}{\partial z} + \frac{\delta v}{\delta \theta} = \nu^* \frac{\partial}{\partial z}\int_0^\theta K(\theta - \theta')v(\theta')d\theta'. \tag{198}$$

Assuming that the function v depends only on the variable $\eta = \theta - zG^{-1}$, and introducing the change of variables $v = 2\Phi(\eta)$, we are led to the equation for determining the structural shock wave

$$-\frac{\partial \Phi^2}{\partial \eta} + G\frac{\partial \Phi}{\partial \eta} = -\nu^* \frac{\partial}{\partial \eta}\int_0^\eta K(\eta - \eta')\Phi(\eta')d\eta', \tag{199}$$

where G is a constant.

Integrating Eq. (199) yields

$$\Phi^2(\eta) = G\left[\Phi(\eta) + e_1 \int_0^\eta K(\eta - \eta')\Phi(\eta')d\eta'\right], \tag{200}$$

where $e_1 = \nu^* G^{-1}$.

At $\eta = 0$, we have

$$\Phi_0^2 = G\Phi_0,$$

whence it follows that

$$\Phi_0 = 0 \quad \text{or} \quad \Phi_0 = G, \tag{201}$$

where $\Phi_0 = \Phi(0)$.

From two values of $\Phi_0 = \Phi(0)$ governed by (201) $\Phi_0 = 0$ should be chosen, since discontinuities could not propagate in hereditarily elastic media with a singular kernel of heredity [55].

In order to find the asymptotic magnitude of the desired function Φ at $\eta \to \infty$, we will consider Volterra operators K^* with a positive kernel $K(t)$, which not only obeys the condition of fading memory $K(\infty) = 0$, but also satisfies the condition of boundedness of the integral

$$\lim_{t \to \infty}(K^* \cdot 1) = \int_0^\infty K(t)dt = K_\infty. \tag{202}$$

We will name such integrals as bounded integrals.

Let us show that

$$\lim_{t \to \infty}\left(\ni_\gamma^*(\tau_i^\gamma) \cdot 1\right) = \int_0^\infty \ni_\gamma\left(-t/\tau_i\right)dt = 1. \tag{203}$$

Really, Laplace transformation of the product $\ni_\gamma^*(\tau_i^\gamma) \cdot 1$ has the form

$$\overline{\ni_\gamma^*(\tau_i^\gamma) \cdot 1} = \frac{\tau_i^{-\gamma}}{p(p^\gamma + \tau_i^{-\gamma})}. \tag{204}$$

Applying the limiting theorem of the Laplace transform

$$\lim_{p \to 0} p \left[\ni_\gamma^* (\tau_i^\gamma) \cdot 1 \right] = \lim_{t \to \infty} \left(\ni_\gamma^* (\tau_i^\gamma) \cdot 1 \right) = \lim_{p \to 0} \frac{\tau_i^{-\gamma}}{p + \tau_i^{-\gamma}} = 1, \qquad (205)$$

results in relationship (203).

Further we will introduce a class of functions G such that if the function $g(t) \in G$, then at any choice of the positive value ζ there exists such a number g_∞, and it is possible to indicate such a magnitude $t = t_*$ that at $t > t_*$ the inequality

$$|g(t) - g_\infty| < \zeta \qquad (206)$$

is valid.

Now we will prove the following two theorems stated by Rabotnov [48].

Theorem 1. Let two bounded operators L^* and M^* are specified, and their product $L^* \cdot M^*$ is defined, then at $t \to \infty$ the following limiting equality is fulfilled:

$$(L^* \cdot M^*) \cdot 1 = (L^* \cdot 1) (M^* \cdot 1) \quad (t \to \infty). \qquad (207)$$

To prove the theorem, let us represent the kernels of the operators L and M via Laplace integrals

$$L(t) = \int_0^\infty \bar{L}(p) e^{-pt} dp, \qquad M(t) = \int_0^\infty \bar{M}(q) e^{-qt} dq. \qquad (208)$$

Integrating (208) over t from the left and from the right, we obtain

$$L^* \cdot 1 = \int_0^\infty \frac{\bar{L}(p)}{p} \left(1 - e^{-pt} \right) dp, \qquad M^* \cdot 1 = \int_0^\infty \frac{\bar{M}(q)}{q} \left(1 - e^{-qt} \right) dq. \qquad (209)$$

Tending t to ∞ in formulas (209), we have

$$L^* \cdot 1 = \int_0^\infty \frac{\bar{L}(p)}{p} dp, \qquad M^* \cdot 1 = \int_0^\infty \frac{\bar{M}(q)}{q} dq. \qquad (210)$$

Now we could calculate the kernel of the product of operators $L^* \cdot M^*$, which, as a rule, has the form [48]:

$$N(t - \tau) = \int_\tau^{t'} L(t - s) \tau M(s - \tau) ds. \qquad (211)$$

Considering (208), formula (211) could be written as follows:

$$N(t - \tau) = \int_\tau^t \int_0^\infty \int_0^\infty \bar{L}(p) \bar{M}(q) e^{-p(t-s)} e^{-q(s-\tau)} dp \, dq \, ds. \qquad (212)$$

Changing the order of integration in (212), i.e., integrating first over t, we reduce (212) to the form

$$N(t - \tau) = \int_0^\infty \int_0^\infty \bar{L}(p) \bar{M}(q) \frac{1}{p - q} \left(e^{-q(t-\tau)} - e^{-p(t-\tau)} \right) dp \, dq. \qquad (213)$$

Putting $\tau = 0$ in (213) and integrating the obtained relationship in terms of t, we find

$$(L^* \cdot M^*) \cdot 1 = \int_0^t N(t)dt = \int_0^\infty \int_0^\infty \bar{L}(p)\bar{M}(q) \frac{1}{p-q} \left[\frac{1}{q}\left(1-e^{-qt}\right) - \frac{1}{p}\left(1-e^{-pt}\right) \right] dpdq. \tag{214}$$

Tending t to ∞ in (214) and considering (210), we obtain

$$\lim_{t\to\infty} (L^* \cdot M^*) \cdot 1 = \int_0^\infty \int_0^\infty \frac{\bar{L}(p)\bar{M}(q)}{pq}\,dpdq = \int_0^\infty \frac{\bar{L}(p)}{p}\,dp \int_0^\infty \frac{\bar{M}(q)}{q}\,dq$$

$$= \lim_{t\to\infty} (L^* \cdot 1) \cdot \lim_{t\to\infty} (M^* \cdot 1). \tag{215}$$

Relationship (215) coincides with (207) what proves the stated theorem.

Theorem 2. If operator K^* is bounded and $g(t) \in G$, then at $t \to \infty$ the following equality is fulfilled:

$$K^*g = K_\infty g_\infty. \tag{216}$$

To prove the theorem, we put

$$L^* = K^*, \qquad M(t) = g'(t). \tag{217}$$

Then the kernel of the operator $L^* \cdot M^*$, according to (211) and (217), takes the form

$$N(t-\tau) = \int_\tau^t K(t-s)g'(s-\tau)ds, \tag{218}$$

while relationship $(L^* \cdot M^*) \cdot 1$ with due account for (218) could be written as

$$(L^* \cdot M^*) \cdot 1 = \int_0^t N(t)dt = \int_0^t \int_0^t K(t-s)g'(s)dsdt. \tag{219}$$

Making the change

$$t - s = \tau, \quad s = t - \tau, \quad ds = -d\tau$$

in the double integral, we rewrite (219) as

$$(L^* \cdot M^*) \cdot 1 = \int_0^t \int_0^t K(\tau)g'(t-\tau)d\tau dt = \int_0^t K(\tau)\left[g(t-\tau) - g(-\tau)\right]d\tau$$

$$= \int_0^t K(\tau)g(t-\tau)d\tau - g(0)\int_0^t K(\tau)d\tau. \tag{220}$$

Since the function $g(t)$ for negative magnitudes of the argument was determined, then we have prolonged it in the negative domain putting $g(-t) = g(0)$.

Using Theorem 1 and considering that

$$L^* \cdot 1 = \int_0^t K(\tau)d\tau, \qquad M^* \cdot 1 = g(t) - g(0),$$

as well as relationship (220), we have

$$\lim_{t\to\infty}\left[\int_0^t K(t-\tau)g(\tau)d\tau - g(0)\int_0^t K(\tau)d\tau\right] = \lim_{t\to\infty}\left(g(t)-g(0)\right)\lim_{t\to\infty}\int_0^t K(\tau)d\tau,$$

whence it follows equality (216), hence Theorem 2 has been proved.

Using formula (216) and tending the value $\eta \to \infty$ in Eq. (200), we obtain

$$\Phi_\infty = G(1 + e_1 K_\infty), \tag{221}$$

where $\Phi_\infty = \Phi(\infty)$.

If as a relaxation kernel we use the fractional-exponential function, then $K_\infty = 1$, and formula (221) takes the form

$$\Phi_\infty = G(1 + e_1). \tag{222}$$

Thus, formulas (201) and (222) define the limiting locations of the stationary shock wave profile.

8. Application of Rabotnov's Operators in Problems of Impact Response of Thin Structures

The approach existing for studying the impact response of viscoelastic engineering structures is considered below in this Section by the example of the dynamic response of a viscoelastic Bernoulli-Euler beam, which Young's modulus is the time-dependent operator and the bulk modulus is considered to be constant, transversely impacted by an elastic sphere [67].

Following Timoshenko [80] who considered the problem on a transverse impact of an elastic sphere upon an elastic Bernoulli-Euler beam, let us formulate the problem on the transverse impact response of a viscoelastic beam, the viscoelastic features of which are described by a certain viscoelastic operator. In this case, the equations of motion of an elastic spherical impactor of radius R and the viscoelastic beam of length L have, respectively, the form

$$m\ddot{w}_2 = -P(t), \tag{223}$$

$$\widetilde{E}I\frac{\partial^4 w_1}{\partial x^4} + \varrho A\ddot{w}_1 = P(t)\delta\left(x - \frac{L}{2}\right), \tag{224}$$

where m is the mass of the sphere, w_2 is the displacement of the sphere, $P(t)$ is the contact force, $w_1(x,t)$ is the displacement of the beam at the contact point, $\widetilde{E}$ is a certain viscoelastic operator, I is the moment of inertia of the beam's cross section, A is the beam's cross sectional area, ϱ is its density, $\delta(x - \frac{L}{2})$ is the Dirac delta-function, x is the longitudinal coordinate, and an overdot denotes partial time-derivative.

Equations (223) and (224) are subjected to the following initial conditions:

$$w_1(x,0) = 0, \quad \dot{w}_1(x,0) = 0, \quad w_2(0) = 0, \quad \dot{w}_2(0) = V_0, \tag{225}$$

where V_0 is the initial velocity of the impactor at the moment of impact.

Integrating twice Eq. (223) yields

$$w_2(t) = -\frac{1}{m} \int_0^t P(t')(t - t')dt' + V_0 t. \tag{226}$$

Substituting the solution for a simply-supported Bernoulli-Euler beam

$$w_1(x, t) = \sum_{n=1}^{\infty} T_n(t) \sin\left(\frac{n\pi}{L} x\right) \tag{227}$$

in Eq. (224), and considering the orthogonality condition for the eigenfunctions $\sin\left(\frac{n\pi}{L} x\right)$ on the segment from 0 to L, we are led to the infinite set of uncoupled equations

$$\ddot{T}_n(t) + \Omega_n^2 \widetilde{E} T_n(t) = F_n P(t), \quad (n = 1, 2, ...) \tag{228}$$

each of which describes force driven vibrations of the viscoelastic oscillator, where

$$\Omega_n^2 = \frac{E_1 I}{\varrho A} \left(\frac{n\pi}{L}\right)^4, \quad F_n = \frac{2}{\varrho A L} \sin\frac{n\pi}{2},$$

and E_1 is the elastic modulus.

For those operators $\widetilde{E}$, which will be considered below, the Green function $G_n(t)$ for each oscillator from (228) has the form [67]

$$G_n(t) = A_{0n}(t) + A_n e^{-\alpha_n t} \sin(\omega_n t - \varphi_n), \tag{229}$$

where the index n indicates the ordinal number of the oscillator, and all values entering in (229) have the same structure and the same physical meaning as the corresponding values in Eq. (162) discussed in Sect. 6.

Thus, from (229) it is seen that the Green function possesses two terms, one of which, $A_{0n}(t)$, describes the drift of the equilibrium position and is represented by the integral involving the distribution function of dynamic and rheological parameters, while the other term is the product of two time-dependent functions, exponent and sine, and it describes damped vibrations around the drifting equilibrium position, where A_n is the amplitude, α_n is the damping coefficient, and ω_n and φ_n are the frequency and phase, respectively. The first term is governed by an improper integral taken along two sides of the cut along the negative real semi-axis of the complex plane (see Fig. 2), while the second term is determined for each n by two complex conjugate roots of the characteristic equation, which locate in the left half-plane of the complex plane.

Knowing the Green functions, the solution of Eq. (224) takes the form

$$w_1(x, t) = \sum_{n=1}^{\infty} \sin\left(\frac{n\pi}{L} x\right) \int_0^t G_n(t - t')P(t')dt'. \tag{230}$$

Let us introduce the value characterizing the relative approach of the sphere and beam, i.e., penetration of the beam by the sphere, is

$$y(t) = w_2(t) - w_1\left(\frac{L}{2}, t\right), \tag{231}$$

which is connected with the contact force by the Hertz law

$$P(t) = ky^{3/2}, \tag{232}$$

where

$$k = \frac{4}{3}\sqrt{R}E^* \tag{233}$$

is the operator involving the geometry of the impactor and the elastic features of the impactor and viscoelastic features of the target, which are described due to the Volterra correspondence principle by the operator E^*

$$\frac{1}{E^*} = J^* = \frac{1 - \nu_2^2}{E_2} + \frac{1 - \widetilde{\nu}_1^2}{\widetilde{E}_1}, \tag{234}$$

ν_2 and E_2 are constant Poisson's coefficient and Young's modulus, respectively, for the elastic sphere (impactor), while $\widetilde{\nu}_1$ and $\widetilde{E}_1$ are the operators for the viscoelastic beam (target).

Further in order to obtain the integro-differential equation for the values $y(t)$ and $P(t)$, it is necessary to assign the form of the operator $\widetilde{E}_1$.

Phillips and Calvit [45] were probably the first to investigate the response of a viscoelastic infinitely extended plate to impact of a rigid sphere. They used the Hertz's contact law in its hereditary form [45]. This problem is an immediate extension of Zener's approach [90] for the dynamic rigid spherical-indenter problem for the case of a thin elastic plate [61]. Assuming a falling body to be rigid, the function k (233) in the formula for the contact force in the Hertzian contact law (232) has been represented in [45] by the integral operator with a kernel of heredity based on the constant mechanical loss tangent model.

Ingman and Suzdalnitsky [29] considered dynamic response of a circular viscoelastic plate, viscoelastic features of which are described using the fractional derivative Kelvin-Voigt model, subjected to the impact of a falling elastic sphere following Timoshenko approach [80] but without considering viscoelastic features of the target in the Hertz's contact law. The authors of [29] referring to [92] wrote that

> "experimental investigations with a steel sphere and a circular composite barrier showed that Hertz's law is applicable not only in the case of static contact of elastic bodies, but also in problems of response of composite plates to a low-velocity impact,"

and made the conclusion that this argument could justify the choice of Eq. (232) with a constant stiffness coefficient k. However, firstly, the problems of viscoelasticity have not been considered in [92] (only targets made of elastic isotropic or anisotropic materials with and without account for plastic features in the contact region were utilized in this collective monograph), and secondly, Hunter [28] and Phillips and Calvit [45] showed that the local viscoelastic damping associated with deformation in the contact zone is essential at least on the first stage of active loading, since its ignorance in reducing plate impact data results in large error in the calculation of loss tangent and other characteristic values.

Following Rossikhin and Shitikova [67], we will use the governing equations of the viscoelastic material of the target in terms of Rabotnov's fractional exponential operators

(23) involving one term, i.e.,

$$\tilde{E} = E_\infty \left[1 - \nu_\varepsilon \ni^*_\gamma (\tau^\gamma_\varepsilon) \right], \tag{235}$$

utilizing the algebra of such operators presented in Sect 4.

Now we write Eq. (228) in terms of the Green function $G_n(t)$ using operator (235) as the operator $\tilde{E}$. As a result we obtain

$$\ddot{G}_n(t) + \Omega^2_{\infty n} \left[1 - \nu_\varepsilon \ni^*_\gamma (\tau^\gamma_\varepsilon) \right] G_n(t) = F_n \delta(t), \tag{236}$$

where $\Omega^2_{\infty n} = \frac{E_\infty I}{\varrho A} \left(\frac{n\pi}{L} \right)^4$.

Applying the Laplace transform to Eq. (236) yields

$$\bar{G}_n = \frac{F_n \left(\ae_n + p^\gamma \right)}{p^{2+\gamma} + \ae_n p^2 + \Omega^2_{\infty n} p^\gamma + \Omega^2_{0n} \ae_n}, \tag{237}$$

where $\ae_n = \tau^{-\gamma}_\varepsilon$, and $\Omega^2_{0n} = \frac{E_0 I}{\varrho A} \left(\frac{n\pi}{L} \right)^4$.

The solution of the characteristic equation

$$p^{2+\gamma} + \ae_n p^2 + \Omega^2_{\infty n} p^\gamma + \Omega^2_{0n} \ae_n = 0, \tag{238}$$

and the inversion of the expression (238) on the first sheet of the Riemannian surface via Mellin-Fourier inversion formula (150), results in the desired relationship (229), where the function $A_{0n}(t)$ is defined according to

$$A_{0n}(t) = \int_0^\infty \tau^{-1} B_n(\tau, \ae_n) e^{-t/\tau} d\tau, \tag{239}$$

with the following distribution of the relaxation-retardation parameters:

$$B_n(\tau, \ae_n) = \frac{\sin \gamma \pi}{\pi} \frac{\nu_\epsilon \Omega^2_{\infty n} F_n [\theta_{\infty n}(\tau)]^{-1} [\theta_{0n}(\tau)]^{-1} \tau^3}{\theta_{\infty n}(\tau) [\theta_{0n}(\tau)]^{-1} (\tau/\tau_\epsilon)^{-\gamma} + \theta_{0n}(\tau) [\theta_{\infty n}(\tau)]^{-1} (\tau/\tau_\epsilon)^\gamma + 2 \cos \pi \gamma}, \tag{240}$$

where

$$\theta_{\infty n}(\tau) = \tau^2 \Omega^2_{\infty n} + 1, \quad \theta_{0n}(\tau) = \tau^2 \Omega^2_{0n} + 1,$$

while the amplitude and phase of vibrations have, respectively, the following form:

$$A_n = 2F_n \left[(a_n^2 + b_n^2)^{-1} (\ae_n^2 + r_n^{2\gamma} + 2\ae_n r_n^\gamma \cos \gamma \psi_n) \right]^{1/2}, \tag{241}$$

$$\tan \varphi_n = -\frac{\ae_n \cos \beta_n + r_n^\gamma \cos(\beta_n - \gamma \psi_n)}{\ae_n \sin \beta_n + r_n^\gamma \sin(\beta_n - \gamma \psi_n)}, \quad \tan \beta_n = \frac{b_n}{a_n}, \tag{242}$$

where

$$a_n = (2 + \gamma) r_n^{1+\gamma} \cos(1 + \gamma) \psi_n + 2\ae_n r_n \cos \psi_n + \gamma \Omega^2_{\infty n} r_n^{\gamma-1} \cos(\gamma - 1) \psi_n,$$

$$b_n = (2 + \gamma) r_n^{1+\gamma} \sin(1 + \gamma) \psi_n + 2\ae_n r_n \sin \psi_n + \gamma \Omega^2_{\infty n} r_n^{\gamma-1} \sin(\gamma - 1) \psi_n,$$

$$r_n^2 = \omega_n^2 + \alpha_n^2, \quad \tan \psi_n = -\omega_n \alpha_n^{-1}.$$

If we omit the number n in (237)–(242), then all relationships will coincide with formulas (164) and (165) devoted to the vibrations of a viscoelastic oscillator based on Rabotnov relaxation operator with the root locus at $n = 1$ presented in Fig. 4.

Assuming that the bulk modulus is a constant value, i.e., relationship (51) is fulfilled, the operator E^{*-1} is determined according to formula (234) with due account for (80). Thus we are led to the following functional equation for determining the contact force $P(t)$:

$$
\left(\frac{3}{4\sqrt{R}}\right)^{2/3} \left[\left(\frac{1-\nu_2^2}{E_2} + \frac{1-\nu_\infty^2}{E_\infty}\right) P(t) + \frac{(1-2\nu_\infty)^2\nu_\varepsilon}{4E_\infty} \int_0^t \ni_\gamma \left(-\frac{t-t'}{\tau_\varepsilon}\right) P(t')dt' \right.
$$

$$
\left. + \frac{3\nu_\sigma}{4E_\infty} \int_0^t \ni_\gamma \left(-\frac{t-t'}{\tau_\sigma}\right) P(t')dt'\right]^{2/3} = -\frac{1}{m}\int_0^t P(t')(t-t')dt' + V_0 t
$$

$$
- \sum_{n=1}^{\infty} \sin\left(\frac{n\pi}{2}\right) \int_0^t G_n(t-t')P(t')dt'. \tag{243}
$$

9.   Conclusion

Decoding of different viscoelastic operators has been carried out, and in particular, of the operator of cylindrical rigidity and its reverse operator, in the case when the operator $\tilde{E}$ is given on the basis of the Rabotnov model, while the bulk operator $\tilde{K} = const$. It is also proposed how to decode different viscoelastic operators, and in particular, Poisson's operator $\tilde{\nu}$, if operators $\tilde{\mu}$ and $\tilde{K}$ are given by the Rabotnov model. It is shown that consideration for the bulk relaxation results in the appearance of the second peak in the frequency dependence of the tangent of mechanical loss angle.

It is shown that even if one proceeds from the simple Rabotnov model, then during calculation of such intricate operators as an operator of cylindrical rigidity, it is a need to utilize the generalized Rabotnov model, involving at least sums of two, and sometimes of three or more fractional operators with one and the same fractional parameter. It is proved that the Koeller model is physically admissible only when it is reduced to the generalized Rabotnov model.

Using fractional operators it is possible to describe not only damped vibrations of mechanical systems, but aperiodic motions of these systems as well.

It is shown that stationary shock waves with null discontinuities could propagate in nonlinear hereditary media with a weakly singular kernel of heredity.

Acknowledgments

References

[1] B.N.N. Achar, J.W. Hanneken, T. Clarke, "Response characteristics of a fractional oscillator," *Physica A*, vol. 309, pp. 275–288, 2002.

[2] B.N.N. Achar, J.W. Hanneken, T. Clarke, "Damping characteristics of a fractional oscillator," *Physica A*, vol. 339, pp. 311–319, 2004.

[3] B.N.N. Achar, J.W. Hanneken, T. Enck, T. Clarke, "Dynamics of the fractional oscillator," *Physica A*, vol. 297, pp. 361–367, 2001.

[4] R.L. Bagley, P.J. Torvik, "A generalized derivative model for an elastomer damper," *Shock and Vibration Bulletin*, vol. 49(2), pp. 135–143, 1979.

[5] R.L. Bagley, P.J. Torvik, "On the fractional calculus model of viscoelastic behavior," *Journal of Rheology*, vol. 30(1), pp. 133–155, 1986.

[6] M.A. Belov, A.E. Bogdanovich, "Numerical inversion of Laplace transform by the method of asymptotic extension of the interval in dynamic viscoelasticity problems," *Mechanics of Composite Materials* (Engl transl), vol. 12(5), pp. 762–768, 1976.

[7] H. Beyer, S. Kempfle, "Definition of physically consistent damping laws with fractional derivatives," *ZAMM*, vol. 75(8), pp. 623–635, 1995.

[8] G.W. Scott Blair, "Analytical and integrative aspects of the stress-strain-time problem," *Journal of Scientific Instruments*, vol. 21(5), pp. 80–84, 1944.

[9] P.W. Buchen, F. Mainardi, "Asymptotic expansions for transient viscoelastic waves," *Journal de Mecanique*, vol. 14(4), pp. 597–608, 1975.

[10] A.A. Burenin, Yu.A. Rossikhin, "The effect of viscosity on the character of the propagation of a plane longitudinal shock wave," *Journal of Applied Mechanics and Technical Physics* (Engl. transl.), vol. 31(6), pp. 807–810, 1990.

[11] M. Caputo, "Linear models of dissipation whose Q is almost frequency independent - II," *Geophysics Journal of the Royal Astronomy Society*, vol. 13(5), pp. 529–539, 1967.

[12] M. Caputo, "Vibrations of an infinite viscoelastic layer with a dissipative memory," *Journal of the Acoustical Society of America*, vol. 56(3), pp. 897–904, 1974.

[13] M. Caputo, "Vibrations of an infinite plate with a frequency independent Q," *Journal of Acoustical Society of America*, vol. 60(3), pp. 634–639, 1976.

[14] M. Caputo, F. Mainardi, "A new dissipation model based on memory mechanism," *Pure and Applied Geophysics*, Vol. 91(1), 134–147, 1971.

[15] M. Caputo, F. Mainardi, "Linear models of dissipation in inelastic solids," *La Rivista del Nuovo Cimento*, vol. 1(2), 161–198, 1971.

[16] F. Dal, "Multiple time scale solution of an equation with quadratic and cubic nonlinearities having fractional-order derivative," *Mathematical and Computational Applications*, vol. 16(1), pp. 301–308, 2011.

[17] D.D. Demir, N. Bildik, B.G. Sinir, "Linear vibrations of continuum with fractional derivatives," *Boundary Value Problems*, 2013:104, pp.1–15, 2013.

[18] J. Engelbrecht, *Nonlinear Wave Processes of Deformation in Solids*, Pitman, London, 1983.

[19] A. Gemant, "A method for analyzing experimental results obtained from elasto-viscous bodies," *Physics*, vol. 7, pp. 311–317, 1936.

[20] A.N. Gerasimov, "A generalization of linear laws of deformation and its application to the problems of internal friction" (in Russian), *Prikladnaya Matematika i Mekhanika*, vol. 12, pp. 251–260, 1948.

[21] B. Gross, "On creep and relaxation," *Journal of Applied Physics*, vol. 18(2), pp. 212–221, 1947.

[22] V.L. Gonsovkii, S.I. Meshkov, Yu.A. Rossikhin, "Impact of a viscoelastic rod onto a rigid target," *Soviet Applied Mechanics* (Engl. transl.), vol. 8(10), pp. 1109–1113, 1972.

[23] V.L. Gonsovskii, Yu.A. Rossikhin, "On the propagation of an impulsive load in a viscoelastic medium" (in Russian), in: *Proceedings of the Scientific-Research Institute of Mathematics of Voronezh University*, No. 6, pp. 63–66, 1972.

[24] V.L. Gonsovkii, Yu.A. Rossikhin, "Stress waves in a viscoelastic medium with a singular hereditary kernel," *Journal of Applied Mechanics and Technical Physics* (Engl. transl.), vol. 14(4), pp. 595–597, 1973.

[25] B. Hartmann, G.F. Lee, J.D. Lee, "Loss factor height and width limits for polymer relaxations," *Journal of the Acoustical Society of America*, vol. 95(1), pp. 226–233, 1994.

[26] S. Havriliak, S. Negami, "Analysis of α-dispersion in some polymer systems by the complex variables method," *Journal of Polymer Science (C)*, vol. 14, pp. 99–117, 1966.

[27] S. Havriliak, S. Negami, "On the equivalence of dielectric and mechanical dispersions in some polymers; e.g. poly(*n*-octyl methacrylate)', *Polymer*, vol. 10(10), pp. 859–872, 1966.

[28] S.C. Hunter, "The Hertz problem for a rigid spherical indenter and a viscoelastic half space," *Journal of Mechanics and Physics of Solids*, vol. 8, pp. 219–234, 1960.

[29] D. Ingman, J. Suzdalnitsky, "Response of viscoelastic plate to impact," *ASME Journal of Vibration and Acoustics*, vol. 130, pp. 011010-1–8, 2008.

[30] K. Iosida, *Functional Analysis*, 1967.

[31] A. Jeffrey, T. Kawahara, *Asymptotic Methods in Nonlinear Wave Theory*, Pitman, London, 1982.

[32] S. Kempfle, "Causality criteria for solutions of linear fractional differential equations," *Fractional Calculus Application and Analysis*, vol. 1(4), pp. 351–364, 1998.

[33] R.C. Koeller, "Applications of fractional calculus to the theory of viscoelasticity," *ASME Journal of Applied Mechanics*, vol. 51, pp. 299–307, 1984.

[34] R.C. Koeller, "Polynomial operators, Stieltjes convolution, and fractional calculus in hereditary mechanics," *Acta Mechanica*, vol. 58(3-4), pp. 251–264, 1986.

[35] M.A. Krasnosel'skii, P.P. Zabreiko, E.I. Pystul'nik, P.E. Sobolevskii, *Integral Operators in Spaces of Summing Functions* (in Russian), Moscow, Nauka, 1966.

[36] V.M. Mal'kov, "The viscoelasticity equations of an elastomer layer," *Journal of Applied Mathematics and Mechanics* (Engl. transl.), vol. 59(2), pp. 209–216, 1995.

[37] R.P. Meilanov, M.S. Yanpolov, "Features of the phase trajectory of a fractal oscillator," *Technical Physics Letters* (Engl transl), vol. 28(1), pp. 30–32, 2002.

[38] S.I. Meshkov, "Description of internal friction in the memory theory of elasticity using kernels with a weak singularity," *Journal of Applied Mechanics and Technical Physics* (Engl. transl.), vol. 8(4), pp. 100–102, 1967.

[39] S.I. Meshkov, G.N. Pachevskaya, "Allowance for bulk relaxation by the method of internal friction," *Journal of Applied Mechanics and Technical Physics* (Engl. transl.), vol. 8(2), pp. 47–48, 1967.

[40] S.I. Meshkov, G.N. Pachevskaya, V.S. Postnikov, Yu.A. Rossikhin, "Integral representation of $\ni_\gamma$-functions and their application to problems in linear viscoelasticity," *International Journal of Engineering Science*, vol. 9, pp. 387–398, 1971.

[41] S.I. Meshkov, G.N. Pachevskaya, Y.D. Shermergor, "Internal friction described with the aid of fractionally-exponential kernels," *Journal of Applied Mechanics and Technical Physics* (Engl. transl.), vol. 7(3), pp. 63–65, 1966.

[42] S.I. Meshkov, Yu.A. Rossikhin, "Propagation of acoustic waves in a hereditarily elastic medium," *Journal of Applied Mechanics and Technical Physics* (Engl. transl.), vol. 9(5), pp. 589–592, 1968.

[43] S.I. Meshkov, Yu.A. Rossikhin, "Temperature dependence of the damping coefficients for a dynamical system with a singular kernel," *Journal of Engineering Physics and Thermophysics* (Engl. transl.), vol. 21(2), pp. 1090, 1971.

[44] E. Pelinovski, V. Fridman, J. Engelbrecht, *Nonlinear Evolution Equations* (in Russian), Valgus, Tallinn, 1984.

[45] J.W. Phillips, H.H. Calvit, "Impact of a rigid sphere on a viscoelastic plate," *ASME Journal of Applied Mechanics*, vol. 34, pp. 873–878, 1967.

[46] Yu.N. Rabotnov, "Equilibrium of an elastic medium with after-effect" (in Russian), *Prikladnaya Matematika i Mekhanika*, vol. 12(1), pp. 53–62, 1948.

[47] Yu.N. Rabotnov, *Creep Problems in Structural Members*, (Engl. transl. by Transcripta Service LTD, London, F.A. Leckie, ed.), North-Holland Series in *Applied Mathematics and Mechanics*, **7**, North-Holland Publishing, Amsterdam-London. Originally published in Russian in 1966 as *Polzuchest' Elementov Konstruktsii*, Nauka, Moscow, 1969.

[48] Yu.N. Rabotnov, *Elements of Hereditary Solid Mechanics*, Nauka, Moscow (Engl. transl. by Mir Publishers, Moscow in 1980) 1977.

[49] A.R. Rhzanitsyn, *Some Problems of the Mechanics of Systems Deformable with Time* (in Russian), Gostekhizdat, Moscow, 1949.

[50] Yu.A. Rossikhin, "Reflections on two parallel ways in the progress of fractional calculus in mechanics of solids," *Applied Mechanics Reviews*, vol. 63(1), pp. 010701-1–12, 2010.

[51] Yu.A. Rossikhin, M.V. Shitikova, "On the structure of waves in a nonlinear elastic medium," *Facta Universitatis. Series "Mechanics, Automatic Control and Robotics"*, vol. 1(4), pp. 437–449, 1994.

[52] Yu.A. Rossikhin, M.V. Shitikova, "Ray method for solving dynamic problems connected with propagation of wave surfaces of strong and weak discontinuities," *Applied Mechanics Reviews*, vol. 48(1), pp. 1–39, 1995.

[53] Yu.A. Rossikhin, M.V. Shitikova, "Derivation of nonlinear evolutionary equations for a shock layer of finite thickness," in: *Nonlinear Acoustics in Perspective, Proc. 14th Int. Symp. on Nonlinear Acoustics* (R.J. Wei, Ed.), Nanjing University Press, Nanjing, pp. 270–274, 1996.

[54] Yu.A. Rossikhin, M.V. Shitikova, "Application of fractional derivatives for the analysis of nonlinear damped vibrations of suspension bridges," in: *Proc. 1997 Int. Symp. on Nonlinear Theory and its Applications*, vol. 1, pp. 541–544, Honolulu, USA, Nov 29 - Dec 2, 1997.

[55] Yu.A. Rossikhin, M.V. Shitikova, "Applications of fractional calculus to dynamic problems of linear and nonlinear hereditary mechanics of solids," *Applied Mechanics Reviews*, vol. 50(1), 15–67, 1997.

[56] Yu.A. Rossikhin, M.V. Shitikova, "Application of fractional operators to the analysis of damped vibrations of viscoelastic single-mass systems," *Journal of Sound and Vibration*, vol. 199(4), pp. 567–586, 1997.

[57] Yu.A. Rossikhin, M.V. Shitikova, "Application of fractional derivatives to the analysis of damped vibrations of viscoelastic single-mass systems," *Acta Mechanica*, vol. 120, pp. 109–125, 1997.

[58] Yu.A. Rossikhin, M.V. Shitikova, "Application of fractional calculus for analysis of nonlinear damped vibrations of suspension bridges," *ASCE Journal of Engineering Mechanics*, vol. 124 (9), pp. 1029–1036, 1998.

[59] Yu.A. Rossikhin, M.V. Shitikova, "Analysis of rheological equations involving more than one fractional parameters by the use of the simplest mechanical systems based on these equations," *Mechanics of Time-Dependent Materials*, Vol. 5, pp. 131–175, 2001.

[60] Yu.A. Rossikhin, M.V. Shitikova, "Analysis of the viscoelastic rod dynamics via models involving fractional derivatives or operators of two different orders," *The Shock and Vibration Digest*, vol. 36(1), pp. 3–26, 2004.

[61] Yu.A. Rossikhin, M.V. Shitikova, "Transient response of thin bodies subjected to impact: Wave approach," *Shock and Vibration Digest*, vol. 39, pp. 273–309, 2007.

[62] Yu.A. Rossikhin, M.V. Shitikova, "Comparative analysis of viscoelastic models involving fractional derivatives of different orders," *Fractional Calculus & Applied Analysis*, vol. 10, pp. 111–121, 2007.

[63] Yu.A. Rossikhin, M.V. Shitikova, "Free damped vibrations of a viscoelastic oscillator based on Rabotnov's model," *Mechanics of Time-Dependent Materials*, vol. 12, pp. 129–149, 2008.

[64] Yu.A. Rossikhin, M.V. Shitikova, "Application of fractional calculus for dynamic problems of solid mechanics: Novel trends and recent results," *Applied Mechanics Reviews*, vol. 63(1), pp. 010801-1–52, 2010.

[65] Yu.A. Rossikhin, M.V. Shitikova, "Analysis of free vibrations of a viscoelastic oscillator via the models involving several fractional parameters and relaxation/retardation times," *Computes and Mathematics with Applications*, vol. 59, pp. 1727–1744, 2010.

[66] Yu.A. Rossikhin, M.V. Shitikova, "On fallacies in the decision between the Caputo and Riemann-Liouville fractional derivatives for the analysis of the dynamic response of a nonlinear viscoelastic oscillator," *Mechanics Research Communications*, vol. 45, pp. 22–27, 2012.

[67] Yu.A. Rossikhin, M.V. Shitikova, "Two approaches for studying the impact response of viscoelastic engineering systems: An overview," *Computes and Mathematics with Applications*, vol. 66, pp. 755–773, 2013.

[68] Yu.A. Rossikhin, M.V. Shitikova, T.A. Shcheglova, "Control of dynamic response of a fractional oscillator via rheological parameters variation," in: *Proceedings of the 4th European Conference of Structural Control* (A.K. Belyaev and D.A. Indeitsev, eds), St. Petersburg, Russia, Sept. 8-12, 2008, vol. 2, pp. 719–726, 2008.

[69] Yu.A. Rossikhin, M.V. Shitikova, T.A. Shcheglova, "Forced vibrations of a nonlinear oscillator with weak fractional damping," *Journal of Mechanics of Materials and Structures*, vol. 4(9), pp. 1619–1636, 2009.

[70] M.I. Rozovskii, S.E. Sinaiskii, "Vibrations of an oscillator with residual creep," *Journal of Applied Mathematics and Mechanics* (Engl. transl.), vol. 30(3), pp. 696–703, 1966.

[71] A.R. Rzhanitsyn, *Some Questions of Mechanics of Systems Deformable in Time* (in Russian), Moscow: Gostekhizdat, 1949.

[72] A.R. Rzhanitsyn, *Theory of Creep* (in Russian), Moscow: Stroiizdat, 1968.

[73] S. G. Samko, A. A. Kilbas and O. I. Marichev, *Fractional Integrals and Derivatives. Theory and Applications* (in Russian), Nauka i Tekhnika, Minsk 1988 (Engl. transl. by Gordon and Breach Science Publ.)

[74] M.F. Selivanov, Effective properties of a linear viscoelastic composite, *International Applied Mechanics*, vol. 45, pp. 1084–1091, 2009.

[75] M.F. Selivanov, Y.O. Chornoivan, Computational optimization of characteristics for composites of viscoelastic components, *Journal of Engineering Mathematics*, vol. 74, 91–100, 2012.

[76] D.T. Shermergor, "On the use of fractional differentiation operators for the description of elastic-aftereffect properties of materials," *Journal of Applied Mechanics and Technical Physics* (Engl. transl.), vol. 7(6), pp. 85–87, 1966.

[77] G.I. Slonimsky, "Laws of mechanical relaxation processes in polymers," *Journal of Polymer Science*, Part C vol. 16, pp. 1667–1672, 1967.

[78] W. Smit, H. de Vries, "Rheological models containing fractional derivatives," *Rheologica Acta*, vol. 9, pp. 525–534, 1970.

[79] A.A. Stanislavsky, "Fractional oscillator," *Physical Review E*, vol. 70, pp. 051103-1–6, 2004.

[80] S.P. Timoshenko, "Zur Frage nach der Wirkung eines Stosses auf einen Balken" (in German), *Zeitschrift für Mathematik und Physik*, vol. 62, pp. 198–209, 1913.

[81] T.Y. Thomas, *Plastic Flow and Fracture in Solids*, Academic Press, New York, 1961.

[82] A. Tofighi, "The intrinsic damping of the fractional oscillator," *Physica A*, vol. 329, pp. 29–34, 2003.

[83] P.J. Torvik, R.L. Bagley, "On the appearance of the fractional derivative in the behavior of real materials," *ASME Journal of Applied Mechanics*, vol. 51, pp. 294–298, 1984.

[84] P.J. Torvik, R.L. Bagley, "A different view of viscous damping," *Shock and Vibration Bulletin*, vol. 55(3), pp. 81–84, 1985.

[85] T. Usuki, "Dispersion curves of viscoelastic plane waves and Rayleigh surface wave in high frequency range with fractional derivatives," *Journal of Sound and Vibration*, vol. 332, pp. 4541–4559, 2013.

[86] S.Z. Vulfson, "Thermal stresses in concrete solid masses with due account for creep in concrete" (in Russian), *Izvestija Akademii Nauk SSSR Mekhanika i Mashinostroenie*, Issue 1, pp. 162–165, 1960.

[87] G.M. Zaslavsky, A.A. Stanislavsky, M. Edelman, "Chaotic and pseudochaotic attractors of perturbed fractional oscillator," *Chaos*, vol. 16, pp. 013102-1–6, 2006.

[88] V.M. Zelenev, S.I. Meshkov, Yu.A. Rossikhin, "Effect of the ∋-function singularity parameters on the damped vibrations of elastic systems with aftereffect," *Mechanics of Solids* (Engl. transl.), vol. 5(3), pp. 92-94, 1970.

[89] V.M. Zelenev, S.I. Meshkov, Yu. A. Rossikhin, "Damped vibrations of hereditary-elastic systems with weakly singular kernels," *Applied Mechanics and Technical Physics* (Engl. transl.), vol. 11(2), pp. 290–293, 1970.

[90] C. Zener, "The intrinsic inelasticity of large plates," *Physics Reviews*, vol. 59, pp. 669–673, 1941.

[91] C. Zener, *Elasticity and Anelasticity of Metals*, the University of Chicago Press, Chicago, 1948.

[92] J.A. Zukas, T. Nicholas, H.F. Swift, L.B. Greszczuk, D.R. Curran, *Impact Dynamics*, Wiley, New York, 1982.

[93] D.R. Bland, *The Theory of Linear Viscoelasticity*, International series of Monographs on *Pure and Applied Mathematics*, vol. 10, (I.N. Sneddon and S. Ulam, General Editors), Pergamon Press, Oxford, 1960.

Chapter 9

THEORY OF DIFFUSIVE STRESSES BASED ON THE FRACTIONAL ADVECTION-DIFFUSION EQUATION

Yuriy Povstenko[*]
Institute of Mathematics and Computer Science
Jan Długosz University in Częstochowa, Poland

Abstract

Conventional theory of diffusive stresses is based on the principles of the classical theory of diffusion, specifically on the classical Fick law, which relates the matter flux to the concentration gradient. In combination with the balance equation for mass, this law leads to the classical diffusion equation. We study time-nonlocal generalizations of the diffusive flux governed by the Fick law and of the advection flux associated with the velocity field. The nonlocal constitutive equations with the long-tail power memory kernel result in the time-fractional advection-diffusion equation. The nonlocal constitutive equations with the middle-tail memory kernel expressed in terms of the Mittag-Leffler function lead to the fractional advection-diffusion equation of the Cattaneo type. The theory of diffusive stresses based on the fractional advection-diffusion equation is formulated.

Keywords: Fractional calculus, advection-diffusion, diffusive stresses, Mittag-Leffler function

1. Introduction

The classical Fourier law constitutes the relation between the heat flux $\mathbf{q}$ and the temperature gradient

$$\mathbf{q} = -k \operatorname{grad} T. \tag{1}$$

In combination with a law of conservation of energy, equation (1) leads to the parabolic heat conduction equation

$$\frac{\partial T}{\partial t} = a_{\mathrm{T}} \Delta T \tag{2}$$

---

[*]E-mail address: j.povstenko@ajd.czest.pl

with a_T being the heat diffusivity coefficient.

From the mathematical point of view, the Fourier law in the theory of heat conduction corresponds to the Fick law in the theory of diffusion

$$\mathbf{j} = -a \operatorname{grad} c, \tag{3}$$

where $\mathbf{j}$ is the matter flux, c is the concentration. In combination with the balance equation for mass, equation (3) results in the classical diffusion equation:

$$\frac{\partial c}{\partial t} = a \, \Delta c \tag{4}$$

with a being the diffusivity coefficient.

The classical heat conduction and diffusion equations based on the Fourier and Fick laws, respectively, are quite acceptable for different physical situations. However, many theoretical and experimental studies testify that in media with complex internal structure the standard parabolic equations are no longer accurate enough. In nonclassical theories, the Fourier and Fick laws as well as the parabolic heat conduction and diffusion equations are replaced by more general equations. Some of these theories were formulated in terms of the theory of heat conduction, other in terms of diffusion. For an extensive bibliography on this subject and further discussion see Chandrasekharaiah (1986, 1998), Ignaczak and Ostoja-Starzewski (2010), Joseph and Preziosi (1989), Metzler and Klafter (2000, 2004), Zaslavsky (2002) and references therein.

Gurtin and Pipkin (1968) proposed the general time-nonlocal dependence between the heat flux vector and the temperature gradient. Nigmatullin (1984a, 1984b) considered the following general form of such an equation:

$$\mathbf{q}(t) = -k \int_0^t K(t - \tau) \operatorname{grad} T(\tau) \, \mathrm{d}\tau \tag{5}$$

resulting in the heat conduction equation with memory

$$\frac{\partial T}{\partial t} = a_T \int_0^t K(t - \tau) \, \Delta T(\tau) \, \mathrm{d}\tau. \tag{6}$$

Nigmatullin (1984a) and Green and Naghdi (1993) proposed the constitutive equation of heat conduction in the case of constant kernel (full memory with no memory decay)

$$\mathbf{q}(t) = -k \int_0^t \operatorname{grad} T(\tau) \mathrm{d}\tau. \tag{7}$$

The wave equation for temperature

$$\frac{\partial^2 T}{\partial t^2} = a_T \, \Delta T \tag{8}$$

obtained from Eq. (7) is a constituent part of thermoelasticity without energy dissipation developed by Green and Naghdi (1993).

Cattaneo (1948) introduced the generalized constitutive equation for the heat flux which can be rewritten in a non-local form with the "short-tail" exponential time-nonlocal kernel

$$\mathbf{q}\,(t) = -\frac{k}{\zeta} \int_0^t \exp\left(-\frac{t-\tau}{\zeta}\right) \operatorname{grad} T(\tau)\,\mathrm{d}\tau, \tag{9}$$

where ζ is a nonnegative constant. This equations leads to the telegraph equation for temperature

$$\frac{\partial T}{\partial t} + \zeta \frac{\partial^2 T}{\partial t^2} = a_\mathrm{T}\,\Delta T. \tag{10}$$

Based on this equation, Lord and Shulman (1967) proposed the generalized theory of thermoelasticity.

The time-nonlocal dependences between the heat flux vector and the temperature gradient with the "long-tail" power kernel (see Povstenko (2005, 2009a, 2013))

$$\mathbf{q}\,(t) = -\frac{k}{\Gamma\,(\alpha)} \frac{\partial}{\partial t} \int_0^t (t-\tau)^{\alpha-1} \operatorname{grad} T(\tau)\,\mathrm{d}\tau, \quad 0 < \alpha \le 1, \tag{11}$$

$$\mathbf{q}\,(t) = -\frac{k}{\Gamma\,(\alpha-1)} \int_0^t (t-\tau)^{\alpha-2} \operatorname{grad} T(\tau)\,\mathrm{d}\tau, \quad 1 < \alpha \le 2, \tag{12}$$

can be interpreted in terms of fractional calculus

$$\mathbf{q}\,(t) = -k\,D^{1-\alpha} \operatorname{grad} T(t), \qquad 0 < \alpha \le 1, \tag{13}$$

$$\mathbf{q}\,(t) = -k\,I^{\alpha-1} \operatorname{grad} T(t), \qquad 1 < \alpha \le 2, \tag{14}$$

and result in the time-fractional heat conduction equation

$$\frac{\partial^\alpha T}{\partial t^\alpha} = a_\mathrm{T}\,\Delta T, \qquad 0 < \alpha \le 2, \tag{15}$$

or in terms of diffusion

$$\frac{\partial^\alpha c}{\partial t^\alpha} = a\,\Delta c, \qquad 0 < \alpha \le 2, \tag{16}$$

with the particular cases corresponding to subdiffusion (weak diffusion) ($0 < \alpha < 1$); normal diffusion ($\alpha = 1$); superdiffusion (strong diffusion) ($1 < \alpha < 2$), and ballistic diffusion ($\alpha = 2$).

In Eqs. (13)–(15) $I^\alpha f(t)$, $D^\alpha f(t)$ and $\dfrac{\mathrm{d}^\alpha f(t)}{\mathrm{d}t^\alpha}$ are the Riemann-Liouville fractional integral, Riemann-Liouville fractional derivative and the Caputo fractional derivative, respectively (Kilbas et al. (2006), Podlubny (1999)):

$$I^\alpha f(t) = \frac{1}{\Gamma(\alpha)} \int_0^t (t-\tau)^{\alpha-1} f(\tau)\,\mathrm{d}\tau, \qquad \alpha > 0, \tag{17}$$

$$D^\alpha f(t) = \frac{\mathrm{d}^m}{\mathrm{d}t^m} \left[\frac{1}{\Gamma(m-\alpha)} \int_0^t (t-\tau)^{m-\alpha-1} f(\tau)\,\mathrm{d}\tau \right], \qquad m-1 < \alpha < m, \tag{18}$$

$$\frac{\mathrm{d}^\alpha f(t)}{\mathrm{d}t^\alpha} = \frac{1}{\Gamma(m-\alpha)} \int_0^t (t-\tau)^{m-\alpha-1} \frac{\mathrm{d}^m f(\tau)}{\mathrm{d}\tau^m}\,\mathrm{d}\tau, \qquad m-1 < \alpha < m. \tag{19}$$

The general fractional Cattaneo-type equations were considered by Povstenko (2012, 2013):

$$\mathbf{q}\,(t) = -\frac{k}{\zeta} \int_0^t (t-\tau)^{\beta-2} \, E_{\beta-\alpha,\,\beta-1} \left[-\frac{(t-\tau)^{\beta-\alpha}}{\zeta} \right] \operatorname{grad} T(\tau)\, d\tau, \qquad (20)$$

where $E_{\alpha,\beta}\,(z)$ is the two-parameter Mittag-Leffler function (see Kilbas et al. (2006), Podlubny (1999))

$$E_{\alpha,\beta}\,(z) = \sum_{n=0}^{\infty} \frac{z^n}{\Gamma\,(\alpha n + \beta)}, \quad \alpha > 0, \quad \beta > 0, \qquad (21)$$

being the generalization of the exponential function. The constitutive equation (20) leads to the fractional telegraph equation for temperature

$$\frac{\partial^\alpha T}{\partial t^\alpha} + \zeta \frac{\partial^\beta T}{\partial t^\beta} = a_{\scriptscriptstyle\mathrm{T}} \, \Delta\, T. \qquad (22)$$

Several particular casers of Eqs (20) and (22) corresponding to the different choise of α and β were analyzed by Povstenko (2011) (see also Compte and Metzler (1997)) and were used in construction of the corresponding theories of thermoelasticity (Yussef (2010), Sherief et al. (2010), Povstenko (2011)). Analysis of space-fractional generalizations of the Fourier law and the heat conduction equation as well as of the thermoelasticity theories based on these equations can be found in Povstenko (2009a, 2009b, 2012, 2013).

2. Time-fractional Advection-diffusion Equation

Consider the following constitutive equation for the matter flux (see, for example, Kaviany (1995)):

$$\mathbf{j} = -a \operatorname{grad} c + \mathbf{v}c, \qquad (23)$$

where $\mathbf{v}$ is the velocity vector.

In combination with the balance equation for mass we get

$$\frac{\partial c}{\partial t} = a\, \Delta c - \operatorname{div}(\mathbf{v}c) \qquad (24)$$

or

$$\frac{\partial c}{\partial t} = a\, \Delta c - (\operatorname{div} \mathbf{v})\, c - \mathbf{v} \cdot \operatorname{grad} c. \qquad (25)$$

Supposing $\mathbf{v} = \mathrm{const}$ (or $\operatorname{div} \mathbf{v} = 0$ for generality), we obtain the standard advection-diffusion equation

$$\frac{\partial c}{\partial t} = a\, \Delta c - \mathbf{v} \cdot \operatorname{grad} c \qquad (26)$$

which has several physical interpretations in terms of Brownian motion, diffusion or heat transport with external force or with additional velocity field, diffusion of charge in the electrical field on comb structure, transport processes in porous media, groundwater hydrology, etc. (Bird et al. (2002), Feller (1971), Kaviany (1995), Nield and Bejan (2006), Risken (1989), Scheidegger (1974), Van Kampen (1981)).

In the case of one spatial coordinate x, equation (26) has the following form

$$\frac{\partial c}{\partial t} = a\,\frac{\partial^2 c}{\partial x^2} - v\,\frac{\partial c}{\partial x}. \tag{27}$$

The constitutive equation (23) as well as the advection-diffusion equation (26) can be generalized like the Fick law (3) and the standard diffusion equation (4) similarly to equations considered in the previous section. We will restrict our consideration to the case $\mathbf{v} = $ const. For example, the constitutive equation

$$\mathbf{j}(t) = \int_0^t K\,(t-\tau)\,[-a\,\mathrm{grad}\,c(\tau) + \mathbf{v}c(\tau)]\,\mathrm{d}\tau \tag{28}$$

leads to the advection-diffusion equation with the general memory kernel:

$$\frac{\partial c}{\partial t} = \int_0^t K\,(t-\tau)\,[a\,\Delta c(\tau) - \mathbf{v}\cdot\mathrm{grad}\,c(\tau)]\,\mathrm{d}\tau. \tag{29}$$

Equations describing the ballistic advection-diffusion have the following form:

$$\mathbf{j}\,(t) = \int_0^t [-a\,\mathrm{grad}\,c(\tau) + \mathbf{v}c(\tau)]\,\mathrm{d}\tau\,, \tag{30}$$

and

$$\frac{\partial^2 c}{\partial t^2} = a\,\Delta c - \mathbf{v}\cdot\mathrm{grad}\,c. \tag{31}$$

The time-nonlocal constitutive equation with the "short-tail" exponential kernel

$$\mathbf{j}\,(t) = \frac{1}{\zeta}\int_0^t \exp\left(-\frac{t-\tau}{\zeta}\right)[-a\,\mathrm{grad}\,c(\tau) + \mathbf{v}c(\tau)]\,\mathrm{d}\tau \tag{32}$$

results in the telegraph advection-diffusion equation

$$\frac{\partial c}{\partial t} + \zeta\frac{\partial^2 c}{\partial t^2} = a\,\Delta c - \mathbf{v}\cdot\mathrm{grad}\,c. \tag{33}$$

The time-nonlocal constitutive equations for the matter flux with the "long-tail" power kernel

$$\mathbf{j}\,(t) = D^{1-\alpha}\,[-a\mathrm{grad}\,c(t) + \mathbf{v}c(t)]\,, \qquad 0 < \alpha \leq 1, \tag{34}$$

$$\mathbf{j}\,(t) = I^{\alpha-1}\,[-a\mathrm{grad}\,c(t) + \mathbf{v}c(t)]\,, \qquad 1 < \alpha \leq 2, \tag{35}$$

give the time-fractional advection-diffusion equation

$$\frac{\partial^\alpha c}{\partial t^\alpha} = a\,\Delta c - \mathbf{v}\cdot\mathrm{grad}\,c, \qquad 0 < \alpha \leq 2. \tag{36}$$

Time-fractional generalizations of the advection-diffusion equation were considered by many authors (Barkai (2001), Barkai et al. (2000), Huang and Cao (2013), Huang and Liu (2005), Jumarie (1992), Karatay and Bayramoglu (2012), Liu et al. (2003), Metzler et al. (1999), Zheng and Wei (2010)). In majority of the abovementioned papers, the

fractional generalizations of the one-dimensional equation (27) were considered. It should be noted that interesting results were also obtained for fractional reaction-diffusion systems (see Datsko and Gafiychuk (2012), Gafiychuk and Datsko (2010)).

Lastly, the constitutive equation

$$\mathbf{j}\,(t) = \frac{1}{\zeta} \int_0^t (t-\tau)^{\beta-2} \, E_{\beta-\alpha,\beta-1} \left[-\frac{(t-\tau)^{\beta-\alpha}}{\zeta} \right] [-a \operatorname{grad} c(\tau) + \mathbf{v} c(\tau)] \, \mathrm{d}\tau \quad (37)$$

produces the following fractional telegraph equation with the advection term:

$$\frac{\partial^\alpha c}{\partial t^\alpha} + \zeta \frac{\partial^\beta c}{\partial t^\beta} = a \, \Delta c - \mathbf{v} \cdot \operatorname{grad} c. \tag{38}$$

3.   Theory of Diffusive Stresses

The theory of diffusive strain and stress is governed by a system of partial differential equations consisting of the equations of elasticity with gradient of concentration taken into account. The problem can be treated as an uncoupled in the case when the influence of the time change of strain on the matter flux is neglected. The first theoretical investigation of diffusive stresses dates back to Podstrigach (1961, 1963, 1965). For additional references, further generalizations and discussion see Nowacki (1974), Nowacki and Olesiak (1991), Podstrigach and Povstenko (1985), among others.

Povstenko (2005) proposed the theory of thermoelasticity based on the time-fractional heat conduction equation. A comprehesive review of further generalizations of fractional thermoelasticity (fractional theory of diffusive stresses) can be found in Povstenko (2013).

The stressed-strained state of a solid is governed by the equilibrium equation in terms of displacements

$$\mu \Delta \mathbf{u} + (\lambda + \mu) \operatorname{grad} \operatorname{div} \mathbf{u} = \beta_c K \operatorname{grad} c, \tag{39}$$

the stress-strain-concentration relation

$$\boldsymbol{\sigma} = 2\mu \mathbf{e} + (\lambda \operatorname{tr} \mathbf{e} - \beta_c K c) \mathbf{I} \tag{40}$$

and the corresponding equation describing diffusion. In this paper we will use the time-fractional advection-diffusion equation

$$\frac{\partial^\alpha c}{\partial t^\alpha} = a \, \Delta c - \mathbf{v} \cdot \operatorname{grad} c. \tag{41}$$

Here $\mathbf{u}$ is the displacement vector, $\boldsymbol{\sigma}$ the stress tensor, $\mathbf{e}$ the linear strain tensor, λ and μ are Lamé constants, $K = \lambda + 2\mu/3$, β_c is the diffusion coefficient of volumetric expansion, $\mathbf{I}$ denotes the unit tensor.

As in the case of classical thermoelasticity or the standard theory of diffusive stresses we can use the representation of stresses in terms of the displacement potential Φ (Parkus (1959))

$$\boldsymbol{\sigma} = 2\mu \left(\nabla \nabla \Phi - \mathbf{I} \, \Delta \Phi \right), \tag{42}$$

where ∇ stands for the gradient operator. The displacement potential is determined from the equation

$$\Delta \Phi = mc, \qquad m = \frac{1+\nu}{1-\nu} \frac{\beta_c}{3} \tag{43}$$

with ν being the Poisson ratio.

3.1. The Time-fractional Advection-diffusion Equation in a Plane

Consider the time-fractional advection diffusion equation

$$\frac{\partial^\alpha c}{\partial t^\alpha} = a \left(\frac{\partial^2 c}{\partial x^2} + \frac{\partial^2 c}{\partial y^2} \right) - v \frac{\partial c}{\partial x} - v \frac{\partial c}{\partial y}, \quad -\infty < x < \infty, \ -\infty < y < \infty, \quad (44)$$

under initial condition

$$t = 0: \quad c = p_0 \, \delta(x) \, \delta(y). \tag{45}$$

Here $\delta(x)$ is the Dirac delta function. In (45) we have introduced the constant multiplier p_0 to obtain the nondimensional quantities displayed in Figures.

The zero conditions at infinity are also imposed:

$$\lim_{x \to \pm\infty} c(x, y, t) = 0, \qquad \lim_{y \to \pm\infty} c(x, y, t) = 0. \tag{46}$$

In this paper, we will use the integral transform technique. Recall that the Caputo fractional derivative for its Laplace transform rule requires the knowledge of the initial values of the function $f(t)$ and its integer derivatives of order $k = 1, 2, \ldots, m - 1$ (see Kilbas et al. (2006), Podlubny (1999)):

$$\mathcal{L} \left\{ \frac{\mathrm{d}^\alpha f(t)}{\mathrm{d}t^\alpha} \right\} = s^\alpha f^*(s) - \sum_{k=0}^{m-1} f^{(k)}(0^+) s^{\alpha - 1 - k}, \qquad m - 1 < \alpha < m, \tag{47}$$

where s is the transform variable, the asterisk denotes the Laplace transform.

The exponential Fourier transform

$$\mathcal{F}\{f(x)\} = \widetilde{f}(\xi) = \frac{1}{\sqrt{2\pi}} \int_{-\infty}^{\infty} f(x) \, \mathrm{e}^{ix\xi} \, \mathrm{d}x \tag{48}$$

is used in the domain $-\infty < x < \infty$ and has the inverse

$$\mathcal{F}^{-1}\left\{ \widetilde{f}(\xi) \right\} = f(x) = \frac{1}{\sqrt{2\pi}} \int_{-\infty}^{\infty} \widetilde{f}(\xi) \, \mathrm{e}^{-ix\xi} \, \mathrm{d}\xi . \tag{49}$$

The Fourier transform of the mth derivative of a function has the form

$$\mathcal{F}\left\{ \frac{\mathrm{d}^m f(x)}{\mathrm{d}x^m} \right\} = (-i\xi)^m \widetilde{f}(\xi). \tag{50}$$

Applying to Eq. (44) the Laplace transform with respect to time t and the double Fourier transform with rspect to the space coordinates x and y gives

$$\widetilde{c}^*(\xi, \eta, s) = \frac{p_0}{2\pi} \frac{s^{\alpha - 1}}{s^\alpha + a(\xi^2 + \eta^2) - iv(\xi + \eta)}. \tag{51}$$

or after inversion of transforms

$$c(x, y, t) = \frac{p_0}{4\pi^2} \int_{-\infty}^{\infty} \int_{-\infty}^{\infty} E_\alpha \left\{ - \left[a\left(\xi^2 + \eta^2 \right) - iv(\xi + \eta) \right] t^\alpha \right\} \mathrm{e}^{-ix\xi - iy\eta} \, \mathrm{d}\xi \, \mathrm{d}\eta, \tag{52}$$

where the following formula (Kilbas et al. (2006), Podlubny (1999))

$$\mathcal{L}^{-1}\left\{\frac{s^{\alpha-1}}{s^\alpha + b}\right\} = E_\alpha\left(-bt^\alpha\right) \tag{53}$$

has been used with $E_\alpha(z)$ being the Mittag-Leffler function in one parameter α

$$E_\alpha(z) = \sum_{k=0}^\infty \frac{z^k}{\Gamma(\alpha k + 1)}, \quad \alpha > 0, \; z \in C. \tag{54}$$

The substitution

$$\xi' = \xi - i\frac{v}{2a}, \quad \eta' = \eta - i\frac{v}{2a}$$

allows us to get

$$c(x,y,t) = \frac{p_0}{4\pi^2} \exp\left[\frac{v(x+y)}{2a}\right] \int_{-\infty}^\infty \int_{-\infty}^\infty E_\alpha\left\{-\left[a(\xi^2 + \eta^2) + \frac{v^2}{2a}\right]t^\alpha\right\}$$

$$\times \cos(x\xi)\,\cos(y\eta)\,\mathrm{d}\xi\,\mathrm{d}\eta, \tag{55}$$

where the primes have been omitted for brevity sake.

Next we introduce the polar coordinates in the (ξ, η)–plane:

$$\xi = \rho\cos\theta, \quad \eta = \rho\sin\theta,$$

thus obtaining:

$$c(x,y,t) = \frac{p_0}{4\pi^2} \exp\left[\frac{v(x+y)}{2a}\right] \int_0^\infty \int_0^{2\pi} E_\alpha\left[-\left(a\rho^2 + \frac{v^2}{2a}\right)t^\alpha\right]$$

$$\times \cos(x\rho\cos\theta)\,\cos(y\rho\sin\theta)\,\rho\,\mathrm{d}\rho\,\mathrm{d}\theta. \tag{56}$$

Due to periodic properties of the integrand

$$\int_0^{2\pi} \cos(x\rho\cos\theta)\,\cos(y\rho\sin\theta)\,\mathrm{d}\theta = 4\int_0^{\pi/2} \cos(x\rho\cos\theta)\,\cos(y\rho\sin\theta)\,\mathrm{d}\theta. \tag{57}$$

Changing variables $w = \sin\theta$ and taking into account the following integral (Prudnikov et al. (1981))

$$\int_0^1 \frac{\cos\left(p\sqrt{1-x^2}\right)}{\sqrt{1-x^2}}\,\cos(qx)\,\mathrm{d}x = \frac{\pi}{2} J_0\left(\sqrt{p^2 + q^2}\right), \tag{58}$$

where J_n is the Bessel function of the first kind of the order n, we get

$$c(x,y,t) = \frac{p_0}{2\pi} \exp\left[\frac{v(x+y)}{2a}\right] \int_0^\infty E_\alpha\left[-\left(a\rho^2 + \frac{v^2}{2a}\right)t^\alpha\right] J_0\left(\sqrt{x^2 + y^2}\,\rho\right)\rho\,\mathrm{d}\rho. \tag{59}$$
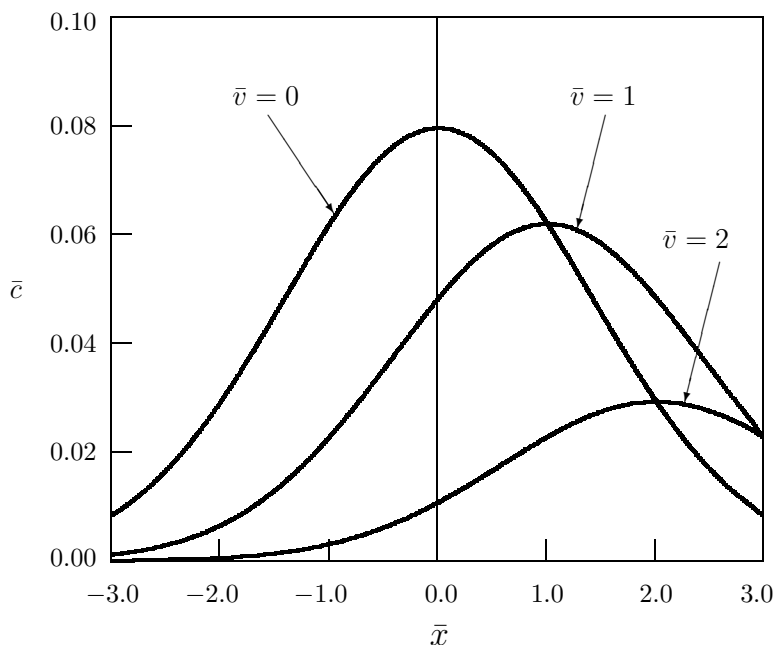
Figure 1. Dependence of the fundamental solution to the Cauchy problem on distance (the classical advection-diffusion equation, $\alpha = 1$).

Let us analyze several particular cases of the solution (59). In the case of standard advection-diffusion equation ($\alpha = 1$ and $E_1(-x) = \mathrm{e}^{-x}$), evaluating the integral (Prudnikov et al. (1983))

$$\int_0^\infty x\,\mathrm{e}^{-px^2} J_0(qx)\,\mathrm{d}x = \frac{1}{2p}\,\exp\left(-\frac{q^2}{4p}\right), \quad p > 0, \quad q > 0, \tag{60}$$

we arrive at

$$c(x, y, t) = \frac{p_0}{4\pi at}\,\exp\left[-\frac{(x - vt)^2 + (y - vt)^2}{4at}\right]. \tag{61}$$

In the case $\alpha = 1/2$ the Mittag-Leffler function can be represented as

$$E_{1/2}(-x) = \frac{2}{\sqrt{\pi}}\int_0^\infty \mathrm{e}^{-u^2 - 2xu}\mathrm{d}u \tag{62}$$

and the corresponding solution reads

$$c(x, y, t) = \frac{p_0}{4a\sqrt{t}\pi^{3/2}}\int_0^\infty \frac{1}{u}\,\mathrm{e}^{-u^2}\exp\left[-\frac{(x - 2v\sqrt{t}u)^2 + (y - 2v\sqrt{t}u)^2}{8a\sqrt{t}u}\right]\mathrm{d}u. \tag{63}$$

The results of numerical computations of concentration for $y = 0$ are presented in Fig. 1 for $\alpha = 1$ and in Fig. 2 for $\alpha = 0.5$. The following nondimensional quantities

$$\bar{c} = \frac{at^\alpha}{p_0}\,c, \qquad \bar{v} = \frac{t^{\alpha/2}}{\sqrt{a}}\,v, \qquad \bar{x} = \frac{x}{\sqrt{a}t^{\alpha/2}}, \qquad \bar{y} = \frac{y}{\sqrt{a}t^{\alpha/2}} \tag{64}$$

have been introduced.
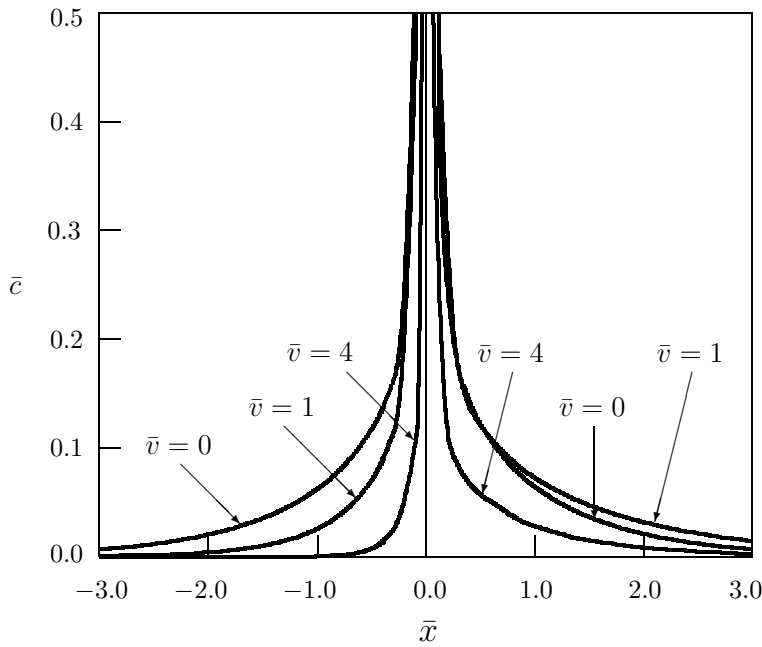
Figure 2. Dependence of the fundamental solution to the Cauchy problem on distance (the time-fractional advection-diffusion equation, $\alpha = 0.5$).

4. Diffusive Stresses

The double Fourier transform applied to Eq. (43) gives:

$$\widetilde{\widetilde{\Phi}} = -\frac{m}{\xi^2 + \eta^2} \widetilde{\widetilde{c}} \tag{65}$$

and after inverting the transforms

$$\Phi = -\frac{mp_0}{4\pi^2} \int_{-\infty}^{\infty} \int_{-\infty}^{\infty} E_\alpha \left\{ -\left[a\left(\xi^2 + \eta^2\right) - iv(\xi + \eta) \right] t^\alpha \right\} \frac{e^{-ix\xi - iy\eta}}{\xi^2 + \eta^2} \, d\xi \, d\eta. \tag{66}$$

The corresponding stress components are calculated according to (42) and have the following form:

$$\sigma_{xx} = -\frac{2\mu m p_0}{4\pi^2} \int_{-\infty}^{\infty} \int_{-\infty}^{\infty} E_\alpha \left\{ -\left[a\left(\xi^2 + \eta^2\right) - iv(\xi + \eta) \right] t^\alpha \right\} \frac{\eta^2 e^{-ix\xi - iy\eta}}{\xi^2 + \eta^2} \, d\xi \, d\eta, \tag{67}$$

$$\sigma_{yy} = -\frac{2\mu m p_0}{4\pi^2} \int_{-\infty}^{\infty} \int_{-\infty}^{\infty} E_\alpha \left\{ -\left[a\left(\xi^2 + \eta^2\right) - iv(\xi + \eta) \right] t^\alpha \right\} \frac{\xi^2 e^{-ix\xi - iy\eta}}{\xi^2 + \eta^2} \, d\xi \, d\eta, \tag{68}$$

$$\sigma_{xy} = \frac{2\mu m p_0}{4\pi^2} \int_{-\infty}^{\infty} \int_{-\infty}^{\infty} E_\alpha \left\{ -\left[a\left(\xi^2 + \eta^2\right) - iv(\xi + \eta) \right] t^\alpha \right\} \frac{\xi\eta e^{-ix\xi - iy\eta}}{\xi^2 + \eta^2} \, d\xi \, d\eta. \tag{69}$$
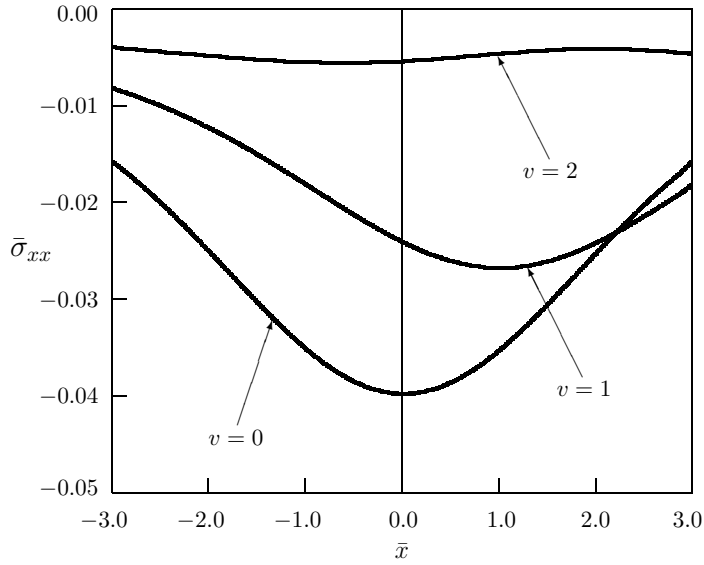
Figure 3. Dependence of the stress component σ_{xx} on distance ((the classical advection-diffusion equation, $\alpha = 1$).

In the particular case of diffusive stresses caused by the solution to the standard advection-diffusion equation ($\alpha = 1$) we obtain

$$
\begin{aligned}
\sigma_{xx} = {} & -\frac{\mu m p_0}{\pi} \Bigg\{ \frac{1}{2at} \frac{(y - vt)^2}{(x - vt)^2 + (y - vt)^2} \, \exp\left(-\frac{(x - vt)^2 + (y - vt)^2}{4at} \right) \\
& + \frac{(x - vt)^2 - (y - vt)^2}{[(x - vt)^2 + (y - vt)^2]^2} \left[1 - \exp\left(-\frac{(x - vt)^2 + (y - vt)^2}{4at} \right) \right] \Bigg\}.
\end{aligned}
\tag{70}
$$

$$
\begin{aligned}
\sigma_{xy} = {} & \frac{\mu m p_0}{\pi} \frac{(x - vt)(y - vt)}{(x - vt)^2 + (y - vt)^2} \Bigg\{ \frac{1}{2at} \, \exp\left(-\frac{(x - vt)^2 + (y - vt)^2}{4at} \right) \\
& - \frac{2}{(x - vt)^2 + (y - vt)^2} \left[1 - \exp\left(-\frac{(x - vt)^2 + (y - vt)^2}{4at} \right) \right] \Bigg\}.
\end{aligned}
\tag{71}
$$

$$
\sigma_{yy} = -2\mu m c - \sigma_{xx}.
\tag{72}
$$

To get the stress components (70)–(71) the polar coordinates in the (ξ, η)-plane have been inroduced and the following integrals (Prudnikov et al. (1981))

$$
\begin{aligned}
& \int_0^1 \sqrt{1 - x^2} \cos{(bx)} \, \cos\left(c\sqrt{1 - x^2} \right) \mathrm{d}x \\
& = \frac{\pi}{2} \left[\frac{c^2}{b^2 + c^2} \, J_0\left(\sqrt{b^2 + c^2} \right) + \frac{b^2 - c^2}{(b^2 + c^2)^{3/2}} \, J_1\left(\sqrt{b^2 + c^2} \right) \right]
\end{aligned}
\tag{73}
$$
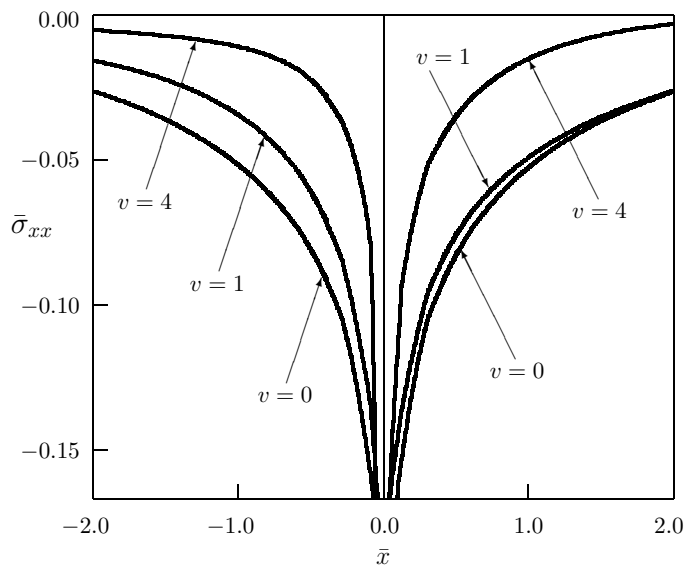
Figure 4. Dependence of the the stress component σ_{xx} on distance (the time-fractional advection-diffusion equation, $\alpha = 0.5$).

and Prudnikov et al. (1983)

$$\int_0^\infty \mathrm{e}^{-px^2} J_1(qx)\,\mathrm{d}x = \frac{1}{q}\left[1 - \exp\left(-\frac{q^2}{4p}\right)\right], \quad p > 0, \quad q > 0, \tag{74}$$

have been used.

Additionally,

$$\int_0^1 x \sin(bx) \sin\left(c\sqrt{1-x^2}\right)\mathrm{d}x$$
$$= \frac{\pi}{2}\frac{bc}{b^2+c^2}\left[-J_0\left(\sqrt{b^2+c^2}\right) + \frac{2}{\sqrt{b^2+c^2}}J_1\left(\sqrt{b^2+c^2}\right)\right]. \tag{75}$$

Another particular case $\alpha = 1/2$ results in the stress component

$$\sigma_{xx} = -\frac{2\mu m p_0}{\pi^{3/2}}\int_0^\infty \mathrm{e}^{-u^2}\left\langle \frac{\left(y-2v\sqrt{t}u\right)^2}{4a\sqrt{t}u\left[\left(x-2v\sqrt{t}u\right)^2 + \left(y-2v\sqrt{t}u\right)^2\right]} \right.$$

$$\times \exp\left[-\frac{\left(x-2v\sqrt{t}u\right)^2 + \left(y-2v\sqrt{t}u\right)^2}{8a\sqrt{t}u}\right]$$

$$+ \frac{\left(x-2v\sqrt{t}u\right)^2 - \left(y-2v\sqrt{t}u\right)^2}{\left[\left(x-2v\sqrt{t}u\right)^2 + \left(y-2v\sqrt{t}u\right)^2\right]^2}$$

$$\times \left.\left\{1 - \exp\left[-\frac{\left(x-2v\sqrt{t}u\right)^2 + \left(y-2v\sqrt{t}u\right)^2}{8a\sqrt{t}u}\right]\right\}\right\rangle. \tag{76}$$

Dependence of the nondimensional quantity

$$\bar{\sigma}_{xx} = \frac{at^\alpha}{2\mu m p_0}\, \sigma_{xx}$$

on the nondimensional coordinate $\bar{x}$ for $\bar{y} = 0$ is shown in Fig. 3 for $\alpha = 1$ and in Fig. 4 for $\alpha = 0.5$.

5.   Conclusion

We have analyzed the time-nonlocal generalizations of the constitutive equation for the matter flux resulting in fractional advection-diffusion equation. The theory of diffusive stresses associated with fractional advection-diffusion equation has been proposed. The fundamental solution to the Cauchy problem for such an equation has been considered in the case of two space variables, which has been solved using the integral transform technique. It should be emphasized that the fundamental solution to the Cauchy problem in the case $0 < \alpha < 1$ has the logarithmic singularity at the origin:

$$c(x, y, t) \sim -\frac{p_0}{2\pi\Gamma(1-\alpha)at^\alpha}\, \exp\left[\frac{v(x+y)}{2a}\right] \ln\left(\sqrt{1 + \frac{v^2 t^\alpha}{2a}\,\frac{\sqrt{x^2+y^2}}{\sqrt{a}t^{\alpha/2}}}\right). \quad (77)$$

This result is similar to the case of the time-fractional diffusion equation when $v = 0$ (see Povstenko (2005) and Schneider (1990)). Such a singularity disappears only for the classical advection diffusion equation ($\alpha = 1$). Due to singularity of the solution at the origin, in the case $0 < \alpha < 1$ drift caused by the quantity v is less noticeable than in the case $\alpha = 1$ (compare Figs. 1 and 2 and Figs. 3 and 4).

References

Barkai, E., (2001). Fractional Fokker-Planck equation, solution, and application. *Phys. Rev.* 63, 046118.

Barkai, E., Metzler, R., Klafter, J., (2000). From continuous time random walks to the fractional Fokker-Planck equation. *Phys. Rev. E* 61, 132-138.

Bird, R.B., Stewart, W.E., Lightfoot, E.N., (2002). *Transport Phenomena*, 2nd ed. John Wiley & Sons, Inc., New York.

Cattaneo, C., (1948). On the conduction of heat. *Atti Sem. Mat. Fis. Univ. Modena*, 3, 83-101.

Chandrasekharaiah, D.S., (1986). Thermoelasticity with second sound: a review. *Appl. Mech. Rev.* 39, 355-376.

Chandrasekharaiah, D.S., (1998). Hiperbolic thermoelasticity: a review of recent literature. *Appl. Mech. Rev.* 51, 705-729.

Compte, A., Metzler, R., (1997). The generalized Cattaneo equation for the description of anomalous transport processes. *J. Phys. A: Math.Gen.* 30, 7277-7289.

Datsko, B., Gafiychuk, V., (2012). Complex nonlinear dynamics in subdiffusive activator-inhibitor systems. *Commun. Nonlinear Sci. Numer. Simulat.* 17, 1673-1680.

Feller, W., (1971). *An Introduction to Probability Theory and Its Applications*, 2nd ed. John Wiley & Sons, New York.

Gafiychuk, V., Datsko, B., (2010). Mathematical modeling of different types of instabilities in time fractional reaction-diffusion systems. *Comput. Math. Appl*. 59, 1101-1107.

Green A.E., Naghdi, P.M., (1993), Thermoelasticity without energy dissipation. *J. Elast*. 31, 189-208.

Gurtin, M.E., Pipkin, A.C., (1968). A general theory of heat conduction with finite wave speeds. *Arch. Rational Mech. Anal*. 31, 113-126.

Huang, H., Cao, X., (2013). Numerical method for two dimensional fractional reaction subdiffusion equation. *Eur. Phys. J. Special Topics* 222, 1961-1973.

Huang, F., Liu, F., (2005). The time fractional diffusion equation and the advection-dispersion equation. *ANZIAM J.* 46, 317-330.

Ignaczak, J., Ostoja-Starzewski, M., (2010). *Thermoelasticity with Finite Wave Speeds*. Oxford University Press, Oxford.

Joseph, D.D., Preziosi, L., (1989). Heat waves. *Rev. Modern Phys.* 61, 41-73.

Jumarie, G., (1992). A Fokker-Planck equation of fractional order with respect to time. *J. Math. Phys.* 33, 3536-3542.

Karatay, I., Bayramoglu, S.R., (2012). An efficient scheme for time fractional advection dispersion equations. *Appl. Math. Sci.* 6, 4869-4878.

Kaviany, M., (1995). *Principles of Heat Transfer in Porous Media*, 2nd ed. Springer, New York.

Kilbas, A.A., Srivastava, H.M., Trujillo, J.J., (2006). *Theory and Applications of Fractional Differential Equations*. Elsevier, Amsterdam.

Liu, F., Anh, V., Turner, I., Zhuang, P., (2003). Time-fractional advection-dispersion equation. *J. Appl. Math. Comput.* 13, 233-245.

Lord, H.W., Shulman, Y., (1967). A generalized dynamical theory of thermoelasticity. *J. Mech. Phys. Solids* 15, 299-309.

Metzler, R., Klafter, J., (2000). The random walk's guide to anomalous diffusion: a fractional dynamics approach. *Phys. Rep.* 339, 1-77.

Metzler, R., Klafter, J., (2004). The restaurant at the end of the random walk: recent developments in the description of anomalous transport by fractional dynamics. *J. Phys. A: Math. Gen.* 37, R161-R208.

Metzler, R., Barkai, E., Klafter, J., (1999). Anomalous diffusion and relaxation close to thermal equilibrium: a fractional Fokker-Planck equation approach. *Phys. Rev. Lett.* 82, 3563-3567.

Nield, D.A., Bejan, A., (2006). *Convection in Porous Media*, 3rd ed. Springer, New York.

Nigmatullin, R.R. (1984a). To the theoretical explanation of the "universal response". *Phys. Stat. Sol. (b)* 123, 739-745.

Nigmatullin, R.R. (1984b). On the theory of relaxation for systems with "remnant" memory. *Phys. Stat. Sol. (b)* 124, 389-393.

Nowacki, W., (1974). Dynamical problems of thermodiffusion in solids. *Bull. Acad. Polon. Sci., Sér. Sci. Techn*. 23, 55-64, 129-135, 257-266.

Nowacki, W., Olesiak, Z.S., (1991). *Thermodiffusion in Solids*. Polish Scientific Publishers (PWN), Warsaw. (In Polish).

Parkus, H., (1959). *Instationäre Wärmenspannungen*. Springer, Wien.

Podlubny, I., (1999). *Fractional Differential Equations*. Academic Press, San Diego.

Podstrigach, Ya.S., (1961). Differential equations of thermodiffusion problem in isotropic deformable solid. *Dop. Ukrainian Acad. Sci.* 2, 169-172. (In Ukrainian).

Podstrigach, Ya.S., (1963). Differential equations of the diffusive strain theory of a solid. *Dop. Ukrainian Acad. Sci.* 3, 336-339. (In Ukrainian).

Podstrigach, Ya.S., (1965). Diffusion theory of inelasticity of metals. *J. Appl. Mech. Techn. Phys.* 2, 67-72. (In Russian).

Podstrigach, Ya.S., Povstenko, Y.Z., (1985). *Introduction to Mechanics of Surface Phenomena in Deformable Elastic Solids.* Naukova Dumka, Kiev. (In Russian).

Povstenko, Y., (2005). Fractional heat conduction equation and associated thermal stresses. *J. Thermal Stresses* 28, 83-102.

Povstenko, Y., (2009a). Thermoelasticity which uses fractional heat conduction equation. *J. Math. Sci.* 162, 296-305.

Povstenko, Y., (2009b). Theory of thermoelasticity based on the space-time fractional heat conduction equation. *Phys. Scr. T* 136, 014017.

Povstenko, Y., (2011). Fractional Cattaneo-type equations and generalized thermoelasticity. *J. Thermal Stresses* 34, 97-114.

Povstenko, Y., (2012). Theories of thermal stresses based on space-time-fractional telegraph equations. *Comp. Math. Appl.* 64, 3321-3328.

Povstenko, Y., (2013). Fractional thermoelasticity. In: *Encyclopedia of Thermal Stresses*, vol. 4. R.B. Hetnarski (ed.), Springer, Berlin, pp. 1778-1787.

Prudnikov, A.P., Brychkov, Yu.A., Marichev, O.I., (1981). *Integrals and Series. Elementary Functions*. Nauka, Moscow. (In Russian).

Prudnikov, A.P., Brychkov, Yu.A., Marichev, O.I., (1983). *Integrals and Series. Special Functions*. Nauka, Moscow. (In Russian).

Risken, H., (1989). *The Fokker-Planck Equation*. Springer, Berlin.

Scheidegger, A.E., (1974). *The Physics of Flow Through Porous Media*, 3rd ed. University of Toronto Press, Toronto.

Schneider, W.R., (1990). Fractional diffusion. In: R. Lima, L. Streit and R. Vilela Mendes (Eds.), *Dynamics and Stochastic Processes*, Lecture Notes in Physics, vol. 355, pp. 276–286. Springer, Berlin.

Sherief, H.H., El-Sayed, A.M.A., Abd El-Latief, A.M., (2010). Fractional order theory of thermoelasticity. *Int. J. Solids Struct.* 47, 269-275.

Van Kampen, N.G., (1981). *Stochastic Processes in Physics and Chemistry*. North-Holland, Amsterdam.

Youssef, H.M., (2010). Theory of fractional order generalized thermoelasticity. *J. Heat Transfer* 132, 061301.

Zaslavsky, G.M., (2002). Chaos, fractional kinetics, and anomalous transport. *Phys. Rep.* 371, 461-580.

Zheng, G.H., Wei, T., (2010). Spectral regularization method for a Cauchy problem of the time fractional advection-dispersion equation. *J. Comput. Appl. Math.* 233, 2631-2640.

Chapter 10

MODELLING DRUG EFFECT USING FRACTIONAL CALCULUS

Clara M. Ionescu[*]

Ghent University, Department of Electrical Energy,
Systems and Automation, Zwijnaarde, Belgium

Abstract

Closed loop control of depth of anesthesia (DOA) implies a good knowledge of the patient pharmaco-kinetics and -dynamics, i.e., the availability of a reliable model of the patient. This is necessary since prediction of drug effect in the body is essentially the main component of regulating DOA. Hitherto, this is done in a complex clinical environment, involving the anesthesiologist as a main decision-maker element. Obviously, the decision of administrating hypnotic and opioid drugs is a difficult one, since over- and under-dosing are a peril for patient's wellbeing and recovery. The expertise of the anesthesiologist and human factor make this decision a subjective one and may be difficult to justify in a mathematical framework. This chapter introduces emerging tools available on the 'engineering market' imported from the area of fractional calculus. Drug diffusion compartmental models are introduced and a novel interpretation of the classical drug-effect curve given. By employing tools from fractional calculus, model nonlinearity is avoided, allowing linear control strategies for automatic control of DOA systems.

Keywords: Analgesia, nonlinear dynamics, closed loop anesthesia, multivariable control, depth of anesthesia, drug effect interaction, fractional order impedance

Introduction

The emerging concepts of fractional calculus (FC) in biology and medicine have shown a great deal of success, explaining complex phenomena with a startling simplicity (Magin, 2006; Ionescu, 2013). It is clear that a major contribution of the concept of FC has been and remains still in the field of biology and medicine (West, 1990; Machado et al., 2013).

---

[*] Corresponding Author address: Email: claramihaela.ionescu@ugent.be.

Fractional calculus generously allows integrals and derivatives to have any order, hence the generalization of the term *fractional-order* to that of *general-order*. Of all applications in biology, diffusion is the one most appealing from modeling point of view, since it allows characterizing a relatively complex process with parsimonious models.

Modeling drug dynamics in the body using compartmental models is perhaps one of the most popular modeling approaches (Jacques, 1985). These models are based on mathematical characterization of molecular biochemistry and transport phenomena in the body (Macheas & Iliadis, 2006). As such, diffusion plays an important role in drug assimilation, transport and clearance, and it is a physiological process, which can be well described by means of fractional calculus (Trujillo, 2006).

In this chapter, a fresh view upon the models for drug release and their effect will be given in the application of depth of anesthesia regulation. Although in this chapter only hypnosis will be discussed, general anesthesia consists of three components acting simultaneously on the patient's vital signals, leading to an overall state of a) hypnosis b) neuromuscular blockade and c) analgesia (i.e., pain relief level).

Hypnosis is a general term indicating unconsciousness and the level of hypnosis is related to the infusion of hypnotic drug. Hypnosis is relatively well characterized and sensors to measure it by means of electroencephalogram (EEG) data are currently employed in standard clinical practice (Liu et al., 2011; Struys et al. 1998) and have been proven useful in closed-loop control of anesthesia (Ionescu et al. 2008; Ionescu et al. 2011).

Neuromuscular blockade ensures that the patient remains paralyzed during surgical procedures and is also a relatively well-characterized process with standard sensors available (EMG-electromyography) (Ozcan et al., 2012). Analgesia represents the loss of pain sensation that results from a interruption in the nervous system pathway between the sense organ and the brain. Finally, sedation refers to a combined effect of hypnosis and analgesia (Kress et al., 2002). From the point of view of detection and measurement, analgesia is the sole component remaining to be de-mystified.
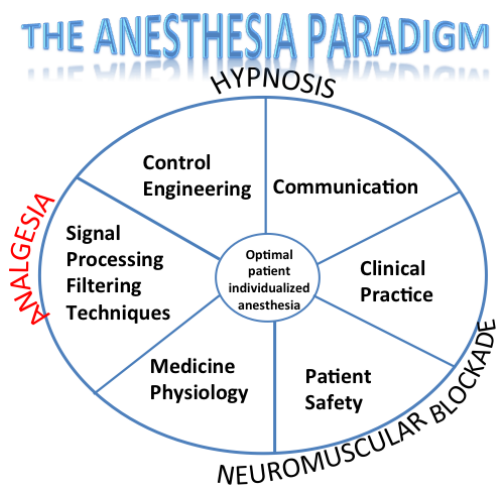
Figure 1. A personal view upon the high interdisciplinarity required to obtain a comprehensive picture of the anesthesia paradigm.

If one would like to have optimal drug infusion rates into a patient with avoiding over- and under-dosing, then accurate patient models are necessary (although not sufficient, since a good control methodology is also required) (Absalom et al., 2011). Accurate models may hold a realistic dynamic perspective for average populations datasets, but they are by far sub-optimal when patient-individualized control is envisaged. This is due to the fact that inter-patient variability has a strong impact on the perception and effectiveness of the drug into the body of the patient (i.e., drug effect, patient sensitivity to the drug, etc.). A schematic representation of the anesthesia paradigm in terms of its components is given in Figure 1. The hypnosis and neuromuscular blockade are well characterized, yet the analgesia component remains challenging for control purposes because no direct output measure is available. Hence, no specific models are yet available for analgesia effect in the human body during general anesthesia (i.e., unconsciousness).
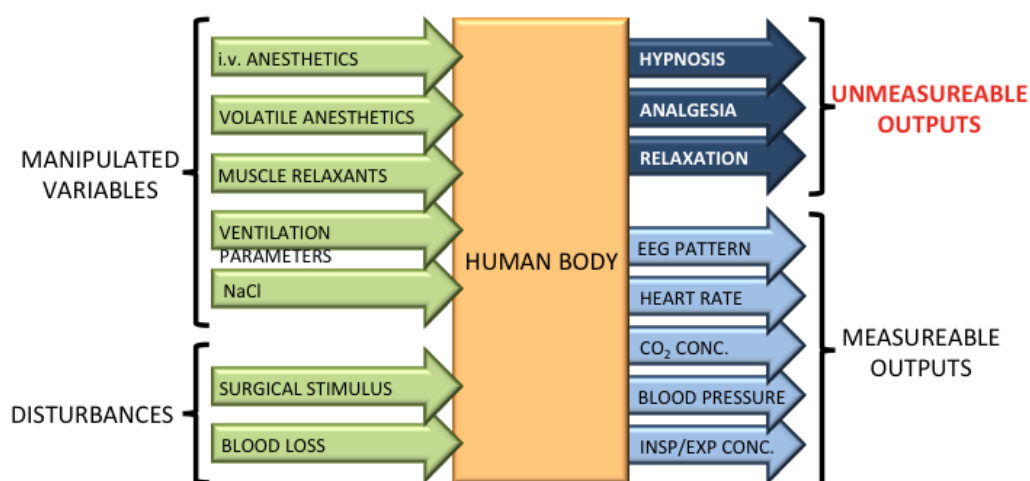
Figure 2. An overview of inputs and outputs in the complex dynamic system of the human body during surgery and general anesthesia.

The absence of more objective measures and decision-making elements in the DOA regulating system is justified by the lack of direct measures of hypnosis and analgesia, as depicted in Figure 2. Hypnosis is a state of (un)consciousness and this is currently measured via an indirect measure, the electroencephalogram. Analgesia is a state of insensibility to pain stimuli (mechanical, thermal, etc.) and is measured via indirect measures such as facial stress, reaction to speech, reaction to electrical stimulation in the hand of the patient, etc. Clearly, of these two components, analgesia is the most subjective measurement. Efforts are being made to develop new sensor techniques and new horizons are explored for modeling this intricate process and to provide mathematical models to replace these subjective evaluations.

The pharmacokinetic (PK) models available in the literature are linear in terms of model parameters and dynamics (Schnider et al, 1998; 1999). Their frequency response is quasi-identical, less for a scaling factor in the gain (this accounts in part for the sensitivity to the drug with respect to the body mass index of the patient). The pharmacodynamic (PD) models are usually represented by nonlinear Sigmoid (Hill) curves and represent the relationship of the drug concentration to the drug effect in each patient. From patient-individualized control

point of view, PD models are the most challenging part of the patient model andpose most challenges for control (i.e., highly nonlinear characteristic).

Fractional calculus offers tools to model such nonlinear characteristics as those of the PD models with less degree of nonlinearity in model parameters (Ionescu, 2013). The original purpose of this chapter is to put forward a fresh view to these models and to suggest how they can be integrated in the control paradigm of depth of anesthesia regulation.

The chapter is structured as follows: next, a brief introduction on the fractional calculus tools for modeling drug release and its effect is given. Section III depicts the classical methodology for PK-PD models in anesthesia and section IV presents the proposed PD modeling approach and some simulation results. Current limitations for the use of these models in a closed loop control paradigm are given and a conclusion section summarizes the main outcome of this paper.

Methods

Emerging Tools in the Field of Bio-Engineering

Pure empirical models such as input - output models are rather descriptive with loss of physiological insight into the drug absorption, transport, diffusion and release. However, from control point of view they are the most simple to obtain and to deliver information to the controller for deciding the optimal drug infusion rate necessary for the specific patient whose model is available. On the other hand, physiologically and bio-chemically based models are difficult to attain due to the extraordinary complexity of this process. For instance, the pathway of pain signaling into the body is depicted in Figure 3. It can be observed the various flows and complex bio-chemical reactions necessary to be modeled.
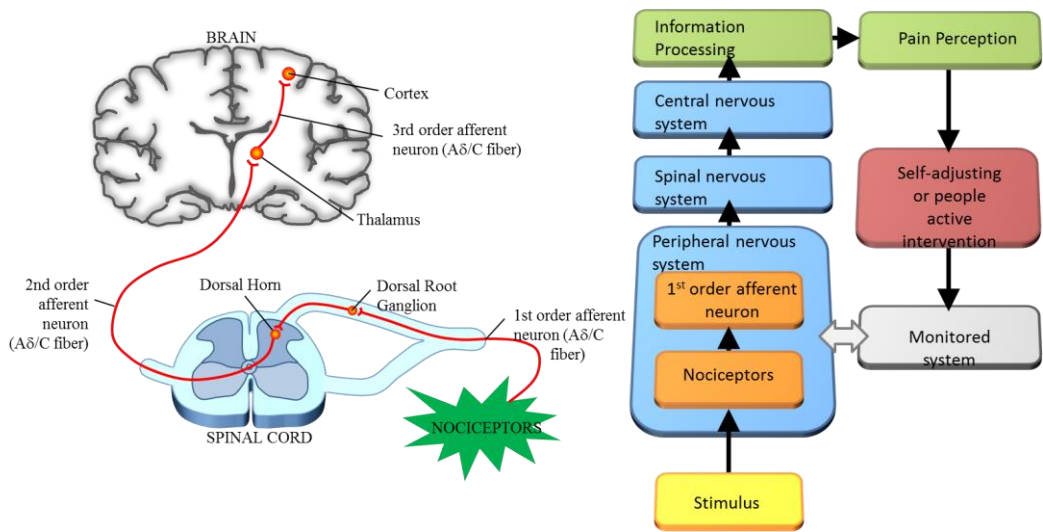
Figure 3. A diagram of the pathways of pain signaling in the human body.

In general, pain is a complicated process that involves an intricate interaction between a number of important chemicals found naturally in the brain and spinal cord. These chemicals,

called neurotransmitters, transmit nerve impulses from one cell to another. The complex process of pain awareness can be divided in three main phases: (i) transduction, (ii) transmission and (iii) perception. The first phase, transduction, begins when a painful or noxious stimulus causes tissue damage. The damaged cells release substances that lead to the generation of an electric action potential. In the next phase (i.e., transmission of the pain signal) the electric action potential continues from the site of damage to the spinal cord, where it ascends up the spinal cord to higher centers in the brain. The third phase, perception, is the conscious awareness of pain. Treatment of pain-related suffering requires knowledge of how pain signals are initially interpreted and subsequently transmitted and perpetuated. Therefore, it is mandatory to first understand how an analgesic drug diffuses into the human body and how we can build models of pain signaling and transmission.

An intermediate solution is perhaps the use of semi-empirical models. Such a fairly simple model to employ in characterizing drug release is the power-law model:

$$\frac{M_t}{M_\infty} = kt^n \tag{1}$$

where M_t and M_∞ are cumulative amounts of drug released at time t and infinite time, respectively; and k is a constant reflecting the structural and geometrical characteristics of the system, and n is the *release exponent* (Higuchi, 1961). For purely diffusion-controlled release, $n=0.5$, while other values of n may be indicative of various diffusion conditions. These features of this model are of special interest in our study since we would like to look at the inter-patient variability from this standpoint.

Following the fundamental law of physics which applies to well stirred, homogeneous systems, it follows that the mean square displacement of the walker, $<x^2>$ in the random walk model is proportional to time (Kopelman, 1988; Rinaki et al., 2003):

$$<x^2> \approx t \tag{2}$$

However, in disordered systems, such as most biological environments, this is no longer proportional with time, but with the fractal walk dimension of the walker:

$$<x^2> \approx t^{D_w} \tag{3}$$

with $D_w \neq 2$. This property implies that scaling laws such as power laws are associated with kinetics of various processes taking place in the (biological) environment (i.e., tissue). Most biological tissues can be approximated in their properties by polymers. As such, the spatio-temporal porosity of a dynamically changing polymer is close to the percolation threshold for non-classical diffusion effects impinging on release kinetics.

Fractional calculus has shown in several (non)biological applications that classical diffusion as well as non-classical diffusion can be characterized by fractional order differ-integrals models (Machado et al, 2013; Trujillo, 2006). It is possible to derive further the model from (1) in its Laplace equivalent, as indicated in (Magin, 2006). This result has regained the attention of the research community and current efforts are being directed

towards providing pharmacokinetic models with fractional order differ-integrals (Dokoumetzidis and Macheras, 2009; Kytariolos et al, 2010; Dokoumetzidis et al., 2010; Popovic et al., 2011; Hennion and Hanert, 2013; Popovic et al, 2013; Copot et al., 2013; Ionescu et al., 2013), and their equivalent Laplace models of non-integer order, coined in the literature as FOIMs (fractional order impedance models) (Ionescu, 2013).

Classical PK-PD Models for Drug Diffusion

In order to control the depth of sedation based on predictive control strategies, a model capturing the dynamics of the patient is required. The selection of the model's input and output variables is crucial for optimal control. Propofol is a commonly used hypnotic drug to induce general anesthesia (Absalom et al., 2011; Bailey & Haddad, 2005) and is also used to avoid awareness of pain. Sometimes is used together with Remifentanil, a strong opioid, to emphasize analgesia (i.e., pain relief). The two drugs have a synergic effect, obeying exactly the same behavior as that discussed in this section. For sake of simplicity, only the effects of one drug (i.e., Propofol) will be considered hereafter.

Using the electroencephalogram (EEG), several derived, computerized parameters like the BIS have been tested and validated as a promising measure of the hypnotic component of anesthesia. BIS values lie in the range of 0-100; whereas 90-100 range represents fully awake patients; 60-70 range and 40-60 range indicate light and moderate hypnotic state, respectively (Struys et al., 2003).

PK-PD blocks denote compartmental models. The PK-PD models most commonly used for propofol and remifentanil are the 4th order compartmental model described by Schnider et al., (1998, 1999) and they have the structure depicted in Figure 4:
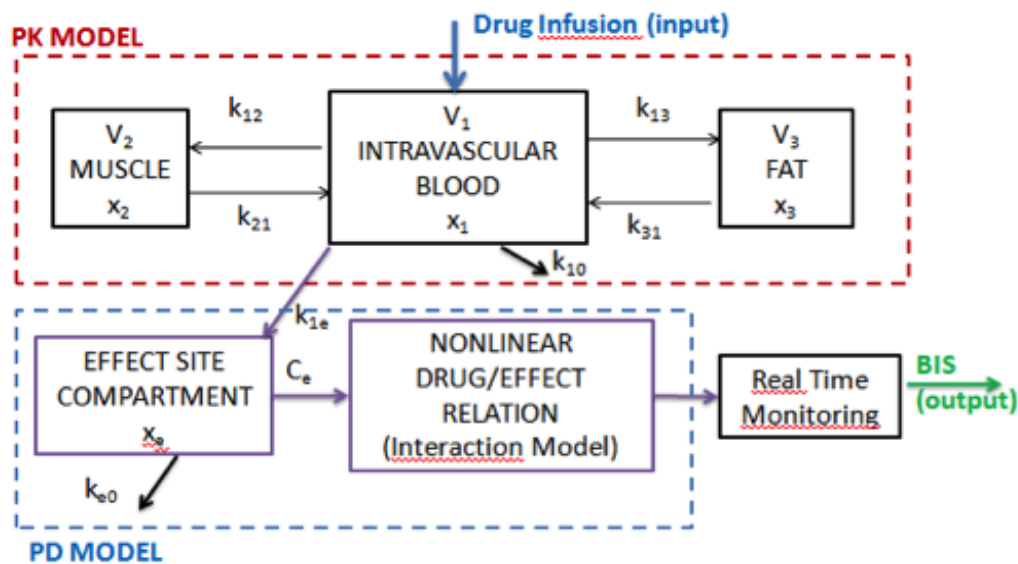
Figure 4. General compartmental model of the patient, where PK denotes the pharmacokinetic model and PD denotes the pharmacodynamic model of an infused drug.

In this figure x_1 [mg] denotes the amount of drug in the central compartment. The blood concentration is expressed by x_1/V_1. The peripheral compartments 2 and 3 model the drug exchange of the blood with well and poorly diffused body tissues. The masses of drug in fast and slow equilibrating peripheral compartments are denoted by x_2 and x_3, respectively. The parameters k_{ji}, for $i \neq j$, denote the drug transfer frequency from the jth to the ith compartment and $u(t)$ [mg/s] is the infusion rate of the anesthetic drug into the central compartment. An additional hypothetical effect compartment was proposed to represent the lag between drug plasma concentration and drug response. The parameters k_{ij} of the PK models depend on age, weight, height and gender and the relations can be found in (Schnider 1998; 1999). The PK-PD model is represented by the following equations:

$$\dot{x}_1(t) = -\left[k_{10} + k_{12} + k_{13}\right]x_1(t) + k_{21}x_2(t) + k_{31}x_3(t) + \frac{u(t)}{V_1}$$

$$\dot{x}_2(t) = k_{12} \cdot x_1(t) - k_{21} \cdot x_2(t) \qquad\qquad (4)$$

$$\dot{x}_3(t) = k_{13} \cdot x_1(t) - k_{31} \cdot x_3(t)$$

$$\dot{x}_e(t) = -k_{e0} \cdot C_e(t) + k_{1e} \cdot x_1(t)$$

The effect compartment receives drug from the central compartment by a first-order process and it is regarded as a volumeless additional compartment. Therefore, the drug transfer frequency from the central compartment to the effect-site compartment is equal to the frequency of drug removal from the effect-site compartment: $k_{e0}=k_{1e}=0.456$ [min^{-1}] (Struys et al. 2003). Drug concentration in the effect site compartment is denoted by the variable C_e. The parameters k_{ij} of the PK models depend on age, weight, height and gender and can be calculated for Propofol:

$$V_1 = 4.27 \; [l]; \quad V_3 = 2.38 \; [l]; \quad V_2 = 18.9 - 0.391 \cdot (age - 53) \; [l]$$

$$C_{l1} = 1.89 + 0.0456(weight - 77) - 0.0681(lbm - 59) + 0.0264(height - 177) \; [l/\min]$$

$$C_{l2} = 1.29 - 0.024(age - 53) \; [l/\min]; \qquad C_{l3} = 0.836 \; [l/\min]$$

$$k_{10} = \frac{C_{l1}}{V_1} \; \left[\min^{-1}\right]; \quad k_{12} = \frac{C_{l2}}{V_1} \; \left[\min^{-1}\right]; \quad k_{13} = \frac{C_{l3}}{V_1}\left[\min^{-1}\right];$$

$$k_{21} = \frac{C_{l2}}{V_2} \; \left[\min^{-1}\right]; \quad k_{31} = \frac{C_{l3}}{V_3}\left[\min^{-1}\right]$$

where C_{l1} is the rate at which the drug is cleared from the body, and C_{l2} and C_{l3} are the rates at which the drug is removed from the central compartment to the other two compartments by distribution. The lean body mass *(lbm)* for women and men are: $1.1 \cdot weight - 128 \cdot \frac{weight^2}{height^2}$ and

$1.07 \cdot weight - 148 \cdot \frac{weight^2}{height^2}$, respectively.

The relation between the effect site concentration C_e and the BIS is given by a nonlinear sigmoid Hill curve:

$$BIS(t) = E_0 - E_{max} \cdot \frac{C_e^{\gamma}(t)}{C_e^{\gamma}(t) + C_{50}^{\gamma}} \qquad (5)$$

where E_0 is the BIS value when the patient is awake; E_{max} is the maximum effect that can be achieved by the infusion of Propofol; C_{50} is the Propofol concentration at half of the maximum effect and γ is a parameter which together with the C_{50} determines the patient sensitivity to the drug. Usually, E_0 and E_{max} are usually considered equal to 100.

As explained earlier, the main challenge for control standpoint is the nonlinearity of the Hill curve given by (5) and the inherent inter-patient variability. To illustrate this to the reader, a realistic set of typical and atypical patients has been used, with the parameter values given in Table 1. The resulted Hill curves by simulating the PKPD model of these patients is shown in Figure 5.
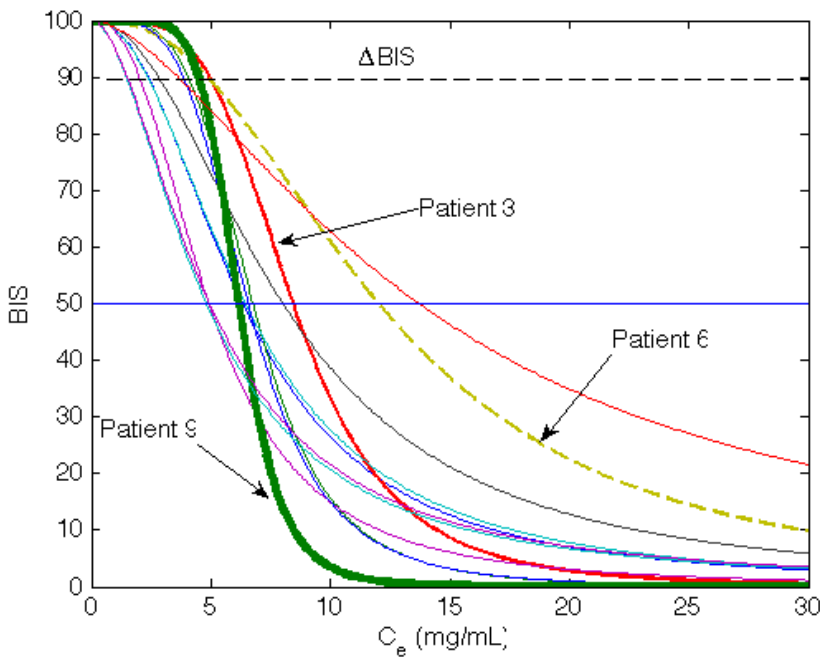
Figure 5. Example of Hill curves from various patients illustrating the high-degree of interpatient variability.

For instance, Patient 3 and patient 9 require the same amount of effect site concentration before they start to react, but they have significantly different sensitivity to the drug effect. On the other hand, patient 6 requires less effect site concentrations to initiate the reaction in BIS, but the response is very slow. Moreover, it can be generalized that below a certain threshold value for the effect site concentration, the BIS(t) does not vary significantly. Such a threshold interval is used in practice to apply target-controlled infusion, which is in fact an open loop control policy. This specific intial strategy provides a desired effect site concentration in the patient, but does not take into account the actual measured BIS. Obviously, this is only useful in the induction phase of anesthesia, i.e., until a certain ΔBIS is achieved.

Table 1. Characteristic variables for each of the virtual realistic 12 patients used in this study as from (Ionescu et al, 2008)

Patient	Age	Length	Weight	Gender	C50	E0	Emax	Gamma
P1	40	163	54	F	6.33	98.8	94.1	2.24
P2	36	163	50	F	6.76	98.6	86	4.29
P3	28	164	52	F	8.44	91.2	80.7	4.1
P4	50	163	83	F	6.44	95.90	102.00	2.18
P5	28	164	60	M	4.93	94.70	85.30	2.46
P6	43	163	59	F	12.10	90.20	147.00	2.42
P7	37	187	75	M	8.02	92.00	104.00	2.10
P8	38	174	80	F	6.56	95.50	76.40	4.12
P9	41	170	70	F	6.15	89.20	63.80	6.89
P10	37	167	58	F	13.70	83.10	151.00	1.65
P11	42	179	78	M	4.82	91.80	77.90	1.85
P12	34	172	58	F	4.95	96.20	90.80	1.84

It is obvious that all these differences in reactions from patients to the same amount of drug infused in their body require a high degree of robustness from the controller. The drawback is a conservative control, which may not always deliver the expected performance, e.g., when disturbances need to be removed fast to avoid awareness in the patient. Consequently, a significant strain is put on the controller's task to keep the closed loop performance within the same specifications for all types of patients.

Hybrid Models emerging from Classical PK-PD and FOIMs

The interwoven thread connecting these models is based on the theory of fractional calculus and fractal walk dynamics (West, 1990; Magin, 2006). An interesting feature of systems characterized by fractal dynamics is the following: represented on a log-log plot, their characteristic becomes linear. This feature is of special interest for us, especially if the reader may recall the Hill curve from Figure 5. Of course, it would be very nice if the strong nonlinearity and inter-patient variability depicted in this figure would be diminished, or even better, simply vanish into thin air. In this section, some ideas will be put forward which will lead the reader through this new approach of viewing Hill curves from a different perspective.

Based on (1) one can write the same relationship for the Hill curve:

$$\frac{C_e(t)}{BIS(t)} = k \times t^n \tag{6}$$

where k and n are varying on the patient PK-PD characteristics. If one compares (5) with (6) it can be recognized the resemblance in the power term and observe in fact a simplification of the model from (5) in terms of parameter number. From a structural point of view, there is no difference between the models, since both are semi-empirical models. The term $C_e(t)/BIS(t)$ denotes the concentration-to-effect ratio (CER) and its units are [mg/ml/%].

The profile of $C_e(t)$ may differ depending on the type of depth of anesthesia regulation that can occur in practice. Usually, in target-controlled infusion systems, drug is infused in the patient in open loop (i.e., no feedback from the patient is explicitly taken into account!) and is the most widely applied in clinical practice. Averaged population models are used to predict the concentration in the blood and thus in the effect site compartment from (4) and their corresponding BIS effect. If one represents this in time, it appears as a train of steps of different values; i.e., the anesthesiologist changes the value of the targetted concentration depending on the reactions in biological signals from patient (e.g., heart rate, respiratory rate, blood pressure, cardiac output, oxigen concentration, etc.).

In order to verify the validity of the above assumptions, a simulation study has been performed. Values for the effect site concentration $C_e(t)$ have been given in the range from 0.01-20, linear distribution of 2000 points. $BIS(t)$ has been calculated with parameters from Table 1 and formula from (5). The purpose of k is that of a scaling factor, so a common value has been identified for all patients: 5.45^{-10}. The identified values for the parameter n are illustrated in Figure 4. From Figure 5 one may recall the specificity of patients 3, 6 and 9. Their corresponding values are $n=3.88$, $n=2.72$ and $n=4.45$, respectively.

The results of the model identification from (5) are given in figures 6-11. Notice that somewhat less accurate model is identified for patient 9 and patient 10. Looking back in Table 1, these patients have the highest, respectively the lowest values for the *Gamma* parameter, which give the slopes of the Hill curve in Figure 5. Correlating this with the results of the identification from Figure 12, we observe that also the highest, respectively the lowest value for the n parameter is obtained for the same patients. We conclude that the n parameter holds a similar significance in (6) as that of the *Gamma* parameter in (5).
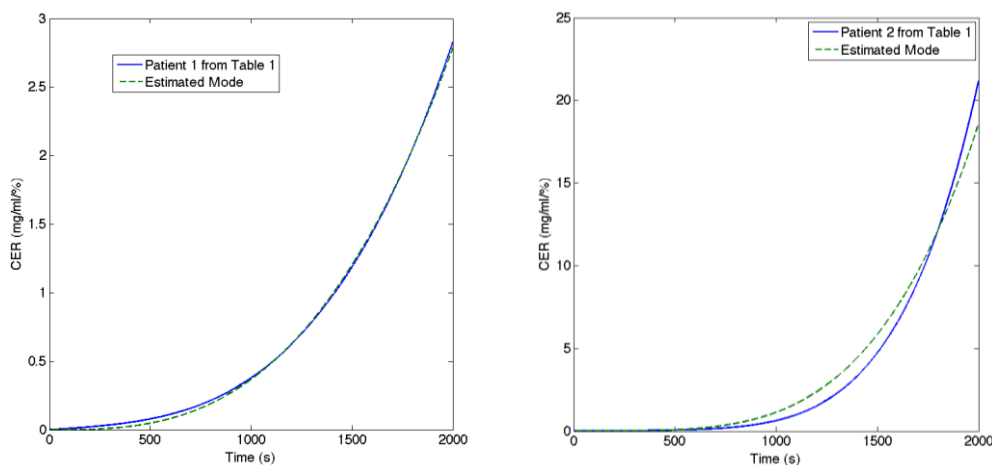
Figure 6. Illustration of identification result for Patient 1 and Patient 2 from Table 1.

Discussion

It may be possible to replace (5) by some form (6), since the fractional order impedance can account for time-varying dynamics by having a variable fractional order value n. This idea is a good incentive for further thought.
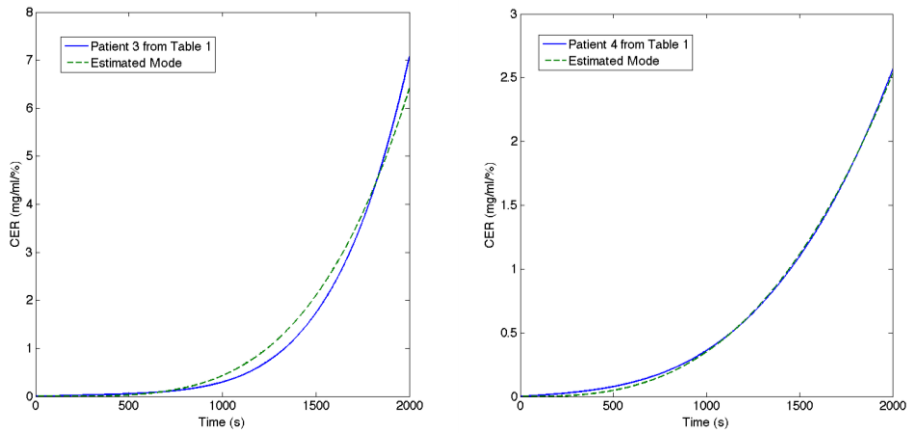
Figure 7. Illustration of identification result for Patient 3 and Patient 4 from Table 1.
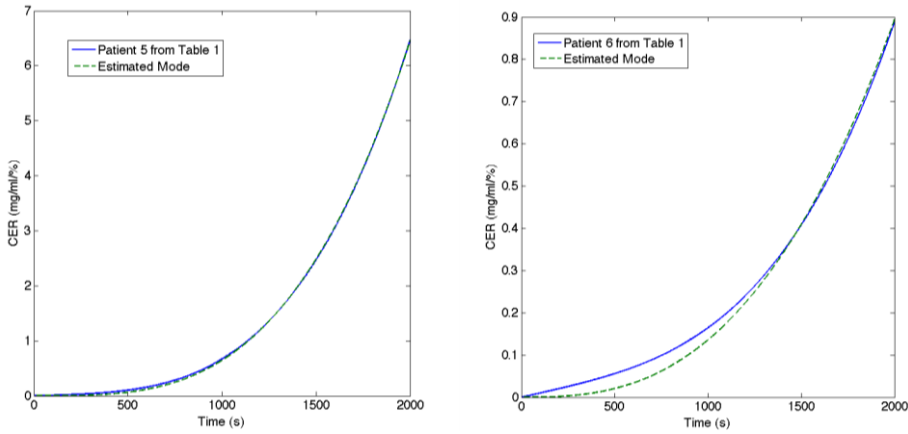
Figure 8. Illustration of identification result for Patient 5 and Patient 6 from Table 1.
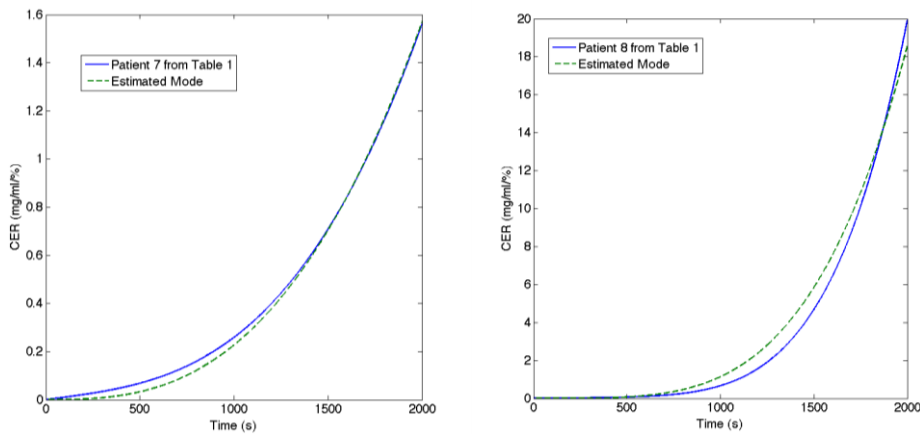
Figure 9. Illustration of identification result for Patient 7 and Patient 8 from Table 1.
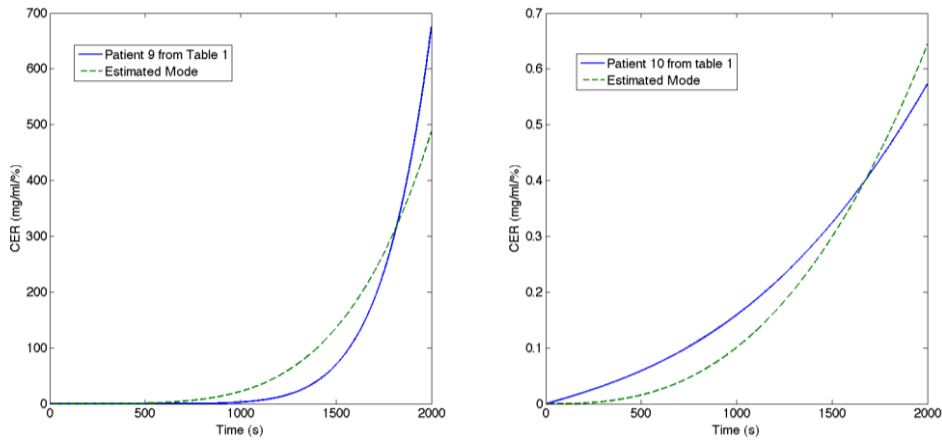
Figure 10. Illustration of identification result for Patient 9 and Patient 10 from Table 1.
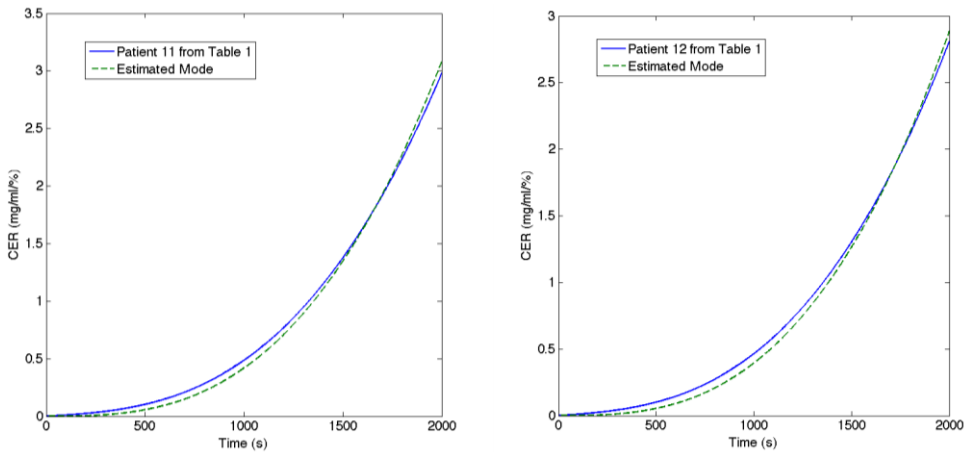
Figure 11. Illustration of identification result for Patient 11 and Patient 12 from Table 1.

It is obvious that i) closed loop control is necessary and ii) an averaged patient model will deliver sub-optimal results since they require a robust, conservative controller able to deal with the inter-patient variability. Moreover, it is also clear that the inter-patient variability may vary quite significantly and that one single controller (without online adaptation) will never suffice in practice.

A first problem is to find online adaptation algorithms which may adapt the model parameters k and n to the patient characteristics. Identification from logarithmically sampled data has been proposed in (De Keyser et al., 2011) and represents a good framework for developing the online identification algorithm.

Another problem is to find a solution to integrate the model from (6) into a closed loop control system taking into account the requirement for a logarithmic sample time (i.e., in order to maintain linearity). It has already been shown in various examples that a Riemann sampling rate (i.e., linear periodic) may be outperformed by a Lebesque sampling rate (i.e., event-triggered) in several applications (Goodwin et al., 2013). Since the Lebesque sampling rate is an event trigerred rate used successfully in practice in closed loop control (e.g.,

networked control, sensor networks), it may be revealing to look into the possibility of a logarithmic sampling rate.
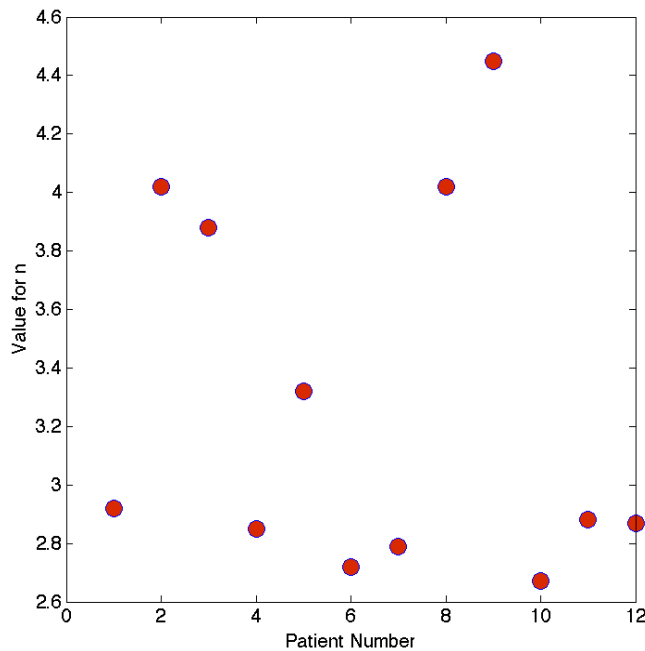
Figure 12. Identified values of the n parameter from the power law model in (6) for all patients given in Table 1.

Conclusion

This chapter presented the available tools emerging from fractional calculus to model the nonlinear characteristics of the pharmacokinetic and pharmacodynamic patient models. Advantages and challenges have been discussed. Results suggest that the high degree of inter-patient variability and nonlinearity may be avoided, leading to linear control techniques instead of advanced, complex control techniques.

This fresh view upon the patient models enables further optimization of the multiple input (i.e., two drugs) single output (i.e., their synergic effect) until the analgesia sensor becomes available for a fully multivariable input-output control of anesthesia.

Acknowledgment

References

Absalom, A., De Keyser, R., Struys, M., (2011). Closed Loop Anesthesia: Are We Getting Close to Finding the Holy Grail? *Anesthesia and Analgesia*, 112(3), 364-381.

Bailey, J.M., Haddad, W.M., (2005). Drug dosing control in clinical pharmacology, *IEEE Control Systems Magazine*, 25(2), 35-51.

Copot, D., Chevalier, A., Ionescu, C., De Keyser, R., (2013). A two-compartment fractional derivative model for propofol diffusion in anesthesia, *Proc. Conference on Systems and Control*, Hyderabad, India, 28-31 August, 264-269.

De Keyser, R., Ionescu, C., Festila, C., (2011). A one-step procedure for frequency response estimation based on switch-mode transfer function analyzer, *Proc. IEEE-CDC Conf on Decision and Control joint with ECC-European Control Conf.,* December 12-15, Orlando, Florida, 1189-1194.

Dokoumetzidis A., Macheras P., (2009). Fractional kinetics in drug absorption and disposition processes, *J. Pharmacokinet Pharmacodyn.*, 36, 165-178.

Dokoumetzidis A., Magin R., Macheras P., (2010), Fractional kinetics in multi-compartmental systems, *J. Pharmacokinet. Pharmacodyn.*, 37, 507-524.

Goodwin, G., Aguero, J.C., Cea-Garrido, M.E., Salgado, M.E., Yuz, J.I., (2013). Sampling and sampled-data models, *IEEE Control Systems Magazine*, 33(5), 34-53.

Hennion M., Hanert E. (2013), How to avoid unbounded drug accumulation with fractional pharmacokinetics, J. Pharmacokinet Pharmacodyn, 40, 691-700.

Higuchi, T., (1961). Rate of release of medicaments from ointment bases containing drugs in suspension, *J. Pharm Sci,* 50, 874-875.

Ionescu, C., De Keyser, R., Torrico, B., De Smet, T., Struys M., Normey-Rico, J., (2008). Robust Predictive Control Strategy Applied for Propofol Dosing using BIS as a Controlled Variable during Anesthesia, *IEEE Transactions on Biomedical Engineering*, 55, 2161-2170.

Ionescu C., Hodrea R., De Keyser R., (2011), Variable time-delay estimation for anesthesia control during intensive care, *IEEE Transaction on Biomedical Engineering*, 58(2), 363-369.

Ionescu, C., (2013). The human respiratory system: an analysis of the interplay between anatomy, structure, breathing and fractal dynamics Springer, Series in BioEngineering 2013, Print ISBN 978-1-4471-5387-0, On- line ISBN 978-1-4471-5388-7.

Ionescu, C.M., Copot, D., De Keyser, R., (2013). Three compartmental model for propofol diffusion during general anesthesia, *Discontinuity, Nonlinearity and Complexity*, 2(4), 357-368.

Jacques, J.A., (1985). Compartmental analysis in biology and medicine, University of Michigan Press.

Kopelman, R., (1988). Fractal reaction kinetics, *Science*, 241, 1620-1626.

Kress JP, Pohlman AS, Hall JB, (2002), Sedation and analgesia in the intensive care unit, *American Journal of Respiratory Critical Care Medicine*; 166, 1024-8.

Kytariolos J., Dokoumetzidis A., Macheras P., (2010). Power law IVIVC: an application of fractional kinetics for drug release and absorption, *Eur. J. of Pharmaceutica.l Sci.,* 41, 299-304.

Liu N, Chazot T, Genty A, Landais A, Restoux A, McGee K, Laloe PA, Trillat B, Barvais L, Fischler M, (2011), Closed-loop co-administration of Propofol and Remifentanil guided

by Bispectral index: a randomized multicenter study, Anesthesia and Analgesia, 112(3), 546-557.

Macheas, P., Iliadis, A., (2006). Modeling in Biopharmaceutics, Pharmacokinetics, and Phamacodynamics: Homogeneous and Heterogeneous Approaches. Springer Verlag, New York.

Magin, R. (2006). Fractional Calculus in Bioengineering. Begell House Publishers.

Ozcan A, Ozcan N, Gulec H, Yalcin F, Basar H, (2012), Comparison of the effects of fentanyl, remifentanil, and dexmedetomidine on neuromuscular blockade, *Journal of Anesthesia*, 26(2), 196-199.

Popovic J., Dolicanin D., Rapaic M., Popovic S., Pilipovic S., Atanackovic T., (2011), A nonlinear two compartmental fractional derivative model, *Eur. J. Drug Metab*. Pharmacokinet., 36, 189-196.

Popovic J., Posa M., Popovic K., Popovic D., Milosevic N., Tepavcevic V., (2013), Inidividualization of a pharmacokinetic model by fractional and nonlinear fit improvement, *Eur. J. Drug Metab. Pharmacokinet*., 38, 69-76.

Rinaki, E., Valsami, G., Macheras, P., (2003). The power law can describe the 'entire' drug release curve from HPMC-based matrix tablets: a hypothesis, *Int. J. of Pharmaceutics*, 255, 199-207.

Schnider, T.W., Minto, C.F., Gambus, P.L. , Andresen, C, Goodale, DB , Youngs, EJ, (1998). The influence of method of administration and covariates on the pharmacokinetics of Propofol in adult volunteers, *Anesthesiology*, 88: 1170-1182.

Schnider, TW., Minto, CF, Shafer, SL, Gambus, PL, Andresen, C, Goodale, DB, Youngs, EJ, (1999). The influence of age on Propofol pharmacodynamics, *Anesthesiology*, 90:1502-1516.

Struys M, Versichelen L, Byttebier G, Mortier E, Moerman A, Rolly G, (1998), Clinical usefulness of the bispectral index for titrating propofol target effect-site concentration, *Anaesthesia*, 53, 4-12.

Struys, M., Vereecke, H., Moerman, A., Jensen, E., Verhaeghen, D., De Neve, N., Dumortier F., Mortier E., (2003). Ability of the bispectral index, autoregressive modelling with exogenous input-derived auditory evoked potentials, and predicted propofol concentrations to measure patient responsiveness during anesthesia with propofol and remifentanil, *Anesthesiology,* 99, 802-814.

Tenreiro Machado, J.A., Kiryakova, V., Mainardi, F., (2013). Recent history of fractional calculus, *Communications in Nonlinear Science and Numerical Simulation*, 16(3), 1140-1153.

Trujillo, J.J., (2006). Fractional models: Sub and super-diffusives, and undifferentiable solutions, *Innovation in Engineering Computational Technology*, pp. 371-401.

West, B.J., (1990). Fractal physiology and chaos in medicine, Studies of nonlinear phenomena in life sciences vol.1. Singapore: World Scientific.

Chapter 11

FUZZY FRACTIONAL PID CONTROLLERS: ANALYSIS, SYNTHESIS AND IMPLEMENTATION

*Ramiro S. Barbosa**and *Isabel S. Jesus*†

GECAD − Knowledge Engineering and Decision Support Research Center
Institute of Engineering / Polytechnic of Porto (ISEP/IPP)
Dept. of Electrical Engineering, Porto, Portugal

Abstract

Fuzzy logic controllers (FLC) have developed greatly in recent years. They offer easy and robust solutions to complex problems, allowing human reasoning to be applied to the control of systems. This chapter introduces the concepts of fractional calculus in FLC. The resulting fuzzy fractional PID controllers are investigated in terms of their structures and respective digital implementations. In the first part of chapter, a simple and effective tuning methodology is proposed and compared with traditional approaches. The methodology for tuning the fuzzy controllers is based on the prior knowledge of integer/fractional-order control strategy, making the procedure adequate to replace an existent controller in order to improve the system control performance. In the second part of chapter, are devised optimal fuzzy fractional PID controllers by using a particle swarm optimization algorithm. A comparative study between fuzzy integer and fractional PID controllers is presented. The feasibility and effectiveness of the proposed controllers are tested on several benchmark systems that are representative of industrial processes. The simulation results show the better performance of fractional controllers over the conventional PID or fuzzy PID controllers.

PACS: 05.45-a, 52.35.Mw, 96.50.Fm

Keywords: fuzzy control, PID controller, fractional PID control, fractional calculus, fuzzy fractional PID control, optimization

1. Introduction

In recent years, fractional-order (FO) PID controllers have been a fruitful field of research [3, 50, 51]. However, no effective and simple tuning rules still exist for these con-

---

*E-mail address: rsb@isep.ipp.pt
†E-mail address: isj@isep.ipp.pt

trollers as those given for the integer PID controllers [2]. The FO-PID controller involves an integrator/differentiator of real, irrational or, even, of complex order [11, 50]. It has been demonstrated the good performance of this type of controller, in comparison with the conventional PID algorithms. The FO-PID extends the capabilities of the classical counterpart and, thus, have a wider domain of application, such as in suspension systems, robotics, signal processing, control and diffusion [44, 50, 51, 33]. On the other hand, the FLC have also been successfully applied in the control of many physical systems, particularly those with uncertainty, unmodelled, disturbed and/or nonlinear dynamics [36, 37, 18, 27].

Fuzzy control emerged on the foundations of Zadeh's fuzzy set theory [43, 12, 22]. This kind of control is based on the ability of a human being to find solutions for particular problematic situations. It is well know from our experience, that humans have the ability to simultaneously process a large amount of information and make effective decisions, although neither input information nor consequent actions are precisely defined. Through multivalent fuzzy logic, linguistic expressions in antecedent and consequent parts of IF-THEN rules describing the operator's actions can be efficaciously converted into a fully-structured control algorithm. The fuzzy method offer a systematic procedure to design controllers for many kind of systems, that often leads to a better performance than that of the conventional PID controller. It is a methodology of intelligent control that mimics human thinking and reacting by using a multivalent fuzzy logic and elements of artificial intelligence. Many applications using FLC can be found in [40, 36, 48, 53, 27].

It has been proved that the use of the fuzzy fractional controllers improved the results for many kind of systems, since it gives additional flexibility to the design. In this line of thought, many applications using this type of controllers were developed in the last few years [6, 3, 28, 4, 5, 17, 16, 47, 29, 30]. In [6, 3], the authors proposed the use of fuzzy fractional PD and PID controllers in the control of integer plants. They proved their effectiveness and superior robustness when compared with conventional integer or fuzzy PID controllers. In [4, 5] the fuzzy FO-PID controllers are tested on several fractional-order plants showing their superior control system performance. In [29, 30] are devised optimal fuzzy FO-PID controlers for nonlinear control systems. The above studies are devoted to discrete fractional-order PID controllers and their digital implementation. Other studies using continuous fuzzy FO-PID controllers are found in [18, 17, 16, 47].

In the first part of chapter, are combined the features of fuzzy controllers with those of fractional controllers of PID-type. The resulting fuzzy FO-PID controller is investigated in terms of its digital implementation and robustness. The combined advantages of the two controllers results in a better controller with superior robustness and wider domain of application. The tuning methodology of these controllers is based on the prior knowledge of integer or fractional-order control. First, a fractional-order controller is built and tuned (or used one already implemented). Then, we replace it with a linear fuzzy fractional controller displaying exactly the same step response. After, we make the controller nonlinear and fine tune it in order to get better control of the system. The fuzzy fractional controller will give, at least, the same performance of its linear counterpart.

In the second part of chapter, are designed optimal fuzzy FO-PID controllers by using particle swarm optimization (PSO) algorithm. PSO is one of the latest evolutionary techniques inspired by social bahavior of bird flocking or fish schooling [20, 21, 35]. A fractional nonlinear control system with saturation in actuator is analyzed in terms of step

responses, variation of controller parameters and time domain specifications as the fractional order of the fuzzy controller is changed. The influence of the order of the discrete rational approximations in control system performance is also studied.

The chapter is organized as follows. Section 2 presents the fundamentals of continuous and discrete fractional-order PID controllers. Section 3 outlines a tuning methodology for the design of fuzzy FO-PID controllers. Two decomposed structures for fuzzy FO-PID controllers are presented. In section 4, are devised optimal fuzzy FO-PID controllers using the PSO algorithm. The proposed fuzzy FO-PID controllers are tested and assessed their effectiveness and robustness in the control of integer and fractional-order plants commonly found in industry. Finally, section 5 draws the main conclusions.

2.   Basics of Fractional PID Controllers

The fractional-order controller of PID-type, usually named $PI^\lambda D^\mu$ controller, may be given as [51, 3]:

$$C\left(s\right) = \frac{U\left(s\right)}{E\left(s\right)} = K_p + \frac{K_i}{s^\lambda} + K_d s^\mu \tag{1}$$

where λ and μ are the orders of the fractional integrator and differentiator, respectively. The parameters K_p, K_i and K_d are correspondingly the proportional, integral and derivative gains of the controller. Clearly, taking $\left(\lambda,\ \mu\right) \equiv \left\{\left(1,1\right),\ \left(1,0\right),\ \left(0,1\right),\ \left(0,0\right)\right\}$ we get the classical {PID, PI, PD, P}-controllers, respectively. Other PID controllers are possible, namely: PD^β controller, PI^α controller, PID^β controller, and so on. The $PI^\lambda D^\mu$-controller is more flexible and gives the possibility of adjusting more carefully the dynamical proprieties of a control system [51, 6].

The time domain equation of the $PI^\lambda D^\mu$ controller is:

$$u\left(t\right) = K_p e\left(t\right) + K_i D^{-\lambda} e\left(t\right) + K_d D^\mu e\left(t\right) \tag{2}$$

where $D^{\left(*\right)}\ \left(\equiv {}_0 D_t^\alpha\right)$ denotes the differential operator of integration and differentiation (differintegral) to a fractional-order $\alpha = \left\{-\lambda,\ \mu\right\} \in \Re$.

The two most commonly used definitions for the differintegral are the Riemann-Liouville definition and the Grünwald-Letnikov definition [44, 42]. The Riemann-Liouville definition of a fractional derivative is $\left(\alpha > 0\right)$:

$$D^\alpha f\left(t\right) = \frac{1}{\Gamma\left(n-\alpha\right)}\frac{d^n}{dt^n}\int_0^t \frac{f\left(\tau\right)}{\left(t-\tau\right)^{\alpha-n+1}}d\tau \tag{3}$$

where $n-1 < \alpha < n$, n is an integer, $f(t)$ is the applied function, and $\Gamma(x)$ represents the Gamma function of x.

The Grünwald-Letnikov definition is $\left(\alpha \in \Re\right)$:

$$D^\alpha f\left(t\right) = \lim_{h\to 0}\frac{1}{h^\alpha}\sum_{j=0}^{[t/h]}\left(-1\right)^j \binom{\alpha}{j} f\left(t-jh\right) \tag{4a}$$

$$\binom{\alpha}{j} = \frac{\Gamma\left(\alpha+1\right)}{\Gamma\left(j+1\right)\Gamma\left(\alpha-j+1\right)} \tag{4b}$$

where h is the time increment and $[v]$ means the integer part of v.

The "memory" effect of these operators is demonstrated by above equations, where the convolution integral in (3) and the infinite series in (4), reveal the unlimited memory of these operators, ideal for modeling hereditary and memory properties in physical systems and materials.

The fractional integrals and derivatives can also be defined in the s-domain. Considering null initial conditions, they are given by the simple form ($\alpha \in \Re$):

$$D^\alpha f(t) = L^{-1}\{s^\alpha F(s)\} \tag{5}$$

where L represents the Laplace operator and $F(s) = L\{f(t)\}$. Definition (5) gives an easily interpretation of the fractional-order operator in the frequency domain. In fact, the open-loop Bode diagrams of amplitude and phase of s^α have correspondingly a slope of 20α dB/dec and a constant phase positionated at $\alpha\pi/2$ rad over the entire frequency domain [46, 7, 15].

From a control (and signal) processing perspective, approach (4) seems to be the most useful and intuitive, particularly for a discrete-time implementation [10, 39]. Thus, using (4), a discrete fractional PI$^\lambda$D$^\mu$ control equation can be obtained from (2) as ($h \approx T$, T is the sampling period):

$$u(k) = K_p e(k) + K_i D^{-\lambda} e(k) + K_d D^\mu e(k) \tag{6}$$

with

$$D^\alpha e(k) \approx \frac{1}{T^\alpha} \sum_{j=0}^{k} (-1)^j \begin{pmatrix} \alpha \\ j \end{pmatrix} e(k-j) \tag{7}$$

Replacing (7) in (6), the discrete PI$^\lambda$D$^\mu$ controller is then expressed as:

$$u(k) = K_p e(k) + \frac{K_i}{T^{-\lambda}} \sum_{j=0}^{k} (-1)^j \begin{pmatrix} -\lambda \\ j \end{pmatrix} e(k-j) + \frac{K_d}{T^\mu} \sum_{j=0}^{k} (-1)^j \begin{pmatrix} \mu \\ j \end{pmatrix} e(k-j) \tag{8}$$

The control equation (8) shows that the current value of control signal $u(k)$ depends on all previous values of error $e(k)$, making the computation too heavy as time increases and so unsuitable for a practical implementation of these algorithms. This fact illustrates the global character (i.e., unlimited memory) of the fractional-order operators. For practical implementation of fractional integral and derivative (7) we often apply the "short memory principle" [50], resulting in expression:

$$u(k) = K_p e(k) + \frac{K_i}{T^{-\lambda}} \sum_{j=v}^{k} c_j^{(-\lambda)} e(k-j) + \frac{K_d}{T^\mu} \sum_{j=v}^{k} c_j^{(\mu)} e(k-j) \tag{9}$$

where $v = 0$ for $k < L/T$ or $v = k - L/T$ for $k > L/T$; L is the memory length and $c_j^{(\alpha)} = (-1)^j \begin{pmatrix} \alpha \\ j \end{pmatrix}$ are the binomial coefficients which may be calculated recursively as:

$$c_0^{(\alpha)} = 1; \quad c_j^{(\alpha)} = \left(1 - \frac{1+\alpha}{j}\right) c_{j-1}^{(\alpha)}, \quad j = 1, 2, \cdots \tag{10}$$
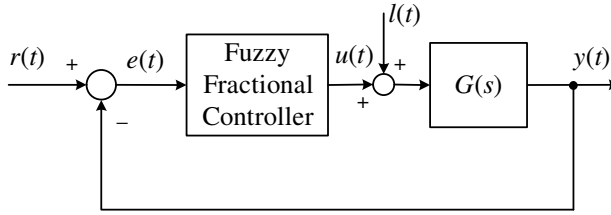
Figure 1. Fuzzy fractional PID controlled system.

Note that (9) is given in the form of a FIR filter [24]. Other discrete-time approximations in the form of IIR filters are also possible [54, 8, 9, 10, 13, 14, 45]. In section 4 is presented a method to obtain digital rational approximations of fractional-order derivatives and integrals.

3.   Tuning Methodology for Fuzzy Fractional PID Controllers

In this section, we will apply fuzzy logic control (FLC) for the design of fuzzy FO-PID controlled systems [36, 48]. Despite of variety of possible fuzzy controller structures, the controller is usually arranged in cascade with the system being controlled. This type of arrangement is shown in Figure 1 and will be used in this study. Other fuzzy schemes may be adopted such as fuzzy supervisory control and adaptive fuzzy control [48, 40, 26].

The main idea here is to explore the fact that the FLC, under certain conditions, is equivalent to a PID controller [43, 37, 26] and to extrapolate this fact for the case of fractional-order controllers. In a certain sense, the fuzzy PID controllers are a special case of the more general fuzzy FO-PID controllers, in which are involved two extra tuning parameters: the fractional orders (λ, μ) of controller equation (6).

The basic form of a fuzzy controller is illustrated in Figure 2 [48], consisting of a fuzzy rule base, an inference mechanism, and fuzzification and defuzzification interfaces. In general, the mapping between the inputs and the outputs of a fuzzy system is nonlinear [23, 26]. However, it is possible to construct a rule base with a linear input-output mapping [43, 26]. For that, the following conditions must be fulfilled:

- Use triangular input sets that cross at the membership value 0.5

- The rule base must be complete AND combination (cartesian product) of all input families

- Use the algebraic product (*) for the AND connective

- Use output singletons, positioned at the sum of the peak positions of the input sets

- Use sum-accumulation and centre of gravity for singletons (COGS) defuzzification

It seems reasonable to start with the design of a conventional integer/fractional PID controller and from there to proceed to a fuzzy control design. In this way, the linear fuzzy
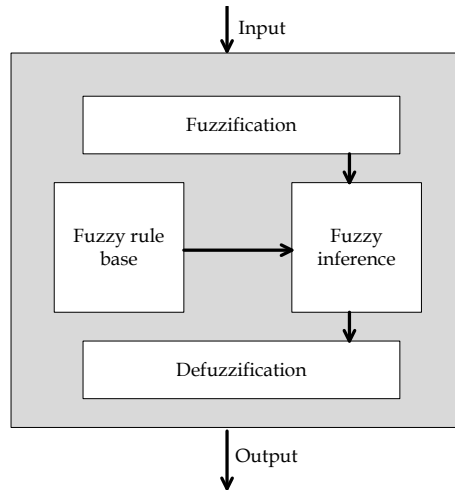
Figure 2. Structure of a fuzzy controller.

controller may be used in a design procedure based on integer/fractional PID control, as follows [26, 6, 3]:

1. Build and tune an integer/fractional PID controller

2. Replace it with an equivalent linear fuzzy controller

3. Make the fuzzy controller nonlinear

4. Fine-tune it

With the above procedure, the design of fuzzy FO-PID controllers will be greatly simplified, particularly if the controller was already implemented and it is desirable to enhance its performance. Moreover, this new type of controllers extends the potentialities of both fuzzy and fractional controllers and performs, at least, as well as its linear counterpart [26, 6, 3].

3.1. Fuzzy Fractional PD Controller

The time-domain equation of a fractional PD$^{\mu}$-controller is given by ($K_i = 0$ in (2)):

$$u\left(t\right) = K_p e\left(t\right) + K_d D^{\mu} e\left(t\right) \tag{11}$$

The corresponding discrete-time fractional PD$^{\mu}$-controller is:

$$u\left(k\right) = K_p e\left(k\right) + K_d D^{\mu} e\left(k\right) \tag{12}$$

Figure 3 illustrates the block diagram of the fuzzy fractional PD$^{\mu}$ (FF-PD$^{\mu}$) controller. As can be seen, the controller acts on the error, $e(k)$, and on the fractional change of error,
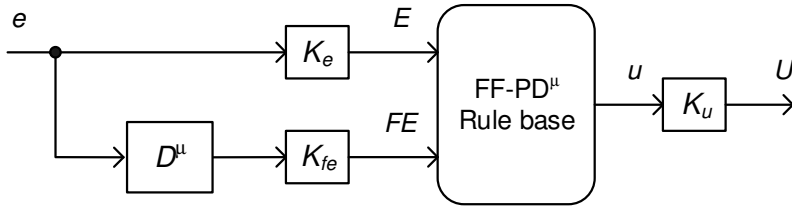
Figure 3. Fuzzy fractional PD$^{\mu}$-controller.

$D^{\mu}e(k)$. The control signal is U. The controller has three tuning gains, K_e and K_{fe}, corresponding to the inputs and K_u to the output. The following relations are thus verified:

$$E = K_e e, \quad FE = K_{fe}D^{\mu}e, \quad U = K_u u \qquad (13)$$

where E and FE represent the terms of error and fractional change of error, respectively.

The control signal U is generally a nonlinear function of E and FE:

$$U = f(E, FE)K_u = f(K_e e, \ K_{fe}D^{\mu}e) K_u \qquad (14)$$

With a proper choice of design, a linear approximation can be obtained as:

$$f(K_e e(k), \ K_{fe}D^{\mu}e(k)) \approx K_e e(k) + K_{fe}D^{\mu}e(k) \qquad (15)$$

and

$$U(k) = (K_e e(k) + K_{fe}D^{\mu}e(k)) K_u = K_e K_u e(k) + K_{fe}K_u D^{\mu}e(k) \qquad (16)$$

Comparing (16) with (12), it yields the relation between the gains of the conventional and fuzzy PD$^{\mu}$ controllers:

$$\begin{aligned} K_e K_u &= K_p \\ K_{fe} K_u &= K_d \end{aligned} \qquad (17)$$

The linear FF-PD$^{\mu}$-controller provides all the advantages of the conventional fractional PD$^{\mu}$-controller.

For an equivalent linear FF-PD$^{\mu}$-controller, the conclusion universe should be the sum of the premise universes and the input-output mapping should be linear. Table 1 lists a linear rule base for the FF-PD$^{\mu}$ controller composed of four rules. There are only two fuzzy labels (Negative and Positive) used for the fuzzy input variables and three fuzzy labels (Negative, Zero and Positive) for the fuzzy output variable. This rule base should satisfy above mentioned conditions in order to provide a linear mapping.

Scaling the input gains may be necessary to preserve the linearity of the fuzzy controller. However, that should be made without affecting the tuning [6, 3]. For example, considering (16), and a scale factor M $(M > 0)$:

$$U(k) = (K_e e(k) + K_{fe}D^{\mu}e(k)) K_u = (MK_e e(k) + MK_{fe}D^{\mu}e(k)) \frac{K_u}{M} \qquad (18)$$

This scaling has some advantages, as it will avoid saturation and will provide a simpler design, since the universes ranges of inputs and outputs are normalized to a prescribed interval, say percentage of full scale $[-100, 100]$.

Table 1. Rule base for the FF-PD$^\mu$ controller.

Rule 1	If E is N and FE is N then u is N
Rule 2	If E is N and FE is P then u is Z
Rule 3	If E is P and FE is N then u is Z
Rule 4	If E is P and FE is P then u is P

3.2. Fuzzy Fractional PID Controller

The inclusion of an integral action is necessary whenever the closed-loop system exhibits a steady-state error. The fuzzy fractional PD$^\mu$+I$^\lambda$ (FF-PD$^\mu$+I$^\lambda$) controller combine the fractional-order integral action with a fuzzy PD$^\mu$-controller, as illustrated in Figure 4.

The control signal U is generally a nonlinear function of error E, fractional change of error *FE*, and fractional integral of error *FIE*:

$$U = (f(E, FE) + FIE) K_u = \left(f\left(K_e e(k), K_{fe} D^\mu e(k)\right) + K_{fie} D^{-\lambda} e(k) \right) K_u \tag{19}$$

Adopting the linear approximation (15) it yields the discrete control equation:

$$U(k) \approx \left(K_e e(k) + K_{fe} D^\mu e(k) + K_{fie} D^{-\lambda} e(k) \right) K_u$$
$$= K_u K_e e(k) + K_u K_{fe} D^\mu e(k) + K_u K_{fie} D^{-\lambda} e(k) \tag{20}$$

Comparing (20) with the discrete fractional PI$^\lambda$D$^\mu$-controller (6), it yields the relation between the gains of the conventional and fuzzy fractional PID controllers:

$$K_e K_u = K_p$$
$$K_{fie} K_u = K_i$$
$$K_{fe} K_u = K_d \tag{21}$$

The linear FF-PD$^\mu$+I$^\lambda$ controller provides all the advantages of the conventional fractional PI$^\lambda$D$^\mu$-controller.

3.3. Illustrative Examples

In this section we apply the proposed fuzzy FO-PID controllers in the control of integer and fractional-order plants. In all experiments, the simulation parameters are: absolute memory computation of approximation (7), scale factor $M = 0.1$, and sampling period $T = 0.05$ s.

3.3.1. Example 1: Integer-Order Plant

Consider the normalized transfer function of a double integrator plant, which serves as a model of many dynamic systems:

$$G_1(s) = \frac{1}{s^2} \tag{22}$$
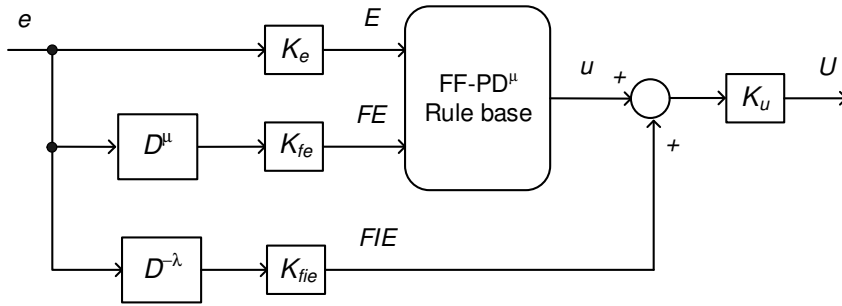
Figure 4. Fuzzy fractional PD$^\mu$+ I$^\lambda$ controller.

For the control of plant (22) a fractional PD$^\mu$ controller was designed in [6]:

$$C_{PD^\mu}(s) = K_P + K_D s^\mu = 0.5 + 0.5 s^{0.7} \tag{23}$$

Let us design an equivalent linear FF-PD$^\mu$-controller. By configuring the fuzzy inference system (FIS) and selecting three scaling factors, we obtain a FF-PD$^\mu$-controller that reproduces the exact control performance as the fractional PD$^\mu$-controller. We first fix $K_e = 100$, since the error universe is chosen to be percentage of full scale [-100, 100], and the maximum error to a unit step is 1. The values of K_{fe} and K_u are obtained using expressions (17). Figure 5 shows the input families and the linear control surface obtained by using the rule base of Table 1 while satisfying the conditions of linear mapping; E is the error, FE is the fractional derivative of error and u is the output of the fuzzy PD$^\mu$ controller. Note that this result represents the step 2 – replace the conventional controller with an equivalent linear fuzzy controller – of the design procedure.

In order to enhance the performance of the control system we now proceed to step 3 of the design – make the fuzzy controller nonlinear. Thus, after verifying that the linear FF-PD$^\mu$-controller is properly designed, we may adjust the FIS settings such as its style, membership functions and rule base to obtain a desired nonlinear control surface. In this work, we choose to change the fuzzy rule base, as illustrated in Table 2. This rule base is commonly used in fuzzy control systems and consists of 49 rules with 7 linguistic terms (NL – Negative large, NM – Negative medium, NS – Negative small, ZR - Zero, PS – Positive small, PM – Positive medium and PL – Positive large). The membership functions for the premises and consequents of the rules are shown in Figure 6a). With two inputs and one output the input-output mapping of the fuzzy logic controller is described by the nonlinear surface of Figure 6b). For the defuzzication process we use the centroid method.

Figure 7 shows the step responses of both linear and nonlinear fuzzy PD$^\mu$ ($\mu = 0.7$) controllers. We verify that the nonlinear controller improves the system control performance, namely the overshoot and settling time.

For comparison purposes, we also compute the integral of the absolute error (IAE):

$$\text{IAE} = \int_0^t |e(t)| dt \tag{24}$$

For $t = 20$ s we get IAE (linear) = 2.84 and IAE (nonlinear) = 2.00.

(a)　　　　　　　　　　　　　(b)
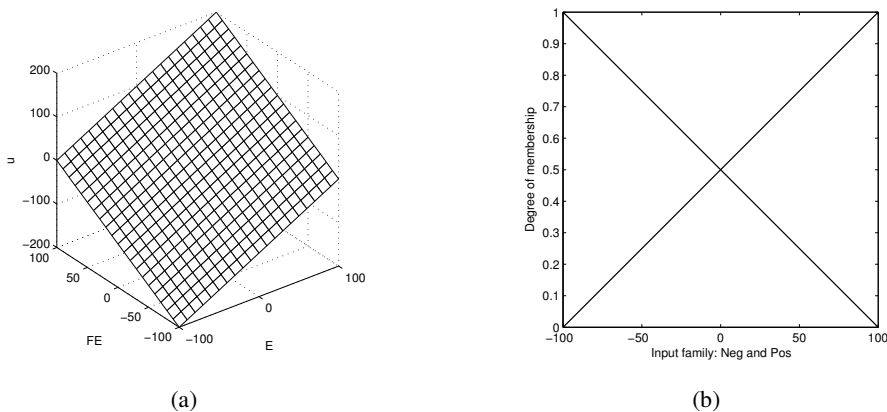
Figure 5. Linear surface (a) with the corresponding input families (b).

Table 2. Fuzzy control rules.

E/FE	NL	NM	NS	ZR	PS	PM	PL
NL	NL	NL	NL	NL	NM	NS	ZR
NM	NL	NL	NL	NM	NS	ZR	PS
NS	NL	NL	NM	NS	ZR	PS	PM
ZR	NL	NM	NS	ZR	PS	PM	PL
PS	NM	NS	ZR	PS	PM	PL	PL
PM	NS	ZR	PS	PM	PL	PL	PL
PL	ZR	PS	PM	PL	PL	PL	PL

The system performance can be further improved. For that, we go to step 4 (and last) of the design procedure – fine tune the controller. The nonlinear fuzzy controller will be adjusted by changing the parameter values of K_e, K_{fe}, and K_u. In this study we propose the use of a genetic algorithm (GA) to fine tune the gains of the controller. A GA is a search technique used in computer science to find approximate solutions in optimization and search problems. GA are a particular class of evolutionary algorithms that use techniques inspired by evolutionary biology such as inheritance, mutation, natural selection, and crossover, established by the Darwin's theory of evolution [19, 38, 41, 32]. The advantage of GA is in their parallelism. GA is travelling in a search space using more individuals than other methods. However, GA also have disadvantages, namely the computational cost, because many times these algorithms are slower than other methodologies.

The GA fitness function corresponds to the minimization of the integral absolute error (IAE) criterion (as defined in (24)):

$$\text{IAE}(K_e, K_{fe}, K_u) = \int_0^\infty |e(t)| dt \tag{25}$$

where (K_e, K_{fe}, K_u) are the fuzzy fractional PD$^\mu$ controller parameters to be optimized.
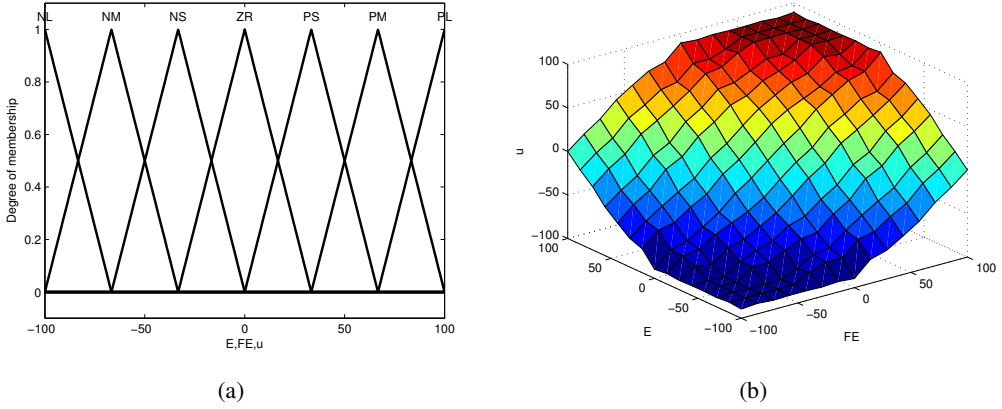
Figure 6. Memberships functions for *E*, *FE* and *u* (a) Nonlinear control surface (b).

In Figure 7, the comparison of the unit-step responses of the closed-loop system with $G_1(s)$ controlled by the linear and nonlinear PD^μ-controllers, and with the optimal nonlinear FF-PD^μ ($\mu = 0.7$) controller is given. We establish the following values for the GA parameters: population size $P = 20$, crossover probability $C = 0.8$, mutation probability $M = 0.05$ and number of generations $N_g = 50$. The interval of the FLC parameters used in the GA optimization are defined around 10% of the nominal parameters obtained with the linear controller. In this case IAE (optimal) = 0.075. As can be seen, the optimal nonlinear controller improves significantly the control system performance, in terms of overshoot, rise time, and settling time, when compared with other fuzzy controllers. In this way, the fuzzy fractional controller provides greater flexibility than the integer/fractional controller and can be used to better adjust the dynamical properties of a control system.

3.3.2. Example 2: Fractional-Order Plant

Many real dynamical processes are modeled by fractional-order transfer functions [50, 44, 25]. Here we consider the fractional-order plant model given in [51]:

$$G_2(s) = \frac{1}{0.8s^{2.2} + 0.5s^{0.9} + 1} \tag{26}$$

An integer-order PD controller and a fractional-order PD^μ-controller were designed in [51]:

$$C_{PD}(s) = K_P + K_D s = 20.5 + 2.7343s \tag{27}$$

$$C_{PD^\mu}(s) = K_P + K_D s^\mu = 20.5 + 3.7343s^{1.15} \tag{28}$$

Figure 8 shows the unit-step responses of the closed-loop fractional-order system with the conventional PD-controller and with the PD^μ-controller for $G_2(s)$. The comparison shows that for satisfactory feedback control of the fractional-order system is better to use a fractional-order controller instead of a classical integer-order controller. Note, however,
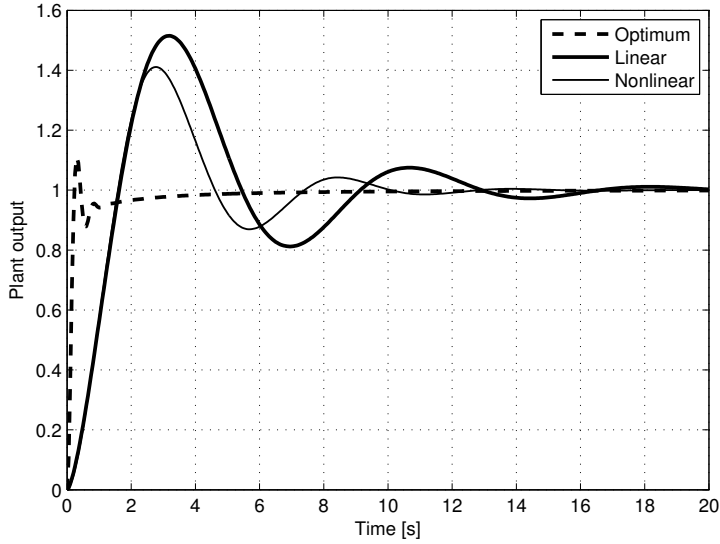
Figure 7. Unit step responses of system with $G_1(s)$ and with the linear, nonlinear and optimum fuzzy fractional PD$^\mu$ ($\mu = 0.7$) controllers.

that the control system presents a steady-state error, since no integral action is employed. In this case, for $t = 6$ s: IAE (PD) = 0.86 and IAE(PD$^\mu$) = 0.55.

Let us now design an equivalent linear FF-PD$^\mu$ controller. As in previous example, we fix $K_e = 100$. The values of K_{fe} and K_u are obtained using expressions (17). The input families and the linear control surface are illustrated in Figure 5. This result represents the step 2 of the design procedure. In order to enhance the performance of the control system we proceed to step 3 of the methodology.

For obtaining the desired surface control, we apply again the nonlinear fuzzy rule base of Table 2. The corresponding membership functions and surface control are shown in Figures 6.

In Figure 8, the comparison of the unit-step responses of the closed-loop system with $G_2(s)$ controlled by the linear and nonlinear FF-PD$^\mu$ ($\mu = 1.15$) controllers is given. We verify that the nonlinear controller improved the overshoot, settling time, and steady-state error, when compared with the linear fuzzy controller. In this case IAE (nonlinear) = 0.40, which is smaller than the linear counterpart.

To further improve the system performance we fine tune the controller (step 4, and last, of the design procedure). The fuzzy controller parameters (K_e, K_{fe}, K_u) are tuned using a GA while minimizing the IAE index (25). Figure 8 shows the unit-step responses of the closed-loop system with $G_2(s)$ controlled with the optimum nonlinear FF-PD$^\mu$ ($\mu = 1.15$) controller. The GA parameters are: population size P=20, crossover probability $C = 0.8$, mutation probability $M = 0.05$ and number of generations $N_g = 25$. The interval of the FLC parameters used in the GA optimization are defined around 10% of the nominal parameters obtained with the linear controller. In this case IAE (optimal) = 0.037. Clearly,
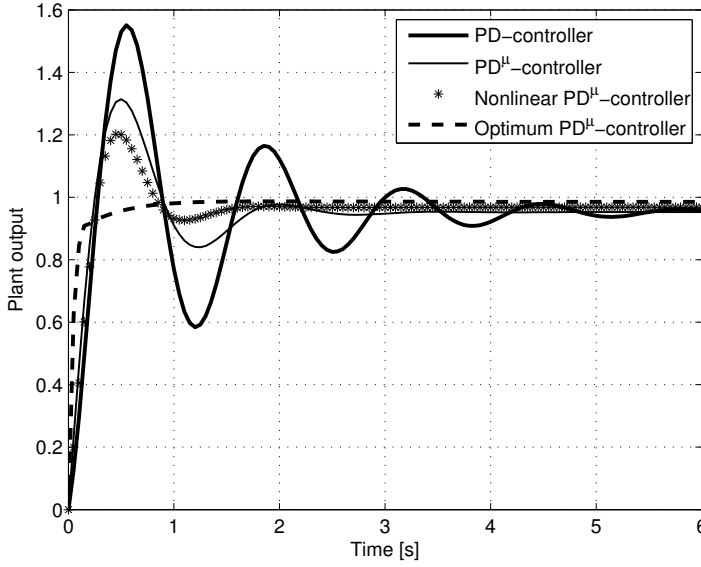
Figure 8. Unit step responses of system with $G_2(s)$ with PD-controller, and with the linear, nonlinear and optimal fuzzy fractional PD$^\mu$ ($\mu = 1.15$) controllers.

the optimal nonlinear controller produced better results than other fuzzy controllers, since the transient response (namely the overshoot, rise time, settling time, and steady-state error) and the error IAE are smaller.

Now, let us consider the FF-PD$^\mu$+I$^\lambda$-controller. In order to test the robustness of the fuzzy controller, we introduce a load disturbance of amplitude $l = -2$ after 8 seconds in system of Figure 1. We use the same (K_p, K_d) parameters of the linear FF-PD$^\mu$ ($\mu = 1.15$) controller and tuned the (K_i, λ) for a satisfactory control response. The final tuned parameters are $(K_i, \lambda) = (10, 0.8)$. With $K_e = 100$, and using (21) we obtain K_{fe}, K_u, and K_{fie} of the fuzzy controller.

Figure 9 shows the step and load responses of closed-loop system with FF-PD$^\mu$+I$^\lambda$ controller, $(\mu, \lambda)=(1.15, 0.8)$, for the linear and nonlinear control surfaces. We observe the better response of the fuzzy controller to the reference and disturbance inputs with the non-linear rule base (Table 2) compared to their linear counterpart (Table 1). If further improved is needed, we can fine tune it using the GA while minimizing the IAE criterion (25), as done in previous examples. Once more, we demonstrate the robustness and effectiveness of these controllers.

4.   Optimal Fuzzy Fractional PID Controllers

In this section we design optimal fuzzy fractional PID controllers by using PSO algo-rithm [39, 31, 29, 30, 28].
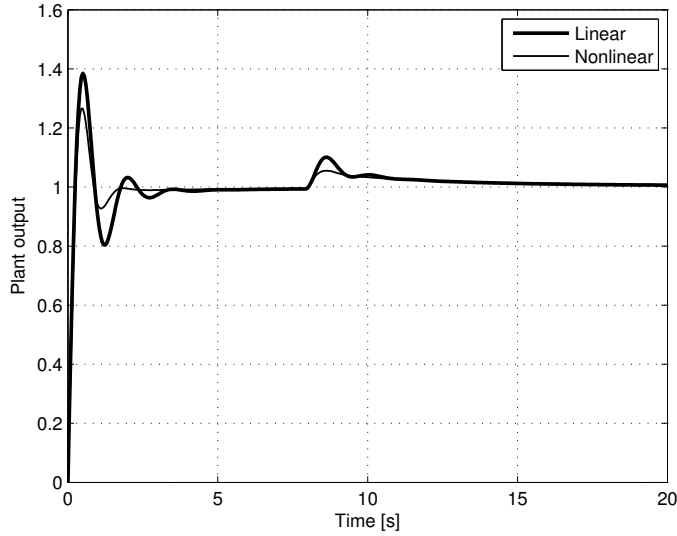
Figure 9. Unit-step and load responses of the fractional control system with $G_2(s)$ and with the linear and nonlinear FF-PD$^\mu$+I$^\lambda$ controllers.

4.1. Approximations by Rational Functions

In this study we adopt discrete integer-order approximations to the fundamental element s^α ($\alpha \in \Re$) of a fractional-order control (FOC) strategy. The usual approach for obtaining discrete equivalents of continuous operators of type s^α adopts the Euler, Tustin and Al-Alaoui generating functions [10, 54, 14].

It is well known that rational-type approximations frequently converge faster than polynomial-type approximations and have a wider domain of convergence in the complex domain. Thus, by using the Euler operator $w(z^{-1}) = (1-z^{-1})/T_c$, and performing a power series expansion of $[w(z^{-1})]^\alpha = [(1-z^{-1})/T_c]^\alpha$ gives the discretization formula corresponding to the Grünwald-Letnikov definition (4):

$$D^\alpha\left(z^{-1}\right) = \left(\frac{1-z^{-1}}{T_c}\right)^\alpha = \sum_{k=0}^{\infty}\left(\frac{1}{T_c}\right)^\alpha (-1)^k \left(\begin{array}{c} \alpha \\ k \end{array}\right) z^{-k} = \sum_{k=0}^{\infty} h^\alpha(k) z^{-k} \quad (29)$$

where T_c is the sampling period and $h^\alpha(k)$ is the impulse response sequence.

A rational-type approximation can be obtained through a Padé approximation to the impulse response sequence $h^\alpha(k)$, yielding the discrete transfer function:

$$H\left(z^{-1}\right) = \frac{b_0 + b_1 z^{-1} + \ldots + b_m z^{-m}}{1 + a_1 z^{-1} + \ldots + a_n z^{-n}} = \sum_{k=0}^{\infty} h(k) z^{-k} \quad (30)$$

where $m \leq n$ and the coefficients a_k and b_k are determined by fitting the first $m + n + 1$ values of $h^\alpha(k)$ into the impulse response $h(k)$ of the desired approximation $H(z^{-1})$.

Thus, we obtain an approximation that matchs the desired impulse response $h^\alpha(k)$ for the first $m + n + 1$ values of k [10]. Note that the above Padé approximation is obtained by considering the Euler operator but the determination process will be exactly the same for other types of discretization schemes [10].

4.2.   Fuzzy Fractional Control System

Figure 10 presents the block diagram of the fuzzy control system to be analyzed, where $G(s)$ is the process transfer function. The gains of the fuzzy fractional PD$^\beta$+I controller will be tuned through the application of a PSO algorithm in order to achieve a superior control performance of system of Figure 10. Note the presence of a saturation nonlinearity.

The generalized PI$^\alpha$D$^\beta$ controller is given here as [51]:

$$G_c\left(s\right) = \frac{U(s)}{E(s)} = K_p + \frac{K_i}{s^\alpha} + K_d s^\beta, \qquad \alpha, \beta > 0 \tag{31}$$

where the fractional-order operators are implemented by rational approximations of type (30).

In the system of Figure 10, we apply a fuzzy logic control (FLC) for the PD$^\beta$ actions and the integral of the error is added to the output in order to find a fuzzy PD$^\beta$ + I controller [6]. In fact, we can have a fuzzy PD$^\beta$+I$^\alpha$ controller, *i.e.* an added fractional integral action, as presented in [5]. This is the FLC of Figure 4 with an integer integral action in the feedforward path ($\alpha = 1$). The block diagram of Figure 11 illustrates the configuration of the proposed fuzzy controller. In this controller, the control actions are the error e, the fractional derivative of e and the integral of e. The U represents the controller output. Also, the controller has four gains to be tuned, K_e, K_{ie}, K_{ce} corresponding to the inputs and K_u to the output.

The control action U is generally a nonlinear function of error E, fractional change of error CE, and integral of error IE:

$$U\left(k\right) = [f\left(E, CE\right) + IE]\,K_u = \left[f\left(K_e e\left(k\right), K_{ce} D^\beta e\left(k\right)\right) + K_{ie} Ie\left(k\right)\right] K_u \tag{32}$$

where D^β is the discrete fractional derivative implemented as rational approximation (30) using the Euler scheme (29); the integral of error is calculated by rectangular integration:

$$I\left(z^{-1}\right) = \frac{T_c}{1 - z^{-1}} \tag{33}$$

To further illustrate the performance of the fuzzy PD$^\beta$+I a saturation nonlinearity is included in the closed-loop system of Figure 10, and inserted in series with the output of the fuzzy controller. The saturation element is defined as:

$$n\left(u\right) = \left\{ \begin{array}{ll} u, & |u| < \delta \\ \delta\,sign\left(u\right), & |u| \geq \delta \end{array} \right. \tag{34}$$

where u and n are respectively the input and the output of the saturation block and $sign(u)$ is the signum function.
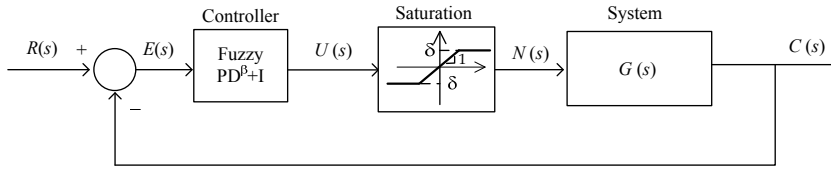
Figure 10. Block diagram of the fuzzy control system.
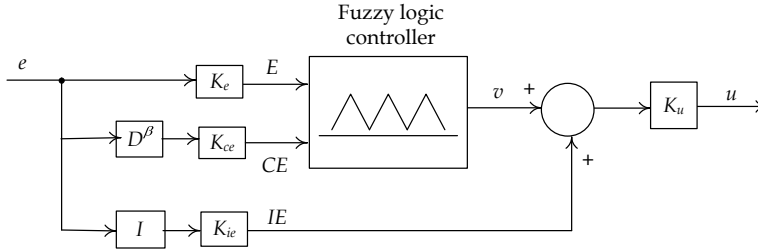
Figure 11. Fuzzy PD$^\beta$ + I controller.

Here we give an emphasis of the proposed FLC presented in Figure 11. The basic structure for FLC is illustrated in Figure 2. The fuzzy rule base, which reflects the collected knowledge about how a particular control problem must be treated, is one of the main components of a fuzzy controller. The other parts of the controller perform make up the tasks necessary for the controller to be efficient. The rule base for the fuzzy PD$^\beta$+I controller is presented in Table 2. The membership functions for the premises and consequents of the rules are shown in Figure 12a). With two inputs and one output the input-output mapping of the fuzzy logic controller is described by a nonlinear surface, presented in Figure 12b).

The fuzzy controller will be adjusted by changing the parameter values of K_e, K_{ce}, K_{ie} and K_u. The fuzzy inference mechanism operates by using the product to combine the conjunctions in the premise of the rules and in the representation of the fuzzy implication. For the defuzzification process we use the centroid method.

4.3.   Particle Swarm Optimization

In this study we use a particle swarm optimization (PSO) algorithm for the tuning of a fractional order controller, applied to a system. The PSO is one of the latest evolutionary techniques developed by Dr. Eberhart and Dr. Kennedy in 1995, inspired by social behaviour of bird flocking or fish schooling. The PSO scheme optimizes searching by virtue of the swarm intelligence produced by the cooperation and competition among the particles of a species [20, 35, 21]. The social system is discussed through the collective behaviours of simple individuals interacting with their environment and each other. Examples of this are the bird flock or fish school. Some applications of PSO are found in the field of nonlinear dynamical systems, data analysis, electrical engineering, function optimization, artificial neural network training, fuzzy control and many others in real world applications [20, 21, 49, 55, 28].

It is important to mention that a reliable execution and analysis of a PSO usually re-
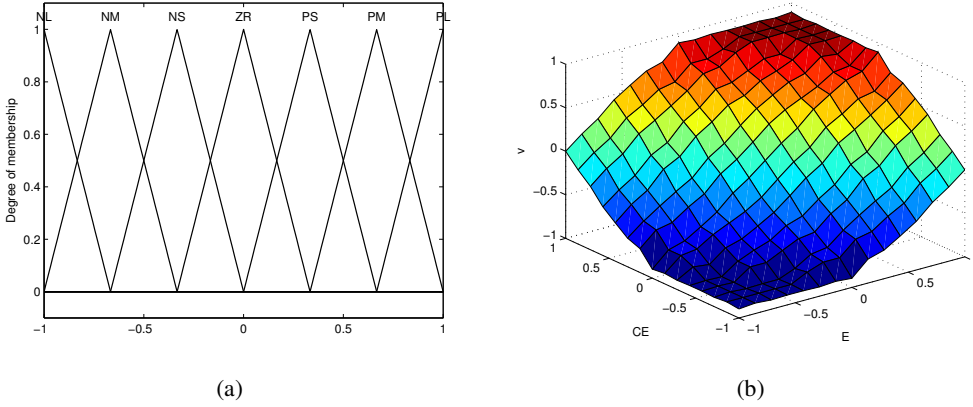
Figure 12. Memberships functions for *E*, *CE* and *v* (a) Nonlinear control surface (b).

quires a large number of simulations to provide that stochastic effects have been properly considered. In the PSO algorithm, all particles represent a potential solution to a problem, which is performed by adjusting their position taking into account both personal and group experiences [21, 28, 52]. In each iteration, the velocity (v) is actualized by expression (35a). The new particle position (cp_{k+1}) is found by adding their actual position with the new velocity, as shown in (35b).

$$v_{k+1} = w * v_k + c_1 * r_1(lbp - cp_k) + c_2 * r_2 * (gbp_k - cp_k) \tag{35a}$$

$$cp_{k+1} = cp_k + v_{k+1} \tag{35b}$$

where ω is the inertia weight, c_1 and c_2 are the individual and sociality weights coefficients for modelling attractive forces from the local and global best, respectively; r_1 and r_2 are aleatory numbers between [0, 1], lbp is the local best position, cp is the current position, and gbp is the global best position [28]. The inertia term, forces the particle to move in the same direction as before by adjusting the old velocity. The cognitive term (personal best), forces the particle to go back to the previous best position. On the other hand, the social learning term (global best), forces the particle to move to the best previous position of its neighbors. The PSO optimizes an objective function by iteratively improving a swarm of solutions, called particles, based on special management of memory. Each particle is modified by referring to the memory of individual swarm's best information. Due to the collective intelligence of these particles, the swarm is able to repeatedly improve its best observed solution and converging to an optimum.

4.4.   Objective Function for Optimization

The optimization fitness function corresponds to the minimization of the integral time absolute error (ITAE) criterion, that measure the response error as defined as [29]:

$$J\left(K_e, K_{ce}, K_{ie}, K_u\right) = \int\limits_0^\infty t\left|r\left(t\right) - c\left(t\right)\right| dt \tag{36}$$

where $(K_e, K_{ce}, K_{ie}, K_u)$ are the PD$^\beta$+I controller parameters to be optimized. Other criteria are possible like the integral time square error (ITSE), integral absolute error (IAE), integral square error (ISE), among others [31, 34, 17, 16].

4.5.   Case Studies

We analyze the closed-loop system of Figure 10 with a fuzzy fractional PD$^\beta$ + I controller (Figure 11). In all the experiments, the fractional order derivative D$^\beta$ in scheme of Figure 11 is implemented by using a 4th order Padé discrete rational transfer function $(m = n = 4)$ of type (30). It is used a sampling period of $T_c = 0.1$ s. The PD$^\beta$+I controller is tuned through the minimization of the ITAE (36) using a PSO. We use $\delta = 15.0$. We establish the following values for the PSO parameters: population number $PN = 25$, $c_1 = c_2 = 1$, $\omega = 0.9$ and a maximum number of iterations $I_{Max} = 50$. For guarantee that stochastic effects are properly considered, the experiments consist on executing the PSO 10 times, and we get the best result, *i.e.* the simulation that leads to the smaller J, and consequently a combination of controller gains, that leads to a better transient and steady state responses.

4.5.1.   Example 1. High-Order Transfer Function

In the first case, we compare a fuzzy fractional PD$^\beta$+I controller which leads to the lower error ($\beta = 0.9$), with a fuzzy integer PID controller ($\beta = 1$). Figure 13a) shows the unit step responses of both controllers. The plant system $G_3(s)$ used is represented by a high$-$order transfer function [1]:

$$G_3(s) = \frac{1}{(s + 1)(1 + 0.5s)(1 + 0.5^2s)(1 + 0.5^3s)} \tag{37}$$

The controller parameters, corresponding to the minimization of the ITAE index, lead to the values for the fuzzy integer PID controller: $\{K_e, K_{ce}, K_{ie}, K_u\} \equiv \{$ 1.0705, 3.8194, 0.4206, 4.4784 $\}$, with $J = 2.3763$, and for the fuzzy fractional PD$^\beta$+I controller to the following values: $\{K_e, K_{ce}, K_{ie}, K_u\} \equiv \{0.7193, 0.3551, 0.2702, 3.2029\}$, with $J = 0.8409$. These values lead us to conclude that the fuzzy fractional order controller produced better results than the integer one, since the transient response (namely, the settling time, rise time and overshoot) and the error J are smaller, as can be seen in Figure 13a). Figure 13b) shows the ITAE error as function of β. The graph shows that lowest error is produced for $\beta = 0.9$. We also see that the fractional controller is always better than its integer version (considering $0 < \beta \le 1$).

Figure 14 illustrates the variation of FLC parameters (K_e, K_{ce}, K_{ie}, K_u) as function of the order's derivative β, while Figure 15 shows the variation of the transient response parameters, namely the settling time t_s, rise time t_r, peak time t_p and overshoot $ov(\%)$ *versus* β, for the closed-loop step response, when minimizing the ITAE index. The variation of FLC parameters and the transient response parameters reveal a smooth variation with β.

(a)

(b)
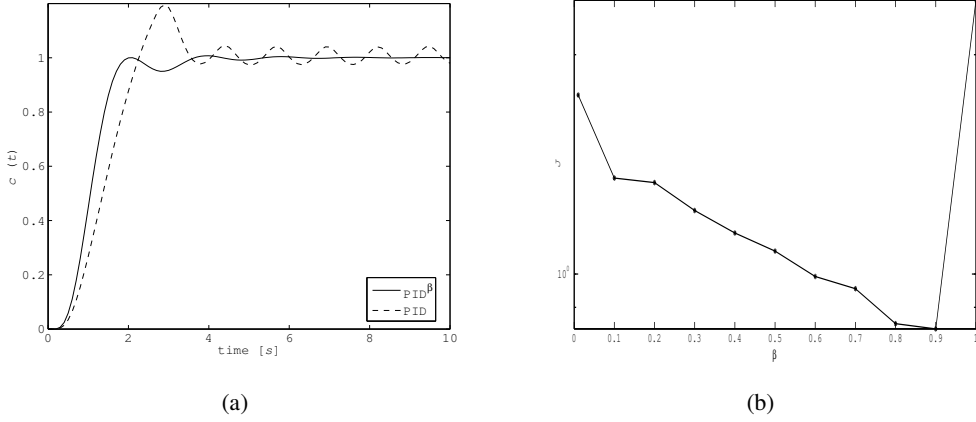
Figure 13. Step responses of the closed-loop system with a fuzzy PD+I and PD$^\beta$+I ($\beta = 0.9$) controllers (a) Error J versus β for $G_3(s)$ (b).

4.5.2.   Example 2. Non-Minimum Phase System

In a second experiment, we consider a fuzzy PD$^\beta$+I controller which leads for lower error to $\beta = 0.8$, applied to a process $G_4(s)$ represented by a non−minimum system given by the transfer function (38) [1].

$$G_4(s) = \frac{1 - 5s}{(s+1)^3} \tag{38}$$

Once again, we consider for comparison the corresponding integer version ($\beta = 1$). Figure 16a) shows the unit step responses of both controllers.

The controller parameters, corresponding to the minimization of the ITAE index, lead to the values for the fuzzy integer controller: $\{K_e, K_{ce}, K_{ie}, K_u\} \equiv \{$ 0.9953, 1.3058, 0.4360, 0.1991 $\}$, with $J = 70.9016$, and for the fuzzy fractional controller: $\{K_e, K_{ce}, K_{ie}, K_u\} \equiv \{0.0873, 0.0569, 0.0417, 2.5740\}$, with $J = 35.4189$. These values lead us to remain the previously conclusions drawn for $G_3(s)$, namely that the fuzzy fractional order controller produced better results than the integer one, since the transient response (in particular the settling time, rise time and overshoot) and the error J are smaller. Figure 16b) shows the ITAE error as function of β. The graph shows a lowest error for $\beta = 0.8$. Also, the fractional controller (for $0 < \beta \leq 1$) is always better than the conventional fuzzy PID controller.

Figure 17 illustrates the variation of FLC parameters (K_e, K_{ce}, K_{ie}, K_u) as function of the order's derivative β, while Figure 18 shows the variation of the transient response parameters, namely t_s, t_r, t_p and $ov(\%)$ *versus* β, for the closed-loop step response, when minimizing the ITAE index. The variation of FLC parameters and the transient response parameters reveal a smooth variation with β.
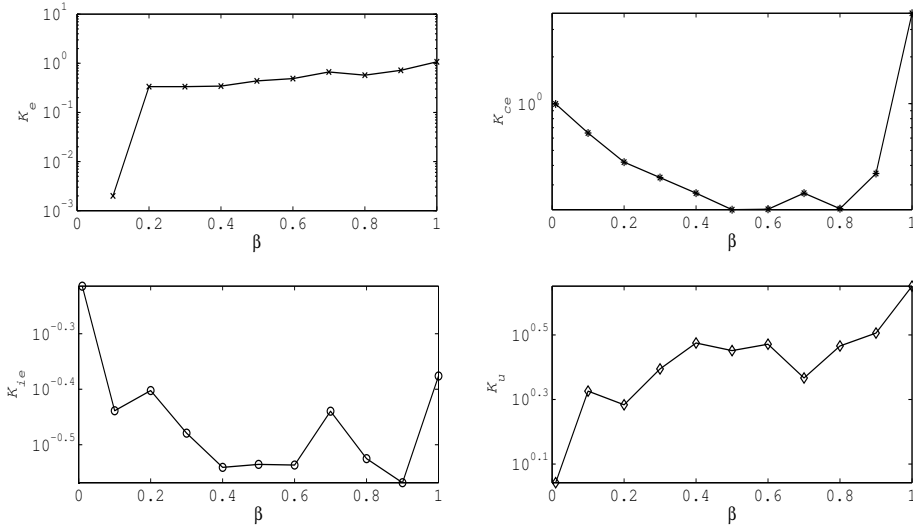
Figure 14. The PD$^\beta$+I parameters (K_e, K_{ce}, K_{ie}, K_u) $versus$ β for $G_3(s)$.

4.5.3. Example 3. Second-Order Transfer Function With Time Delay

In a third experiment, we consider a fuzzy PD$^\beta$+I controller which leads for lower error to $\beta = 0.9$, applied to a process $G_5(s)$ represented by a second-order transfer function with a time delay (39).

$$G_5(s) = \frac{e^{-s}}{4s^2 + 4s + 1} \tag{39}$$

Once more time, we consider for comparison the corresponding integer version ($\beta = 1$). Figure 19 a) shows the unit step responses of both controllers.

The controller parameters, corresponding to the minimization of the ITAE index, lead to the values for the fuzzy integer controller: $\{K_e, K_{ce}, K_{ie}, K_u\} \equiv \{1.1616, 1.0076, 0.1993, 1.3628\}$, with $J = 8.3228$, and for the fuzzy fractional controller: $\{K_e, K_{ce}, K_{ie}, K_u\} \equiv \{0.6600, 0.7851, 0.1171, 2.7525\}$, with $J = 5.8728$. These values lead us to remain the previously conclusions drawn for $G_3(s)$ and $G_4(s)$, namely that the fuzzy fractional order controller produced better results than the integer ones, since the transient response (in particular the settling time, rise time and overshoot) and the error J are smaller. Figure 19b) shows the ITAE error as function of β. The graph shows that for this process we have a lower error for $\beta = 0.9$.

Figure 20 illustrates the variation of FLC parameters (K_e, K_{ce}, K_{ie}, K_u) as function of the order's derivative β, while Figure 21 shows the variation of the transient response parameters, namely t_s, t_r, t_p and $ov(\%)$ $versus$ β, for the closed-loop step response, when minimizing the ITAE index. The variation of FLC parameters and the transient response parameters reveal a smooth variation with β.

In conclusion, with the fuzzy fractional PD$^\beta$+I controller we get the best controller tuning, superior to the performance revealed by the integer-order scheme. Moreover, we prove the effectiveness of this control structure when used in systems with time delay. In fact, sys-
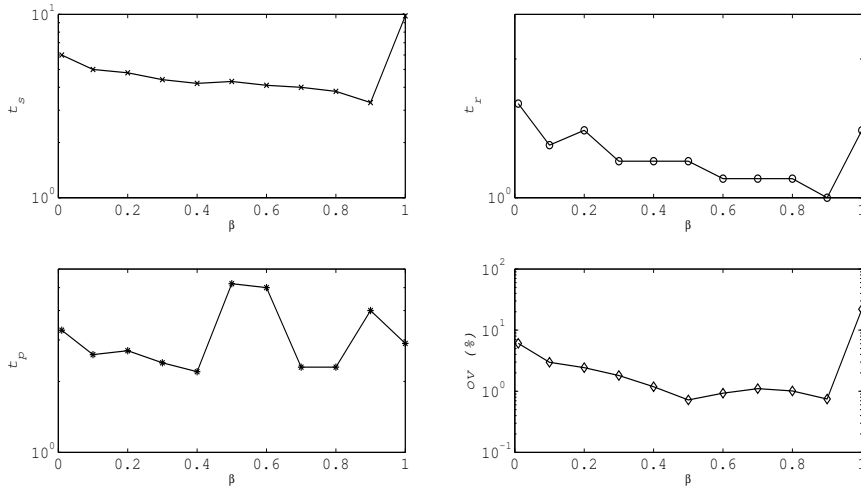
Figure 15. Parameters t_s, t_r, t_p, $ov(\%)$ *versus* β of the step responses of the closed-loop system with $G_3(s)$ and with a fuzzy PD$^\beta$+I controller.
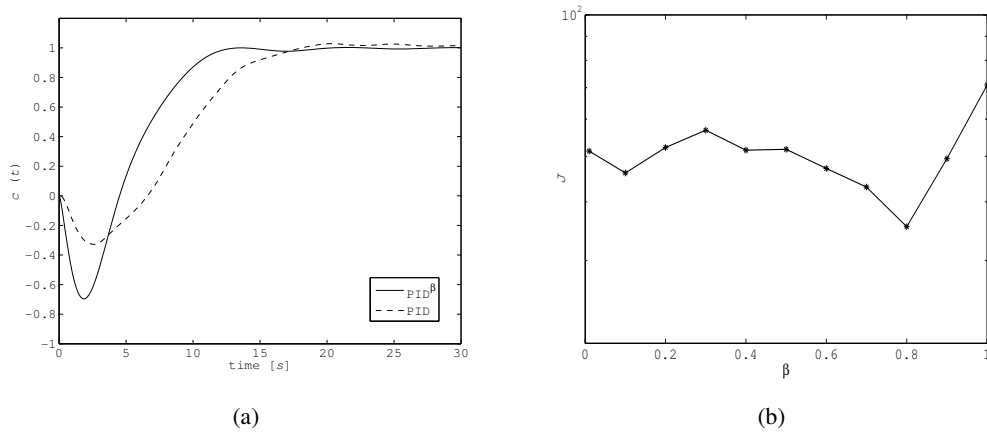
Figure 16. Step responses of the closed-loop system with fuzzy PD+I and PD$^\beta$+I ($\beta = 0.8$) controllers (a) Error J versus β for $G_4(s)$ (b).

tems with time delay are more difficult to be controlled with the classical methodologies, however the proposed algorithm reveals that is very effective in the control of this type of systems.

4.6. Influence of Order of Rational Approximations

Here we analyze the influence of the order of rational approximations used in the simulations for different values of $m = n$. In the experiments, the controller performance is evaluated for several values of order $m = n = \{1, 2, ..., 10\}$. For this study we use the
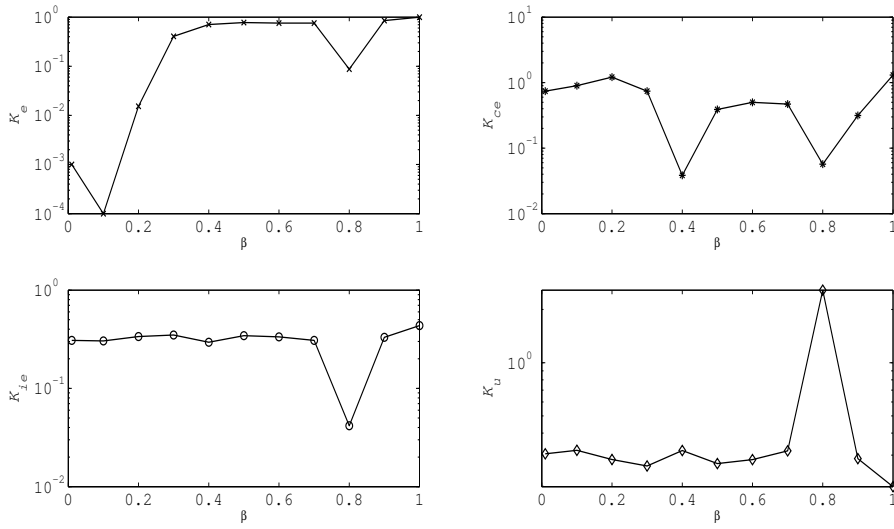
Figure 17. The PD$^{\beta}$+I parameters (K_e, K_{ce}, K_{ie}, K_u) $versus$ β for $G_4(s)$.
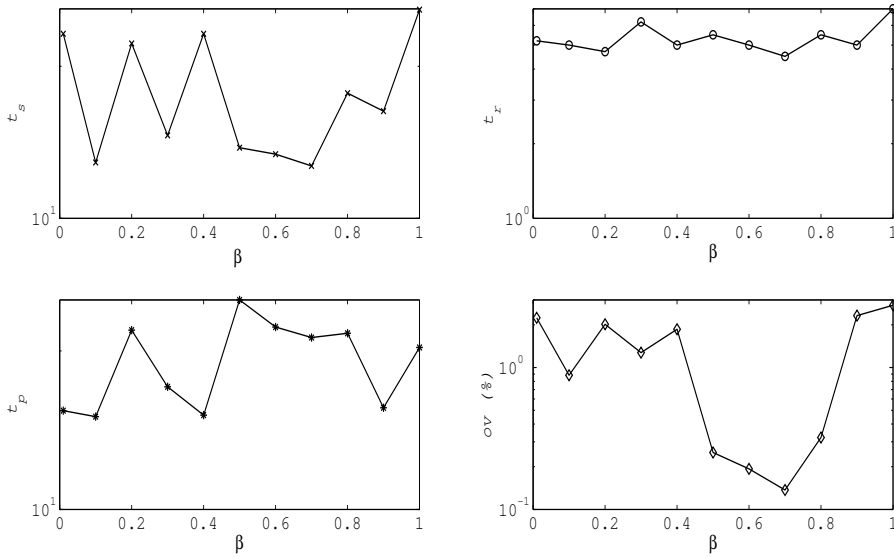
Figure 18. Parameters t_s, t_r, t_p, $ov(\%)$ $versus$ β of the step responses of the closed-loop system with $G_4(s)$ and with a fuzzy PD$^{\beta}$+I controller.

second-order transfer function with time delay $G_5(s)$.

Figure 22 shows the unit step responses of PD$^{\beta}$+I controller for various orders of approximations m, and for the best case of 10 experiments, $i.e.$ the simulation that leads to the smaller J. We observe that the responses are very similar varying slightly with order m.
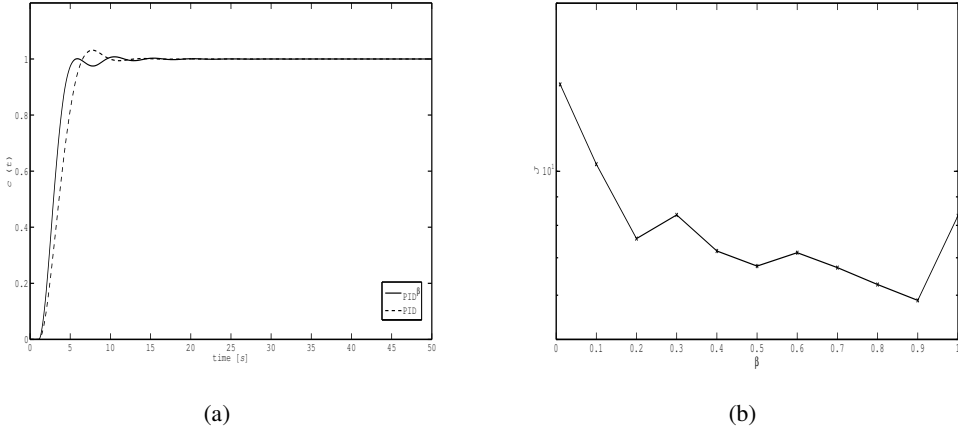
(a)

(b)

Figure 19. Step responses of the closed-loop system with fuzzy PD+I and PD$^\beta$+I ($\beta = 0.9$) controllers (a) Error J versus β for $G_5(s)$ (b).
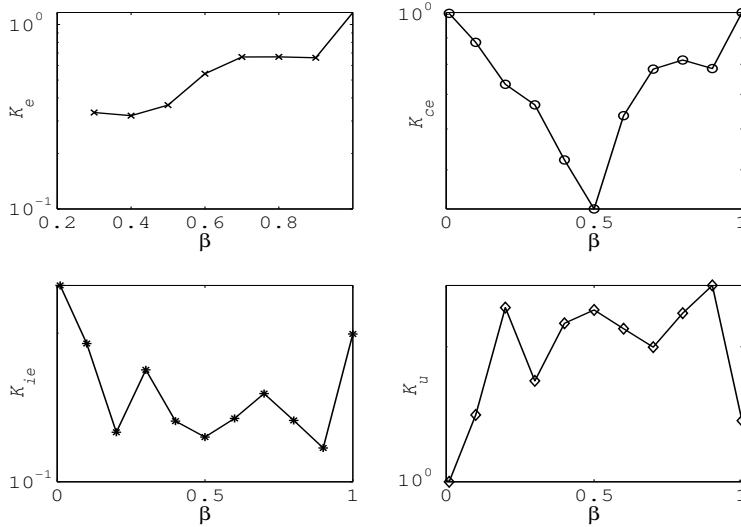
Figure 20. The PD$^\beta$+I parameters (K_e, K_{ce}, K_{ie}, K_u) $versus$ β for $G_5(s)$.

For this process we have a lower error for β between 0.8 and 0.9 as function of m. These facts can also be seen in Figure 23 that shows the ITAE error as function of β and m. From the graph, it is clear that the best approximations are found for $2 \leqslant m \leqslant 5$.

Figure 24 illustrates the variation of FLC parameters (K_e, K_{ce}, K_{ie}, K_u) as function of order's derivative β and order of approximation m, while Figure 25 shows the variation of the transient response specifications, namely t_s, t_r, t_p and $ov(\%)$ $versus$ β and m, for the closed-loop step response. It is observed that the FLC parameters and the transient response specifications varies with β and m. For instance, the system overshoot is lower for relatively high values of β and wide range of order's $2 \leqslant m \leqslant 10$, as seen in Figure 25.
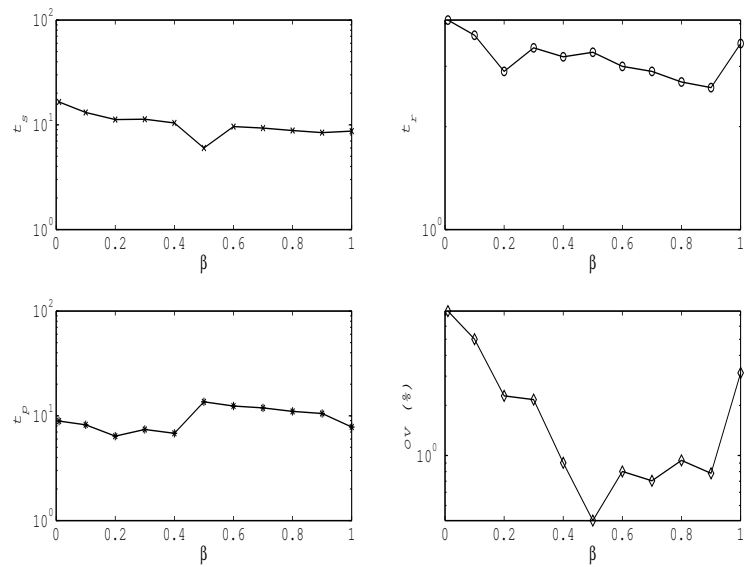
Figure 21. Parameters t_s, t_r, t_p, *ov*(%) *versus* β of the step responses of the closed-loop system with $G_5(s)$ and with a fuzzy PD$^\beta$+I controller.
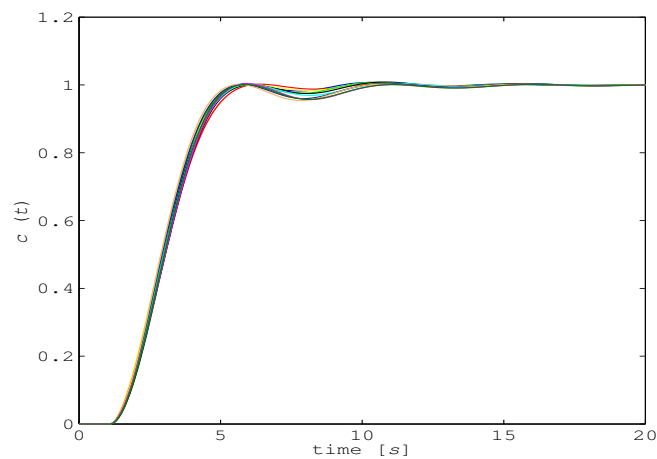
Figure 22. Step responses of the closed-loop system with fuzzy PD$^\beta$+I controller *versus* order m for $G_5(s)$.

The same analysis can be done for other parameters.
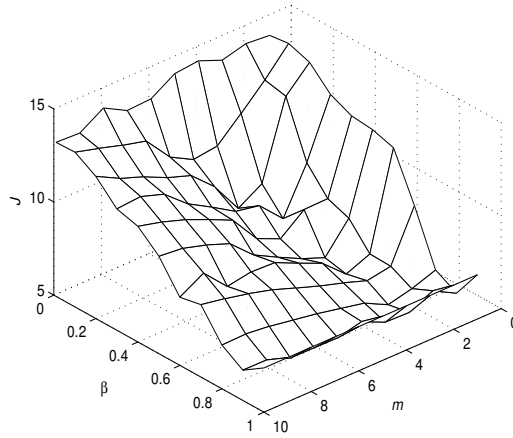
Figure 23. Error $J\ versus\ \beta$ and m for $G_5(s)$.
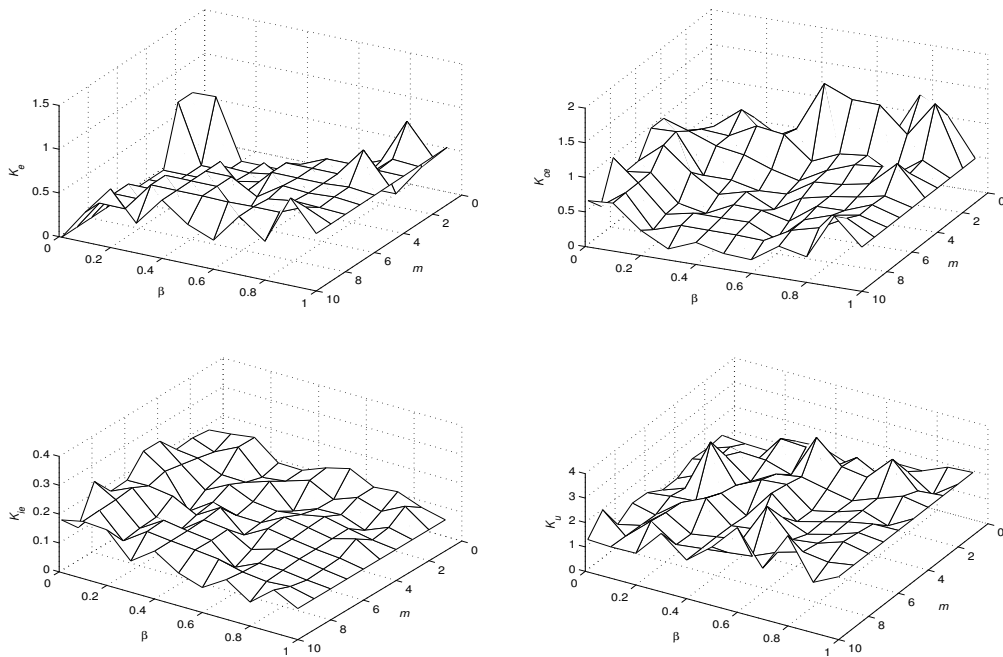
Figure 24. The PD$^\beta$+I parameters (K_e, K_{ce}, K_{ie}, K_u) $versus$ β and m for $G_5(s)$.

5. Conclusion

This chapter has presented several fuzzy control structures with fractional-order derivative and integral actions combined to form a PID-type controller. Comparison with conventional fuzzy and PID controllers is performed to illustrate the effectiveness and robustness of the proposed algorithms. Another distinguished feature of this study is the use of discrete
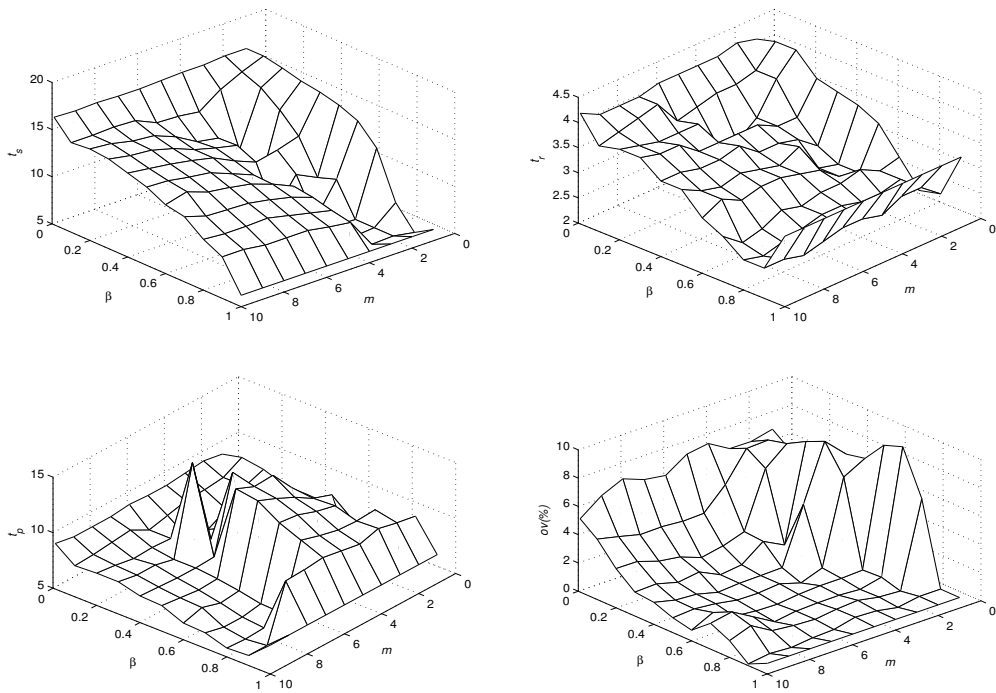
Figure 25. Parameters t_s, t_r, t_p, $ov(\%)$ *versus* β and m of the step responses of the closed-loop system with $G_5(s)$ and with a fuzzy PD$^\beta$+I controller.

fuzzy fractional-order controllers in the form of series and rational approximations which reveals useful for a digital implementation of these algorithms.

In the first part of chapter, a methodology for tuning fuzzy fractional PID controllers is introduced. This methodology is simple and effective and can be used to replace an existent integer/fractional PID controller in order to enhance system performance. Also, it was demonstrated that, with this approach, the designed controllers are equivalent to the conventional fractional PD/PID controllers by using a linear input-output mapping of the rule base of the fuzzy fractional controller. Moreover, by making the controller nonlinear, the performance of the control system proves to be, in most systems, better than its linear counterpart.

In the second part of chapter, were developed optimal fuzzy fractional PID controllers in which the parameters were tuned through a PSO algorithm. A nonlinear fuzzy control system with saturation in actuator is analyzed. In general, the control strategies presented, give better results than those obtained with conventional integer control structures, showing, once more, its effectiveness in the control of nonlinear systems. An analysis study regarding the influence of order of discrete rational approximations is also provided.

Certainly, the incorporation of fuzzy reasoning into fractional-order controllers will increase the applicability of these controllers.

References

[1] Kiam Heong Ang and Gregory Chong, *PID control system analysis, design, and technology*, IEEE Transactions on Control Systems Technology 13 (2005), 559–576.

[2] K. J. Astrom and T. Hagglund, *PID controllers: Theory, design, and tuning*, Instrument Society of America, USA, 1995.

[3] Ramiro S. Barbosa, *On linear fuzzy fractional PD and PD+I controllers*, Proceedings of FDA'10, 4th IFAC Workshop Fractional Differentiation and its Applications (Badajoz, Spain), October 18-20, pp. 1–6.

[4] Ramiro S. Barbosa and Isabel S. Jesus, *Application of fuzzy fractional PD+I controllers tuned by a genetic algorithm*, 39th Annual Conference of the IEEE Industrial Electronics society-IEEE-IECON'13 (2013), 3333–3338.

[5] ———, *A methodology for the design of fuzzy fractional PID controllers*, 10th International Conference on Informatics in Control, Automation and Robotics - ICINCO 2013 (2013), 276–281.

[6] Ramiro S. Barbosa, Isabel S. Jesus, and Manuel F. Silva, *Fuzzy reasoning in fractional-order PD controllers*, Proceedings of AIC'10, 10th WSEAS International Conference on Applied Informatics and Communications - New Aspects of Applied Informatics, Biomedical Electronics Informatics and Informatics and Communications (Taipei, Taiwan), August 20-22, 2010, pp. 252–257.

[7] Ramiro S. Barbosa, J. A. Tenreiro Machado, and Isabel M. Ferreira, *Tuning of PID controllers based on bode's ideal transfer function*, Nonlinear Dynamics 38 (2004), 305–321.

[8] ———, *Least-squares design of digital fractional-order operators*, Proceedings of the First IFAC Workshop on Fractional Differentiation and its Applications (FDA'04) (Bordeaux, France), July 19-21, 2004, pp. 434–439.

[9] ———, *Pole-zero approximations of digital fractional-order integrators and differentiators using signal modeling techniques*, 16th IFAC World Congress (Prague, Czech Republic), July 4-8, 2005.

[10] Ramiro S. Barbosa, J. A. Tenreiro Machado, and Manuel F. Silva, *Time domain design of fractional differintegrators uing least-squares*, Signal Processing 86 (2006), 2567–2581.

[11] ———, *Discretization of complex-order algorithms for control applications*, Journal of Vibration and Control 14 (2008), no. 9/10, 1349–1361.

[12] James Carvajal, Guanrong Chen, and Haluk Ogmen, *Fuzzy PID controller: Design, performance evaluation, and stability analysis*, Journal of Information Science 123 (2000), 249–270.

[13] Y. Q. Chen and B. M. Vinagre, *A new IIR-type digital fractional order differentiator*, Signal Processing 83 (2003), no. 11, 2359–2365.

[14] Y. Q. Chen, B. M. Vinagre, and I. Podlubny, *Continued fraction expansion approaches to discretizing fractional order derivatives-an expository review*, Nonlinear Dynamics 38 (2004), 155–170.

[15] YangQuan Chen and Kevin L. Moore, *Relay feedback tuning of robust PID controllers with iso-damping property*, IEEE Transactions on systems, Man, and Cybernetics-Part B: Cybernetics 35 (1) (2005), 23–31.

[16] S. Das, I. Pan, and S. Das, *Performance comparison of optimal fractional order hybrid fuzzy PID controllers for handling oscillatory fractional order processes with dead time*, ISA Transactions 52 (2013), 550–566.

[17] S. Das, I. Pan, and A. Gupta, *A novel fractional order fuzzy PID controller and its optimal time domain tuning based on integral performance indices*, Engineering Applications of Artificial Intelligence 25 (2012), 430–442.

[18] H. Dekavari, R. Ghaden, A. Ranjbar, and S. Momani, *Fuzzy fractional order sliding mode controller for nonlinear systems*, Comunications in Nonlinear Sicence and Numerical Simulation 15 (2010), no. 4, 963–978.

[19] Goldberg E., *Genetic algorithms in search optimization and machine learning*, Addison-Wesley, 1989.

[20] R. C. Eberhart and J. Kennedy, *A new optimizer using particle swarm theory*, Sixth International Symposium on Micro Machine and Human Science (1995), 39–43.

[21] R. C. Eberhart and Y. Shi, *Particle swarm optimization: developments, applications and resources*, Congress on Evolutionary Computation (2001).

[22] I. Eker and Torun Yunis, *Fuzzy logic control to be conventional methods*, Energy Coversion and Management 47 (2006), 377–394.

[23] S. Glichet and L. Foulloy, *Fuzzy controllers: Synthesis and equivalences*, IEEE Transactions on Fuzzy Systems 3 (1995), no. 2, 140–148.

[24] Monson H. Hayes, *Statistical digital signal processing and modeling*, Wiley & Sons, New York, 1996.

[25] R. Hilfer, *Applications of fractional calculus in physics*, World Scientific, Singapore, 2000.

[26] J. Jantzen, *Foundations of fuzzy control*, Wiley and Sons, Chichester, England, 2007.

[27] David F. Jenkins and Kevin M. Passino, *An introduction to nonlinear analysis of fuzzy control systems*, Engineering and Technology 7 (1999), no. 1, 75–103.

[28] Isabel S. Jesus, *Application of PSO algorithm for the study of fractional order electrical potential*, 18th IFAC World Congress - IFAC-WC'11 (2011), 10812–10817.

[29] Isabel S. Jesus and Ramiro S. Barbosa, *Application of fuzzy fractional PD+I controllers tuned by a genetic algorithm*, 39th Annual Conference of the IEEE Industrial Electronics society-IEEE-IECON'13 (2013), 3333–3338.

[30] ———, *Tuning of fuzzy fractional PD+I controllers by genetic algorithm*, 10th International Conference on Informatics in Control, Automation and Robotics - ICINCO 2013 (2013), 282–287.

[31] Isabel S. Jesus and J. A. Tenreiro Machado, *Application of fractional calculus in the control of heat systems*, Journal of Advanced Computational Intelligence and Intelligent informatics 11(9) (2007), 1086–1091.

[32] ———, *Implementation of fractional-order electromagnetic potential through a genetic algorithm*, Journal of Communications in Nonlinear Science and Numerical Simulation 14 (2009), 1838–1843.

[33] Isabel S. Jesus, J. A. Tenreiro Machado, and Ramiro S. Barbosa, *Fractional order nonlinear control of heat system*, 13rd workshop on Fractional Differentiation and its Applications - IFAC-FDA'08 (Ankara, Turkey), 2008.

[34] Isabel S. Jesus, J. T. Machado, and Ramiro S. Barbosa, *On the fractional order control of heat systems*, Intelligent Engineering Systems and Computational Cybernetics, Springer, Netherlands, 2008.

[35] J. Kennedy and R. C. Eberhart, *Particle swarm optimization*, IEEE international conference on neural networks IV (1995), 1942–1948.

[36] C. C. Lee, *Fuzzy logic in control systems: fuzzy logic controller-part I and II*, IEEE Transactions on System Man, and Cybernetics-Part B: Cybernetics 20 (1990), no. 2, 404–435.

[37] H.-H Li and H. B. Gatland, *Conventional fuzzy control and its enhancement*, IEEE Transactions on System Man, and Cybernetics-Part B: Cybernetics 26 (1996), no. 5, 791–797.

[38] Mitchell M., *An introduction to genetic algorithms*, SMIT Press, 1998.

[39] J. A. Tenreiro Machado, *Analysis and design of fractional-order digital control systems*, SAMS Journal of Systems Analysis, Modelling and Simulation 27 (1997), 107–122.

[40] G. K. I. Mann, B.-G Hu, and R. G. Cosine, *Analysis of direct action fuzzy PID controller structures*, IEEE Transactions on Systems, Man, and Cybernetics-Part B: Cybernetics 29 (1999), no. 3, 371–388.

[41] Z. Michalewicz, *Genetic algorithms + data structures = evolution programs*, Springer-Verlag, 1996.

[42] K. S. Miller and B. Ross, *An introduction to the fractional calculus and fractional differential equations*, Wiley & Sons, New York, 1993.

[43] M. Mizumoto, *Realization of PID control by fuzzy control methods*, Fuzzy Sets and Systems 70 (1995), 171–182.

[44] K. B. Oldham and J. Spanier, *The fractional calculus*, Academic Press, New York, 1974.

[45] Manuel D. Ortigueira and António J. Serralheiro, *New insights into pseudo-fractional* ARMA *modelling*, Proceedings of the Second IEEE International Conference on Computational Cybernetics (ICCC 2004) (Vienna, Austria), August 30-September 1, 2004, pp. 391–394.

[46] A. Oustaloup, *La dérivation non entière: Théorie, synthèse et applications*, Editions Hermès, Paris, 1995.

[47] I. Pan and S. Das, *Intelligent fractional order systems and control: An introduction*, Springer, Berlin, 2013.

[48] K. M. Passino and S. Yurkovich, *Fuzzy control*, Addison-Wesley, Menlo Park, California, 1998.

[49] Eduardo S. Pires, Paulo B. Moura de Oliveira, J. A. Tenreiro Machado, and Isabel S. Jesus, *Fractional order dynamics in a particle swarm optimization algorithm*, Seventh International Conference on Intelligent Systems Design and Applications- IEEE - ISDA'07 (2007), 703–708.

[50] I. Podlubny, *Fractional differential equations*, Academic Press, San Diego, 1999.

[51] _____, *Fractional-order systems and $PI^\lambda D^\mu$-controllers*, IEEE Transactions on Automatic Control 44 (1999), no. 1, 208–214.

[52] H. Shayeghi, A. Safari, and H. A. Shayanfar, *Multimachine power system stabilizers design using PSO algorithm*, International Journal of Electrical Power and Energy Systems Engineering 1 (2008), 703–708.

[53] M.-Y. Shieh and T.-H. S. Li, *Design and implementation of integrated fuzzy logic controller for a servomotor system*, Mechatronics 8 (1998), 217–240.

[54] B. M. Vinagre, Y. Q. Chen, and I. Petras, *Two direct tustin discretization methods for fractional-order differentiator/integrator*, Journal of the Franklin Institute 340 (2003), 349–362.

[55] Z. H. Zhan, J. Zhang, Y. Li, and H. S. H Chung, *Adaptive particle swarm optimization*, IEEE Transactions on Systems, Man, and Cybernetics 39 (2009), 1362–1381.

INDEX

D

E

F